University of Southampton

Faculty of Medicine

Clinical and Experimental Sciences

Investigating macrophage-pathogen interactions in asthma

by

Jodie Ackland

ORCID ID: 0000-0003-3120-3620

Thesis for the degree of Doctor of Philosophy

January 2021

University of Southampton

Abstract

Faculty of Medicine
Clinical and Experimental Sciences
Thesis for the degree of Doctor of Philosophy
Investigating macrophage-pathogen interactions in asthma
By Jodie Ackland

The pathobiont, Nontypeable *Haemophilus influenzae* (NTHi), colonises the airway of individuals with chronic respiratory disease and is particularly associated with severe, neutrophilic, steroid-resistant asthma. Although NTHi has been implicated in asthma, respiratory tract viral infections remain the main aetiological agent of asthma exacerbations. However, it is now becoming clear that the presence of potentially pathogenic bacteria, such as NTHi, are present in the airway prior to respiratory tract viral infections. The macrophage is the predominant immune cell in the airway, yet accumulating evidence suggests NTHi is able to infect and persist within macrophages, which are also a target of the influenza A virus (IAV). It is unclear whether NTHi infection and persistence modulates macrophage responses to respiratory tract viral infections.

The aim of this thesis was to investigate modulation of macrophage gene expression during intracellular NTHi infection and how this interaction impacts on the response of these cells to subsequent infection with IAV. In addition, this thesis aimed to investigate transcriptomic alterations of NTHi during intracellular infection of macrophages, in order to identify mechanisms of persistence.

To achieve these aims, dual RNASeq analysis of an NTHi-monocyte-derived macrophage (MDM) infection model was performed. Transcriptomic analysis of NTHi-infected MDM identified enrichment of macrophage intracellular immune response pathways. Use of WGCNA identified *CASP4*, *PNRC1* and *SGPP2* to be the central MDM genes in the gene module most significantly associated with NTHi infection. Despite activation of MDM innate immune responses, NTHi was still able to persist within these cells. NTHi adaptation to persistence was associated with modulation of bacterial pathways involved in metabolic and stress responses, and downregulation of NTHi ribosomal protein genes. However, validation of the top NTHi differentially expressed genes *bioC, mepM* and *dps*, found strain-dependent expression of NTHi genes. Validation of select macrophage intracellular immune response genes demonstrated conservation of the MDM transcriptomic response when challenged with additional clinical strains of NTHi. Furthermore, NTHi presence was detected by FISH in 56% of severe asthma bronchoalveolar lavage (BAL) samples, which was associated with increased neutrophil inflammation ($p=0.0462$) and asthma duration ($p=0.0436$). Elevated *IL1B* ($p=0.0041$), *GBP1* ($p=0.0477$) and *SGPP2* ($p=0.0221$) gene expression was detected in samples determined as NTHi positive compared to NTHi negative, indicating modulation of airway inflammation by NTHi. Adaptation of the MDM model to incorporate the IAV following NTHi infection resulted in further modulation of the infection process; IAV replication levels decreased ($p=0.0049$), whereas NTHi load increased ($p=0.0313$). Decreased IAV levels was suggested to be due to NTHi-mediated upregulation of macrophage anti-viral immunity, specifically the type I IFN pathway, prior to IAV infection. Increased NTHi presence was associated with transcriptomic changes in NTHi genes previously identified to be involved in NTHi adaptation to intracellular persistence, *bioC* and *mepM*. Consequently, NTHi-infected macrophages exhibited a sustained inflammatory response, compared to MDM infected with IAV-alone.

The data in this thesis indicate the ability of NTHi to adapt in order to persist within macrophages, despite activation of macrophage intracellular immune response pathways. The subsequent modulation of IAV infection and NTHi colonisation during co-infection resulted in sustained macrophage inflammation that was not sufficient to completely clear either pathogen. Modulation of macrophage responses prior to and during bacterial-viral co-infection could have important implications for designing future studies to better our understanding of multiple host-pathogen interactions in the lung.

Table of Contents

Table of Tables

Table of Figures

Research Thesis: Declaration of Authorship

Print name: Jodie Ackland

Title of thesis: Investigating macrophage-pathogen interactions in asthma

I declare that this thesis and the work presented in it are my own and has been generated by me as the result of my own original research.

I confirm that:

1. This work was done wholly or mainly while in candidature for a research degree at this University;
2. Where any part of this thesis has previously been submitted for a degree or any other qualification at this University or any other institution, this has been clearly stated;
3. Where I have consulted the published work of others, this is always clearly attributed;
4. Where I have quoted from the work of others, the source is always given. With the exception of such quotations, this thesis is entirely my own work;
5. I have acknowledged all main sources of help;
6. Where the thesis is based on work done by myself jointly with others, I have made clear exactly what was done by others and what I have contributed myself;
7. None of this work has been published before submission.

Signature: .....Date:.....

Acknowledgements

My first thanks must go to my main supervisor Dr. Karl Staples. Thank you for your substantial support, invaluable guidance and continual encouragement throughout my PhD. I must also thank the other members of my supervisory team, Dr. David Cleary, Professor Myron Christodoulides and Professor Tom Wilkinson for all of their support and advice. I am very grateful to have had this opportunity, which would not have been possible without an Asthma UK-funded studentship.

The work in this thesis could not have been carried out without the tireless efforts of numerous individuals involved in ensuring the maintenance and smooth running of equipment and facilities, as well as providing me with technical and scientific advice and support. Namely, I need to thank Richard Jewell, Dr. Carolann McGuire, Dr Laurie Lau, Dr. Regina Teo and Dr. Dave Johnston. I must acknowledge the work of Dr. Karen Osman in sequencing and characterising the NTHi strains used in this thesis, as well as Rebecca Anderson for her support in NTHi culture. The sequencing in this thesis was performed by Novogene Ltd., I must thank the team involved at Novogene for their advice and support. The bioinformatics analysis in this thesis would not have been possible without Dr. Ashley Heinson, without whom I would have stumbled at the first bioinformatic-shaped hurdle. Thank you for your valuable time, patience and guidance.

I am truly grateful to all of the individuals who donated and/or took blood as part of this work – without you, this work could not have been carried out. Similarly, I must thank all of the volunteers and study staff involved in the WATCH study. Special thanks must go to Clair Barber for her assistance in this aspect, but most especially for the emotional support in the form of encouraging chats and emails along the way.

The biggest cohort of people that I must thank are all of the past and present members of the Pulmonary Immunology group. In particular, I must thank Dr Doriana Cellura who reassuringly keeps the lab smoothly running. I am truly thankful for all of your technical advice over the years, but most importantly, for your continual encouragement and for often helping me put things into perspective. Thanks must go to Dr. C. Mirella Spalluto for her crucial and insightful molecular biology advice. I must thank Dr. Aishath Fazleen, Dr. Alastair Watson, Dr. Anna Freeman and Dr. Hannah Burke for their support and engaging office/lab chats – from scientific discussions to engaging sport debates. For both academic and emotional support, Dr. Grace Cooper and Sruthymol Lukose were absolute rocks. It was an absolute pleasure working with both of you. Grace, thank you for your technical help, particularly surrounding flow cytometry, and for our many Tapas Tuesday (or any day) trips after a long day in the lab. Sruthy, thank you for your invaluable help and advice with image analysis. Our coffee chats were welcome breaks during those long incubation times, not to mention acting as a venting outlet, whilst our continual meme exchanges provided some much needed comic relief.

My initial passion for scientific research was kindled by Dr. Julia Rey-Nores, without whom I would not have had the confidence to apply for a PhD. I would like to recognise and thank Julia, for her encouragement and for helping me find my resolve and take the first steps on this path.

Of course, thanks must go to my family and friends for their love and support throughout my PhD.

My most unreserved thanks are saved for Dr. Joshua Wallington. Thank you, not just for your assistance in the thesis proof-reading process, previously teaching me lab techniques and acting as a sounding board for scientific discussions, but for your unconditional love and support throughout my PhD. Your endless patience, understanding, positivity and rational voice of reason gave me strength and kept me grounded and focussed right to the very end.

Abbreviations

ACP ..... Acyl Carrier Protein
ACQ ..... Asthma Control Questionnaire
ALI ..... Air Liquid Interface
AM ..... Alveolar Macrophage
B2M ..... Beta-2 Microglobulin
BAL ..... Bronchoalveolar Lavage
BD ..... Bronchodilator
BDP ..... Beclometasone Dipropionate
BHI ..... Brain Heart Infusion
BMI ..... Body Mass Index
BP ..... Biological Process
BSA ..... Bovine Serum Albumin
CARD9 ..... Caspase-associated recruitment domain 9
CC ..... Cellular component
CCL ..... Chemokine (C-C motif) Ligand
CD ..... Cluster of Differentiation
cDNA ..... complementary DNA
CF ..... Cystic Fibrosis
CFU ..... Colony Forming Unit
ChIP-seq ..... Chromatin Immunoprecipitation followed by sequencing
CHOC ..... Chocolate Agar
ChoP ..... Phosphorylcholine
CLR ..... C-type Lectin Receptor
CO_2 ..... Carbon dioxide
COPD ..... Chronic Obstructive Pulmonary Disease
CpG ..... 5'—Cytosine—phosphate—Guanine—3’
CPM ..... Counts Per Million
Ct ..... Cycle Threshold
CXCL ..... Chemokine (C-X-C motif) Ligand
DAMPs ..... Damage Associated Molecular Patterns
DAPI ..... 4',6-Diamidino-2-Phenylindole
DEG ..... Differentially Expressed Gene
DNA ..... Deoxyribonucleic Acid
dNTP ..... Deoxyribonucleotide Triphosphate
dsRNA ..... double stranded RNA

EDTA.....Ethylenediaminetetraacetic Acid
ELISA.....Enzyme-Linked Immunosorbent Assay
EPS.....Extracellular Polymeric Substance
ER .....Endoplasmic Reticulum
Fab.....Fragment antigen-binding
FACS .....Fluorescence-Activated Cell Sorting
FBS.....Fetal Bovine Serum
FC .....Fold Change
FcγR .....Fc gamma Receptor
FcεRI .....Fc epsilon Receptor I
FDR .....False Discovery Rate
FEV1 .....Forced expiratory volume in one second
FISH .....Fluorescence *in situ* hybridization
FITC.....Fluorescein isothiocyanate
FVC .....Forced Vital Capacity
GBP.....Guanylate binding Protein
GFP .....Green Fluorescent Protein
GM-CSF.....Granulocyte-Macrophage Colony-Stimulating Factor
GO .....Gene Ontology
GS .....Gene Significance
HA.....Hemagglutinin
Hap .....*Haemophilus influenzae* adhesion protein
HGF.....Hepatocyte Growth Factor
HiB .....*Haemophilus influenzae* type b
HMW .....High Molecular Weight
IAV.....Influenza A virus
IBV .....Influenza B virus
ICAM-1 .....Intercellular Adhesion Molecule 1
IPF.....Idiopathic pulmonary fibrosis
IFN .....Interferon
Ig.....Immunoglobulin
IL.....Interleukin
IQR.....Interquartile Range
IRF .....Interferon Regulatory Factor
ISG .....Interferon Stimulated Gene
IU .....Infectious Units
JAK.....Janus Kinase
KEGG .....Kyoto Encyclopaedia of Genes and Genomes

KO ..... Knockout

LABA..... Long Acting Beta Agonist

LAMA ..... Long Acting Muscarinic Antagonist

LAMP..... Lysosome-Associated Membrane Proteins

LBP ..... LPS Binding Protein

LC ..... Lysis Control

LDH ..... Lactate Dehydrogenase

LIMS ..... Leukocytes: Inflammation Model Systems

LLOQ ..... Lower Limit of Quantification

lncRNA ..... long noncoding RNA

LOS..... Lipooligosaccharide

LPS ..... Lipopolysaccharide

MACS ..... Magnetic-Activated Cell Sorting

MAVS ..... Mitochondrial antiviral-signalling protein

MARCO ..... Macrophage Receptor with Collagenous Structure

MCC ..... Maximal Clique Centrality

MDCK..... Madin-Darby Canine Kidney

MDM..... Monocyte-Derived Macrophage

MF..... Molecular Function

MICL..... Myeloid Inhibitory C-type Lectin-like Receptor

miRNA..... microRNA

MLST ..... Multilocus Sequence Typing

MM ..... Module Membership

MOI..... Multiplicity Of Infection

mRNA..... messenger RNA

Mtb ..... *Mycobacterium tuberculosis*

MTS..... 3-(4,5-dimethylthiazol-2-yl)-5-(3-carboxymethoxyphenyl)-2-(4-sulfophenyl)-2H-tetrazolium

MyD88 ..... Myeloid differentiation primary response 88

NA ..... Neuraminidase

NAD..... Nicotinamide Adenine Dinucleotide

ncRNA ..... noncoding RNA

NEP..... Nuclear Export Protein

NF-κB ..... Nuclear Factor kappa-light-chain-enhancer of Activated B Cells

NK cell..... Natural Killer cell

NLR..... NOD-like Receptor

NLRP3 ..... Nucleotide-binding oligomerization domain, Leucine-Rich repeat, Pyrin domain containing 3

NOD ..... Nucleotide binding Oligomerization Domain
NP ..... Nucleoprotein
NRAD ..... National Review of Asthma Deaths
NS ..... Nonstructural
NTHi ..... Nontypeable *Haemophilus influenzae*
OD ..... Optical Density
OMP ..... Outer membrane protein
OMV ..... Outer membrane vesicles
OVA ..... Ovalbumin
PA ..... Polymerase Acidic protein
PB ..... Polymerase Basic protein
PAF ..... Platelet Activating Factor
PAMP ..... Pathogen-Associated Molecular Pattern
PBMC ..... Peripheral Blood Mononuclear Cells
PBS ..... Phosphate-Buffered Saline
PCA ..... Principal Component Analysis
PCR ..... Polymerase Chain Reaction
pe ..... Protein E
PFA ..... Paraformaldehyde
PFU ..... plaque forming units
PresRAT ..... Predicting small RNAs and their Targets
PRR ..... Pattern Recognition Receptor
PVE ..... Proportion of Variance Explained
PW ..... PermWash™
QC ..... Quality control
qPCR ..... Quantitative PCR
RdRP ..... RNA-dependent RNA Polymerase
RIG ..... Retinoic Acid-inducible Gene
RILP ..... Rab7-Interacting Lysosomal Protein
RIN ..... RNA Integrity Number
RIPK2 ..... Receptor-Interacting Protein Kinase 2
RLR ..... Retinoic Acid-inducible Gene-I-Like Receptor
RNA ..... Ribonucleic Acid
RNP ..... Ribonucleoprotein
ROS ..... Reactive Oxygen Species
RPMI ..... Roswell Park Memorial Institute
RSH ..... Rel/Spo Homolog
rRNA ..... ribosomal Ribonucleic Acid

RS ..... Reduced Serum
RSV ..... Respiratory Syncytial Virus
S1P ..... Sphingosine 1-Phosphate
scRNASeq ..... single cell RNA Sequencing
SD ..... Standard Deviation
SR ..... Scavenger Receptor
sRNA ..... small RNA
SNP ..... Single Nucleotide Polymorphism
ssRNA ..... single stranded RNA
ST ..... Sequence Type
STAT ..... Signal Transducer and Activator of Transcription
Streptavidin-HRP ..... Streptavidin-Horseradish Peroxidase
TCID ..... Tissue Culture Infectious Dose
TGF- β ..... Transforming Growth Factor beta
T1/2/17 ..... Type 1/2/17
Th ..... T Helper
TLR ..... Toll-like Receptor
TMB ..... 3,3',5,5'-Tetramethylbenzidine
TMM ..... Trimmed Mean of M-values
TNF ..... Tumour Necrosis Factor
TOM ..... Topological Overlap Matrix
Treg ..... Regulatory T cells
TRIF ..... TIR-domain-containing adapter-inducing interferon-β
tRNA ..... transfer RNA
ULOQ ..... Upper Limit of Quantification
VEGF ..... Vascular Endothelial Growth Factor
WASP ..... World ASthma Phenotypes
WATCH ..... Wessex AsThma CoHort of difficult asthma
WHO ..... World Health Organization
WGCNA ..... Weighted Gene Correlation Network Analysis

Chapter 1 Introduction

1.1 Asthma

1.1.1 Overview of asthma

Asthma is a complex, heterogeneous disease of the airways characterised by episodic and reversible airway obstruction, hyper-resp

onsiveness and inflammation[1]. A variety of factors have been implicated in the onset of asthma including genetics, allergen exposure, infection, pollution, diet, hormones as well as stress and psychological factors[2]. Asthma can be diagnosed by clinical assessment of patient history, spirometry and allergic sensitivities[3]. Atopy is the term given to the genetic predisposition to mount high immunoglobulin (Ig) E responses against environmental allergens, which can result in the development of allergic diseases including allergic rhinitis, atopic dermatitis (eczema) and allergic asthma[4].These allergic sensitivities are a risk factor for asthma development and can be tested for using the skin prick test, which measures reactions to a variety of common environmental allergens[5], or measuring serum levels of IgE[6]. However, non-allergic (or non-atopic) forms of asthma can develop following exposure to a non-allergic environmental trigger. Clinically defining asthma can be complex due to a various number of clinical asthma phenotypes displaying different disease pathologies[7].

There is no current cure for asthma, with therapies only designed to manage symptoms. These include inhaled/oral corticosteroids and leukotriene modifiers to control airway inflammation and bronchodilators such as β_2-agonists or anticholinergics for immediate relief of asthma symptoms[8]. However, some phenotypes of asthma appear to be steroid-resistant and unresponsive to treatment[9]. The future of asthma treatment is moving towards modulating specific components of the immune system involved in asthma pathogenesis by use of monoclonal antibodies targeting inflammatory pathways[10,11]. However there is still an unmet need for better preventative treatments[2].

1.1.2 Epidemiology and burden of asthma

Asthma affects 300 million people worldwide, with 1 in 10 children and 1 in 12 adults affected[1,12]. In the UK, the majority of the estimated £1.1 billion cost of asthma per annum is generated by delivering primary care preventative treatments to manage and ease symptoms[13]. Despite this cost, approximately 75% of asthma hospital admissions could be avoided with improved or better primary care[14]. Deaths caused by asthma are rare but are a leading cause of preventable deaths and the UK-wide National Review of Asthma Deaths (NRAD) found that up to two thirds of asthma-associated deaths could have been prevented if the appropriate care was given, with the number of reported deaths in the UK amongst the highest in Europe[14,15]. Following on from this 2015 NRAD

review, Gupta *et al.* (2018) identified the influence of socio-economic factors on the development of asthma and impact subsequent access to treatment, with asthma more prevalent in disadvantaged communities in England[16]. The 20th century saw a dramatic rise in asthma, with childhood asthma rates doubling between the 1980s and 2009[17,18]. One theory that attempts to explain the increased incidence of asthma is the 'hygiene hypothesis', which suggests that modern day cleanliness and sterile environments have promoted the development of allergic diseases such as asthma by reducing the exposure of individuals to non-infectious organisms during childhood[19]. The hygiene hypothesis is backed by a body of evidence showing that individuals in different living environments, such as farms, were exposed to microbial organisms in early life and were less likely to go on to develop asthma[20–23]. The link between microbes and asthma has been further demonstrated over the last decade, with a number of studies indicating that the composition of the lung microbiome is associated with development of asthma in later life[24,25]. This concept will be discussed further in Section 1.2.

1.1.3 Airway inflammation and asthma phenotypes

The heterogeneous nature of asthma renders it difficult to clinically group patients, resulting in a spectrum of asthma phenotypes[26]. A call for studies focused on working towards gaining a better understanding and recognition of the various asthma phenotypes resulted in the establishment of the World ASthma Phenotypes (WASP) study in 2016[7,27]. Despite the evolving understanding of asthma phenotypes, two commonly used definitions focus on allergic and non-allergic asthma[26].

The allergic asthma phenotype is the classical form of asthma most widely recognised and is implicated in 50-80% of asthma cases[28]. Allergic asthma is induced by common environmental allergens including house dust mite, pollen, mould and ragweed and is characterised by type 2 (T2) inflammation[26]. T2 inflammation is driven by cytokines such as interleukin (IL)-4, IL-5 and IL-13 released by T helper (Th) 2 cells which increase the recruitment and survival of eosinophils, an innate inflammatory immune cell. T2 inflammation promotes the pathophysiological features of eosinophilic asthma including increased basement membrane thickness and corticosteroid responsiveness[7,26,29,30]. As such, a number of therapeutics used in asthma aim to reduce the number of eosinophils and T2 cytokines[31]. However, despite elevated eosinophils levels in asthma, the functional role of eosinophils in asthma remain unclear. Observations that IL-5-specific blocking antibodies reduce blood and sputum eosinophil levels, but not airway hyper-responsiveness or asthma symptoms, provides uncertainty about the pathological role of eosinophils in asthma[32].

The cytokine IL-9 was originally considered a member of the T2 cytokine family, produced by Th2 cells, however it was identified that a specific subset of Th cells, Th9 cells, are the main source of IL-9[33]. Enhanced expression of IL-9 has been identified in the lungs of asthmatic patients with

increased mast cell and eosinophil accumulation, mucus hypersecretion and airway hyper-responsiveness[34]. Unlike eosinophils, mast cells appear to be present in the airways of asthmatics irrespective of disease phenotype or severity[35]. Mast cells are produced and mature in the bone marrow and are crucial effector and regulatory cells during T2 responses. In particular, mast cells are responsible for airway bronchoconstriction following exposure to an environmental trigger such as an allergen[36]. The IgE antibody, which is released from activated B cells, attaches to Fc epsilon Receptor I (FcεRI) on mast cells[37]. Upon binding of the allergen to the exposed fragment antigen-binding (Fab) region of the antibody, the mast cell is activated and undergoes degranulation releasing bronchoconstrictors including histamine, leukotrienes and prostaglandins[36,37]. Mast cells also release cytokines including tumour necrosis factor (TNF) α/β and IL-4, -5, -6, -1β and -13. These cytokines have a range of effects on eosinophil production and regulation (IL-5) and stimulate the proliferation and differentiation of activated B-cells (IL-4, 5 and 6)[36,37]. Mast cell release of the aforementioned mediators alters permeability and adhesiveness of the vascular endothelium, allowing for circulating inflammatory cells to adhere to and migrate into the tissue. A higher degree of mast cell degranulation has been shown to occur in asthmatic patients compared to healthy controls[38], suggesting ongoing mast cell activation in the asthmatic airway promotes the characteristic chronic inflammation of the airways[37,38].

The role of the Th subset of regulatory cells (Tregs) is suppression of effector cells in order to maintain low levels of airway hyper-responsiveness and limit the above described T2-mediated inflammation of the airways[34,39]. Treg cells are a source of 'suppressive' cytokines such as Transforming Growth Factor (TGF)-β, IL-10 and IL-35 which act to suppress the local immune response[22]. Lower levels of Tregs have been identified in the blood and lung of individuals with asthma, with the isolated Tregs displaying heterogenic functional phenotypes and impaired responses[40,41]. As a result, Treg dysfunction is associated with the failure to suppress an excessive T2 response, resulting in asthma development[22].

Although asthma pathogenesis has long been associated with an excessive T2 response and increased eosinophil levels, an increasing number of studies now challenge this view, with non-T2 inflammation evident in some asthma patients[31]. A literature search conducted by Douwes *et al.* (2002) discovered that only 50% of published asthma cases were associated with eosinophilic asthma[42]. Since the publication of this aforementioned review, it has been recognised that neutrophilic inflammation also plays a significant role in asthma and is more commonly associated with severe asthma phenotypes, linked to more severe airflow obstruction, steroid resistance and increased presence of potentially pathogenic bacteria[43,4444,45]. Although the neutrophilic asthma phenotype is not the most common form of disease (5-20% of all cases), individuals with severe

asthma have increased risk for hospitalisation and account for 50-80% of the health care burden of asthma[46].

Neutrophils are an innate immune cell involved in microbial killing using an array of intracellular and secreted effector molecules[47]. However, dysregulated release of these neutrophil effector molecules can cause further unwarranted inflammation leading to tissue damage and progressive loss of lung function. Confirmation of neutrophil infiltration into the lung by analysing bronchial biopsies and induced sputum obtained from severe asthma patients found that neutrophilic inflammation was mediated by elevated T1/17 immune responses[26,30,36,48].

T17 cytokines include IL-17A, IL-17F and IL-22, however the primary cellular source of these cytokines remain unclear. Th17 cells can produce T17 cytokines upon activation, with increased frequency of Th17 cells found in the airways of asthmatics. Conversely, both macrophages and the epithelium have also been implicated as sources of T17 cytokines[49,50]. Regardless of the cellular source, these T17 cytokines indirectly promote recruitment of neutrophils to the airway by increasing the secretion of neutrophil chemokines, such as CXCL8/IL-8, from airway epithelial cells[51]. IL-8 is a potent chemoattractant for neutrophils, highlighted by a >50% reduction in neutrophil migration following IL-8 inhibition[52]. The crucial relationship between IL-8 and neutrophils was further highlighted in a study by Hosoki *et al.* (2015), who investigated a panel of 48 cytokines and chemokines in BAL fluid to determine which inflammatory mediator(s) could be used as a diagnostic marker[53]. An increase in IL-8 and neutrophil levels together was the only inflammatory marker that could distinguish between the severities of asthma phenotypes. Those with more severe forms of asthma also exhibit increased inflammasome responses, with elevated expression of IL-1β at both the protein and messenger RNA (mRNA) level[54]. Elevated expression of other inflammasome components detected in severe asthma sputum including nucleotide-binding domain, leucine-rich repeat, pyrin domain containing 3 (NLRP3), caspase-1 and caspase-4 further suggest a role for the inflammasome in severe asthma[55].

Although eosinophil and neutrophil sputum proportions are often used as a marker to differentiate between asthma phenotypes, the two inflammatory phenotypes are not mutually exclusive. Patients can also display high proportions of both immune cells (mixed granulocytic) or low/no proportion of both immune cells (paucigranulocytic). The heterogeneous, complex milieu of inflammatory cells in asthma highlight the difficulties in pinpointing the exact underlying mechanism of asthma pathogenesis.

1.1.4 Asthma exacerbations

An asthma exacerbation is characterised by a worsening of symptoms following exposure to a trigger and can be graded in severity as mild, moderate, severe or life-threatening[56]. Symptoms

include wheeze, shortness of breath and chest tightness and are induced by airway inflammation, resulting in airflow obstruction and increased airway responsiveness[57,58]. With approximately 65,000 hospital admissions yearly in the UK, exacerbations contribute to the considerable health care burden of asthma, with the added economic impact due to lost productivity of workers[59]. In general, exacerbations heavily and negatively affect quality of life. Triggers of asthma exacerbations include air pollution, cigarette smoking, allergens and bacteria/virus infections[1].

Recognition of air pollution as a cause of an exacerbation can be difficult as there can be a delay between a peak in air pollution and a peak in hospitalisations due to an exacerbation event[60]. Pollution sources can be separated into outdoor and indoor pollution. Outdoor sources includes pollutants from combustion of natural gas and vehicle fuel, ozone and particulate matter whilst indoor sources include fireplaces, heaters and gas stoves[1]. Cigarette smoking is associated with more severe symptoms of asthma and an accelerated decline in lung function, including an unexplained impaired response to corticosteroid treatment[61]. Common allergens such as dust mite, cockroach, pet hair/fur, mould and grass pollen are associated with increased asthma-related admissions to hospital[62].

Respiratory tract infections have also been identified as a cause of asthma exacerbations. Seasonal variations in exacerbation-related hospital admissions occur due to the seasonal nature of some circulating pathogens[58]. In children, seasonal peaks occur in line with the school calendar, whereas in older adults, a peak is seen in the winter months, which aligns with increases in circulating viruses such as rhinovirus and influenza[1]. Although the exact role of bacterial infections in exacerbations is unclear, various bacteria have been isolated during an exacerbation. The atypical bacterial pathogens *Mycoplasma pneumoniae* and *Chlamydia pneumoniae* were originally associated with exacerbations of asthma[63], however numerous other bacterial pathogens now implicated in asthma exacerbations include *Haemophilus influenzae, Moraxella catarrhalis, Streptococcus pneumoniae, Haemophilus parainfluenzae, Klebsiella pneumoniae* and *Bordetella pertussis*[64–66]. The role of bacteria and the microbiome in asthma will be discussed further in Section 1.2.

1.1.5 Viral exacerbations of asthma

Despite isolation of bacteria during asthma exacerbations, the most commonly identified organisms during exacerbation are viruses, with up to 80% of exacerbations driven by viral respiratory tract infections[67,68]. Viruses are often difficult to detect by standard culture methods, however the advent of sensitive molecular techniques led to an increased detection of respiratory viruses from samples[69]. In some cases, polymerase chain reaction (PCR) based techniques identified almost ten times more positive samples than culture-dependent methods[69]. The mechanisms of viral-induced exacerbations appear to differ from exacerbations induced by non-infective triggers[68]. A study by

Wark *et al.* (2002) found increased neutrophil and neutrophil elastase levels during an infective exacerbation, whereas exacerbations due to non-infective causes resulted in increased eosinophil levels and the number of IL-5+ cells[68]. Furthermore, it appears that different viruses induce distinct airway responses; influenza infection results in increased epithelial cell lysis comparative to rhinovirus infection[58]. In order to develop targeted therapeutics to decrease the incidence of exacerbations and improve the quality of life for individuals with asthma[58], the exact mechanisms by which different triggers cause exacerbations requires clarification.

A systematic review by Papadopoulos *et al.* (2011) found no less than 11 viruses associated with exacerbations of asthma[70]. Interestingly, Papadopoulos *et al.* found differences in the prevalence of viruses between adults, children (6 – 17 years old) and infants (<6 years old). High rhinovirus prevalence was detected in 55% of children, whereas in adults, rhinovirus prevalence was only 29%. Respiratory syncytial virus (RSV) was also lower in adults compared to infants (3% to 19%) with prevalence in children also low at 4%. Conversely, detection of influenza virus was higher in adults (23%) compared to both infants and children (3% and 2.5% respectively). Depending on the study included in the aforementioned systematic review, the reported percentage of each specific virus detected during an exacerbation varied. This could be due to numerous differences in each study design including sample size, demographics, seasonality and methodologies.

1.2 Lung Microbiome

1.2.1 Overview

The dogma of lung sterility has prevailed since the late 19th century, supported by the lack of sensitivity of culture-dependent methods when sampling for bacteria. Subsequent misapplication and misinterpretation of microbiology testing and the belief that positive results were due to contamination of samples from the upper airway furthered the notion of lung sterility[71]. The level of agreement with this notion was such that the Human Microbiome Project in 2007 did not include the lungs amongst the 18 body sites initially sampled[71]. However, the advent of culture-independent methods have refuted the dogma of lung sterility by demonstrating that a diverse community of bacteria reside in the airways[72]. Advances in our understanding of the lung microbiome have originated largely through sequencing techniques such as 16s RNA sequencing which is a much more sensitive method of detecting bacteria in samples compared to conventional culture methods[73,74]. Expanding on 16s RNA sequencing, metagenomics allows for sequencing of all genes to allow for exploration of the metabolic and functional profile of the microbial community sampled, whereas metatranscriptomics reveals the active functional profile of the community which can be compared across different conditions, such as between health and disease[73].

The study of the lung microbiome is a relatively young field, and as such, faces technical and methodological challenges[72]. The increased sensitivity of culture-independent techniques detects

contaminants in samples, which can confound the study results[75]. A variety of contamination sources can be introduced during airway sampling and subsequent sample preparation including the tools used during bronchoscopy sampling, the bronchoscope rinse fluid, plastic consumables, reagents including DNA extraction kits or PCR mastermixes and even researchers themselves[75,76]. Sterile laboratory reagents can contain small amounts of bacterial DNA, therefore reagents used for sampling need to be considered as controls for microbiome sequencing experiments to ensure that any novel bacteria found are not due to reagent contamination[75,77]. Contamination by upper respiratory tract microbes can occur during sampling of the lower respiratory tract which cause difficulties in distinguishing between the microbiome of the upper and lower respiratory tract[76]. Incorporating appropriate controls into microbiome studies is particularly important due to the low biomass of the lung microbiome which could otherwise make it difficult to clearly determine the microbiome signature above sequencing noise[75]. Avoiding sample contamination is crucial given the observation that even within the lung, bacterial communities differ between anatomical sites[78]. Despite these technical obstacles, studies are now identifying common lung microbiome profiles which allows for comparison of the microbiome between health and disease[72].

1.2.2 Development and composition of the lung microbiome

The mechanisms of lung microbiome development are not entirely clear; it was originally believed that the healthy human foetus develops within a bacteria-free environment and acquires a microbiome following birth[79]. Delivery mode impacts on the acquisition and structure of the lung microbiome, suggesting that following birth there is a maternal-newborn transfer of microbes in which environmental factors influence microbiome acquisition[79]. However, recent work has shown that the lung microbiome of vaginally-delivered and caesarean section-delivered babies were similar, suggesting that the lung microbiome was developed *in utero*[80]. This is consistent with a previous study showing the placental microbiome bears resemblance to the human oral microbiome, suggesting the airway microbiome is transplacentally-derived[81]. Conversely, a more recent study found no substantial evidence of bacteria or a structured microbiome in the placenta of humans[82]. The ongoing controversy surrounding placental microbiome presence highlights the need for appropriate controls when attempting to characterise environments with low microbial biomass.

The composition of the lung microbiome is influenced by three factors; microbial immigration, microbial elimination and the relative reproduction rate of it members[71]. The primary source of microbial immigration is believed to be through microaspiration and direct mucosal dispersion. Microbes are cleared (eliminated) mechanically by mucociliary clearance and the innate and adaptive immune response within the respiratory tract. Finally, microbial growth/reproduction rates vary depending on pressures exerted on microbial communities by the lung environment and

the immune response. Microbiome studies at various anatomical sites have found the existence of a core microbiome at each location in healthy individuals[74]. Interestingly, within the lung it appears that the core lung microbiome includes potential respiratory tract pathogens[25,72,83,84]. The composition of the lung microbiome is altered in individuals with chronic lung disease, such as asthma, which can be further modified during exacerbated periods of disease[85].

1.2.3 Microbiome in asthma

The last decade has heralded a surge in lung microbiome studies to investigate the relationship between the microbiome and health and disease. One of the first studies investigating the structure of the microbiome in asthma was published in 2010 by Hilty *et al.* (2010) who found differences in the composition of the microbiome between asthmatics and healthy controls, with an increased presence of Proteobacteria[25]. Subsequent studies have confirmed the increased abundance of Proteobacteria in asthma[45], with specific Proteobacteria such as *H. influenzae,* associated with more severe, neutrophilic phenotypes of asthma[46,86,87].

The increased presence of specific potentially pathogenic bacteria in the lungs of children have been suggested to predispose individuals to development of asthma. Bisgaard *et al.* (2007) found that children who were colonised with these potentially pathogenic bacteria within 1 month of life were more likely to develop asthma by the age of 5[24]. It remains unclear as to how bacteria influence the development of asthma. However, studies using murine models have suggested that an altered microbiome structure favouring potentially pathogenic bacteria, instead of commensal organisms such as *Prevotella* spp. results in an altered immune response to infection. As such, the type of colonising microbes may influence host immune development and training[88,89]. Larsen *et al.* (2014) demonstrated that Peripheral Blood Mononuclear Cells (PBMC) isolated from children prior to asthma development in later life displayed aberrant immune responses to potentially pathogenic bacteria such as *H. influenzae, M. catarrhalis,* and *S. pneumoniae*. Thus, it is possible that modulation of immune responses by colonising bacteria in early life may predispose individuals to asthma, but the exact mechanisms for this modulation remain elusive.

Nonetheless, modulation of the host immune response by potentially pathogenic bacteria is suggested to contribute to the persistent airway inflammation in individuals that have already developed asthma. This concept was proposed by Folsgaard *et al.* (2013) who found that airway colonisation by *H. influenzae* and *M. catarrhalis* was associated with increased inflammation, including a mixed T1/T2/T17 response with high levels of IL-1β and TNF-α[90]. The increased presence of *H. influenzae* in particular has been associated with some of the main clinical features of asthma including increased bronchial hyperresponsiveness[91], increased airway inflammation including inflammasome activation[91] and elevated pro-inflammatory cytokines[86] and increased influx of

inflammatory cells such as neutrophils[87]. As individuals with asthma are treated with steroids to reduce airway inflammation, it is possible that the immunosuppressive effects of treatment result in the ability of Proteobacteria such as *H. influenzae* to better colonise the airway. As such, Marri *et al.* (2013) sought to determine whether the microbiome of steroid-naïve asthmatic patients was also perturbed[92]. In concordance with the previous studies, a higher prevalence of Proteobacteria was also found in the airways of steroid-naïve asthmatic patients compared to healthy controls. This suggests that the altered airway microbiome is not due to any immunomodulatory effects caused by steroid treatment and rather that microbiome dysbiosis is a feature of asthma.

1.2.4 Host-microbiome interactions

Although the importance of the composition of the lung microbiome between health and disease is becoming apparent, the complexities of host-microbiome interactions are only now beginning to be appreciated. Increasing evidence indicates that the gut microbiome modulates the host mucosal defence response, however less is known about the role of the lung microbiome in regulating the host immune response[93]. Human lung microbiome studies have mainly consisted of using metagenomics on large cohorts to identify the microbiome composition. Although metagenomics is a powerful tool, simply characterising the microbiome of individuals within cohorts does not ascertain any meaningful interactions between the host and resident microbes. A study by Franzosa *et al.* (2014) showed that using metagenomics or determining the relative abundance of a species in a sample does not necessarily correlate with the activity of the present microbes as measured using metatranscriptomics[94]. Determining microbial activity could better unveil the functional relevance of a particular microbe within a microbiome and whether modulation of host responses occur.

Recent studies have begun to correlate microbial activity with host gene expression. Using a combination of shotgun RNA sequencing for microbial identification and host differential gene expression, Castro-Nallar and colleagues (2015) identified a host gene profile in response to the presence of Proteobacteria[95]. Expanding on this work, Perez-Losada *et al.* (2015) used a dual transcriptomic profiling technique to simultaneously assess differences in the host and microbial functional properties of asthmatic children and healthy controls[96]. They found differences in bacterial metabolism-associated genes between the metatranscriptomes of asthmatic and non-asthmatic subjects, with host *IL1A* expression associated with bacterial adhesion[96]. Although studies such as the ones described above have now begun to associate the functional implications of the structure of distinct microbial communities in individuals, further work utilising metatranscriptomics is needed to determine the exact impact of these altered microbiome profiles in the development and progression of asthma and modulation of host immune responses. As accumulating evidence implicates certain Proteobacteria species such as *H. influenzae* in asthma,

the impact of the presence of certain pathogens must now be explored utilising experimental models aimed at elucidating the mechanisms behind host-pathogen interactions in asthma pathogenesis.

1.2.5 Overview of nontypeable *Haemophilus influenzae* (NTHi)

Haemophilus influenzae is a gram negative coccobacillus and a human-restricted pathobiont[97]. H. *influenzae* is a fastidious organism requiring both hemin (factor X) and nicotinamide adenine dinucleotide (NAD, factor V) for growth[98]. Transmission of *H. influenzae* occurs via respiratory droplets and is commonly isolated from the nasopharynx, middle ear and respiratory tract[99–101]. *H. influenzae* can be divided into typeable and nontypeable strains depending on the presence or absence of a polysaccharide capsule. This capsule is used to classify the encapsulated strains into six serotypes (a-f), with those strains not in possession of a capsule unable to be serotyped in this manner and are designated as nontypeable *Haemophilus influenzae* (NTHi).

NTHi strains are extremely diverse and are given Sequence Type (ST) numbers by multilocus sequence typing (MLST)[102]. The *H. influenzae* genome is estimated to consist of between 1,700 – 1,900 genes, however it has been suggested that the NTHi core genome is comprised of only 75% of these genes[103]. The remaining genes are accessory genes which form the supragenome (alternatively known as the pan-genome) and are interchangeable[104,105]. The natural competence ability of NTHi allows for acquisition of accessory genes that can be advantageous for survival or persistence in a particular environment, which results in vast NTHi strain diversity[103]. As well as vast genomic diversity, phase variation also generates heterogeneity. Phase variation involves a reversible ON/OFF switching of gene expression, resulting in a heterogenic phenotype within a clonal bacterial population[106]. The resulting heterogenic population increases the ability of bacteria to survive and persist by allowing for rapid adaptation to a changing environment and evasion of host immune responses[107].

NTHi infection is associated with various diseases including pneumonia, meningitis, sinusitis, otitis media and exacerbations of chronic respiratory diseases such as chronic obstructive pulmonary disease (COPD) and asthma[64,99,108–110]. Until recently, *H. influenzae* type b (Hib) was the predominant cause of *H. influenzae*-associated disease and morbidity and mortality amongst children[101]. However, the introduction of the Hib vaccine has been successful in reducing Hib-associated disease such as meningitis, septicaemia, pneumonia and epiglottitis[111]. A longitudinal study by Adam *et al.* (2010) found that prior to the vaccine, 64.9% of *H. influenzae* causing invasive disease was Hib, which dropped to 9.4% following the introduction of the Hib vaccine[112]. Carriage of Hib appears to decrease and eventually disappear within 24 months from the start of vaccination[113].

The widespread use of the Hib vaccine could contribute to lung microbiome dysbiosis through the removal of Hib, causing microbiome restructuring and expansion of NTHi into the ecological niche Hib previously occupied. Increasing incidence of NTHi since the introduction of the Hib vaccine is apparent; the percentage of invasive disease cases involving NTHi has risen from 29.9% to 70.3%[112]. Elsewhere, Langereis and Jonge (2015) report that in the twenty years following the implementation of the Hib vaccine, the number of cases of NTHi infection increased almost 6-fold[114]. The Hib vaccine targets the polysaccharide capsule, which is absent in NTHi. As such, other vaccine candidates need to be considered for an effective NTHi vaccine. However, the vast antigenic heterogeneity of NTHi strains renders it challenging to create an effective vaccine[115]. For this reason, coupled with the increasing prevalence of ampicillin-resistant strains, NTHi was classified as a priority pathogen by the World Health Organisation (WHO)[116].

1.2.6 NTHi infection of the respiratory tract

The first step in establishing infection is adherence to host airway cells[110]. NTHi express a repertoire of cell surface proteins that are important during adherence to and invasion of the respiratory tract. These adhesins include pili[117], *H. influenzae* adhesion protein (Hap)[118], High Molecular Weight (HMW) protein 1/2[119], Hia[120], P4/lipoprotein e, P5[121,122] and lipoolygosaccharide (LOS)[123], which can facilitate NTHi adherence to a variety of airway structures. The outer membrane lipoprotein e (P4), encoded by the *hel* gene, adheres to components of the extracellular matrix[124,125], whereas P5 interacts with intracellular adhesion molecule 1 (ICAM-1/CD54) expressed on epithelial cells[121]. Similarly, NTHi pili can bind to ICAM-1[126] and also human respiratory mucins which are the major component of airway mucus[127]. The HMW proteins and Hia bind to host cell sialic acid, which is found in high abundance in the human respiratory tract[128–130].

NTHi expression of LOS differs from lipopolysaccharide (LPS) which is expressed by the majority of gram-negative bacteria, due to the lack of the O-antigen[131]. The structure of LOS varies between NTHi strains due to phase variation, resulting in multiple heterogeneous LOS glycoforms[132]. The expression of phosphorylcholine (ChoP) on LOS allows NTHi to interact with a host cell surface receptor called platelet-activating factor (PAF), enabling adherence and invasion of host cells[133]. As such, elevation of the PAF receptor in the chronically inflamed airway could explain persistent colonisation by NTHi[133]. The duration of NTHi airway colonisation varies, with longitudinal studies of cystic fibrosis and COPD suggesting persistence ranges from months up to as long as 7 years[134–136].

One method by which some bacteria are able to persist within the airway is by formation of a biofilm. A biofilm can defined as an aggregation of microorganisms that adhere to each other and/or a surface surrounded by an extracellular polymeric substance (EPS)[137]. One of the most

studied biofilm formers within the lung is *Pseudomonas aeruginosa,* which is able to adapt to the cystic fibrosis airway and persist through biofilm formation[138]. The first evidence of NTHi airway biofilm formation *in vivo* was provided in bronchoalveolar lavage samples from cystic fibrosis patients[139]. However, the majority of work contributing to our current understanding of NTHi biofilm formation is in the context of otitis media[101]. Nonetheless, the ability of NTHi to form lung biofilms remains a controversial concept.

NTHi has traditionally been considered an extracellular pathogen, however an increasing number of reports suggest that NTHi is able to invade cells to enhance airway persistence and survival[140]. Geme *et al.* (1990) first used an *in vitro* model to demonstrate NTHi adherence and invasion of epithelial cells[141]. NTHi entry into cells consists of various mechanisms including receptor-mediated endocytosis[142] and macropinocytois[143,144] and often requires substantial cell cytoskeletal rearrangements. Early studies using epithelial cell lines showed NTHi persistence both paracellularly and intracellularly for up to 7 days post initial infection[145]. Ren *et al.* (2012) later expanded on this work and detected viable NTHi 10 days after infection in an air-liquid interface (ALI) co-culture model[146]. Intracellular residence of NTHi within airway epithelial cell membrane-bound vacuoles was also demonstrated by use of transmission electron microscopy[143].

One of the first indications of NTHi invasion of phagocytic cells was provided by Forsgren *et al.* (1994) who used transmission electron microscopy to visualise replicating, intracellular NTHi within macrophage-like cells isolated from adenoid tissue[147]. Early work by Ahren *et al.* (2001) found that in contrast to the invasion of epithelial cells as reported by Swords *et al.* (2000), the PAF receptor on monocytes was not involved with NTHi invasion of monocytes[133]. Instead, NTHi entered monocytes through receptor-mediated endocytosis mediated by interactions with a β-glucan receptor[142]. Furthermore, evidence for NTHi entry into macrophages by lipid-raft mediated endocytosis has been shown, with lipid raft inhibitors blocking invasion of NTHi into alveolar macrophages[148]. Following invasion of phagocytic cells, NTHi is able to persist intracellularly, with Craig *et al.* (2001) demonstrating the varying ability of different clinical isolates to survive inside mouse cell line macrophages for up to 24 h[149].

It is not clear how NTHi is able to survive once inside a macrophage. However gene expression studies have shown that modulation of NTHi gene expression contributes to enhanced intracellular survival by upregulation of stress response genes and metabolic pathways[150,151]. One adaptation identified is regulation of NTHi carbonic anhydrase expression, which plays a role in enhancing NTHi survival within THP-1 cells and in environments with low CO_2 levels[152]. Furthermore, when faced with a low nutrient environment, NTHi promoted the preferential route of macropinocytosis to enter epithelial cells, resulting in NTHi avoiding host cell degradation mechanisms[144]. Together,

these studies highlight the capacity of NTHi to adapt when challenged by environmental or host immune pressures during infection of the respiratory tract.

1.2.7 NTHi and asthma

Numerous studies have isolated NTHi from the airway of individuals with asthma, with NTHi presence suggested to be associated with the development and progression to more severe disease. Childhood NTHi carriage is a risk factor for the development of asthma in later life[24,25], with the seminal paper by Hilty *et al.* (2010), finding a *Haemophilus*-dominant microbiome in the airway of individuals with asthma[25]. A Danish study that sampled children at 1 month of age found that colonisation by NTHi was associated with increased risk of developing asthma in the first 5 years of life[24]. Building on these observations in humans, a murine model of airway disease demonstrated a potential functional consequence of NTHi colonisation. Mice colonised with NTHi after 3 days of life exhibited an exacerbated response when later challenged with an allergen, suggesting NTHi contribution to aberrant host immune development[109]. However the exact role of NTHi colonisation of the airways of infants in early life and subsequent development of asthma is still unclear.

NTHi has been implicated in asthma exacerbations, but has also been isolated from the airways of asthmatics during stable periods of disease[1,65,66,86,153]. In particular, NTHi has been associated with neutrophilic, steroid-resistant asthma[64]. Experimental models trying to unpick the observations of NTHi and neutrophilic inflammation in cohort studies have confirmed this association. Murine models of allergic airways disease found that NTHi infection of mice drove the development of steroid-resistant neutrophilic inflammation[154,155]. However it remains unclear whether, in humans, NTHi contributes to the progression of severe, neutrophilic, steroid resistant asthma or if NTHi takes advantage of the chronically inflamed and damaged airway that is characteristic of severe asthma.

Neutrophilic asthma is also less responsive to treatment and is often associated with corticosteroid resistance. Development of steroid resistance in asthma has been suggested to be due to increased NLRP3, caspase-1 and IL-1β responses to NTHi infection[54]. Suppression of IL-1β-mediated responses in mice also prevented the development of the steroid resistant features of asthma. Thus, minimising the burden of NTHi infection in severe asthma could reduce the development of steroid-resistance and improve outcomes for patients requiring steroids to manage their symptoms.

1.3 Immune response of the respiratory tract

The respiratory tract is constantly exposed to the dangers of the external environment[156]. To protect the body from foreign particles, the respiratory tract initially utilises physical barrier mechanisms. Layers of epithelial cells line the respiratory tract and adhere to neighbouring cells, forming a tight barrier. Within this barrier, specialised epithelial cells known as goblet cells produce mucus to trap any large foreign particles. Through use of cilia on the epithelial cell surface, the

trapped particles are mechanically shifted upwards are expelled from the body by expectoration[156]. This physical mechanism, known as mucociliary clearance, is not always impenetrable and small foreign bodies, including pathogens, can bypass this mechanism[156,157]. An immunological defence is required to prevent any further spread of infection, which is composed of two response arms; the innate and the adaptive response. Each arm performs specialised functions responsible for ensuring the body remains protected from infection. The innate immune response is the first line of defence against pathogens and in the lung is composed of leukocytes and epithelial cells that line the alveolar surface and airways[158]. The role of the innate response is to respond immediately and non-specifically to potential threats through recognition of common microbial ligands and initiation of a broad anti-microbial response[158]. In contrast, the adaptive response has evolved to respond to and remember specific microbial antigens in order to induce a targeted immune response towards the detected threat. These two arms of the immune system are exquisitely linked; cells of the innate arm such as macrophages and dendritic cells ingest and present components of foreign particles to cells of the adaptive immune arm such as T cells and B cells. These adaptive immune cells are recruited and further activated by innate immune cell release of cytokines, chemokines and growth factors which promote the specialized responses of the adaptive immune response[159].

1.3.1 Development of macrophages

The predominant innate immune cell in the healthy respiratory tract is the macrophage, which is a critical regulator of the innate arm of the immune response[160]. Macrophages belong to the mononuclear phagocyte system and were once believed to arise from bone marrow progenitors[161]. However, it has recently been identified that this mononuclear phagocyte system arises from at least three sources: the yolk sac, the fetal liver and the bone marrow[162]. Progenitors that arise from the yolk sac are believed to be tissue-resident cells which persist throughout life and self-maintain the macrophage population in each cellular compartment independently from hematopoietic input[161,162]. Monocytes generated in the fetal liver are believed to be precursor for alveolar macrophages, as determined by fate-mapping studies[163,164]. Finally, bone marrow derived progenitors give rise to circulating monocytes which can be recruited to tissues during infection and develop into macrophages. It is believed that these monocyte-derived macrophages have a shortened life-span compared to embryonic-derived macrophages[161].

Macrophages have a wide array of functions specific to the anatomical niche in which they are resident of, with differing macrophage populations present throughout organs in the body; alveolar macrophages populate the lung, Kupffer cells in the liver, osteoclasts in the bone and microglia in the brain[161,165]. Alveolar macrophages self-replicate by a Granulocyte-Macrophage Colony-Stimulating Factor (GM-CSF)-dependent mechanism, which is crucial for the development and maintenance of alveolar macrophage function[163166]. The importance of GM-CSF signalling for

maintenance of macrophage function is shown by the rare disease pulmonary alveolar proteinosis, which results in accumulation of alveoli surfactant due to defective macrophage function as a result of the loss of GM-CSF signalling[167]. Furthermore, GM-CSF knockout (KO)-mice exhibit other macrophage functional abnormalities including defective phagocytosis, decreased oxygen radical production and abnormal cytokine responses to lung infection which can be corrected by administration or rectification of GM-CSF expression[166].

1.3.2 Role of macrophages in innate immunity

Macrophages orchestrate the airway immune defence response, regulate inflammation and maintain homeostasis and participate in immune resolution processes[168]. The defensive role of macrophages allows for effective detection and recognition of pathogens, production of pro-inflammatory mediators to recruit and activate other components of the immune response, and phagocytosis of pathogens to prevent further spread of infection[160,169,170]. The role of macrophages in immune balance and regulation ensures that inflammatory responses are controlled and not excessive in order to prevent unnecessary damage to the local tissue. However, when tissue damage occurs, macrophages are involved in immune resolution processes such as efferocytosis. This process results in clearance of apoptotic cells to prevent release of the contents of dying cells to the external environment, which could propagate local inflammation[171]. Macrophages can also produce anti-inflammatory mediators such as IL-10 and TGF-β which can signal to dampen pro-inflammatory response and restore homeostatic balance[172]. These secreted molecules, along with growth factors such as vascular endothelial growth factor (VEGF) and hepatocyte growth factor (HGF) can also promote tissue repair following acute lung injury[173].

Although the adaptive arm of the immune system is more likely to be associated with immune memory, recent studies have demonstrated the ability of macrophages to undergo innate immune training. Immune training involves epigenetic modifications following initial challenge, which results in altered responsiveness upon secondary stimulation[174]. The type of immune training macrophages undergo depends on the type of stimulus and the local microenvironment and can either be termed immune memory or tolerance[174]. For example, stimulation of macrophages using different types of receptor ligands resulted in development of immune tolerance and differential repression of pro-inflammatory responses[175]. Although suppression of macrophage pro-inflammatory responses in the lung may help prevent excessive tissue damage from unwarranted inflammation, slower or delayed responses to further stimulation may result in increased susceptibility to bacterial infection, a phenomenon commonly observed following viral infection[176]. On the other hand, trained immunity inducing memory can result in enhanced pro-inflammatory responses upon re-stimulation, which can be beneficial. Stimulation with B-glucan results in 'priming' of macrophages with enhanced pro-inflammatory responses upon secondary challenge[177].

Within the lung, macrophages have a high degree of plasticity, allowing them to alter their functional phenotype depending on the airway inflammatory environment[178]. Previous macrophage nomenclature classified macrophages into 'M1' and 'M2' phenotypes. M1 macrophages were defined as 'classically activated' (LPS + Interferon (IFN)-γ) and mediated pro-inflammatory, anti-microbial effector responses. In contrast, M2 macrophages were classed as 'alternatively activated' (IL-4 + IL-13) and defined as mediating inflammation resolution and tissue repair responses[179]. However, recent studies have shown a diverse spectrum of macrophage activation states, suggesting the M1-M2 polarisation model is too simple to be applied to macrophage phenotypes[180–182]. An elegant transcriptome-based network analysis study by Xue *et al.* (2014) provided transcriptomic evidence for this spectrum of macrophage activation states[180]. By exposing macrophages to a variety of stimuli, Xue *et al.* identified a number of diverse macrophage activation programmes, far more complex than the originally proposed M1/M2 activation axis. Macrophage phenotyping is further complicated when macrophages isolated from disease, such as asthma, have an altered phenotype when compared to healthy controls[183]. The role of the macrophage in the context of NTHi infection will be discussed further below.

1.3.3 Recognition of pathogens

Upon encountering a pathogen, macrophages recognise conserved molecular structures called pathogen-associated molecular patterns (PAMPs) found in microorganisms, using a repertoire of germline-encoded pattern recognition receptors (PRRs)[184]. There are different classes of PRRs including Toll-like receptors (TLRs), NOD-like receptors (NLRs), retinoic acid-inducible gene (RIG)-I-like receptors (RLRs) and C-type lectin receptors (CLRs). These receptors recognise a diverse array of PAMPs or damage associated molecular patterns (DAMPs), which will be discussed in more detail below.

To date, 13 TLRs have been identified, however only 10 of these have shown to be expressed in humans[185]. TLRs recognise an assortment of ligands from various microorganisms and are traditionally expressed either on the cell surface, or on the membrane of intracellular compartments, such as endosomes[185]. The initial detection of NTHi by macrophages occurs through TLR2 or TLR4. TLR2 is an extracellular TLR and forms heterodimers with TLR1 and TLR6 and is able to detect NTHi ligands such as lipoproteins[169,186,187]. TLR4 is also an extracellular TLR which typically recognises bacterial LPS or LOS[169]. The importance of TLR2 and TLR4 in the immune response to NTHi has been shown in mouse KO studies; TLR2 or TLR4 KO mice infected with NTHi have decreased production of TNF-α, IL-1β and IL-6 and impaired bacterial clearance compared to control mice[188,189]

Although TLR2 and TLR4 are traditionally known to recognise bacterial PAMPs, they have also been implicated in detection of viral pathogens[190]. TLR4 was the first TLR to be shown to respond to virus; TLR4-mediated production of IL-6 from monocytes was detected in response to RSV fusion protein[191]. Furthermore, single nucleotide polymorphisms (SNPs) in TLR4 have resulted in reduced responses to both the traditional TLR4 ligand LPS and the RSV fusion protein[192,193]. TLR2 can also recognise viral envelope proteins, viral capsid proteins or viral proteins released from cells[194]. In mouse KO studies, TLR2 KO mice showed a reduced response to RSV[195], whereas mice treated with the TLR2 agonist Pam2Cys showed enhanced viral clearance and antiviral activity, suggesting a role for TLR2 in antiviral immunity[196].

Intracellular TLRs include TLR3, 7, 8 and 9, which are expressed on the membrane of endosomes and are responsible for monitoring these compartments for the presence of intracellular pathogens. TLR3 recognises double stranded RNA (dsRNA), whereas TLR7 and TLR8 are structurally similar receptors and recognise single stranded RNA (ssRNA). All three TLRs were traditionally implicated in detection of viral pathogens[190]. However, these TLRs are also able to detect bacterial pathogens. Expression of TLR3 was found to be upregulated in epithelial cells following NTHi infection[197], and when an anti-TLR3 monoclonal antibody was used to inhibit TLR3, decreased production of NTHi-induced chemokine (C-C motif)-ligand (CCL)5 and chemokine (C-X-C motif) ligand (CXCL)10 was observed[198]. The gene expression of *TLR7* was also shown to be upregulated in macrophages infected with NTHi[199]. TLR9 detects unmethylated 5'—Cytosine—phosphate—Guanine—3' (CpG) DNA but a role for responding to NTHi infection is unclear. Purified NTHi DNA was shown to induce Nuclear Factor kappa-light-chain-enhancer of Activated B Cells (NF-κB) activation via TLR9, however this stimulation was absent when cells were stimulated with whole, live NTHi[200]. Furthermore, in TLR9 KO mice, no difference in alveolar macrophage response to NTHi where found compared to wild-type mice[201]. Although TLR9 is traditionally implicated in detection of bacterial pathogens, it has also been shown to play an important role in the detection of CpG DNA from viruses[202].

In addition to TLRs, RLRs are cytoplasmic sensors of viral RNA, crucial in triggering antiviral responses. A member of the RLR family, RIG-I, has shown to be induced by both viral and bacterial PAMPs, despite traditionally being considered a cytosolic viral sensor[203]. Macrophages infected with *Legionella pneumophila* produced a RIG-I-dependent interferon response[204], with another bacterial pathogen, *Salmonella enterica* serovar Typhimurium, also activating a RIG-I-dependent interferon response in non-phagocytic cells[205]. The expression of RIG-I has been shown to be increased in macrophages exposed to NTHi[199].

Similarly to RLRs, NLRs are cytosolic intracellular receptors, however NLRs detect peptidoglycan, a component of the bacterial cell wall[206]. The most well characterised NLRs are NOD1 and NOD2, which have been suggested to synergise with TLR signalling to augment host responses[206]. As well as stimulation of pro-inflammatory cytokines and chemokines via NF-κB, NOD pathway activation can also increase IFN-β production, as demonstrated following intracellular infection by *Listeria monocytogenes* or *Mycobacterium tuberculosis*[207]. Evidence for NOD1/2 signalling in the host defence against NTHi has also been shown in a murine NTHi infection model[208].

Within the NLR family are a subset of NLRs that form part of the multiprotein assembly known as the inflammasome, a cytosolic complex involved in the activation of innate inflammatory immune responses[209]. Inflammasome assembly following recognition of bacteria results in activation of caspase-1, which promotes cleavage of the pro-IL-1β and pro-IL-18 inflammatory cytokines into their mature forms and subsequent amplification of pro-inflammatory responses[209]. This version of inflammasome activation is termed canonical inflammasome activation. In contrast, upon detection of cytosolic LPS, caspase-4 and -5 (caspase-11 in mice) can induce noncanonical inflammasome activation[210,211]. The noncanonical pathway can be activated by direct detection of LPS by caspase-4/5 independent of TLR4[212] or through interactions with guanylate-binding proteins (GBPs)[213]. GBPs are a family of interferon inducible proteins involved in the host defence against intracellular pathogens[214]. GBPs can be recruited to pathogen-containing vacuoles or can bind to intracellular pathogens to facilitate recruitment of caspase-4 to the bacterial cell surface and subsequent activation of the noncanonical inflammasome pathway resulting in caspase-1 activation, pyroptosis and IL-1β maturation[215,216]. Components of the inflammasome are upregulated by both a macrophage cell line and human alveolar macrophages in response to NTHi infection[217].

Finally, CLRs are a large family of transmembrane or soluble receptors which play an important role in maintaining homeostasis through recognition of both exogenous (non-self) and endogenous (self) carbohydrate ligands[218]. In the context of responding to pathogens, CLRs sense carbohydrate structures on pathogens and trigger signalling pathways to modulate cellular responses[219]. Dectin-1 is a CLR expressed in the lung and shown to be involved in modulating the pro-inflammatory response to NTHi[220] and is also a receptor used by NTHi to invade monocytic cells[142].

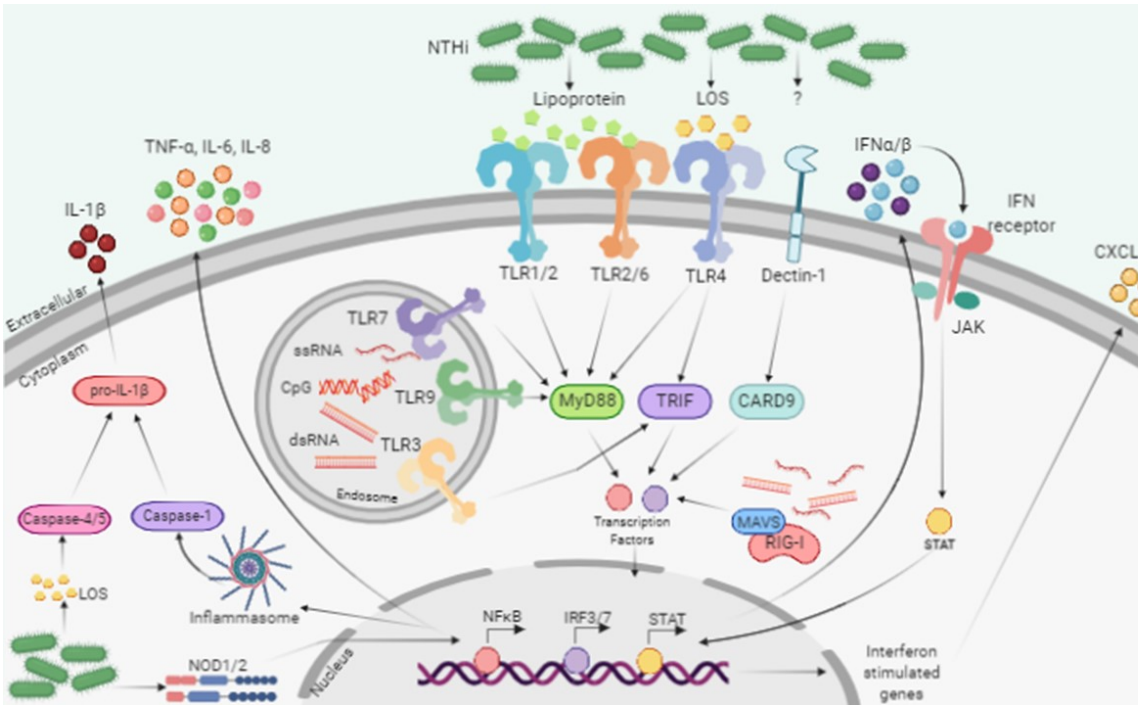

Figure 1.1. Generalised overview of the macrophage inflammatory response to NTHi . Macrophages sense NTHi via a wide array of PRRs including TLRs (1-7, 9), CLRs (Dectin-1), NLRs (NOD1/2) and RLRs (RIG-I). Upon recognition of extracellular NTHi ligands including lipoprotein (TLR1/2 and TLR2/6), LOS (TLR4) and carbohydrate moieties (Dectin-1) or NTHi-derived genetic material within an endosome (TLR3/7/9) or in the cytosol (RIG-I, NOD1/2), downstream signalling events via MyD88, TRIF or CARD9 occur. These signalling pathways either converge on the transcription factor NF-κB, which causes an upregulation in the transcription and production of pro-inflammatory mediators such as TNF-α, IL-6 and IL-8, or on IRF transcription factors which results in an increase in the production of IFN. These IFN act upon the macrophage in an autocrine or paracrine manner via the JAK-STAT pathway, upregulating the expression of interferon stimulated genes and the release of inflammatory mediators such as CXCL10. Signalling events and detection of cytosolic LOS upregulates members of the inflammasome pathway, which results in caspase-mediated cleavage of pro-IL-1β into mature IL-1β. NTHi = Nontypeable *Haemophilus influenzae*, LOS = lipoolygosaccharide, TLR = toll like receptor, CLRs = C-type lectin receptors, NLRs = NOD-like receptors, RLRs= RIG-I-like receptors, IRF = interferon regulatory factor, NOD = nucleotide binding oligomerization domain, MyD88 = Myeloid differentiation primary response 88, TRIF = TIR-domain-containing adapter-inducing interferon-β, CARD9 = caspase-associated recruitment domain 9, JAK = Janus kinase, STAT = signal transducer and activator of transcription, RIG-I = retinoic acid-inducible gene I, MAVS = Mitochondrial antiviral-signalling protein. Figure created using BioRender.com.

1.3.4 Production of pro-inflammatory mediators

Upon recognition of PAMPs by PRRs, signalling pathways are activated for the downstream production of pro-inflammatory mediators (Figure 1.1). Adaptor proteins such as Myeloid differentiation primary response 88 (MyD88), TIR-domain-containing adapter-inducing interferon-β (TRIF) and caspase-associated recruitment domain 9 (CARD9) act downstream of PRRs and are important in signal transduction and triggering of immune responses. All TLRs signal via the MyD88-dependent pathway, except TLR3 which signals via the TRIF-dependent pathway[190] and TLR4 which can stimulate both the MyD88-depedent and TRIF-dependent pathways[221]. In contrast, Dectin-1 signals via CARD9, however in macrophages, Dectin-1 activation of pro-inflammatory responses has been suggested to require additional TLR co-stimulation via MyD88[222]. NLRs can also signal via CARD9, however the primary adaptor protein involved in NLR signalling is the receptor-interacting protein kinase 2 (RIPK2)[223]. Finally, RLR signalling, such as the RIG-I signalling pathway can occur via the adaptor mitochondrial antiviral-signalling protein (MAVS)[224].

These aforementioned adaptor proteins facilitate induction of downstream signalling resulting in the activation of NF-κB and interferon regulatory factors (IRFs), which are transcription factors responsible for the regulation of pro-inflammatory cytokines and chemokines[184]. The role of NF-κB as a central transcription factor in the response to NTHi has been demonstrated. Following binding of NTHi to TLR2/4, signalling is induced by NF-κB leading to increased production of macrophage inflammatory mediators such as TNF-α, IL-6 and IL-8[186,217,225,226]. However, certain NTHi antigens stimulate an enhanced response compared to others; NTHi outer membrane protein (OMP) P6 selectively induces IL-8 and TNF-α, whereas NTHi OMP P2 is a weak inducer of these mediators[225]. Alternatively, whereas TLR4/MyD88 signalling and NF-κB activation results in upregulation of pro-inflammatory genes, TLR4/TRIF-dependent signalling results in IRF-mediated upregulation of IFN responses[169]. As such, production of IFN can be induced in a TLR-dependent manner by TLR 3, 4, 7, and 9 or a TLR-independent manner by RIG-I, either via NF-κB or IRF activation of IFN genes[227,228].

There are three types of IFN (I, II and III) which when released, can act on cells in an autocrine or paracrine manner to activate and amplify the anti-viral immune response. Following PRR detection of a pathogen, signalling cascades result in upregulation of type I IFN gene expression and protein release. These IFN proteins can then bind to the IFN receptor and amplify the IFN response by stimulation of the JAK-STAT signalling pathway, resulting in the upregulation of numerous interferon stimulated genes (ISGs) which further enhances pathogen detection and innate immune signalling[227,229,230]. Although the initiation of the IFN pathway is traditionally associated with anti-viral immunity, the upregulation of IFNs has been detected in response to NTHi[227,231]. One mechanism in which NTHi activates anti-viral responses is through NTHi DNA triggering type I IFN signalling, resulting in upregulated *CXCL10* expression[231]. CXCL10 is traditionally expressed

following viral infection and recruits T cells and Natural Killer (NK) cells to the source of infection[232,233]. Moreover, infections of macrophages using live NTHi showed a downregulation of *IFNB* gene expression levels, suggesting that NTHi is able to modulate macrophage anti-viral pathways[234].

1.3.5 Macrophage phagocytosis

Phagocytosis is a mechanism utilised by a subset of specialised immune cells known as 'professional phagocytes' which includes macrophages, dendritic cells and neutrophils[235]. When macrophages were first discovered by Ellie Metchnikoff, they were described as 'big eaters', referring to their phagocytic ability[236]. Phagocytosis is defined as the uptake of particulates (>0.5 μm) within a plasma membrane envelope[237]. There are a variety of uptake mechanisms that depend on particle size, receptor-ligand interactions and cytoskeleton rearrangements[237].

Phagocytosis is composed of a series of complex and sophisticated events. Macrophages express an array of dedicated phagocytic receptors for microbial ligands which include lectin-like receptors including CD169 and CD206, scavenger receptors (SR) such as SR-A, Macrophage Receptor with Collagenous Structure (MARCO) and CD36 and C-type lectins such as Dectin-1 and Myeloid Inhibitory C-type Lectin-like Receptor (MICL)[237–240]. The importance of these receptors to macrophage phagocytosis is highlighted by *in vitro* studies; modulation of macrophage MARCO expression by altering calcium levels *in vitro* found that phagocytosis of NTHi was higher in those macrophages with increased surface level expression of MARCO[241]. The aforementioned receptors play a role in non-opsonized phagocytosis, however macrophages express immunoglobulin receptors including Fc gamma Receptor (FcγR)IIa which participate in enhancing phagocytosis of microbes that have been opsonized by antibodies or components of the complement system[170]. In contrast, FcγRIIb is an inhibitory receptor, which downregulates FcγR-mediated phagocytosis[242].

Once the pathogen is bound to a receptor, cytoskeletal membrane rearrangements bring the pathogen into the macrophage resulting in the production of an internal vesicle known as a phagosome[237]. Pathogens can also enter macrophages by endocytic pathways, resulting in localisation of pathogens within an endosomal compartment. Through a series of maturation and fusion events, the phagosome or endosome matures into an acidic compartment known as the phago/endolysosome[170]. A number of proteins are involved in coordination of this maturation process, including the Rab GTPases. Identification of early or late stages or maturation can be detected through the presence of 'early' markers such as Rab5 which is lost upon compartment maturation which gain 'late' markers such as Rab7[243]. The Rab7-interacting lysosomal protein (RILP) facilitates fusion of late endosomes/phagosomes with lysosomes. Within this matured compartment, the pathogen is neutralised to prevent any further spread of infection and is

processed for antigen presentation. This series of events is simplified and is highlighted in Figure 1.2, however, the exact mechanisms of pathogen internalisation is complex and is dependent on both the pathogen itself and the receptors that initiate phagocytosis[235,237].

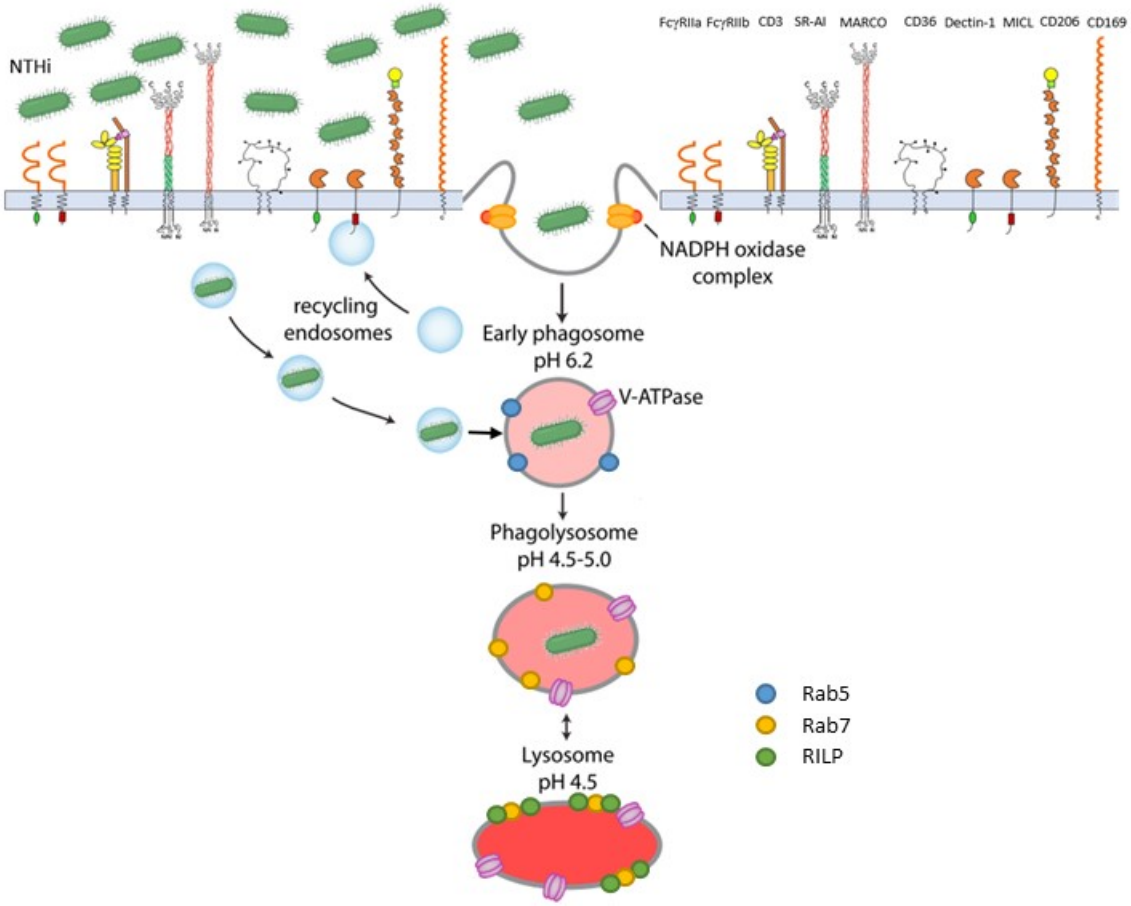

Figure 1.2. **Mechanism of NTHi clearance by macrophages**. Upon recognition of NTHi by an array of dedicated phagocytic receptors including FcγRIIa, CD3, SR-AI, MARCO, CD36, Dectin-1, MICL, CD206 and CD169, NTHi is brought into a macrophage phagosome through a series of cytoskeletal re-arrangements. NTHi can also enter via endocytic pathways. NTHi containing compartments such as endosomes or phagosomes are initially decorated with early protein markers such as Rab5, which are subsequently lost upon maturation of compartments and acquisition of the late protein marker Rab7. Final stages of maturation involves fusion of late compartments with lysosomes which is facilitated by Rab7-interacting lysosomal protein (RILP). Following phagosome/endosome fusion with a lysosome, the compartment matures into a phago/endolysosome, an acidic compartment which results in the destruction of NTHi. FcγRIIa = Fc fragment of IgG receptor IIa/b, CD = Cluster of Differentiation, SR-AI = Scavenger Receptor AI, MICL = Myeloid inhibitory C type-like lectin. Adapted from Gordon (2016)[237].

1.3.6 Macrophage impairment in asthma

Although fundamental to the airway immune response, macrophages have an altered phenotype in asthma[183]. As previously described, macrophages are a major source of pro-inflammatory cytokines in the lung. Increased levels of TNF-α, IL-1β, IL-6 and IL-8 were found in the airway of asthmatic patients compared to healthy controls[36]. Furthermore, increased presence of IL-17+ macrophages has been found in the BAL of asthmatic patients suggesting that macrophages play a role in shaping the T17 response in asthmatics and promoting neutrophilic inflammation[49]. On the other hand, a role for macrophages in eosinophilic airway inflammation has also been suggested. Macrophages in the asthmatic airway can be activated by IL-4 and IL-13, which induces macrophage production of eotaxin, a chemoattractant for eosinophils[244]. Depleting macrophages from allergen-sensitized and challenged mice showed a reduction in eosinophilic infiltration and inflammation[245]. A similar decrease in eosinophil recruitment and eotaxin production was observed following transfer of naïve macrophages to sensitised mice[246]. These studies suggest that macrophage dysfunction and phenotype could be central in promoting specific types of airway inflammation in asthma.

Monocyte-derived macrophages from the blood of asthma patients also exhibit reduced phagocytic activity, indicating that functional impairment of phagocytic cells in asthmatics is not limited to the lung[247]. This phagocytic defect appeared to be more pronounced in macrophages obtained from severe asthma patients, but did not appear to extend to inert particles, suggesting the defect is pathogen-specific[247]. Furthermore, alveolar macrophages from individuals with severe asthma show impaired phagocytosis of apoptotic cells in comparison to macrophages from healthy controls or mild asthmatics[248]. A similar defect in phagocytic capacity has also been reported in patients with COPD, with reduced uptake of NTHi by both alveolar macrophages and monocyte-derived macrophages[249,250]. Impairment in macrophage regulation and clearance of NTHi in the asthmatic airway could contribute to persistent and chronic NTHi colonisation of the lung. In addition, this macrophage impairment could prevent viral clearance of the airways, allowing viral infection to occur and potentially contribute to a viral-driven exacerbation of asthma.

1.4 Influenza

1.4.1 Pathology of influenza infection

Influenza is a seasonal virus, with epidemics in non-tropical regions occurring annually during the colder months of autumn and winter[251]. Epidemics in tropical climates are not as common, however can occur during the rainy season[252]. The WHO estimates that annual influenza epidemics cause 3-5 million cases of severe illness, resulting in 290,000 – 650,000 deaths[253]. Influenza is highly contagious and spreads through aerosolised droplets produced by an infected individual[254]. The virus infects the respiratory tract, resulting in the sudden onset of symptoms such as fever, cough,

headache, sore throat, runny nose, muscle and joint pain and malaise[253]. After 1-2 weeks, influenza infection is self-limiting in healthy adults, however those in 'at-risk' groups such as the young, elderly, immunocompromised or those with chronic medical conditions, such as asthma, can suffer from a more severe illness or secondary complications[253,255,256].

The emergence of a novel influenza strain which the population has little immunity against is characterised as a pandemic[252]. Unlike seasonal strains, pandemics are thought to occur in cycles[257]. Pandemics are often major causes of mortality and morbidity and result in high financial burden due to health care cost and lost productivity of workers[252]. Although there are four subtypes of influenza, A-D, the influenza A virus is most commonly associated with respiratory illness in humans[258]. In the 20th Century, the most devastating influenza A pandemics occurred in 1918, 1957, 1968 and 1977[259]. The 1918 pandemic killed approximately 50 million people and is regarded as the mostly deadly pandemic on record to date[260]. Although the influenza virus itself causes severe illness and respiratory tract damage, the majority of deaths during the 1918 pandemic appeared to be as a result of secondary bacterial infection leading to pneumonia[261].

1.4.2 Influenza structure

The influenza virus is a small, enveloped virus belonging to the *Orthomyxoviridae* family[262]. The influenza viral genome is composed of eight segments of negative sense, single-stranded RNA (Figure 1.3)[263]. These segments encode for viral proteins including three viral RNA-dependent RNA polymerase (RdRP) proteins, polymerase acidic protein (PA) and polymerase basic protein (PB) 1 and 2 which form the ribonucleoprotein (RNP) complex[264,265]. Two segments encode for viral cell surface proteins hemagglutinin (HA) and neuraminidase (NA) and another segment encodes nucleoprotein (NP), which is also a component of the RNP complex[266]. Both HA and NA undergo antigenic drift and shift, resulting in a high mutation rate in these proteins[267]. The variation in these proteins allows for classification of influenza by the subtype of HA and NA on the cell surface[267]. Although there are many genetically distinct subtypes – 16 HA and 9 NA, only three HA (H1, H2 and H3) and two NA (N1 and N2) subtypes are commonly implicated in human epidemics [257,264]. Another genome segment encodes for two proteins crucial for influenza replication, the M1 matrix protein and the M2 ion-channel protein[267–269]. Finally, the smallest segment encodes for influenza non-structural (NS) proteins NS1 and NS2, which is alternatively known as nuclear export protein (NEP)[264]. Although it is described here that 8 RNA segments encode for 10 proteins, the proteome of the influenza virus appears to be more complex than originally believed. A further 7 'accessory' proteins arising from alternative splicing and frameshift mutations have been discovered: PB1-F2, PB1-N40, PA-X, PA-N155, PA-N182, M42, and NS3[270].

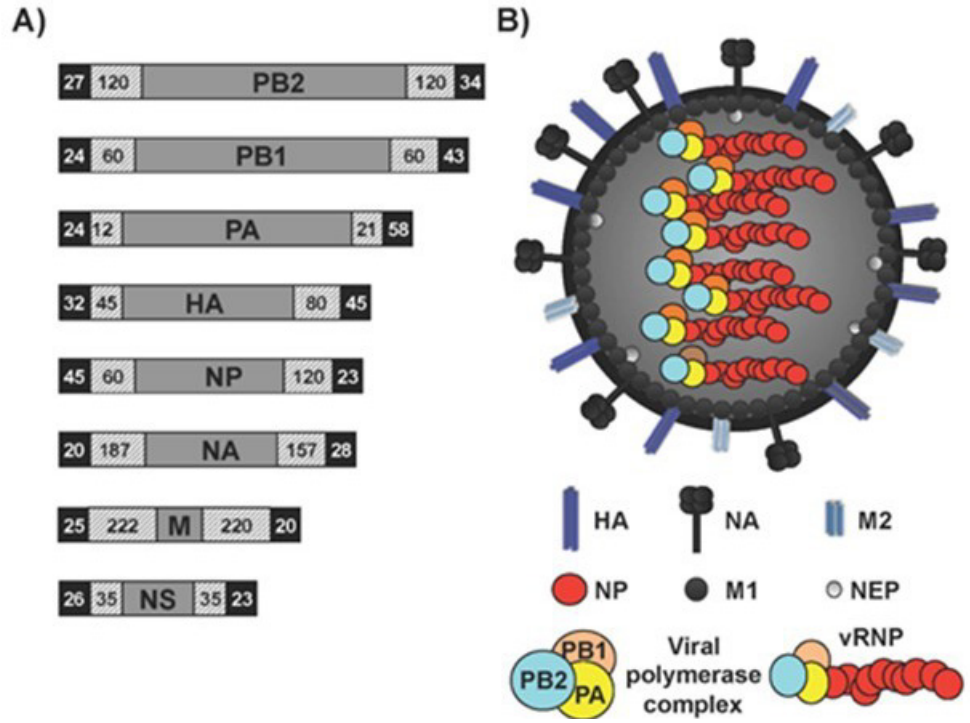

Figure 1.3. Influenza A virus genome and virion structure. (A) Genome structure highlighting the eight viral RNA segments (PB2, PB1, PA, HA, NP, NA, M and NS). Black boxes indicate the non-coding regions, the hatched boxes represent the packaging signals responsible for packaging into virions. The numbers indicate the nucleotide length. (B) Virion structure of IAV. HA, NA and the M2 channel are inserted into the lipid bilayer. An inner surface envelope made up of M1 protein sits below the lipid bilayer, with NEP also a component of the inner surface. The eight RNA segments are enclosed with NP which is associated with the viral RNA-dependent RNA polymerase complex which is composed of PB1, PB2 and PA. HA = hemagglutinin, NA = neuraminidase, M1/2 = matrix 1/2, NEP = nuclear export protein, NP = nucleoprotein. Image from Breen *et al.*, (2016)[263] CCBY 4.0

1.4.3 Influenza infection of the respiratory tract

The influenza virus is transmissible in droplets produced by infected individuals and is able to gain access to and infect the respiratory tract[254]. The influenza virus first adheres to host cells through binding of viral HA, to sialic acid residues on the host cell, which triggers viral entry via endocytosis[271]. The virus is then trafficked to an endosome where acidification changes the environmental pH, which activates the M2 ion channel protein and induces dissociation of the viral RNP core[272]. This core complex is then transported to the nucleus where viral replication occurs[265,267]. The M1 matrix protein interacts with viral RNA and NP and in association with NS2/NEP, facilitates the export of the RNP complex into the cytosol[267,269,273]. Production of new viral progeny is generated in the cytosol and concentrates at lipid rafts near the surface of the cell, where budding of the plasma membrane occurs, forming a complete new viral particle[269,274]. As these particles are linked to the cell surface through HA binding to sialic acid, NA cleaves these linkages

to release the new viral particle, which can then infect other cells[275]. This type of infection is termed 'productive' as new infectious virions are released from infected cells[276].

Although responsible for prevention of respiratory infection, lung macrophages are often targets of influenza infection[276–278]. Attachment to macrophages is achieved through binding to sialic acid residues on the cell surface[279], however a sialic-independent attachment can occur via macrophage C-type lectin receptors which also mediate viral entry[280,281]. Despite influenza attachment and entry into macrophages, there is debate on the ability of influenza to infect macrophages. Some studies suggest that infection is abortive[282,283] whilst others report productive infection [277,278,284]. Notably, Marvin *et al.* (2017) tested a panel of 28 distinct influenza viruses and found that only a small subset were able to productively infect macrophages, suggesting varying pathogenesis of influenza strains[285]. In a mouse model of influenza infection, Le *et al.* (2013) demonstrated contrasting murine respiratory tract pathology caused by two genetically similar strains of influenza virus[286]. Infection with one influenza strain induced higher levels of cytokines such as CXCL10, IL-6, TNF-α, an increased number of infiltrating inflammatory immune cells and increased tissue damage throughout the lung compared to the other tested influenza strain[286]. Furthermore, Campbell *et al.* (2015) found that macrophage phenotype was a determinant of the ability of influenza to infect cells[287]. Together, these studies suggest that influenza-macrophage interactions are complex and depend on both virus strain and macrophage origin and phenotype.

1.4.4 Treatment and vaccine strategies

There are two main classes of antiviral drugs that have shown to be effective in treating influenza infection: M2 inhibitors and neuraminidase inhibitors[288]. Both antiviral drug classes prevent the establishment of influenza infection by inhibiting components of viral replication. However, resistance to these drugs can occur and become persistent in circulating strains[288,289]. Discovering new classes of drugs against influenza is hampered by rapid evolution of resistance in strains. An example of this is the broad-spectrum anti-viral favipiravir, which is a nucleoside analog targeting the viral RNA-dependent RNA polymerase. Although no reports have indicated favipiravir resistance so far, it has been shown *in vitro* that mutations in the viral polymerase can potentially lead to resistance[290].

Due to the rapid evolution of the influenza virus resulting in increasingly limited efficacy of anti-viral drugs, vaccination remains the primary strategy for prevention and control of influenza[291]. Although the influenza virus has strong immunogenic surface proteins, both HA and NA undergo antigenic shift and drift, resulting in mutation of these vaccine target sites[267]. Therefore, a seasonal influenza vaccine is generated annually by predicting which exact strains will be in circulation in the upcoming year[292]. Individuals given the seasonal vaccine may not be protected from an emerging

pandemic strain as it is unlikely to be included in the seasonal vaccine[291]. Due to the unpredictability of emerging strains and the year-by-year variation in vaccine efficacy, it is important to pursue alternative treatment strategies to reduce the impact of influenza infections by determining the conserved mechanisms by which influenza is able to establish infection in the airway.

1.4.5 Influenza and asthma

As discussed above, reducing influenza burden is currently attempted through vaccination. Individuals with asthma are regarded as an 'at risk' group so are recommended the seasonal vaccine. Vaccination has shown to prevent 59-78% of hospitalisations associated with asthma exacerbations[293], however, vaccination coverage rate in children is low. An investigation into vaccination rates in Europe found that only 6.1% of children received the annual vaccine[294]. Children are vehicles for the dissemination of viruses within communities, as highlighted by peaks in hospitalisation for viral induced exacerbations reflecting the school calendar[295]. Thus, increasing influenza immunisation of children could provide herd immunity to fellow classmates and adults who do not receive the vaccine[296].

The importance of reducing annual influenza burden is clear, as asthma is one of the most common risk factors for hospitalisation with seasonal influenza[297–299]. Observational studies show that 1.5% to 23% of samples tested from patients admitted to hospital presenting with an asthma exacerbation were positive for the influenza A virus[70,300–303]. The systematic review by Papadopolous *et al.* (2011) previously discussed in Section 1.1.5, identified a lower proportion of exacerbations associated with influenza in children. However, a more recent analysis of the 2003 – 2009 influenza seasons found that 32% of children aged 17 years or younger hospitalised due to influenza also had asthma[304]. The variation in influenza detection rates could be due to differences in sample size, demographics, seasonality and the methodologies used. Dawood *et al.* (2011) suggest that changes in testing practices, increased influenza awareness and availability of sensitive PCR testing for influenza viruses, may have resulted in a higher proportion of hospitalisations and exacerbations to be associated with the influenza virus[304].

The most recent 2009 H1N1 pandemic caused an estimated 575,000 deaths[305,306], which has resulted in the 2009 pandemic being labelled as 'mild' when compared to the estimated 50 million deaths caused by the infamous H1N1 pandemic in 1918[260]. Despite the 'mild' label, asthma was the most common risk factor associated with hospitalisation during the 2009 H1N1 influenza pandemic[307–309], with some studies suggesting that between 22-29% of patients admitted to hospital with influenza also had asthma[310,311]. Asthmatics appear to be more susceptible to influenza infection, perhaps as a consequence of the chronic inflammation that is characteristic of the asthmatic airway, resulting in damaged airways better allowing for IAV attachment and entry

into host cells. Conversely, the IFN response in asthma airway bronchial epithelial cells is impaired, with lower amounts of IFNs produced following viral stimulation[312]. Given that innate IFN responses are crucial in restricting influenza infection[313], this IFN defect in the asthmatic airway could account for the susceptibility of asthmatics to viral infections such as influenza.

1.4.6 Macrophage immune response to influenza

Macrophage depletion studies have shown that macrophages are crucial responders to influenza. In influenza-infected animal models, macrophage depletion resulted in reduced viral clearance and increased morbidity and mortality[314,315]. As described previously, GM-CSF is a cytokine that promotes the survival, proliferation and function of lung macrophages[166]. Treatment of mice with GM-CSF increased numbers of macrophages and conferred protection against influenza, highlighting the fundamental role of macrophages in controlling influenza infection[316,317].

Macrophages detect influenza infection through RIG-I and TLR7, however the gene expression of these PRRs vary between early and late infection, suggesting these receptors play different roles during infection[318]. RIG-I detects the 5'-triphosphorylated RNA of the replicating influenza genome within the cytosol of infected cells, whereas TLR7 detects viral RNA that has been taken up into the endosome[319,320]. Following detection of influenza, macrophages respond by secretion of a number of cytokines including TNF-α, IL-1β, IL-6, IL-12, IL-15, IL-18, IL-27 and IL-29[318,321,322] and increased expression of the chemokines CCL2, CCL4, CCL5, CXCL8, CXCL9, CXCL10 and CXCL11[318,322,323]. Influenza induces the expression and release of interferons from macrophages, with IFN-α and IFN-β both upregulated following influenza infection[318]. Interferons stimulate the expression of ISGs in neighbouring cells, which prime cells into an antiviral state[319].

Despite the fundamental role of macrophages in controlling influenza infection, excessive responses or immune cell infiltration could in fact contribute to the pathology caused by the virus[324]. In murine models, immune cell infiltration by macrophage and neutrophils and increased release of pro-inflammatory mediators including TNF-α, IL-1β, IL-6, IL-12, CXCL10 and IFN-β following influenza infection were associated with severe lung pathology[324–326]. Despite increased immune cell infiltration and inflammatory responses, viral titres in the lungs of mice were not reduced[324].

An important immune function of macrophages to reduce viral tires is phagocytosis of influenza-infected cells. Macrophages phagocytose influenza-infected cells undergoing apoptosis which prevents the virus from producing new virions and therefore limits viral spread[327]. Using a mouse model, Hashimoto *et al.* (2007) showed that inhibiting phagocytosis increased the mortality rate of mice infected with influenza[328]. Given the previously described deficiency in asthmatic macrophage phagocytosis and the dysregulated immune response observed during influenza infection,

macrophage impairment could dually contribute to the chronic inflammation of the asthmatic airway and susceptibility to a viral infection, resulting in a viral-driven exacerbation.

1.4.7 Co-infection in the airway

With the expanding knowledge of the lung microbiome[71], and the increasing number of airway observational studies reporting the presence of bacteria and virus simultaneously[329–333], the original paradigm of infection models only using a single pathogen to model airway host-pathogen interactions needs to be reconsidered. It is apparent that influenza infection does not occur in isolation, but rather on a background of bacterial colonisation. In asthma, NTHi is detected in up to 60% of patients with severe, neutrophilic, steroid resistance asthma[46]. Co-infection of bacteria and virus results in more severe exacerbations and hospital readmission of individuals with chronic respiratory disease[334]. As individuals with more severe forms of asthma account for up to 80% of the health care burden and associated costs[46], the impact of NTHi colonisation and viral infections on the immune response and development of exacerbations requires urgent investigation.

Interactions between bacteria and viruses in asthma have been investigated more widely in early life development studies. Early life viral respiratory tract infections have been suggested to lead to development of asthma in later life[335]. The majority of studies investigating this have focussed on RSV and more recently rhinovirus infection. However, a recent study suggests that no specific viral trigger, but rather, the number of respiratory episodes predisposes individuals to asthma in later life[335]. As Bisgaard *et al.* (2007) demonstrated that presence of Proteobacteria such as NTHi resulted in increased risk of asthma development in later life[24], the modulation of host immune development and responses by colonising bacteria prior to early life viral infection must be considered more extensively.

Given the observation of increased NTHi in the asthmatic airway and the increased risk associated for individuals with asthma for hospitalisation with influenza infection[24,25,46,304], the interactions of these two pathogens and implications for the host airway immune response requires further investigation. Observational studies have identified the presence of *H. influenzae* during influenza infection[65,336–338]. Co-infection with influenza and *H. influenzae* increases severity of disease, compared to infection by each pathogen alone[252]. It is not clear how NTHi modulates the immune response to viral infection in asthma, however associations between NTHi and viral infection have been demonstrated in COPD, with presence of NTHi and rhinovirus associated with lower lung function, increased exacerbation risk and increased airway inflammation[332,339].

Traditionally, investigations of co-infection in the airway have focussed on influenza and secondary bacterial infection, of which *H. influenzae* is often implicated[252]. However, it is now clear that the presence of bacteria precede viral infection. As a result, studies are now beginning to investigate

the influence of the microbiome and specific bacteria on shaping the immune response to a viral challenge. Ichinohe *et al.* (2011) found mice commensal gut microbiota regulate the immune defence against influenza. After oral antibiotics were used to deplete commensal bacteria, defective anti-viral immunity from CD4+ T-, CD8+ T- and B-cells was detected, which resulted in increased viral titres[88]. Building on this work Abt *et al.* (2012) used transcriptional profiling and functional assays following antibiotic depletion of gut commensal bacteria in mice, and found a defect in macrophage anti-viral immune signalling, particularly in the interferon signalling pathway[340]. This defect was apparent prior to viral infection as decreased macrophage responsiveness to virus was associated with a reduction in steady-state transcription of anti-viral pathways. In these murine studies, it is not clear which specific commensals are involved in attenuating the immune response, and how the gut-lung microbiome axis influences lung immune responses. However, it is implied that dysbiosis of the microbiome could render individuals more susceptible to viral infection. More functional studies in the human lung are required to determine whether the shift in the structure of the asthmatic microbiome towards an overgrowth of Proteobacteria, in particular increased presence of NTHi[25], also results in modulation of host immune responses to viral infection that was observed in the aforementioned murine studies.

Limited studies specifically investigating NTHi-influenza-macrophage interactions have been performed, however different combination of pathogens and host cells indicate the potential for prior bacterial colonisation or infection of the host to affect the subsequent immune response to a viral infection. For example, the potential of macrophage-bacteria interactions shaping the immune response has been shown by Wang *et al.* (2013) who demonstrated that *S. aureus* priming recruits monocytes which mature into a macrophage phenotype capable of inhibiting influenza-mediated inflammation[341]. More recently, two studies have investigated the effect of host cell co-infection with the influenza A virus (IAV) and respiratory tract pathogens such as *S. pneumoniae* and NTHi. Both studies demonstrated a physical interaction between bacteria and IAV which enhanced *S. pneumoniae* adherence to epithelial cells[342], influenza infection of Madin-Darby Canine Kidney (MDCK) cells and influenza uptake and internalization by THP-1 cells[343]. In contrast, earlier work did not pre-incubate pathogens prior to infection of host cells and found differing results in infection dynamics. One study found no effect of prior NTHi infection of epithelial cells on IAV replication[344], whereas another study found NTHi infection inhibited subsequent RSV replication and infection[345], but rendered epithelial cells more susceptible to rhinovirus infection[346]. Overall, there appears to be contrasting results of protection or synergism between different combinations of pathogens depending on the experimental infection model used. Further work is required to fully elucidate the modulation of macrophage responses to influenza infection by pre-colonising NTHi.

1.5 Summary

The role of the lung microbiome in the development and modulation of immune responses are not well understood. In chronic respiratory diseases such as asthma, the microbiome is perturbed, with an increased abundance of potentially pathogenic Proteobacteria, such as NTHi, detected even during stable periods of disease[25,65,86,347]. In particular, NTHi is associated with more severe forms of asthma and a neutrophilic, steroid-resistant asthma inflammatory phenotype[54,293,347]. It is not clear how NTHi is able to persist in the respiratory tract, but has been suggested to reside intracellularly within host cells, such as macrophages[147,149,348] and is able to regulate gene expression to enhance intracellular persistence[150]. It is unknown whether NTHi intracellular persistence modulates the macrophage immune response and contributes to asthma progression or exacerbations. Although up to 80% of exacerbations are virally driven[67,68], increasing evidence suggests the presence of potentially pathogenic bacteria precedes the arrival of a virus in the respiratory tract. It is unclear whether this colonising bacteria modulates host responses to a virus, potentially resulting in dysregulation of inflammatory responses and exacerbation of disease.

1.6 Aims and hypothesis

This project has two main hypotheses:

1) *Both macrophage and NTHi gene expression will be modulated during intracellular infection.*
2) *NTHi infection of macrophages compromises the ability of macrophages to respond to a subsequent viral challenge*.

The specific aims for this project are:

1. Develop a model of NTHi intracellular persistence within monocyte-derived macrophages (MDM)
2. Characterise the MDM response to NTHi infection
3. Determine changes in the gene expression of MDM during infection with NTHi by dual RNASeq
4. Validate macrophage genes of interest in the NTHi-MDM infection model
5. Determine changes in the gene expression of NTHi during infection of MDM by dual RNASeq
6. Validate NTHi genes of interest in the NTHi-MDM infection model using additional clinical strains of NTHi
7. Assess the ability of influenza to infect macrophages following NTHi infection of macrophages
8. Investigate MDM and NTHi gene expression in severe asthma BAL samples

To achieve these aims, the impact of NTHi intracellular infection of macrophages will be explored using dual RNASeq to determine transcriptomic changes in both host and pathogen gene expression during infection. Firstly, an NTHi-macrophage infection model will be optimised using a MDM model. MDM have previously been extensively used to model macrophage-pathogen interactions for a variety of organisms including NTHi, *M*. *catarrhalis*, *S. pneumoniae*, RSV and IAV[240,349–352]. However in order to ensure successful sequencing of NTHi-MDM infection, various factors require optimisation. Most importantly, MDM and NTHi need to remain viable throughout infection, allowing for sufficient RNA to be recovered for sequencing. Once optimised, multiple clinical strains will be used to assess MDM responses, to ensure comparable responses are detected to heterogeneous NTHi strains.

Transcriptomic analysis of MDM and NTHi gene expression will be performed using R packages such as edgeR and DESeq2 for differential gene expression analysis[353,354]. The biological relevance of differentially expressed genes will be explored using freely available online gene ontology tools. Validation of the top differentially expressed genes will confirm whether the expression of MDM genes in response to additional clinical strains of NTHi is conserved, assessing whether macrophages are able to mount similar transcriptomic responses to diverse clinical NTHi strains. Additionally, validation of NTHi gene expression across multiple NTHi strains, as well as comparing expression of genes between intracellular and extracellular, planktonic state NTHi will identify conserved genes important for intracellular survival which could potentially be therapeutically targeted to reduce the burden of chronic NTHi infection.

Once NTHi-MDM interactions have been characterised by bioinformatic analysis of the dual RNASeq data, the impact of NTHi infection of macrophages prior to influenza A infection will be assessed. MDM previously infected with NTHi will be incubated with IAV and assessed for viral replication, regulation of immune responses and NTHi viability by flow cytometry, quantitative PCR (qPCR), Lactate Dehydrogenase (LDH) assay, Luminex/Enzyme-Linked Immunosorbent Assay (ELISA) and live viable counting.

Finally, the expression of MDM and NTHi genes identified in the dual RNASeq analysis and subsequent modelling with IAV will be investigated in severe asthma BAL samples to determine whether NTHi modulation of macrophage gene expression during a stable period of asthma can be detected and correlate with patient symptoms and clinical characteristics.

Chapter 2 Materials and Methods

2.1 Ethics and patient recruitment

Blood was collected from healthy volunteers in accordance with the Leukocytes: Inflammation Model Systems (LIMS) protocol approved by the Hampshire A Research Ethics Committee (13/SC/0416). The inclusion criteria for healthy donors includes a) individuals between the ages of 18 - 65, b) individuals able to give informed consent and c) individuals who the research team believe will comply with the study. The exclusion criteria include a) individuals who have had respiratory infection in the previous month, b) individuals using anti-inflammatory, antibacterial or antiviral medication currently or in the previous month, c) individuals that have evidence of drug abuse and d) individuals the research team deem unsuitable for the study.

Bronchoalveolar lavage (BAL) samples were obtained from a sub cohort of patients undergoing bronchoscopy as part of the Wessex Asthma Cohort of Difficult Asthma (WATCH) study in accordance with the protocol approved by the West Midlands – Solihull Research Ethics Committee (REC reference: 14/WM/1226), as per Azim *et al.* (2019)[355].

2.2 Isolation and differentiation of monocyte derived macrophages (MDM)

After individuals gave written informed consent, 120 ml blood was obtained using BD vacutainer lithium heparin blood collection tubes (BD Biosciences, Oxford, UK). Blood was diluted with Dulbecco's Phosphate-Buffered Saline (PBS) (Sigma-Aldrich, Gillingham, UK) before carefully layered onto Ficoll Plaque-Plus (GE Healthcare, Little Chalfont, UK) and subjected to density centrifugation at 800 *g* for 30 min at 20°C. Peripheral blood mononuclear cells (PBMC) were harvested from the interface and washed in PBS and centrifuged at 400 *g* for 10 min. Harvested PBMC were counted on a haemocytometer and washed in PBS, followed by centrifugation at 400 *g* for 5 min before being resuspended in 80 µl magnetic-activated cell sorting (MACS) buffer (2mM EDTA, 0.5% (v/v) Bovine Serum Albumin (BSA) in PBS) per 10^7 PBMC and 10 µl CD14+ magnetic microbeads (Miltenyi Biotec, Surrey, UK) per 10^7 PBMC. PBMC were incubated on ice for 20 min before washing with MACS buffer and centrifuged at 400 *g* for 5 min. PBMC were resuspended in 500 µl MACS buffer per 10^8 PBMC and run through a pre-washed LS MACS column (Miltenyi Biotec). To flush unlabelled cells through the column, 3 ml MACS buffer was washed through the column three times. To remove the retained $CD14^+$ positive cells from the column, the column was transferred to a fresh falcon tube and 5 ml of MACS buffer was added before firm application of the plunger. The 5 ml cell suspension was made up to 10 ml with PBS and counted on a haemocytometer. CD14+ monocytes were resuspended at 10^6 cells per ml in RPMI media (Sigma-Aldrich) supplemented with 2 mg/ml L-glutamine, 0.05 U/ml penicillin, 50 µg/ml streptomycin, 0.5 µg/ml amphotericin B (all Sigma-Aldrich), 10% (v/v) heat-inactivated foetal bovine serum (FBS) and 2 ng/ml GM-CSF (R&D Systems, Abingdon, UK), known as MDM culture media. Monocytes were

seeded at 5 x 10^5 cells per well in 48-well culture plates, incubated at 37°C, 5% CO_2, and differentiated into MDM over 12 days, with culture media replaced every 48 h. This method of differentiation generates macrophages exhibiting a 'lung-like' macrophage phenotype which has previously been described to resemble human alveolar macrophages[250,356,357]. GM-CSF differentiated MDM and human alveolar macrophages (AM) are phenotypically comparable, including similar phagocytic capacity[250], cytokine production[356] and expression of functional cell surface markers[358]. Furthermore, GM-CSF is crucial in regulating AM function *in vivo*[166,167] and is abundantly expressed in the asthmatic lung[359], thus the use of GM-CSF to generate MDM phenotypically similar to AM from asthma was chosen to better represent macrophage-pathogen interactions in asthma using an *in vitro* model.

2.3 Lung sample processing from WATCH study

BAL was collected from patients and stored on ice until processing by members of the WATCH study team. Briefly, samples were filtered using a 100 µm cell strainer and centrifuged at 790 *g* for 10 min at 4°C. The cell pellet was resuspended in PBS and a cell count using the trypan blue exclusion method was performed to assess cell viability, which identified a median BAL cell viability of 77% (Figure 2.1). Subsequently, the cell suspension was adjusted to 5 x 10^5 cells per ml in PBS. Cell cytospins were generated, with 75 µl of the cell suspension added to a cytospin funnel and subjected to centrifugation using a Shandon Cytospin® centrifuge at 450 rpm for 6 min. Slides were left to air dry at room temperature for at least 2 h before use or stored at -20°C until required for Fluorescence *in situ* hybridization (FISH, as described in 2.24). The remaining cell suspension was resuspended to allow for a minimum of 5 x 10^5 cells per ml and centrifuged at 790 *g* for 10 min at 4°C. The sample was resuspended in 500 µl QIAzol and vortexed for 30 s. Samples were stored at -80°C until RNA isolation was performed (as described below in 2.9).

Sputum was also collected and processed for each patient, and although sputum samples were not used in this thesis, the differential sputum cell counts were used to determine patient inflammatory phenotypes. Briefly, sputum was obtained by members of the WATCH study team and was stored on ice until processing. Sputum was weighed and diluted with 2 volumes of 0.2% (w/v) dithiothreitol (DTT) to processed sputum weight (g) and vortexed for 15 s. Sample was placed on a bench roller in ice for 30 min. The sample was then passed through a 100 µm cell strainer and centrifuged at 790 *g* for 10 min at 4°C. The cell pellet was resuspended and a cell count using the trypan blue exclusion method was performed to assess cell viability, which indicated a median sputum cell viability of 70% (Figure 2.1). Cells were resuspended to a concentration of 5 x 10^5 cells per ml to generate cytospin slides, with 75 µl of the cell suspension added to a cytospin funnel and subjected to centrifugation using a Shandon Cytospin® centrifuge at 450 rpm for 6 min. Slides were left to air dry at room temperature for at least 2 h before use or stored at -20°C until required.

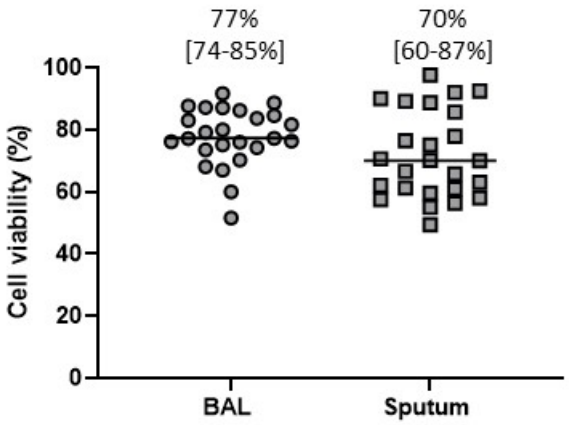

Figure 2.1. Viability of BAL and sputum cells. The trypan blue exclusion method was used to assess cell viability of cells obtained from both BAL and sputum. The median percentage cell viability for BAL cells (77%) and sputum cells (70%) indicate good viability was retained during sampling and processing. N=25.

2.3.1 Enumeration of cells in lung samples

For both BAL and sputum differential cell counts using the stored cytospin slides, a rapid Romanowsky stain was used to visually identify cells[360]. Cytospin slides were fixed in methanol for 30 s and left to air dry. Slides were next stained for 30 s in eosin, blotted to remove excess solution before staining in methylene blue solution for 1 min. Slides were then rinsed under running tap water and left to air dry overnight. Once dry, slides were manually counted under a light microscope, with a total of 400 cells manually counted to determine the proportion of macrophages, neutrophils, eosinophils, lymphocytes and epithelial cells present in each sample. Sputum cell counts were used to determine the inflammatory phenotype of patients using published cut off values[361–363]:

Inflammatory phenotype	Sputum percentage cut off
Neutrophilic asthma	≥40% neutrophils
Eosinophilic asthma	≥3% eosinophils
Mixed granulocytic asthma	≥40% neutrophils and ≥3% eosinophils
Paucigranulocytic asthma	<40% neutrophils and <3% eosinophils

2.4 Culture and storage of NTHi strains

The NTHi strains used in this study were ST942, 203, 103, 1447, 408, 14, 201 and a Green Fluorescent Protein (GFP)-labelled strain 375^{SR}. All NTHi were cultured from Southampton COPD patients[352,364], apart from GFP-375^{SR}, which was received as a kind gift from Dr. Derek Hood (MRC Harwell). GFP-375^{SR} is a GFP-tagged streptomycin resistant strain of NTHi-375, a clinical otitis media isolate from a Finnish study on children undergoing tympanocentesis between 1994 to 1995[365,366]. Characterisation of the Southampton NTHi strains, including whole genome sequencing and antimicrobial resistance testing, was performed by Dr. K. Osman and Rebecca Anderson (University

of Southampton)[367,368]. Only ST14, ST201, ST408 and GFP-375^{SR} were used for *in vitro* experiments. NTHi stocks of these four strains were grown and frozen for long term storage according to an established method published by Kirkham and colleagues[369]. Briefly, NTHi was cultured from frozen stock on to chocolate blood agar plates (CHOC, Oxoid, Basingstoke, UK) and incubated overnight at 37°C, 5% CO_2. Single NTHi colony forming units (CFU) were selected and inoculated in supplemented Brain Heart Infusion (BHI) media (30 mg/L Hemin (Sigma-Aldrich, Paisley, UK), 10 mg/L β-Nicotinamide adenine dinucleotide (β-NAD, Sigma) and 44 ml/L glycerol at 37°C, 5% CO2 for 8 hours before addition of heat inactivated FBS (20%) for storage at -80°C in 1 ml aliquots. Kirkham *et al.* (2013), have shown that NTHi retains viability when stored this way[369]. Counts of frozen NTHi stocks were routinely performed to determine the concentration of aliquots prior to use and to ensure NTHi viability remained stable over time (Figure 2.2).

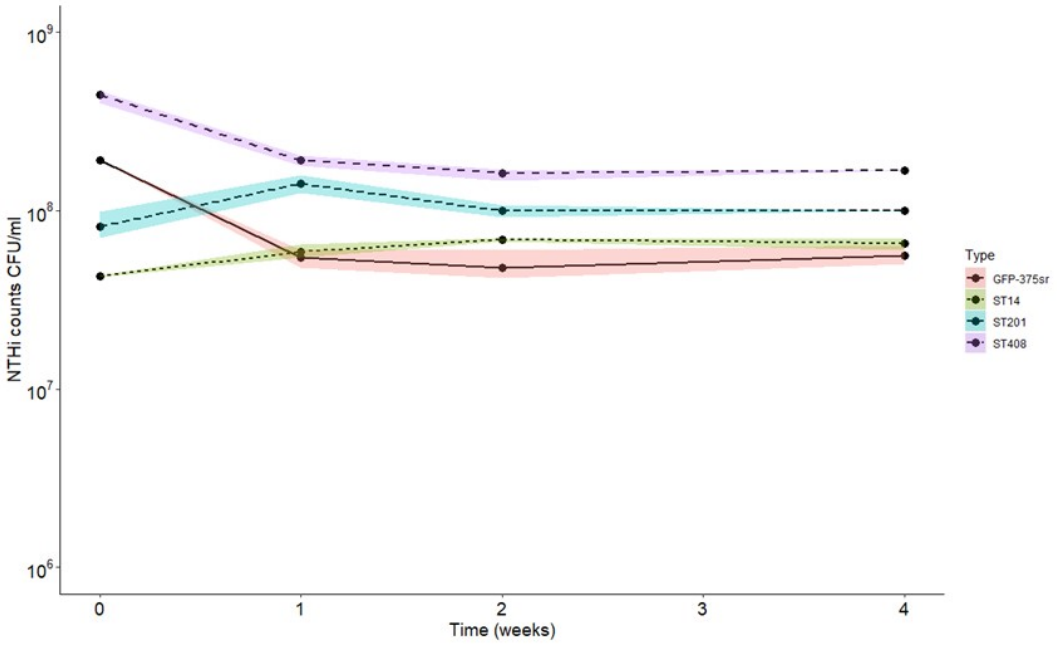

Figure 2.2. Live viable counts of frozen stocks of the four NTHi strains used for *in vitro* infection experiments throughout this thesis. Frozen stocks of NTHi ST14, ST408, ST201 and GFP-375SR were grown as per Kirkham *et al.*[369]. Three aliquots of each strain were thawed at each indicated time point and assessed for viability by live viable counting. Dots indicate median values of three individual replicate aliquots for each strain at each time point, with lower and upper lines of the colour band for each strain show interquartile range (IQR, 25th and 75th percentile respectively).

2.5 Assessment of NTHi strain diversity

To assess NTHi strain diversity, the ParSNP package from the Harvest suite[370] was used to analyse 7 clinical isolates of NTHi that had previously been whole genome sequenced[367]. Strain 86-028NP was used as a reference genome, as it was the first NTHi strain to be completely sequenced and as such as been extensively used as a reference strain in the literature[104,371,372]. The 86-028NP genome file, (GenBank number CP000057.2), was downloaded from https://www.ncbi.nlm.nih.gov/nuccore. Default parameters were used to analyse these strains to construct an assembly-based core-SNP phylogeny. The resulting data file was inputted to FigTree version 1.4.4 to visualise results as a phylogenetic tree. From this analysis, three strains isolated from different anatomical locations and identified on three different clades of the constructed phylogenetic tree were chosen to infect MDM as described below for strain comparison infection experiments.

2.6 Infection of MDM

2.6.1 NTHi infection of MDM

For infection assays using NTHi, MDM culture media was removed and wells were washed twice with PBS. This removed any remaining antibiotics that could hamper NTHi infection. Infection media containing 2 mg/ml L-glutamine and 0.1% (v/v) FBS in RPMI was added to wells. This media is known as Reduced Serum (RS) RPMI due to the decreased amount of FBS and was only used for infection assays, not for routine MDM culturing. The appropriate number of NTHi vials required to achieve the desired multiplicity of infection (MOI) for experiments were defrosted and transferred to a fresh tube containing 500 µl PBS and centrifuged at 800 *g* for 10 min, 4°C to pellet the bacteria. The remaining supernatant was discarded and the pellet was resuspended in RS-RPMI. The appropriate amount of NTHi was added to each well depending on the MOI required. Wells were made to a total volume of 500 µl with RS-RPMI.

To stop the infection, the RS-RPMI media was removed and cells washed twice with PBS before RS-RPMI with 1% (v/v) gentamicin was added to wells for 90 min in order to kill and remove extracellular bacteria. Depending on the type of experiment, cells were washed and left in RS-RPMI either with or without gentamicin until 24 h, or a gentamicin protection assay was performed (described in 2.7). For experiments incorporating subsequent IAV infections, cells were incubated in gentamicin for 2 h.

2.6.2 Influenza A virus (IAV) infection of MDM

At 24 h post initial NTHi infection, NTHi- infected or uninfected MDM were washed twice with PBS before 450 µl of RS-RPMI was added to the wells. Frozen aliquots of H3N2 Influenza A/Wisconsin/67/2005 (Virapur, San Diego, CA) supplied at a TCID50 (Tissue Culture Infectious Dose required to kill 50% of cells) of 3.6 x 10^8 IU/ml (infectious units/ml) MDM were infected with 3.6 x 10^4 Plaque Forming Units (PFU)/ml for 2 h. After 2 h of infection, extracellular IAV was removed by washing twice with 500 µl PBS and replacement of antibiotic free RS-RPMI for a further 22 h. At 24 h post IAV infection (final endpoint time 48 h), cells were harvested either for viable NTHi counting

by gentamicin protection assay (as described below in 2.7), or MDM were harvested into polypropylene FACS tubes (BD Biosciences, Oxford, UK) using 200 µl non-enzymatic cell dissociation solution (Sigma) for flow cytometry staining (described in 2.23).

2.7 Gentamicin protection assay

MDM were infected as described in Section 2.6. After 90 min incubation with RS-RPMI containing gentamicin, cells were washed twice with PBS and incubated with PermWash™ (PW, BD Biosciences), diluted to a 1 x solution (v/v) for 20 min. Cells were then scratched gently from wells and 25 µl of serially diluted cell suspension was plated on CHOC agar plates (Oxoid) and incubated at 37°C, 5% CO_2 overnight. CFU on each plate were counted and final counts were expressed as CFU/ml following correction for dilution and amount (25 µl) plated.

2.8 Visualisation of infected MDM

For visualisation of NTHi-infected MDM, MDM were infected with GFP-375^{SR} as described in 2.6.1. MDM were harvested following the gentamicin wash at 6 h or at 24 h post initial infection and were incubated with 200 µl Cell Dissociation Solution (Sigma) for 20 min at 37℃. The wells were lightly scratched with a pipette to gently remove cells. The cell suspension was transferred to a fresh tube with 800 µl fresh PBS and centrifuged at 800 *g* for 10 min, 4℃. The supernatant was removed and the subsequent cell pellet was resuspended in 50 µl PBS and mixed well. From this, 10 µl was added onto PolyFrost Microslides (Solmedia, Shrewsbury, UK) and left until completely dried. Once dry, 4% paraformaldehyde (PFA) was added to the spot for 15 min. Excess PFA was removed and slides were quickly washed in PBS and left until completely dry. Once dry, 25 µl Vectashield® Mounting Medium solution containing DAPI nuclear stain (1.5 µg/ml) (Vector Laboratories, Inc. Burlingame, CA) was added to each spot and a glass coverslip mounted on top. Slides were visualised using Axioscope KS400 fluorescence microscope using Carl Zeiss Axioscope 3.0 software.

2.9 RNA isolation

Following infection, MDM samples were harvested in 500 µl TRIzol® (Thermo Fisher Scientific, MA, USA) and frozen at -80°C. BAL cell pellets in 500 µl QIAzol were kindly provided by the WATCH study team. When required, samples were thawed and 0.2 ml chloroform (Sigma) per 1 ml TRIzol/QIAzol was added to the sample and vortexed. Tubes were left at room temperature for 8 min before centrifugation at 12,000 *g* at 4°C for 10 min. The resulting aqueous phase was harvested into 0.5 ml isopropanol (Sigma) per 1 ml TRIzol and 4 µl glycogen (Applied Biosystems, Paisley, UK) to precipitate the RNA. Following incubation at -20°C for a minimum of 1 h, the samples were centrifuged at 12,000 *g* at 4°C for 10 min. The resulting RNA pellet was washed twice with 75% ethanol (Sigma) for at least 1 h each time. After ethanol removal, the pellet was air dried and resuspended in RNase free water (Sigma). RNA concentration was determined using NanoDrop 1000 software (Thermo Fisher Scientific).

For samples to be used for dual RNASequencing, RNA extraction was performed using a miRNeasy kit (QIAGEN®, Manchester, UK), according to the manufacturer's instructions. Due to the differences in protocol between the standard phenol-chloroform extraction (above) and the column extraction method, it is possible that these different methods could be a source of variation. However, the column method was used in order to ensure high quality extraction of total RNA and successful sequencing of samples.

Briefly, 0.1 ml chloroform per 0.5 ml TRIzol® was added to each sample and shaken vigorously by hand for 30 s before incubation at room temperature for 3 min prior to centrifugation at 12,000 *g* at 4°C for 15 min. The resulting aqueous phase was harvested into fresh tubes and washed with a volume of 100% ethanol determined as 1.5 x the total amount of aqueous phase recovered. This mixture was transferred to RNeasy MinElute spin column and centrifuged at 10,000 *g* for 15 s at room temperature. At this stage, samples were treated with DNase I (QIAGEN®), to remove any contaminating genomic DNA which could impact on sequencing. DNAse I stock was prepared as per the manufacturer's instructions, with the lyophilized DNase I (1500 Kunitz units) dissolved with 550 µl RDD buffer. Briefly, 350 µl RWT buffer was added to the spin column and centrifuged at 10,000 *g* for 15 s at room temperature. The collection tube was discarded and replaced with a fresh tube, with 10 µl of DNase stock diluted with 70 µl RDD buffer, with 80 µl added to each column and incubated at room temperature for 15 min. After this incubation, 500 µl of RWT buffer was added to each column prior to centrifugation at 10,000 *g* for 15 s at room temperature. The flow through in the collection tube was re-applied to the spin column and again centrifuged at 10,000 *g* for 15 s at room temperature. The collection tube containing flow through was discarded and the miRNeasy protocol re-commenced, with 500 µl RPE buffer added to the columns and centrifuged at 10,000 *g* for 15 s at room temperature. The flow through was discarded and 500 µl ethanol (80%) was added to the columns and centrifuged at 10,000 *g* for 2 min at room temperature. The flow through was again discarded and samples centrifuged at 10,000 *g* for 5 min at room temperature. A new collection tube replaced the old tube and samples were left to air dry for up to 15 min at room temperature. Samples were resuspended with 15 µl pre-heated RNase-free water (QIAGEN®) for 10 min at room temperature. Samples were centrifuged at 10,000 *g* for 1 min at room temperature twice, with the flow through reapplied to the column between centrifugations. Isolated RNA was stored at -80°C until required.

2.10 Assessment of RNA quality and quantity for dual RNASeq samples

The guidelines from the sequencing company chosen to carry out sequencing of samples for this project (Novogene, Hong Kong) stated several specifications that were required to be met in order for the isolated RNA to be sequenced. This included:

1. RNA concentration >50 ng/µl in a minimum of 20 µl RNase free water
2. Total RNA content >2.5 µg
3. A260/280 >2.0
4. RNA Integrity Number (RIN) score >6.5

2.10.1 Assessment of RNA concentration, total RNA content and A260/280 ratios: NanoDrop

RNA concentration and total RNA content was assessed using NanoDrop 1000 software (ThermoFisher Scientific). In order to meet the minimum requirements for total RNA per sample for sequencing, each biological replicate (n=5) was performed in quadruple for each condition (uninfected at 6 h, NTHi-infected at 6 h, uninfected at 24 h and NTHi-infected at 24 h). Immediately following RNA isolation, samples in 15 µl RNAse free water (QIAGEN®) representing four technical repeats for each experiment were combined. This resulted in total RNA diluted in approximately 60 µl RNase-free water, which ensured sufficient sample was present to be used for quality control checks prior to shipping, upon arrival at Novogene for further quality checks and finally sequencing. The measured RNA concentration, total RNA content and A260/280 ratios met the required guidelines (Table 2.1).

2.10.2 Assessment of RNA quality: RNA Integrity Score (RIN)

The Agilent 2100 Bioanalyzer System (Agilent Technologies, Cheshire, UK) with the Agilent RNA 6000 Nano Kit (Agilent Technologies) was used to assess the quality of the RNA from samples to be sent for sequencing. Briefly, all required reagents were brought to room temperature, in the dark, for 30 min prior to use. A 65 µl aliquot of pre-prepared filtered gel was combined with 1 µl of RNA 6000 Nano dye concentrate and mixed thoroughly. The gel-dye mix was centrifuged for 10 min at 13000 *g*. Meanwhile, a new RNA Nano chip with 16 wells was installed onto the chip priming station and once centrifuged, 9 µl of the gel-dye mix was added to the indicated well. The priming station was closed and the plunger of the syringe was pressed down until it was held by the priming station latch. After exactly 30 s, the plunger was released and allowed to move upwards for 5 s, until it was manually pulled back up to the 1 ml position. A further 9 µl of gel-dye mix was added to the two remaining wells. In the other 13 wells that did not contain the gel-dye mix, 5 µl of the RNA 6000 Nano marker was added. RNA ladder aliquots that were heat denatured for 2 min at 70°C prior to freezing, were thawed on ice and 1 µl of RNA ladder was added to the well which was marked with a ladder symbol. In the remaining 12 wells, 1 µl of sample was added. The RNA chip was vortexed for 1 min before being inserted into the receptacle of the Agilent 2100 Bioanalyzer and the run was processed using the 2100 expert software. The software output also allows for visual inspection of

the run as a gel (Figure 2.3A) or as an electropherogram (Figure 2.3B) which indicates two ribosomal peaks (18S and 28S) for eukaryotic RNA. An NTHi-only control was used as a marker to determine the presence of prokaryotic RNA (Figure 2.3A), which can also be faintly observed in some of the infected MDM samples. The presence of both prokaryotic and eukaryotic RNA in mixed samples, such as infected cells, has been suggested to erroneously lower the RIN quality score[373]. The guidelines given by Novogene for sequencing instructed that samples should have a minimum of 6.5 RIN score to be of sufficient quality to be successfully sequenced. All samples received high RIN scores, ranging between 9.3 to 10 (Table 2.1).

Table 2.1. RNA quantity and quality for sequencing. RNA was isolated from MDM from 5 individual healthy donors infected with NTHi MOI 100 for 6 h, or left uninfected, followed by a 90 min gentamicin wash and left to incubate in antibiotic free media until 24 h. Samples were harvested using TRIzol at either 6 h or 24 h, resulting in a total of 20 samples, with 4 conditions per donor. Nucleic acid concentration and A260/280 ratios were determined by NanoDrop, RNA integrity number (RIN) was determined using Agilent Bioanalyser.

Sample Number	Nucleic Acid (ng/µl)	Total RNA (µg)	A260/A280	RNA Integrity number (RIN)
Sample 1	119.76	7.18572	1.99	10
Sample 2	99.05	5.943	1.99	9.5
Sample 3	119.81	7.18866	2.01	10
Sample 4	74.43	4.46556	2.04	9.3
Sample 5	126.22	7.57302	1.99	10
Sample 6	118.15	7.08918	2.03	10
Sample 7	111.05	6.66312	2.01	10
Sample 8	78.05	4.68312	2.00	10
Sample 9	80.36	4.82172	2.02	10
Sample 10	105.20	6.31194	2.01	9.6
Sample 11	110.66	6.63978	2.00	10
Sample 12	71.62	4.2969	2.02	10
Sample 13	80.69	4.8414	1.99	10
Sample 14	110.20	6.61212	1.99	10
Sample 15	66.93	4.01574	1.97	10
Sample 16	84.69	5.08128	2.03	10
Sample 17	104.52	6.27114	2.02	10
Sample 18	113.18	6.79056	2.03	9.5
Sample 19	121.23	7.27392	2.03	10
Sample 20	92.25	5.53506	2.00	9.8

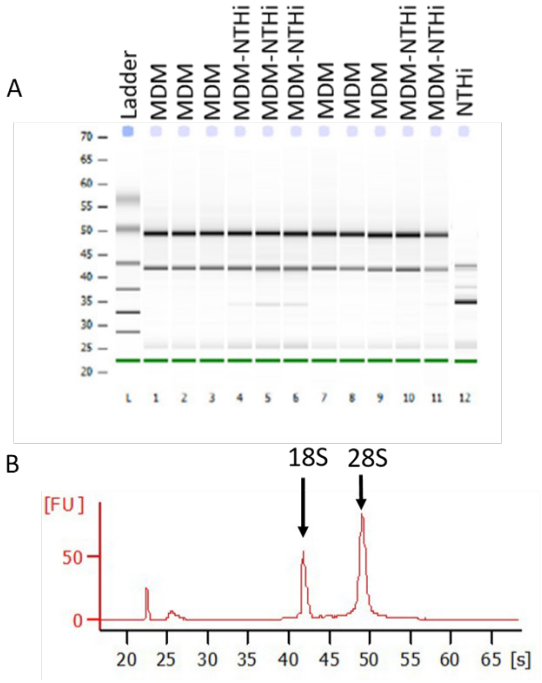

Figure 2.3. Output of the Agilent 2100 Bioanalyzer run for RNA integrity analysis, generated by Agilent expert software.(A) Representative gel image of run showing the ladder (Ladder), a mixture of uninfected (MDM) and NTHi-infected (MDM-NTHi) samples and NTHi-only control (NTHi). (B) Representative electropherogram of a MDM sample with a RIN score of 10, highlighting the 18S and 28S eukaryotic ribosomal peaks.

2.10.3 Novogene Quality Control of RNA

Upon arrival at Novogene, samples again underwent quality control checks to ensure the RNA was of sufficient quality and quantity post-shipping to Hong Kong. RNA degradation and contamination was assessed using 1% agarose gel (Figure 2.4). Novogene also assessed RNA integrity using the RNA Nano 6000 Assay Kit of the Bioanalyzer 2100 system (Figure 2.5). Although the RIN scores assessed by Novogene ranged from 7.10 to 9.50, which were lower than the RIN scores generated before shipping (Table 2.1), they were still above the required standard for sequencing.

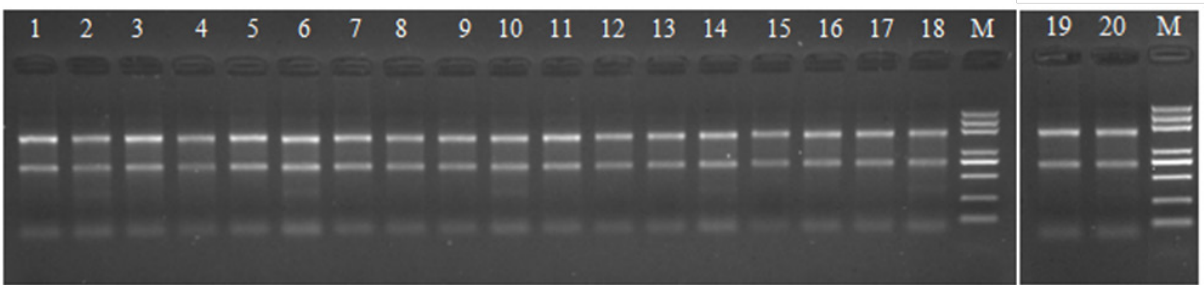

Figure 2.4. Agarose gel of samples run by Novogene to determine RNA degradation and contamination. Samples 1 – 20 are mixed MDM/NTHi. M is DNA ladder. Gels were 1% agarose and run for 16 min at 180v using 1 µl of sample.

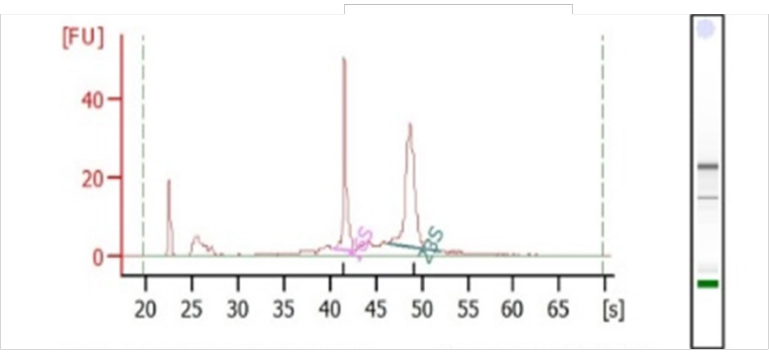

Figure 2.5. Representative output of the Agilent 2100 Bioanalyzer run by Novogene for determination of RNA integrity. Electropherogram of a MDM sample with a RIN score of 9.4, highlighting the 18S and 28S eukaryotic ribosomal peaks.

RNA quantification was assessed using the Bioanalyzer to ensure a sufficient quantity of RNA was present in each sample. The median RNA concentration across samples measured by Novogene was slightly lower (95 ng/µl compared to 104.9 ng/µl, not significant, Table 2.2) as was the total RNA measured (5.7 µg compared to 6.3 µg, not significant, Table 2.2). The RIN scores measured by Novogene were significantly lower for all samples (median RIN score of 9 versus 10, $p<0.001$). However, these differences could be attributed to different sensitivities of the lab equipment used, rather than any degradation or loss of samples during transport to Novogene in Hong Kong. Nonetheless, all 20 samples were deemed to be of satisfactory quality and quantity to proceed with sequencing.

Table 2.2. Comparison of quality control measures. Pre- (in Southampton) and post- (Novogene) shipping quality control checks including RNA concentration per sample, RIN scores, and the total amount of RNA per sample. Values shown are medians [IQR].

	Southampton	Novogene
Concentration (ng/µl)	104.9 [80.4 – 117]	95 [79.5 – 116]
Total amount of RNA (µg)	6.3 [4.8 – 7]	5.7 [4.7 – 6.9]
RIN score	10 [9.9 – 10]	9 [8.4 – 9.3]

2.11 Library preparation and RNA sequencing

All samples successfully passed quality control (QC) checks and underwent library preparation by Novogene. Briefly, ribosomal RNA (rRNA) was removed from all samples using Ribo-Zero™ Magnetic Kit (New England BioLabs (NEB), USA). Next, libraries were generated using the NEBNext®Ultra™ Directional RNA Library Prep Kit for Illumina® (NEB, USA) following manufacturer's instructions. Library quality was assessed on the Agilent Bioanalyzer 2100 system and quantified using a Qubit 2.0 fluorometer (Life Technologies) which determined the amount of each sample to be fed into the Illumina machine for sequencing. Sequencing was performed using NovaSeq 6000 Illumina platform and 150-base pair (bp) paired end reads were generated in a FASTQ format using a sequencing depth of 90 million reads.

2.11.1 Quality control of sequenced data

An overview of the workflow used to analyse the sequenced data is shown as a flow chart in Figure 2.6. For clarity, the analysis performed solely by Novogene is highlighted. For quality control of the sequenced data, Novogene used an in-house Perl script to obtain clean reads by removing reads containing adapter sequences, reads containing poly-N and reads with low quality. The overall contribution of these reads to total number of reads was low, indicating good sequencing quality (Figure 2.7). The overview of data quality measurements performed by Novogene is shown in Table 2.3. The error rate for each base call was determined using the Illumina CASAVA software. Each nucleotide base call is assigned a Phred score during sequencing, also known as a Quality or Q score, which is given as an integer indicating the probability that the base call is incorrect. The scores given here are Q20 and Q30 which indicates that the reads respectively have a 1% (or 1 in 100) or 0.1% (1 in 1000) probability of being called incorrectly; more than 92% of reads achieved a Q30 score, indicating good sequencing accuracy (Table 2.3).

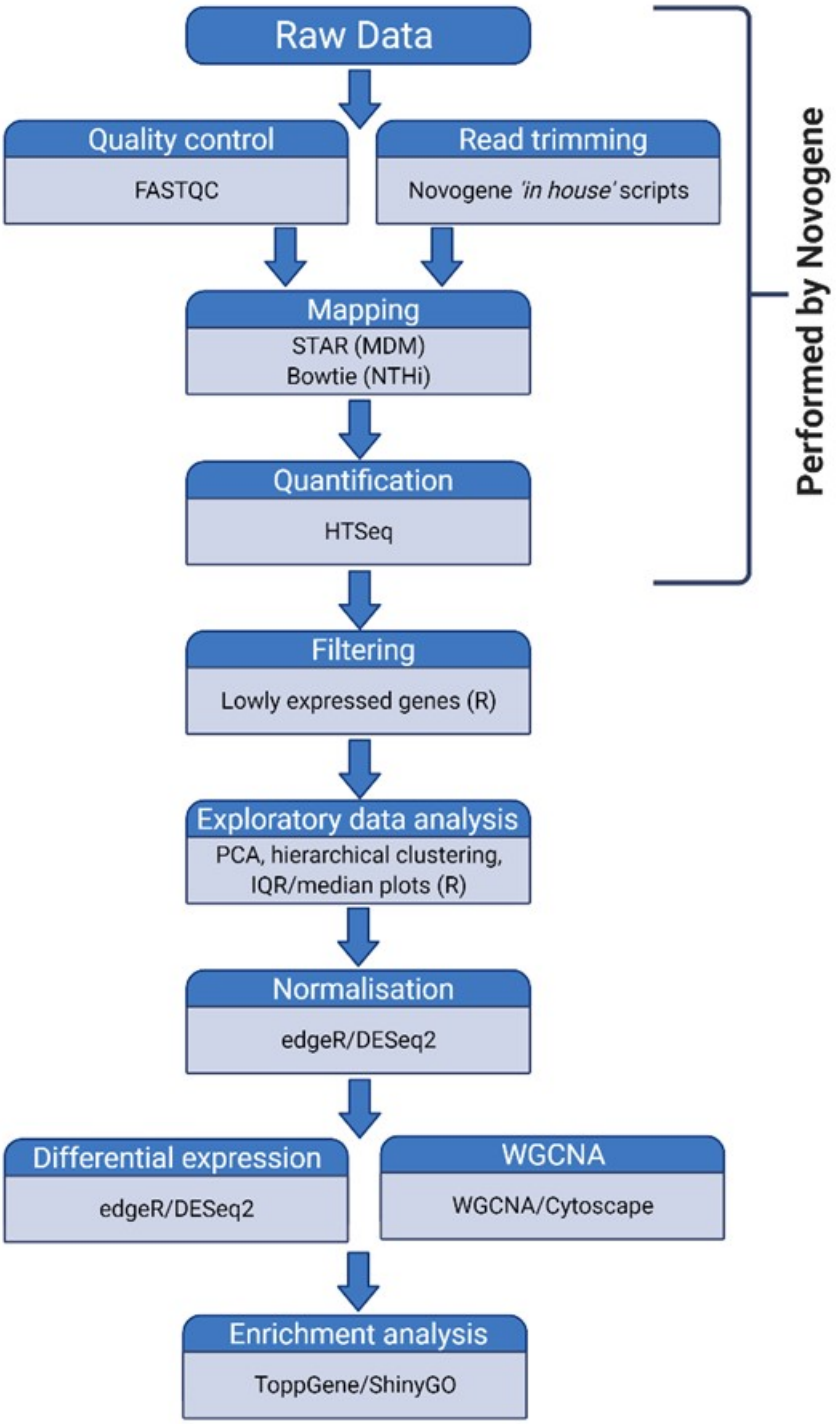

Figure 2.6. Workflow overview of the analysis performed on the dual RNASeq data set. As indicated, Novogene performed read quality control (QC), trimming, mapping and quantification. The analysis described in this thesis commenced from the filtering step using the read count file generated by Novogene during read count quantification. Figure created using BioRender.com

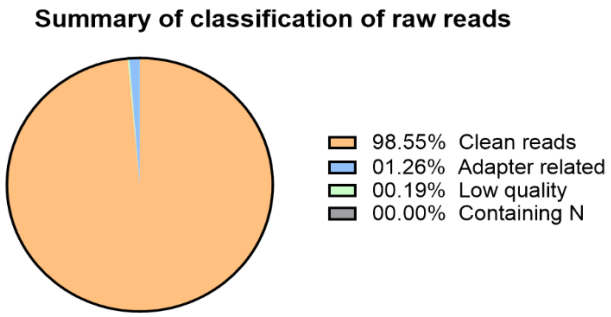

Figure 2.7. Summary of the raw read classification. Clean reads (orange) passed quality control and were taken forward for downstream analysis. The remaining low number of discarded reads where reads containing uncertain nucleotides (N) was more than 10% of the read (grey), reads where low quality nucleotides constituted more than 50% of the read (green) and reads with adapter contamination (blue).

Sequencing errors can arise as a result of the sequencing machinery, reagent availability and quality of samples, which can lead to errors in base incorporation at the end of the run when sequencing reagents begin to run out or particularly when longer read lengths are being used. Additionally, these factors can affect the nucleotide distribution at the start of the run, where higher number of errors occur due to the use of random primers during library construction. However, the error rate remained low at 0.04% for all samples sequenced (Table 2.3).

Table 2.3. Overview of raw data quality. The raw reads indicate the original number of read counts, whereas clean reads indicate the number of reads left after filtering. Q20 and Q30 indicate the percentage of bases whose correct base recognition rates were greater than 99% and 99.9% respectively.

Sample	Raw reads	Clean reads	Error rate (%)	Q20 (%)	Q30 (%)	GC content (%)
C_6h_005	99652897	98039267	0.04	98.05	94.24	52.3
T_6h_005	107614701	106636728	0.04	97.77	93.51	48
C_24_005	94189759	92754579	0.04	97.8	93.79	54.12
T_24_005	92516671	91154148	0.04	97.75	93.69	52.53
C_6h_016	99552909	97818883	0.04	97.37	92.78	49.6
T_6h_016	100745342	99225211	0.04	97.35	92.65	46.97
C_24_016	97327140	95733486	0.04	97.44	92.95	50.03
T_24_016	97676657	96311615	0.04	97.6	93.26	49.49
C_6h_082	102249423	100538771	0.04	97.94	94.1	54.09
T_6h_082	110185024	108971501	0.04	97.43	92.84	49.57
C_24_082	112923232	111135717	0.04	98.06	94.36	53.75
T_24_082	99235578	97693743	0.04	98.2	94.59	52.31
C_6h_104	92938591	91489427	0.04	98.07	94.39	54.02
T_6h_104	94238136	93125481	0.04	97.59	93.15	49.24
C_24_104	100189134	98954889	0.04	97.73	93.62	51.76
T_24_104	114876917	113157353	0.04	97.66	93.43	51.25
C_6h_124	92353829	91092015	0.04	97.37	92.84	53.32
T_6h_124	113796943	112442213	0.04	97.89	93.76	45.95
C_24_124	112035097	110546365	0.04	97.55	93.25	52.91
T_24_124	93527361	91611161	0.04	97.66	93.48	52.55

2.12 Mapping to reference genome

Mapping of the raw data to the each reference genome was performed separately by Novogene, with only clean reads used for mapping. The Spliced Transcripts Alignment to a Reference (STAR) software (version 2.5)[374] was used to map reads to the human genome (hg38, from NCBI/UCSC/Ensembl), whereas Bowtie2 (version 2.2.3)[375] was used to map reads to the NTHi genome. The genome sequence of the exact NTHi strain used for the sequencing (ST14) was generated by Dr. K. Osman[367] and was kindly provided by Dr. D Cleary following annotation of this strain using the command line software tool *Prokka*[376] as follows:

```
prokka Genomes/MICA_10_contigs.fasta --outdir MICA_10_ann --
force --prefix MICA_10 --compliant --cpus 0 --genus
Haemophilus --species influenzae --strain MICA_10 --usegenus
--locustag UoS_HiMICA_10
```

It is expected that 70-90% of RNASeq reads will map to the human genome[377]. The total mapping percentages here vary from 67.58% - 97.59% (Figure 2.8A, Table 2.4). The lower total mapping percentages occur when the samples have been infected with NTHi, as the total read population will also include NTHi reads. As the bacterial RNA will not be mapped to the human genome, this will result in lower mapping percentages to the human genome. Samples that were not infected with NTHi consistently mapped over 90% to the human genome, ranging from 90.42% to 93.94%. Conversely, the samples that were not infected with NTHi had very low mapping to the NTHi ST14 genome (Figure 2.8B, Table 2.4). The total mapping percentages to the NTHi genome of uninfected samples varied from 0% to 1.95%, whereas the NTHi-infected samples total mapping percentages ranged from 2.11% - 19.08%.

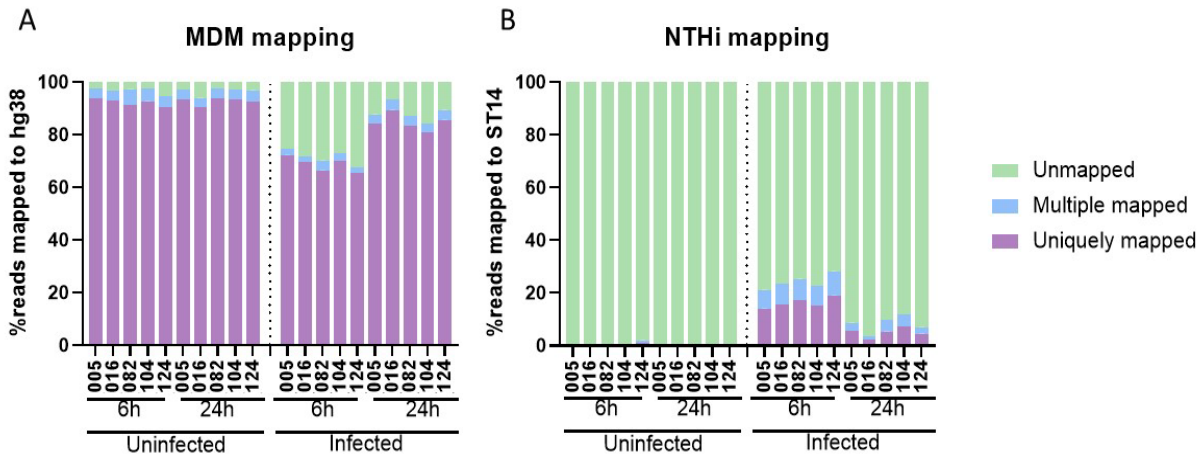

Figure 2.8. Percentage of the total sequenced reads mapped to hg38 or NTHi ST14 reference genomes. (A) Reads mapped to hg38, representing MDM reads for each samples and (B) Percentage of reads mapped to ST14, representing NTHi reads for each sample. Green = unmapped reads, blue = multiple mapped reads, purple = uniquely mapped reads.

Table 2.4. Summary of number of reads mapped to NTHi ST14 or hg38 reference genomes.

	Total reads	Total mapped		Multiple mapped		Uniquely mapped	
Sample ID		ST14	hg38	ST14	hg38	ST14	hg38
C_6h_005	196078534	7760	191127978	7620	6940438	140	184187540
T_6h_005	213273456	45129607	159183320	15113398	4763874	30016209	154419446
C_24_005	185509158	11653	180036244	11500	7026036	153	173010208
T_24_005	182308296	15721523	159983084	5714574	6661024	10006949	153322060
C_6h_016	195637766	4353	189116938	4221	7014188	132	182102750
T_6h_016	198450422	46667409	142590574	15841418	4654314	30825991	137936260
C_24_016	191466972	804365	179985314	781401	6863826	22964	173121488
T_24_016	192623230	6878041	179801994	2811869	7496056	4066172	172305938
C_6h_082	201077542	5304	195777696	5126	12424384	178	183353312
T_6h_082	217943002	55195640	153124456	17928964	8088254	37266676	145036202
C_24_082	222271434	6375	216800092	6224	8206182	151	208593910
T_24_082	195387486	18858689	170352376	8527572	7355278	10331117	162997098
C_6h_104	182978854	5651	178569730	5505	8795118	146	169774612
T_6h_104	186250962	42369625	136169134	14218699	5788696	28150926	130380438
C_24_104	197909778	4201	192401562	4100	7253916	101	185147646
T_24_104	226314706	26550693	190915920	10040812	7693880	16509881	183222040
C_6h_124	182184030	3559174	172213550	1323198	7403058	2235976	164810492
T_6h_124	224884426	63428580	151971478	20525200	4679512	42903380	147291966
C_24_124	221092730	5606	214390472	5460	9393454	146	204997018
T_24_124	183224322	12967154	163929522	4859983	6962114	8107171	156967408

2.13 Visualisation of data distribution and variance

Following mapping and alignment of clean, raw data to the respective reference genomes by Novogene, a read count table was produced and from this point, I analysed the RNASeq data using Rstudio® (version 3.6.1) and code developed with Dr. A. Heinson (University of Southampton). To inspect the quality and distribution of the data, multiple methods were used including basic quality control plots, IQR vs median plots, hierarchical clustering and principal component analysis (PCA). As the initial macrophage read count data file provided by Novogene was extensive (60k genes), it became apparent that this file included long non coding (lnc) RNA and pseudogenes. As these genes were not of interest to the main analysis, these genes were removed using the *grep* command line function and the dual RNASeq analysis proceeded with a read count data set containing 19795 genes.

2.13.1 Basic quality control plots

The distribution of the raw count data for each sample was first plotted as a boxplot, using the inbuilt boxplot function in R. The data distribution appeared to be skewed, likely due to the high amount of genes in the data set that were lowly or not expressed (Figure 2.9). Therefore filtering of the data set was next performed to remove these lowly expressed genes. The MDM data was filtered using a cut-off value of 10, and the NTHi data was filtered using a cut-off value of 5. These values determine that a gene must have a read count of greater than 10 (MDM) or 5 (NTHi) across all samples to be retained in the data set; essentially it must be expressed in half of the samples in the respective data set. The code used for filtering MDM data in R is below:

```
> values<-t(values)
> Filter <-10
> keep_tags<-rowSums(values>1)>=Filter
> values_filtered<-values[keep_tags,]
```

The code used for filtering NTHi genes was the same, apart from the filter was set to 5, rather than 10. Prior to filtering, the MDM count matrix contained 19795 genes. After lowly expressed genes were filtered out and removed, 15048 genes remained. Similarly, after filtering, 1611 genes were retained in the NTHi data set from a starting count matrix of 2148 genes. These filtered genes were separately saved as a new count matrix (known as *values_filtered*) and were used for further data exploration.

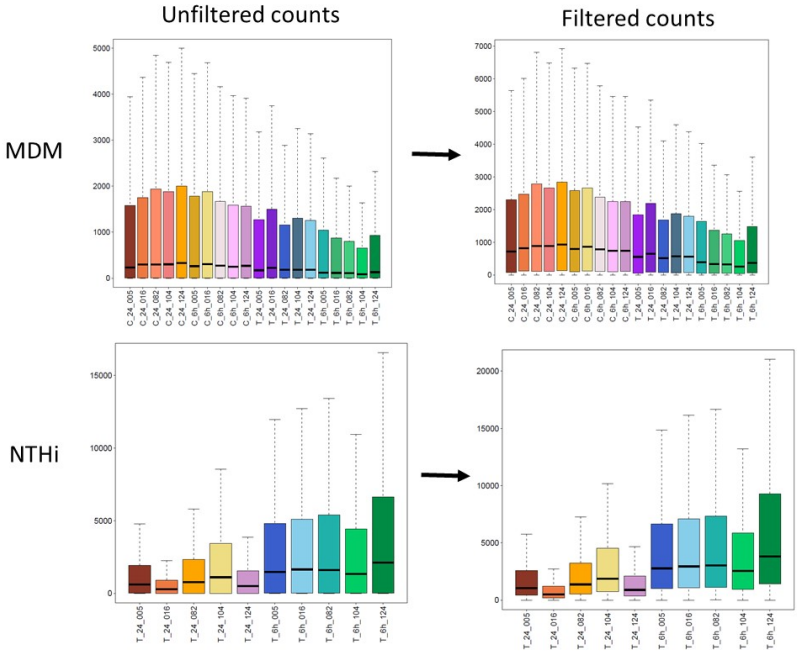

Figure 2.9. **Filtering of lowly expressed genes.** Genes were filtered from the MDM data set to reduce the number of lowly expressed genes impacting on downstream differentially expressed genes analysis. MDM data set (top), NTHi data set (bottom).

2.13.2 IQR vs median plot

The IQR vs median plots can be used to visually inspect the spread of data across samples in both data sets separately, and identify any potential outliers. The filtered count matrix was set as *values_filtered*, with the following code used:

```
> IQR_samples<- apply(values_filtered, 1, IQR)
> Median_samples<- apply(values_filtered, 1, median)
> SD_IQR<-sd(IQR_samples)
> SD_Median<-sd(Median_samples)
> Mean_IQR<-mean(IQR_samples)
> Mean_Median<-mean(Median_samples)
# for 1 standard deviation:
> SD_1_IQR<-c((Mean_IQR - SD_IQR), (Mean_IQR + SD_IQR))
> SD_1_Median<-c((Mean_Median - SD_Median), (Mean_Median +
SD_Median))
# for 2 standard deviations:
> SD_2_IQR<-c((Mean_IQR - (2 * SD_IQR)), (Mean_IQR + (2
*SD_IQR)))
> SD_2_Median<-c((Mean_Median - (2 * SD_Median)),
(Mean_Median
    + (2 * SD_Median)))
```

2.13.3 Hierarchical clustering

To observe the similarities between the samples, hierarchical clustering using the Euclidean method and Ward linkage was performed on the filtered data *(values_filtered)* using the packages *amap* and *dendextend*:

```
> hc_euc_ward<-hcluster(values_filtered, method='euclidean',
link="ward")
> plot(hc_euc_ward, main="genes_filtered Euclidean Ward",
hang=-1)
```

2.13.4 Principal component analysis (PCA)

To visualise the variance in the data, PCA was used on the filtered MDM and NTHi data sets. PCA reduces the dimensions of the data set and allows visualisation of the variance in the data as discrete principal components. PCA was performed on the filtered count matrix *(values_filtered)* using the *prcomp* function in R studio®, with the Proportion of Variance Explained (PVE) by the principal components (*pcs*) also determined:

```
> pcs<-prcomp(values_filtered)
> PC1<-pcs$x[,1]
> PC2<-pcs$x[,2]
> PC3<-pcs$x[,3]
> PCA_details<-cbind(PC1,PC2,PC3)
> pca<-merge(PCA_details,info,by="row.names",all=FALSE)
> row.names(pca)<-pca$Row.names
> pca<-pca[,-1]

> PC1<-pca$PC1
> PC2<-pca$PC2> PC3<-pca$PC3
> plot(PC1,PC2)
# Plotting the proportion of variance explained by the PCs
> pve<-data.frame(summary(pcs)$importance)
> prop<-pve[3,]
```

```
> barplot(as.numeric(prop),names.arg = colnames(prop), las=2,
cex.names=0.7, xlab="Principal Components", ylab="Percentage
of Variance Explained", main="PCA Percentage of Variance
Explained")
```

2.14 Data normalisation and differential gene expression analysis

Normalisation of the RNASeq data was performed using two Bioconductor packages: *edgeR*[353] and *DESeq2*[378]. Both methods were used to normalise the RNASeq data set and perform differentially expressed gene (DEG) analysis for both the MDM and NTHi data set. The code for both packages is below, with *pheno* representing the sample information file and *values_filtered* the filtered count matrix.

2.14.1 MDM differential gene expression analysis

```
> # edgeR for MDM #
> # Setting up confounding variables
> Condition<-as.factor(paste(pheno$Condition,"_",pheno$Time,
   sep=""))
> Donor<-as.factor(pheno$Donor)
># Create model
> design<-model.matrix(~0+Condition+Donor)
> eds<-t(values_filtered)
 > eds_filtered<-DGEList(counts=eds, genes=rownames(eds))
> ## Normalise the data to account for different library
sizes
> eds_filtered<-calcNormFactors(eds_filtered,method="TMM")
> # Calculate Differentially Expressed Genes:
> eds_filtered<- estimateDisp(eds_filtered, design)
> # Fit data to model
> fit <- glmQLFit(eds_filtered, design)
> my.contrasts<-makeContrasts(
   Infection_v_Control_6=ConditionT_6-ConditionC_6,
   Infection_v_Control_24=ConditionT_24-
   ConditionC_24,levels=design)
>#Pull out comparisons from model
> qlf6h <- glmQLFTest(fit,contrast=my.contrasts
   [,"Infection_v_Control_6"])
>qlf24h <- glmQLFTest(fit, contrast=my.contrasts
   [,"Infection_v_Control_24"])
> all_genes6h<-as.data.frame(topTags(qlf6h,
   n=nrow(eds_filtered)))
> all_results6h<-(all_genes6h)
> all_genes24h<-as.data.frame(topTags(qlf24h,
   n=nrow(eds_filtered)))
> all_results24h<-(all_genes24h)
> #Extract only the genes differentially expressed with an
FDR
   corrected p-value <0.05
>#6h comparison
> DE_results6h<-all_results6h[all_results6h[,"FDR"]<=0.05,]
> # 24h comparison
> DE_results24h<-
all_results24h[all_results24h[,"FDR"]<=0.05,]
> # END edgeR #
> # DESeq2 for MDM #
> #Setting up confounding variables
> Condition<-as.factor(paste(pheno$Condition,"_",pheno$Time,
```

```
   sep=""))
> Donor<-as.factor(pheno$Donor)
> pheno$Condition_Time<-as.factor
   (paste(pheno$Condition,"_",pheno$Time,sep=""))
> pheno$Donor<-as.factor(pheno$Donor)
> # Setting up a DESeqDataSet
> dds <- DESeqDataSetFromMatrix(countData = t_matrix, colData
= pheno,design = ~ Condition_Time +Donor)
> # Performing differential expression testing.
> dds <- DESeq(dds)
> # END DESeq2 #
```

2.14.2 NTHi differential gene expression analysis

```
> # edgeR for NTHi #
> #Setting up confounding variables
> Time<-as.factor(pheno$Time)
> Donor<-as.factor(pheno$Donor)
> # Create model
> design<-model.matrix(~0+Time+Donor)
> eds<-t(values_filtered)
> eds_filtered<-DGEList(counts=eds, genes=rownames(eds))
> ## Normalise the data to account for different library
sizes
> eds_filtered<-calcNormFactors(eds_filtered,method="TMM")
> #Calculating Differentially Expressed Genes:
> eds_filtered<- estimateDisp(eds_filtered, design)
> # Fit data to model
> fit <- glmQLFit(eds_filtered, design)
> my.contrasts<-makeContrasts(Time24-Time6,levels=design)
> #Pull out comparison from model
> qlf <- glmQLFTest(fit, contrast=my.contrasts)
> all_genes<-as.data.frame(topTags(qlf,
n=nrow(eds_filtered)))
> all_results<-(all_genes)
> #Extract only the genes differentially expressed with an
FDR
   p-value <0.05
> all_genes<-as.data.frame(topTags(qlf,
n=nrow(eds_filtered)))
> DE_results<-all_results[all_results[,"FDR"]<=0.05,]
> # END edgeR #

> # DESeq2 for NTHi #
> # Setting up confounding variables
> Condition<-as.factor(paste(pheno$Condition,"_",pheno$Time,
sep=""))
> Donor<-as.factor(pheno$Donor)
> pheno$Condition_Time <-
as.factor(paste(pheno$Condition,"_",pheno$Time, sep=""))
> pheno$Donor<-as.factor(pheno$Donor)
> # Setting up a DESeqDataSet
> dds <- DESeqDataSetFromMatrix(countData = t_matrix, colData
   = pheno, design = ~ Condition_Time + Donor)
> # Performing differential expression testing.
> dds <- DESeq(dds)
> # END DESeq2 #
```

A normalised data set containing counts per million (CPM) values was extracted from the edgeR analysis method for the MDM and NTHi data sets using:

```
> # Extracting edgeR normalized / filtered cpm matrix
> counts.per.m <- cpm(eds_filtered,
normalized.lib.sizes=TRUE)
```

Similarly, normalised counts were extracted from the DESeq2

```
> # Extracting DESeq2 normalised counts
> counts<-counts(dds, normalized=TRUE)
```

The data sets containing the CPM values were used to visualise data distribution as a box plot, using the inbuilt R boxplot function to inspect the normalisation process of each method.

2.15 Weighted gene correlation network analysis (WGCNA)

To identify genes important for the MDM response to NTHi infection, weighted gene correlation network analysis (WGCNA) was performed using the *WGCNA* R package[379]. The expression data required for this analysis were the normalised CPM values generated during the *edgeR* analysis (Section 2.14). MDM CPM values were log transformed in R using the function (log2(data +1) before using WGCNA. Sample trait data were also loaded into R, which contained information about the samples (donor ID, infection status and time point). The expression file was termed *datExpr* and sample data file was termed *traitData*. Data were first checked for outliers by plotting a clustering dendrogram using hierarchical clustering and the average linkage method, as suggested by the WGCNA guide:

```
> sampleTree = hclust(dist(datExpr0), method = "average")
```

2.15.1 Automatic network construction and module detection.

Construction of the gene network was performed using the WGCNA automatic network construction method, which is a 1-step network construction and module detection function. To construct the network, WGCNA uses Pearson's correlation to assess gene expression profiles. The resulting correlation matrix was used to calculate the adjacency matrix by selecting a soft thresholding power for analysis of network topology. A soft thresholding power was chosen based on the scale-free topology fit output of the *pickSoftThreshold* function using default values provided by the WGCNA package:

```
> # Choose a set of soft-thresholding powers
> powers = c(c(1:10), seq(from = 12, to=20, by=2))
> # Call the network topology analysis function
> sft=pickSoftThreshold(datExpr,powerVector=powers,verbose=5)
> # Plot the results
># Sclae-free fit index
> plot(sft$fitIndices[,1], -
sign(sft$fitIndices[,3])*sft$fitIndices[,2], xlab="Soft
Threshold (power)",ylab="Scale Free Topology Model Fit,signed
R^2",type="n", main = paste("Scale independence"));
> text(sft$fitIndices[,1], -
sign(sft$fitIndices[,3])*sft$fitIndices[,2],
```

```
labels=powers,cex=cex1,col="red");
> # this line corresponds to using an R^2 cut-off of h
> abline(h=0.90,col="red")
> # Mean connectivity
> plot(sft$fitIndices[,1], sft$fitIndices[,5],  xlab="Soft
Threshold (power)",ylab="Mean Connectivity", type="n",  main
= paste("Mean connectivity"))
> text(sft$fitIndices[,1], sft$fitIndices[,5], labels=powers,
cex=cex1,col="red")
```

The trade-off between a higher R^2 value and mean connectivity could result in a low number of connections and thus render it difficult to identify modules. However, a power of 18 was chosen for construction of the gene network as it was the lowest power to completely intersect the high value red line (R^2 = 0.9) on the scale independence plot (Figure 2.10A), whilst maintaining a mean connectivity score above 0 (Figure 2.10B). The following code was used to construct the gene network using default values, except the above pre-specified soft thresholding power (power = 18) and the *maxBlockSize*, which was increased to 16000 in order to analyse all the genes (15048) in the data set concurrently, not as separate 'blocks':

```
> # Construct gene network
> net = blockwiseModules(datExpr, power = 18,  maxBlockSize =
16000, TOMType = "unsigned", minModuleSize = 30,
reassignThreshold = 0, mergeCutHeight = 0.25, numericLabels =
TRUE, pamRespectsDendro = FALSE, saveTOMs = TRUE,
saveTOMFileBase = "MDM_TOM", verbose = 3)
```

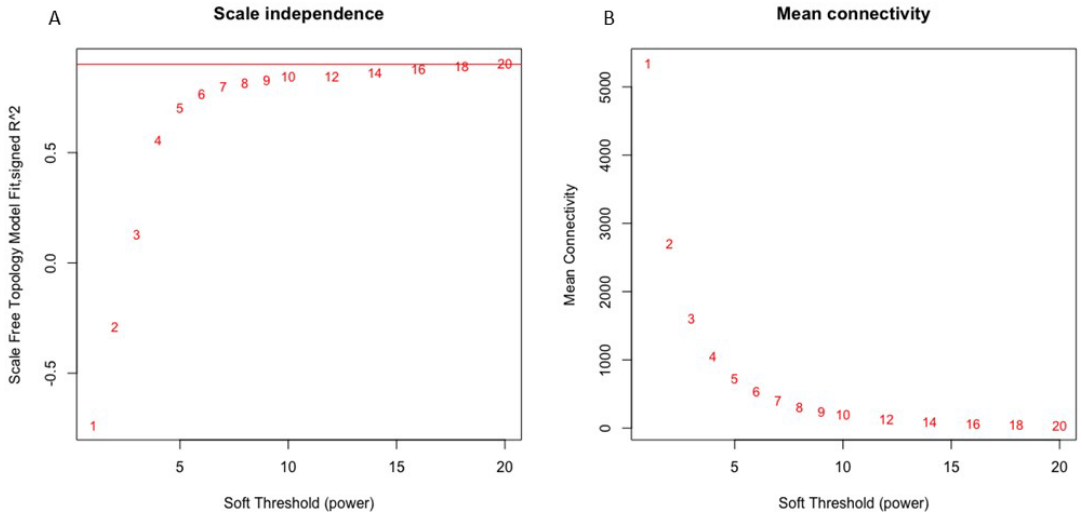

Figure 2.10. Network topology analysis for determining the soft-threshold power to be used for construction of the gene network . (A) scale-free fit index (y axis) as a function of the soft-thresholding power (x axis). (B) Mean connectivity degree (y axis) as a function of the soft thresholding power (x axis). Red line indicates R^2 = 0.9.

To visualise the clustering of modules and strength of gene connections, the TOM matrix was transformed to a dissimilarity TOM (*dissTOM*), which was transformed for better visualisation and to make moderately strong connections more visible in the heatmap (Figure 2.11):

```
> dissTOM = 1-TOMsimilarityFromExpr(datExpr, power = 18);
> plotTOM = dissTOM^7
> diag(plotTOM) = NA
> # plot heatmap
> TOMplot(plotTOM, geneTree, moduleColors, main = "Network
heatmap plot, all genes")
```

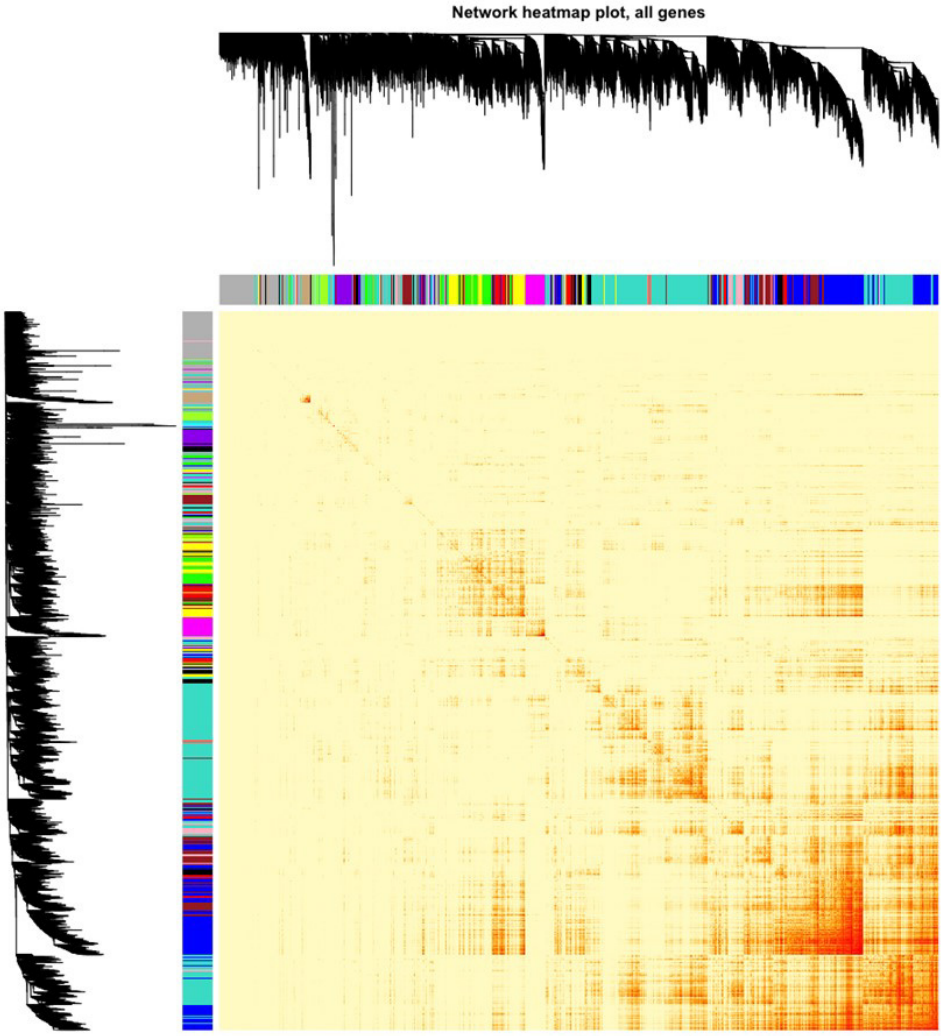

Figure 2.11. **Visualisation of the Topological Overlap Matrix (TOM) of the MDM gene set**. Accompanying gene module colour assignments and dendrogram are shown along the side and top of the heatmap. Lighter yellow colour indicates low overlap (low connections between genes), whereas darker colours (darker orange/red) represent higher overlap (higher connections between genes).

2.15.2 Relating modules to sample traits

Identification of modules that are associated with sample traits was performed by correlating module eigengenes (first principal component of the module) with trait information.

```
> # Relating modules to external clinical traits
> # Quantifying module-trait associations
> nGenes = ncol(datExpr)
> nSamples = nrow(datExpr)

> # Recalculate MEs with color labels
> MEs0 = moduleEigengenes(datExpr, moduleColors)$eigengenes
> MEs = orderMEs(MEs0)
> moduleTraitCor = cor(MEs, traitData, use = "p")
> moduleTraitPvalue = corPvalueStudent(moduleTraitCor,  )
> # Display the correlation values within a heatmap plot
> textMatrix = paste(signif(moduleTraitCor, 2),
    "\n(",signif(moduleTraitPvalue, 1), ")", sep = "")
> dim(textMatrix) = dim(moduleTraitCor)
> labeledHeatmap(Matrix = moduleTraitCor, xLabels =
names(traitData), yLabels = names(MEs), ySymbols =
names(MEs), colorLabels = FALSE, colors = blueWhiteRed(50),
textMatrix = textMatrix, setStdMargins = FALSE, cex.text =
0.5, zlim = c(-1,1), main = paste("Module-trait
relationships"))
```

2.15.3 Association of gene significance and module membership

To identify whether a gene assigned to a module is a significant member of the module, the gene significance (GS) and module membership (MM) was calculated. GS is the correlation between the gene and sample trait (e.g. infection status, time point). The MM is the correlation of the module eigengene and the gene expression profile. The relationship between MM and GS is important to ascertain gene importance in a specific module; a higher and more significant positive correlation, the more important the gene. The association of individual genes with the trait *Infection* was quantified using the code below.

```
> Infection = as.data.frame(traitData$Infection);
> names(Infection) = "Infection"
> # names (colors) of the modules
> modNames = substring(names(MEs), 3)
> geneModuleMembership = as.data.frame(cor(datExpr0, MEs, use
= "p"))
>MMPvalue=as.data.frame(corPvalueStudent(as.matrix(geneModule
Membership), nSamples))
> names(geneModuleMembership) = paste("MM", modNames, sep="")
> names(MMPvalue) = paste("p.MM", modNames, sep="")
> geneTraitSignificance = as.data.frame(cor(datExpr0,
Infection, use = "p"))
> GSPvalue=as.data.frame(corPvalueStudent(as.matrix
(geneTraitSignificance), nSamples))
> names(geneTraitSignificance) = paste("GS.", names(Time),
sep="")
> names(GSPvalue) = paste("p.GS.", names(Infection), sep="")
```

2.15.4 Identifying intra-modular relationships with sample traits

To study the relationships between modules, the module similarity by eigengene correlation was quantified and visualised as a dendrogram and heatmap. Additionally, the sample trait of infection was added to the analysis to identify which module, or cluster of modules, NTHi infection was most highly associated with. The module eigengenes were recalculated to include the infection trait to determine where the trait clusters within the eigengene dendrogram and heatmap.

```
> # Recalculate module eigengenes
> MEs = moduleEigengenes(datExpr0, moduleColors)$eigengenes
> # Isolate trait (Infection or infection) from the clinical
traits
> Infection = as.data.frame(traitData$Infection)
> names(Infection) = "Infection"
> Infection = as.data.frame(traitData$Infection)
> names(Infection) = "Infection"
> # Add the trait to existing module eigengenes
> METInfection = orderMEs(cbind(MEs, Infection))
> METinfection = orderMEs(cbind(MEs, Infection))
> # Plot the relationships among the eigengenes and the trait
> > plotEigengeneNetworks(MEinfection, "", marDendro =
  c(0,4,1,2), marHeatmap = c(3,4,1,2), cex.lab = 0.8,
  xLabelsAngle= 90)
```

2.15.5 Export of networks for visualisation in Cytoscape

In order to visualise the gene networks within each module, the network file was exported into Cytoscape. As each module contained differing number of genes, topological overlap thresholds were manually judged for each module to ensure a minimum of 40 nodes and 100 edges were present; too low a threshold and the network would be indecipherable and too high a threshold would remove any meaningful network interactions. The code below is using the '*blue'* module as an example of network export from R into a file format usable by Cytoscape. To assess the most highly connected genes in the exported networks, the cytoHubba plugin in Cytoscape was used, with the Maximal Clique Centrality (MCC) scoring method used to rank all nodes present in the network[380].

2.16 Gene ontology analysis

To explore the biological relevance of the significant differentially expressed genes found in the WGCNA and DEG analysis, gene list enrichment analysis and Kyoto Encyclopaedia of Genes and Genomes (KEGG) pathway analysis was performed using online tools such as ToppFunn, which is part of the ToppGene Suite[381] and ShinyGo[382] using default parameter settings (FDR multiple correction method and enrichment significance cut off level 0.05). Both online tools use hypergeometric distribution with False Discovery Rate (FDR) correction as the method for determining statistical significance of functionally enriched pathways. Clustering of the top gene ontology terms was performed in Cytoscape using the EnrichmentMap and AutoAnnotate plugins.

2.17 Reverse transcription

Reverse transcription to produce complementary DNA (cDNA) was carried out in 20 µl volumes with the following reagents; 2 µl 10 x RT random primers, 2 µl 10 x RT buffer, 0.8 µl deoxyribonucleotide triphosphate (dNTP) mix, 1 µl RNAse inhibitor and 1 µl Multiscribe Reverse Transcriptase (all Applied Biosystems) with 250 ng RNA added to each reaction and the remaining volume (up to 20 µl) supplemented with RNase-free water (Sigma). Reverse Transcription was performed at 25°C for 10 min, 37°C for 2 h and 85°C for 5 min using a DNA Engine Thermal Cycler (MJ Research/Bio-Rad Laboratories CA, USA).

2.18 Quantitative PCR (qPCR)

Quantitative PCR (qPCR) was performed in 5 µl reactions using previously generated cDNA (as described in Section 2.17). Briefly, for qPCR to analyse MDM or NTHi gene expression, 2.5 µl TaqMan Universal Master Mix II (Applied Biosystems) was added to 1.25 µl RNAse-free water (Sigma) and 0.25 µl of appropriate TaqMan primers. MDM primers are shown in Table 2.5 and NTHi primer sequences are shown in Table 2.6 and were designed by Applied Biosystems using the gene sequences from the ST14 draft genome assembly. The qPCR reactions were performed at 95°C for 10 min and 40 cycles of 95°C for 15 s and 60°C for 1 min using a 7900HT Fast Real-Time PCR System.

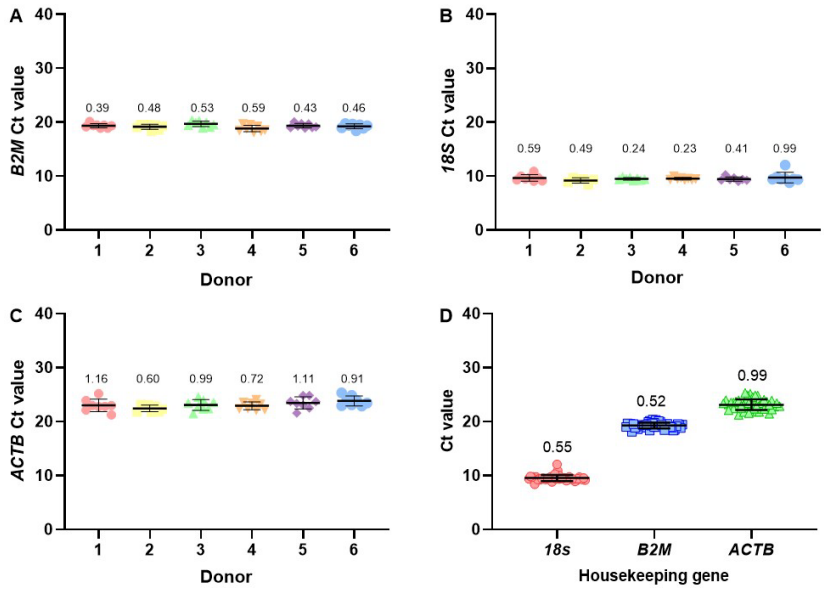

Figure 2.12. Assessment of housekeeping gene stability for qPCR. Three commonly used housekeeping genes were assessed for stability across the conditions used in this thesis (Section 2.6). The Ct values for *18S* (A), *B2M* (B) and *ACTB* (C) were measured across 6 healthy MDM donors individually, due to the inherent variability between donors. Each donor sample consists of 8 conditions: 6h uninfected, 6h NTHi infected, 24h uninfected, 24h NTHi infected, 48h uninfected, 48h NTHi infected, 48h IAV-infected and 48h co-infected (NTHi+IAV). (D) Ct values for all donors and conditions were combined to assess stability of housekeeping genes including donor variability. Lines indicate mean and error bars and values show standard deviation.

Host gene expression results were normalised to housekeeping gene beta-2-microglobulin (*B2M*) using the delta-delta cycle threshold (Ct) method:

2^-(experimental gene of interest – experimental housekeeping gene) - (uninfected gene of interest – uninfected housekeeping gene).

Use of *B2M* as a suitable housekeeping gene for macrophages has been demonstrated previously in the literature[383–385] and has routinely been used in the lab[199,234,240,351,352] as a housekeeping gene for MDM gene expression work. Comparison of housekeeping gene stability across individual MDM donors in response to the infection conditions and time points used in this thesis (Section 2.6) confirmed stability of *B2M* in this model. *B2M* (Figure 2.12A) outperformed *18S* (Figure 2.12B) and *ACTB* (Figure 2.12C), maintaining the lowest variability as measured by the standard deviation (Figure 2.12D). As such, *B2M* was pragmatically chosen as the single housekeeping gene of choice for this work, in order to minimise the cost of reagents. NTHi gene expression results were either normalised to *B2M* (chapter 3) or the NTHi *rho* gene (chapter 5 onwards), as expression of *rho* was determined not to significantly change between 6 h and 24 h in the dual RNASeq analysis. Statistical analysis was performed on delta-delta Ct values. Values were then transformed using *2^-* deltadelta Ct to graphically express results as fold change.

Table 2.5. List of MDM primers for qPCR. All from Applied Biosystems.

Gene	Accession Number
18s	Hs09003631_g1
ACOD1	Hs00985781_m1
ACTB	Hs99999903_m1
B2M	Hs00984230_m1
CASP4	Hs01031951_m1
CXCL10	Hs00171042_m1
DDX58	Hs01061436_m1
GBP1	Hs00977005_m1
IFNA	Hs00256882_s1
IFNB	Hs01077958_s1
IFNG	Hs00989291_m1
IL1B	Hs01555410_m1
IRF1	Hs00971965_m1
IRF3	Hs01547288_m1
IRF7	Hs00185375_m1
LAMP3	Hs01111316_m1
MX1	Hs00895608_m1
PNRC1	Hs00199095_m1
RELA	Hs01042010_m1
SGPP2	Hs00544786_m1
TLR2	Hs00152932_m1
TLR4	Hs00152939_m1
TLR7	Hs01933259_s1

Table 2.6. List of NTHi primers for qPCR. All NTHi primers were from Applied Biosystems. Primer sequences for *bioC, mepM, dps, yadA* and *rho* were obtained using sequences from the ST14 draft assembly genome and were used by Applied Biosystems to design primers. The specific primer/probe sequences for *hel* were from Coughtrie *et al.*[386].

Gene	Assay ID	Forward Primer	Reverse Primer	Probe
bioC	APH6EPN	GCACTGGAGGGCATTTACAACTTTA	TCGGAAAGATCGGTTCCAATTACTTT	CCGCCCCTCGTTCTAA
mepM	APKA9AK	GGCGAACGTATTGCACTTTCTG	ACAGCTCGACCGTTAATATGAAATTCA	TAACACGGGCATTTCT
yadA	APNKWFF	GTGAGGCATCGAAAAGCTATACAGT	CGGCTGATGATTTTAAGGCTTTTGC	CCCCTTACCAATTGCT
hel	APKA9AH	CCGGGGTGCGGTAGAATTTAATAA	CTGATTTTTCAGTGCTGTCTTTGC	ACAGCCACAACGGTA AAGTGTTCTACG
dps	APMF2VH	GAGGCTATCACTGGAACATTAAAGGT	AGCCACTTCATCAACTCTAGCAATT	ACACGCAAAATTTG
rho	AP2XDRH	AGGCAATGGCTCAACAGAAGATTTA	CAAACCACGTTGACCTTTACCAATT	ACCGCACGTATTTTG

2.19 Lactate Dehydrogenase (LDH) assay

LDH release into culture supernatants was assessed by the CytoTox 96® Non-Radioactive Cytotoxicity Assay according to the manufacturer's instructions (Promega, Madison, USA). Briefly, 50 µl of harvested supernatant and 50 µl CytoTox 96® Reagent was added to a 96 well plate and incubated for 30 min in the dark at room temperature. 50 µl of stop solution was added and the absorbance read on a microplate reader at 490 nm (Multiskan Ascent, Agilent Technologies, Wokingham, UK). Optical Density (OD) reading of the media only control was regarded as background and subtracted from sample values.

2.20 Metabolic activity assay

To assess MDM metabolic activity, a CellTiter 96® AQ_{ueous} One Solution Cell Proliferation Assay (Promega), known as a MTS (3-(4,5-dimethylthiazol-2-yl)-5-(3-carboxymethoxyphenyl)-2-(4-sulfophenyl)-2H-tetrazolium, inner salt) assay, was used according to the manufacturer's instructions. Briefly, MDM were seeded at 2.5 x 10^4 cells per well, which was pre-determined by optimisation of the cell number required to allow accurate absorbance reading. MDM were infected with NTHi or left uninfected, as described in 2.6.1. At 24 h, media was removed and 100 µl fresh RS-RPMI was added, along with 20 µl MTS Solution Reagent, to each well and incubated for 1 h at 37°C, 5% CO_2. After 1 h, absorbance was read on a microplate reader (Multiskan Ascent) at 490 nm.

2.21 Enzyme-Linked Immunosorbent Assay (ELISA)

To determine release of MDM inflammatory mediators, culture supernatants were harvested frozen at -80°C until needed. IL-1β, IL-6, IL-8 and CXCL10 release was determined by use of a DuoSet® ELISA kit (R&D Systems) according to manufacturer's instructions. Briefly, Nunc™ MaxiSorp™ ELISA plates (Biolegend) were coated with 100 µl capture antibody and incubated overnight at room temperature. Plates were washed in PBS containing 0.05% Tween-20 (known as Wash Buffer). Plates were blocked using 200 µl PBS containing 1% (v/v) BSA at room temperature for 1 h. Plates were again washed with Wash Buffer before addition of 100 µl of appropriately diluted samples and standards and incubated at room temperature for 2 h. Plates were then

washed with Wash Buffer and incubated with 100 µl appropriate detection antibody at room temperature for 2 h. Following washing with Wash Buffer, 100 µl streptavidin-horseradish peroxidase (streptavidin-HRP) was added and incubated in the dark at room temperature for 20 min. After a final wash with Wash Buffer, 100 µl 3,3',5,5'-Tetramethylbenzidine (TMB) substrate solution was added to wells and incubated in the dark at room temperature for up to 20 min. The reaction was stopped by addition of 50 µl 'stop solution' / 1M H_2SO_4. Absorbance was read on a microplate reader (Multiskan Ascent) at 450 nm using 550 nm wavelength correction.

2.22 Luminex Assay

Analysis of MDM cell culture supernatants was also performed using a customised 14-plex Luminex Human Magnetic Assay according to the manufacturer's instructions (R&D Systems). Briefly, 50 µl of the premixed microparticle cocktail was added to each well of a 96 well plate and incubated with 50 µl of neat MDM culture supernatant or the pre-prepared standard at 4°C overnight. The plate was then washed with 100 µl Wash Buffer (R&D Systems) whilst attached to a Handheld Magnetic Washer, which held the microparticles and bound sample analytes to the bottom of the plate to prevent them washing away. The biotin antibody cocktail provided was diluted with the provided diluent concentrate (R&D Systems) and 50 µl was added to each well and incubated for 1 h on a plate shaker. The plate was again washed as described above, before 50 µl of Streptavidin-PE was added and again incubated for 30 min on a plate shaker. The plate was read using a Bio-Plex 200 system (Bio-Rad), with the concentration of each analyte calculated from the concentration of the 1 in 3 diluted standard curve for each analyte. The lower and upper limit of quantitation (LLOQ and ULOQ) for each analyte is indicated in Table 2.7.

Table 2.7. The lower and upper limit of quantitation (LLOQ and ULOQ) for each analyte (pg/ml).

Analyte	Lower Limit of Quantification	Upper Limit of Quantification
CCL20	8.558	2169.997
IFN-α	3.497	2657.992
IFN-β	3.786	2999.998
IFN-γ	18.040	13434.827
IL-1β	5.801	4347.716
IL-10	1.313	942.046
IL-15	2.171	1540.061
IL-17C	4.919	4085.088
IL-23	45.919	34817.527
IL-27	92.344	72333.779
IL-33	3.791	2824.383
IL36β	1.026	829.974
TLSP	0.862	630.293
TNF-α	2.190	1660.525

2.23 Flow Cytometry

Flow cytometry was used to assess IAV or GFP-NTHi infection of MDM. For GFP-NTHi infections, MDM were infected with GFP-NTHi as described in Section 2.6.1 and harvested at 6 h (after the 90 min gentamicin wash) and 24 h. To analyse IAV infection of MDM, MDM were infected as described in 2.6.2 and harvested 24 h post initial IAV incubation (at 48 h). MDM were harvested in both instances using 200 µl non-enzymatic cell dissociation solution (Sigma) for 20 min at 37°C. After 20 min, cells were gently removed from wells into 5 ml polypropylene tubes (BD). Cells were washed and centrifuged at 400 *g*, 4°C for 5 min in Fluorescence-Activated Cell Sorting (FACS) buffer (2mM EDTA, 0.5% (w/v) BSA in PBS) and resuspended in 200 µl Cytofix/Cytoperm™ Fixation and Permeabilization Solution (BD Biosciences) and incubated on ice for 20 min. At this point, for the GFP-NTHi infections, cells were washed and resuspended in 250 µl FACS buffer, as no antibody staining was necessary due to the GFP-tag present on the GFP-NTHi strain. For analysis of IAV infection, cells were washed and centrifuged and stained with 2 µl Fluorescein isothiocyanate (FITC) labelled anti-NP-1 antibody (Abcam) in 100 µl 1 x PermWash™ (BD Biosciences) for 30 min on ice. Cells were washed in 2 ml 1 x PermWash™ and resuspended in 250 µl FACS buffer. Acquisition was performed using 9-colour FACSAria (BD Biosciences), with FlowJo software (Version 10) used for analysis. A reference gating strategy for determining IAV or GFP-NTHi infection is shown in Figure 2.13. Firstly, gating was used to select MDM and not debris (Figure 2.13A). Subsequently, the uninfected MDM at the appropriate time point for each experiment was used as the gating control for negative FITC-fluorescent signal to assess GFP-NTHi infection at 6 h (Figure 2.13B) or 24 h (Figure 2.13C) or IAV infection at 48 h (Figure 2.13D).

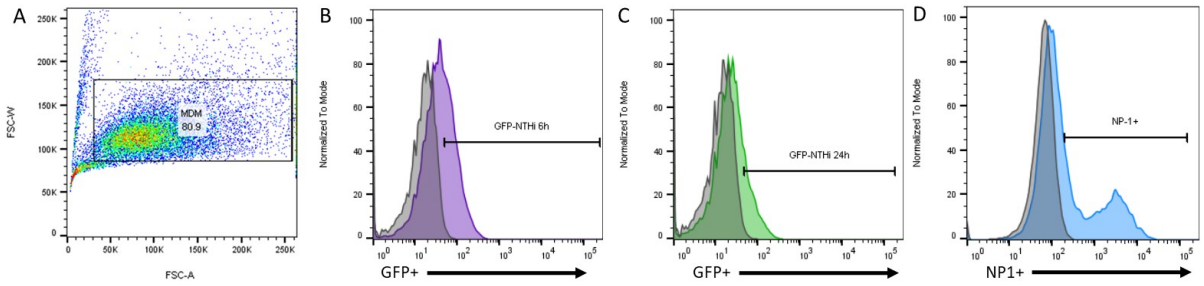

Figure 2.13. Representative flow cytometry gating strategy for determining NP-1+ MDM. Cells were first gated by size to exclude any debris. Uninfected MDM were then used to gate as a negative control to identify NP-1+ MDM.

2.24 Fluorescent in situ hybridisation (FISH)

Stored BAL cytospin slides (Section 2.3) were thawed and allowed to come to room temperature. Slides were washed in PBS before being fixed in a paraformaldehyde-acetic acid fixative solution (36.5M paraformaldehyde and 5% acetic acid in PBS) for 15 min. Slides were subsequently washed twice in PBS for 5 min, before two final quick washes in water. Slides were dehydrated using an ethanol gradient of 70% ethanol for 5 min, 90% ethanol for 5 min and 100% ethanol for 5 min before being left to completely air dry. The NTHi specific probe HAIN16S1251 and the pan-bacteria probe EUB338A (Table 2.8) were diluted to a concentration of 50 µg/µl in hybridization buffer (0.9 M NaCl, 20 mM Tris/HCl, 0.01% SDS, and 30% formamide pH 7.5) and 20 µl added to each slide. Hybridization was performed for 2 h at 46˚C using a ThermoBrite StatSpin humid chamber before being washed for 15 min in wash buffer (80 mM NaCl, 20 mM Tris- HCl pH 8, 5 mM EDTA, and 0.01% SDS) at 48˚C. Slides were again washed in PBS before addition of 150 µl of Vector® TrueVIEW® Autofluorescence Quenching reagent (Vectorlabs) for 4 min. Slides were washed in PBS before glass coverslips were added using Vectashield mounting solution containing 4',6-Diamidino-2-Phenylindole (DAPI) nuclear stain (Vectorlabs). Slides were stored at 4˚C until visualisation occurred using a Zeiss Axioskop2 Mot fluorescence microscope using x 40 magnification immersion oil objective. Images were acquired using Micro-Manager and analysed in ImageJ. Bacteria-only controls were used to ensure specific binding of the NTHi-specific probe to NTHi. All bacteria used were stained by DAPI. *Escherichia coli* BL21 (kindly provided by Dr. A Watson, University of Southampton) and *Streptococcus pneumoniae* D39 serotype 2 (kindly provided by Dr. G Cooper, University of Southampton[240]) were detected by the FITC-pan probe, but not the CY3 NTHi-specific probe (shown as green only in the merged images, Figure 2.14A-B). In contrast, NTHi was detected by both probes, as indicated by the yellow-orange colour in the merged images (Figure 2.14C).

Table 2.8. Probe sequences used for FISH. HAIN16S1251 is an NTHi-specific probe and EUB338A is a pan-bacteria probe. FITC= Fluorescein isothiocyanate.

Probe	Probe Sequence	Fluorophore
HAIN16S1251	5’ TCGCAGCTTCGCTTCCCT 3’	CY3
EUB338A	5’ GCTGCCTCCCGTAGGAGT 3’	FITC

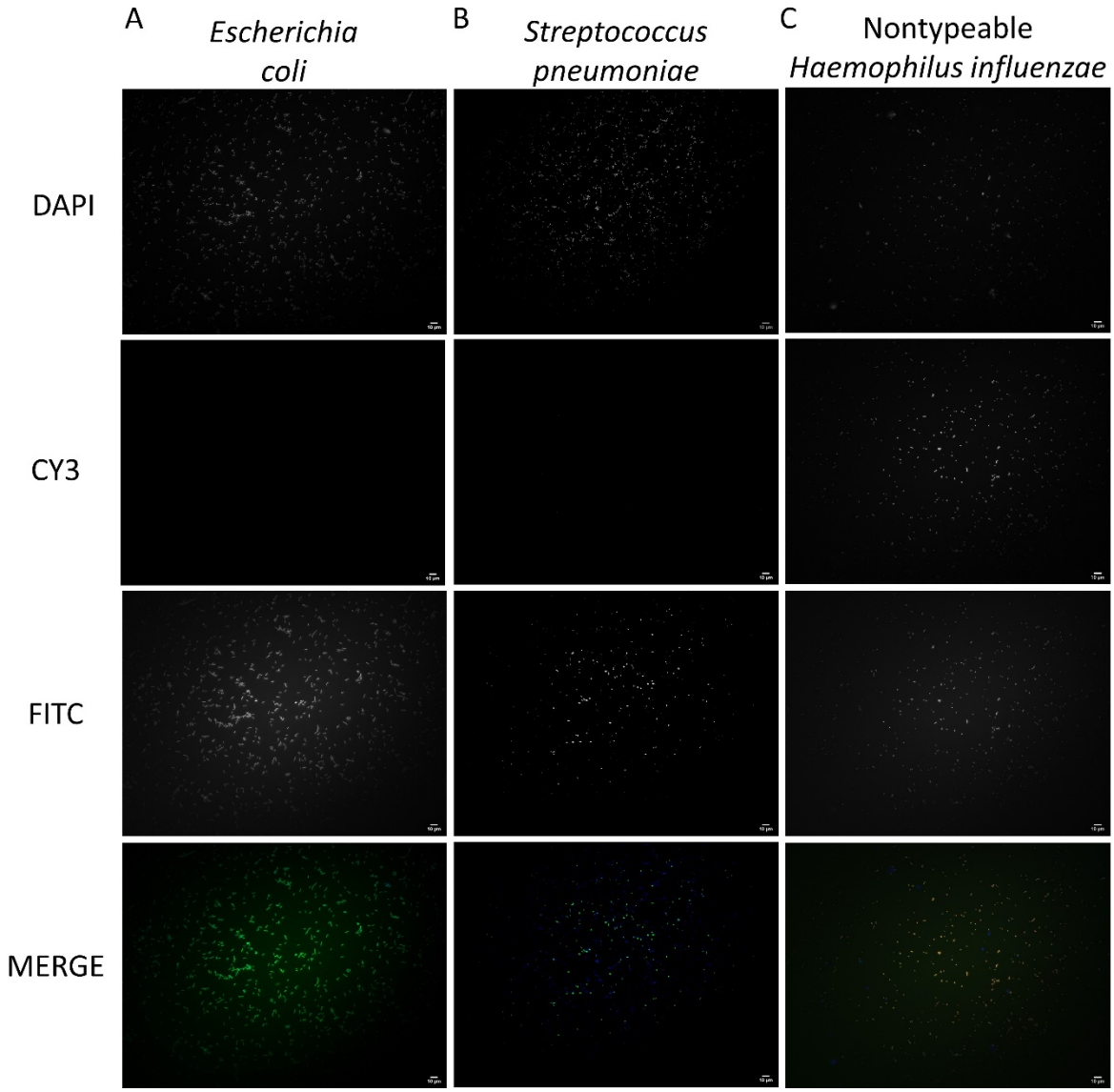

Figure 2.14. Bacteria only controls for FISH. To determine whether any signal from the Cy3 NTHi specific probe could be detected in the presence of other bacteria, slides containing bacteria only were prepared using (A) *Escherichia coli*, (B) *Streptococcus pneumoniae* and (C) Nontypeable *Haemophilus influenzae* as a positive control. FISH was performed using the pan bacteria probe (FITC) and the NTHi-specific probe (Cy3). All slides were counterstained with the nuclear stain DAPI. Images taken using 40x oil immersion objective. Scale bar shows 10 µm. FITC= Fluorescein isothiocyanate, DAPI = 4',6-Diamidino-2-Phenylindole.

2.24.1 Quantification of NTHi colonisation in BAL samples

FISH was performed as described above. For quantification, all images were acquired using the same exposure settings for each individual fluorescent channel. Quantification of the presence of NTHi for each individual was performed in ImageJ/FIJI (National Institutes of Health, USA, version 1.53c) [387,388]. The number of macrophages in each image, represented by DAPI staining of single cell nucleus, was quantified using the Analyse Particles in-built ImageJ tool (Figure 2.15A). This was achieved by setting the threshold for each image and running the 'Convert to Mask' and 'Erode' functions before the 'Analyse Particles' function to count the individual nuclei. The CY3 NTHi-specific signal was next quantified using the Find Maxima in-built ImageJ tool (Figure 2.15B). Firstly, each image was adjusted using the 'Enhance Contrast', 'Smooth' and 'Gaussian Blur' in-built ImageJ functions. The 'Find Maxima' function was then used to identify the CY3 signal that passed a set 'prominence' level, which was set to reduce potential background or autofluorescence being counted as NTHi. The output of DAPI and CY3 signal quantification (Figure 2.15D) was then used to determine the number of DAPI-stained cells associated with the CY3-NTHi signal, which was expressed as a percentage of cells colonised with NTHi.

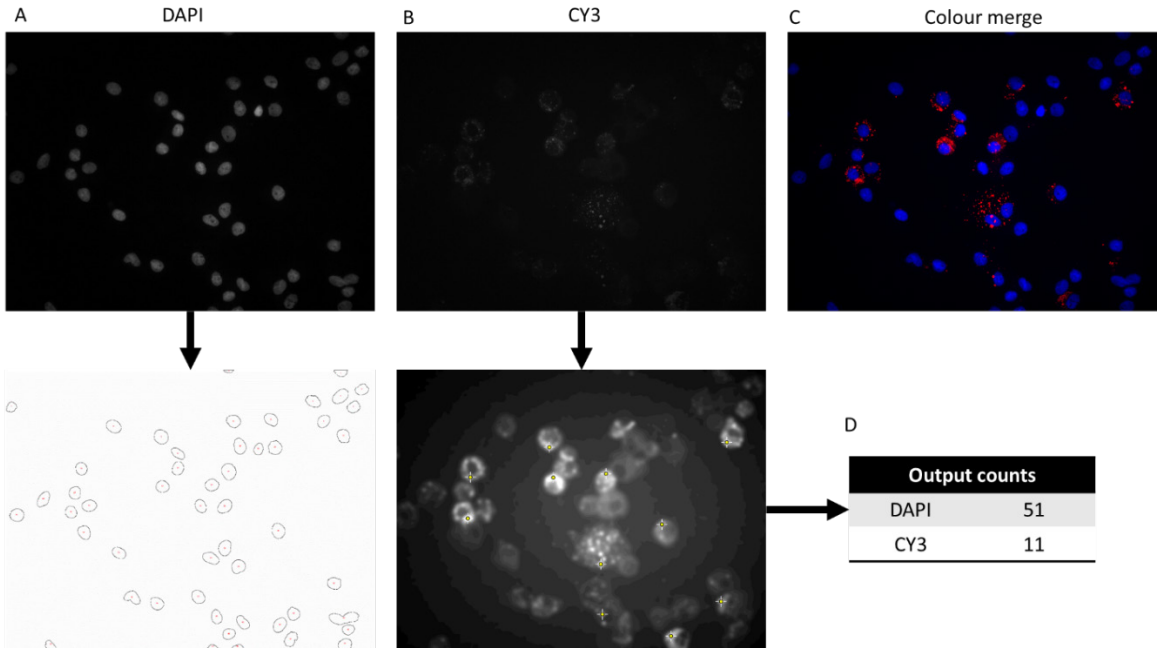

Figure 2.15. Quantification analysis of a representative FISH image. (A) The number of host cells was first quantified using the Analyse Particles function, which returned a count for each DAPI-stained nuclei, which represents a single cell. (B) The CY3 signal was quantified using the in-built Find Maxima Image J tool and the Gaussian Blur filter function, in order to only count a single Cy3 signal for each cells. The crosses present on the image show the Cy3 signal passing the set prominence level, which was set to reduce the potential of autofluorescence or background signal counting as NTHi. (C) The colour composite merged image showing the CY3-NTHi signal associating with a single DAPI-strained nuclei. (D) The count output for this individual sample indicates that out of the 51 total cells detected, 11 were colonised with NTHi = 22% NTHi+ cells. DAPI = 4',6-Diamidino-2-Phenylindole

2.25 Crystal violet staining to detect NTHi in cell culture wells

To visualise and quantify NTHi viability in the absence of MDM, wells that did not contain MDM were incubated with NTHi at MOI 10, 100 or infection media alone for 2 h, 6 h or 24 h at 37℃, 5% CO_2. After each time point, the supernatant was removed and wells washed twice with PBS and left to air dry for 15 min. Once dry, 200 µl of 0.2% crystal violet (v/v) (Sigma) was added and incubated at 37℃ for 15 min. After 15 min, the crystal violet solution and wells were washed three times with 500 µl PBS to remove excess crystal violet. To quantify NTHi presence in wells, 200 µl 75% ethanol was added to solubilise the crystal violet stain and 100 µl was removed and added to a fresh 96 well plate and read on a plate reader at 590nm (Multiskan Ascent).

2.26 Overview of packages and software

All packages and software used for analysis in this thesis are displayed in Table 2.9. As not all packages have citable publications, the URL link to the package description page is included alongside the version number of the tool used in this thesis, with references included in the author list where available.

2.27 Statistical Analysis

Statistical analysis was performed using GraphPad Prism (version 8 GraphPad Software, San Diego, USA) and statistical significance was determined as $p<0.05$. Due to low sample sizes throughout this thesis, data were treated as non-parametric for statistical analysis. For paired data, Wilcoxon matched-pairs signed rank test between two groups or Friedman test with Dunn's post hoc test for multiple comparison testing between more than two groups for one independent variable were used. For analysis of data with more than one independent variable, a two way ANOVA, with Tukey's multiple comparisons post hoc test was used. For unpaired data, Mann Whitney U test between two groups or Kruskal-Wallis with Dunn's post hoc test for multiple comparison testing between more than two groups were used. Correlation analyses were performed using Spearman rank correlation coefficient. For analysis of categorical data, Fisher's exact test was used.

For analysis of DEG and enrichment analysis, statistically significant differentially expressed genes were determined as FDR corrected $p<0.05$, using the Benjamini-Hochberg correction method.

Table 2.9. Overview of the bioinformatic tools and software used in this thesis.The version number indicates the version of the software/tool that was used at the time of analysis so may not represent the most up to date version available. The URL included is the software or package website which has more information about how to download and use the software, including vignettes or manuals detailing the functions and uses of the package and associated code. References for published literature are included where available, if not, the names of the authors/creators for each package/tool are included. NA = Software version not available

R packages	Version	URL	Author and/or reference
amap	0.8-18	https://CRAN.R-project.org/package=amap	A.Lucas
corrplot	0.84	https://CRAN.R-project.org/package=corrplot	T.Wei, V.Simko V, M.Levy *et al.*
dbplyr	2.0.0	https://CRAN.R-project.org/package=dbplyr	H.Wickham and E.Ruiz
dendextend	1.13.4	https://cran.r-project.org/package=dendextend	T.Galili, Y.Benjamini, G.Simpson *et al.*[389]
DESeq2	1.24.0	https://bioconductor.org/packages/DESeq2	M.Love, C.Ahlmann-Eltze, K.Forbes *et al.*[378]
dplyr	1.0.2	https://CRAN.R-project.org/package=dplyr	H.Wickham, R.François, L.Henry *et al.*
edgeR	3.26.8	https://bioconductor.org/packages/edgeR	Y.Chen, A.T.L Lun, D.J.McCarthy *et al.*[353]
ellipse	0.4.2	https://CRAN.R-project.org/package=ellipse	D.Murdoch and E.D.Chow
EnhancedVolcano	1.2.0	https://bioconductor.org/packages/EnhancedVolcano	K.Blighe
factoextra	1.0.7	https://CRAN.R-project.org/package=factoextra	A. Kassambara and F.Mundt
FactoMineR	2.3	https://CRAN.R-project.org/package=FactoMineR	F.Husson, J.Josse, S. Le and J.Mazet
ggalluvial	0.12.2	https://CRAN.R-project.org/package=ggalluvial	J.C.Brunson and Q.D.Read
ggplot2	3.3.2	https://CRAN.R-project.org/package=ggplot2	H.Wickham, W.Chang, L.Henry *et al.*
ggpubr	0.4.0	https://CRAN.R-project.org/package=ggpubr	A.Kassambara
ggrepel	0.8.2	https://CRAN.R-project.org/package=ggrepel	K.Slowikowski, A.Schep, S.Hughes *et al.*
ggridges	0.5.2	https://CRAN.R-project.org/package=ggridges	C.O.Wilke
GOplot	1.0.2	https://CRAN.R-project.org/package=GOplot	W.Walter and F.Sanchez-Cabo[390]
gplots	3.0.4	https://CRAN.R-project.org/package=gplots	G.R.Warnes, B.Bolker, L.Bonebakker *et al.*
Hmisc	4.4-0	https://CRAN.R-project.org/package=Hmisc	F.E.Harrell Jr
hrbthemes	0.8.0	https://CRAN.R-project.org/package=hrbrthemes	B.Rudis, P.Kennedy, P.Reiner *et al.*
RcolorBrewer	1.1-2	https://CRAN.R-project.org/package=RColorBrewer	E.Neuwirth
rgl	0.103.5	https://CRAN.R-project.org/package=rgl	D.Adler and D.Murdoch
scales	1.1.1	https://CRAN.R-project.org/package=scales	H.Wickham, D.Seidel and RStudio
stats	3.6.1	https://www.rdocumentation.org/packages/stats	R Core Team and contributers worldwide
viridis	0.5.1	https://CRAN.R-project.org/package=viridis	S.Garnier, N.Ross, B.Rudis *et al.*
WGCNA	1.69	https://CRAN.R-project.org/package=WGCNA	P.Langfelder and S.Horvath[379]
Command line tools	**Version**	**URL**	**Author and/or reference**
Gingr	1.3	https://github.com/marbl/gingr	B.D.Ondov, T.J.Treangen, A.M.Phillippy[370]
Harvest	1.1.2	https://github.com/marbl/harvest-tools	B.D.Ondov, T.J.Treangen, A.M.Phillippy[370]
ParSNP	1.2	https://github.com/marbl/parsnp	B.D.Ondov, T.J.Treangen, A.M.Phillippy[370]
Software	**Version**	**URL**	**Author and/or reference**
AutoAnnotate	1.3	http://apps.cytoscape.org/apps/autoannotate	M.Kucera, R.Isserlin, A.Arkhangorodsky *et al.*[391]
clusterMaker2	0.9.5	http://apps.cytoscape.org/apps/clustermaker2	J.H.Morris, L.Apeltsin, A.M.Newman *et al.*[392]
cytoHubba	0.1	http://apps.cytoscape.org/apps/cytohubba	Chia-Hao Chin, Shu-Hwa Chen, Hsin-Hung Wu.[380]
Cytoscape	3.8.2	https://cytoscape.org	P.Shannon, A.Markiel, O.Ozier *et al.*[393]
EnrichmentMap	3.3	http://apps.cytoscape.org/apps/enrichmentmap	D.Merico,R.Isserlin, O.Stueker, A.Emili and G.Bader[394]
WordCloud	3.1.0	http://apps.cytoscape.org/apps/wordcloud	L.Oespe, D.Merico, R.Isserlin and G.D.Bader.[395]
VennDIS	1.0.1	http://kislingerlab.uhnres.utoronto.ca/projects	V.Ignatchenko, A.Ignatchenko, A.Sinha *et al.*[396]
Online tools	**Version**	**URL**	**Author and/or reference**
Intererome	2.01	http://www.interferome.org/interferome/	I.Rusinova, S.Forster, S. Yu *et al.*[397]
PresRAT	NA	http://www.hpppi.iicb.res.in/presrat/	K.Kumar, A.Chakraborty and S.Chakrabarti[398]
ShinyGo	0.61	http://bioinformatics.sdstate.edu/go	S.X.Ge, D.Jung and R.Yao.[382]
ToppGene	NA	https://toppgene.cchmc.org	J.Chen, E.Bardes, B.Aronow and A.G.Jegga.[381]
Venny	2.1	https://bioinfogp.cnb.csic.es/tools/venny/	J.C.Oliveros.[399]

Chapter 3 Optimisation of an NTHi-MDM intracellular infection model

3.1 Introduction

The main aim of this thesis was to investigate NTHi-macrophage interactions and the impact on subsequent viral infection, which is a main driver of asthma exacerbations. Although NTHi presence in the airways of individuals with asthma is now being widely reported during both stable and exacerbated periods of disease, NTHi presence is associated with more severe disease, steroid resistance and neutrophilic inflammation[86,400]. It is not understood whether NTHi infection and residence with airway macrophages modulates the immune response, contributing to chronic airway inflammation and exacerbations in asthma. As such, this chapter will focus on optimisation of an *in vitro* monocyte-derived macrophage (MDM)-NTHi infection model. This model will be subsequently used to investigate both host and pathogen transcriptomic changes associated with infection by dual RNASeq.

A challenging and limiting factor of dual RNASeq is that bacterial RNA can make up less than 1% of the total RNA in an infected cell[373]. Furthermore, 95% of total RNA in an infected cell is host ribosomal RNA, further reducing the ratio of bacterial RNA of interest[401]. Therefore, it is likely that in this system, macrophage RNA will vastly outweigh the amount of NTHi RNA present. To overcome this, the NTHi transcriptome must be sequenced in enough depth to determine biologically significant changes in NTHi gene expression above any noise in the data set[402].

A MDM infection model previously established in the lab comprises of a 2 h infection period with either a virus or bacteria, followed by a 22 h incubation period in antibiotic containing media[199,240,349,350,352,403]. However, this infection model was primarily used to investigate the MDM response to the pathogen in question, with only low amounts of viable NTHi recovered from MDM[234]. In order to reduce the potential increased costs that occur with increasing sequencing depth to ensure adequate coverage of the NTHi transcriptome, in addition to the host transcriptome, the infection model first required optimisation. This chapter will detail optimisation of an intracellular infection model, ensuring a sufficient amount of live, viable NTHi was present for sequencing, without compromising the viability of the macrophage.

3.2 Results

3.2.1 Optimising recovery of NTHi from infected MDM

A commonly used method of quantifying live intracellular NTHi is the gentamicin protection assay[123,141,142,144,149]. Gentamicin has been reported to be less able to cross the cell membrane of the host cell than other antibiotics and therefore not impact on the viability of intracellular bacteria[147,404]. Previously published studies using gentamicin protections assays to assess the number of intracellular bacteria have used a variety of infection times, ranging from 1 h to 24 h[123,140,405–407]. As mentioned above, the previous work in the lab using MDM demonstrated only

approximately 1 x 10^3 CFU/ml of NTHi was able to be recovered after infection of MDM for 2 h using a MOI of 1[234]. Therefore, to ensure sufficient quantities of NTHi will be present within MDM to accurately quantify and identify changes between the desired tested conditions, the infection model was optimised using higher MOIs of 10 and 100 using an intermediate time point of 6 h.

To investigate the effect of antibiotics on the recovery of viable intracellular NTHi, MDM were infected with NTHi at MOI 10 or MOI 100 for 6 h before being incubated with either penicillin/streptomycin or gentamicin for 90 min. MDM were then lysed using 1 x PermWash™ (PW) and plated onto CHOC agar plates overnight at 37°C, 5% CO_2. The amount of NTHi recovered from MDM incubated with gentamicin was significantly higher compared to MDM incubated with penicillin/streptomycin (Figure 3.1A & B, p=0.0313 for both MOIs).

The gentamicin concentration was tested to ensure the effectiveness of concentrations used to kill all extracellular NTHi. MDM were incubated for 90 min in concentrations ranging from 5 µg/ml to 500 µg/ml following infection with NTHi for 6 h (Figure 3.2A and B). For both MOIs, lower amounts of NTHi were recovered using higher gentamicin concentrations, however this was not significant. To ensure that extracellular NTHi was removed or killed during the antibiotic wash, culture supernatants were harvested and plated onto CHOC agar plates. NTHi was still detectable at the lower concentration of gentamicin (Figure 3.2C and D). NTHi counts were observed in particular for MDM infected with NTHi at MOI 100 and then incubated with the lower concentration (5 µg/ml) of gentamicin compared to 500 µg/ml (p=0.0104), suggesting that the slightly higher counts recovered from within MDM at the lower gentamicin concentrations may be due to the presence of extracellular NTHi in culture supernatants (Figure 3.2A and B)

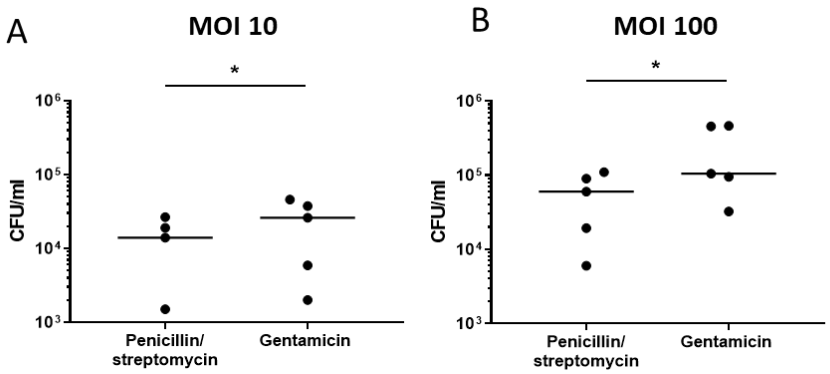

Figure 3.1. Comparing the effects of penicillin/streptomycin (PS) and gentamicin on intracellular NTHi counts. MDM were infected with NTHi at MOI 10 (A) or MOI 100 (B) for 6 h before incubation with either penicillin/streptomycin or gentamicin for 90 min before being lysed for plate counting. Recovered counts are expressed as CFU/ml. Uninfected controls were also performed but NTHi was not detected (not shown on graphs). Graphs show paired data and lines indicate medians. N=5. Where fewer data points are shown, NTHi was not detected (ND). Data were analysed by Wilcoxon signed-rank test; *p<0.05.

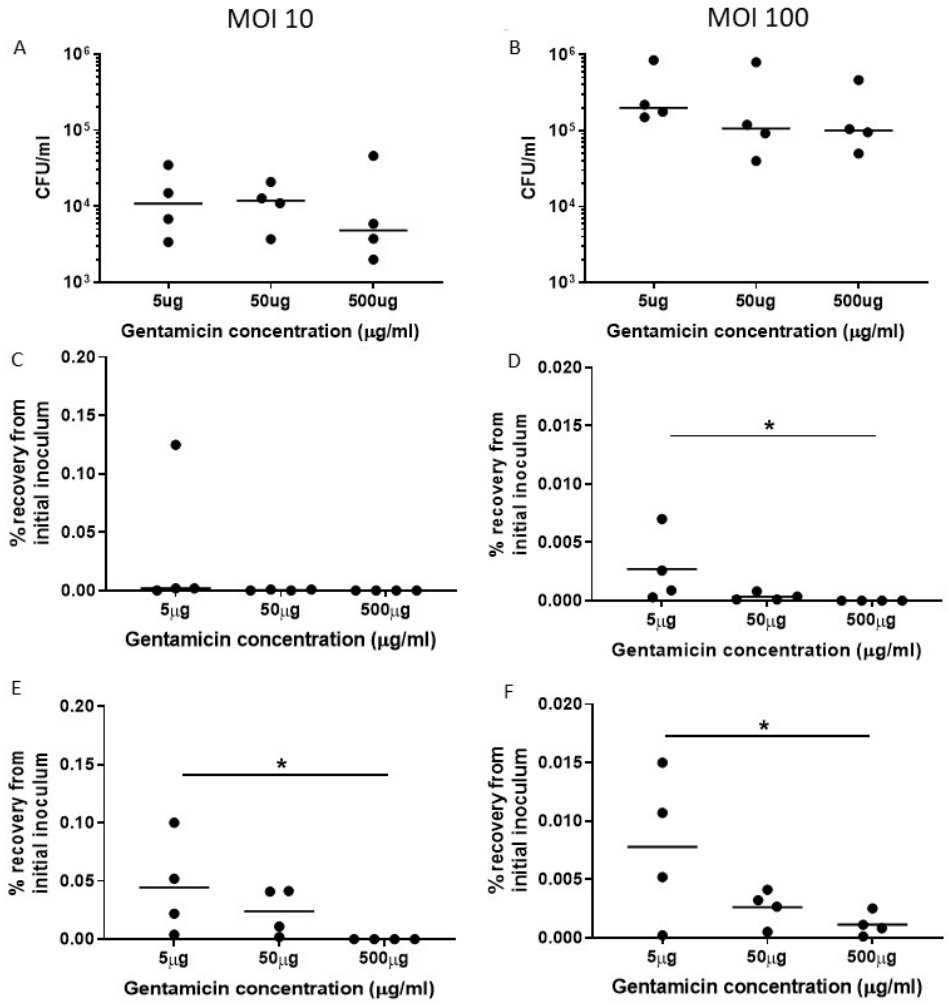

Figure 3.2. Optimising gentamicin concentration for recovery of intracellular NTHi. MDM were infected with NTHi at either MOI 10 or 100 for 6 h before incubation with different concentrations of gentamicin for 90 min. (A) and (B) counts recovered from lysed MDM following incubation with different gentamicin concentrations for 90 min. (C) and (D) the supernatants from the wells were plated to determine presence of live NTHi in and is expressed as a percentage of the initial inoculum. (E) and (F) culture supernatants were harvested, centrifuged and the resulting pellet resuspended in PBS and plated out. Results are expressed as a percentage of the initial inoculum. N=4. Uninfected controls were also performed but NTHi was not detected (not shown on graphs). Graphs show paired data and lines indicate medians. Data were analysed by Friedman test with Dunn's multiple comparison test; *p<0.05

As this experiment was performed by directly harvesting the contents of the gentamicin-containing infection culture media and plating on CHOC agar plates, the presence of gentamicin could potentially prevent the growth of NTHi on CHOC agar plates and result in an underestimation of the amount of live, extracellular NTHi present in the supernatants. To determine the presence of remaining live NTHi, culture supernatants were harvested into sterile tubes and subjected to centrifugation for 10 min at 800 *x g* to pellet bacteria. The gentamicin-containing supernatant was discarded and the cell pellet was resuspended in fresh PBS before being plated onto CHOC agar plates. Unlike previously, presence of NTHi was detected in supernatants containing the higher

concentrations of gentamicin (Figure 3.2E & F). Nonetheless, higher NTHi counts were still detected using the lower concentration of gentamicin compared to the highest concentration (p=0.0104 for MOI 10, p=0.04 for MOI 100). These results suggest that the gentamicin present in the supernatants impacted on NTHi growth on plates. However, when comparing the amount of NTHi detected in the supernatant to the initial amount of NTHi (MOI) added, the amount was negligible as the highest percentage recovery was less than 0.15% (Figure 3.2C).

These data indicate that 500 µg/ml gentamicin was the optimum concentration to remove extracellular NTHi, therefore infected MDM were incubated with 500 µg/ml gentamicin for 30, 60 or 90 min to determine the length of time required to kill all extracellular NTHi, without impacting on intracellular NTHi viability. No significant differences in the amount of NTHi recovered from MDM after 30, 60 or 90 min of gentamicin treatment was detected (Figure 3.3A and B). However, the presence of NTHi was still detected in the supernatants after 30 and 60 min of gentamicin treatment, but not 90 min (Figure 3.3C & D). Therefore, 30 and 60 min were not sufficient gentamicin incubation times for removal of all extracellular NTHi. In contrast, no extracellular NTHi was detected in the supernatants after 90 min and no significant decrease in intracellular NTHi viability was detected.

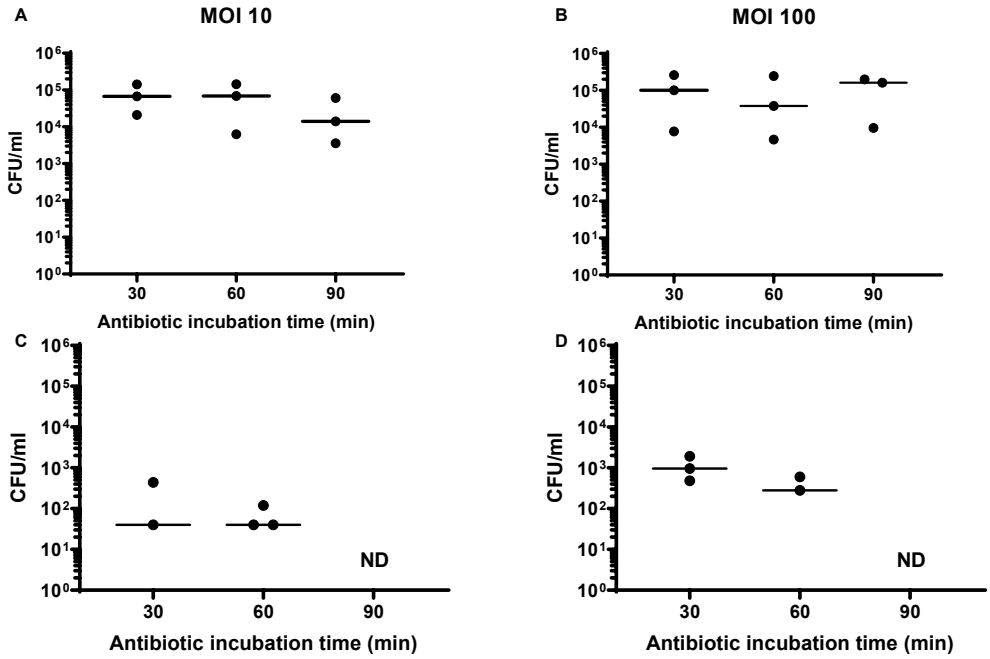

Figure 3.3. Optimisation of gentamicin incubation time. MDM were infected with NTHi at MOI 10 or 100 for 6 h before incubation with gentamicin for either 30, 60 or 90 min. (A) and (B) to determine intracellular NTHi, MDM were lysed after each incubation time and plated out. (C) and (D) to ensure that no extracellular NTHi remained following gentamicin incubation, MDM supernatants were harvested and plated out. N=3, where there are fewer data points, NTHi was not detected (ND). Uninfected controls were also performed but NTHi was not detected (not shown on graphs). Graphs show paired data and lines indicate medians. Data were analysed by Friedman test.

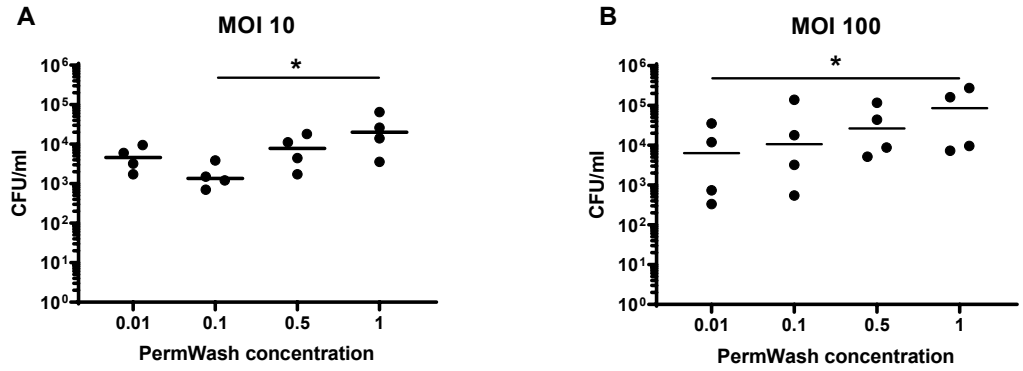

Figure 3.4. Optimisation of MDM lysis for NTHi recovery. MDM were infected with either MOI 10 (A) or MOI 100 (B) NTHi for 6 h and incubated in gentamicin for 90 min. To lyse MDM, cells were incubated with different PermWash™ (PW) concentrations for 20, min and plated onto CHOC agar plates. Both (A) and (B) indicate that 1x PW allowed for highest recovery of NTHi. Graphs show paired data and lines indicate medians. Uninfected controls were also performed but NTHi was not detected (not shown on graphs). Data were analysed by Friedman test with Dunn's multiple comparison test; *p<0.05

The final factor optimised to enable effective assessment of intracellular NTHi was the concentration of PW used to lyse and release intracellular NTHi from MDM. PW contains saponin, and previous work by Morey *et al.* (2011) indicated that lower concentrations of saponin increased bacterial recovery[140]. To assess the concentrations required for adequate MDM lysis to release and recover NTHi, PW concentrations ranging from 0.01 to 1 x PW were used. In contrast to the aforementioned work by Morey *et al.* (2011), significantly higher NTHi CFU counts were recovered using higher concentrations of PW (Figure 3.4A and B, p=0.0370 between 0.1 x PW and 1 x PW at MOI 10, and p=0.0155 between 0.01 x PW and 1 x PW at 100 MOI). Henceforth, experiments involving the use of the gentamicin protection assay, used conditions of 500 µg/ml gentamicin for 90 min before lysis of MDM with 1 x PW.

3.2.2 NTHi viability decreases over time in the absence of MDM

As previously mentioned, the formerly established infection model developed in the laboratory used a 2 h infection period, with minimal amounts of NTHi detected[199,240,349,350,352]. To determine the duration of the infection period required for the highest amount of NTHi to be recovered from MDM and therefore be detected by sequencing, a time course experiment was performed. However, the ability of NTHi to be cultured over an extended period of time in the presence of MDM first required testing. To assess this, NTHi was incubated with either MDM (+MDM) or infection media alone (-MDM)(Figure 3.5). The amount of NTHi recovered from culture supernatants was measured at early (2 h), intermediate (6 h) and late (24 h) infection time points by live viable counting. Intriguingly, lower NTHi counts were recovered from MDM-free supernatants, compared to counts obtained from supernatants containing NTHi cultured with MDM, which was significant at 6 h and 24 h (p=0.0183 and 0.0073, respectively), but not 2 h. This suggests that over time, NTHi viability decreases when not cultured with host cells such as MDM.

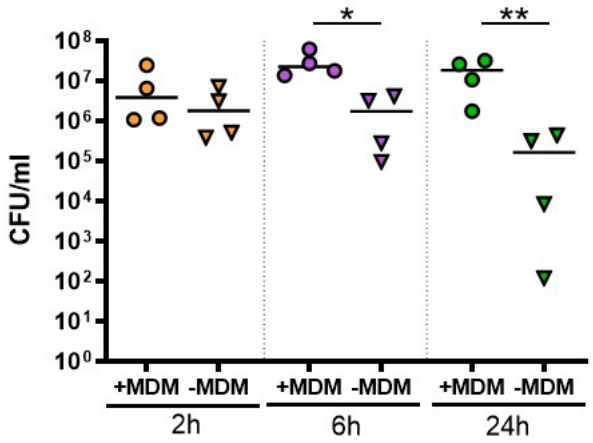

Figure 3.5. NTHi viability decreases in the absence of MDM. NTHi viable counts recovered from well supernatants with (+MDM, circles) or without (-MDM, triangles) MDM present. Infections occurred as previously described, but here, NTHi at MOI 10 was incubated in wells containing MDM or wells that just contained infection media. Graphs show paired data and lines indicate medians. N=4. Asterisk indicates statistical significance performed by Friedman test with Dunn's multiple comparison test; *p<0.05, **p<0.01

To determine whether the decrease in CFU/ml counts was simply due to NTHi adherence to the plastic of the culture plate or forming aggregates, at each time point the well culture media was removed and 0.2% crystal violet added to visualise NTHi. However, even at the longer 24 h time point, no crystal violet staining was observed, with absorbance values below the culture media-only control well (n=2, data not shown). This suggests that the lower NTHi counts in supernatants from MDM-free wells were not due to NTHi adherence to the well plastic. Nonetheless, viable NTHi was able to be recovered from wells containing MDM from the early 2 h time point to the late 24 h time point.

3.2.3 NTHi intracellular recovery was highest after 6 h infection

Following confirmation of live, viable NTHi presence following incubation with MDM until 24 h, a time course experiment was performed whereby MDM were infected with NTHi at MOI 1, 10 or 100 for 2, 6 or 24 h. At each time point several variables were assessed. Firstly, the amount of NTHi present in the culture supernatants was determined by sampling the media and plating out (Figure 3.6A). Secondly, to account for NTHi associated with MDM, which includes intracellular and membrane-bound extracellular NTHi (regarded as 'associated' NTHi), cells were washed with PBS only and immediately incubated with PW and plated (Figure 3.6B). Finally, MDM were subjected to the fully optimised gentamicin protection assay protocol described above, washed again with PBS to remove any remaining antibiotics and then incubated in 1 x PW prior to being plated out for viability counting (Figure 3.6C). The counts recorded here are regarded as 'intracellular' NTHi. For clarity, Figure 3.6D, E and F are graphical representations of NTHi location for each condition.

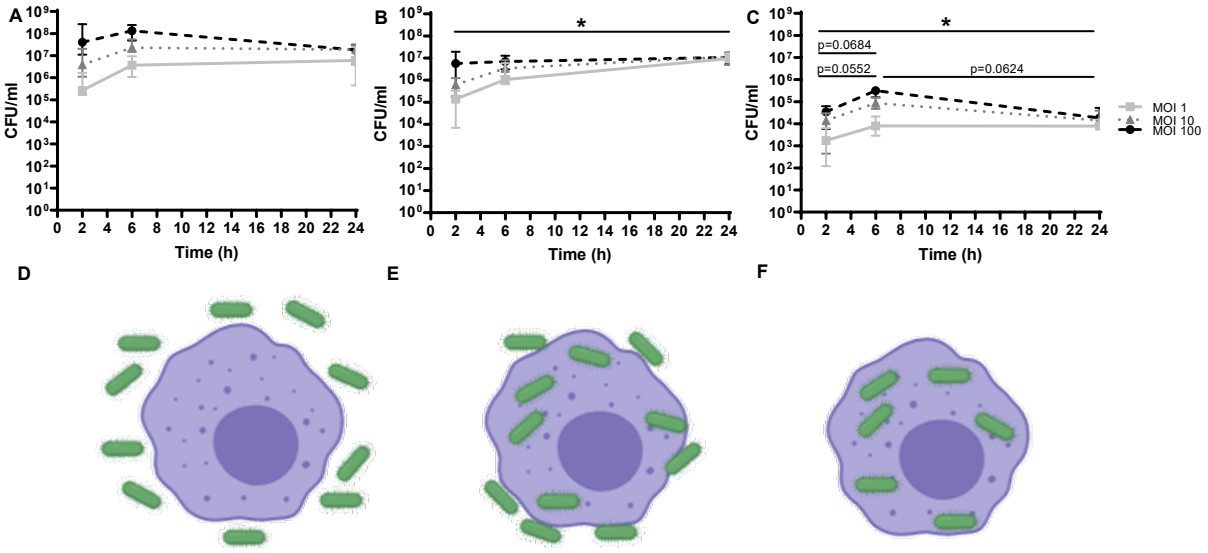

Figure 3.6. Time course of NTHi-MDM infection. MDM were infected with NTHi at MOI 1, 10 or 100 for 2 h, 6 h or 24 h. (A) Supernatants were harvested at these time points to show the amount of NTHi in the well not in contact with the MDM (B) MDM were washed with PBS and immediately lysed to determine the amount of NTHi associated with the macrophage (both extracellular membrane-bound and intracellular NTHi). (C) MDM were washed and incubated for 90 min with gentamicin to remove extracellular NTHi in order to recover only intracellular NTHi. D-F show the locations of NTHi sampled in graphical format for clarity. Uninfected controls were also performed but NTHi was not detected (not shown on graphs). Each point represents the median of 4 experiments and lower and upper whiskers indicate IQR (25^{th} and 75^{th} percentile). Data were analysed by Two-Way ANOVA, with Tukey's multiple comparisons test to compare the effect of infection time on NTHi number for each MOI; *p<0.05. For B, significance is for MOI 1, 2 h v 24 h. For C, the top line row is for MOI 1 comparisons, middle line is for MOI 10 and the bottom line row is for MOI 100 comparisons. Bottom panel created using Biorender.com

No significant differences in the amount of NTHi recovered from the culture supernatants at 2 h, 6 h or 24 h for any MOI was detected (Figure 3.6A). However, the recovery of NTHi associated with MDM significantly increased between the 2 h and 24 h time point for MOI 1 (Figure 3.6B, p=0.0458), whereas counts for MOI 10 and 100 appeared to be consistent between 6 h and 24 h. Finally, the amount of intracellular NTHi peaked at 6 h compared to 2 h (p = 0.0684 and p = 0.0552 for MOI 10 and 100 respectively) and 24 h (p=0.0624 for MOI 100) whereas higher amounts of NTHi were recovered at 24 h compared to 2 h for MOI 1 (Figure 3.6C, p=0.0213).

3.2.4 Live NTHi was not detected following an extended incubation period with antibiotics

As the aim of developing the current model is to assess both NTHi and MDM responses, it is possible that investigating a single 6 h time point may be too early to characterise the MDM response to NTHi infection[408,409]. This infection model was adapted further to include an extended period of incubation following the initial 6 h NTHi infection, to better model persistent NTHi infection. As mentioned in Section 3.1, this current model is being adapted from models previously used in-

house, which often used a '24 h' end time point for immune response readouts. As 24 h has previously proven successful to investigate MDM responses, this current model was extended to include a 24 h time point. In contrast to the previously established models that incubated MDM in penicillin-streptomycin containing media following the initial 2 h infection period[234,240,349,352,403], gentamicin was used as this current work has shown the viability of intracellular NTHi is less affected when gentamicin is used (Figure 3.1).

Previous optimisation of gentamicin concentration found that using 500 µg/ml gentamicin for 90 min was sufficient to kill all extracellular NTHi. However, continually using this high concentration of gentamicin for 18 h could impact the ability of NTHi to persist within MDM. To test this, MDM were infected with NTHi at MOI 10 or 100 for 6 h, before incubation with either 5, 50 or 500 µg/ml gentamicin for 18 h. MOI 1 was not used as the time course experiment indicated that low amounts of intracellular NTHi were recovered at 6 h compared to MOI 10 and 100. The gentamicin-containing media was removed and cells were washed twice with PBS to remove any residual gentamicin in the well and cells were lysed with PW for plate counting. NTHi was recovered at 6 h, but NTHi was unable to be detected at 24 h for either MOI 10 or 100, despite the inclusion of lower gentamicin concentrations (Figure 3.7A & B). This indicates that the continued presence of gentamicin in this model does not allow for NTHi persistence.

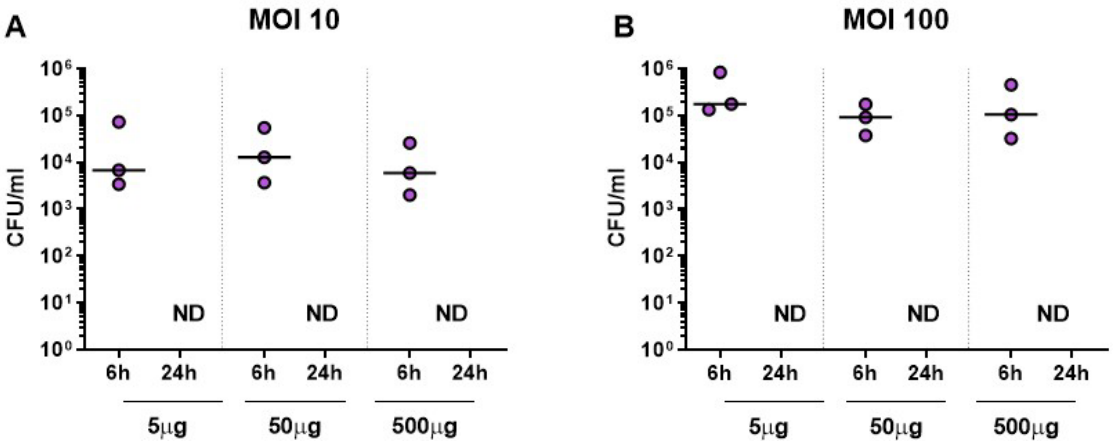

Figure 3.7. Viable NTHi was not recovered from MDM following an extended incubation period in antibiotic-containing media. Comparison of gentamicin concentration during extended gentamicin incubation period. MDM were infected with either MOI 10 (A) or 100 (B) NTHi for 6 h and then incubated with 5, 50 or 500 µg/ml gentamicin for a further 18 h, before MDM were harvested for live plate counting of NTHi. Despite lower concentrations of gentamicin, no NTHi was recovered at the 24 h time points. ND = Not Detected. N=3. Uninfected controls were also performed but NTHi was not detected (not shown on graphs). Graphs show paired data and lines indicate medians.

3.2.5 NTHi can persist until 24 h post infection in the absence of antibiotics

As the presence of gentamicin hinders NTHi infection and persistence in MDM, the infection model was further altered to remove the extended period of antibiotic incubation. However, as the aim of the dual RNA-sequencing is to determine changes associated with intracellular infection, a 90 min gentamicin wash (500 µg/ml) will still be used at 6 h in order for only NTHi that has been internalised within MDM to remain within the culture well and subsequently be sequenced.

To determine whether removing the extended antibiotic incubation period allowed for NTHi persistence, MDM were infected with NTHi at MOI 10 or 100 for 6 h. Four separate conditions were then investigated: i) NTHi counts at 6 h (6h); ii) NTHi counts at 24 h after an extended gentamicin incubation period (24h+G); iii) NTHi counts at 24 h after a 90 min gentamicin wash at 6 h and extended incubation in antibiotic free media (24h-G); and iv) NTHi counts at 24 h after a 90 min gentamicin wash, extended incubation in antibiotic free media and a final gentamicin wash at 24 h (24h-G+G). For clarity, these conditions are shown as a graphical explanation (Figure 3.8A).

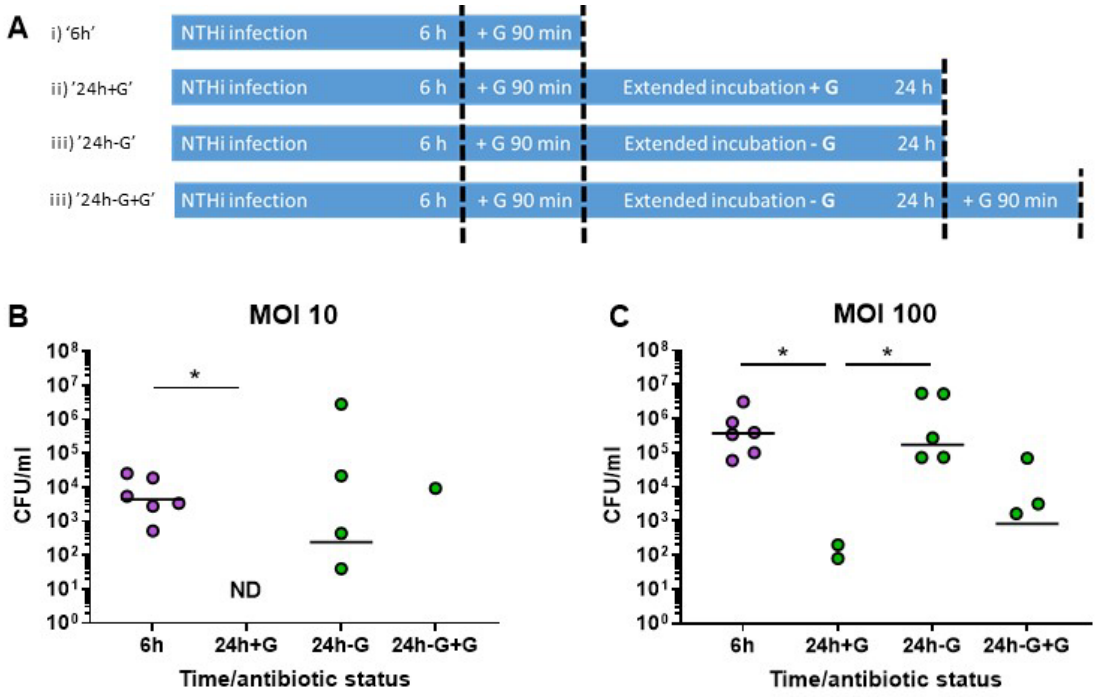

Figure 3.8. Viable NTHi was recovered from MDM not subject to an extended gentamicin incubation period.

MDM were infected with NTHi for 6 h before being subjected to various conditions (A) at either MOI 10 (B) or MOI 100 (C). After 6 h NTHi infection, MDM were either i) subject to a 90 min gentamicin wash, lysed and plated out (6h), ii) incubated in gentamicin for 18 h and lysed and plated out at 24 h (24h+G), iii) incubated in gentamicin for only 90 min, then left in antibiotic free media until 24 h when MDM were lysed and plated (24h-G) or iv) incubated in gentamicin for only 90 min, then left in antibiotic free media until 24 h when MDM were subject to a 90 min gentamicin wash and then lysed and plated out (24h-G+G). ND = Not Detected. N=6. Uninfected controls were also performed but NTHi was not detected (not shown on graphs). Graphs show paired data and lines indicate medians. Data were analysed by Friedman test with Dunn's multiple comparison test; *p<0.05

NTHi was recovered at 6 h for both MOIs (Figure 3.8B & C). Similarly to previous results, no counts were recovered at 24 h using MOI 10 and a low number of NTHi were recovered using MOI 100 following an extended period of gentamicin incubation. However, when a gentamicin wash was used to remove extracellular NTHi at 6 h prior to an extended incubation period in antibiotic free media, NTHi was detectable at both MOIs (Figure 3.8B & C, 24h-G). The final condition (24h-G+G) was used to determine whether the NTHi detected in the third condition was intracellularly located. To achieve this, prior to MDM lysis and plating at 24 h, a 90 min gentamicin wash was used to kill extracellular NTHi. Live counts were not obtained for all experiments in this condition for either MOI (Figure 3.8B & C).

Importantly, higher levels of NTHi were recovered at 24 h following a 90 min gentamicin wash and extended incubation in the absence of gentamicin, compared to NTHi counts obtained in the continued presence of gentamicin ($p=0.0437$). Therefore, the 6 h time point (with a 90 min gentamicin wash) and a 24 h time point (with a 90 min gentamicin wash and extended incubation period in antibiotic-free media) will be taken forward in this work (shown in Figure 3.8A iii).

As live NTHi was detected at both 6 h and 24 h by viable counting, it was next determined whether NTHi RNA was also detectable at both of these time points. Detection of NTHi RNA was crucial, given that the aim of optimising this model was to sequence NTHi during infection. MDM were infected as before at MOI 10 or 100 for 6 h, followed by a 90 min gentamicin wash and were either harvested or further incubated in antibiotic-free media until 24 h. RNA was harvested at both 6 h and 24 h. The NTHi *hel* gene was used to detect NTHi RNA by PCR. The *hel* gene codes for a conserved outer membrane lipoprotein expressed by NTHi and has been used previously for detection of NTHi in clinical samples[386,410].

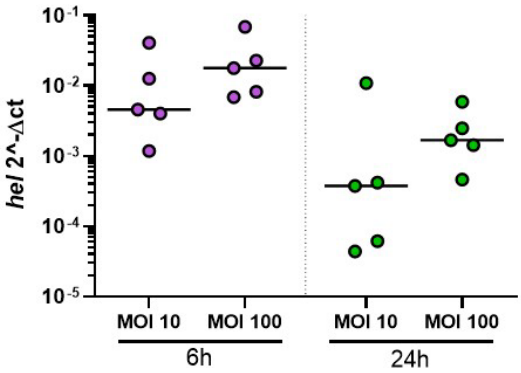

Figure 3.9. Detection of NTHi presence in the absence of antibiotics was detected by qPCR. MDM were infected with NTHi at MOI 10 or 100 for 6 h, subject to 90 min gentamicin and then either immediately harvested or were subject to a further incubation period in antibiotic free media until harvest at 24 h. Expression of the NTHi *hel* gene was normalised to MDM *B2M* housekeeping gene. N=5. Uninfected controls were also performed but NTHi RNA was not detected (not shown on graphs). Graphs show paired data and lines indicate medians. Data were analysed by Friedman test.

NTHi was detected by qPCR at both time points, with higher levels of *hel* expression detected using MOI 100 compared to MOI 10, however this was not statistically significant at either time point (Figure 3.9). Nonetheless, higher levels of NTHi RNA will be more suitable for sequencing, therefore MOI 100 will be used for the remainder of this thesis.

3.2.6 MDM viability was not affected, but metabolic activity increased in response to infection.

To ensure that the infection conditions deemed to be suitable to assess intracellular NTHi infection were not detrimental to macrophages, MDM viability during infection was assessed. For this, a lactate dehydrogenase (LDH) assay was used to assess LDH release into the culture supernatants over the course of infection. LDH release is a commonly used marker of cytotoxicity, with increased LDH release suggesting that cells are less viable and less structurally intact and therefore releasing LDH into the culture environment. LDH release was normalised to the uninfected control at the appropriate time point to express the results as fold change relative to the control. No statistically significant changes in LDH release were detected between 6 h and 24 h, suggesting that NTHi persistence does not impact MDM viability (Figure 3.10).

Slight increases in LDH release were detected for some samples at 6 h, therefore the ability of NTHi to contribute to the overall LDH levels was tested. As a lower level of LDH release by NTHi was expected compared to MDM, multiple MOIs of NTHi were used to ensure that NTHi LDH release could be quantified. Thus, NTHi was cultured in the absence of MDM for 6 h at an equivalent of MOI 1, 10 or 100. At 6 h, the supernatants were harvested and assessed for LDH release. A positive lysis control demonstrated the maximal capability of NTHi to produce LDH at each MOI, which confirmed LDH produced by this particular strain of NTHi was able to be measured by the LDH assay (Figure 3.11).

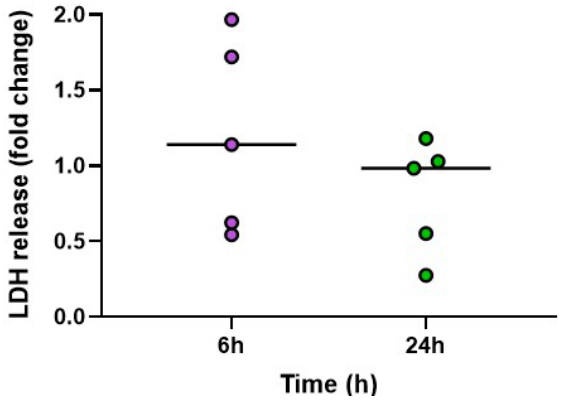

Figure 3.10. Assessment of MDM viability by LDH assay. MDM were infected with NTHi at MOI 100 for 6 h, subject to 90 min gentamicin and then either immediately harvested or were subject to a further incubation period in antibiotic free media until harvest at 24 h. Supernatants were harvested at both time points and assessed for differences in LDH release, with LDH release normalised to the uninfected control for each time point. N=5. Graphs show paired data and lines indicate medians. Data were analysed by Wilcoxon signed rank test.

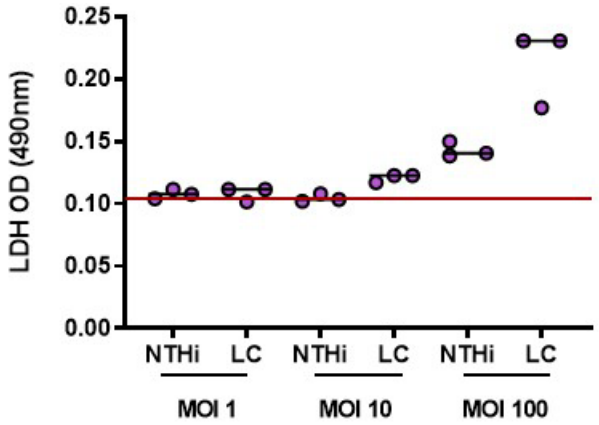

Figure 3.11. LDH release by NTHi during 6 h incubation. NTHi was incubated in the absence of MDM for 6 h. The amount of NTHi used was equivalent to the MOI used to infect MDM. To determine the ability of NTHi to release LDH, NTHi at each MOI were lysed with the provided lysis control (LC). The remaining data at each MOI indicate the amount of LDH released by NTHi over 6 h and is expressed as the OD value. The red line indicates the OD reading of the negative media control. N=3. Graphs show paired data and lines indicate medians.

However, minimal amounts of LDH were released during culture for MOI 1 and MOI 10, with higher amounts of LDH release detected using MOI 100 most likely due to the increased number of NTHi present. Due to the inability of the LDH assay to discriminate between host and pathogen LDH release, the change in NTHi LDH release during co-culture with MDM was unable to be assessed. Nonetheless, the presence of NTHi, particularly MOI 100, may contribute to the overall level of LDH released into supernatants, which could falsely indicate modulation of MDM viability during infection.

Although increased LDH release is suggested to relate to decreased cell viability, LDH is an important enzyme in cellular glycolysis[411]. Therefore, modulation of LDH release could also be due to increased metabolism of MDM in response to NTHi infection, rather than decreased MDM viability. To assess MDM metabolic activity, a colorimetric MTS assay was next used. As the quantity of final product in the MTS assay is directly proportional to the number of viable cells, the number of MDM to be used for this assay first required optimisation. To optimise MDM number, cells were seeded in a 96 well culture plate ranging from 5×10^3 to 1×10^5 MDM per well. As the manufacturer instructions stated the MTS reagent incubation time could vary depending on cell type used, optical density readings were taken at hourly intervals to determine the optimum assay end point. As such, 1 h incubation provided sufficient time to assess the colorimetric change, particularly using MDM quantities ranging from 2.5×10^4 to 1×10^5 per well (Figure 3.12A). As 5×10^4 MDM were the highest quantity of cells at the 1 h time point still on the exponential phase of the curve and had not yet plateaued, this number was chosen to take forward and infect with NTHi to determine whether there are any changes in metabolic activity due to infection.

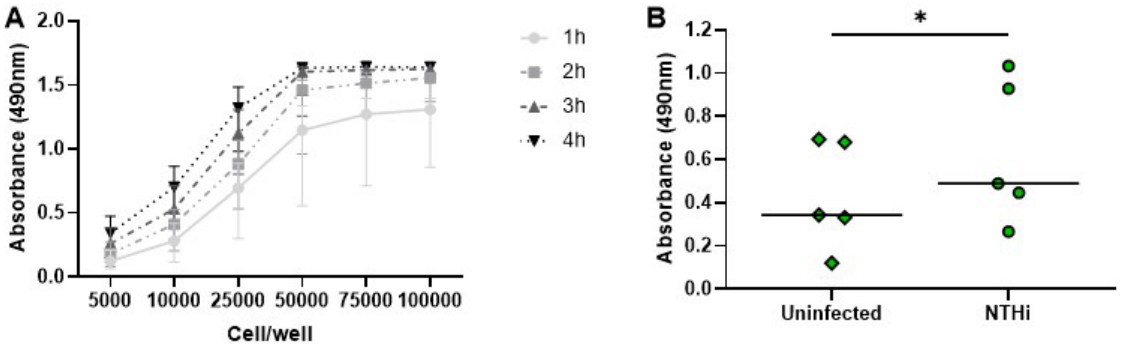

Figure 3.12. Metabolic activity of MDM increases following infection. (A) Optimisation of MTS assay using different quantities of MDM ($5x10^3$ – $1x10^5$ MDM) and reagent incubation times (1 h – 4 h). (B) $5x10^4$ MDM were infected with NTHi at MOI 100 for 6h, washed with gentamicin for 90 min and incubated in antibiotic free media until 24 h. At 24 h, MDM were washed and incubated in 100 µl antibiotic free media and 20 µl MTS reagent for 1 h. After 1 h, absorbance was read at 490 nm on a microplate reader. Graphs show paired data, shapes (A)/lines (B) indicate medians and error bars show IQR. Data were analysed by Wilcoxon signed-rank test; *p<0.05

Following infection with NTHi at MOI 100, a significant increase in metabolic activity was measured in infected MDM compared to uninfected MDM at 24 h (Figure 3.12B). This suggests that the increased LDH measurements do not necessarily indicate decreased MDM viability, but rather increased metabolic activity as a result of NTHi infection.

3.2.7 NTHi infection of MDM can be visualised using GFP-NTHi

To demonstrate that NTHi was physically associated with MDM at 6 h and 24 h, a fluorescently labelled NTHi strain (GFP-NTHi-375^{SR}, a kind gift from Dr. Derek Hood, MRC Harwell) was used to visualise infection of MDM by fluorescence microscopy. The fluorescent label is a green fluorescent protein (GFP) that NTHi-375 has been genetically modified to constitutively express. MDM were infected as previously described and were harvested at 6 h and 24 h before being streaked and fixed onto glass sides and stained with DAPI.

Using fluorescent microscopy, it was evident that uninfected MDM did not have any presence of green fluorescent bacteria and instead, only the blue DAPI-stained nucleus was visible (Figure 3.13A). In contrast, MDM infected with GFP-NTHi had clear evidence of GFP fluorescence at both 6 h (Figure 3.13B) and 24 h (Figure 3.13C), which was closely associated with the macrophage nuclei. The use of a gentamicin wash indicates that NTHi present in this model have resided intracellularly within MDM, which was further confirmed by recovery of live GFP-NTHi at 6 h and 24 h by viable counting (Figure 3.13D).

To quantify the percentage of GFP-NTHi+ MDM, MDM were infected as described and harvested for analysis by flow cytometry. The uninfected MDM at each time point was used as a GFP-NTHi negative gating control (Figure 3.13E). The number of GFP-NTHi+ MDM at 6 h was 18.9%, which

decreased at 24 h to 12.4% (Figure 3.13F).Together, these results suggest that when sequenced not only will a number of MDM be infected by NTHi, but the NTHi sequenced will have been associated with MDM over the course of the infection period. This will allow for assessment of NTHi and MDM interactions through analysis of transcriptomic changes during infection.

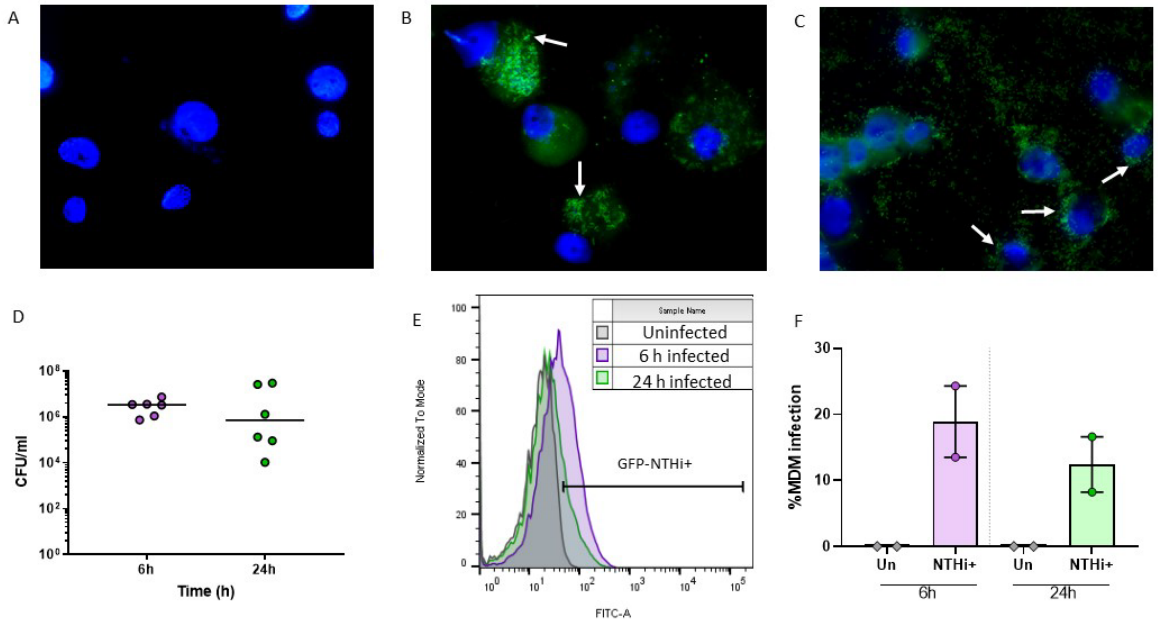

Figure 3.13. Use of GFP labelled NTHi to visualise NTHi infection of MDM. MDM were infected with GFP-NTHi at MOI 100 for 6 h, subject to 90 min gentamicin and then either immediately harvested or were subject to a further incubation period in antibiotic free media until harvest at 24 h. MDM were streaked and fixed onto glass sides and then stained with DAPI and visualised using the AxioScope KS400 fluorescence microscope at 100 x magnification. (A) Uninfected MDM, (B) GFP-NTHi infected MDM at 6 h and (C) GFP-NTHi infected MDM at 24 h. White arrows indicate NTHi associated with the MDM nuclei. (D) MDM were infected as described and harvested for live plate counting to quantify GFP-NTHi recovery from MDM. Graph (N=6) shows paired data and lines indicate medians, 6 h = purple, 24 h = green. Data were analysed by Wilcoxon signed-rank test. (E) To quantify the number of infected MDM at 6 h and 24 h, flow cytometry was used, with the uninfected MDM acting as the negative gating control. (E) Representative histogram plot showing uninfected MDM (grey) 6 h GFP-infected MDM (purple) and 24 h GFP-infected MDM (green). (F) Quantification of MDM infectivity by GFP-NTHi, n=2. Bar shows median and lines indicate interquartile range. Due to low sample number (2) no statistical testing was performed.

3.2.8 MDM responses were observed at both 6 h and 24 h

As the work in this thesis so far has focused on optimising the NTHi-MDM infection model to ensure a sufficient amount of live, viable NTHi could be recovered from MDM, with minimal impact on MDM viability, it is not clear whether macrophage responses to NTHi are detectable at the chosen two time points (6 h and 24 h). To assess activation of MDM responses, the gene expression of the *RELA* subunit of NFκB, the central transcription factor for a variety of immune response pathways, was measured by qPCR. Upregulation of *RELA* was detected at both 6 h and 24 h compared to the uninfected controls (Figure 3.14A). Expression levels did not change between 6 h and 24 h, suggesting continual macrophage activation throughout the infection period in response to the presence of NTHi.

To determine whether changes in protein release by MDM could be detected in response to NTHi, the release of the pro-inflammatory cytokine, IL-1β, was assessed at 6 h and 24 h by ELISA. Detectable levels of IL-1β were measured in culture supernatants, even at the earlier 6 h time point (Figure 3.14B), with levels significantly higher at the 24 h time point (p=0.0312). Together, increased MDM gene expression and inflammatory mediator release in response to NTHi can be detected at both 6 h and 24 h, indicating that this optimised infection model is suitable for assessing MDM-NTHi interactions during persistent infection by sequencing.

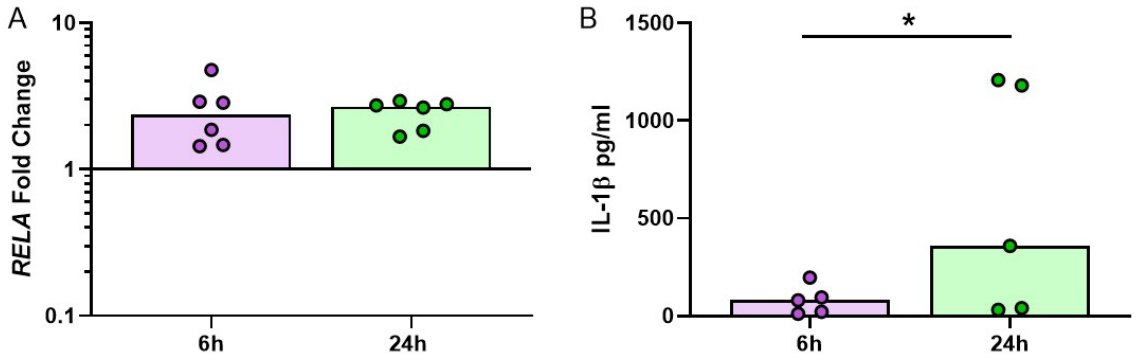

Figure 3.14. MDM inflammatory immune responses are detected in response to NTHi at both 6 h and 24 h. MDM were infected with NTHi at MOI 100 for 6 h, subject to a 90 min gentamicin wash and then either immediately harvested or were subject to a further incubation period in antibiotic free media until harvest at 24 h. RNA was harvested at both time points and the expression of RELA (A) was measured by qPCR. Gene expression was normalized to housekeeping gene *B2M* and is expressed as fold change relative to the uninfected MDM control. Supernatants were harvested at both time points and assessed for levels of IL-1β (B) release by MDM. No release was detected for the uninfected MDM control. Graphs show paired data and bars indicate medians. Data were analysed by Wilcoxon signed-rank test; *p<0.05

3.2.9 Analysis of NTHi strain diversity using ParSNP

NTHi is a heterogeneous organism with vast genetic diversity that has proven challenging to successfully development treatments against. It is not clear whether the diversity of NTHi strains causes a differential immune response, contributing to difficulties in successfully identifying targets for therapeutics. To ensure that the current strain used in this work so far is not extreme in its ability to elicit an immune response (i.e. extremely virulent or not pro-inflammatory at all), MDM responses to different clinical strains of NTHi were assessed.

Seven clinical strains of NTHi that had been isolated either during bronchoscopy sampling, nasal brushing or sputum induction from patients with chronic respiratory disease were available for this work (Figure 3.15A)[364]. These strains had previously undergone whole genome sequencing so the sequences were available as FASTA files. For strain diversity analysis, the ParSNP package from the Harvest Tools suite was used. The sequence files were analysed using the package default parameters and the NTHi reference genome (86-028NP), which is publicly available (https://www.ncbi.nlm.nih.gov) and is a reference strain commonly used[104,371,372,412].

ParSNP is core-genome aligner and uses differences in single nucleotide polymorphisms (SNPs) to infer evolutionary relationships between strains. ParSNP produces output files that can be visualized using the second component of the Harvest Tools suite, Gingr. This output file was input to FigTree (v.1.4.4) to visualize the diversity of these strains as a phylogenetic tree, with no clustering of strains due to sample location apparent (Figure 3.15B).

A

NTHi	Location
ST942	Sputum
ST203	Sputum
ST201	Sputum
ST103	Nasal Brushing
ST408	Nasal Brushing
ST14	Lung
ST1447	Lung

B

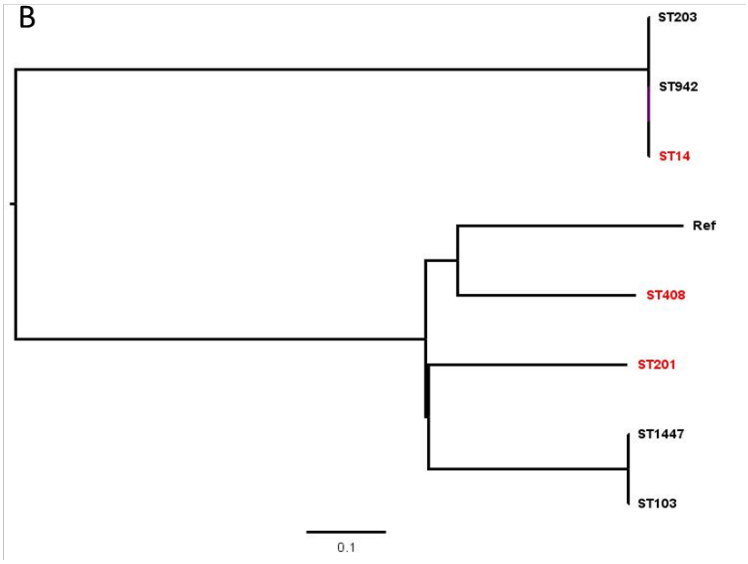

Figure 3.15. Diversity of NTHi strains isolated from individuals with chronic respiratory disease. (A) Sequence type of the NTHi strains used for strain diversity analysis and the sample location from which each strain was isolated. Strains were isolated from either from sputum sample, nasal brushing or protected bronchial brushes of the lung. (B) Phylogenetic tree created in FigTree using ParSNP output files. Strain 86-028NP is the reference NTHi strain used. Strains highlighted in red (ST14, ST408 and ST201) indicate the strains chosen for further *in vitro* experimental analysis.

To determine whether the response of MDM to NTHi is strain-dependent, three strains were chosen for *in vitro* MDM infections based on the diversity inferred from both the phylogenetic tree. Three strains from each clade were chosen, and each strain chosen represents a different anatomical sampling location: ST408 (nasal brushing), ST14 (lung protected brushing), ST201 (sputum). Of note, ST14 was the strain used for the initial set up of this MDM infection model.

3.2.10 NTHi persistence within MDM was strain dependent

The ability of each strain to infect and persist within MDM at MOI 100 was assessed. MDM were infected with either ST408, ST14 or ST201 for 6 h, washed with gentamicin for 90 min and either harvested for live viable counting (6 h time point) or incubated in antibiotic free media until 24 h and harvested for live viable counting (24 h time point).

At 6 h, significantly less ST408 was present compared to ST201 ($p=0.0016$, Figure 3.16A). At 24 h, higher CFU/ml of ST201 was detected compared to ST14 and ST408 (both $p = 0.0281$, Figure 3.16B). Although ST14 and ST408 counts slightly increased by 37% (1.353×10^5 CFU/ml at 6 h compared to 1.855×10^5 CFU/ml at 24 h) and 69% (2.58×10^4 CFU/ml at 6 h compared to 4.35×10^4 CFU/ml at 24 h) respectively, ST201 counts increased by a higher margin of 1171% (5.56×10^5 CFU/ml at 6 h to 7.07×10^6 CFU/ml at 24 h, not statistically significant, $p = 0.1563$).

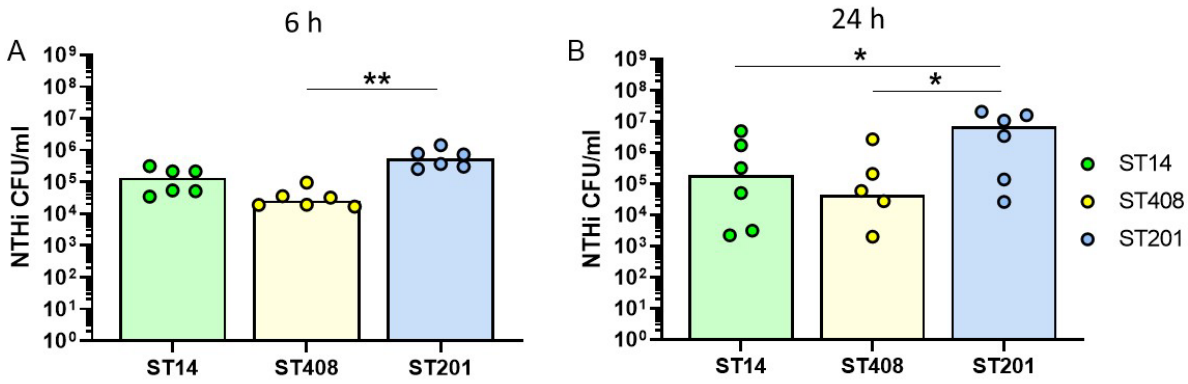

Figure 3.16. Infection and persistence within MDM by different strains of NTHi measured by live viable counts. MDM were infected with ST14 (green), ST408 (yellow) or ST201 (blue) at MOI 100 for 6 h, subject to a 90 min gentamicin wash and then either immediately harvested or subject to a further incubation period in antibiotic free media until harvest at 24 h. Recovered live counts expressed as CFU/ml were detected at both (A) 6 h and (B) 24 h. N=6. Uninfected controls were also performed but NTHi was not detected (not shown on graphs). Graphs show paired data and lines indicate medians. Data were analysed by Friedman test with Dunn's multiple comparison test; *$p<0.05$, **$p<0.01$.

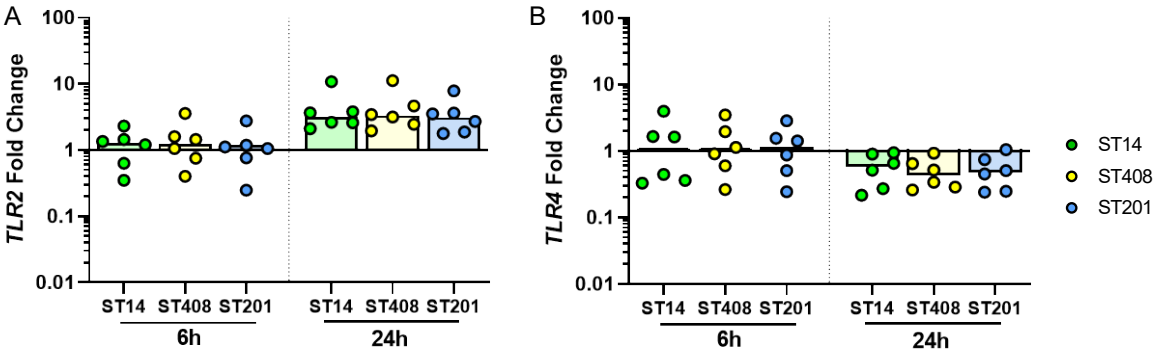

Figure 3.17. MDM immune response to additional clinical strains of NTHi measured by qPCR. MDM were infected with ST14 (green), ST408 (yellow) or ST201 (blue) at MOI 100 for 6 h, subject to 90 min gentamicin and then either immediately harvested or were subject to a further incubation period in antibiotic free media until harvest at 24 h. Expression of (A) TLR2 and (B) TLR4 were normalised to MDM *B2M* housekeeping gene. N=6. Graphs show paired data and lines indicate medians. Data were analysed by Friedman test with Dunn's multiple comparison test.

3.2.11 The MDM immune response to NTHi was not strain-dependent

To determine whether MDM responded to NTHi in a strain-dependent manner, MDM were infected with either ST408, ST14 or ST201 as previously described and harvested for RNA at 6 h and 24 h. Firstly, the expression of MDM immune response genes was assessed by qPCR and normalized to the housekeeping gene *B2M* and respective uninfected control at each time point.

The expression of *TLR2*, a cell surface receptor for bacterial lipoproteins, was upregulated at 24 h compared to 6 h in response to all three strains (Figure 3.17A), whereas in comparison, *TLR4*, a cell surface receptor for LPS, was downregulated at 24 h compared to 6 h for all strains (Figure 3.17B). However, when comparing expression levels of *TLR2* and *TLR4* induced between strains at 6 h or 24 h, no strain-dependent differences were evident.

To investigate whether strain-dependent differences in the MDM immune response could be observed at the protein level, the release of the pro-inflammatory mediators IL-6 and IL-1β by MDM was measured by ELISA using the harvested supernatants from the previously described infections.

Both mediators were detected at 6 h and 24 h, with significantly higher release of both IL-6 (Figure 3.18A; $p<0.05$ for ST14, $p<0.01$ for ST408 and ST201) and IL-1β (Figure 3.18B; $p<0.05$ for ST14 and ST408, $p<0.01$ for ST201) at 24 h compared to the uninfected control. No statistically significant differences in the level of either pro-inflammatory mediator between strains were detected, suggesting the immunogenicity or pathogenesis of the NTHi strain used to optimize the NTHi-MDM infection model (ST14) is not divergent from other respiratory tract NTHi strains and will continue to be used for the remainder of this current work.

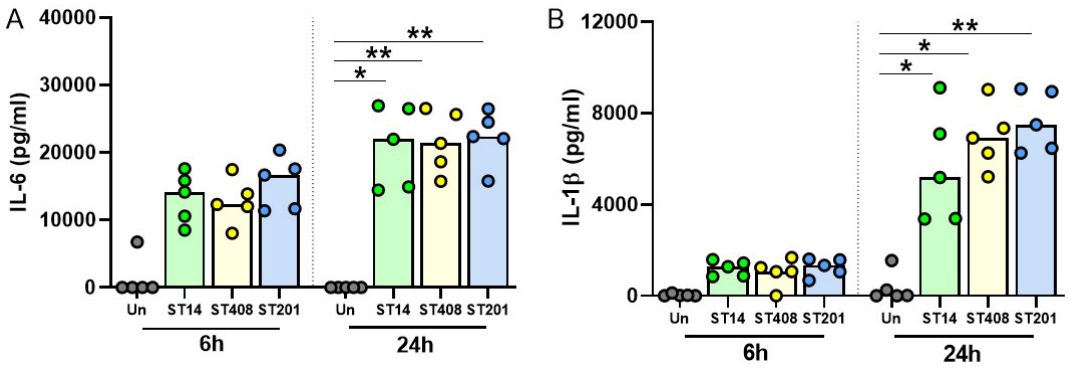

Figure 3.18. Release of MDM pro-inflammatory mediators did not differ between different strains of NTHi.

MDM were infected with ST14 (green), ST408 (yellow) or ST201 (blue) at MOI 100 for 6 h, subject to a 90 min gentamicin wash, incubated in antibiotic free media until 24 h. Well supernatants were harvested at 6 h and 24 h for analysis of pro-inflammatory mediator release of IL-6 (A) and IL-1β (B). N=5. Graphs show paired data and bars indicate medians. Data were analysed by Friedman test with Dunn's multiple comparison test.

3.3 Discussion

There is increasing evidence for NTHi persistent colonisation in the airway of individuals with chronic respiratory diseases, such as asthma[64,65,86,400]. One method of persistence that has been suggested is intracellular residence within host immune cells, with NTHi detected in CD14+ cells isolated from adenoid tissue[147,348]. Further *in vitro* studies have confirmed the ability of NTHi to infect and reside within a number of host cells including epithelial cells, monocytes and macrophages[133,149,150,406,413]. Exactly how NTHi modulates the host cell response and adapts to intracellular persistence is not well understood, thus, one of the main aims of this thesis was to investigate NTHi-MDM interactions using dual RNASeq. The work in this chapter involved optimisation of an NTHi-MDM infection model for dual RNASeq to allow for analysis of both host and pathogen transcriptomic changes during intracellular infection. As such, harvesting only NTHi associated with MDM was essential. If extracellular NTHi that had not interacted with MDM were to be sequenced, the noise of the data set could increase and create difficulties in defining any meaningful NTHi gene signature during infection. Additionally, as previously mentioned, the amount of RNA able to be recovered from live, viable NTHi could be a limiting factor in this model. As such, to ensure the NTHi transcriptome was captured in enough detail to determine differential gene expression during infection, the infection model required careful optimization.

To only recover intracellular NTHi from infected MDM, the gentamicin protection assay was optimised based on an assay protocol utilized previously[240], to ensure that all extracellular NTHi was killed or removed. Although the range of gentamicin concentration in the literature used for this type of assay varies between 50 µg/ml and 300 µg/ml[140,149,150,405], in this model only use of 500 µg/ml clearly showed that extracellular NTHi was no longer detectable. Once this factor was optimised, it was crucial to determine the infection time required to recover the maximum amount of viable NTHi for sequencing. The time points 2 h, 6 h and 24 h were selected to cover a range of early, intermediate and late infection times; similarly to those previously reported by Baddal *et al.* for their dual RNASeq work involving NTHi and epithelial cells[151]. In contrast to continual infection of MDM for 24 h, MDM infection for 6 h yielded the highest recovery of NTHi. Lower amounts of NTHi could be present at 24 h for three reasons; firstly, the macrophages have had sufficient time to respond to the presence of NTHi and are effectively phagocytosing and clearing the bacteria, as shown by Craig *et al.*[149]. Secondly, sequestering of essential nutrients occurs as part of the host immune response to bacteria[414]. As NTHi survival relies on external environmental nutrient sources, the extended infection period could result in fewer nutrients being available to NTHi over time, resulting in decreased NTHi viability and lower amounts of NTHi recovered at 24 h. Thirdly, after a longer infection period, NTHi residing intracellularly could switch to an altered growth state to allow for continued persistence within MDM. This could change the ability of NTHi to be cultured on agar

plates, resulting in lower number of visible colonies, a scenario previously postulated by Clementi and Murphy[413].

Although sequencing of intracellular NTHi will allow for deeper exploration of Clementi and Murphy's postulation, it could be speculated that NTHi intracellular adaptation was already observed in this work by decreased expression of the *hel* gene at 24 h (Figure 3.9, not significant), despite live counts showing only a small decrease in viable NTHi. The *hel* gene encodes for an outer membrane protein lipoprotein e/P4 and has shown to be important in colonisation of the airway by adhering to components of the extracellular matrix[124,125]. Downregulation of genes encoding outer membrane proteins during NTHi infection of epithelial cells has been previously demonstrated[151]. Furthermore, following phagocytosis by macrophages, Craig *et al.* showed that NTHi exhibits differential gene expression, with intracellular survival of NTHi dependent on increased expression of sigma factor σ^E, which promoted the transcription of genes required by NTHi to be able to adapt to an intracellular environment[150]. Together, these studies indicate that NTHi is able to respond to a variety of environmental stimuli through genetic adaptations leading to increased intracellular survival. Changes in the NTHi transcriptome during persistent infection of macrophages will be explored further in this thesis following analysis of the sequencing data.

Of initial concern was the finding that upon extending the infection model to include an extended incubation period in gentamicin-containing media until 24 h, NTHi was unable to be recovered using live counts. Adapting the model to include a 90 min gentamicin wash to remove extracellular bacteria following the initial 6 h infection period, resulted in NTHi persistence up to 24 h. A similar duration of persistence has been previously shown by Craig *et al.,* with persistence even detected up to 72 h after the initial infection[149]. Intracellular persistence has also previously been shown by Forsgren *et al.* who observed intracellular presence of viable NTHi in macrophages derived from adenoid tissue[147]. In this current work, a 90 min gentamicin wash was demonstrated to kill extracellular NTHi at 6 h, therefore, any NTHi recovered at 24 h must have resided intracellularly during the infection process, with any NTHi located extracellularly at 24 h potentially having escaped the antibacterial action of the macrophage. NTHi escaping the immune response has previously been shown, with NTHi residing between epithelial cells protected from antibiotic and antibody action[145]. More recently, it was demonstrated that bacterial pathogens phagocytosed by macrophages resulted in shielding from neutrophils and prevention of excessive inflammation[415]. The macrophage phagocytic impairment in asthma could reduce the number of bacteria 'shielded' within macrophages, with higher numbers of extracellular bacteria present in the airway accounting for the increased influx of neutrophils observed in those with severe asthma and NTHi colonisation. Although macrophage phagocytosis and subsequent shielding of pathogens from neutrophils was suggested to contribute to the macrophage role in maintaining lung homeostasis, intracellular

pathogens able to circumvent the phagocytic process could exploit this to evade the host immune response.

The use of MOI 100 was required to ensure a sufficient amount of NTHi would be present within MDM for sequencing, and changes in NTHi gene expression would be able to be assessed. Although the ratio of macrophage to NTHi during persistent infection in the lung is not known, the MOI used *in vitro* may not be representative of a biologically relevant infection and thus represents a potential limitation of this work[373]. Nonetheless, a similarly high MOI was used by Baddal *et al.* to infect epithelial cells which also allowed changes in NTHi gene expression to be investigated by dual RNASeq[151].

Even though the optimized conditions for NTHi infection allowed for a sufficient amount of viable NTHi to be recovered from MDM, macrophage viability was also an important concern; there would be little point in sequencing an infection model that allowed for sufficient NTHi numbers but was severely detrimental to the macrophage. Despite LDH cytotoxicity assays being commonly used to assess cell viability[416], increases in LDH release could potentially be misleading. Release of LDH into the culture supernatants typically indicates that cells are less structurally intact and thus less viable[417]. However, as LDH is an important enzyme for glycolysis[418], increased presence of the lactate dehydrogenase enzyme could therefore also be due to increased metabolic activity of the macrophage in response to infection. Increased metabolic activity was observed by use of the MTS assay, indicating increased macrophage activity in response to NTHi infection. If MDM were dying, metabolic activity readouts would decrease as fewer MDM would be present, indicating cell viability did not decrease during NTHi infection.

In this system, increased LDH and metabolic activity as assessed by MTS was likely due to activation of the macrophage immune response to NTHi, as LDH has recently been shown to regulate the immune response. Daifuku and colleagues showed that LDH supplementation enhances production of IL-6 and TNF-α, suggesting a role of LDH in regulation of the inflammatory response[419]. Song *et al.* further confirmed this role by inhibiting LDH expression, resulting in a decrease in the production of IL-6, TNF-α and IL-1β[418]. Moreover, microarray results suggest that lactate metabolism is correlated with inflammatory responses[418]. Immunometabolism is an emerging field, with links between modulation of host cell metabolism and intracellular survival of pathogens becoming apparent[420]. The modulation of macrophage metabolic genes in response to infection will be investigated further following sequencing of this infection model.

Although increased metabolic activity suggests increased macrophage activation, it was important to determine whether a detectable immune response to NTHi at the two chosen time points could be measured before sequencing. Upregulation of macrophage responses at 6 h and 24 h was detectable at the gene level and protein level, indicating the validity of the two chosen time points.

This chapter also explored whether there were any NTHi strain-dependent effects on the macrophage immune response. NTHi strains are heterogeneous and it is not clear how this heterogeneity impacts on the ability of NTHi to persist within the airway. The seven strains of NTHi that were available for phylogenetic analysis were all clinical isolates cultured from either lung protective brushings, induced sputum or nasal brushings. Despite these diverse anatomical locations, when the sequenced genome of these strains were analysed to determine strain diversity, the strains did not cluster based on sample location. Although this is a small sample size to draw conclusions from, dissimilarity of NTHi strains derived from the same clinical source has also been shown in two larger studies by Erwin *et al.* and De Chiara *et al.*[372,412]. NTHi evolution perhaps depends on environmental and niche pressures that uniquely vary between individuals, rather than variation between anatomical locations.

The ability of macrophages to clear NTHi infection has been suggested to be strain-dependent[149,406]. Differences in strain persistence *in vitro* were also found in this chapter, further suggesting the varying capability of macrophages to clear NTHi strains. Importantly, strain-dependent persistence has been observed *in vivo* by Pettigrew *et al.* (2018), who found the duration of NTHi airway persistence between strains varied from 2 – 1422 days (median 161 days)[421]. Differences in transcriptomic profiles observed between NTHi could account for the varying ability between NTHi strains to respond to environmental stresses[422]. Elucidating survival mechanisms that are conserved across the majority of NTHi strains could better direct future therapeutics to reduce the burden of NTHi persistence in the airway of individuals with chronic respiratory disease.

Although it is clear that NTHi heterogeneity must be considered, the dual RNASeq work in this thesis was undertaken using only a single strain due to technical and financial limitations. However, validation of the dual RNASeq analysis used the additional clinical strains to determine whether the responses observed for both host and pathogen are conserved. The primary strain that was used for the remainder of this work was ST14, because unlike ST408 and 201, this strain was directly isolated from the human lung. Although ST201 is a sputum isolate, it cannot be definitely stated that this strain is of lung origin. The induced sputum could potentially be contaminated by NTHi located in the upper respiratory tract[71,423,424], resulting in the isolation of NTHi that may not be a true lung-resident strain. As the aim of this work was to model NTHi infection of the lung, the sputum and nasal brushing strains were not as clinically relevant as a lung-derived strain.

3.4 Summary

In this chapter, an NTHi-MDM infection model was optimised for dual RNASeq to investigate changes in both host and pathogen gene expression associated with NTHi intracellular infection of macrophages. This resulted in an infection model comprising of 6 h NTHi infection, a 90 min gentamicin wash to remove all extracellular NTHi, followed either by harvesting of cells for analysis (6 h time point) or an extended incubation in antibiotic-free media until 24 h (24 h time point). At

both 6 h and 24 h, live, viable NTHi was recovered, with NTHi RNA also detected. Macrophage immune responses were detectable and upregulated in response to NTHi at 6 h and 24 h, reflected by increased macrophage metabolic activity. The next chapter will focus on the analysis of the sequenced macrophage transcriptome in response to NTHi infection at 6 h and 24 h.

Chapter 4 Transcriptomic analysis of the macrophage response to NTHi infection

4.1 Introduction

The previous chapter detailed optimisation of an NTHi-MDM infection model for dual RNASeq, comprising of NTHi infection of MDM at MOI 100 for 6 h, followed by a 90 min gentamicin wash and an extended incubation period in antibiotic free media up until 24 h. Subsequently, this infection model was performed using MDM isolated from five different healthy blood donors and the RNA from each experiment was isolated, and the technical repeats were combined and assessed to ensure the RNA was of sufficient quantity and quality prior to shipping to Novogene (Hong Kong) for sequencing. The methodology used by Novogene for quality control of RNA, library generation, quality control of sequenced data and mapping to reference genomes are described in Section 2.10 onwards. This chapter describes the analysis of the macrophage transcriptomic data set performed by myself using Rstudio® (version 3.6.1) and code developed with Dr. A. Heinson (University of Southampton) on the raw, unfiltered read count table generated by Novogene.

4.2 Results

4.2.1 Exploratory data analysis

The starting number of protein-coding genes in the raw MDM data set was 19795, however, as a number of these genes were likely to include lowly expressed genes, the data was filtered (Section 2.13.1). Subsequently, 15048 genes remained in the data set for differential gene expression analysis. The distribution of the expression levels of these 15048 genes was assessed to ensure no sample outliers were present in the dataset. This analysis was performed by creating an interquartile range (IQR) versus median plot, hierarchical clustering and principal component analysis (PCA).

4.2.1.1 Interquartile range (IQR) versus median exploratory plot

The spread of data across samples was visually inspected to determine the presence of any sample outliers. Plotting an IQR vs median graph shows whether any samples fall outside the limit of 2 standard deviations (SD). All samples remained within ± 2SD, indicating data distribution for each sample did not significantly vary and no outliers were present (Figure 4.1).

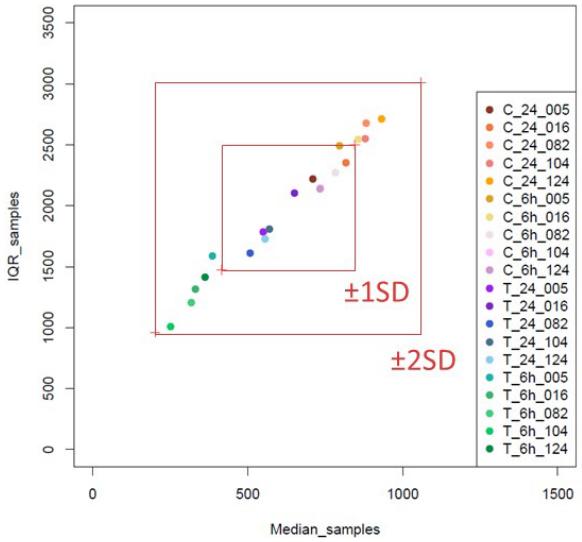

Figure 4.1. Interquartile range (IQR) vs median plot of the filtered MDM data. The IQR of each MDM sample was plotted on the y axis and the median of each sample was plotted on the x axis. The inner red box indicates ± 1 standard deviation (SD) and the outer box indicates ± 2 SD.

4.2.1.2 Hierarchical clustering

Hierarchical clustering allows for visualisation of gene expression patterns between samples[425], as a sample with a gene expression profile too dissimilar from the whole data set would independently cluster and could potentially be considered an outlier. MDM samples clustered depending on infection status (uninfected or infected). However, within these two clusters no clustering of samples based on infection time point (6 h or 24 h) was apparent (Figure 4.2). No sample outliers were detected using this data visualisation method.

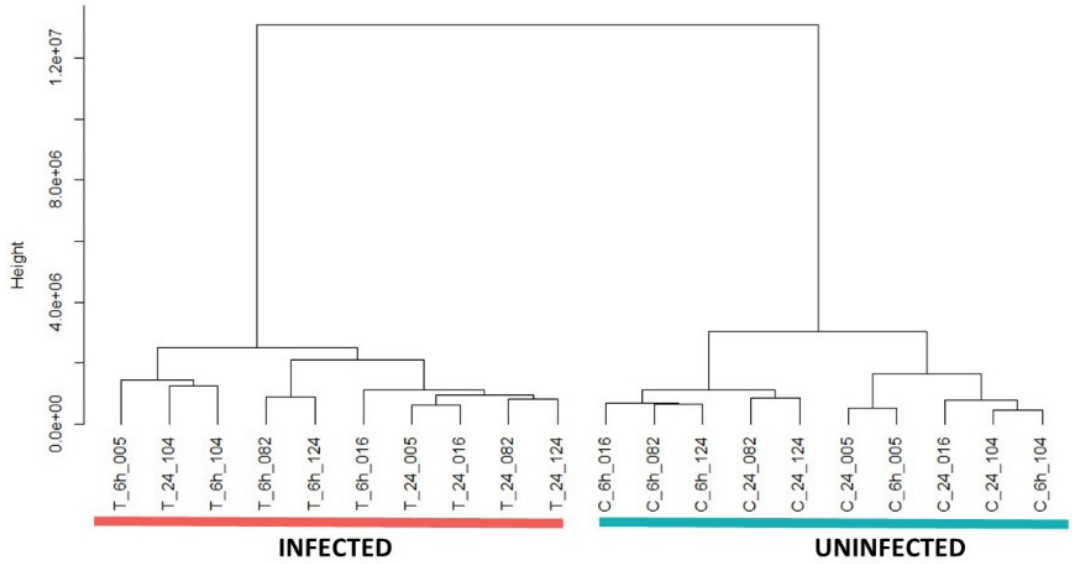

Figure 4.2. Hierarchical clustering of the filtered MDM data. MDM samples clustered based on infection status (infected samples = red, uninfected samples = blue) using Ward linkage and Euclidean distance method.

4.2.1.3 Principal Component Analysis

Principal component analysis (PCA) is another method used to visualise variance in the data set by reducing the data dimensions into discrete principal components[426]. As a result, the first principal component explains the largest source of variation in the data, the second component explains the second largest source of variation and so on[427]. PCA analysis identified two distinct sample clusters separated by the first principal component (PC1, 69.3%, Figure 4.3). Overlaying the associated metadata for each sample indicated these two clusters were infected or uninfected MDM samples (Figure 4.3A) with no clustering associated with time point (Figure 4.3B), in agreement with the previous hierarchical clustering result. Of note, some donors appeared to be clustering together within the individual clusters defined along PC1 (Figure 4.3.C), indicating that the innate biological variance amongst donors remained despite the presence of technical effects of infection and culture time. The Proportion of Variance Explained (PVE) plot indicates that PC1 accounts for the majority of variance in the MDM data (Figure 4.3D).

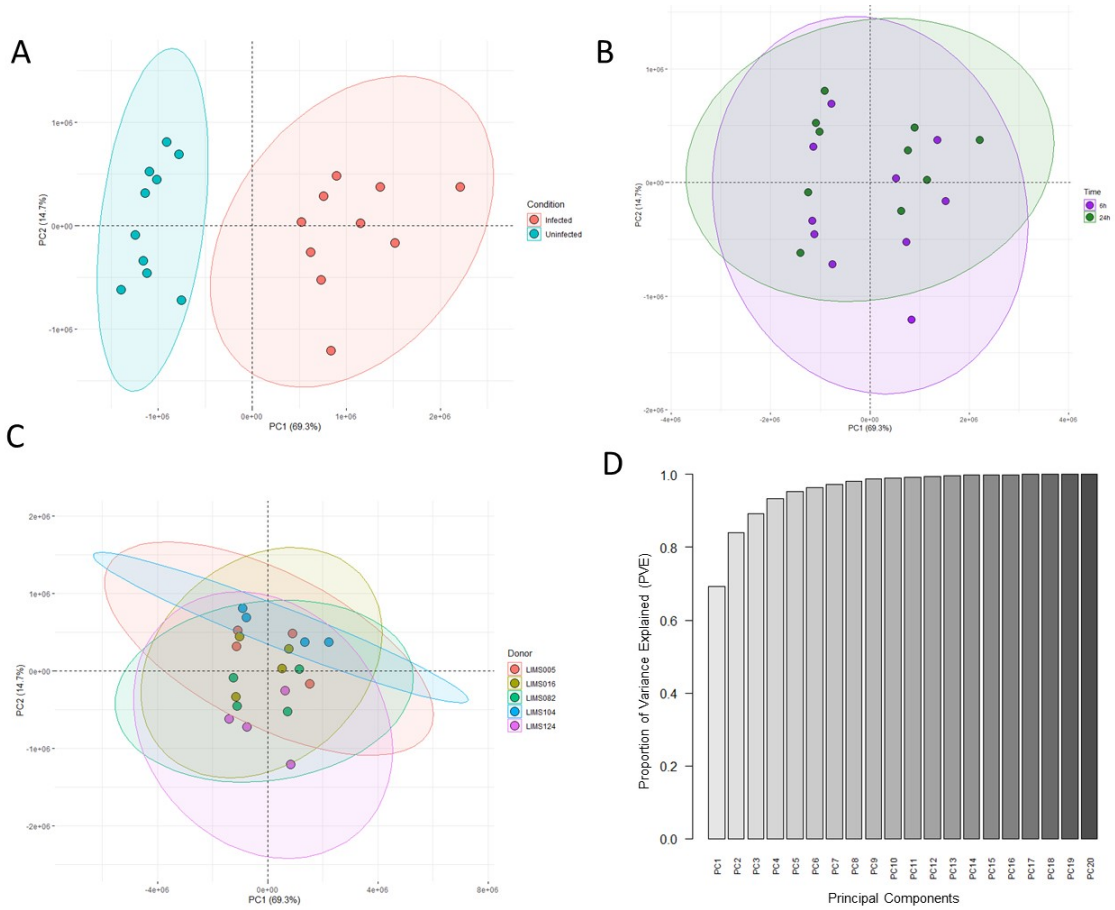

Figure 4.3. **Principal component analysis performed on the filtered MDM data.** The 2D PCA plots are coloured based on overlaid metadata. (A) PCA coloured by infection status (uninfected = blue, infected = red), (B) PCA coloured by time point (6 h samples = green 24 h samples = purple), (C) PCA coloured by each donor as detailed in the accompanying legend. (D) Proportion of Variance Explained (PVE) cumulative plot, indicating the amount of variance explained by each of the individual principal components. PC1 accounts for the majority of the variance in the MDM data set.

Together, the visualisation of data distribution and variance did not identify any sample outliers requiring exclusion from the data set. Therefore, the data was able to pass to the next stage of processing with all 20 samples retained in the MDM data set.

4.2.2 Data normalisation

Normalisation of RNASeq data is important to remove any bias that may have been introduced during sequencing. Sources of bias include library size (between sample differences), gene length and GC content (both within sample differences)[428]. Two Bioconductor packages were used to perform data normalisation: edgeR and DESeq2. Although both packages work on the similar assumption that most genes in a given data set are not differentially expressed and use a negative binomial distribution model, the normalisation strategies used are different; edgeR uses the Trimmed Mean of M-values (TMM) method[429] whereas DESeq2 uses a geometric normalisation strategy[428]. Despite differences in strategies, normalisation of the 15048 MDM genes was consistent across both methods as a more even spread of data was observed in the boxplots following normalisation (Figure 4.4B & C) compared to pre-normalisation (Figure 4.4A).

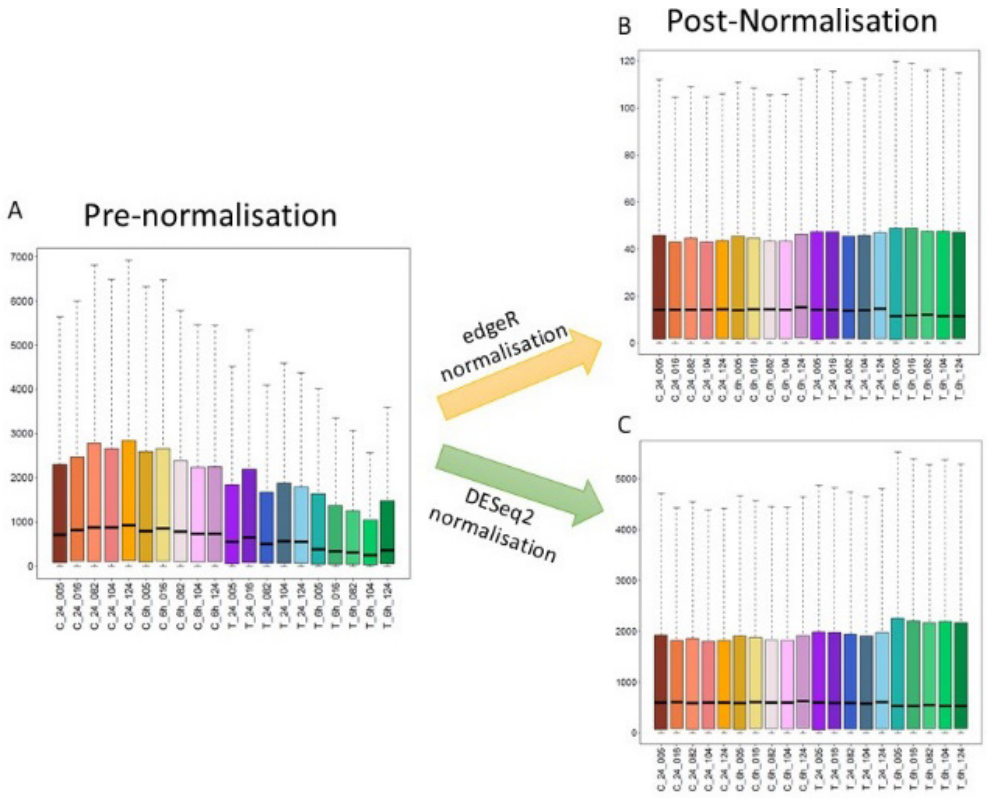

Figure 4.4. Normalisation of the filtered MDM data. (A) Pre-normalised data, (B) data that has been normalised using the edgeR package, (C) data that has been normalised using the DESeq2 package.

4.2.3 Differential gene expression analysis

Following data normalisation, edgeR and DESeq2 were used to determine differentially expressed genes (DEGs) between uninfected and infected macrophages at 6 h and 24 h. Using multiple bioinformatics tools for differential gene analysis is beneficial to reduce the impact of variability between bioinformatics methods by obtaining a conservative DEG list[430]. A small percentage of genes were determined as differentially expressed by edgeR but not by DESeq2, and vice versa (Figure 4.5). The genes determined as differentially expressed by both methods represent 86.4% (8730 genes at 6 h, Figure 4.5A) and 95.7% (8547 genes at 24 h, Figure 4.5B) of the total number of DEGs (10,105 genes at 6 h, 8931 genes at 24 h), suggesting a high amount of convergence between edgeR and DESeq2. Only DEGs identified by both edgeR and DESeq2 were taken forward for further analysis.

The large number of genes determined as differentially expressed (FDR $p<0.05$) could render the data difficult to explore in depth using commonly available gene ontology tools. Therefore, fold change (FC) cut offs were applied to reduce the number of DEGs (Figure 4.6A). Altering FC cut offs can significantly change the interpretation of the data, so must be used with caution; a larger fold change isn't necessarily more biologically significant than a smaller fold change[431]. Previous dual RNASeq studies have used arbitrary $\log_2$ FC cut offs varying from 1 to 2[151,432,433].

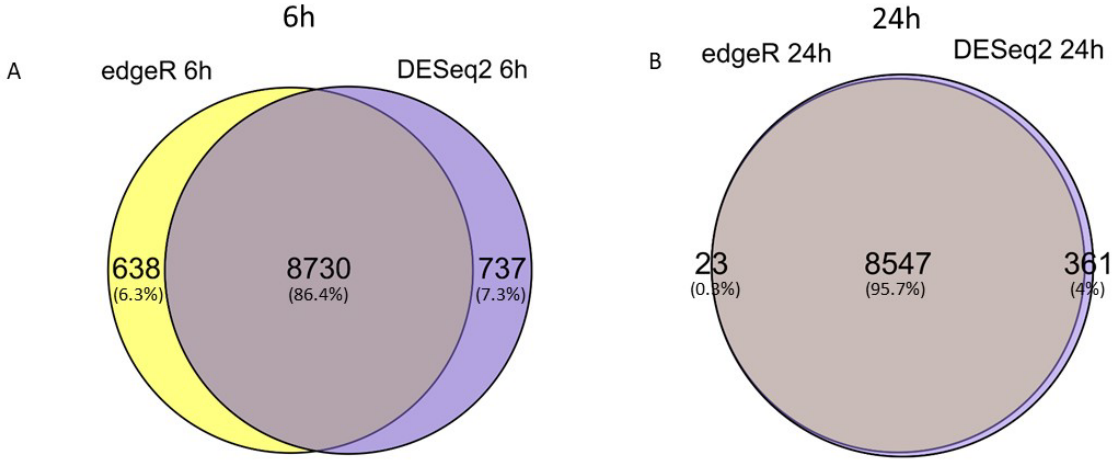

Figure 4.5. Number of differentially expressed genes at 6 h or 24 h. Venn diagrams showing the overlap of genes that are determined as differentially expressed by edgeR (left), DESeq2 (right) or by both packages (middle) at 6 h (A) or 24 h (B). Uninfected samples are compared against infected samples at each time point, with genes determined as differentially expressed with an FDR adjusted p-value <0.05. Created using VennDIS v1.0.1.

A

p<0.05	6h	24h
FC0	8730	8547
FC1	5005	4126
FC1.5	2974	2622
FC2	1802	1763

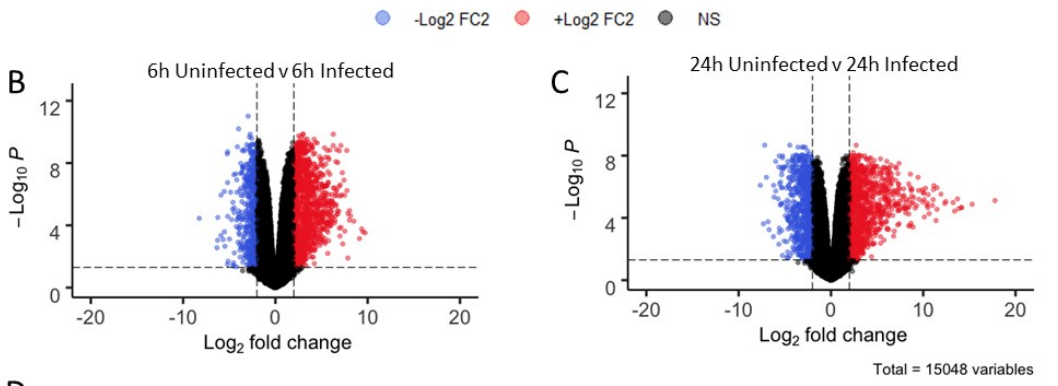

D

	Upregulated	Downregulated	Total
6h	1249	553	1802
24h	1028	735	1763

Figure 4.6. Expression of MDM genes compared between uninfected or infected samples at 6 h or 24 h. Volcano plots created in R using the EnhancedVolcano package showing the expression profile of all 15048 genes. (A) Table of the number of genes determined as differentially expressed (FDR p<0.05) at different $\log_2$ fold change (FC) cut offs. (B) 6 h and (C) 24 h volcano plots highlighting the genes above the $\log_2$ FC cut off of ±2. Red = upregulated genes ($\log_2$ +FC2 and FDR p<0.05), blue = downregulated genes ($\log_2$ FC2 and FDR p<0.05) and black = not significant genes (NS). (D) Table of the number of genes ($\log_2$ FC2 and FDR p<0.05) upregulated or downregulated at 6 h or 24 h.

Applying a $\log_2$ FC cut off of 1 resulted in 5005 (6 h) and 4126 (24 h) genes being retained in the data set (Figure 4.6.A). Increasing the FC cut off to 2 resulted in a smaller number of genes retained at 6 h and 24 h (1802 and 1763, respectively). As the $\log_2$ FC cut off of 2 returned a more manageable number of genes for each time point comparison, this cut off was chosen for determining significantly differentially expressed genes. Although a similar number of DEGs were present at both time points, higher fold changes were apparent at 24 h compared to 6 h (Figure 4.6B & C). Furthermore, a higher number of genes were upregulated (1249 at 6 h, 1028 at 24 h) compared to downregulated (553 at 6 h, 735 at 24 h) in response to NTHi infection (Figure 4.6D). The 1802 6 h DEGs and 1763 24 h DEGs were plotted as a heatmap, which demonstrated clustering of MDM samples according to infection status (Figure 4.7 A & B), suggesting the differential expression of these DEGs was driven by NTHi infection.

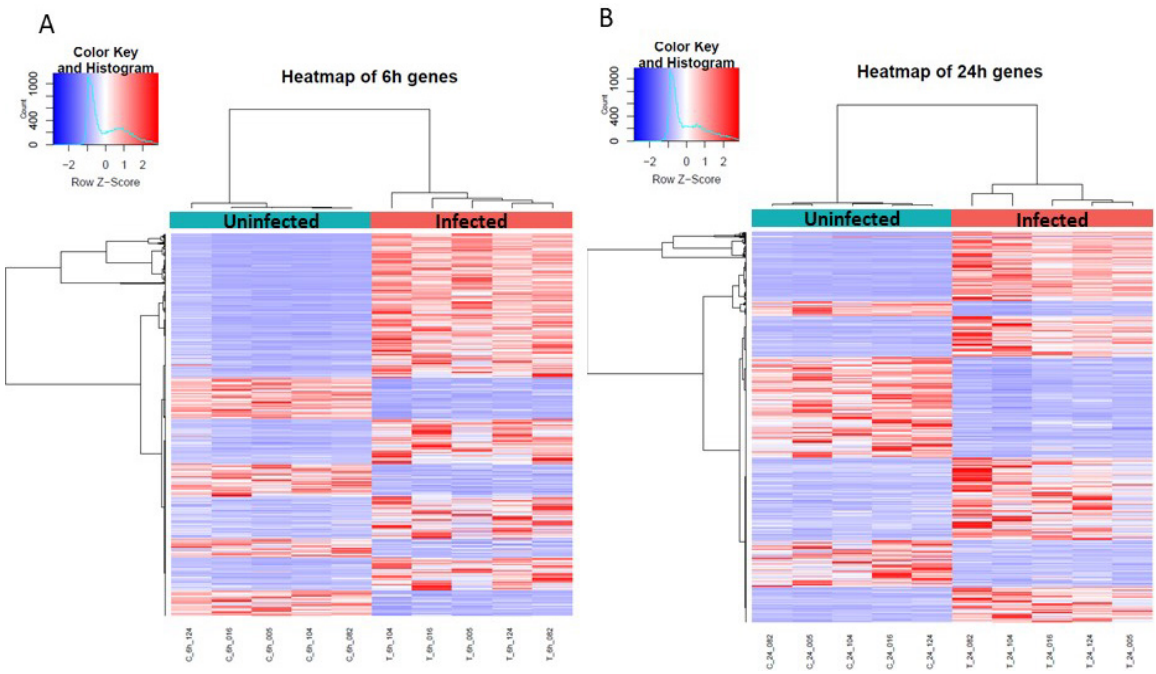

Figure 4.7. Heatmaps of the differentially expressed genes at 6 h or 24 h. Differentially expressed genes determined using log_2 FC2 and FDR p<0.05 cut offs were plotted to display the expression and clustering of samples at 6 h (A, 1802 genes) or 24 h (B, 1763 genes). For both time points, the uninfected and infected samples clustered together.

4.2.4 Time-dependent responses to NTHi infection

To assess whether regulation of the 1802 and 1763 DEGs was conserved across time points or if DEGs were exclusively differentially expressed at a single time point, the 6 h and 24 h gene lists were compared for time-dependent gene expression. This comparison identified 863 genes (hereinafter designated as 'core genes') to be differentially expressed at both 6 h and 24 h (Figure 4.8A). The remaining 1839 genes were differentially expressed at a single point time point only, with 939 genes differentially expressed at 6 h only and 900 genes differentially expressed at 24 h only.

A

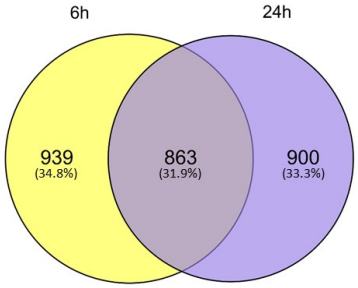

B

	6h only	24h only	6h/24h	
	6h	24h	6h	24h
Upregulated	543	325	706	703
Downregulated	396	575	157	160
Total	939	900	863	

Figure 4.8. Time-dependent expression of significantly differentially expressed genes. (A) Venn diagram indicating the number of genes determined as significantly differentially expressed at 6h only (left), 24h only (right) or across both time points (middle). Created using VennDIS v1.0.1. (B) Table showing the number of upregulated or downregulated genes determined as DEGs at 6 h only, 24 h only or at 6 h and 24 h.

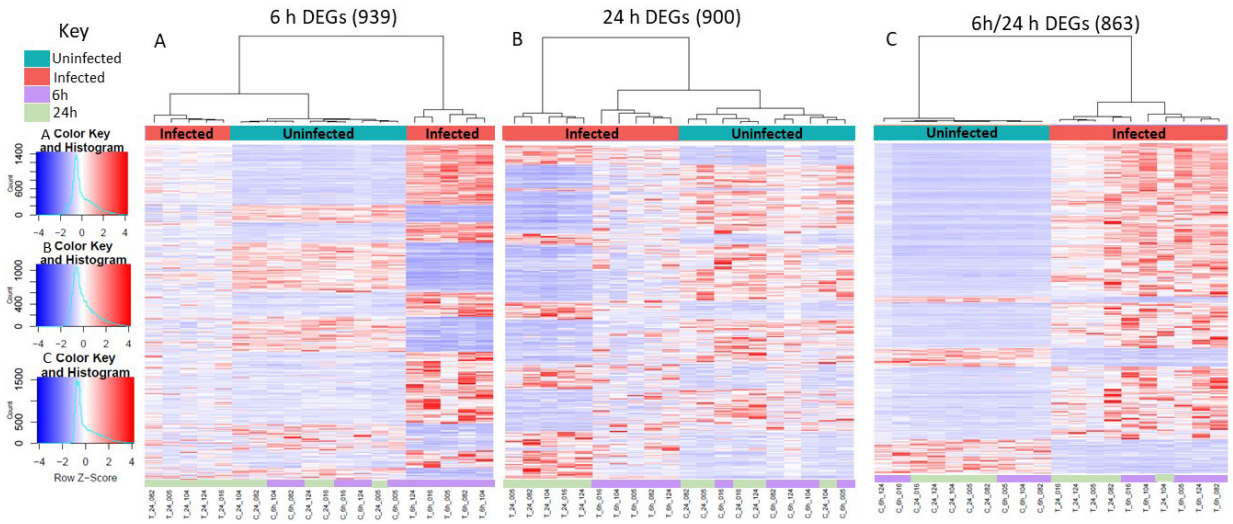

Figure 4.9. **Time-dependent MDM gene expression profiles in response to NTHi infection**. Heatmaps show the expression profile of DEGs at (A) 6 h only, (B) at 24 h only and (C) at both 6 h and 24 h for all 20 MDM samples. Clustering was performed using Euclidean distance and Ward linkage methods. Key indicates the colours used to represent the uninfected (blue) and infected (red), 6 h (purple) and 24 h (green) samples. The colour key and histogram boxes from top to bottom represent A, B and C respectively.

A higher number of DEGs were upregulated (543) compared to downregulated (396) at 6 h, whereas the opposite was observed for 24 h; a higher number of downregulated (575) DEGs were identified compared to upregulated (325) DEGs (Figure 4.8B). The time-dependent expression of these DEGs was further highlighted by the lack of clustering of infected samples across time points. Hierarchical clustering of samples based on the expression of the 6 h only DEGs showed that the 6 h infected samples clustered together, however they also clustered independently of the 24 h infected samples (Figure 4.9A). Similarly, for the 24 h only DEGs, the 24 h infected samples clustered together but away from the 6 h infected samples and the 6 h and 24 h uninfected samples (Figure 4.9B).

In contrast, for the 863 core genes determined as differentially expressed at both 6 h and 24 h, all infected samples clustered together regardless of time point and independently of the uninfected samples (Figure 4.9C). The absence of a strong time point signal within this 863 core gene set was perhaps due to the continued expression of these genes across both 6 h and 24 h, emphasised by only 9 out of the 863 genes changing direction of expression between 6 h and 24 h (Figure 4.10A). Furthermore, 5 out of the top 20 downregulated and 8 out of the top 20 upregulated genes were consistently highly modulated at both 6 h and 24 h (Figure 4.10B). The majority of genes present in the 20 highest upregulated gene list at both 6 h and 24 h (6/8 genes) are involved in macrophage activation and pro-inflammatory processes (*IL6, IL12B, CSF2, CSF3, CCR7* and *SERPINB2*) (Figure 4.10C). The two remaining genes *ACOD1* and *IDO1* are involved in macrophage metabolic processes.

A

Gene	6h logFC	24h logFC
IFNA1	3.664652	-2.30645
PDZRN4	3.209284	-2.19349
OR6N2	2.497279	-4.4499
SMAD3	2.290499	-2.00013
LIMS2	2.206782	-2.59324
PHLDB2	2.11795	-2.30859
PI15	-4.58413	2.21051
CD79B	-2.7861	2.046117
TMEM169	-2.55992	2.095253

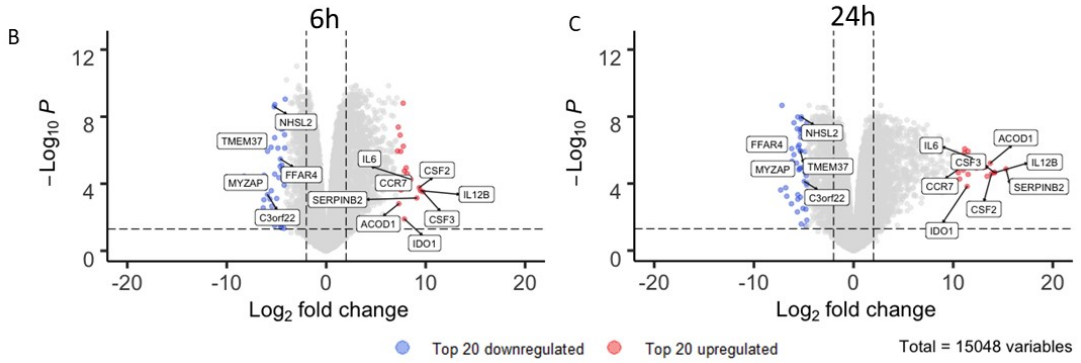

Figure 4.10. **Consistent expression of 863 core MDM genes at 6 h and 24 h**. (A) Table of the 9 genes that change direction of expression between 6 h and 24 h. (B) 6 h and (C) 2 4h volcano plots highlighting the top 20 upregulated (red) and downregulated (blue) genes, with the 13 labelled genes consistently highly up/downregulated at both time points.

To determine whether the time-dependent expression of each DEG set (6 h only, 24 h only and 6 h/24 h) was associated with specific biological responses, gene list enrichment analysis was performed using ToppFunn, which is part of the ToppGene Suite. The ToppGene Suite is useful for determining the functional enrichment of genes in a human data set with a large number of genes[381], as was the case here.

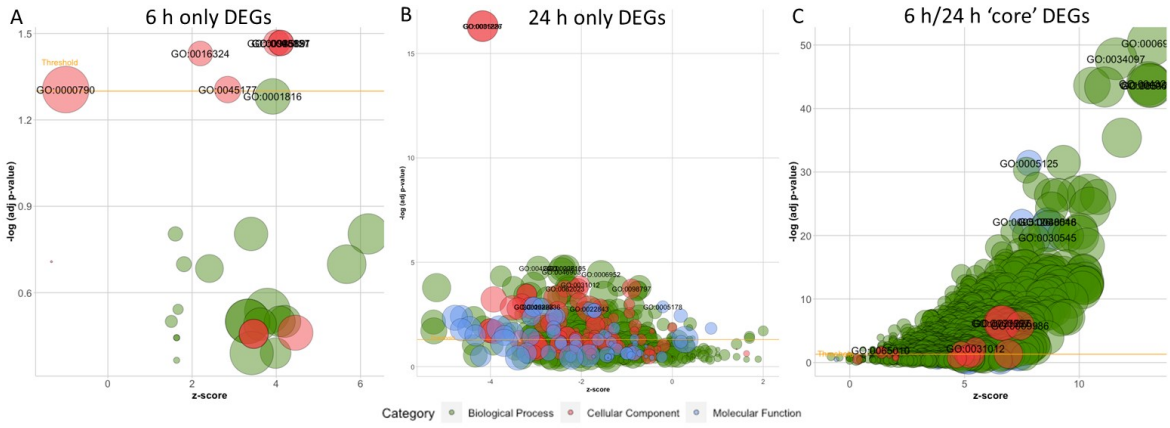

Figure 4.11. Gene Ontology analysis of the differentially expressed genes at each time point. GOPlot of enriched Gene Ontology terms for DEGs at (A) 6 h only, (B) 24 h only and (C) the core DEGs expressed at both 6 h and 24 h following gene list enrichment analysis using ToppFunn. The yellow line indicates significance threshold, as determined by the FDR p-value <0.05, size of dots indicate number of genes present in each term.

Table 4.1. Table of the most significantly enriched MDM gene ontology terms. This table shows the same terms indicated previously in Figure 4.11, but here the GO:ID numbers are accompanied with the GO:terms and functional enrichment FDR value. A maximum of 5 of the most significantly functionally enriched pathways are shown, with fewer terms meaning lower enrichment significance for a specific category or time point. Colours are representative of the category as plotted in Figure 4.11. Genes in input show the number of MDM genes assigned to each term, which were compared against the full gene set for each category used by ToppFunn/ToppGene.

Category	GO:ID	GO:Term	Enrichment FDR	Genes in input	Genes in annotation
6h only DEGs					
GO: Biological Process	GO:0001816	cytokine production	0.05	71	875
GO: Cellular Component	GO:0098589	membrane region	0.03	39	411
	GO:0045121	membrane raft	0.03	37	396
	GO:0098857	membrane microdomain	0.03	37	397
	GO:0016324	apical plasma membrane	0.4	35	373
	GO:0000790	nuclear chromatin	0.5	121	1923
GO: Molecular Function	NA	NA	NA	NA	NA
24h only DEGs					
GO: Biological Process	GO:0022610	biological adhesion	1.93E-05	116	1516
	GO:0042493	response to drug	1.93E-05	97	1194
	GO:0007155	cell adhesion	1.93E-05	115	1509
	GO:0046903	secretion	2.88E-05	132	1835
	GO:0006952	defense response	3.85E-05	132	1850
GO: Cellular Component	GO:0031226	intrinsic component of plasma membrane	4.87E-17	161	1790
	GO:0005887	integral component of plasma membrane	4.87E-17	156	1710
	GO:0031012	extracellular matrix	1.21E-04	55	598
	GO:0098797	plasma membrane protein complex	1.83E-04	61	711
	GO:0062023	collagen-containing extracellular matrix	1.83E-04	46	474
GO: Molecular Function	GO:0005178	integrin binding	1.36E-03	23	146
	GO:0015267	channel activity	1.36E-03	62	705
	GO:0022803	passive transmembrane transporter activity	1.36E-03	62	706
	GO:0022836	gated channel activity	1.36E-03	48	491
	GO:0022843	voltage-gated cation channel activity	1.73E-03	30	245
6h24h ‘core’ DEGs					
GO: Biological Process	GO:0006952	defense response	4.82E-51	228	1850
	GO:0034097	response to cytokine	1.51E-48	183	1287
	GO:0043207	response to external biotic stimulus	1.17E-44	200	1606
	GO:0051707	response to other organism	2.36E-44	199	1604
	GO:0019221	cytokine-mediated signaling pathway	2.36E-44	138	814
GO: Cellular Component	GO:0005887	integral component of plasma membrane	5.91E-07	123	1710
	GO:0031226	intrinsic component of plasma membrane	5.91E-07	127	1790
	GO:0009986	cell surface	1.51E-06	84	1036
	GO:0031012	extracellular matrix	6.59E-03	48	598
	GO:0065010	extracellular membrane-bounded organelle	1.09E-02	5	9
GO: Molecular Function	GO:0005125	cytokine activity	3.92E-32	65	225
	GO:0048018	receptor ligand activity	7.37E-23	82	497
	GO:0005126	cytokine receptor binding	7.40E-23	64	312
	GO:0030546	signaling receptor activator activity	7.40E-23	82	502
	GO:0030545	receptor regulator activity	2.10E-20	82	547

Enrichment analysis found a lack of significantly enriched terms within the 6 h only DEG set; there was no enrichment of Molecular Function gene ontology (GO) terms, one enriched Biological Process and five enriched Cellular Component terms (Figure 4.11A, Table 4.1). The only significantly enriched Biological Process was ‘cytokine production’ (GO:0001816), which was only just determined as significant (p=0.05). In contrast, a higher number of enriched terms were identified for all categories for the 24 h only DEGs (Figure 4.11B, Table 4.1). The top most significantly enriched GO:term for each category (Molecular Function; ‘integrin binding’, Biological Process; ‘biological

adhesion' and Cellular Component; 'integral component of plasma membrane') suggest enrichment of processes involved in macrophage adhesion at 24 h.

Finally, enrichment analysis of the 6 h/24 h DEGs identified significant enrichment of terms in the GO:Biological Process category (Figure 4.11C, Table 4.1). The most significantly enriched processes included macrophage pro-inflammatory immune responses, with 'defense response' the top enriched Biological Process. Other top functionally enriched macrophage biological processes included the terms 'response to cytokine' (GO:0034097) and 'response to other organism' (GO:0051707), which indicated macrophage activation to NTHi infection but also to the secretion of cytokines, potentially in an autocrine or paracrine manner.

4.2.5 Activation of MDM 'intracellular pathogen' immune response pathways in response to NTHi infection

As the 6 h/24 h core DEG set was significantly functionally enriched with immune processes and the conserved differential expression of these 863 core genes across both time points suggests continual modulation in response to the persistent NTHi infection, this core DEG set was taken forward to be explored in further detail. More than 500 GO:terms were significantly functionally enriched in the Biological Process category. Such a high number of terms, combined with the inherent redundancies in gene ontology terms, could render it difficult to extrapolate biologically significant specific immune responses of the macrophage to NTHi infection[434].

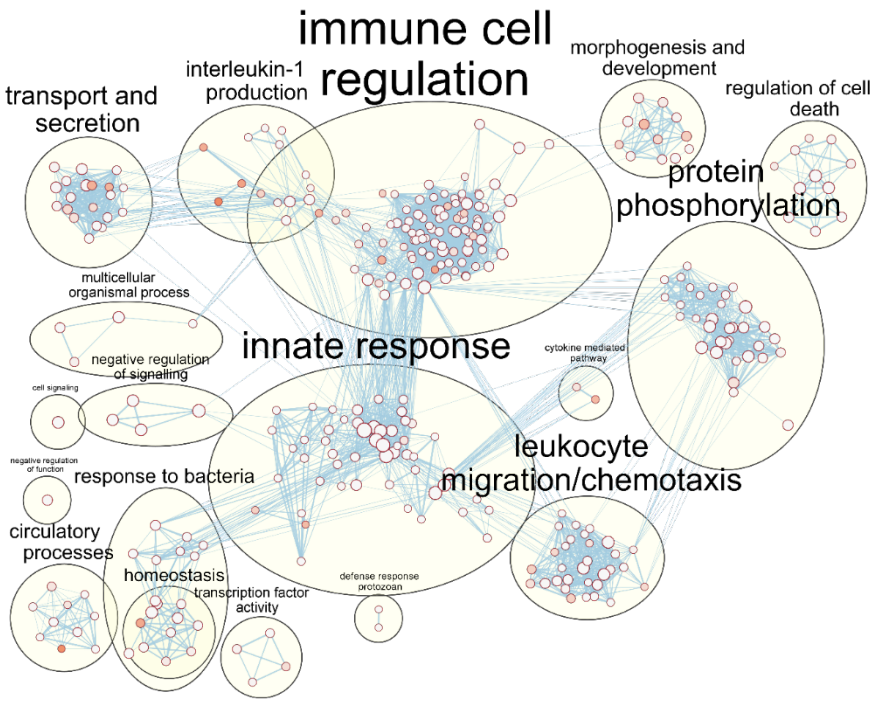

Figure 4.12. Enrichment of immune process across 6 h and 24 h. Clustering of the top 500 enriched Biological Process GO:terms using EnrichmentMap and AutoAnnotate in Cytoscape. Nodes represent individual GO:terms, with size relating to the number of genes in each term and the colour indicating enrichment significance. Larger cluster labels indicate a higher number of terms within the cluster. Edges represent connections between nodes that share genes.

Therefore, a network of the top 500 significantly enriched Biological Process terms was created, which generated clusters of overlapping gene terms to facilitate easier interpretation of gene ontology results. The resulting network further highlighted the immune response signal in the data, with gene terms clustering together under generic immune response phrases such as 'immune cell regulation', 'innate response' and 'response to bacteria' (Figure 4.12). However more specific immune processes such as 'leukocyte migration/chemotaxis' and 'interleukin-1 production' were also identified.

Presence of the 'leukocyte migration/chemotaxis' cluster in Biological Process network could indicate macrophage signalling to other immune cells through secretion of inflammatory mediators. As this is a crucial function of the macrophage immune response, the role of NTHi-infected macrophages in immune cell signalling was explored further. The top 10 significantly enriched leukocyte-related terms were extracted from the 'leukocyte migration/chemotaxis' cluster, which contained a number of terms related to leukocyte and granulocyte migration and chemotaxis (Figure 4.13A). For all 10 terms, gene expression was fairly consistent across the two time points, with expression levels appearing to be slightly lower at 24 h (Figure 4.13B).

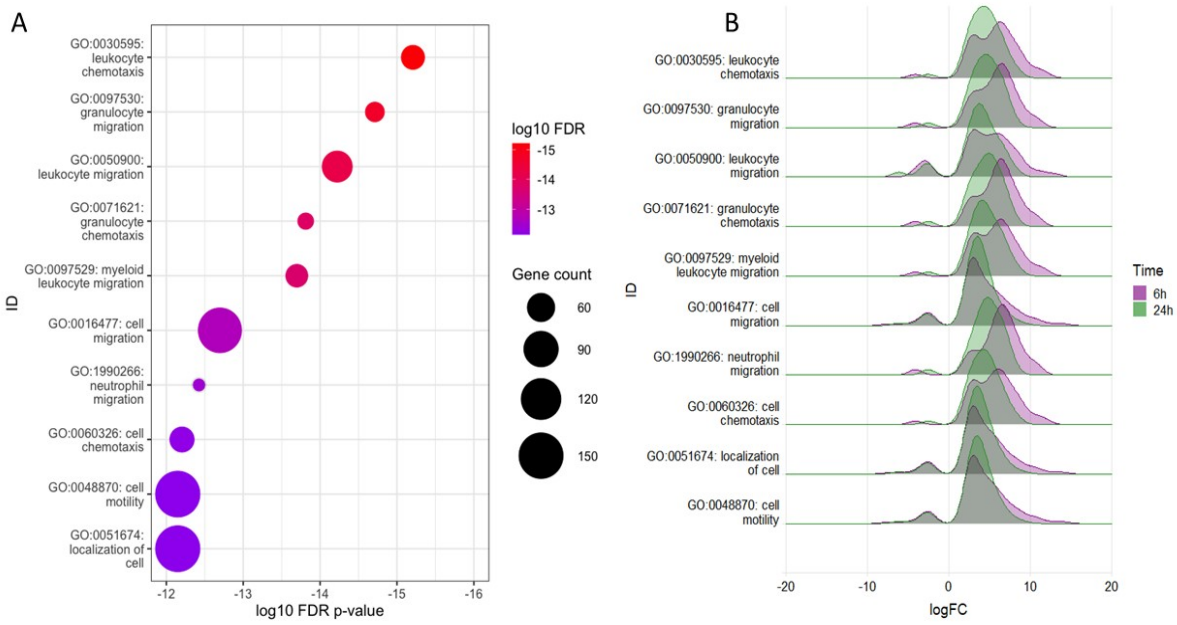

Figure 4.13. **Enrichment of leukocyte-related terms in the Biological Processes category.** (A) The top 10 enriched leukocyte-related Biological Processes in the core gene list in response to NTHi infection. Category IDs are ordered by enrichment significance (FDR) which is indicated by the colour of the dot, with the size of the dot representing the number of genes assigned to each category. (B) The expression of genes at 6 h (purple) and 24 h (green) present in the top 10 leukocyte-related Biological Processes show a higher number of genes are upregulated at both time points, compared to downregulated.

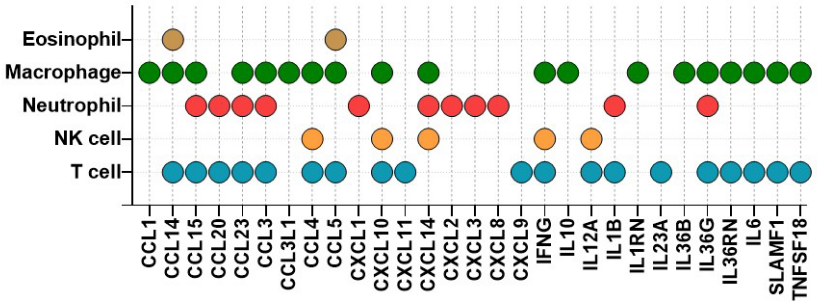

Figure 4.14. Upregulated genes involved in macrophage recruitment and activation of other immune cells. Upregulated macrophage genes encoding for secreted proteins in the leukocyte chemotaxis (GO:0030595) term and the suggested association of the gene product with T cells, NK cells, neutrophils, eosinophils and macrophages/monocytes.

The most significantly enriched term in the cluster was 'leukocyte chemotaxis' (GO:0030595). Out of the 47 genes assigned to this category, 46 were upregulated in response to NTHi infection at 6 h and 24 h. The only downregulated gene was *CXADR*, the coxsackievirus and adenovirus receptor which functions as a cell adhesion molecule[435]. To investigate which specific leukocytes the macrophage may be recruiting, 29 upregulated genes encoding for secreted macrophage proteins within the 'leukocyte chemotaxis' category and the target cell type were identified. The majority of the identified macrophage genes were for chemoattractants for T cells (19 genes) and monocytes/macrophages (19), followed by neutrophils (11), NK cells (5) and eosinophils (2) (Figure 4.14).

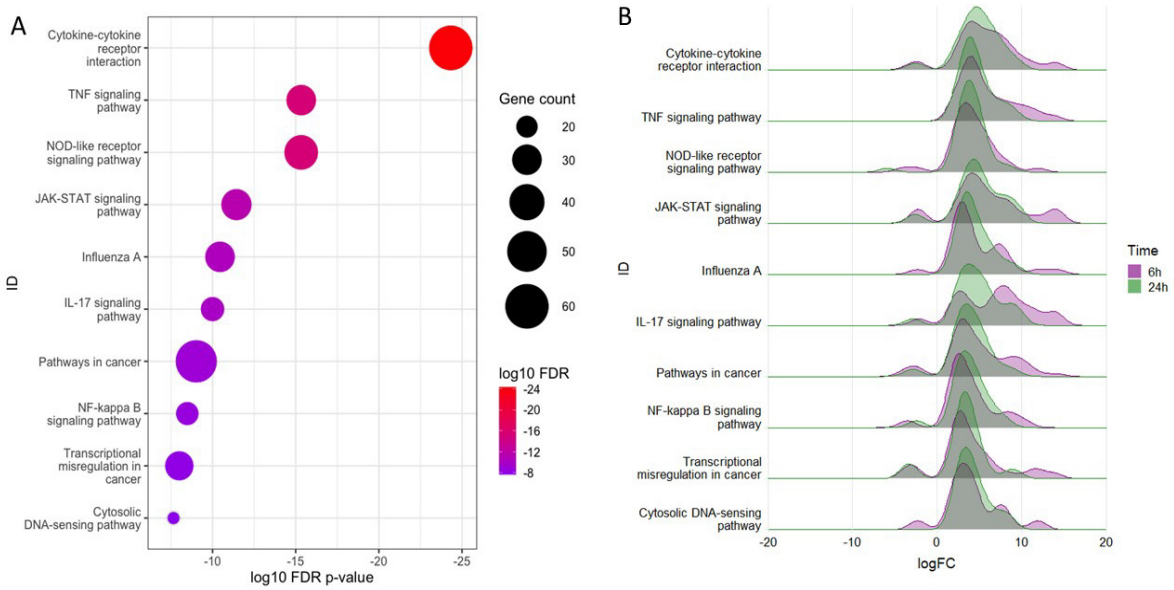

Figure 4.15. Enrichment of MDM KEGG pathways in the core gene list in response to NTHi infection. (A) Pathway/category IDs are ordered by enrichment significance (FDR) which is indicated by the colour of each dot, with the size of the dot representing the number of genes assigned to each pathway/category. Enrichment significance performed using TopFunn. (B) Expression of genes present in the top 10 KEGG pathways at 6 h (purple) and 24 h (green) show a higher number of genes were upregulated at both time points, compared to downregulated.

Although GO enrichment analysis indicates activation of the macrophage immune response during NTHi infection, it is not clear which specific immune response pathways were activated. To determine pathway enrichment, KEGG pathway analysis was performed on the core 863 DEG list using ShinyGo[436]. A total of 75 KEGG pathways were significantly functionally enriched, with the majority of the top 10 functionally enriched pathways indicating activation of immune response pathways (Figure 4.15A). In agreement with the previously identified top enriched GO:terms, the top KEGG pathway was 'cytokine-cytokine receptor interaction'. A higher number of genes in all 10 pathways were upregulated at both time points, compared to downregulated, further showing the continued transcriptomic response to persistent NTHi infection (Figure 4.15B). Enrichment of specific intracellular immune response pathways such as the 'NOD-like receptor signalling', 'Influenza A' and 'Cytosolic DNA-sensing' pathways (all FDR $p<0.05$) indicate activation of macrophage responses to intracellular NTHi.

Enriched terms in the Cellular Component GO category also suggest intracellular presence of NTHi. Cellular Component GO:terms refer to the cellular position in which the product of the gene in the input list performs a function, rather than a process. Within the Cellular Component category, enrichment of the term 'symbiont-containing vacuole' (GO:0020003) was found (FDR $p = 0.0433$, Table 4.2). The genes enriched in this category (*GBP2, GBP4, GBP6,* and *GBP7)* are members of the guanylate-binding protein (GBP) family, which play a role in antibacterial defence against intracellular pathogens[214]. Although not included within this particular GO:term annotation, 3 other GBP family members (*GBP1, GBP3* and *GBP5*) were also statistically significantly upregulated at both 6 h and 24 h (Figure 4.16).

Table 4.2. Significantly enriched GO terms in the Biological Process and Cellular Component categories relating to host-pathogen symbiosis. Top significant functionally enriched GO terms including the term 'symbiont' for the categories Biological Process and Cellular Component for the 863 core genes differentially expressed at 6 h and 24 h (log_2 FC ±2, FDR $p<0.05$).

Category	ID	Term	Enrichment FDR	Genes in input	Genes in annotation
GO: Biological Process	GO:0043903	regulation of symbiosis, encompassing mutualism through parasitism	1.35E-10	38	232
	GO:0044403	symbiotic process	3.57E-04	67	911
	GO:0051817	modification of morphology or physiology of other organism involved in symbiotic interaction	1.57E-02	15	124
GO: Cellular Component	GO:0020005	symbiont-containing vacuole membrane	2.47E-02	4	6
	GO:0020003	symbiont-containing vacuole	4.33E-02	4	7

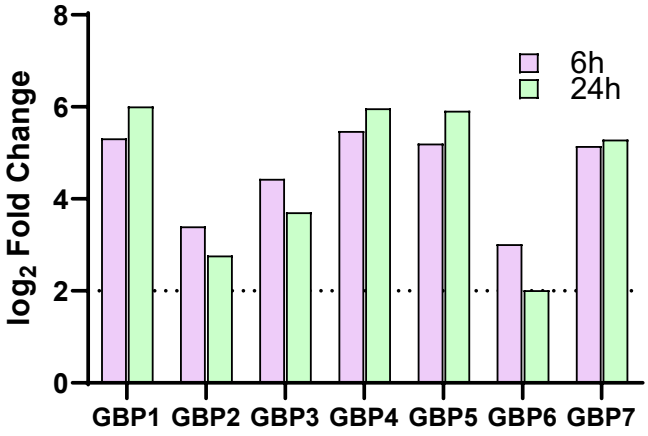

Figure 4.16. Upregulation of host GBPs involved in containing intracellular pathogens. Log fold change values of guanylate-binding protein (GBP) 1-7. Purple bar = 6 h, green bar = 24 h. Dotted line indicates log_2 FC 2 cut off. All genes were statistically significantly upregulated at both time points (FDR $p<0.05$).

4.2.5.1 Modulation of macrophage pathways involved in bacterial clearance

Despite the data so far indicating upregulation of the macrophage response to an intracellular pathogen during NTHi infection, NTHi was still able to persist until 24 h, suggesting inefficient macrophage pathogen clearance. Macrophages play a key role in pathogen clearance by internalising pathogens via an endocytic or phagocytic pathway, eventually resulting in pathogen degradation[437]. However, no enrichment of bacterial internalisation pathways were identified in the core 6 h/24 h DEG data set. As NTHi is capable of entry into host cells through multiple mechanisms, the gene expression of cell surface receptors involved in bacterial internalisation was first investigated to determine whether any regulation of individual genes could be detected.

A total of 30 genes for cell surface receptors were mined from the 'endocytosis', 'phagosome' and 'FcγR-mediated phagocytosis' KEGG pathways. Only 3 genes at 6 h (*FCGR2A, LDLR* and *SIGLEC1*) and 7 genes at 24 h (*CAV1, CD36, FCGR2A, MRC1, OLR1, SCARB1* and *TLR2*) were up or downregulated in response to NTHi infection above the log_2 FC 2 cut off originally applied to the data set (Figure 4.17). Furthermore, only one gene (*FCGR2A*) passed this cut off value at both time points, so would have been the only gene to have been retained in the core 6 h/ 24 h data set, which could partly explain the lack of functional enrichment for macrophage clearance processes in this conserved data set. Nonetheless, a number of genes were determined to be statistically significantly regulated in response to NTHi infection, with a higher number of genes significantly differentially expressed at 24 h (25/30) compared to 6 h (16/30). Of these statistically significantly expressed genes, a similar number of up and down regulated genes were present at both time points; 8 genes were upregulated and 8 genes were downregulated at 6 h, and 13 genes were upregulated and 12 genes downregulated at 24 h.

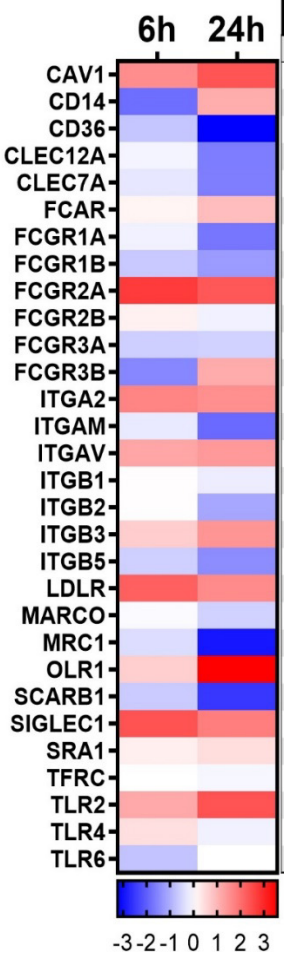

	6h		24h	
	logFC	FDR	logFC	FDR
CAV1	1.566444	**0.007838**	**2.370944**	**0.000976**
CD14	-1.85564	**0.000653**	1.134698	**0.01848**
CD36	-0.74039	**0.006656**	**-3.24649**	**2.30E-08**
CLEC12A	-0.15272	0.619316	-1.66377	**4.27E-05**
CLEC7A	-0.30646	0.132343	-1.65164	**8.04E-07**
FCAR	0.125693	0.65323	0.912609	**0.003031**
FCGR1A	-0.18656	0.428917	-1.74722	**1.87E-06**
FCGR1B	-0.6952	**0.0255**	-1.28432	**0.000447**
FCGR2A	**2.72183**	**5.51E-09**	**2.331498**	**5.85E-08**
FCGR2B	0.188089	0.444369	-0.17074	0.506604
FCGR3A	-0.62924	**0.003295**	-0.57675	**0.006905**
FCGR3B	-1.53656	**0.013543**	1.1525	**0.041851**
ITGA2	1.702383	**0.000592**	1.539936	**0.001685**
ITGAM	-0.26868	0.286141	-1.90702	**1.77E-06**
ITGAV	1.230385	**9.45E-05**	1.412027	**3.36E-05**
ITGB1	0.015805	0.931583	-0.23054	0.188427
ITGB2	0.010293	0.973541	-1.12463	**0.000763**
ITGB3	0.695121	**0.049802**	1.479945	**0.000475**
ITGB5	-0.60258	**0.00236**	-1.46342	**6.88E-07**
LDLR	**2.217889**	**0.000223**	1.618969	**0.003338**
MARCO	-0.06561	0.767417	-0.58379	**0.010906**
MRC1	-0.44123	0.102528	**-2.97329**	**7.25E-08**
OLR1	0.667765	0.077275	**3.561199**	**3.62E-07**
SCARB1	-0.66761	**0.01469**	**-2.55484**	**1.67E-07**
SIGLEC1	**2.388651**	**1.69E-05**	1.788171	**0.000273**
SRA1	0.208899	0.114365	0.457972	**0.002151**
TFRC	-0.01202	0.974649	-0.10356	0.779493
TLR2	1.18365	**0.000174**	**2.399904**	**2.41E-07**
TLR4	0.423717	0.101548	-0.16573	0.539169
TLR6	-0.76976	**0.002046**	-0.00908	0.970606

Figure 4.17. Gene expression of macrophage cell surface receptors involved in bacterial internalisation. Thirty genes for cell surface receptors were mined from the 'endocytosis', 'phagosome' and 'FcγR-mediated phagocytosis' KEGG pathways. Heatmap shows the $\log_2$ FC for each gene at 6 h and 24 h, downregulated genes in blue, upregulated genes in red, as indicated in the key below the heatmap. The accompanying Table shows the $\log_2$ FC values and FDR p-value for each gene. Bold indicates genes that were statistically significantly differentially expressed (FDR $p<0.05$), with genes expressed $\pm\log_2$ FC2 also shown in bold.

Once internalised, pathogens are contained within phagosome or endosome compartments which undergo maturation processes, culminating in pathogen degradation. The transcriptomic regulation of genes involved the maturation of these compartments during NTHi infection was investigated by determining the expression of markers known to define 'early' and 'late' phagosomes/endosomes. The majority of genes for early markers were significantly upregulated at 6 h and 24 h, with the exception of Early Endosome Antigen 1 (*EEA1*) which was upregulated at 6 h, but by 24 h was downregulated (Figure 4.18A). In contrast, the majority of 'late' markers were significantly downregulated at both time points, apart from *RAB7A* which was upregulated at 6 h, but was not differentially expressed at 24 h. *RAB5* encodes for the Rab5 GTPase which defines early endosomes and are removed from the membrane upon maturation. Rab7 replaces Rab5 and characterises maturation to a late endosome[243], however *RAB7B* was the most significantly downregulated 'late' marker (-2.7 $\log_2$FC at 24 h, $p<0.001$).

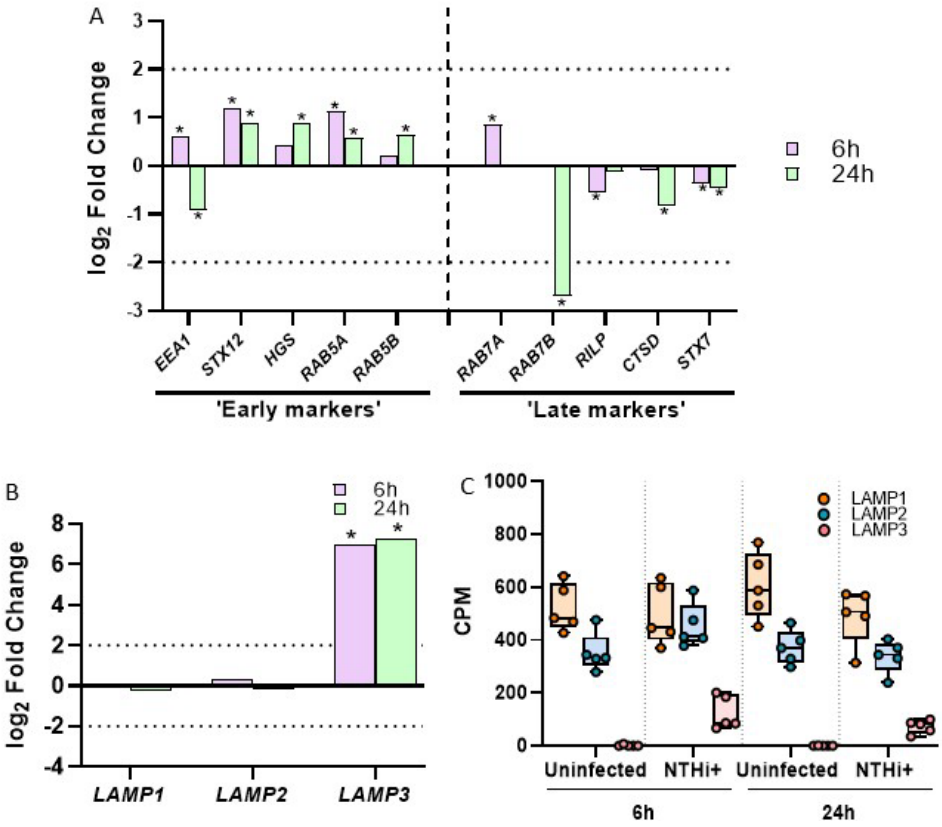

Figure 4.18. Regulation of MDM markers involved in endosome/phagosome maturation. (A) Regulation of select 'early' and 'late' endosome and phagosome markers expressed by MDM in response to NTHi infection. (B) Log_2 FC of *LAMP1*, *2* and *3* at 6 h and 24 h compared to uninfected MDM. For both (A) and (B), asterisk indicates statistically significant differentially expressed genes ($p<0.05$). Dotted line indicates log_2FC cut off. (C) Normalised counts per million (CPM) expression values of *LAMP1*, *2* and *3* in uninfected and infected (NTHi+) MDM across 6 h and 24 h. Dots represent each matched sample, upper and lower whiskers show maximum and minimum values respectively, the middle line is the median value and the lower and upper lines of the box plot are the first and third quartile respectively.

Final endosomal maturation processes include fusion of an endosome or phagosome with a lysosome, which is required for degradation of pathogens. Lysosome-Associated Membrane Proteins (LAMP) 1 and 2 are essential for phagosome-lysosome fusion and maturation from early to late phagosomes[438]. Only small and non-significant changes in *LAMP 1/2* gene expression were detected during NTHi infection (Figure 4.18B). *LAMP3* gene expression on the other hand was significantly upregulated at both 6 h (+7 log_2FC) and 24 h (+7.3 log_2FC). However, differences in LAMP gene regulation could be due to the constitutive macrophage expression of LAMP 1/2 proteins, as indicated by differences in the abundance of normalised read counts (Figure 4.18C).

4.2.5.2 Identification of the key genes involved in the intracellular response to NTHi by WGCNA

Although gene list enrichment analysis and KEGG pathway analysis identified enrichment of macrophage intracellular immune response pathways, the nature of GO tools do not capture the complexity of how genes assigned to significantly enriched GO terms are co-expressed and which genes are the central players within enriched pathways. In order to determine which specific genes were central in the macrophage response to intracellular NTHi infection, weighted gene correlation network analysis (WGCNA) was performed.

WGCNA is an unsupervised analysis method which constructs a gene network based on gene expression profiles to determine co-expression similarity between genes[379]. As such, the recommended starting data set must not have been filtered by differential gene expression profiles, which would likely bias the analysis and result in generation of few highly correlated modules[379]. Therefore, WGCNA analysis was performed on the normalised 15048 gene list that was filtered only to removal lowly expressed genes, which was recommended by the WGCNA package guide[379].

First, network topology analysis assigned MDM genes to discrete modules, of which 15 modules were identified (Figure 4.19A). Each module was designated a colour and is referred to as the designated colour from herein. The grey module was categorised as the 'bin' module containing genes not assigned to any module, with 1750 genes out of 15048 starting genes assigned to the grey module (Figure 4.19B).

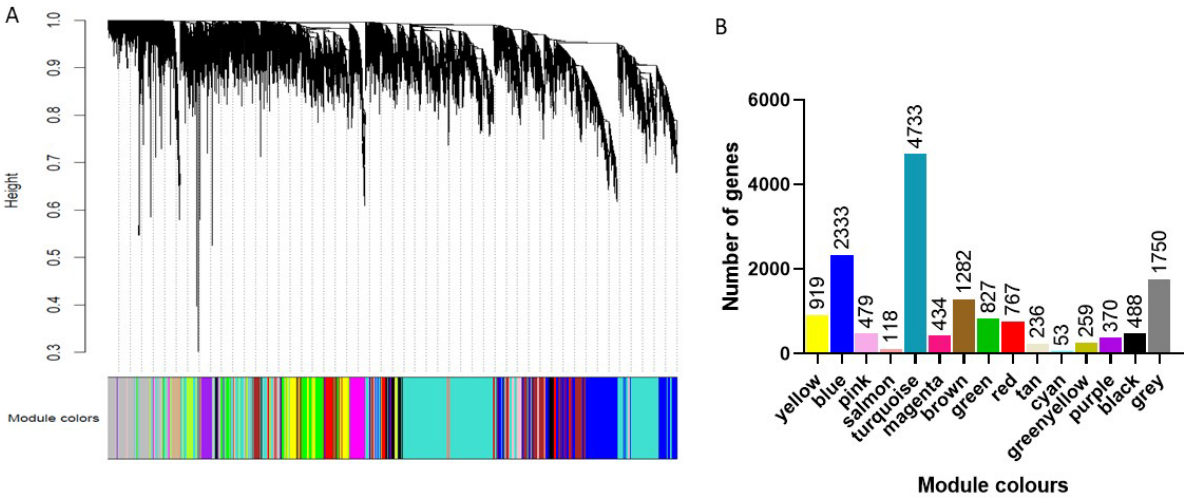

Figure 4.19. Assignment of genes to module colours. (A) Clustering dendrogram of all 15048 genes with dissimilarity based on topological overlap. (B) Bar plot quantifying the number of genes assigned to each module.

Correlation of module eigengenes (first principle component of each module) with trait information (time point, infection status and donor ID) determined a number of modules to be associated with NTHi infection (Figure 4.20). Firstly, no significant correlations between donors and any of the modules were apparent, suggesting little impact of donor-donor variability on the MDM data set. The time trait was significantly correlated (all $p<0.05$) with four modules; magenta, turquoise, tan and pink, however NTHi infection was significantly correlated (all $p<0.05$) with ten modules; black, blue, brown, green, pink, red, salmon, tan, turquoise and yellow.

To determine the significance between the genes assigned to each module and the infection trait, correlation of module membership and gene significance was performed which found that all ten modules were significantly associated with NTHi infection (all $p<0.05$), however correlation score strength varied (Figure 4.21). The strongest correlations were the blue (0.93), brown (0.86), red (0.78) and black (0.67) modules (Figure 4.21, top row), indicating the high significance of genes being assigned to these modules and association with NTHi infection. The yellow (0.61), pink (0.61), green (0.54) and turquoise (0.51) modules were also moderately correlated (Figure 4.21 middle row), with the salmon and tan modules statistically significantly, but more weakly, associated with NTHi infection (0.41 and 0.2 respectively, Figure 4.21, bottom row).

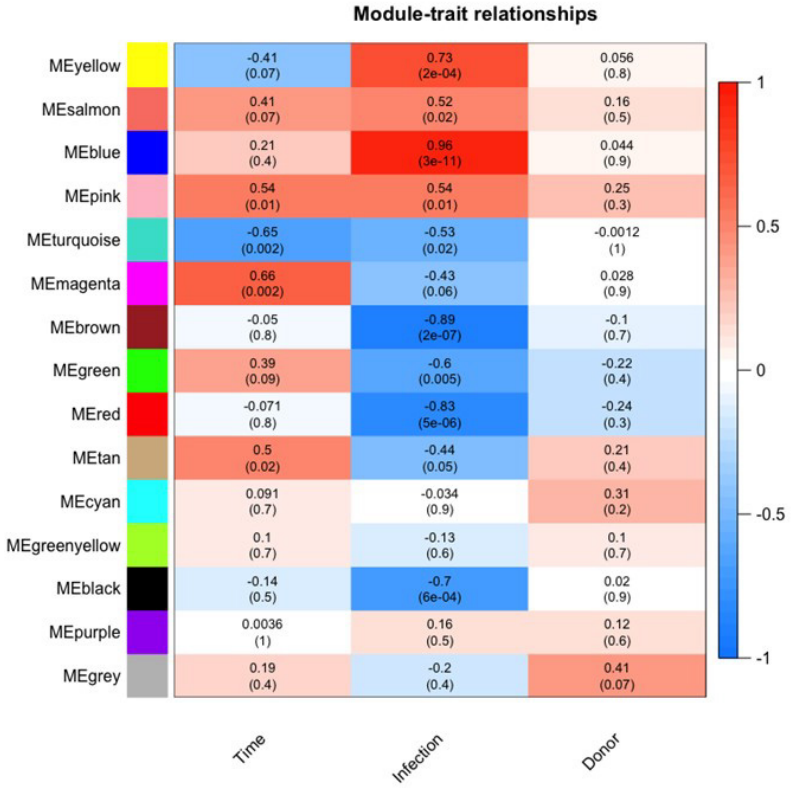

Figure 4.20. **Association between modules and sample trait data.** Each row corresponds to a module eigengene and each column to a trait. Each cell contains the correlation score (top) and p-value (bottom) assigned to each relationship. The module most significantly associated with time is magenta. The module most significantly associated with infection is blue. No modules were significantly associated with donors.

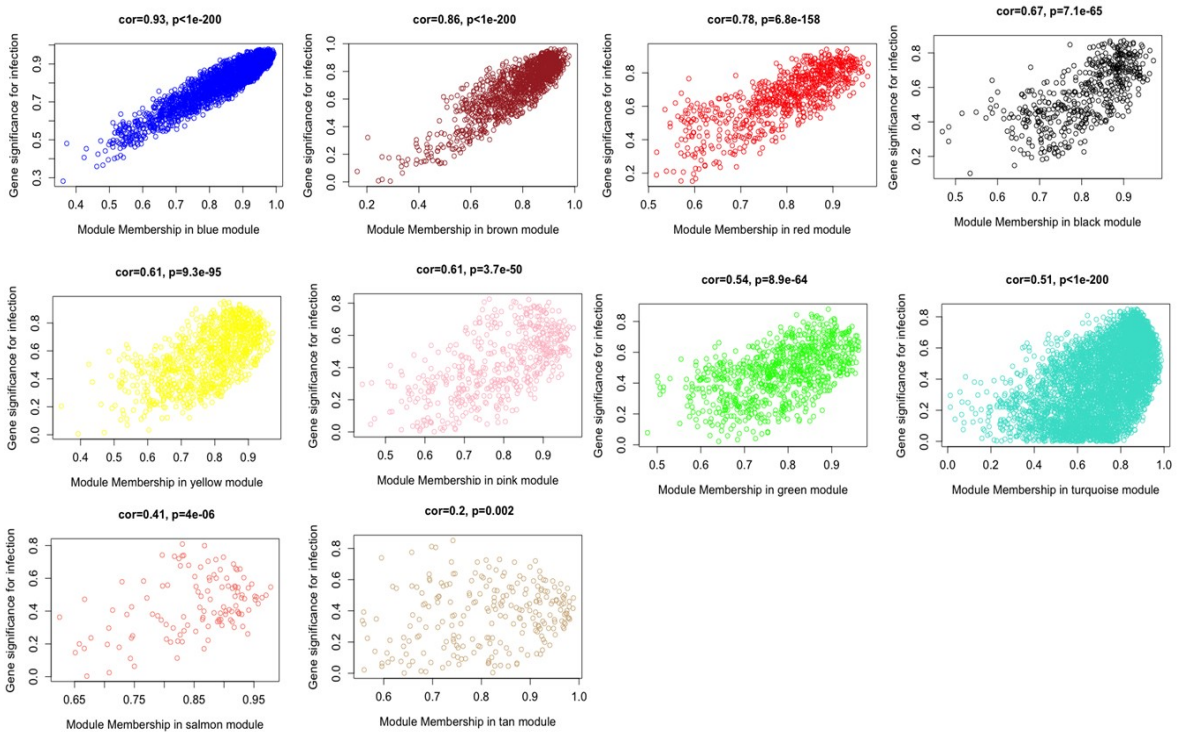

Figure 4.21. Module membership and gene significance correlations for infection. Identification of gene significance in the 10 modules (blue, brown, red, black, yellow, pink, green, turquoise, salmon and tan) found to be significantly correlated with the NTHi infection. Module membership indicates the correlation of each individual gene to the specific module eigengene. The correlation and corresponding p-value for each comparison is present above each scatterplot and modules are ordered based on level of correlation (high to low).

To visualise the relationship between module eigengenes and NTHi infection, module eigengenes were clustered to include the infection trait (Figure 4.22). Four distinct clusters of modules were visible; cluster I (yellow, blue, pink and salmon), cluster II (turquoise), cluster III (magenta, brown, green and red) and cluster IV (tan, cyan, greenyellow, black and purple). Gene list enrichment analysis identified enrichment of divergent processes for each cluster.

Cluster I was functionally enriched with immune response processes, cell activation and metabolic processes involved in responding to an immune stimulus (Figure 4.23A). KEGG pathway analysis identified enrichment of various immune response pathways including 'TNF signalling pathway', 'Influenza A', 'NOD-like receptor signalling pathway', 'JAK-STAT signalling pathway' and 'Cytokine-cytokine receptor interaction'. Enrichment of intracellular immune response terms in cluster I was similar to the immune response enrichment observed in the previous DEG analysis (Section 4.2.5.1).

Cluster II was enriched with pathways associated with cell activation and metabolic processes, including protein transport and cytoskeleton organisation, with an enrichment of non-coding (nc)RNA metabolic processes (Figure 4.23B). Enrichment of the 'Autophagy' KEGG pathway indicated increased cell component turnover, potentially as a result of increased macrophage activation.

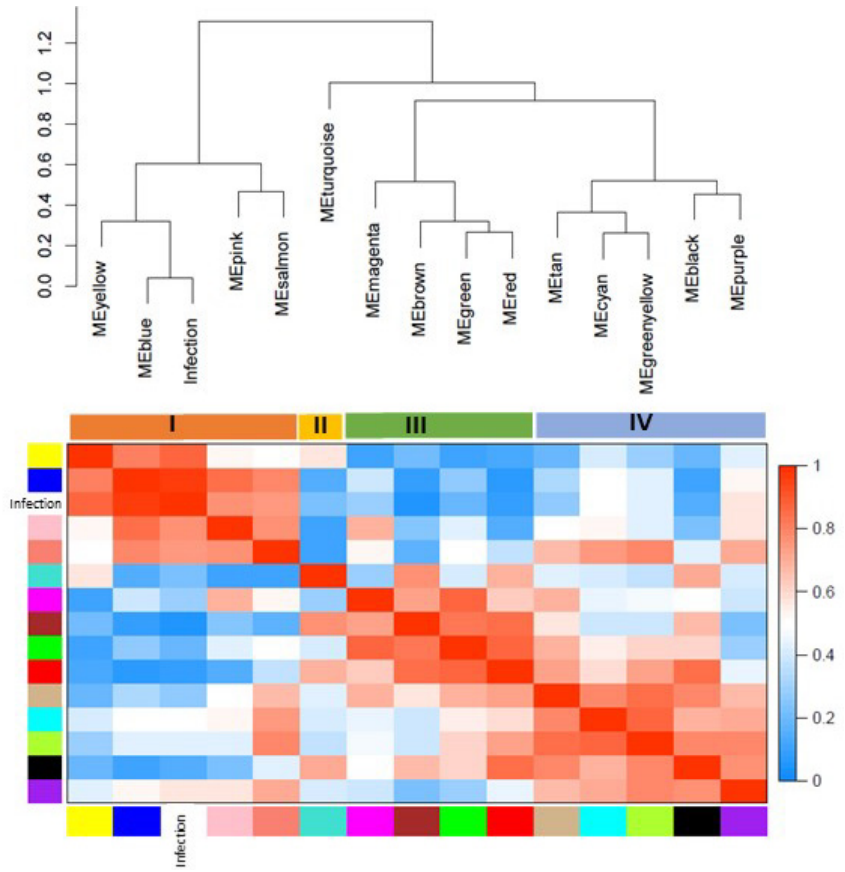

Figure 4.22. Clustering of NTHi infection trait with modules of interest. Visualisation of the eigengene network as a dendrogram and heatmap showing the relationships between individual modules and the NTHi infection trait. Each row and column in the heatmap corresponds to one module eigengene (labelled by colour) or NTHi infection. In the heatmap, blue colour represents low adjacency (negative correlation), while red represents high adjacency (positive correlation).

Cluster III was particularly enriched with gene regulation (transcription and translation) and metabolic processes (Figure 4.23C). The 'Ribosome' KEGG pathway was the most significantly enriched KEGG pathway. Out of 154 genes annotated to the KEGG pathway, 88 macrophage genes were present in cluster III. Numerous GO terms relating to gene and protein regulation were enriched including 'nuclear-transcribed mRNA catabolic process nonsense-mediated decay', 'structural constituent of ribosome', 'co-translational protein targeting to membrane' and 'protein targeting to endoplasmic reticulum (ER)'. Enrichment of metabolic processes was highlighted by enriched molecular function terms such as 'oxidoreductase' and 'NADH dehydrogenase' with various cellular component terms relating to the mitochondrion similarly enriched, corroborating increased MDM activity measured by the MTS assay in Section 3.2.6. KEGG pathways relating to cellular metabolism were enriched, with 'Oxidative Phosphorylation' in the top 5 significantly enriched KEGG pathways.

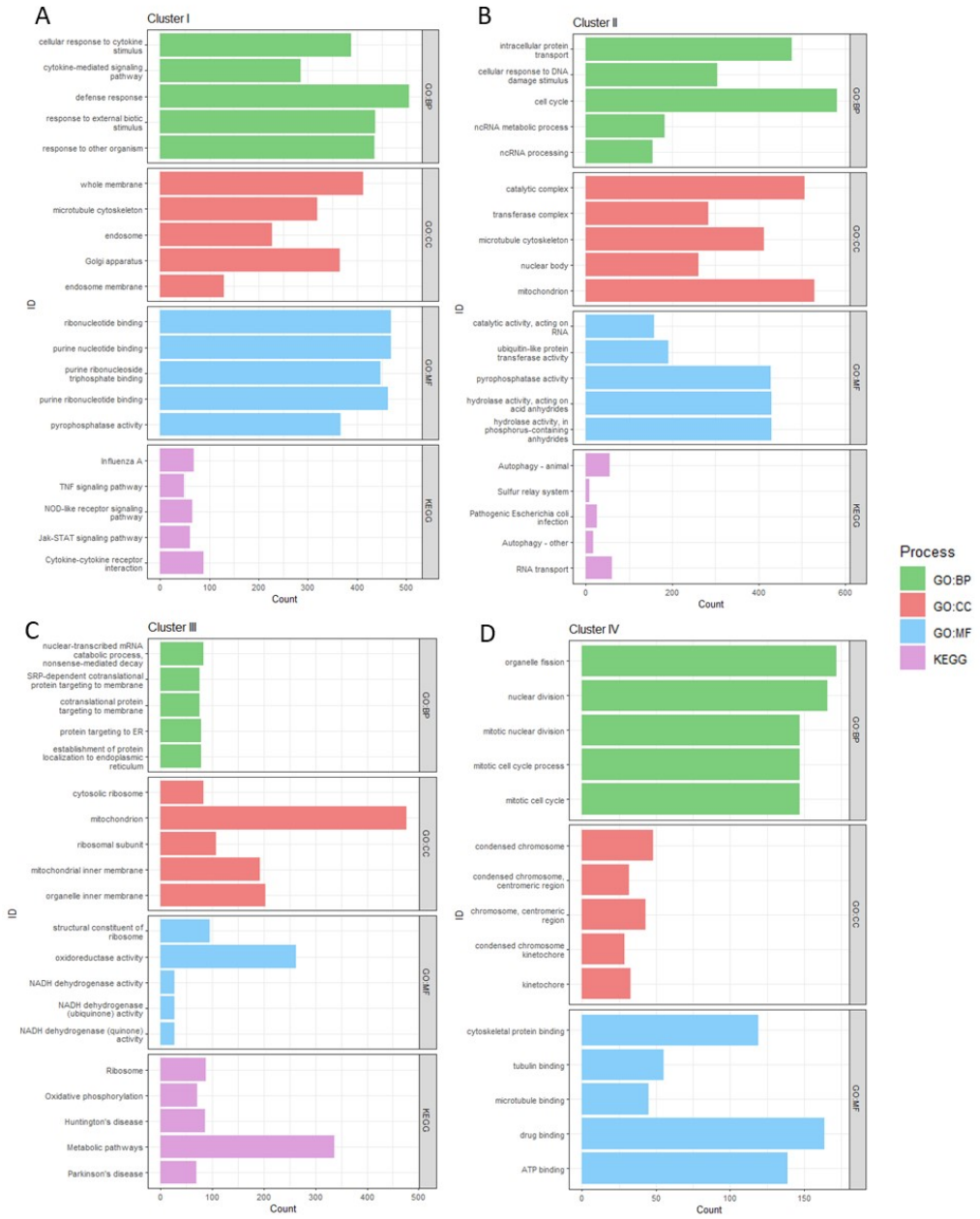

Figure 4.23. Intracellular immune response pathways were modulated in the cluster most highly associated with infection. The top 5 significantly enriched terms for Biological Processes (BP), Cellular Component (CC), Molecular Function (MF) and KEGG pathway are shown for each cluster, with pathway/category IDs ordered by enrichment significance (all shown terms = FDR $p<0.05$). (A) Cluster I was enriched in immune response pathways, (B) Cluster II was enriched in metabolic and cell activation processes, (C) Cluster III was enriched in gene regulation and metabolic processes, (D) cluster IV was enriched in cell cycle processes, however no significant KEGG pathways were identified for this cluster. Gene ontology analysis performed using ToppFunn.

Cluster IV was enriched with cell cycle processes. Enrichment of GO terms involved in cell cycle processes include organelle fission, nuclear division and mitotic cell cycle processes (Figure 4.23D). Genes coding for mitotic spindle, chromosome centromeres and microtubule cytoskeleton indicate the cellular components involved in cell cycle process that were found to be enriched. Despite assignment of 1406 genes to this cluster, no significant enrichment of KEGG pathways were found.

4.2.5.2.1 Identification of blue module 'hub' genes involved in the MDM response to intracellular NTHi infection

As the blue module was highly significantly correlated with NTHi infection and was part of the cluster (I) that was enriched with immune processes, this module was chosen to explore further. The expression pattern of the 2225 genes assigned to the blue module demonstrated similar expression to the core gene set identified previously, with uninfected and infected samples clustering independently, with no time point sub clustering (Figure 4.24A). Similarly, the regulation of gene expression between 6 h and 24 h remained consistent, with a higher number of upregulated genes compared to downregulated genes (Figure 4.24B).

Only 9 upregulated genes at 6 h became downregulated at 24 h, whereas 10 downregulated genes at 6 h became upregulated at 24 h (Figure 4.24C). The blue module was significantly enriched with immune response pathways, suggesting the blue module was driving the enrichment of immune processes in cluster I. In particular, intracellular immune response pathways including 'NOD-like receptor signalling pathway', 'Influenza A', 'Legionellosis', 'Herpes simplex infection' and 'RIG-I-like receptor signalling pathway' were enriched (Figure 4.25A). Enrichment of similar KEGG and GO:terms further confirms the results of the earlier DEG analysis, suggesting the macrophage response to intracellular NTHi infection involves a specific intracellular immune response (Figure 4.25 B, C & D).

A

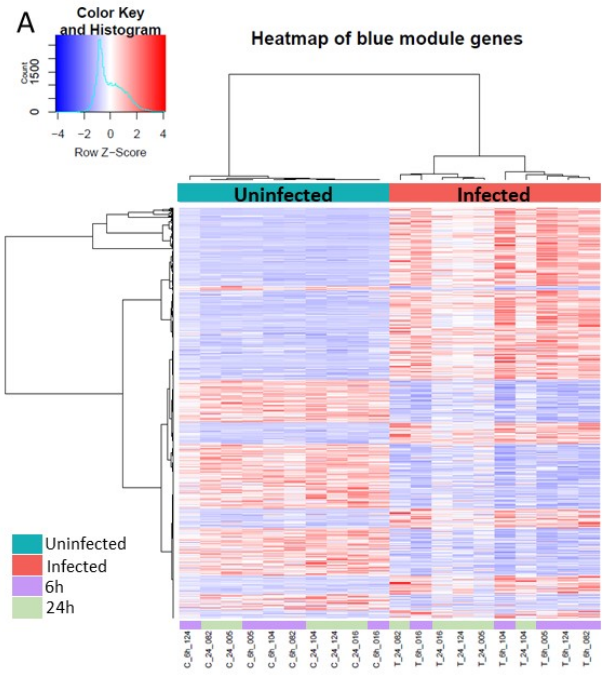

B

	Upregulated	Downregulated	Total
6h	1267	958	2225
24h	1268	957	2225

C

Gene	6h logFC	24h logFC
ZHX1-C8orf76	0.619538	-0.00493
GJB3	2.382888	-0.60505
GRIN2B	2.026339	-0.20012
MGAM	1.161045	-1.65955
NBPF10	0.690979	-0.07866
TAF9	0.535289	-0.68674
RNVU1-4	0.489912	-1.32083
POLG2	0.143048	-0.20826
PSMB3	0.125018	-0.09601
CHKB-CPT1B	-0.01333	1.639682
SLC22A31	-2.59356	1.566758
RDM1	-0.07229	0.996626
ORAI1	-0.4201	0.953198
C11orf98	-3.54872	0.828616
ZNF625	-2.0706	0.578818
NUDT18	-1.25655	0.418032
COL4A2	-1.94759	0.280295
TADA2A	-0.96464	0.14144
PCGF2	-0.84249	0.029799

Figure 4.24. Expression profile of the genes assigned to the blue module. (A) Heatmap of the 2225 genes present in the blue module using Euclidean distance and Ward linkage. (B) Table indicating number of upregulated and downregulated genes at 6 h and 24 h. (C) Table of the 20 genes in the blue module that changed direction of expression (upregulated to downregulated or vice-versa) between 6 h and 24 h.

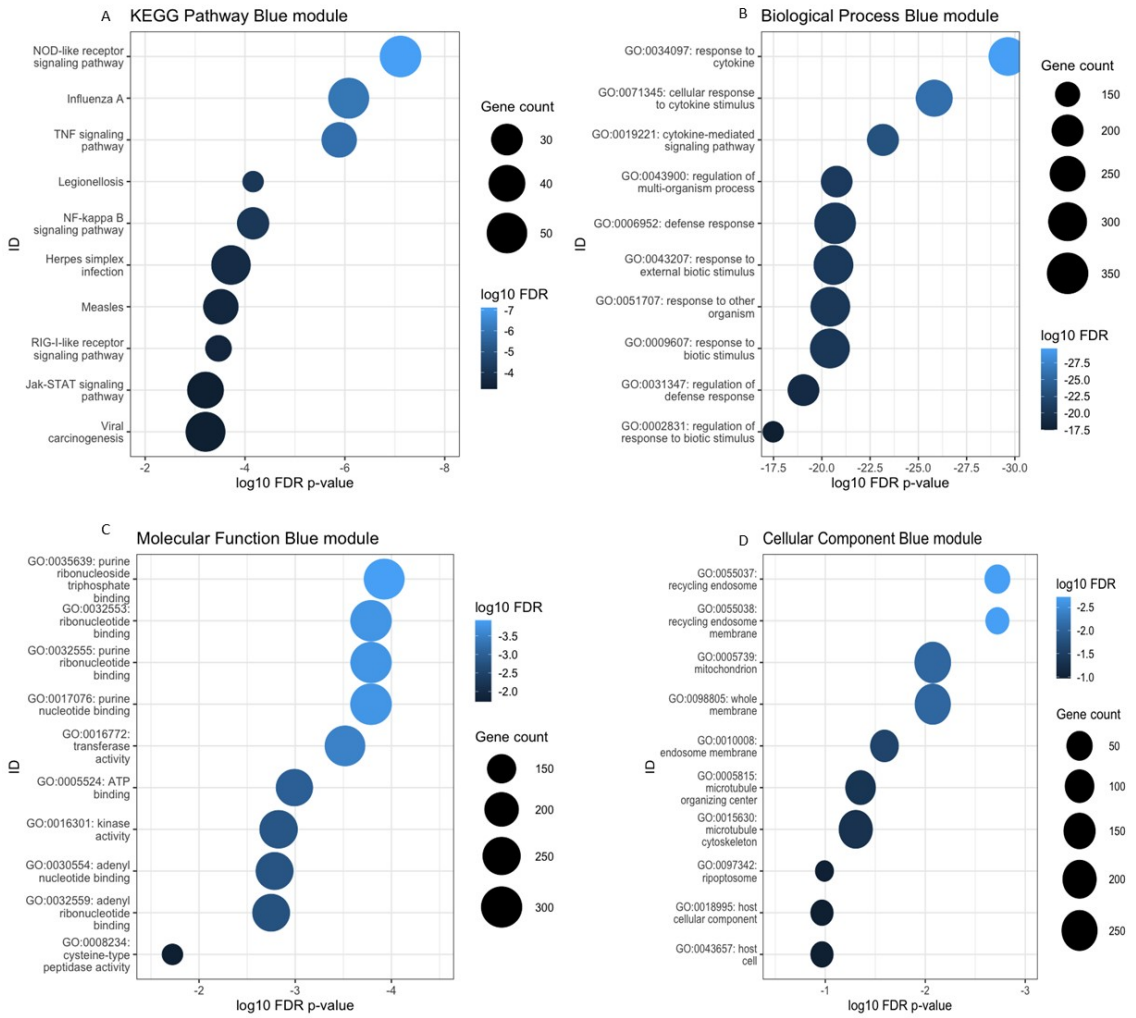

Figure 4.25. The MDM intracellular immune response is driven by genes assigned to the blue module. The top 10 enriched KEGG pathways (A) and GO terms in the (B) Biological Process, (C) Molecular Function and (D) Cell Component categories for the 'blue' module. Pathway/category IDs are ordered by enrichment significance (FDR) which is indicated by the colour of the dot, with the size of the dot representing the number of genes assigned to each pathway/category. Gene list enrichment performed using ToppFunn.

To determine the key genes in the blue module network, the most highly connected genes were extracted from the blue module gene list. The Maximal Clique Centrality (MCC) scoring method ranked the connectivity of the nodes (genes) in the network; key nodes were coloured blue, with lighter colours indicating decreasing network importance and solid lines showing connecting edges/interactions between nodes (Figure 4.26A). Three genes *CASP4, PNRC1* and *SGPP2* were the highest ranked nodes (Figure 4.26B). Furthermore, within the constructed blue module network, *GBP1*, *GBP4* and *GBP5* were present. These genes were also identified earlier in this chapter to suggest presence of intracellular NTHi and subsequent activation of the macrophage response to intracellular infection, which could be mediated by the top ranked hub gene, *CASP4*.

A

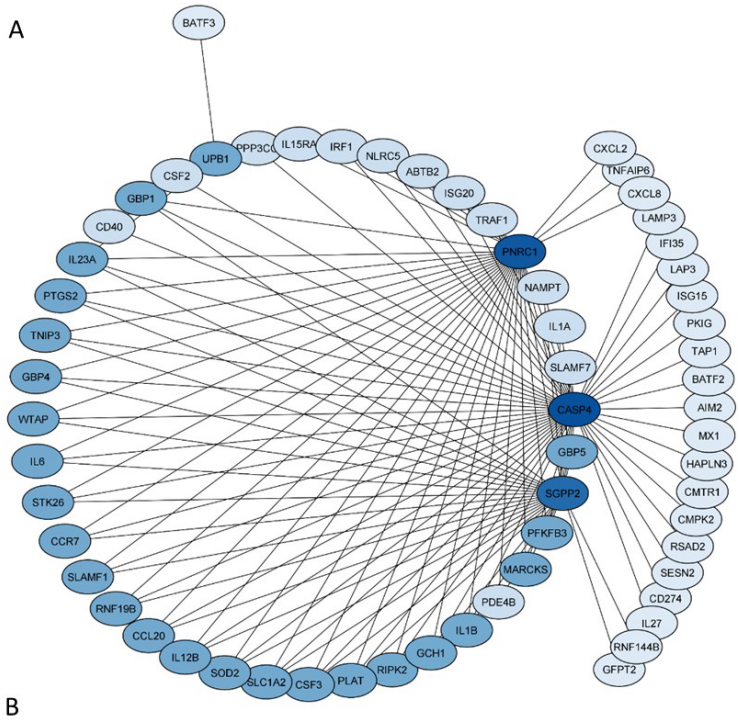

B

Rank	Gene	Score
1	CASP4	28
2	PNRC1	21
3	SGPP2	9
4	GBP5, GBP4	3
6	ABTB2, UPB1, GBP1, RIPK2, GCH1, PLAT, NAMPT, SLC1A2, CCL20, CCR7, STK26, IL6, TRAF1	2
19	CXCL8, PTGS2, PFKFB3, LAMP3, CXCL2, MARCKS, IL23A, MX1, IL1B, ISG15, SOD2, IL12B, IL1A, SLAMF1, PPP3CC, IL15RA, SESN2, GFPT2, RSAD2, CMPK2	1
39	IFI35, ISG20, PDE4B, CD40, BATF3, CSF2, AIM2, BATF2, TAP1, PKIG, CSF3, IL27, RNF19B, CD274, TNFAIP6, IRF1, CMTR1, RNF144B, LAP3, HAPLN3, SLAMF7, NLRC5, WTAP, TNIP3	0

Figure 4.26. **Construction of the blue module gene network identifies CASP4 as the highest connected gene involved in the intracellular immune response to NTHi infection.** (A) Visualisation of the top network connections in the blue module, which is highly correlated with the infection trait, generated in Cytoscape using a topological overlap threshold of 0.34. 62 nodes and 122 edges are shown, with three genes CASP4, *PNRC1* and SGPP2 identified as the highest ranked nodes (in darker blue). (B) Table showing the ranking scores of the 62 blue module genes by Maximal Clique Centrality (MCC) using the cytoHubba plugin in Cytoscape.

4.2.6 Validation of transcriptomic analysis

4.2.6.1 Validation of macrophage gene expression in response to additional clinical strains of NTHi

Although no strain dependent differences in the macrophage response between ST14, ST408 and ST201 were shown in chapter 3, the genes and proteins tested previously were general pro-inflammatory responses already established in the literature to be modulated in response to NTHi *in vitro*[186,187,189,439] . However, a number of the genes in the blue module network have not yet been investigated in the context of macrophage responses to NTHi infection. Therefore it was important to confirm whether the regulation of the genes identified in this chapter were conserved in response to additional strains of clinical NTHi. In total, eight genes were chosen for validation in the

MDM using ST14 and the previously used clinical NTHi strains ST408 and ST201. Seven genes from the blue module network were chosen, including the top three ranked genes *CASP4*, *SGPP2* and *PNRC1*, and four other genes present in the blue module also involved in the response to intracellular pathogens including *IRF1, GBP1, IL1B* and *LAMP3*. The final gene chosen was *ACOD1*, one of the top expressed genes at 6 h and 24 h, involved in immunometabolism and regulation of inflammation (Figure 4.10).

All genes were found to be upregulated at both 6 h and 24 h by MDM in response to all three clinical strains of NTHi (Figure 4.27). Induction of *CASP4* in response to ST201 appeared to be lower compared to ST408 at 6 h (FC 2.5 v 1.8 p=0.0281), and ST14 at 24 h (FC 2.1 v 1.7, p=0.0628), however the fold change differences were only slight. Similarly, *ACOD1* gene expression at 6 h was lower in response to ST201 (FC 107) compared to both ST14 (FC 179, p=0.0117) and ST408 (FC 212, p=0.0628) but these differences were not significant at 24 h. Despite few differences in the level of gene expression induction, infection with all three strains resulted in consistent upregulation of MDM responses, indicating that these genes were conserved in the MDM response to NTHi intracellular infection.

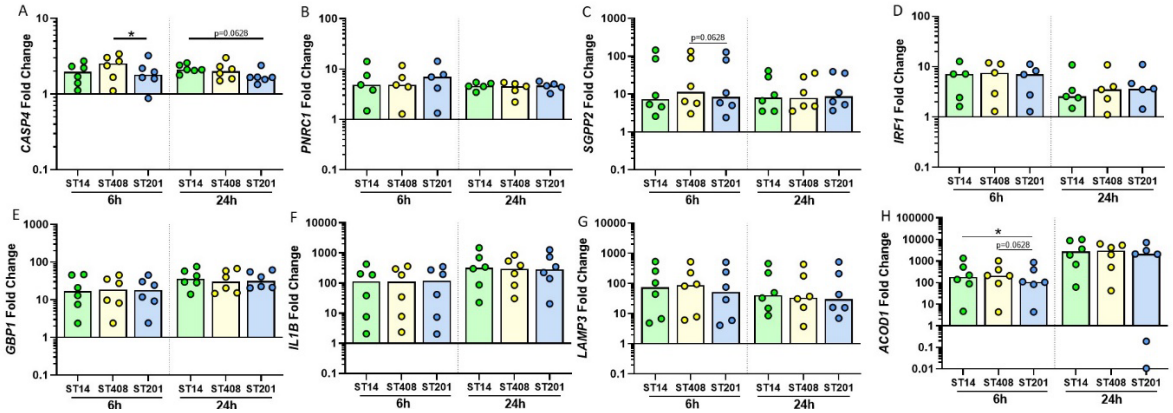

Figure 4.27. MDM intracellular immune response is conserved in response to additional clinical strains of NTHi. To confirm the expression of MDM genes identified in the dual RNASeq analysis in response to additional clinical strains, MDM were infected with ST14 (green), ST408 (yellow) or ST201 (blue) for 6 h, washed with gentamicin for 90 min then left to incubate in antibiotic free media until 24 h. RNA was harvested at 6 h (post gentamicin wash) and at 24 h. Gene expression of (A) *CASP4*, (B) *PNRC1*, (C) *SGPP2*, (D) *IRF1*, (E) *GBP1*, (F) *IL1B*, (G) *LAMP3* and (H) *ACOD1* were measured at both time points by qPCR. Gene expression was normalised to *B2M* and to the uninfected control at the respective time point and is expressed as fold change relative to uninfected control at either 6 h or 24 h. N=5-6. Data were analysed by Friedman test with Dunn's multiple comparisons test; *p<0.05

4.2.6.2 Validation of macrophage pro-inflammatory mediator release in response to NTHi

As macrophage recruitment of immune cells can often result in a dysregulated or exacerbated inflammatory response in individuals with chronic respiratory disease, it was important to validate NTHi-infected MDM release of pro-inflammatory mediators in response to NTHi at 6 h and 24 h. Transcriptomic analysis in this chapter identified an enrichment of terms involved in 'cytokine-mediated signalling pathways' (Figure 4.11 and Table 4.1) and 'leukocyte chemotaxis' (Figure 4.12), with a number of mediators present in the blue module gene network (Figure 4.26). Thus, the gene lists associated with these analyses were mined for genes encoding for macrophage secreted proteins which could be validated by ELISA or Luminex assay.

As such, a small panel of mediators upregulated by MDM in response to NTHi at the transcriptomic level at both 6 h and 24 h were selected to be assessed in cell culture supernatants (Table 4.3). Macrophage mediators could be grouped into general pro-inflammatory mediators (IL-1β, TNFα, IL-6), lymphocyte-related mediators (IL-15, IL-23, IL-27, IL-33, and IL-36β), neutrophil specific mediators (IL-8/CXCL8, IL-17C and CCL20) and anti-inflammatory mediators (IL-10 and TSLP). The majority of pro-inflammatory mediators were detected by Luminex within the lower and upper limit of quantification (LLOQ and ULOQ, respectively) boundaries of each individual analyte assay specificities at 6 h and 24 h. Only IL-33 (Figure 4.28A) was unable to be detected above the LLOQ of the Luminex assay for any time point or condition (uninfected or infected).

Table 4.3. Regulation of dual RNASeq differentially expressed macrophage inflammatory mediator genes to be validated by Luminex or ELISA. Table indicates the gene chosen from the dual RNASeq data set for protein validation by Luminex or ELISA, all genes were statistically significantly upregulated (FDR p-value p<0.05).

	6h		24h	
Gene	**Log_2FC**	**FDR p-val**	**Log_2FC**	**FDR p-val**
CCL20	6.68	p<0.001	9.50	p<0.001
IL1B	6.03	p<0.001	8.18	p<0.001
IL10	5.22	p<0.001	4.26	p<0.001
IL15	3.60	p<0.001	3.24	p<0.001
IL17C	2.00	p<0.05	2.97	p<0.01
IL23	8.02	p<0.001	8.46	p<0.001
IL27	8.14	p<0.001	8.89	p<0.001
IL33	2.22	p<0.05	4.23	p<0.01
IL36B	3.08	p<0.001	2.65	p<0.001
IL6	8.51	p<0.001	11.92	p<0.001
IL8	5.39	p<0.001	8.61	p<0.001
TLSP	7.75	p<0.001	8.69	p<0.001
TNFA	7.10	p<0.001	5.36	p<0.001

In contrast, the high level of CCL20 protein present in all samples resulted in values above the ULOQ of the Luminex assay and was thus unable to be accurately quantified. Nonetheless, this indicates that NTHi-infected macrophages release copious amounts of CCL20, but any future analysis of CCL20 protein will require dilution of culture supernatants to allow for more accurate quantification of this mediator. Levels of the other two neutrophil associated mediators, IL-8 (Figure 4.28B) and IL-17C (Figure 4.28C) were within the assay detection limits. Both IL-8 and IL-17C were released in response to NTHi infection with significantly higher levels detected at 24 h (p=0.0145 and p=0.0044, respectively).

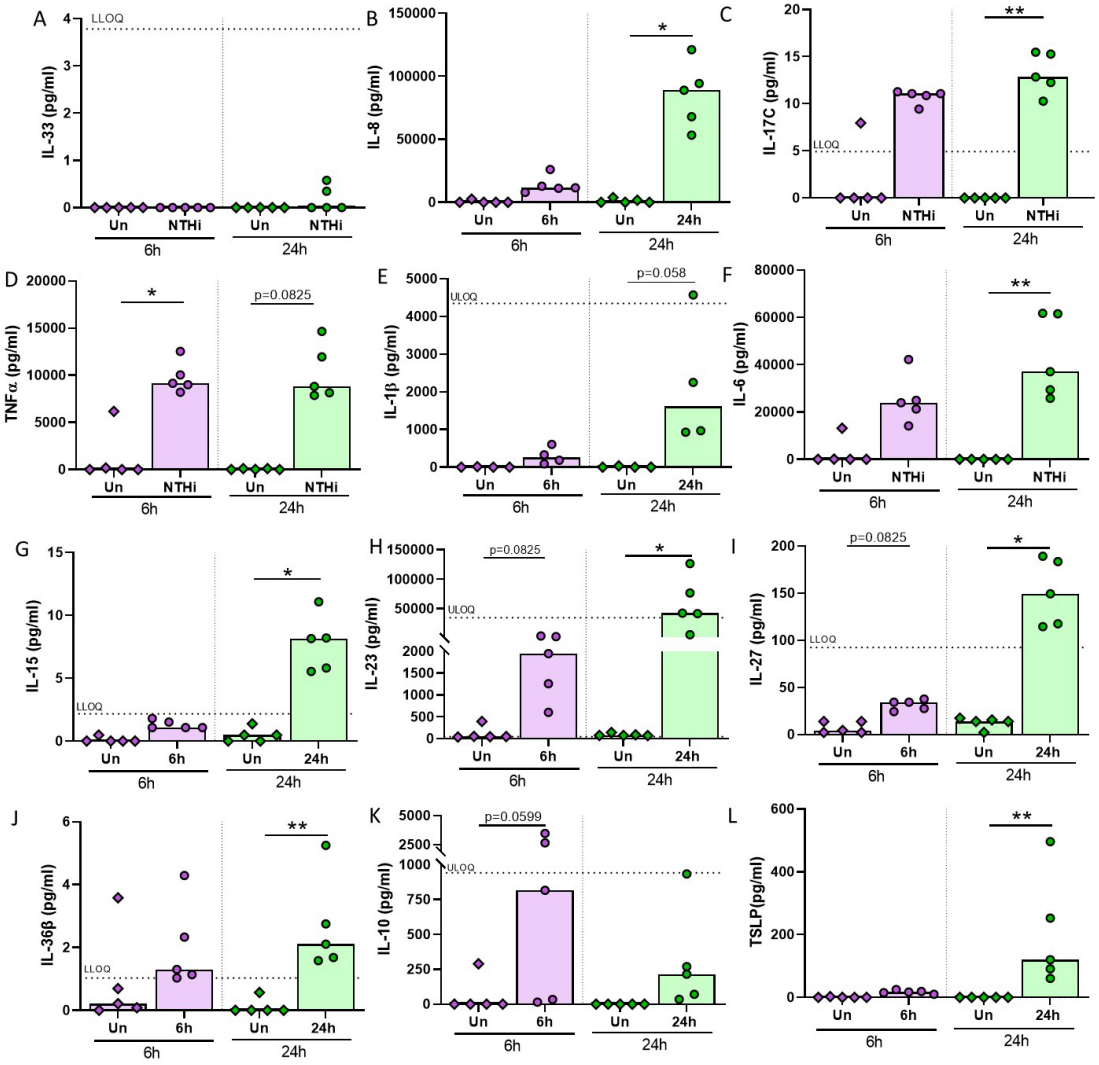

Figure 4.28. MDM release of inflammatory mediators at 6 h and 24 h in response to NTHi infection. MDM release of (A) IL-33, (B) IL-8, (C) IL-17C, (D) TNF-α, (E) IL-1β, (F) IL-6, (G) IL-15, (H) IL-23, (I) IL-27, (J) IL-36β, (K) IL-10 and (L) TSLP into harvested cell culture supernatants in response to NTHi infection at 6 h (purple) or 24 h (green) was measured by Luminex or ELISA (IL-6 and IL-8 only), with horizontal lines on graphs indicating the upper limit of quantification (ULOQ) or lower limit of quantification (LLOQ) of the Luminex assay. N=5, except for IL-1β as one sample was unable to be extrapolated from above the upper limit of quantification. Graphs show paired data and bars indicate median values. Data were analysed by Friedman test with Dunn's multiple comparisons; *p<0.05, **p<0.01

MDM release of general inflammatory proteins such as TNFα, IL-1β and IL-6 were detected at both 6 h and 24 h (Figure 4.28D-F). Similarly, the release of lymphocyte-related proteins IL-15, IL-23, IL-27, and IL-36β in response to NTHi was detected at both time points (Figure 4.28G-J). Although IL-15 and IL-27 were detected in response to NTHi at 6 h, the level of release for each analyte was below the respective LLOQ. However, by 24 h, both IL-15 and IL-27 were able to be detected above the LLOQ and were significantly higher at 24 h compared to the uninfected control ($p=0.0429$ and $p=0.0212$, respectively).

In contrast, both IL-23 and IL-36β release was detected above the LLOQ at both time points, indicating the high upregulation and release of these two proteins in response to NTHi infection. The increased release of IL-23 and IL-36β was significant compared to the uninfected control and 24 h ($p=0.0212$ and $p=0.0028$, respectively). Finally, two mediators involved in regulation of inflammatory process, IL-10 and TSLP, were upregulated at both time points, with IL-10 release higher at 6 h (Figure 4.28K $p=0.0599$) and TSLP release higher at 24 h (Figure 4.28L, $p=0.0066$). The upregulation of these two known inflammatory regulator proteins could indicate the macrophage attempting to maintain balance of inflammation to prevent an exacerbated response to NTHi, highlighting the plasticity of macrophage function during infection.

4.3 Discussion

Analysis of macrophage gene expression in response to NTHi infection in this chapter identified a core transcriptomic gene profile that was consistently upregulated across both 6 h and 24 h. In particular, a macrophage immune response profile specific to responding to an intracellular pathogen was evident. NTHi is still considered an extracellular pathogen, despite increasing evidence of an intracellular lifestyle[140,149,348]. The previous chapter modelled *in vitro* intracellular persistence using three clinical strains of NTHi, which all persisted up until at least 24 h. This chapter further confirmed the intracellular presence of NTHi through transcriptomic activation of various macrophage immune response pathways such as the 'NOD-like' and 'RIG-I-like' receptor signalling pathways which are responsible for intracellular pathogen detection and initiation of responses. Activation of an intracellular immune response was identified using two different analysis methods; differential gene expression analysis (edgeR and DESeq2) and WGCNA. A small panel of selected genes were validated in the MDM model using additional clinical strains of NTHi. Infection with all three strains upregulated the chosen MDM genes in a similar manner, indicating the conserved nature of the macrophage response to NTHi infection.

Although gene list enrichment analysis was useful in highlighting significantly modulated functions or pathways in response to NTHi infection, as a high number of genes were significantly differentially expressed, the specific genes crucial for a particular response were difficult to extrapolate. Use of WGCNA not only reconfirmed the DEG analysis findings of an intracellular immune response to NTHi infection, but also identified the key genes involved. The top hub gene in the blue module gene network was *CASP4*, which encodes for caspase-4, a member of the inflammatory caspase family involved in noncanonical inflammasome activation[211]. Inflammasomes are crucial in the host defence against pathogens through regulation of pro-inflammatory cytokine secretion and pyroptosis induction[440]. Following ligand stimulation, components of the inflammasome machinery are upregulated, culminating in recruitment and activation of caspase-1 and cleavage of pro-IL-1β and IL-18 into their mature forms[441]. In contrast, caspase-4 has emerged as a regulator of noncanonical inflammasome activation, which can directly bind LPS *in vitro* and regulate LPS-induced secretion of pro-inflammatory cytokines[212,213]. The use of caspase-4 as a cytosolic sensor for LPS could account for the lack of differential expression of the primary LPS sensor, TLR4, during NTHi infection in this current work. Recognition of LPS by TLR4 includes binding of LPS by the LPS binding protein (LBP) which then transfers LPS to CD14. CD14 is then able to present LPS to the TLR4-MD-2 complex. All three of these genes varied in expression during NTHi infection; *LBP* was not differentially expressed at 6 h but was significantly upregulated at 24 h (log_2 FC 11.5, FDR $p<0.001$), *CD14* was downregulated at 6 h (log_2 FC -1.86, FDR $p<0.001$) but was upregulated at 24 h (log_2 FC 1.13, FDR $p = 0.018$) and *MD2* was downregulated at 6 h (log_2 FC -1.3, $p<0.001$) and not differentially expressed at 24 h. Further work assessing the protein level of

expression of these sensors would aid in determining the functional response of MDM during NTHi infection.

Pathogenic bacteria prevent host recognition by decorating their LPS (or LOS in the case of NTHi) with molecules including sialic acid and phosphorylcholine (ChoP)[123,133,442]. Caspase-4 could function as a secondary line of defence within the host cell, to detect pathogens that can bypass extracellular detection or are able to escape intracellular containment mechanisms. Gene expression of *CASP4* and *IL1B* has also been found to be elevated in individuals with asthma, compared to healthy controls, with higher levels of expression in neutrophilic asthma compared to eosinophilic and paucigranulocytic asthma[55]. Given the association of NTHi presence and neutrophilic asthma, *CASP4* and *IL1B* gene expression induced by NTHi persistence within macrophages could therefore be a key driver in the development of neutrophilic asthma.

Of note, one NTHi strain, ST201, induced lower levels of *CASP4* compared to ST14 and ST408 during infection of MDM. Although *CASP4* gene expression was still upregulated, the lower expression of this gene could perhaps indicate why ST201 was better able to infect and persist within macrophages, as shown in chapter 3 (Figure 3.16). Therefore, while the differences in *CASP4* gene expression were small, alterations in the expression of this gene could be crucial to investigate further given the apparent importance of this gene in regulating the intracellular immune response to NTHi identified by network analysis.

Murine studies have shown that full activation of the murine caspase-4 homolog, caspase-11, depends on recruitment of interferon-inducible GTPases, guanylate-binding proteins (GBPs)[443]. The DEG analysis in this chapter found 7 GBPs to be significantly differentially expressed at both 6 h and 24 h, with *GBP1*, *4* and *5* also present in the blue module gene network. GBPs are able to restrict intracellular pathogens such as *Mycobacterium bovis* BCG and *Listeria monocytogenes* through recruitment of antimicrobial effectors to bacteria-containing vacuoles[444]. GBPs facilitate rupturing of vacuoles, such as those containing *Salmonella typhimurium*, allowing for release of bacterial content, including LPS, into the cytosol for subsequent detection by caspase-4[215]. GBPs can also bind directly to bacteria present in the cytosol, resulting in bacterial lysis[445]. This bacterial lysis could cause activation of other cytosolic sensors through increased presence of bacterial components in the host cell cytosol; increased exposure of NTHi genetic material which would normally be concealed within NTHi could explain the enrichment of the cytosolic DNA sensing pathway at both 6 h and 24 h. Conversely, recent work has demonstrated that GBPs associate with the bacterial surface moments after it has escaped from the vacuole to promote recruitment of caspase-4 without bacteriolysis[216]. Preventing bacteriolysis of intracellular bacteria could be a control mechanism to avert over activation of immune responses that could occur following bacterial lysis. Increased *CASP4* expression in MDM following NTHi infection in this current model could be driven through NTHi interacting with GBPs, however further work will be needed to confirm NTHi-GBP

physical interactions. Importantly, recruitment of GBPs is dependent on live pathogen presence; previous work showed no association between GBPs and pathogens following use of dead or inactivated bacteria[215]. The continual transcriptomic upregulation of GBPs at 6 h and 24 h further suggests that intracellular NTHi remains live and viable for at least 24 h in the model used in this thesis.

Although the data indicate the intracellular location of NTHi in this model, it is not clear how NTHi enters the macrophage, as determining the route of NTHi entry was not a focus of this current work. However, considering the route of entry by NTHi is important as the mechanism of internalisation could govern the outcome of infection and allow enhanced persistence. For example, endosomes produced via lipid raft-mediated endocytosis are differentially trafficked and have been suggested to avoid the endolysosomal pathway completely[413,446]. Use of this particular pathway by NTHi has been previously suggested, with lipid raft inhibitors preventing NTHi invasion of mouse alveolar macrophages[148]. A component of lipid raft-mediated endocytosis is caveolin, for which the *CAV1* gene was upregulated at both 6 h and 24 h in response to NTHi infection. Potential preferential internalisation via an endocytic pathway enabling NTHi to avoid and eventually escape lysosomal degradation could be a mechanism by which NTHi is able to persist within MDM. Although internalisation of pathogens involves rapid changes in cell surface protein levels, it has been demonstrated that decreasing cell surface levels of CD36 was also accompanied by a decrease in CD36 mRNA levels in response to influenza, a well-known intracellular pathogen[240]. Therefore, changes in the expression of genes involved in bacterial internalisation pathways could give an indication as to the potential mechanism used by NTHi to enter and persist within cells.

Following internalisation of bacteria, phagocytes such as macrophages have a sophisticated process of shuttling bacteria-containing compartments to fuse with lysosomes resulting in degradation and subsequent inactivation of bacteria[438]. Maturation of these compartments are characterised by the presence of certain proteins, which can be divided into 'early' or 'late' markers. This current analysis found the gene expression of early markers to be upregulated, whereas the gene expression of late markers were mostly significantly downregulated. This suggests a decreased number of late or mature endosomes/phagosomes within macrophages for which these markers can be recruited to, although this needs to be confirmed at the protein level. Fewer compartments could be present for a number of reasons; firstly, the upregulation of *CASP4* and *GBPs* could indicate the increased presence of NTHi within the cytosol, potentially following rapid escape from within a compartment shortly after initial entry into the macrophage.

Secondly, delaying or inhibiting compartment maturation is a process employed by other intracellular bacteria to facilitate persistence. The causative agent of tuberculosis, *Mycobacterium tuberculosis* (Mtb), successfully inhibits macrophage phagosome maturation by disrupting the interaction of Rab7 and Rab7-interacting lysosomal protein (RILP, a Rab7 effector), which is

important for the fusion of late endosomes and lysosomes[447]. *Neisseria gonorrhoeae* similarly prevents Rab7 and RILP interaction through degradation of LAMP-1 by the *N. gonorrhoeae*-secreted IgA1 protease, which prevents RILP recruitment[448]. LAMP-1 is also targeted by *Burkholderia cenocepacia*, facilitating escape by delaying the accumulation of LAMP-1[449]. In this current work, *LAMP1/2* transcripts were not differentially expressed at either time point. This could be due to the level of constitutive expression of these two genes, as shown by the high number of transcripts measured in both the uninfected and infected macrophages. LAMP-1/2 are major lysosomal proteins accounting for almost half of the total lysosomal membrane proteins and are responsible for maintenance of lysosomal integrity, pH and catabolism[450]. In contrast, LAMP-3 expression can be induced by bacterial infection, LPS or hypoxic conditions[151,450], which may explain the higher fold change in expression levels of *LAMP3* between uninfected and infected MDM compared to *LAMP1/2*. As changes in mRNA expression levels do not indicate whether LAMP-1/2/3 functionally colocalise with NTHi-containing compartments, imaging of LAMP-1/2/3 at 6 h and 24 h would be important to determine whether these proteins play a role in the macrophage response to NTHi.

LAMP3 gene expression was significantly upregulated at both 6 h and 24 h in response to NTHi infection and was present in the blue module gene network. Baddal *et al.* (2015) also found NTHi infection of epithelial cells induced *LAMP3* expression by more than 20-fold[151]. LAMP-3 is an established marker of dendritic cells[451], but the role of LAMP-3 in macrophages has not been fully explored. Transcriptomic analysis of IFN-γ + LPS stimulated macrophages found novel expression of *LAMP3*, suggesting it plays a role in the macrophage inflammatory response[452]. Recruitment of LAMP-3 to *Salmonella*-containing compartments led to increased recovery of *Salmonella typhimurium* from infected THP-1 cells[450]. However as LAMP-3 localised at the cell surface prior to co-localising with intracellular *Salmonella*, it was proposed that LAMP-3 was involved in the initial steps of bacterial invasion rather than bacterial avoidance of the lysosomal pathway, which could account for the decreased *Salmonella* infection detected following LAMP-3 knockdown.

Macrophages appear to have a limited capacity for intracellular killing, with higher MOIs shown to result in reduced intracellular killing and accumulation of intracellular bacteria[453]. This aforementioned reduction in intracellular killing was associated with reduced phagosomal maturation, which the transcriptomic data in this current chapter suggests may also be occurring during NTHi-MDM infection in this model. Therefore the use of MOI 100, a limitation of this study previously discussed in Section 3.3, may potentially be contributing to the impairment of macrophage clearance mechanisms, but this may not be biologically representative of NTHi-macrophage interactions *in vivo*.

Importantly, macrophage phagocytosis is impaired in asthmatics, which could be how NTHi is able to evade the macrophage immune response and establish persistence[454]. Avoiding phagocytosis routes of entry and entering via an endocytic pathway is suggested to enhance persistence and

survival of NTHi[144]. Both alveolar macrophages and monocyte-derived macrophages isolated from severe asthmatics demonstrated impaired phagocytosis of *H. influenzae*[247]. The phagocytic defect causing this impairment is not known, however Liang *et al.* (2014) showed phagocytosis of polystyrene beads was not affected, suggesting that the phagocytic defect was pathogen-specific[247]. Impaired phagocytosis of NTHi was also observed in COPD[250], potentially due to decreased expression of Siglec-1 by COPD alveolar macrophages[455]. Tanno *et al.* (2020) demonstrated that blocking Siglec-1 expression resulted in decreased NTHi phagocytosis, suggesting *in vivo* reductions of Siglec-1 expression could result in diminished NTHi clearance. This current work shows significant upregulation of *SIGLEC1* gene expression at both 6 h and 24 h, although the limitation of this transcriptomic data is that it does not indicate the cell surface expression of Siglec-1. Furthermore, as the macrophages used in this study were from the blood of healthy donors, characterising the expression of Siglec-1 and other receptors implicated in phagocytosis on the surface of alveolar macrophages from individuals with asthma will give a better indication of whether these receptors are differentially modulated in the asthmatic airway compared to healthy controls. The complex asthmatic airway environment may play a role in modulating the cell surface expression of such receptors; studies investigating airway macrophage PRRs found cell surface expression was modified by cigarette smoke and steroids[456,457]. Continual airway presence by pathogens such as NTHi could also contribute to the impairment of macrophage function over time, which may explain the differences in the level of defect observed between severe and moderate asthmatics[247].

Another important function of macrophages is to orchestrate and regulate the immune response upon infection, which includes recruitment and activation of other immune cells[458]. Upregulation of genes encoding for secreted mediators were primarily chemoattractants for T cells, neutrophils and other monocytes/macrophages. In the lung, infected or activated macrophages can recruit other macrophages or circulating monocytes to the site of infection[459]. However, in this current monolayer model, it is possible that outcome of inflammatory mediator release was paracrine signalling, resulting in priming of neighbouring cells to respond to a potential infection. Here, one of the main limitations of this work is apparent; due to use of bulk RNASeq methodology, the transcriptomic data represent the averaged, global expression profile for each sample. As such, it is unclear as to whether diverse macrophage phenotypes were present in an NTHi-infected sample; uninfected macrophages, NTHi-intracellularly infected macrophages and activated, but not infected macrophages could all be present and differentially responding in this model. The transcriptomic profile of macrophages intracellularly infected with NTHi at 24 h could be significantly different to the transcriptomic profile of neighbouring macrophages activated by the release of inflammatory mediators from infected macrophages. Use of single-cell sequencing would be able to confirm this.

Previous work has shown cross-talk between NTHi-infected MDM and autologous T cells[199,234,352]. The influence of NTHi-infected macrophages on T cell recruitment and activation is an important consideration, given the involvement of T cells in the pathogenesis of asthma[460]. The panel of upregulated inflammatory mediator genes in this work suggests macrophages may contribute to a Th1 response, which is not unexpected given the crucial role of Th1 responses in combating an intracellular infection[461]. However, NTHi persistence has been associated with a switch in Th responses to favour Th17 and neutrophilic inflammation[462]. In this current chapter, transcriptomic analysis found upregulation of macrophage genes for neutrophil chemoattractants, including *CXCL8, IL17C* and *CCL20*, which were validated at the protein level, with high amounts of mediators released in response to NTHi. NTHi-infected macrophages could be the cellular source of these chemoattractants *in vivo*, driving the recruitment of neutrophils to the lung. This has previously been postulated by Song *et al.* 2008, who suggested that alveolar macrophages are the cellular source of increased IL-17 in the BALF of asthmatic patients, not Th17 cells[49]. In contrast, Singhania *et al.* (2018) suggested that activated T cells drive an IL-17 response in severe asthma[463]. As NTHi-infected macrophages have been shown to activate T cells *in vitro*[199,234,352], the complex, inflammatory environment in asthma may be driven by dysregulation of macrophage-mediated recruitment and activation of both neutrophils and T cells.

Both CXCL8/IL-8 and CCL20 sputum levels are associated with increased neutrophils in asthmatic patients, but work by Busse *et al.* (2017) found sputum levels of CCL20 were higher in aged patients, who also had significantly longer duration of asthma and poorer asthma control[464]. Unfortunately the microbial colonisation status of patients was not considered, so it is unclear whether NTHi presence was associated with these clinical measures. Nonetheless, despite increasing evidence of the association between NTHi presence and airway neutrophilia in asthma, the mechanistic relationship between the two has yet to be elucidated.

Finally, although NTHi is a bacterial pathogen, various pathways relating to viral infection were found to be significantly enriched in this work, including the 'Influenza A' KEGG pathway. This enrichment could be due to the inherent redundancies and bias that are common during gene ontology analysis[434]. However, the potential enrichment of macrophage anti-viral pathways could have important ramifications for investigating the primary hypothesis of this project. NTHi infection appears to activate similar macrophage transcriptomic pathways that are activated during influenza A infection, which must be considered when further developing the infection model in this work to determine the impact of NTHi intracellular infection on subsequent viral infection.

4.4 Summary

This chapter has used bioinformatic analysis to identify the macrophage transcriptomic response to intracellular NTHi infection. The MDM response is primarily dominated by a core gene expression profile of 863 genes consistently expressed across both 6 h and 24 h, which was functionally enriched in immune response processes, in particular, immune responses to an intracellular pathogen. This intracellular immune response transcriptomic signal was confirmed by two different analyses, WGCNA and DEG analysis, highlighting the strength of the signal in this data set. WGCNA indicated that the macrophage intracellular immune responses were modulated by *CASP4* and *GBPs.* Validation of select genes indicated that MDM responses were conserved during infection with additional clinical strains of NTHi. Despite transcriptomic activation of the macrophage immune response to an intracellular pathogen, NTHi was still able to persist within this model. Therefore, the next chapter will focus on analysis of NTHi gene expression to determine exactly how NTHi adapts during intracellular infection of MDM.

Chapter 5 Transcriptomic analysis of NTHi adaptation during intracellular persistence

5.1 Introduction

The macrophage response to persistent intracellular NTHi infection in the previous chapter was shown to encompass a core transcriptomic upregulation of various immune response pathways. Enriched immune processes included pathways involved in responding to an intracellular pathogen but despite this apparent robust innate immune response, NTHi was still able to persist within macrophages. This chapter will focus on analysing the NTHi dual RNASeq data to specifically determine how NTHi adapts to persist within MDM, by analysing NTHi transcriptomic changes between 6 h and 24 h during intracellular infection. Unfortunately due to financial limitations, it was not possible to include planktonic NTHi samples for sequencing. Therefore, selected NTHi genes identified in the dual RNASeq analysis will be validated by qPCR using planktonic state NTHi, which will be discussed further in this chapter.

5.2 Results

5.2.1 Exploratory data analysis

The NTHi data set provided by Novogene contained 2148 genes. This data set was filtered to remove any lowly expressed genes, which were determined as genes that were not expressed in at least half of the samples (5/10 samples). As a result, 1611 NTHi genes were retained from the starting number of 2148 NTHi genes. The distribution of these 1611 genes was assessed using IQR, hierarchical clustering and principal component analysis (PCA) to ensure no outliers were present.

5.2.1.1 Interquartile range (IQR) versus median exploratory plot

An IQR vs median graph was plotted to visually inspect the spread of data across samples. All samples remained within two standard deviations (SD), indicating that the data distribution does not vary significantly and no samples were identified as outliers (Figure 5.1).

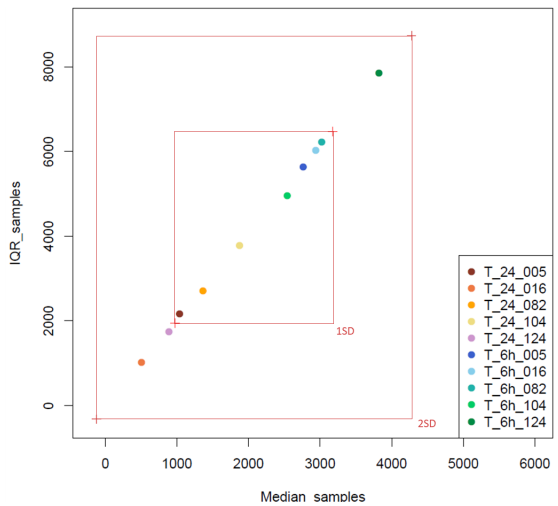

Figure 5.1. Interquartile range (IQR) vs median plot of the pre-normalised, filtered NTHi data. The IQR of each NTHi sample was plotted on the y axis and the median of each sample was plotted on the x axis. The inner red box indicates ± 1 standard deviation (SD), the outer box indicates ± 2 SD

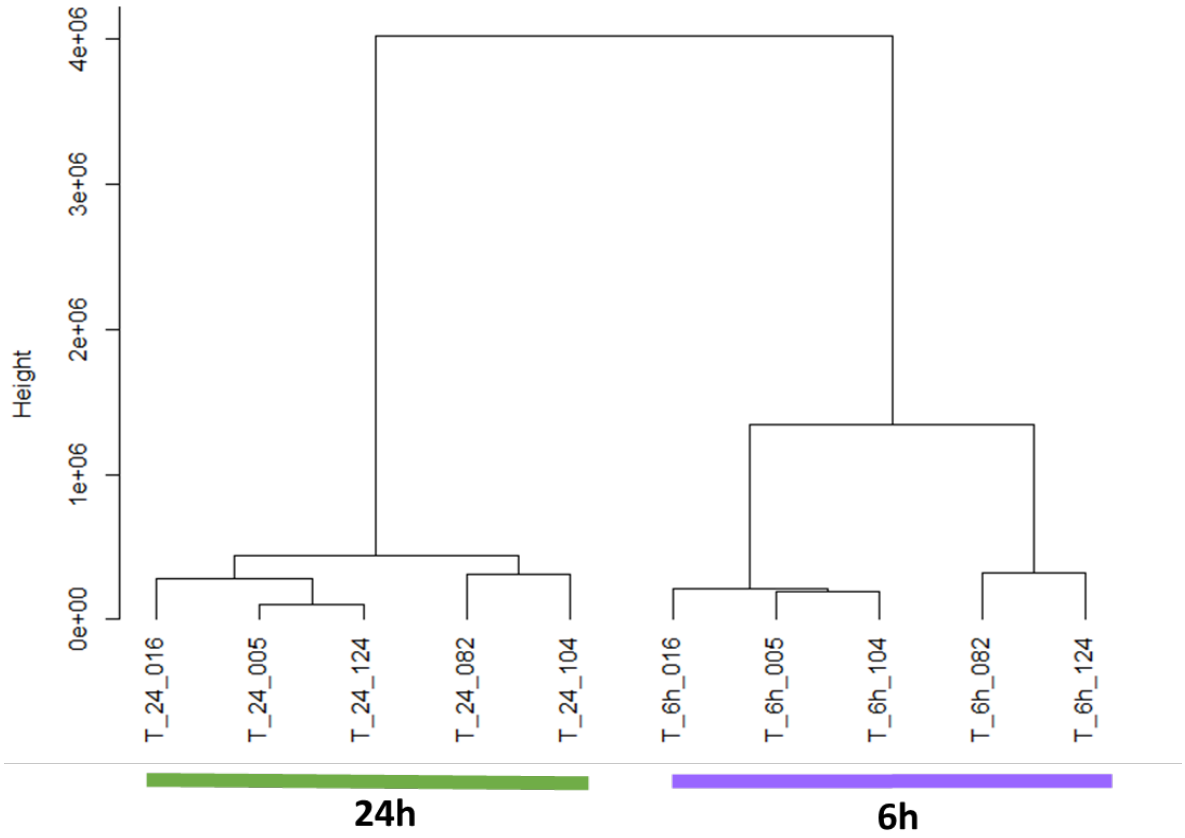

Figure 5.2. Hierarchical clustering of the pre-normalised, filtered NTHi data. Ward linkage and Euclidean distance method was used to construct the clustering. Samples clustered based on time point (6 h samples = purple line, 24 h samples = green line).

5.2.1.2 Hierarchical clustering

Hierarchical clustering of the filtered data was performed using the same parameters used to cluster MDM samples in Figure 4.2 (Euclidean distance and Ward linkage). However, unlike the MDM samples, the NTHi samples clustered based on time point (6 h or 24 h)(Figure 5.2). Again, no outliers were detected using this data visualisation method.

5.2.1.3 Principal Component Analysis

PCA analysis confirmed clustering of samples by time point; two different clusters were visible, being separated by the first principal component (PC1, 94.3%, Figure 5.3A). No donor-specific effect appeared to be present based on PCA clustering (Figure 5.3B).

Together, the visualisation of data distribution and variance demonstrated that although filtering of the data set was required to remove any lowly expressed genes that are uninformative for this analysis, no sample outliers were consistently identified that required removal. Therefore, the data passed to the next stage of analysis with all samples retained in the NTHi data set.

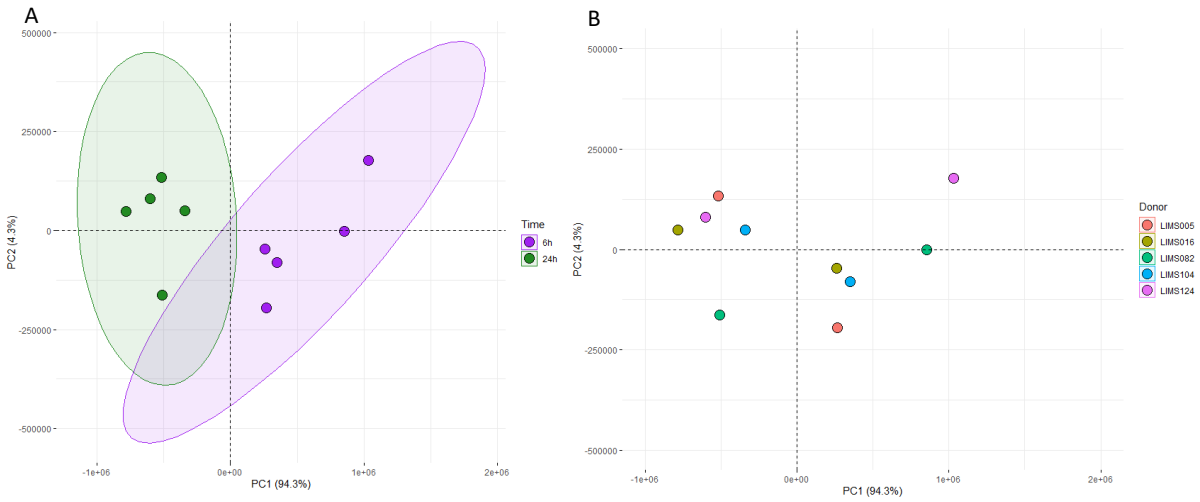

Figure 5.3. Principal component analysis performed on the pre-normalised, filtered NTHi data. The PCA plots are coloured based on overlaid metadata (A) PCA coloured by time point (6 h samples = purple, 24 h samples = green). (B) PCA coloured by each donor as detailed in the accompanying legend.

5.2.2 Data normalisation

The same two Bioconductor packages (edgeR and DESeq2) used to analyse the MDM data were also used for analysis of the NTHi data. Lower number of reads were detected at 24 h, which may have been due to lower presence of NTHi in these samples. Normalisation of the NTHi data set was similar between both packages, with a more even spread of data observed in the boxplots following normalisation (Figure 5.4B & C) compared to pre-normalisation (Figure 5.4A).

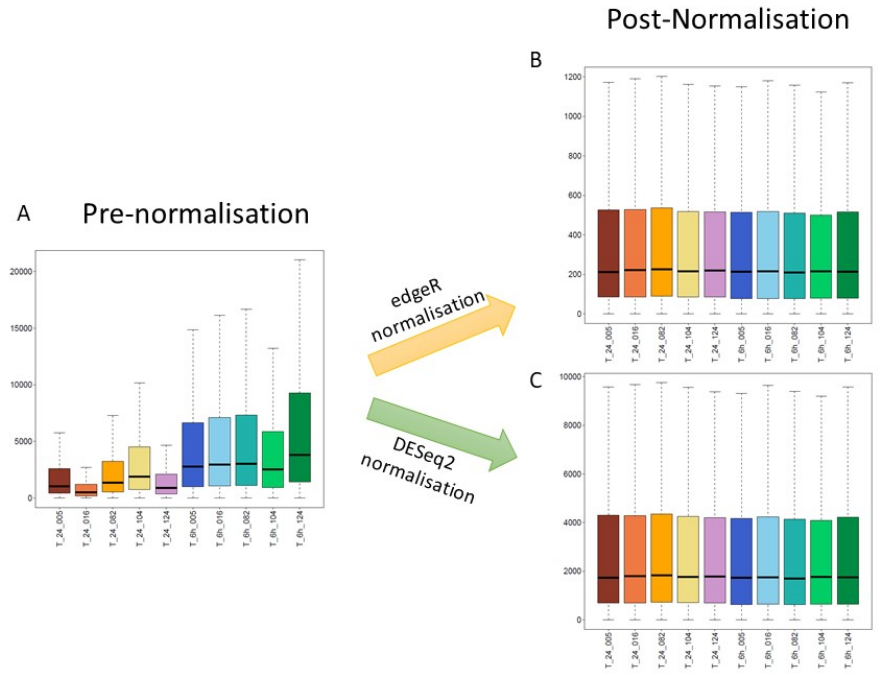

Figure 5.4. Normalisation of the filtered NTHi data. (A) Pre-normalised data, (B) data that has been normalised using the edgeR package, (C) data that has been normalised using the DESeq2 package.

5.2.3 Differential gene expression analysis

The two Bioconductor packages, edgeR and DESeq2, were used to perform differentially expressed gene analysis on the filtered and normalised 1611 NTHi genes, comparing the NTHi gene expression between 6 h and 24 h to investigate changes in expression during intracellular infection. For both edgeR and DESeq2, genes were considered differentially expressed at an FDR adjusted p-value <0.05. Only genes determined as differentially expressed by both packages would be taken forward for further analysis. Out of the normalised 1611 input genes, the total number of genes determined as differentially expressed was 732, with 624 genes (85%) determined as differentially expressed by both methods. No genes were determined as differentially expressed by edgeR only and 108 (15%) genes were determined as differentially expressed by DESeq2 only (Figure 5.5A).

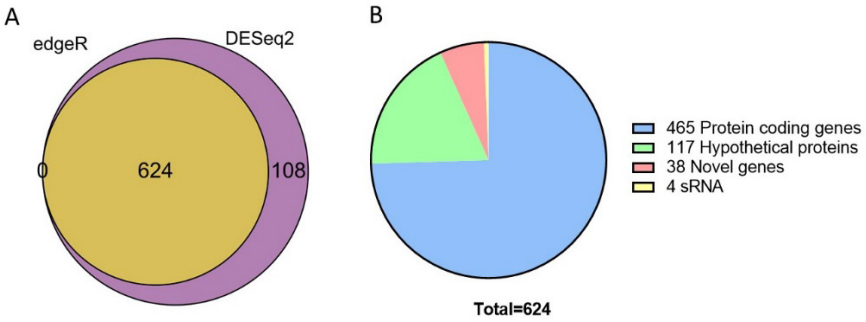

Figure 5.5. Number and type of differentially expressed NTHi genes. Venn diagram showing the overlap of genes that are determined as differentially expressed by edgeR (left), DESeq2 (right) or by both packages (middle). Created using VennDIS v1.0.1. (B) Chart showing the distribution of gene type within the 624 DEG list. Protein coding genes are genes with an assigned annotation name, sRNA = small RNAs, novel genes are novel transcripts not previously identified, and hypothetical protein genes are genes with no known assigned gene name or function.

A

p<0.05	DEG number
FC0	624
FC1	107
FC1.5	28
FC2	4

C

FC1 total genes	107
Upregulated	69
Downregulated	38

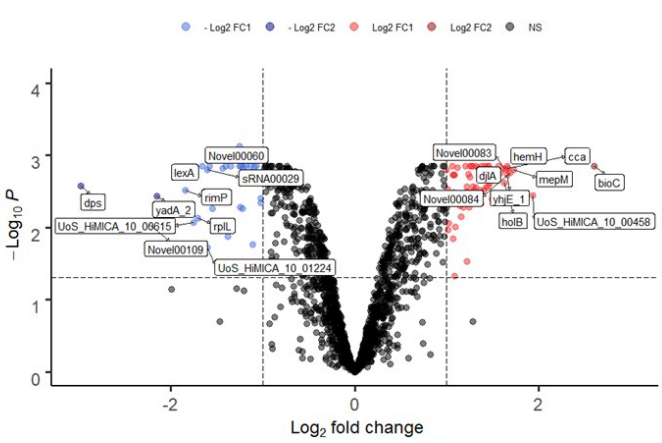

Figure 5.6. Regulation of the NTHi DEGs. (A) Log_2 fold change (log_2 FC) cut offs for NTHi DEGs (FDR p<0.05). (B) The top 10 up and top 10 downregulated DEGs are indicated by labels on the volcano plot. Dotted lines indicate FDR p<0.05 significance value and the log_2 FC 1 cut off; all genes that did not pass both significance measures are represented as black dots. (C) Number of upregulated and downregulated log_2FC 1 DEGs.

Of these 624 genes, the majority of genes (74.64%) were known protein-encoding genes, with 18.62% of genes for hypothetical proteins that currently have no known functional annotation (Figure 5.5B). A smaller number of novel genes (6.1%) were identified, with small (s)RNA making up less than 1% (0.64%) of the genes identified. Unlike the MDM data where numerous genes had high levels of fold change (log_2 FC) in response to NTHi infection, the majority of NTHi gene expression fell between log_2 FC ± 0 – 2. If the same log_2 FC 2 cut off applied to the MDM data set was applied here, only 4 genes (*dps, Novel00109, yadA_2* and *bioC*) would be retained (Figure 5.6A). The top two differentially expressed genes, *bioC* and *dps* had larger changes in expression levels (log_2 FC +2.60 and -2.98 respectively) compared to the other differentially expressed genes (Figure 5.6B). However, to ensure enough genes were present for gene ontology and pathway enrichment analysis, a log_2 FC cut off of 1 was applied, resulting in 107 genes being retained in the NTHi data set. Out of these 107 genes, 69 were upregulated and 38 were downregulated (Figure 5.6C).

5.2.4 NTHi modulation of metabolic processes during intracellular infection of MDM

To determine the biological relevance of these 107 differentially expressed genes, gene list enrichment analysis was performed using ShinyGo. ShinyGo is similar to ToppGene as both perform functional enrichment, however ShinyGo is able to perform functional enrichment analysis of *Haemophilus influenzae* gene lists. The top five significantly enriched Biological Process (BP), Molecular Function (MF) and Cell Component (CC) terms were generic (Figure 5.7 and Table 5.1).

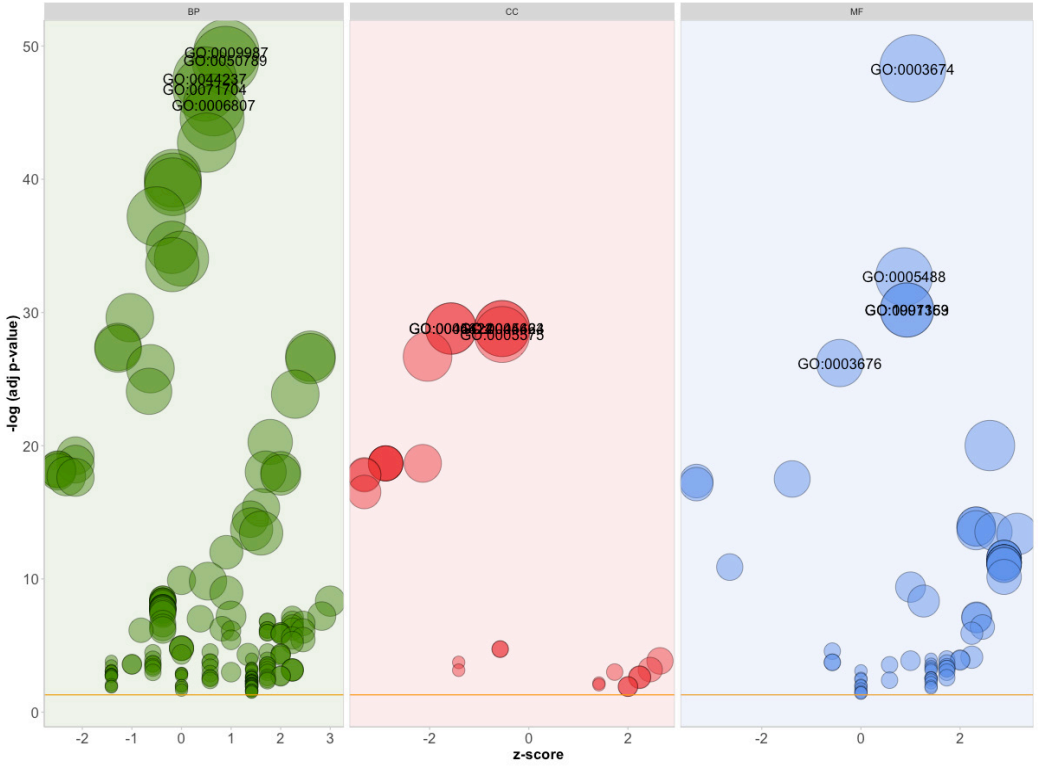

Figure 5.7. Gene ontology analysis of the 107 NTHi differentially expressed genes during infection of MDM. Visualisation of the top significant functionally enriched GO terms for the categories Molecular Function, Biological Process and Cellular component categories. The yellow line indicates 0.05 FDR enrichment p-value, size of dots indicate number of genes present in each term.

Table 5.1. Table of the most significantly enriched NTHi gene ontology terms.This table shows the terms indicated in Figure 5.7, but for clarity, the GO:ID numbers are accompanied with the GO:terms and enrichment FDR value. A maximum of 5 of the most significantly functionally enriched pathways are shown. Colours represent the category in Figure 5.7. Input genes show the number of NTHi genes assigned to each term

Category	GO:ID	GO:Term	Enrichment FDR	Genes in input
GO: Biological Process	GO:0009987	cellular process	2.93E-50	44
	GO:0050789	biological process	1.18E-49	46
	GO:0044237	cellular metabolic process	2.94E-48	41
	GO:0071704	organic substance metabolic process	1.71E-47	41
	GO:0006807	nitrogen compound metabolic process	2.67E-46	38
GO: Cellular Component	GO:0005622	intracellular	1.61E-29	26
	GO:0005623	cell	1.61E-29	31
	GO:0044424	intracellular part	1.61E-29	26
	GO:0044464	cell part	1.61E-29	31
	GO:0005575	cellular component	4.50E-29	31
GO: Molecular Function	GO:0003674	molecular function	4.85E-49	45
	GO:0005488	binding	2.04E-33	33
	GO:0097159	organic cyclic compound binding	6.50E-31	29
	GO:1901363	heterocyclic compound binding	6.50E-31	29
	GO:0003676	nucleic acid binding	6.25E-27	22

Clustering the significantly enriched Biological Process terms identified that the majority of significantly enriched GO terms were in fact metabolic related terms (Figure 5.8). The largest cluster of terms was identified as ‘metabolic process’, which share a high number of genes (edges) with the ‘single organism metabolic process’ cluster, both fairly generic process terms. Enrichment of more specific metabolic pathways were identified with clusters including ‘vitamin biosynthesis’, ‘amino acid metabolism’, ‘nucleoside metabolism’ and ‘fatty acid synthesis’. Enrichment of stress response pathways were also indicated by clusters annotated as ‘stress/stimulus response’ and ‘response to toxic substance’. Processes involved in gene expression and protein synthesis regulation were also enriched, as indicated by the two clusters ‘ribosome biogenesis’ and ‘tRNA/ncRNA processing’.

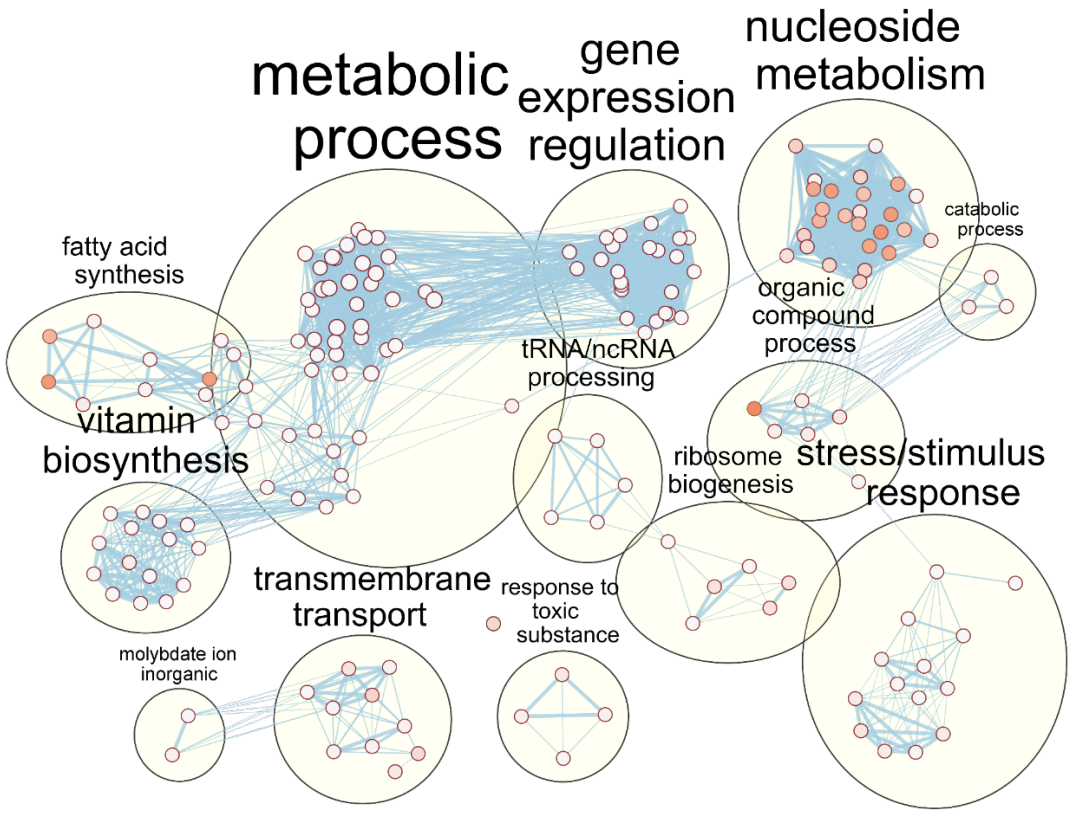

Figure 5.8. Enrichment of NTHi Biological Processes during infection of MDM. Clustering of the enriched Biological Process GO:terms performed using EnrichmentMap and AutoAnnotate in Cytoscape. Nodes represent individual GO:terms, with size relating to the number of genes in each term and the colour indicating enrichment significance. Edges represent connections between nodes that share genes.

Due to the high redundancy and ambiguity surrounding gene ontology terms, the functional role of the 107 DEGs was summarised using the results of the enrichment analysis (Figure 5.9). The highest number of genes (29) were primarily involved in metabolic processes. The remaining genes were involved in regulation of gene expression (23), stress responses (8), virulence (5), replication (5) and protein regulation (2) (Figure 5.9A). The 35 remaining genes were uncharacterised, resulting in no gene name or function available for gene ontology analysis. Of these uncharacterised genes, 22 were hypothetical protein coding genes, 9 were transcripts assigned as novel genes and 2 were sRNA. No clustering of genes according to function was observed, however the data did cluster based on the time point (6 h or 24 h), indicating time dependent gene expression (Figure 5.9B).

The putative function of the 22 uncharacterised hypothetical protein coding NTHi genes was assessed by using the megaBLAST function of the online BLAST suite against the NTHi 86-028NP genome (CP000057.2). All but one gene (*UoS_HiMICA_10_00819*) was detected within the NTHi 86-028NP genome and was assigned an 86-028NP locus tag. The locus tag was then input to the KEGG online search tool to obtain functional information about the gene, if available. As a result, 21/22 uncharacterised genes were given predicted names or functions (Table 5.2).

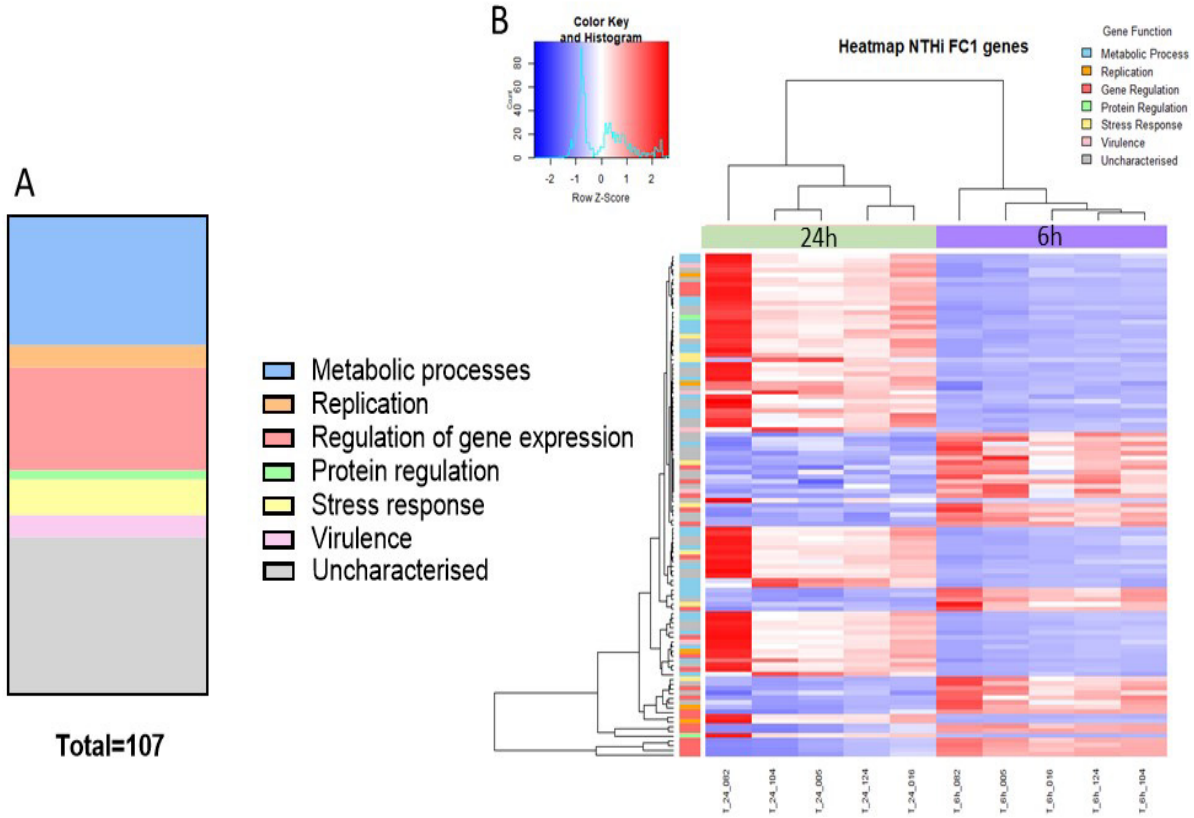

Figure 5.9. Modulation of NTHi processes during infection of MDM. The stacked bar chart highlights the main processes that the 107 NTHi DEGs are involved in. The process with the highest number of genes was metabolic processes (29), followed by regulation of gene expression (23), stress responses (8), virulence (5), replication (5) and protein regulation (2). The remaining genes (35) were uncharacterised (hypothetical or novel gene assignment).

A number of tRNA synthetases were found to be present in the uncharacterised gene list, with two downregulated (*tRNA-Lys* and *tRNA-Met*) and one upregulated (*tRNA-Arg*). The observation of downregulated tRNA is interesting, given not just the role of tRNA in protein synthesis, but also as regulators of the prokaryotic stringent response which is activated by decreased nutrient or substrate availability. Further genes potentially involved in stress responses include *impA* (*NTHI1588*) and *SulA* (*NTHI1379*), with *urvB* (*NTHI1917*) predicted to be involved in DNA repair, which could occur during oxidative stress (Table 5.2). Furthermore, a number of genes potentially encoding for transporter proteins were upregulated, including *sapZ* (*NTHI1396*), which has been implicated in antimicrobial peptide resistance. However, unannotated genes homologous to the NTHi 86-028NP genes *NTHI1325*, *NTHI1330* and *NTHI1331* were predicted to be involved in aerobic metabolism.

Table 5.2. Predicted function of the uncharacterised hypothetical protein coding genes. To determine the putative function of the 22 hypothetical protein genes, the sequence for each gene was compared against the NTHi 86-028NP genome for homologous genes using the megaBLAST function to identify the NTHi 86-028NP (CP000057.2) locus tag which was then used to search for putative functions online using KEGG.

Gene ID	NTHi 86-028NP locus tag	Query cover	Sequence identity	Putative Function	Log_2FC	FDR
UoS_HiMICA_10_00458	NTHI1873	86%	92.62%	probable bacteriophage tail completion protein gpS homolog	1.93	0.004
UoS_HiMICA_10_00452	NTHI1883	100%	95.66%	hypothetical protein	1.55	0.002
UoS_HiMICA_10_00342	NTHI1330	100%	93.54%	conserved hypothetical protein	1.53	0.002
UoS_HiMICA_10_00448	NTHI1888	100%	90.34%	terminase, ATPase subunit	1.43	0.003
UoS_HiMICA_10_00461	NTHI1997	100%	94.61%	predicted Na+-dependent transporters of the SNF family	1.41	0.001
UoS_HiMICA_10_01085	NTHI1917	100%	94.31%	UvrABC system protein B, Nucleotide excision repair	1.38	0.001
UoS_HiMICA_10_00339	NTHI1331	99%	94.96%	conserved FAD/FMN-containing dehydrogenase	1.23	0.003
UoS_HiMICA_10_00795	NTHI1379	100%	95.40%	cell division inhibitor SulA	1.13	0.005
UoS_HiMICA_10_01089	NTHI1915	94%	95.99%	predicted ABC-type transport system, permease component	1.09	0.001
UoS_HiMICA_10_01198	NTHI0490	100%	96.26%	conserved hypothetical protein	1.09	0.002
UoS_HiMICA_10_00453	NTHI1882	100%	94.29%	hypothetical protein	1.08	0.048
UoS_HiMICA_10_00347	NTHI1325	99%	94.45%	transport ATP-binding protein CydC	1.07	0.002
UoS_HiMICA_10_00504	NTHI1396	100%	95.38%	predicted membrane protein sapZ	1.07	0.002
UoS_HiMICA_10_01086	NTHIT0054	100%	100%	tRNA-Asn	1.07	0.014
UoS_HiMICA_10_00545	NTHI1437	100%	98.37%	SH3 domain protein	1.01	0.003
UoS_HiMICA_10_00860	NTHI0339	100%	97.39%	conserved hypothetical protein	-1.02	0.004
UoS_HiMICA_10_01803	NTHI1650	100%	94.13%	conserved hypothetical protein	-1.10	0.001
UoS_HiMICA_10_00819	-	-	-	-	-1.25	0.005
UoS_HiMICA_10_00595	NTHI1588	100%	94.56%	impA peptidase	-1.39	0.001
UoS_HiMICA_10_01837	NTHI1757	91%	90.28%	N4-acetylcytidine amidohydrolase	-1.55	0.005
UoS_HiMICA_10_01224	NTHIT0005	100%	100%	tRNA-Lys	-1.60	0.019
UoS_HiMICA_10_00615	NTHIT0053	100%	100%	tRNA-Met	-1.75	0.009

To further assess the modulation of NTHi metabolic pathways during intracellular infection of MDM, the 29 genes assigned to the metabolic process category were investigated in more detail. These 29 metabolic genes were summarised into 4 distinct metabolic processes: energy metabolism, co-factor and vitamin metabolism, lipid and fatty acid metabolism and metabolite transport (Figure 5.10A). Within the energy metabolism category, genes for aerobic respiration were upregulated, including *rsxC, rsxD, rsxE* and *rsxG*, all genes encoding for a subunit component of the bacterial electron transport complex and *cydD*. NTHi is a facultative anaerobe utilising aerobic respiration, but can switch to fermentation pathways in the absence of oxygen. Upregulation of genes involved in fermentation pathways (*garK, lacC* and *pta*), and metabolite transport proteins (*fruB* and *gntP)* could indicate increased anaerobic respiration/fermentation.

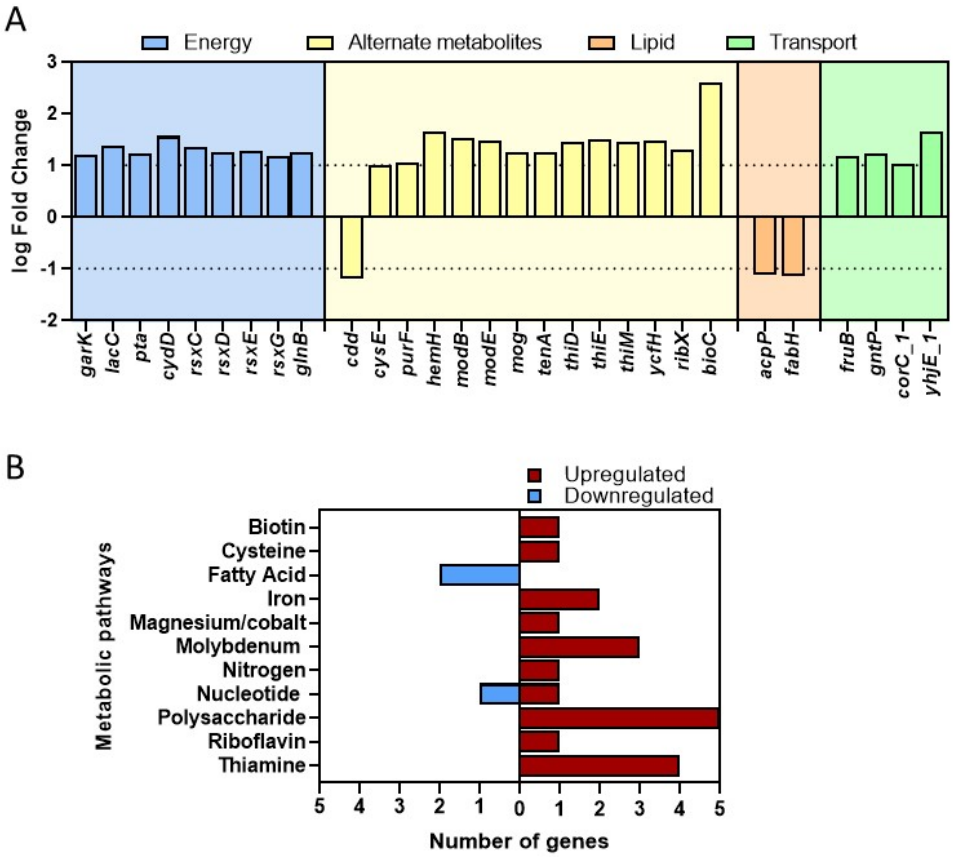

Figure 5.10. NTHi modulation of specific metabolic processes during infection. (A) Overview of the type of role/process of the 29 genes assigned to the metabolic process category. (B) Breakdown of the specific metabolic pathways for the 29 genes, not including the 5 genes involved in the electron transport chain or the one gene which had no specific metabolic pathway assigned. Red = upregulated, blue = downregulated. Dotted line indicates log_2FC 1 cut off.

To determine exactly which alternate metabolic processes the differentially expressed genes were involved in, 23 out of the 29 NTHi metabolic process genes were assigned to a more specific metabolic pathway (Figure 5.10B). The remaining 6 genes not included were the 5 genes previously mentioned as being involved in aerobic respiration and the gene *yhje_1*. Although *yhje_1* was annotated as an 'inner membrane metabolite transport protein', the exact metabolic process this gene is involved in remains unknown. A diverse array of pathways were revealed including vitamin-related pathways including biotin (vitamin B7), riboflavin (vitamin B2) and thiamine (vitamin B1) (Figure 5.10B). These vitamins, along with iron and molybdenum are important constituents of cofactors for various cellular metabolic processes. In contrast, both genes involved in lipid and fatty acid metabolism were downregulated (Figure 5.10A). Upregulation of various vitamin and cofactor-related genes compared to downregulation of lipid/fatty acid metabolism could suggest the increased availability of precursors required for use of certain vitamins and cofactors by NTHi during intracellular infection of MDM.

Table 5.3. Predicted targets of the two differentially expressed NTHi sRNA. The gene targets of the two DE sRNA were assessed by the online tool PresRAT (Predicting small RNAs and their Targets), using the $Pred_{WG}$ function. The reference bacterial genome used was NTHi 86-028NP. All target genes were determined as significantly differentially expressed (all FDR p<0.05), but were below the log_2FC 1 cut off.

Gene ID	NTHi 86-028NP locus tag	Target gene ID in list	Target gene name in list	Putative Function	Log_2FC	FDR
sRNA00003						
tusD	NTHI0709	UoS_HiMICA_10_01564	*tusD*	uncharacterized conserved protein involved in intracellular sulfur reduction	0.92	**0.011**
moaD	NTHI1976	UoS_HiMICA_10_00477	*moaD*	molybdopterin converting factor subunit1	0.73	**0.007**
galK	NTHI0983	UoS_HiMICA_10_00122	*galK*	galactokinase	-0.35	**0.026**
sRNA00029						
tusD	NTHI0709	UoS_HiMICA_10_01564	*tusD*	uncharacterized conserved protein involved in intracellular sulfur reduction	0.92	**0.011**
moaD	NTHI1976	UoS_HiMICA_10_00477	*moaD*	molybdopterin converting factor subunit1	0.73	**0.007**
galK	NTHI0983	UoS_HiMICA_10_00122	*galK*	galactokinase	-0.35	**0.026**
rpmG	NTHI1123	UoS_HiMICA_10_00202	*rpmG*	50S ribosomal protein L33	-0.64	**0.023**
tolR	NTHI0504	UoS_HiMICA_10_00817	*exbD_1*	colicin uptake protein TolR	-0.74	**0.003**

Within the uncharacterised gene list, two sRNAs (*sRNA00003* and *sRNA00029*) were significantly downregulated during infection. The predicted target genes of these two sRNAs were identified using the online tool PresRAT, which predicts sRNA target genes within a bacterial genome using homology based searching[398]. For sRNA00003, three predicted target genes (*tusD, galK* and *moaD*) were identified, whereas five target genes (*tolR*, *tusD, galK, rpmG* and *moaD*) were identified for sRNA00029, with three gene targets (*tusD, galK* and *moaD*) conserved between both sRNAs (Table 5.3). All gene targets were significantly differentially expressed (FDR p<0.05), but expressed varying levels of regulation, with three downregulated and two upregulated target genes. However, these are only predicted targets so further work would be required to confirm the interactions of these sRNA and gene targets.

5.2.5 Modulation of NTHi stress response and virulence genes during intracellular infection

Regulation of virulence factors and stress response pathways are often associated with the ability of bacteria to successfully colonise and adapt to a new environment. A total of 13 NTHi genes were assigned to stress response (8) or virulence (5) categories (Figure 5.11). The only significantly downregulated gene in the virulence category was *YadA_2*, which is a putative trimeric autotransporter adhesion. As previous work[118,119,122,465–467] has indicated the role of NTHi adhesins and outer membrane proteins in virulence and infection, the NTHi data set was examined for other adhesion genes. As the NTHi ST14 genome used for mapping of sequenced reads was a draft genome assembly, it was possible that annotation resulted in assignment of alternative gene names to known NTHi adhesion and outer membrane proteins.

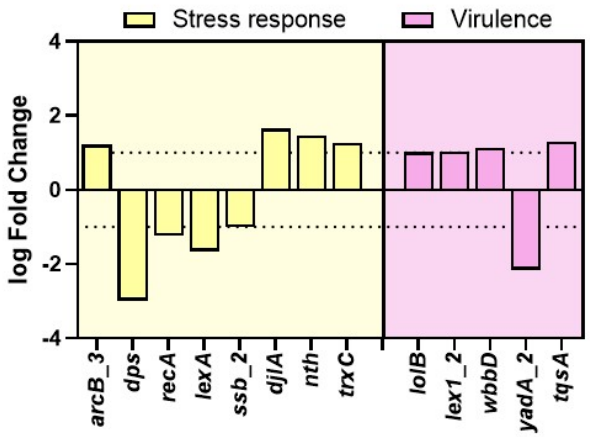

Figure 5.11. NTHi modulation of genes involved in stress response and virulence during intracellular infection. Regulation of differentially expressed genes involved in stress response (yellow) or virulence (pink). Dashed line indicates log_2FC 1 cut off.

To ascertain the presence of adhesins and outer membrane protein, NTHi ST14 gene sequences were compared for sequence identity against a number of known, annotated gene sequences for NTHi adhesins. This identified a number of genes within the NTHi ST14 data set with good sequence homology to known NTHi adhesins and outer membrane proteins (Table 5.4). Only one other NTHi adhesion/outer membrane protein genes, Protein E (*pe*) was significantly differentially expressed (FDR p=0.03) but was below the log_2FC 1 cut off (log_2FC 0.5). The remaining adhesion/outer membrane protein genes were not significantly differentially expressed during intracellular infection of MDM.

Table 5.4 Gene expression of NTHi adhesions and outer membrane proteins during intracellular infection of MDM. The NTHi ST14 genes were checked for sequence identity against known annotated gene sequences (GenBank Accession column) by megaBLAST. All genes were identified with good query cover and sequence identity, confirming the putative role of the ST14 annotated genes. * = genes that were determined as significantly differentially expressed (FDR adjusted p-value <0.05).

Gene	Annotation	Known Gene query	Query cover/ Sequence identity	GenBank Accession	log_2 FC	FDR
UoS_HiMICA_10_00822	*hap*	Hap	85% / 90%	U11024.1	0.17	0.22
UoS_HiMICA_10_00027	*glpQ*	hpd/Protein D	100% / 98%	CP002277.1	0.15	0.64
UoS_HiMICA_10_01205	*hpf*	Hpf/Protein F	100% / 98%	AAZF01000002.1	-0.01	0.94
UoS_HiMICA_10_01479	*ompP1*	omp P1	100% / 93%	CP000057.2	0.25	0.09
UoS_HiMICA_10_01209	-	omp P2	100% / 85%	CP000057.2	0.74	0.21
UoS_HiMICA_10_00023	*hel*	ompP4/lipoprotein e	100% / 98%	M68502.1	-0.17	0.55
UoS_HiMICA_10_00338	*ompA*	omp P5	100% / 91%	L20309.1	-0.27	0.29
UoS_HiMICA_10_01185	-	omp P6	88% / 98%	HM124553.1	0.14	0.59
UoS_HiMICA_10_01395	*pppA*	pilA	100% / 99%	AY816324.1	0.04	0.87
UoS_HiMICA_10_01398	*pilB*	pilB	100% / 96%	AY816324.1	0.35	0.059
UoS_HiMICA_10_01396	*gspF*	pilC	100% / 95%	AY816324.1	0.38	0.13
UoS_HiMICA_10_01398	*pilE*	pilD	100% / 89%	AY816324.1	0.35	0.06
UoS_HiMICA_10_00933	*pe**	Protein E	100% / 95%	CP002276.1	0.51	**0.03**

Other known adhesion genes, *hmw1, hmw2, hia* and *hsf* were not detected in the NTHi ST14 annotated gene list, which was surprising given that approximately 75% of NTHi strains express the *hmw1/2* and the majority of the remaining strains express *hia* or the allelic variant *hsf*. However, within the NTHi ST14 genome annotation file used for mapping sequenced reads was the *Nhha* gene which had sequence identity of 91.78% on the 42% matched query length of *hia* (U38617.2) and identity of 96.85% on 65% matched query length of the allelic variant *hsf* (AY823627.1). Although this suggests presence of a *hia/hsf* homologue annotated as *NhhA* in this particular NTHi ST14 genome, no transcripts were mapped to this gene following dual RNASequencing.

LOS and lipoproteins are also virulence factors required for cell attachment and invasion with genes encoding the biosynthesis of these components (*lolB, lex1_2* and *wbbD*) significantly upregulated at 24 h. However, as well as roles in cell adhesion and attachment, LOS and lipoproteins are integral structural components of the cell wall, protecting the cell from environmental stresses including the host immune response.

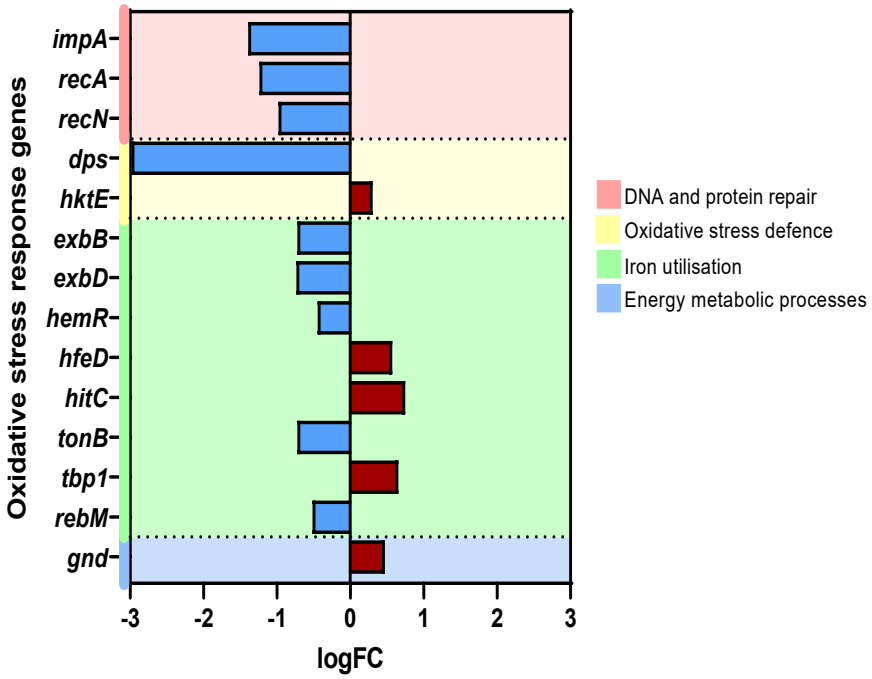

Figure 5.12. NTHi regulation of genes involved in the response to oxidative stress. Only 14/40 genes mined from the study by Harrison *et al.* (2007) who identified upregulated NTHi genes in response to oxidative stress were differentially expressed (FDR $p<0.05$)[468]. Only 3 genes were above the $\log_2$FC 1 cut off (*impA*, *recA* and *dps*). Genes were involved in DNA and protein repair (red), defence against oxidative stress (yellow), iron utilisation (green) and energy metabolism (blue).

Upregulation of *arcB_3*, which encodes for a sensor protein ArcB (Figure 5.11), suggests adaptation of NTHi in response to oxygen levels and Reactive Oxygen Species (ROS) resistance. ArcB is part of the ArcAB two component system with the regulator ArcA which mediates the transition from aerobic to anaerobic metabolism, however, *arcA* was downregulated (-0.44 log_2FC, FDR p=0.007). Also downregulated was the DNA protection during starvation gene (*dps*), a gene also involved in ROS protection. Notably, *dps* was the NTHi gene with the highest fold change difference from 6 h to 24 h (-2.98 log_2FC). Furthermore, two genes encoding for proteins controlling the global bacterial response to DNA damage, the SOS response, were downregulated; *recA* (positive regulator) and *lexA* (repressor). Given that intracellular pathogens are subject to high levels of oxidative stress, the lack of upregulated genes involved in the stress response was investigated further.

The OxyR regulon has been identified to control the expression of genes in response to oxidative stress. Harrison *et al.* (2007) identified a panel of 40 genes upregulated in response to oxidative stress, with 11/40 regulated by OxyR[468]. However in this current work, the global regulator gene, *oxyR*, was not significantly differentially expressed by NTHi (log_2FC 0.05, FDR=0.72). Furthermore, only 3/11 OxyR-regulated genes identified by Harrison *et al.* were upregulated; *gnd*, *hfeD* and *hktE* (Figure 5.12). For the remaining eight OxyR-regulated genes, five genes *(hfeA, hfeB, hfeC, pntA,* and *pntB)* were not significantly differentially expressed (all FDR p>0.05), two genes (*NTHI0705* and *NTHI0684*) were not identified in this data set and the final gene, *dps,* was downregulated, as indicated previously. Genes identified by Harrison *et al.* to be upregulated in response to oxidative stress independent of OxyR were also downregulated in this current work. This included genes involved in DNA and protein repair (*impA, recA* and *recN*) and a number of genes involved in iron utilisation (*exbB, exbD, hemR, tonB,* and *rebM*). In total, 14/40 oxidative stress response genes were differentially expressed by NTHi, with the majority (9/14) downregulated. Although all 14 oxidative response genes were determined to be significantly differentially expressed (FDR p<0.05), only *dps*, *impA* and *recA* were above the log_2FC 1 cut off.

5.2.6 NTHi upregulation of antimicrobial peptide resistance genes

Other than oxidative stress, bacteria have developed systems to combat the antimicrobial host response, of which the *sap* (sensitivity to antimicrobial peptides) family of transporters have been implicated. The gene for a member of this family, *sapZ* was identified as significantly upregulated in the uncharacterised DEG list (Table 5.2). Therefore, the expression of the remaining members of the *sap* operon were investigated. The expression of *sapBCDF* was upregulated, but apart from *sapZ,* the log_2FC values were below the log_2FC 1 cut off (Figure 5.13A). The *sapA* gene was not significantly differentially expressed (log_2FC 0.19, FDR p=0.23). The distribution of transcript expression by NTHi across samples appeared to be fairly consistent for all genes at each time point (Figure 5.13B), suggesting upregulation of the *sap* operon is important during intracellular infection of MDM.

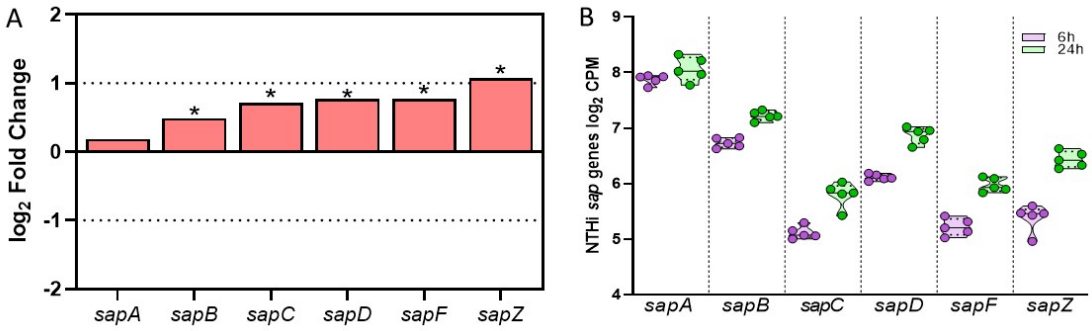

Figure 5.13. NTHi upregulates the gene expression of the antimicrobial resistance sap operon. (A) Log_2FC values of the sap family *sapABCDFZ.* Asterisk indicates genes that were significantly differentially expressed (FDR p<0.05) and dotted lines indicate the log_2FC 1 cut off. (B) log_2 CPM values for each gene at 6 h (purple) and 24 h (green)

5.2.7 NTHi downregulation of ribosomal gene expression during intracellular infection

KEGG pathway analysis was used to determine which specific NTHi pathways were modulated during infection of MDM. As indicated by the Biological Process GO category enrichment of metabolic processes, a number of metabolic KEGG pathways were significantly functionally enriched (Figure 5.14A). The highest number of genes were assigned to the generic 'metabolic pathways' KEGG pathway, with specific pathway terms 'thiamine metabolism' and 'purine metabolism' indicating the type of metabolic KEGG pathways that were determined to be functionally enriched. The enrichment of these pathways, along with the 'microbial metabolism in diverse environments' pathway further indicate the modulation of NTHi metabolic process during infection of MDM. Three of the enriched metabolic KEGG pathways contained a mix of upregulated or downregulated genes, whereas the thiamine and purine metabolic pathways contained all upregulated genes (Figure 5.14B).

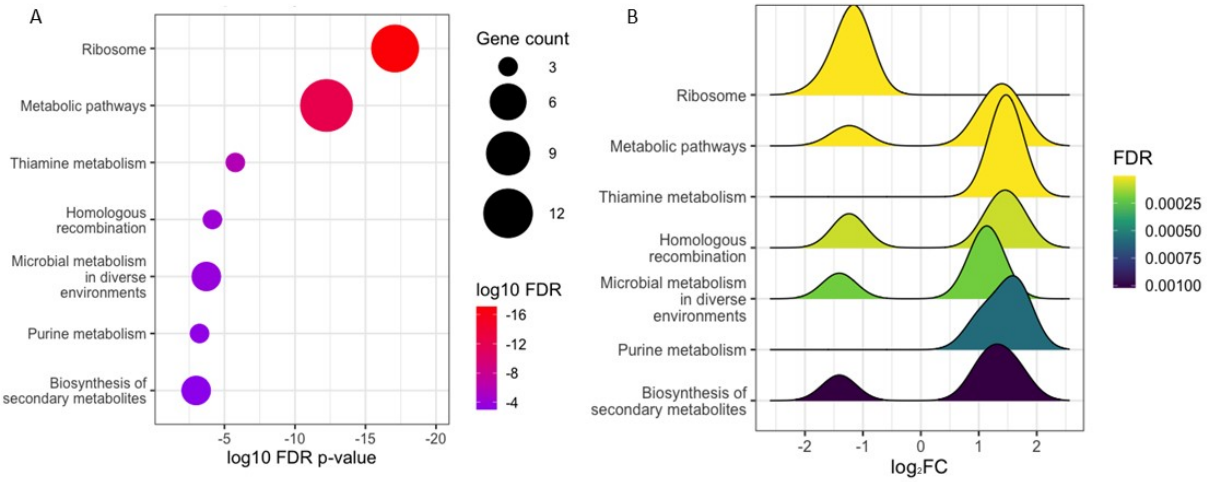

Figure 5.14. Enrichment of NTHi KEGG pathways during infection of MDM. (A) Pathway IDs ordered by enrichment significance (log_{10} FDR) which is indicated by the colour of each dot, with dot size representing the number of genes assigned to each pathway. (B) The expression of genes in the seven enriched KEGG pathways at 24 h. Enrichment performed using ShinyGo.

Table 5.5. NTHi genes assigned to each significantly enriched KEGG functional categories. Table showing the functionally enriched KEGG pathway, FDR and the name of gene assigned to each category.

	KEGG enriched functional category	Name of gene assigned to category	Category Enrichment FDR	Total genes
1	Ribosome	*rplB, rplC, rplD, rplL, rplP, rplV, rplW, rpmC, rpsI, rpsJ, rpsQ,*	8.07E-18	11
2	Metabolic pathways	*bioC, cdd, cysE, dapF, fabH, fruB, hemH, holB, miaA, pta, purF, thiD, thiE, thiM,*	5.82E-13	14
3	Thiamine metabolism	*thiD, thiE, thiM*	1.70E-06	3
4	Homologous recombination	*holB, recA, priA*	7.17E-05	3
5	Microbial metabolism in diverse environments	*cysE, fruB, dapF, pta*	1.94E-04	4
6	Purine metabolism	*hemH, holB, purF*	5.87E-04	3
7	Biosynthesis of secondary metabolites	*miaA, dapF, purF, hemH*	1.02E-03	4

Despite the Biological Processes GO category indicating enrichment of numerous NTHi metabolic processes, the most significantly enriched KEGG pathway was the 'Ribosome' pathway (Table 5.5). All 11 DEGs assigned to this category were downregulated at 24 h (Figure 5.15B). In total, 46 ribosomal protein genes were present in the annotated NTHi gene list, with 37 genes determined as significantly differentially expressed at 24 h (FDR $p<0.05$, Figure 5.15A). However, only 11 of these 37 DEGs (*rplB, rplC, rplD, rplL, rplP, rplV, rplW, rpmC, rpsI,* rpsJ and *rpsQ*) were above the $\log_2$ FC 1 cut off and were subsequently included in the GO and KEGG pathway analysis (Figure 5.15B). Nonetheless, it was clear that during infection of MDM, NTHi globally downregulated ribosomal protein genes.

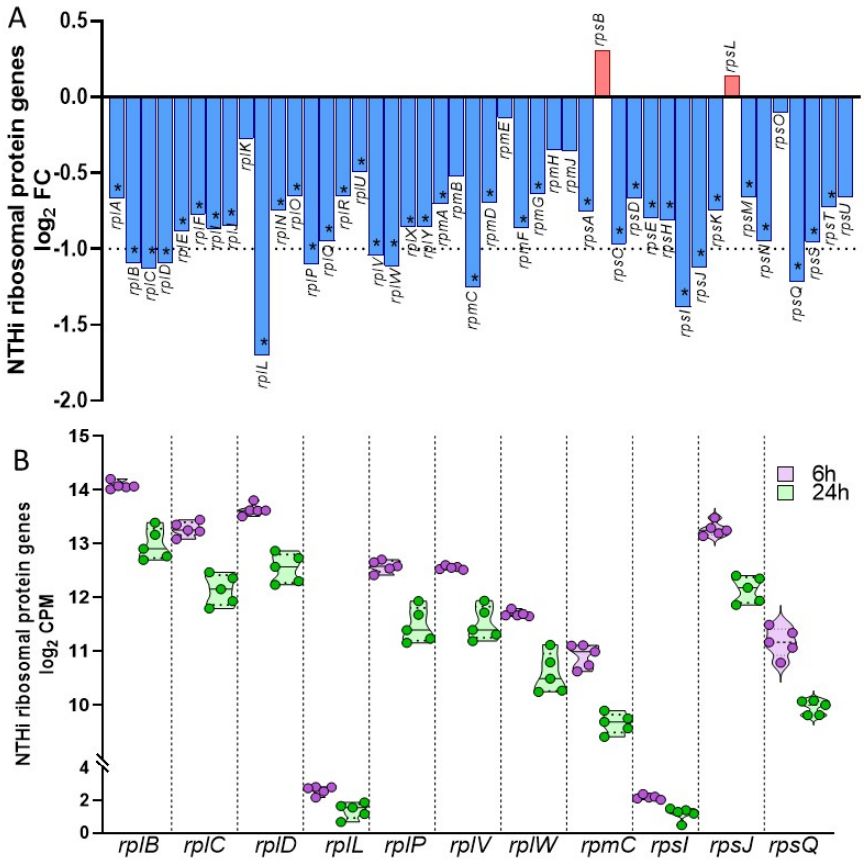

Figure 5.15. Downregulation of NTHi ribosomal protein genes during infection. (A) Log_2 FC values of the 46 ribosomal protein genes detected in the NTHi data set. Dotted line indicates log_2 FC 1 cut off, with asterisk indicating genes (37) that were determined to be significantly differentially expressed at FDR p<0.05. (B) Violin plots of the 11 50S and 30S ribosomal protein genes downregulated by NTHi (log_2 FC 1, FDR p<0.05) between 6 h (purple) and 24 h (green). Dots represent each matched sample and are the log_2 transformed normalised counts per million (CPM) values. Upper and lower whiskers show maximum and minimum values respectively, the middle line is the median and the lower and upper lines of the box plot are the first and third quartile respectively.

5.2.8 Conservation of identified genes across additional clinical strains during intracellular infection of MDM and in planktonic state NTHi

As strains of NTHi are heterogeneous and have been suggested to have different capacities to persist within host cells, it was first assessed whether the expression of the top NTHi genes identified in the dual RNASeq transcriptomic analysis were conserved in additional clinical strains during intracellular infection of MDM at 24 h. The top two upregulated genes, *bioC* and *mepM* and the top two downregulated genes *dps* and *yadA* were chosen to be validated in the MDM model using ST14 and the previously used ST408 and ST201 NTHi strains. The expression of these genes was compared between 6 h and 24 h and expressed as fold change, to mirror the comparison performed in the dual RNASeq analysis.

In agreement with the dual RNASeq analysis, ST14 upregulated expression of *bioC* (FC 1.8, p=0.0156) and *mepM* (FC 2.5, p=0.0313) and significantly downregulated expression of *dps* at 24 h compared to 6 h (FC 0.4, p=0.0156)(Table 5.6). However, no expression of *yadA* was detected for ST14 or the other clinical strains. NTHi ST408 regulated gene expression of *bioC* and *dps* (p=0.0156 and p=0.1, respectively) in the same manner as observed for ST14, however, regulation of *mepM* did not change between 6 h and 24 h (Table 5.6).

In contrast, ST201 significantly downregulated expression of *mepM* between 6 h and 24 h (p=0.0156). As observed for ST14 and ST408, ST201 also downregulated expression of *dps* at 24 h (p=0.0156). Although *bioC* was the top upregulated gene for ST14 in the dual RNASeq analysis, ST201 did not alter the expression of this gene during intracellular infection of MDM.

Table 5.6. Validation of NTHi gene expression using additional clinical strains of NTHi. NTHi gene expression of *bioC, mepM* and *dps* during intracellular infection by NTHi ST14, ST408 and ST201 was measured by qPCR. Expression of gene of interest was normalised to expression of NTHi *rho* gene. Fold change indicates the difference in gene expression between 6 h and 24 h, as was performed in the dual RNASeq analysis. Data were analysed by Wilcoxon signed rank test, statistically significant changes between 6 h and 24 h are indicated in bold.

Gene	Fold Change	p-value
bioC		
ST14	1.8 [1.4 – 5.2]	**0.0156**
ST408	1.9 [1.3 – 3.5]	**0.0156**
ST201	0.95 [0.7 – 1.5]	0.3438
mepM		
ST14	2.5 [1.2 – 3.9]	**0.0313**
ST408	1 [0.9 – 1.5]	0.5625
ST201	0.45 [0.4 – 0.6]	**0.0156**
dps		
ST14	0.4 [0.3 – 0.7]	**0.0156**
ST408	0.5 [0.4 – 0.9]	0.1094
ST201	0.3 [0.1 – 0.4]	**0.0156**

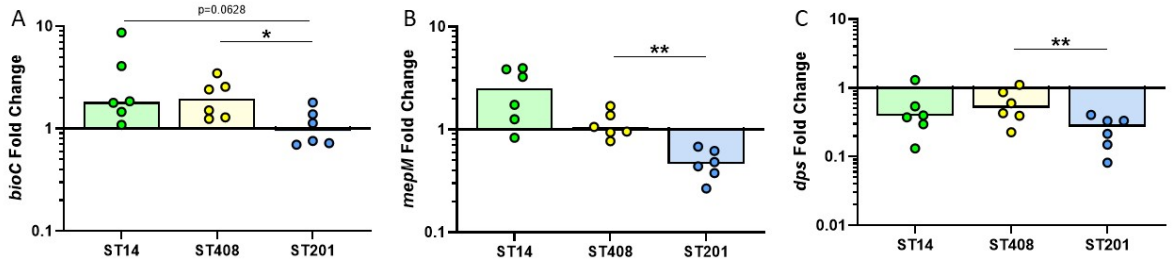

Figure 5.16. The top regulated NTHi ST14 genes were differentially expressed by additional clinical NTHi strains during infection of MDM. MDM were infected as previously described with NTHi ST14 (green), ST408 (yellow) or ST201 (blue) for 6 h, washed for 90 min with gentamicin and incubated in antibiotic free media until 24 h. RNA was harvested from samples at 6 h and 24 h to measure the expression of (A) *bioC*, (B) *mepM* and (C) *dps*. Gene expression was normalised to NTHi *rho* gene and data are shown as fold change in expression from 6 h to 24 h. Graphs show paired data and lines indicate medians. N=6. Data were analysed using Friedman test with Dunn's multiple comparisons; *p<0.05, **p<0.01

When comparing the expression of each gene across the three strains, it was apparent that during intracellular infection of MDM, NTHi ST201 modulated expression of the three genes differently to ST14 and ST408 (Figure 5.16A-C).The disparities in transcriptomic adaptations between NTHi strains during MDM infection could account for the differences in infection levels observed previously (chapter 3, Figure 3.16).

Next, the expression of *bioC, mepM, yadA* and *dps* was measured in NTHi not infecting or associated with MDM, a condition herein known as 'planktonic' state NTHi, in order to confirm that these genes were only differentially expressed during infection. Again, expression of *yadA* was not detected. In contrast, all three genes were upregulated at 6 h compared to planktonic state NTHi ST14. The two upregulated genes *bioC* and *mepM* were more highly expressed at 24 h (p=0.0014 and p=0.0178, respectively), further indicating that the upregulation of these genes were required during ST14 intracellular infection of MDM (Figure 5.17 A & D).

The *dps* gene was more highly expressed by ST14 at 6 h compared to planktonic (p=0.0018), with expression levels decreasing by 24 h (p=0.0954), in line with the fold change decreases detected by dual RNASeq and qPCR validation between 6 h and 24 h (Figure 5.17G). Despite this decrease in expression, *dps* expression levels did not revert back to similar expression levels as planktonic NTHi, further indicating the regulation of these genes during intracellular infection are distinct to planktonic NTHI.

A similar pattern of expression was observed for the other two strains. ST408 differentially expressed *bioC, mepM* and *dps* at 24 h, compared to planktonic NTHi (Figure 5.17B, E & H, respectively). Conversely, ST201 expressed higher levels of *bioC, mepM* and *dps* at 6 h compared to

planktonic (Figure 5.17C, F & I). The *bioC* gene remained elevated at 24 h compared to planktonic, but no differences between 6 h and 24 h were measured, as observed previously (Figure 5.16A). No statistically significant differences in *mepM* and *bioC* expression was measured at 24 h, however expression levels appeared to be lower compared to 6 h. The contrasts between NTHi ST14, ST408 and ST201 gene expression could suggest strain-dependent transcriptomic adaptations result in different mechanisms and outcomes of infection and persistence.

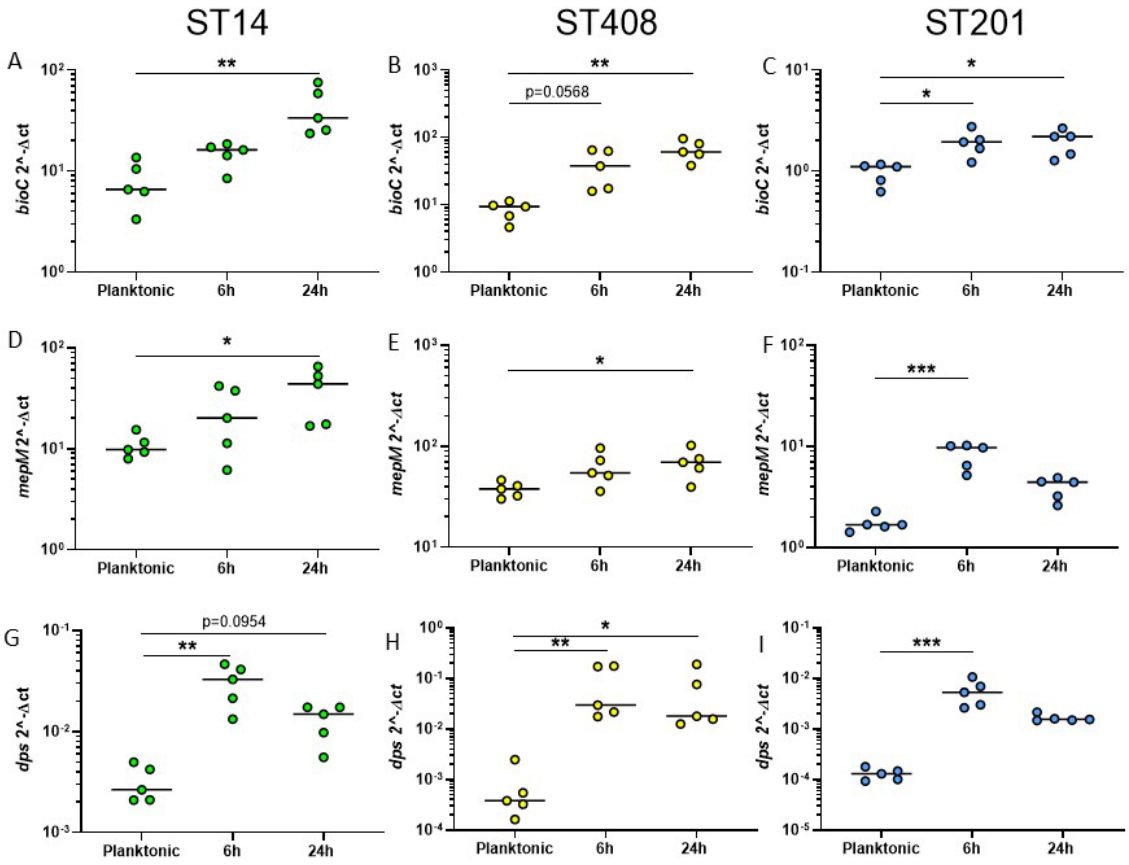

Figure 5.17. NTHi gene expression differs between planktonic NTHi compared to NTHi infecting MDM. MDM were infected with NTHi ST14 (green), ST408 (yellow) or ST201 (blue) as previously described for 6 h, washed for 90 min with gentamicin and incubated in antibiotic free media until 24 h. RNA was harvested at 6 h and 24 h to measure the expression of *bioC*, *mepM* and *dps*. For planktonic NTHi, five independent aliquots of each strain were prepared for infection as normal, but were immediately put in TRIzol. Gene expression was normalised to NTHi *rho* gene. Graphs show unpaired data and lines indicate medians. N=5. Data were analysed using a Kruskal-Wallis test with Dunn's multiple comparisons; *p<0.05, **p<0.01 ***p<0.001.

5.3 Discussion

The mechanisms surrounding NTHi airway persistence *in vivo* are unclear. However, the data presented herein indicates that NTHi transcriptomic changes facilitates persistence within MDM for at least 24 h. Although the amount of NTHi detected slightly decreases between 6 h and 24 h in this work, a significant number of live and viable NTHi were still present by 24 h. This observation is reminiscent of persister cells, whereby a small number of bacteria remain, often in a transient non-growing or dormant state, allowing for proliferation once external conditions or the environment become favourable again[137]. This concept has been demonstrated using a combination of transcriptomic and translational analysis of *Salmonella* intracellular infection of macrophages, which demonstrate *Salmonella* remains metabolically active[469]. The concept of persister cells is often more associated with biofilm growth and antibiotic resistance, however both this current work and that of Stapels *et al.* (2018) demonstrate the ability of pathogens to reside inside immune cells to evade the immune response and antibiotic treatment[469]. *H. influenzae* has previously been demonstrated to shield from antibiotics by residing between lung epithelial cell layers[145]. The presence of persister NTHi cells could account for the ineffectiveness of antibiotic therapy in those with chronic respiratory disease who display a persistent or recurrent NTHi infection[348,470,471]

Although the *Haemophilus influenzae* genome was the first bacterial genome sequenced[472], a number of genes remain uncharacterised and have been assigned predicted functions based on computational and protein prediction analyses. As such, it is possible that uncharacterised genes with no assigned GO or KEGG pathway could alter the outcome of gene ontology analysis if they were functionally annotated and included in the analysis. To try to overcome this, the 22 uncharacterised hypothetical protein genes that were significantly differently expressed (FDR $p<0.05$ and $\log_2$ FC 1) were manually inspected to determine putative functions. It was important to consider the potential functions of these 22 uncharacterised genes, considering that they make up just over 20% of the number of NTHi differentially expressed genes.

The functions of the 22 genes appeared to mirror the enrichment analysis performed on the annotated gene list. A number of genes involved in metabolism, specifically aerobic respiration, were significantly upregulated. Furthermore, genes involved in the stress response and DNA repair processes were differentially expressed, including a number of tRNA. The potential modulation of tRNA could indicate changes in NTHi protein synthesis, which could occur following activation of the stringent response. Activation of the NTHi stringent response during intracellular infection was also suggested by enrichment of genes involved in amino acid biosynthesis pathways and ribosome biogenesis. However, as predicted functions of these uncharacterised genes have not been confirmed or validated, they were not included within the main gene ontology analysis, but can be tentatively discussed within the context of the main findings of the GO and KEGG analyses.

The first stage of NTHi infection and establishing persistence, is adherence to host cells in the respiratory tract. Although multiple studies have identified adhesins and outer membrane proteins to be crucial in promoting attachment to and invasion of host cells[118,120,122,133,467,473,474], the expression of a number of these genes were not significantly differentially expressed at 24 h. This is likely due to the time point used in this work; NTHi was residing intracellularly between 6 h and 24 h, so continual expression of proteins required for attachment to host cells could be energetically expensive and therefore no longer required. Although an earlier time point would have be better suited to assess the transcriptomic regulation of genes involved in attachment and entry of NTHi into cells, the main aim of this work was to determine how NTHi adapts once residing intracellularly.

Modification of outer membrane protein expression has been observed *in vivo*, with NTHi strains serially isolated from patients with COPD exhibiting decreased expression of the HMW1/2 protein over time[475]. A high level of HMW1 or HMW2-specific antibodies were detected in patients, suggesting that the selection pressure for NTHi expressing lower levels of HMW1 or HMW2 resulted in more persistent strains[475]. In this current work, the presence of *hmw1/hmw2* genes were not detected in the NTHi ST14 genome. Instead, adhesion in the respiratory tract may be mediated by expression of the *Hap* or *NhhA* genes, the latter of which was found to have partial sequence identity to *hia* and the allelic variant *hsf*[372]. The duration of lung colonisation of NTHi ST14 prior to its isolation is not known. ST14 could have modulated expression of outer membrane proteins, resulting in changes in the genome sequence of certain genes due to the selective pressures during *in vivo* airway colonisation.

The lack of outer membrane protein and adhesin gene expression during intracellular persistence in this current work could be a crucial finding in regards to therapeutic development. Downregulation, modification or simply lack of expression of these proteins during intracellular residence could result in reduced vaccine efficacy against specific adhesins or outer membrane targets identified as potential NTHi vaccine candidates, in those already chronically colonised with NTHi[421,465]. Therefore, identifying conserved proteins that are crucial for early colonisation of the airway by NTHi may improve vaccine efficacy. As this current work only concerns the transcriptomic regulation of NTHi outer membrane protein genes, it would be of interest to characterise the expression and structure of these proteins during persistent infection *in vitro* and *in vivo*.

One outer membrane protein, *yadA*, was determined to be significantly downregulated in the dual RNASeq analysis, but expression of *yadA* could not be detected by qPCR. A technical reason could explain the lack of detection for this gene. Brief *in silico* analysis of the primer/probe design supplied by Applied Biosystems indicates that the melting temperature of the probe may be incompatible with the protocol setup. As such, more work and optimisation of primer design will be required to validate the expression of *yadA* by NTHi during infection.

Following entry into cells, bacteria are faced with a hostile environment. Metabolic changes are often associated with adaptation of pathogens to persist within an intracellular niche[476]. Baddal *et al.* (2015) used dual RNASeq to investigate NTHi-epithelial cell interactions and also found alterations in metabolism, indicating changes in the availability of host substrates[151]. The transcriptomic analysis in this current chapter highlights a number of genes involved in various metabolic pathways to be modulated between 6 h and 24 h infection. The *bioC* gene displayed the highest level of upregulation in the NTHi data set. Encoding for an O-methyltransferase, *bioC* is involved in generating the pimeloyl acyl carrier protein (ACP) by the fatty acid synthesis pathway and can be used as a precursor for biotin synthesis (also known as vitamin H or B7)[477].

A recent study has shown the ability of the fungal *Candida* spp. to acquire biotin from the host, despite low levels of biotin present in the macrophage phagosome, indicating that biotin is a limited intracellular resource[478]. Pathogens able to scavenge or generate biotin in biotin-restricted environments could therefore be more suited to survive in an intracellular niche. This hypothesis is supported by the discovery that *Mycobacterium* spp. possess a *de novo* biotin synthesis pathway, which when absent, reduces the intracellular fitness of the pathogen[479]. The importance of biotin synthesis and intracellular survival is further demonstrated by the requirement of biotin for the bacteria *Francisella tularensis* escape from phagosomes[480]. The previous chapter detailing MDM transcriptomic changes during NTHi infection highlighted a lack of upregulation of late endosome and phagosome macrophage markers, suggesting a similar mechanism of NTHi subversion or escape from early phagosomes. This escape could be dependent on NTHi biotin biosynthesis regulated by *bioC*, which may explain the significant increase in the expression of this gene during intracellular infection. However the lack of late endosomes and associated markers would need to be determined at the protein level. Using a method such as confocal microscopy to assess presence of early or late markers would also allow visualisation of NTHi co-localisation with specific early/late markers, to better determine the functional role of phagosome and endosome maturation during NTHi infection.

As biotin synthesis pathways are absent in humans, components of the biotin synthesis pathway could be attractive targets for therapeutics against intracellular pathogens. All three clinical NTHi strains expressed higher levels of *bioC* compared to planktonic state NTHi, further indicating the importance of this particular gene for NTHi infection. Although ST201 did not upregulate expression of *bioC* further at 24 h, the initial increase in gene expression suggests *bioC* is an important gene for the early events of infection and adaptation to persistence. However, the importance of biotin, and particularly *bioC*, for NTHi intracellular survival needs to be explored further using NTHi *bioC* mutant knockouts, to determine whether NTHi intracellular persistence changes depending on the ability of NTHi to scavenge host biotin.

The intracellular environment of host cells is only available as a niche for those bacteria able to adapt to unfavourable conditions, such as changes in nutrient or oxygen availability. During intracellular infection of MDM, NTHi appeared to upregulate genes for both aerobic and anaerobic (fermentation) respiration. Although this appears contradictory, NTHi can metabolise carbon sources through a process called respiration-assisted fermentation[481]. Respiration-assisted fermentation has been suggested to contribute to NTHi pathogenesis through degradation of host immune compounds[481]. The ability of NTHi to utilise multiple respiration pathways highlight the adaptability of this pathogen to different oxygen and metabolite levels present in the human respiratory tract and within host cells. However, the transcriptional profile between different *H. influenzae* strains varied in the presence of differing oxygen levels[422]. This observation highlights an important consideration for this current work; NTHi strains may differentially adapt to intracellular residence within MDM and therefore sequencing of additional strains would better identify conserved metabolic pathways or genes regulated during intracellular infection of macrophages.

Furthermore, the two differentially expressed sRNA in this study were predicted to target a number of metabolic genes, suggesting the function of sRNAs in regulating metabolic processes during infection could be an important consideration. However, as the determined gene targets were predicted, further work would be required to confirm the role of these sRNAs in gene expression regulation. Conversely a role for sRNAs in modulating the host immune response, rather than bacterial gene expression has also been found. Packaging of a *P. aeruginosa* sRNA into secreted bacterial outer membrane vesicles (OMVs) attenuated IL-8 secretion in human airway cells and limited neutrophil recruitment in a murine model[482]. Although pathogen OMVs trigger activation of immune responses by host cells, packaging sRNAs into OMVs may be a mechanism allowing for circumvention of this host response to facilitate enhanced bacterial survival.

Other than modulation of metabolic pathways, transcriptomic changes associated with persistence included modulation of NTHi ribosomal protein genes. All 11 ribosomal protein genes assigned to the most significantly enriched ribosome KEGG pathway were downregulated. Further inspection of the NTHi data set found 37 ribosomal protein genes in total were determined to be significantly downregulated by 24 h (FDR $p<0.05$). These 37 genes were all determined to be differentially expressed by significance (FDR $p<0.05$), however only 11 of these were above the $\log_2$ FC 1 cut off originally applied to the data set. Other pathogens including *Bordetella pertussis* and *Leishmania* also downregulate ribosomal proteins or modulate ribosome biogenesis pathways during intracellular infection of macrophages[483,484]. Although functional work is required to confirm the transcriptional analysis indicating that NTHi downregulates ribosomes during intracellular infection, this could be a mechanism of defence against antibiotics, particularly antibiotics targeting protein synthesis.

Downregulation of ribosomal proteins is a component of the stringent response, which is activated by bacteria during times of stress such as nutrient limitation[485]. The stringent response is important in diverting processes away from growth and division to amino acid biosynthesis until external nutrient conditions improve[485]. This mechanism involves two regulatory processes; i) downregulation/repression of genes involved in translation, such as ribosomal protein genes and ii) upregulation of genes in metabolic pathways, particularly genes involved in amino acid biosynthesis[486]. This current work has found evidence of both regulatory processes occurring, suggesting activation of the NTHi stringent response during intracellular infection of MDM.

The role of the stringent response does not appear to as be heavily investigated in NTHi compared to other bacteria. However, the response is conserved amongst bacteria, with the proteins Rel/Spo homolog proteins (known as RSH proteins) have been identified to play a central role in the stringent response[487]. Mycobacteria studies indicate that there is a bistable expression (or phase variation) of Rel across the whole mycobacteria population during nutrient starvation growth conditions[488]. Bistable Rel expression resulted in two different bacterial cell populations which either express a high level of Rel and exhibit a persister cell phenotype or express a low level of Rel and are more likely to be proliferating[488]. The presence of two (or more) different NTHi populations within MDM could result in the transcriptomic changes occurring in each population being missed or averaged during the bioinformatics analysis, due to the bulk sequencing nature of this project. Nonetheless, as the central component of the stringent response, Rel, has been shown to control the emergence of Mtb persister cells and adaptation to an intracellular niche, further investigation of the stringent response during NTHi persistence could better identify NTHi persister cell phenotypes.

Bacteria have developed a repertoire of stress response genes that can be modulated during times of cellular stress to enhance survival. In this current work, NTHi modulated the expression of several different stress response genes, with the *dps* gene exhibiting the highest decrease in log_2FC expression at 24 h. This gene encodes for a DNA protection during starvation protein, and has been suggested to play a role in protecting NTHi from oxidative stress, with NTHi *dps* deletion mutants more sensitive to hydrogen peroxide[489]. The downregulation of *dps*, and a number of genes previously identified by Harrison and colleagues to be upregulated in response to H_2O_2-induced oxidative stress[468], in this current work suggests that NTHi was subject to lower levels of oxidative stress at 24 h, again potentially indicating escape of the bacteria from macrophage intracellular killing mechanisms. This observation could be related to downregulation of macrophage genes involved in maturation of endosomal/phagosomal compartments at 24 h, as indicated in the previous chapter.

Although *dps* was expressed more highly at 6 h compared to planktonic state NTHi, expression levels decreased by 24 h. The expression of *dps* has shown to be crucial for NTHi biofilm growth *in*

vitro[100,490] , a type of growth that does not seem to be occurring in this current model, hence the downregulation of this gene during intracellular infection. The importance of *dps* regulation for NTHi biofilm growth was identified by Pang and colleagues (2012), who also identified upregulation of 25 other genes associated with bacterial-stress response and anaerobic metabolism during biofilm growth[490]. In contrast this current work identified 13/25 of these biofilm-associated genes to be statistically significantly downregulated between 6 h and 24 h infection of macrophages. Of these 13 genes, 4 were above the log_2FC 1 cut off (*impA, rplL, rplP* and *rplD*), whereas the remaining 9 genes (*rpsC* FC -0.97, *clpB* -0.9, *rplJ* -0.85, *dnaK* -0.62, *groS* -0.57, *groL* -0.5, *focA* -0.5 and *rplU* -0.5), were below this fold change cut off. The remaining 12 genes identified by Pang and colleagues (2012) were not significantly differentially expressed. Intracellular infection of macrophages appears to result in a gene expression profile that is distinctive from transcriptomic changes during biofilm growth. However this is only speculative, as confirming differences between planktonic, intracellular and biofilm growth states requires direct comparative experimental work, especially given the observed strain-dependent expression of small number of genes in this work. Nonetheless, identifying NTHi genes crucial for NTHi intracellular persistence *in vitro* and *in vivo* is important, as establishing the importance and conservation of genes during NTHi infection could result in identification of novel antibacterial therapeutic targets.

Other than production of ROS, macrophages can produce antimicrobial peptides in response to infection. Bacteria, including NTHi, have developed effective mechanisms to combat this host response, such as the antimicrobial resistance Sap system encoded by the *sap* operon *sapABCDEFZ*[491]. One of these genes, s*apZ,* was identified in the uncharacterised gene list as significantly upregulated during infection ($p<0.05$ and $> log_2$FC 1), therefore it was of interest to investigate whether the remaining components of the *sap* operon were also differentially regulated. The role of the *sap* operon in antimicrobial resistance was first identified by Groisman *et al.* (1992) in S*almonella*[491]. Mason *et al.* (2005) showed that SapA-deficient NTHi were less likely to persist in the middle ear of a chinchilla model of OM[492], with further work also implicating SapD in enhanced survival *in vivo*[493]. In this current work, *sapA* was not significantly differentially expressed, whereas the remaining *sapB-F* genes were all significantly upregulated at 24 h (all $p<0.05$, but below the log_2FC 1 cut off). Although functions have been described for sapA-F, the function of sapZ is currently unknown[494]. As *sapZ* was the highest significantly upregulated gene of the *sap* operon, further functional work to identify the role of *sapZ* in antimicrobial resistance and intracellular persistence of macrophages is needed.

The second most upregulated gene at 24 h in this current data set was *mepM*, which encodes for a murein/peptidoglycan endopeptidase. Endopeptidases are responsible for incorporation of peptidoglycan into the bacterial cell wall, which is crucial not just for bacterial growth and replication, but also cell viability. Previous work has shown that endopeptidase-deficient E.coli

mutants subjected to stressful conditions undergo rapid cellular lysis[495]. Furthermore, upregulation of genes for macrophage GBPs were identified; these proteins have been shown to directly interact with cytosolic bacteria for recruitment of caspase-4 or for bacteriolysis. Upregulation of not only *mepM,* but *lolB, lex1_2* and *wbbD* could suggest NTHi defence against host immune mechanisms that target the cell wall of bacteria. All three NTHi strains had higher expression levels of *mepM* during infection compared to planktonic state NTHi. Therefore, identifying the role of *mepM* in NTHi infection and intracellular persistence both *in vitro* and *in vivo* could mean it is a novel target for antibacterial therapeutics.

Although this work has attempted to validate the results of the dual RNASeq transcriptomic analysis in planktonic, non-infecting NTHi using qPCR, one of the main limitations of this analysis is the absence of sequenced planktonic comparisons. As previously mentioned, due to financial limitations, it was not possible to include planktonic NTHi samples for sequencing. If planktonic, non-infecting NTHi samples were also sequenced, the validity of the transcriptomic changes associated with intracellular infection would be strengthened. Rather than investigating the expression of only three genes, the global transcriptomic profile between planktonic NTHi, intracellular NTHi at 6 h and intracellular NTHi at 24 h would be compared, to allow for more in depth analysis of gene expression changes associated with intracellular infection. Although this current work indicates how NTHi adapts to intracellular residence between 6 h and 24 h, sequencing planktonic NTHi may have allowed for assessment of gene changes between planktonic and 6 h NTHi, to give a clearer indication of how NTHi initially attaches and enters into the macrophage.

5.4 Summary

This chapter has used bioinformatic analysis to identify transcriptomic adaptations of NTHi during intracellular infection of MDM. NTHi modulates expression of numerous metabolic pathways, stress response genes and ribosomal protein genes during intracellular infection of MDM. Validation using planktonic NTHi indicated that changes in gene expression were associated with intracellular infection of macrophages. However, the regulation of genes was not conserved across multiple clinical strains, suggesting that differences in transcriptomic adaptation during intracellular infection of MDM could explain how some strains are better able to persist in the airway. As the current and preceding chapters have successfully characterised MDM-NTHi interactions during intracellular infection, the next chapter will adapt this infection model further to address the second hypothesis of this work. As such, the next chapter will incorporate the influenza A virus into the NTHi-MDM infection model to investigate whether prior infection of MDM by NTHi influences the progression of IAV infection.

Chapter 6 The impact of NTHi and IAV co-infection of MDM

6.1 Introduction

Although bacterial respiratory tract infections contribute to asthma exacerbations, virally driven exacerbations account for up to 80% of all asthma exacerbations, with RSV, rhinovirus and influenza the most commonly implicated viruses[1,67,70,496] The rise in the number of studies using 16s rRNA sequencing has resulted in an enriched understanding of the lung microbiome, allowing for differences in microbiome composition to be determined not only between healthy individuals and those with chronic lung disease, but during different periods of disease. Potentially pathogenic bacteria, such as NTHi, are not only recovered during exacerbations, but also during stable periods of disease[65,86]. As such, it is becoming apparent that viral respiratory tract infections occur in the presence of colonising airway bacteria. Despite this new wealth of knowledge, it is not clear whether the microbiome and colonising respiratory tract bacterial pathogens modulate the host response or influence the progression of a respiratory tract viral infection.

The data in this thesis so far has demonstrated that NTHi intracellular infection of MDM results in transcriptomic adaptations of both host and pathogen, which could indicate how NTHi is able to persist within the respiratory tract. Although macrophages are important in viral control and clearance, they are also a target of Influenza A virus (IAV) in the airway[278,351]. Therefore this chapter will adapt the previously utilised NTHi-MDM infection model in order to explore IAV infection of NTHi-infected macrophages, to model the dynamics of host-pathogen co-infection in the airway.

6.2 Results

6.2.1 Adaptation of an NTHi-MDM infection model for NTHi-IAV co-infection

6.2.1.1 Model of NTHi-IAV co-infection of MDM

In order to investigate the response of NTHi infection on the MDM response to a subsequent IAV infection, the MDM infection model first required adaption. Briefly, MDM were infected with NTHi at MOI 100 for 6 h as previously described. At the original 24 h infection endpoint, MDM were infected with 3.6 x 10^4 PFU/ml H3N2 Wisconsin IAV for 2 h, an infectious dose similar to that used by Watson *et al*. (2020), which resulted in a 24% median MDM infection[497]. Extracellular IAV was removed and cells were washed to remove excess IAV, before MDM were cultured for a further 22 h to allow for viral replication. Respective uninfected or single pathogen only controls were included for all co-infection experiments. For clarity, a graphical workflow of the adapted infection model is depicted in Figure 6.1.

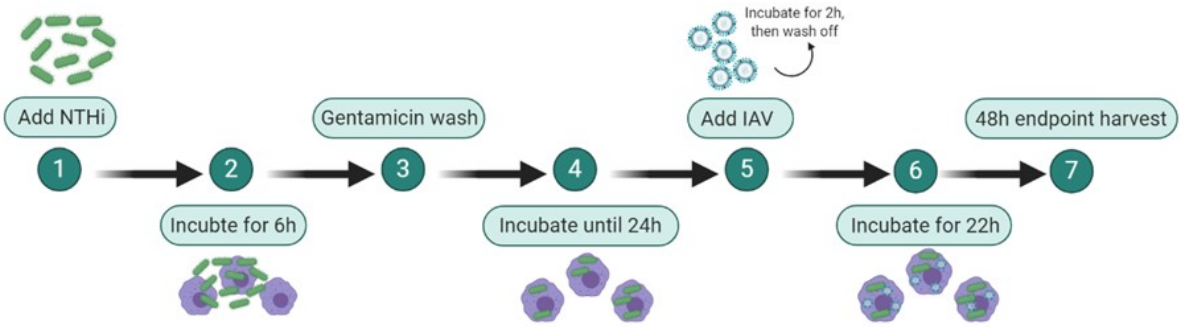

Figure 6.1. Graphical workflow of the adapted infection model used to investigate co-infection of MDM with NTHi and IAV. MDM were infected with NTHi for 6 h, subject to a gentamicin wash and left in antibiotic free media until 24 h when IAV was added for 2 h. After 2 h, excess IAV was washed off and MDM were incubated in antibiotic free media until harvest at 48 h.

6.2.1.2 NTHi persistence in MDM was detected up to 48 h

As the primary aim of adapting this model was to determine the impact of NTHi-IAV co-infection on macrophages, it was important to firstly ensure that NTHi was able to persist within MDM up to the final 48 h endpoint. The NTHi *hel* gene, used previously in chapter 3 to determine presence of NTHi ST14 at 6 h and 24 h, was also detected for all three NTHi strains at 48 h (Figure 6.2A). The levels of *hel* mRNA differed between strains, with *hel* expression decreasing for ST408 between 6 h and 48 h (p=0.0655) and between 6 h and 24 h for ST201 (p=0.0436). However, this decrease in *hel* expression was likely due to transcriptomic adaptation to persistence, as live viable counts did not indicate a significant decrease in NTHi association with MDM and instead demonstrated continual viability of all three strains up until at least 48 h (Figure 6.2B). ST408 and ST14 CFU levels were consistent over the time course, however levels of ST201 CFU appeared to increase over time, with the highest CFU recovered at 48h (p=0.0217 for 6 h v 48 h and p=0.0845 for 24 h v 48 h).

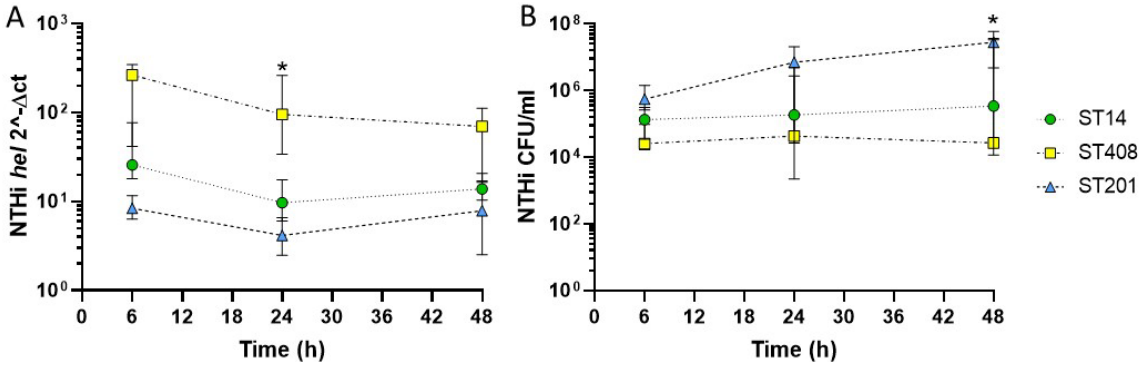

Figure 6.2. NTHi persist within MDM for the duration of the proposed adapted infection model. (A) Detection of the NTHi *hel* gene and (B) live viable counts for ST14 (green), ST408 (yellow) and ST201 (blue) respectively, indicating NTHi association with MDM up to 48 h. NTHi *hel* gene was normalised to NTHi *rho* gene expression at each time point. Graphs show paired data each point represents the median of five biological replicates (n=5), with error bars indicating the IQR. Data were analysed by Two-Way ANOVA with Tukey's multiple comparisons; *p<0.05

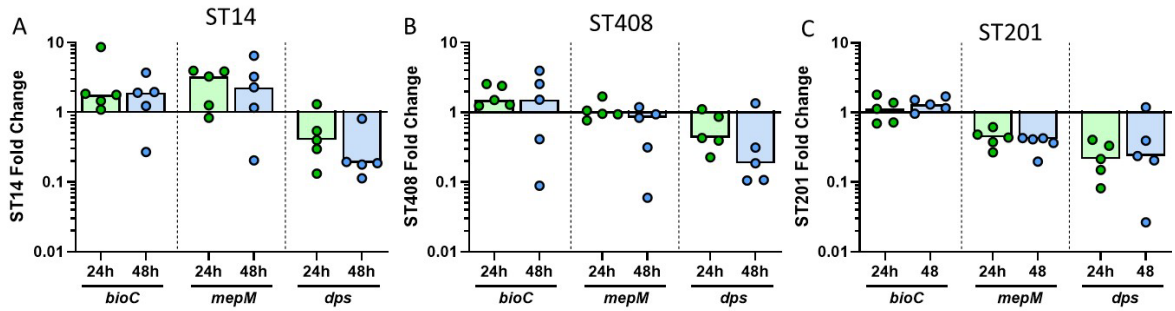

Figure 6.3. NTHi gene expression during persistent infection of MDM. The expression of *bioC, mepM* and *dps* by ST14 (A), ST408 (B) and ST201 (C) at 24 h and 48 h was measured by qPCR. Gene expression was normalised to NTHi *rho* gene and to the expression of each gene at the 6 h time point. Graphs show paired data and bars indicate medians. N=5. Data were analysed by Wilcoxon's signed-rank test with no statistical significance determined between 24 h and 48 h for any gene or NTHi strain.

NTHi persistence was associated with sustained transcriptomic changes of the top regulated NTHi genes identified in the dual RNASeq analysis. For ST14, the upregulation of both *bioC* and *mepM* and downregulation of *dps* in comparison to the initial 6 h time point did not significantly change between 24 h and 48 h (Figure 6.3A). Similarly for ST408, the expression of *bioC* remained upregulated compared to the 6 h time point, but did not significantly change in expression between 24 h and 48 h, whereas mepM was not expressed at all and *dps* remained downregulated (Figure 6.3B). Finally, ST201 continued not to differentially express *bioC* during MDM infection, with both *mepM* and *dps* remaining downregulated at 48 h (Figure 6.3C).

6.2.1.3 MDM viability was not significantly affected during co-infection

To ensure MDM viability was not impacted by co-infection, a LDH assay was used to assess MDM viability. Continual presence of all three NTHi strains did not significantly increase LDH release at 48 h, compared to the uninfected control (Figure 6.4; ST14 = 0.9 FC, ST408 = 1.2 FC and ST201 = 1.4). IAV infection alone slightly increased MDM LDH release (1.4 FC). IAV co-infection with ST14 or ST408 did not impact on LDH release, whereas ST201 and IAV co-infection resulted in a slightly higher increase of LDH release (1.8 FC) compared to ST201 (1.4 FC) and IAV (1.4FC) alone ($p>0.99$). Higher levels of LDH release in response to ST201 compared to ST14 and ST408 could be due to the higher presence of ST201 at 48 h. Overall, no statistically significant increase in LDH release was measured from single pathogen infected or co-infected MDM, indicating that MDM viability was not affected by the continual NTHi presence in the model, or by the addition of IAV.

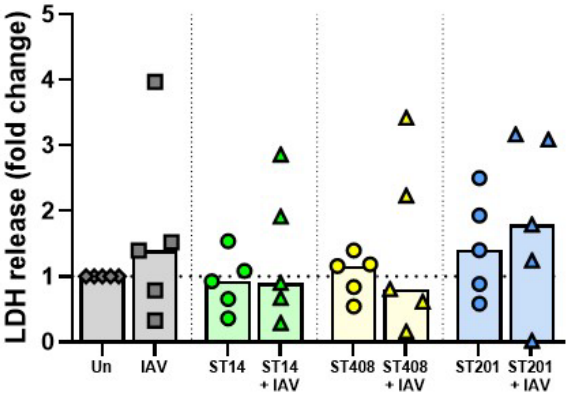

Figure 6.4. MDM remained viable at 48 h, despite IAV, NTHi and co-infection. MDM were infected with ST14 (green), ST408 (yellow), ST201 (blue) or left uninfected (grey), followed by addition of IAV at 24 h, as described in Figure 6.1. At 48 h, culture supernatants were harvested and analysed by a LDH assay. LDH release is expressed as fold change relative to the uninfected control, which is represented by the horizontal dotted line. Graphs show paired data and bars indicate medians. N=5. Data were analysed by Friedman test with Dunn's multiple comparisons test.

6.2.2 Decreased NP-1+ levels were detected in co-infected MDM at 48 h

IAV infection of MDM was measured at the 48 h infection assay endpoint by flow cytometry. Briefly, MDM were harvested from wells, fixed, permeabilised and stained with an anti-nucleoprotein (NP)-1 antibody. NP-1 is a marker of IAV replication so will only be present within IAV-infected MDM. This has been confirmed previously by inactivation of influenza virus by UV irradiation which abrogated NP detection[351,498]. In addition, Lonsdale *et al.* showed that no NP-1 signal was measured when cells were not permeabilised, indicating that NP is a good marker for detection of replication-competent influenza particles inside cells by flow cytometry[498].

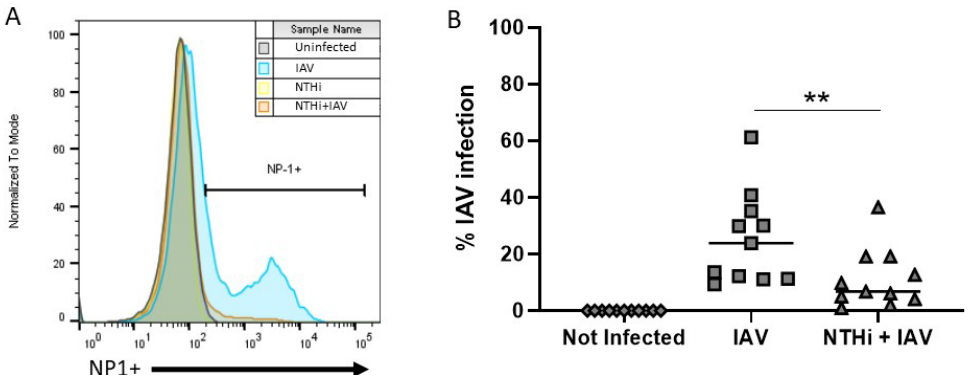

Figure 6.5. NP-1+ levels were lower in co-infected MDM. MDM were infected with NTHi ST14 as previously described and harvested at the final 48 h time point for flow cytometry analysis of IAV infection. A FITC labelled anti-NP-1 antibody was used to determine levels of IAV NP-1 within MDM. (A) Representative histogram showing a second peak for IAV only infected MDM (blue) and a smaller second peak for NTHi and IAV infected MDM (orange). Graph key in top right corner indicates the four conditions tested: uninfected MDM, IAV only, NTHi only and co-infected MDM. Uninfected MDM were used as the NP-1 negative control for gating. (B) Percentage of NP1+ MDM. N=11. Graphs show paired data and lines indicate medians. Data were analysed by Wilcoxon signed-rank test; **p<0.01

To determine the proportion of NP-1+ MDM, the uninfected MDM control was used as the negative control for NP-1 (Figure 6.5A). Two single pathogen only controls were included: NTHi only infected MDM and IAV only infected MDM. For both the uninfected MDM and NTHi-only infected MDM controls, no NP-1 signal was detected. In contrast, for MDM infected only with IAV and MDM co-infected with both NTHi and IAV, there was clear detection of NP-1. Strikingly, decreased NP-1+ levels were detected in co-infected MDM compared to IAV-only infected MDM (Figure 6.5B). The median %NP-1+ MDM infected with IAV only at the 24 h time point was 23.90%, which significantly decreased to a median infection level of 6.76% NP-1+ co-infected MDM (p=0.0049, Figure 6.5B). A reduction in %NP-1+ MDM was also observed following co-infection with ST408 or ST201 with median 4.77% and 5.56% %NP-1+ co-infected MDM detected compared to IAV alone (Figure 6.6A, both p<0.05). Diminished IAV levels in co-infected samples was further assessed by measuring the IAV HA gene by qPCR, which confirmed lower levels of IAV in ST14 (p=0.0291), ST408 (p=0.0417) and ST201 (p=0.1325) co-infected MDM (Figure 6.6B). Co-infections with the three NTHi strains all demonstrated comparable levels of IAV infection, with no strain-dependent differences detected.

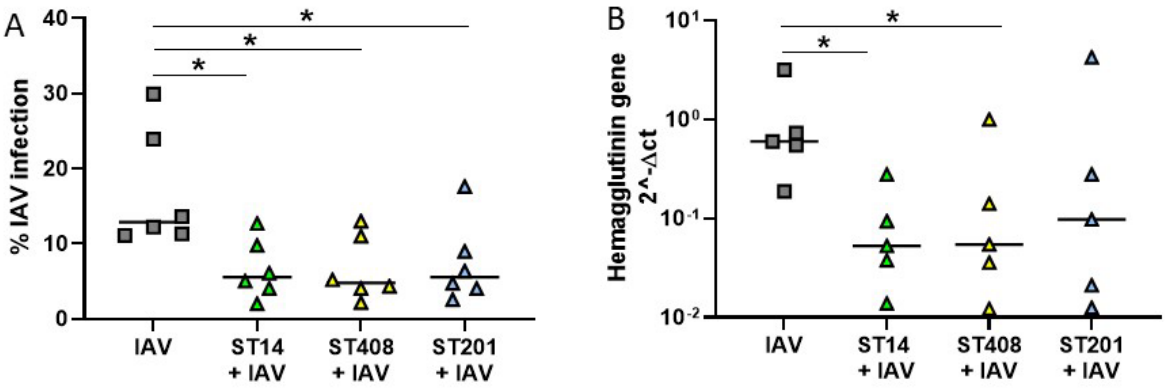

Figure 6.6. Decreased IAV infection was also observed following infection of MDM with additional clinical strains of NTHi. The level of IAV infection at 48 h was measured by detection of IAV NP-1 by flow cytometry (A) and expression of the IAV hemagglutinin (HA) gene by qPCR (B). MDM were infected with NTHi ST14, ST408, ST201 or media control for 6 h. Following an extended incubation period until 24 h, IAV was added at 24 h for 2 h, before removal and washing of extracellular virus and incubation of MDM for a further 22 h to allow for viral replication. IAV HA gene is normalised to MDM housekeeping gene *B2M*. N=5-6. Graphs show paired data and lines indicate medians. Data were analysed by Friedman test with Dunn's multiple comparisons; *p<0.05

6.2.3 Modulation of IFN pathways during NTHi-IAV co-infection of MDM

6.2.3.1 Differential interferon immune responses to NTHi, IAV or co-infection at 48 h

Given that a robust interferon response is important in the defence against influenza infection[229,313], it was hypothesised that the combination effect of NTHi and IAV would result in a higher interferon response by co-infected MDM allowing for better inhibition of IAV infection at this time point, explaining the reduced IAV infection levels seen above (Section 6.2.2). The pattern of *IFNA, IFNB* and *IFNG* gene expression regulation was unique for all three pathogen combinations at 48 h (Table 6.1). MDM infected with IAV-alone upregulated *IFNA* (p=0.0417), *IFNB* (p=0.011) and *IFNG* (p=0.1720), whereas MDM infected with NTHi alone did not upregulate *IFNA* expression (0.8 FC, p>0.99) and only slightly, but not significantly, upregulated *IFNB* gene expression (FC 1.5 p>0.99) compared to the uninfected control. In contrast, MDM *IFNG* gene expression was significantly upregulated in response to NTHi alone (FC 9.6, p=0.0417) and was further elevated in co-infected MDM (FC 72.6, p=0.0156). Co-infected MDM modestly upregulated *IFNA* and *IFNB* (FC 2.1 and 3.2, respectively), but this increase was not significant compared to uninfected MDM.

Although IAV infection resulted in higher levels of *IFNA* and *IFNB* gene expression compared to NTHi infection in particular (Figure 6.7A & B; both p=0.0628), co-infected MDM did not mount a similar magnitude of response, despite the addition of IAV. In contrast, MDM upregulation of *IFNG* was higher in co-infected MDM (72.6 FC) compared to both IAV alone (4.1 FC) and NTHi alone (9.6 FC) infected MDM. However these differences in expression were not significant, most likely due to the heterogeneous spread of *IFNG* gene expression values, particularly in co-infected samples (Figure 6.7C).

MDM gene expression for NTHi alone or NTHi+IAV co-infections also did not significantly differ in response to different NTHi strains for *IFNA* (Figure 6.7D), *IFNB* (Figure 6.7E) or *IFNG* (Figure 6.7F), suggesting MDM regulation of IFN genes in response to NTHi was conserved amongst strains at 48 h. The heterogeneity in gene expression data could be as a result of different levels of NTHi presence at 48 h, as shown previously (Figure 6.2).

Table 6.1. Regulation of IFN gene expression in IAV-alone, NTHi-alone or co-infected MDM compared to uninfected control at 48 h. Values are median [IQR] fold changes of *IFNA*, *IFNB* and *IFNG* gene expression relative to the uninfected control. N=5. Asterisk indicates statistical significance determined between uninfected controls and IAV-, NTHi- and co-infected (NTHi+IAV) samples Data were analysed by Friedman test with Dunn's multiple comparisons.

Gene	IAV	NTHi	NTHi+IAV
IFNA	4.8 [1.7 – 38.7] *** p=0.0417**	0.8 [0.2 – 1.4] p>0.9999	2.1 [0.6 – 6.9] p=0.8
IFNB	18.6 [1.8 – 63.7] *** p=0.0110**	1.5 [0.6 – 3.3] p>0.9999	3.2 [1.8 – 8.5] p=0.2209
IFNG	4.1 [1.8 – 5] p=0.1720	9.6 [2.9 – 65.4] *** p=0.0417**	72.6 [3 – 132.1] *** p=0.0156**

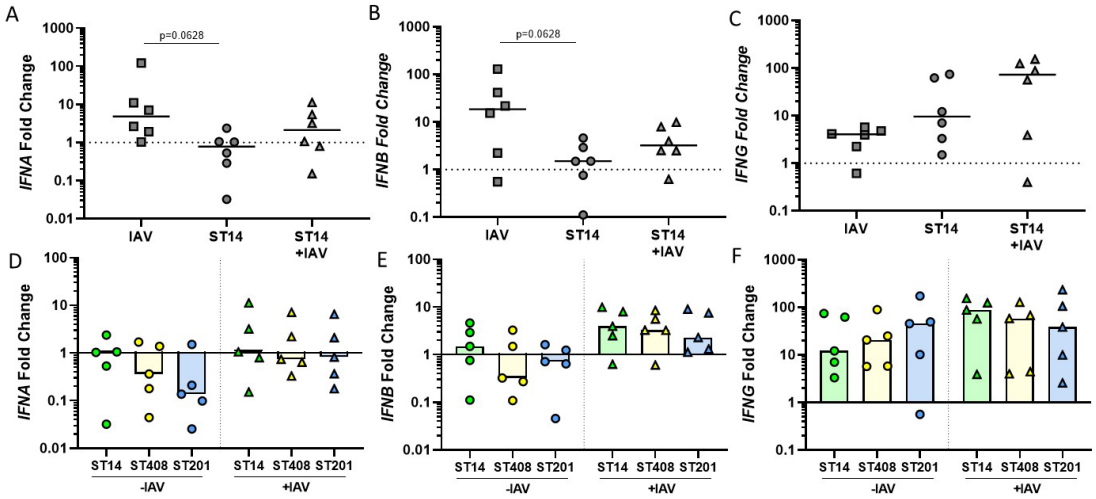

Figure 6.7. MDM expression of IFNs in response to NTHi, IAV or co-infection (NTHi+IAV) at 48 h. MDM were infected with NTHi or media control, followed by addition of IAV at 24 h as described in Figure 6.1. (A) and (D) *IFNA* gene expression, (B) and (E) *IFNB* gene expression and (C) and (F) *IFNG* gene expression. Top row indicates IFN gene expression for IAV, NTHi ST14 and co-infected MDM, bottom row indicates MDM IFN gene expression compared across additional clinical strains of NTHi (ST14 = green, ST408 = yellow and ST201 = blue). Genes of interest were normalised to housekeeping gene *B2M* and are expressed as fold change relative to the uninfected control, which is shown as a dotted line, where appropriate. N=5-6. Graphs show paired data and lines indicate medians. Data were analysed by Friedman test with Dunn's multiple comparisons.

As changes in gene expression do not necessarily relate to changes in the protein product of the gene, a Luminex assay was used to measure release of IFN-α, IFN-β and IFN-γ at 48 h in response to IAV alone, NTHi ST14 alone or co-infection. Only a single strain (ST14) was used for protein level assays due to technical and financial limitations. IAV infection induced higher amounts of IFN-α and IFN-β release compared to NTHi alone and co-infected MDM at 48 h (Figure 6.8A & B). IFN-γ release was also significantly upregulated in NTHi- and co-infected MDM compared to IAV-infection alone (Figure 6.8C; p=0.0599 and 0.0303 respectively).

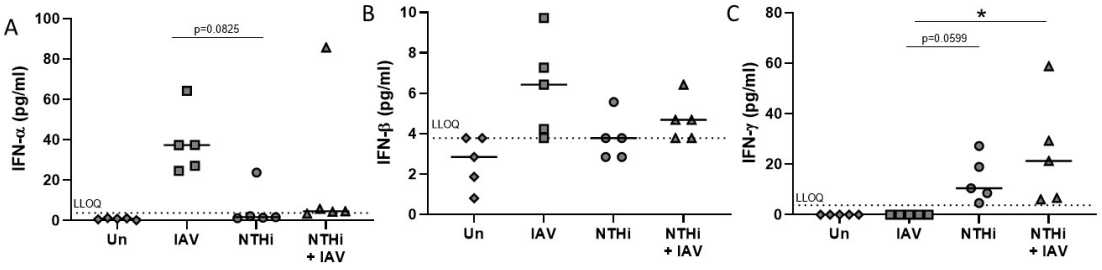

Figure 6.8. MDM differentially released IFNs in response to NTHi, IAV or co-infection (NTHi+IAV). MDM were infected with NTHi ST14 or left uninfected, followed by addition of IAV at 24 h as described in Figure 6.1. Release of IFN-α (A), IFN-β (B) and IFN-γ (C) was assessed by Luminex assay using 48 h culture supernatants. Dotted lines on graphs indicate the specific lower limit of quantification (LLOQ) for each analyte. N=5. Graphs show paired data and lines indicate medians. Data were analysed by Friedman test with Dunn's multiple comparisons; *p<0.05

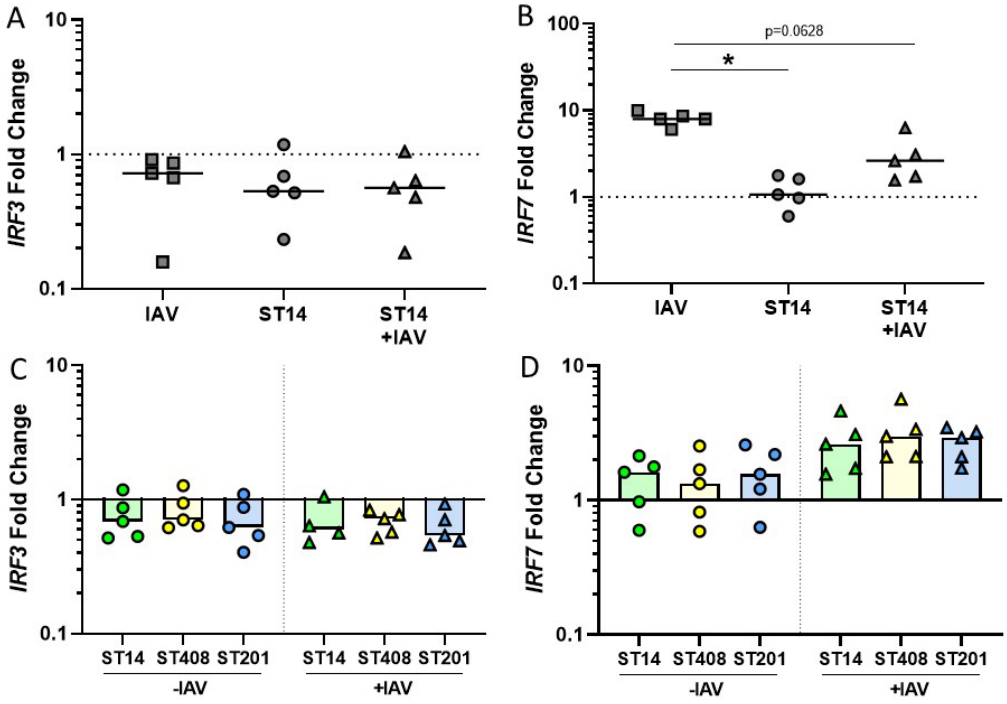

Figure 6.9. MDM expression of IRFs following IAV, NTHi or co-infection at 48h. MDM were infected with NTHi or media control, followed by addition of IAV at 24 h as described in Figure 6.1. The levels of MDM (A) *IRF3* and (B) IRF7 gene expression in response to IAV, ST14 or co-infection were measured by qPCR at 48 h. The expression of (C) IRF3 and (D) and IRF7 were also measured at 48 h following infection with additional clinical strains of NTHi, ST14 (green), ST408 (yellow), ST201 (blue) with and without influenza (- or + IAV). Genes of interest were normalised to housekeeping gene *B2M* and are expressed as fold change relative to the uninfected control, which is shown as a dotted line, where appropriate. N=5-6. Graphs show paired data and lines indicate medians. Data were analysed by Friedman test with Dunn's multiple comparisons; *p<0.05

Modulation of IFN responses by IRFs are crucial for initiating and sustaining an efficient anti-viral response to a pathogen. As such, it was next assessed whether *IRF3* and *IRF7*, two IRFs crucial for efficient IFN production[499], were differentially expressed at 48 h. MDM *IRF3* gene expression was downregulated by all pathogen combinations at 48 h (Figure 6.9A), which was also observed in response to additional clinical strains of NTHi (Figure 6.9C). In contrast, *IRF7* was more highly upregulated in response to IAV infection compared to NTHi infected MDM (p=0.0177) and co-infected MDM (p=0.0628) (Figure 6.9B). Upregulation of *IRF7* was consistent for all strains, with no strain-dependent differences in the level of expression detected (Figure 6.9D).

To confirm the downstream functional effects of IFN signalling, MDM release of the ISG CXCL10 into culture supernatants was assessed by ELISA. Levels of CXCL10 release at 48 h was different for all three pathogen combinations. The highest amount of CXCL10 was released by IAV-infected MDM compared to NTHi-infected MDM (Figure 6.10, p=0.0133). Although co-infected MDM also released a higher amount of *CXCL10* compared to NTHi infection (201.6 pg/ml v 113 pg/ml, not significant), co-infected MDM CXCL10 release was ten times lower compared to response to IAV-alone (201.6 pg/ml v 2188 pg/ml, p=0.1733). This again indicates reduced activation of IFN pathways in co-infected MDM at 48 h, compared to IAV alone infected MDM, despite reduced IAV infection levels.

Together, the MDM IFN gene expression and protein release data indicated that all three pathogen combinations resulted in a differential IFN response. Unsurprisingly, IAV infection resulted in the highest induction of IFN responses, particular type I IFNs, whereas co-infected MDM more highly upregulated type II IFNs. However, the IFN response from co-infected MDM was more similar to that of the MDM response to NTHi alone, despite the presence of IAV. It was therefore likely that the type I IFN response measured at 48 h in co-infected MDM was not responsible for the inhibition of IAV infection.

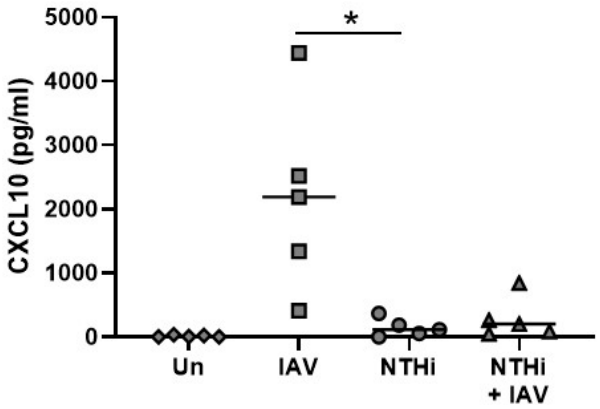

Figure 6.10. MDM release of CXCL10 in response to NTHi, IAV and co-infection at 48 h. MDM were infected with NTHi ST14 or media control (Un) for 6 h washed in gentamicin, and incubated in antibiotic free media until 24 h. At 24 h post initial NTHi-infection, IAV was added for 2 h and cells were washed to remove excess IAV and incubated in antibiotic free media for a further 22h (end time point 48 h). Release of CXCL10 was assessed by ELISA using harvested culture supernatants at 48 h. N=5. Graphs show paired data and lines indicate medians. Data were analysed by Friedman test with Dunn's multiple comparison test; *p<0.05

6.2.3.2 Prior NTHi-modulation of macrophage IFN responses during intracellular infection.

As the IFN response did not appear to play a role in restricting IAV infection in co-infected MDM at 48 h, the upregulation of IFNs in response to NTHi prior to the addition of IAV was next investigated. At 6 h, all three NTHi strains upregulated *IFNA, IFNB* and *IFNG* macrophage gene expression relative to the uninfected control (Table 6.2). However, by 24 h the expression of both *IFNA* and *IFNB* was downregulated by all three NTHi strains. In contrast, *IFNG* was consistently highly upregulated at both 6 h and 24 h by all three NTHi strains. When comparing the level of expression across strains at each time point, no strain-dependent differences in *IFNA* or *IFNB* gene expression were detected (Figure 6.11A & B). The only difference in expression for *IFNG* was between ST14 and ST201, with ST14 inducing a 111-fold increase in *IFNG* gene expression compared to 66.4-fold increase in response to ST201 (Figure 6.11C; p=0.0281).

Table 6.2. Early upregulation of IFN gene expression by MDM in response to different clinical strains of NTHi at 6 h and 24 h. *IFNA, IFNB* and *IFNG* gene expression which were normalised to housekeeping gene *B2M* and are expressed as fold change relative to the uninfected control at the respective time point. The associated p-value indicates the significance of changes in gene expression compared to the uninfected control (bold font p<0.05). N=5. Values are medians [IQR]. Data were analysed by Friedman test with Dunn's multiple comparisons.

	6h			24h		
	ST14	**ST408**	**ST201**	**ST14**	**ST408**	**ST201**
IFNA	2.7 [1.1 – 10.7] p=0.2209	4.4 [2.3 – 10.6] **p=0.011**	3.3 [1.2 – 10.5] **p=0.0417**	0.2 [0.2 – 0.6] p=0.076	0.5 [0.2 – 2.3] p=0.5391	0.3 [0.1 – 0.9] p=0.2209
IFNB	11.2 [5.1 – 101.3] **p=0.011**	11.74 [2.6 – 124.6] **p=0.0052**	19.8 [6.1 - 67] p=0.135	0.7 [0.5 – 0.9] **p=0.0417**	0.7 [0.6- 1] p=0.2209	0.4 [0.4 – 0.7] **p=0.011**
IFNG	126.5 [42.6 – 381.2] **p=0.001**	71.7 [33.8 – 356.2] **p=0.011**	51.98 [14.5 – 99.1] p=0.3526	111 [47.9 – 229.1] **p=0.001**	72.9 [40.4 – 152.3] **p=0.0417**	66.4 [30.7 – 117.2] p=0.1325

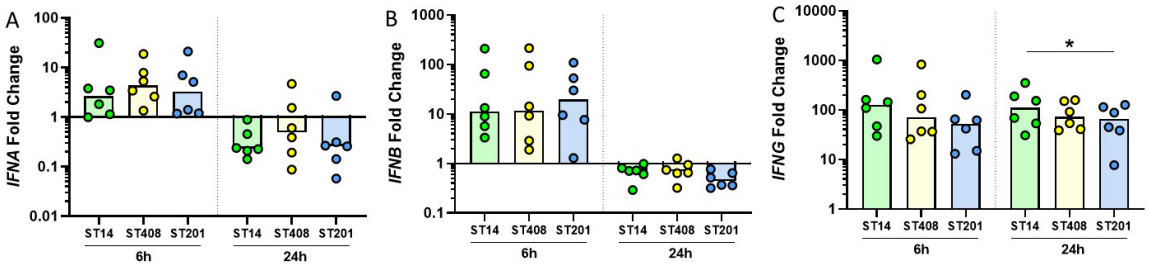

Figure 6.11. Early upregulation of IFN response was consistent across additional strains of NTHi. Expression of *IFNA* (A), *IFNB* (B) and *IFNG* (C) at 6 h and 24 h in response to ST14 (green), ST408 (yellow) or ST201 (blue). Gene of interest was normalised to housekeeping gene *B2M* and data shown as fold change relative to the uninfected control at each respective time point. N=6. Graphs show paired data and bars indicate medians. Data were analysed by Friedman test with Dunn's multiple comparisons; *p<0.05

To confirm that early upregulation of IFN gene expression resulted in production and release of IFN protein, a Luminex assay was used to assess IFN release into the culture supernatants by MDM in response to NTHi ST14 infection at 6 h and 24 h. At 6 h, release of IFN-α was not detected above the lower limit of quantification (LLOQ) (Figure 6.12A). Although IFN-α was trending towards significantly higher release at 24 h in response to NTHi infection compared to the uninfected control (Figure 6.12A, p = 0.0599), the level of IFN-α was also below the limit of the assay and therefore must be interpreted with caution.

In contrast, levels of IFN-β at both 6 h and 24 h were detected above the LLOQ. A statistically significant increase in IFN-β levels was detected at 6 h compared to the uninfected control (Figure 6.12B; p = 0.0212). Although IFN-β was still detected in higher amounts compared to the uninfected control at 24 h, this was not significant (p = 0.1). On the other hand, IFN-γ release at 24 h was statistically significantly higher compared to the uninfected control at 24 h (Figure 6.12C; p = 0.0313), whereas no release above the LLOQ was detected at 6 h.

Next, it was investigated whether this early upregulation of IFN gene expression and subsequent IFN protein release resulted in global modulation of macrophage IFN-related anti-viral pathways in response to NTHi infection. Previous transcriptomic analysis of the MDM response to intracellular NTHi infection in chapter 4 highlighted the 'Influenza A' KEGG pathway as one of the top functionally enriched KEGG pathways. Therefore, the dual RNASeq MDM enrichment analysis using the 'core' gene list was further inspected specifically for enrichment of MDM anti-viral responses across both 6 h and 24 h. The gene list enrichment analysis previously performed using the 'core' DEG list identified a number of significantly enriched interferon-related GO:terms in the Biological Processes category.

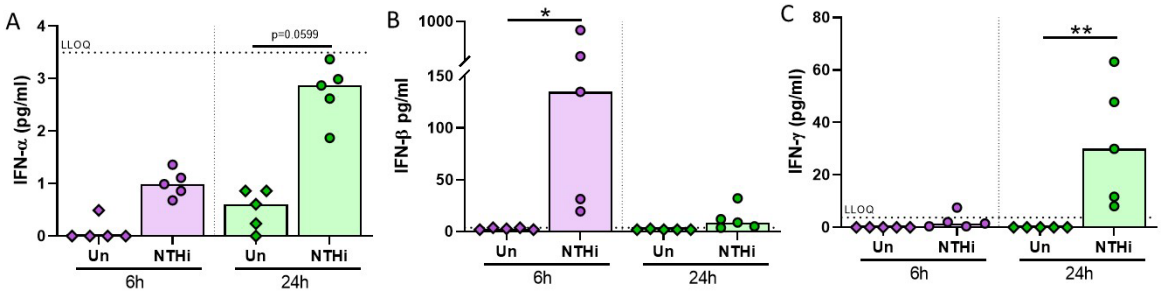

Figure 6.12. MDM released IFNs in response to NTHi infection. MDM release of (A) IFN-α, (B) IFN-β and (C) IFN-γ at 6 h and 24 h in response to NTHi ST14. MDM were infected with NTHi ST14 or media control (Un) for 6 h. MDM were subject to a gentamicin wash and incubated in antibiotic free media until 24h. Supernatants were harvested at 6 h and 24 h for analysis by a Luminex assay. LLOQ is shown on graphs, where appropriate, by a horizontal dotted line. N=5. Graphs show paired data and bars indicate medians. Data were analysed by Friedman test with Dunn's multiple comparisons; *p<0.05, **p<0.01

Overall, 19 terms directly related to interferon signalling were significantly enriched (Figure 6.13C; FDR <0.05), which could be divided into the type I interferon or type II interferon pathway (Figure 6.13A & B). Across these 19 terms, a total of 103 individual genes were assigned. These 103 genes overlapped a number of IFN type I or type II related GO:terms, likely due to the redundancy of gene ontology terminology as has been previously discussed. Of these 103 genes, 18 (17.5%) genes were assigned to both type I and type II IFN pathway terms, whereas the remaining genes were type I (27 genes; 26.2%) or type II (58 genes; 56.3%) only.

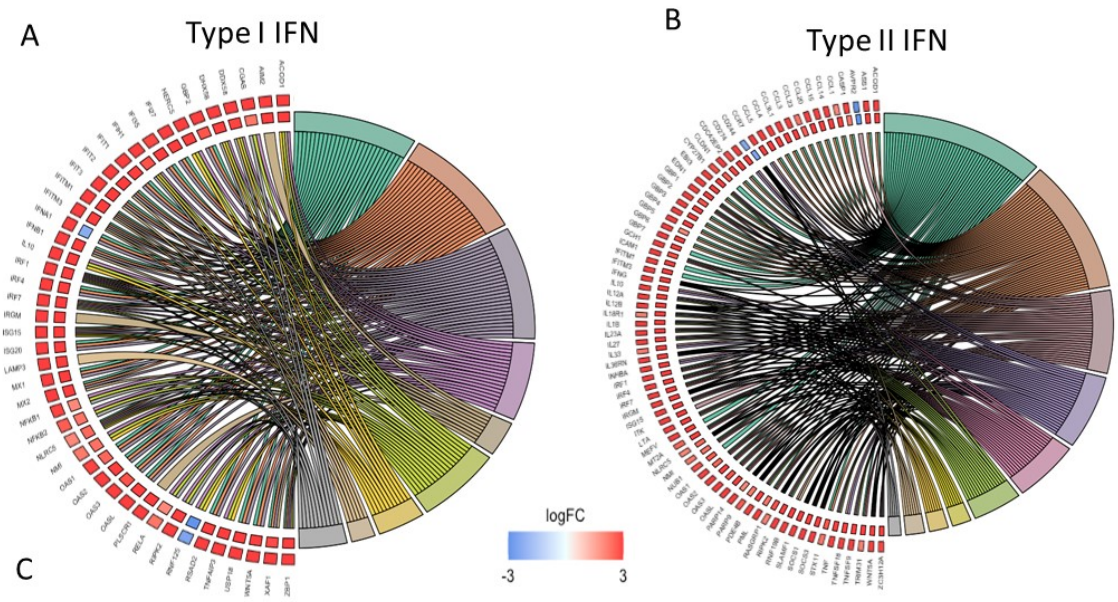

	GO:ID	GO:Term	Genes in input	Genes in annotation	Enrichment FDR
Type I interferon pathways	GO:0060337	type I interferon signaling pathway	27	95	5.12E-13
	GO:0071357	cellular response to type I interferon	27	95	5.12E-13
	GO:0034340	response to type I interferon	27	99	1.41E-12
	GO:0032479	regulation of type I interferon production	19	133	3.25E-04
	GO:0035456	response to interferon-beta	9	30	3.30E-04
	GO:0032606	type I interferon production	19	136	4.41E-04
	GO:0032480	negative regulation of type I interferon production	11	49	5.40E-04
	GO:0035455	response to interferon-alpha	6	22	1.82E-02
	GO:0032481	positive regulation of type I interferon production	11	81	3.64E-02
Type II interferon pathways	GO:0034341	response to interferon-gamma	50	208	2.60E-21
	GO:0071346	cellular response to interferon-gamma	44	189	4.66E-18
	GO:0032609	interferon-gamma production	28	133	3.48E-10
	GO:0032649	regulation of interferon-gamma production	25	118	4.45E-09
	GO:0060333	interferon-gamma-mediated signaling pathway	21	92	3.74E-08
	GO:0032729	positive regulation of interferon-gamma production	16	79	2.12E-05
	GO:0060330	regulation of response to interferon-gamma	7	26	6.86E-03
	GO:0060334	regulation of interferon-gamma-mediated signaling pathway	7	26	6.86E-03
	GO:0072643	interferon-gamma secretion	7	28	1.04E-02
	GO:1902713	regulation of interferon-gamma secretion	5	18	4.87E-02

Figure 6.13. Enrichment of MDM IFN pathways during NTHi infection. Enrichment of (A) Type I and (B) Type II IFN responses was detected in the MDM core gene set. Chord plots indicate that the genes in all processes are shared across multiple different IFN response GO:terms. The expression of all identified genes is indicated by the coloured block next to each gene, with red indicating upregulated and blue indicating downregulated genes, as shown in the log_2FC scale bar. The majority of genes are upregulated at 6 h (outer blocks) and 24 h (inner blocks), with little change in expression. (C) Table indicating name and enrichment significance of each GO:term, with the associated term colour matched to the Chord plot for clarity.

The majority of genes involved in both type I and II interferon responses were consistently upregulated at both 6 h and 24 h, except *RNF125* (type I), *CD244* and *AVPR2* (both type II) which were downregulated at both time points and *IFNA1* (type I) which was upregulated at 6 h, but downregulated at 24 h. No significant enrichment of type III IFN responses, including *IFNL* gene expression, were detected in this current analysis.

As mentioned previously, following IFN interaction with their specific receptor, downstream signalling pathways are activated, resulting in modulation of various genes known as interferon stimulated genes (ISGs). To investigate ISG upregulation in response to NTHi infection prior to IAV challenge, the number of ISGs present in the dual RNASeq data set at 6 h and 24 h were investigated using the online tool Interferome. Interferome is an online, open access database detailing type I, II and III ISGs, created by collating information about gene expression data sets involving IFN treatment of cells[397].

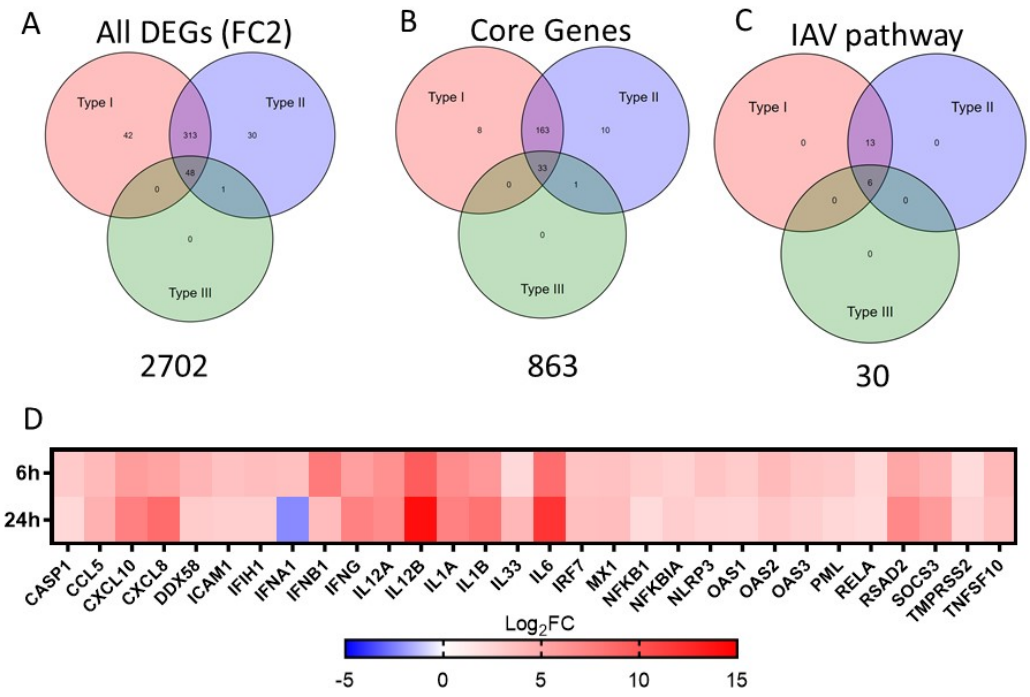

Figure 6.14. Upregulation of MDM interferon stimulated genes (ISGs) following NTHi infection. Venn diagrams show the number of ISGs and the interferon type (I, II or III) associated with the gene stimulation present in (A) the full gene list containing all 2702 differentially expressed genes ($p<0.05$) at a $\log_2$ FC cut off value of 2, (B) the 863 'core' genes consistently expressed across 6 h and 24 h and (C) the Influenza A KEGG pathway generated from the core gene list. Numbers below all Venn diagrams indicated the starting input number of the gene list for each comparison. (D) Heatmap indicating the fold change of all 30 MDM genes in response to NTHi infection that were present in the enriched 'Influenza A' KEGG pathway. ISG detection performed using the online tool Interferome.

By restricting this analysis to genes only present in the 'core' gene list, any potential differences in the temporal expression and regulation of ISGs following the initial activation of the macrophage IFN response may be overlooked or missed. Therefore all 2702 genes differentially expressed at either 6 h, 24 h or across both time points (log_2FC2, FDR p<0.05) were first assessed.

Out of a total of 2702 genes, 434 genes were identified to be stimulated by interferons (Figure 6.14A). This accounted for 16% of all DEGs regulated in response to NTHi infection. Furthermore, a similar pattern of stimulation was observed for the 863 core gene set, with a quarter of genes (215; 25%) present in the core gene set deemed to be stimulated by interferons, indicating a sustained transcriptomic regulation of the interferon response to NTHi infection (Figure 6.14B). In agreement with the enrichment of interferon signalling pathways (Figure 6.13), no activation of type III IFN pathways were detected. The significantly functionally enriched 'Influenza A' KEGG pathway was assigned 30 genes from the core gene list, of which, 19 (63%) were identified as ISGs (Figure 6.14C). Only one gene (*IFNA1*) displayed downregulation (24 h only, log_2FC = -2.3), whereas the remaining 29 genes were consistently upregulated at both 6 h and 24 h (Figure 6.14D).

The interferome platform allows for identification of transcription factors that interact with the genes present in a user-submitted gene list. Within the IAV KEGG pathway gene list (Figure 6.14D), two transcription factors (*RELA* and *IRF7*) were present. A further nine transcription factors were predicted to interact with the 17 remaining ISGs in the IAV KEGG pathway. Therefore, the expression of these eleven transcription factors in response to NTHi infection at 6 h and 24 h were investigated using the dual RNASeq data set (Figure 6.15). Eight out of the eleven transcription factors were upregulated at both 6 h and 24 h in response to NTHi (Figure 6.15). *IRF3* was significantly downregulated at 6 h, but was upregulated at 24 h, whereas *IRF8* was upregulated at 6 h but was no longer differentially expressed at 24 h. Finally, *SIRT6* was not differentially expressed at either time point.

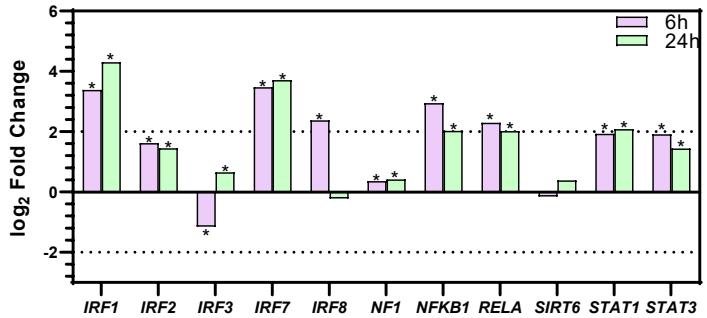

Figure 6.15. Transcription factors involved in modulation of IFN stimulated genes (ISGs) were upregulated in response to NTHi at 6 h and 24 h. Expression of MDM transcription factors that were present in the dual RNASeq data set at 6 h (purple) and 24 h (green). Asterisk indicates statistically significant differentially expressed genes (p<0.05). Dotted line indicates log_2 FC 2 cut off.

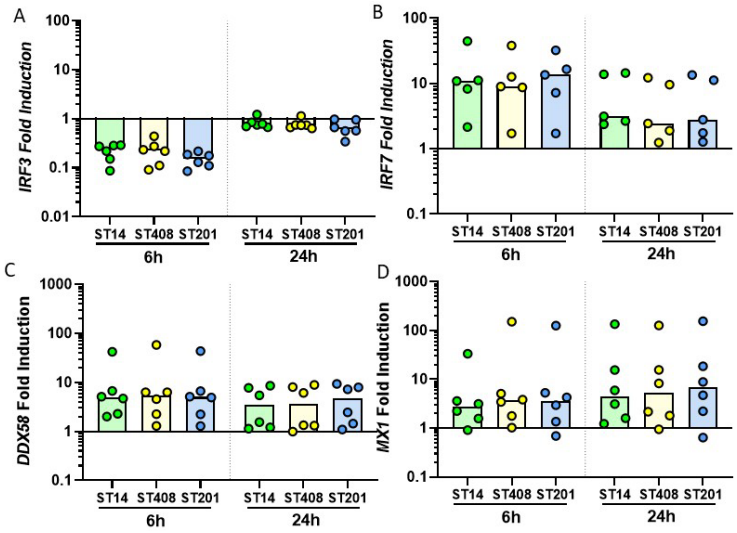

Figure 6.16. Regulation of MDM anti-viral immunity in response to NTHi strains at 6 h and 24 h. Expression of transcription factors (A) *IRF3* and (B) *IRF7* and interferon stimulated genes (C) *DDX58* and (E) *MX1* in response to ST14 (green), ST408 (yellow) or ST201 (blue) at 6 h and 24 h were measured by qPCR. Gene expression was normalized to housekeeping gene *B2M* and to the uninfected MDM control at the respective time point. Graphs show paired data and lines indicate medians. N=5-6. Data were analysed by Friedman test with Dunn's multiple comparisons.

To confirm that MDM regulation of transcription factors was conserved in response to additional clinical strains of NTHi at 6 h and 24 h, *IRF3* and *IRF7* expression levels were measured by qPCR. As shown for previous genes, infection with any strain resulted in the same direction of IRF gene expression (i.e. upregulated or downregulated), suggesting modulation of anti-viral genes by MDM is conserved during infection with multiple clinical strains of NTHi (Figure 6.16A-B). Of note, validation of the gene expression of the transcription factor, *IRF1,* in chapter 4 also demonstrated upregulation of this transcription factor at both 6 h and 24 h (Figure 4.27D).

The expression of MDM ISGs following infection with ST14, ST408 and ST201 was assessed by qPCR at 6 h and 24 h. Two ISGs from the IAV KEGG pathway, *DDX58* and *MX1,* were chosen to be investigated as these two ISGs were previously shown to be upregulated in response to IAV and IFN-β stimulation[497]. Both *DDX58* (Figure 6.16C) and *MX1* (Figure 6.16D) were upregulated at both 6 h and 24 h, with no statistically significant differences in the level of expression between strains observed

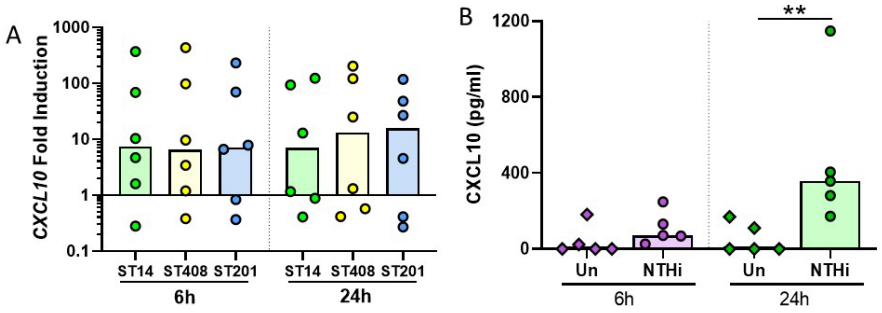

Figure 6.17. MDM upregulation of CXCL10 in response to NTHi infection. (A) Gene expression of *CXCL10* in response to NTHi ST14 (green), ST408 (yellow) or ST201 (blue) at 6 h and 24 h was measured by qPCR. (B) MDM release of CXCL10 protein into cell culture supernatants in response to NTHi ST14 infection at 6 h and 24 h was assessed by ELISA. Gene expression was normalized to housekeeping gene *B2M* and to the uninfected MDM control at the respective time point. Graphs show paired data and lines indicate medians. N=5-6. Data were analysed by Friedman test with Dunn's multiple comparisons; **p<0.01

It was previously shown that MDM release of the protein product of the ISG *CXCL10* was higher in response to IAV alone, compared to MDM infected with NTHi. Thus, it was next investigated whether MDM upregulated CXCL10 gene and protein expression in response to NTHi infection at 6 h and 24 h prior to IAV infection. First, the upregulation of *CXCL10* gene expression in response to additional clinical strain of NTHi was assessed. All three strains upregulated *CXCL10*, with no apparent differences in the level of *CXCL10* induction between strains at 6 h or 24 h (Figure 6.17A). Next, culture supernatants were assessed for CXCL10 release in response to ST14 NTHi infection at 6 h and 24 h by ELISA (Figure 6.17B). Although CXCL10 release was detected at 6 h (71.2 pg/ml), higher release of CXCL10 was measured at 24 h (357.2 pg/ml) which was significant compared to the uninfected control (p=0.0044). Together, these data suggest early NTHi-modulation of macrophage anti-viral pathways, specifically IFN pathways, may prime MDM into an anti-viral state that better enables macrophages to respond to a subsequent viral challenge.

6.2.4 Increased presence of NTHi following IAV co-infection at 48 h

The data in this chapter so far show that previous NTHi infection of MDM results in a diminished IAV infection. It is known that secondary bacterial infections often occur following influenza infection, but is often associated with new, opportunistic pathogen arriving after the initial viral infection. However, this current MDM model was designed to investigate co-infection in the context of a bacterial pathogen (NTHi) already present in the airway. Therefore, the effect of adding IAV on the NTHi already intracellularly residing within MDM was next investigated.

NTHi viable counting was performed to quantify recovery of live NTHi following IAV infection at 48 h. MDM were infected as previously described but at the 48 h endpoint, MDM were lysed to release NTHi for live viable counting. In contrast to decreasing IAV infection levels in co-infected MDM, the presence of NTHi increased. Increased presence was demonstrated by recovery of higher CFU/ml

counts at 48 h for all three strains when IAV was added at 24 h, compared to counts recovered from MDM that were infected with NTHi alone (Figure 6.18A).

The recovery of ST14 from co-infected MDM compared to ST14-alone MDM increased significantly by 209%, with counts increasing threefold from 4.12 x 10^5 CFU/ml to 1.275 x 10^6 CFU/ml (Figure 6.18B; p=0.0313). ST408 counts recovered from co-infected MDM increased the most out of all three strains, with recovered median counts increasing from 4.84 x 10^4 CFU/ml in MDM infected with ST408 alone compared to 5.15 x 10^5 in the presence of IAV, a percentage increase of 964% (Figure 6.18B; p=0.0313). However, the overall distribution of recovered counts for ST408 were extremely variable from MDM both infected with ST408 alone and co-infected with IAV, which could contribute to this large percentage increase. In contrast, recovered counts of ST201 only increased by 25% in co-infected samples compared to ST201-alone infected MDM, but this was still a statistically significant increase (Figure 6.18B; p=0.0313). Generally, viable counts for ST201 were higher than both ST14 and ST201 at 48 h, as originally demonstrated earlier in this chapter (Figure 6.2B). As postulated previously, this confirmed increase of ST201 presence in co-infected samples may account for the higher levels of LDH release previously detected (Figure 6.4).

A

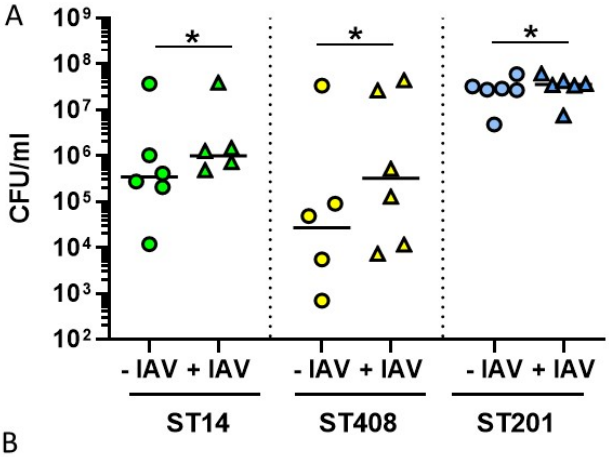

B

Strain	– IAV	+ IAV	% Increase
ST14	4.12 x 10^5 [2.4 x 10^5 – 1.9 x 10^7]	1.275 x 10^6 [6.03 x 10^5 – 2.03 x 10^7]	209%
ST408	4.84 x 10^4 [3.1 x 10^3 – 1.7 x 10^7]	5.15 x 10^5 [7 x 10^4 – 3.5 x 10^7]	964%
ST201	2.92 x 10^7 [2.7 x 10^7 – 4.6 x 10^7]	3.64 x 10^7 [3.4 x 10^7 – 5.2 x 10^7]	25%

Figure 6.18. Increased NTHi counts were recovered from co-infected MDM compared to MDM infected with NTHi alone. MDM were infected with ST14 (green), ST408 (yellow), ST201 (blue) or left uninfected, followed by addition of IAV at 24 h as described in Figure 6.1. Recovery of live NTHi following infection of MDM either only with NTHi (-IAV) or with IAV added at 24 h (+IAV) was measured by viable counting at 48 h (A). N=6. Graphs show paired data and lines indicate medians. Data were analysed by Wilcoxon signed-rank test; *p<0.05. (B) Table indicates the percentage increase in counts for each strain. Values reported are medians [IQR].

6.2.5 NTHi transcriptomic adaptation during NTHi-IAV co-infection of MDM

The three previously identified and validated genes from the NTHi dual RNASeq analysis (*bioC, mepM* and *dps*) showed no significant modulation between 24 h and 48 h for any strain (Figure 6.3). To determine whether IAV presence results in NTHi transcriptomic changes that may explain increased NTHi recovery from MDM at 48 h, the expression of these three genes by ST14, ST408 and ST201 during co-infection was assessed by qPCR.

The ST14 NTHi strain expressed lower levels of both *bioC* and *mepM* during co-infection, compared to ST14 infecting MDM alone (Figure 6.19A; p=0.0313 and Figure 6.19B; p=0.0625 respectively). The expression of *bioC* and *mepM* did not alter for ST408 and ST201 during co-infection with IAV. ST14 and ST201 expression of *dps* did not change, regardless of IAV presence but ST408 *dps* expression increased in co-infected samples (Figure 6.19C; p=0.0313). Changes in the expression of these select few NTHi genes could indicate further global transcriptomic changes during co-infection of MDM, resulting in NTHi outgrowth and proliferation.

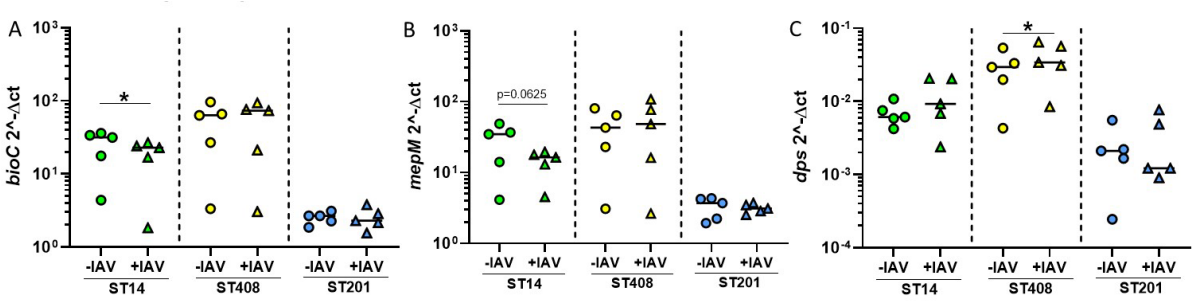

Figure 6.19. Modulation of NTHi gene expression during co-infection. MDM were infected with ST14 (green), ST408 (yellow), ST201 (blue) or left uninfected, followed by addition of IAV at 24 h as described in Figure 6.1. At 48 h, RNA was harvested from each well. Gene expression of NTHi (A) *bioC*, (B) *mepM* and (C) *dps* was measured by qPCR and normalised to NTHi *rho* gene. N=5. Graphs show paired data and lines indicate medians. Data were analysed by Wilcoxon signed-rank test; *p<0.05

6.2.6 NTHi presence resulted in a sustained macrophage inflammatory response

Although NTHi infection appeared to prime the macrophages to better respond to a subsequent viral challenge, as a consequence, MDM appeared less capable of controlling NTHi infection once IAV was added to the infection culture. To ascertain whether this increase was due to co-infection-dependent modulation of MDM genes previously identified as important for the macrophage response to NTHi intracellular infection, the eight previously validated MDM genes in chapter 4 were also investigated in IAV-infected, NTHi-infected and co-infected macrophages at 48 h.

As upregulation of these eight macrophage genes in response to NTHi infection has already been identified in the dual RNASeq analysis and validated in MDM using additional clinical strain of NTHi, it was important to first characterise the regulation of these genes in response to IAV infection at 48 h. The top ranked hub gene in the MDM blue module network, *CASP4*, was significantly upregulated at 48 h in response to IAV infection alone (Table 6.3, p=0.0313). In contrast, the other two top ranked genes, *PNRC1* and *SGPP2*, as well as *IL1B*, were not significantly regulated in response to IAV infection. The two remaining blue module genes, *GPB1* and *IRF1* were significantly upregulated in response to IAV infection (p=0.0156 and p=0.313, respectively), with *LAMP3* also upregulated, but not statistically significant (p=0.1094). *ACOD1* was the most highly upregulated gene, demonstrating a 103-fold increase in response to IAV compared to the uninfected control (p=0.0156).

Table 6.3. The impact of IAV infection on NTHi-specific intracellular immune response MDM genes at 48 h.

The eight genes identified as important for macrophage response to NTH in the dual RNASeq analysis were measured in MDM infected with IAV alone. Data are expressed as median fold change relative to the uninfected control at 48 h, [IQR]. Data were analysed by Wilcoxon signed-rank test. Statistically significant fold changes (p<0.05) are indicated in bold.

Gene	Fold Change v Uninfected	p-value
CASP4	1.53 [1.27 – 2.06]	**0.0313**
SGPP2	0.84 [0.52 – 1.5]	0.4063
PNRC1	1.42 [0.64 – 2.26]	0.2813
IL1B	1.99 [1.04 – 3.29]	0.0781
GBP1	76.76 [28.5 – 133.3]	**0.0156**
LAMP3	4.12 [1.4 – 15.1]	0.1094
IRF1	2.25 [1.47 – 5.36]	**0.0313**
ACOD1	103.4 [19.08 – 235.8]	**0.0156**

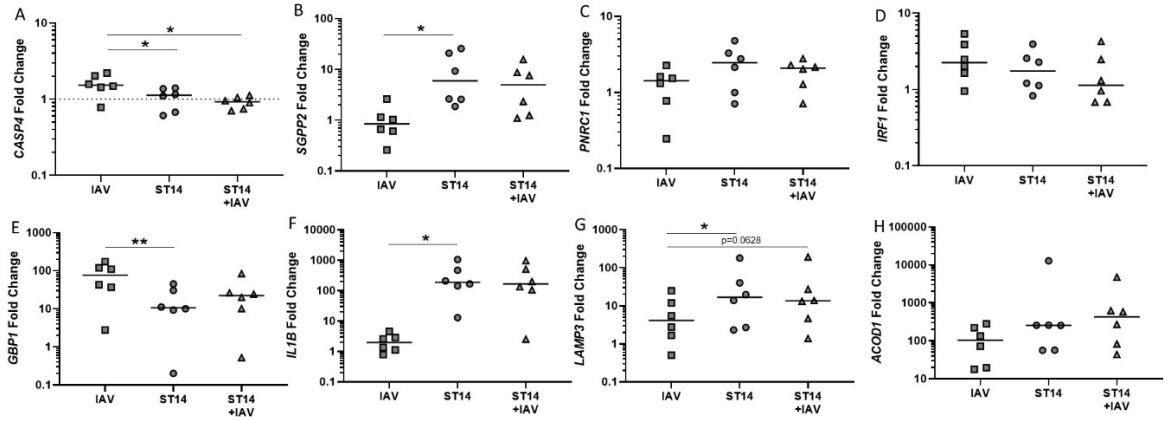

Figure 6.20. Differential modulation of the macrophage immune response between IAV, NTHi and co-infected MDM. The expression of (A) *CASP4*, (B) *SGPP2*, (C) *PNRC1*, (D) *IRF1*, (E) *GBP1*, (F) *IL1B*, (G) *LAMP3* and (H) *ACOD1* which were identified in the dual RNASeq analysis as important in the macrophage response to NTHi ST14 were measured at 48 h following infection with IAV (square), NTHi (circle) or both pathogens (triangle). Genes of interest were normalised to housekeeping gene *B2M* and are expressed as fold change relative to the uninfected control, which is shown as a dotted line, where appropriate. N=6. Graphs show paired data and lines indicate medians. Data were analysed by Friedman test with Dunn's multiple comparisons; *p<0.05, **p<0.01

The regulation of the eight aforementioned genes were next compared between IAV-infected, NTHi-infected and co-infected MDM at 48 h. Infection with IAV alone resulted in higher levels of *CASP4* gene expression compared to NTHi-infection alone (p=0.0281, Figure 6.20A). *CASP4* gene expression was also significantly lower in co-infected MDM compared to IAV-infected MDM (p=0.0281). As *CASP4* was identified as central to the macrophage response to intracellular NTHi infection, lower *CASP4* expression may explain increased NTHi presence in co-infected samples at 48 h.

Subsequently, modulation of the remaining MDM genes (Figure 6.20B-H) in NTHi-infected and co-infected samples compared to the uninfected controls, indicate that NTHi presence results in a sustained activation of macrophage inflammatory genes. *SGPP2, IL1B* and *LAMP3* gene expression was significantly higher in MDM infected with NTHi only, compared to IAV-infection alone (all p<0.05). Activation of macrophage inflammatory genes at 48 h, regardless of IAV presence, was similar following MDM infection with additional NTHi strains, with no strain-dependent differences in expression detected for any of the genes measured (Figure 6.21A-H).

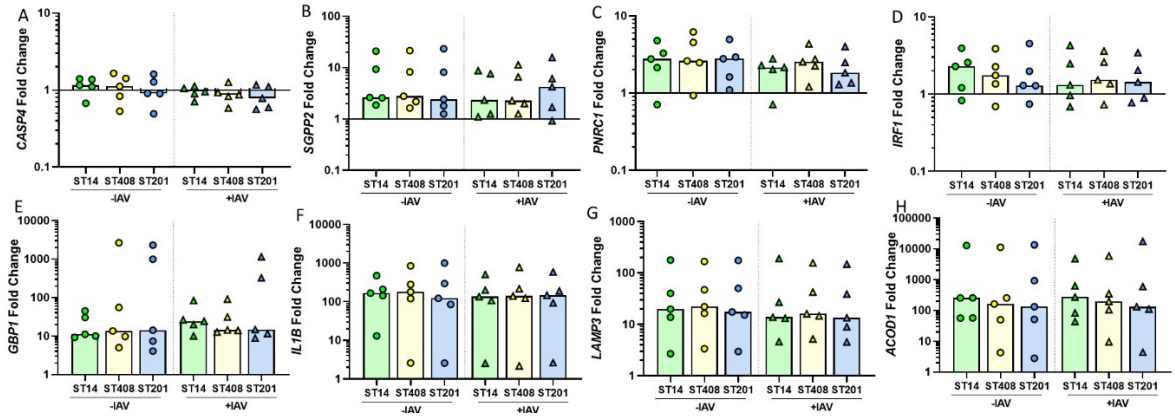

Figure 6.21. MDM gene expression during NTHi-only or NTHi-IAV co-infection was not strain-dependent. The expression of (A) *CASP4*, (B) *SGPP2*, (C) *PNRC1*, (D) *IRF1*, (E) *GBP1*, (F) *IL1B*, (G) *LAMP3* and (H) *ACOD1* following infection with additional clinical strains of NTHi, with and without influenza A infection (+IAV or –IAV respectively) were measured at 48 h. N=5. Graphs show paired data and lines indicate medians. Data were analysed by Friedman test with Dunn's multiple comparisons.

To confirm the sustained upregulation of macrophage inflammatory responses at 48 h, the release of macrophage inflammatory mediators in response to the three different pathogen combinations was next assessed. The transcriptomic analysis in chapter 4 highlighted a number of upregulated genes involved in cytokine production and recruitment of other immune cells, an important effector function of the macrophage immune response. A small panel of mediators were validated by Luminex or ELISA in chapter 4, which demonstrated upregulation of all mediators in response to NTHi at 6 h and 24 h, except for IL-33, which was not detected at either time point (Section 4.2.6.2).

MDM release of these same mediators from chapter 4 was next assessed in response to co-infection at 48 h. Again, IL-33 was not detected at 48 h in response to single or dual pathogen combinations (Figure 6.22A). As previously observed at 6 h and 24 h, MDM CCL20 release in response to NTHi and co-infection at 48 h was above the ULOQ and unable to be accurately quantified (data not shown). However, infection with IAV resulted in MDM release of 67.04 pg/ml at 48 h, which was within the range of quantification for this analyte (8.558 pg/ml – 2169.997 pg/ml). Although CCL20 release was significantly lower in response to IAV than in response to NTHi infection, due to the high abundance of CCL20 protein above the upper limit of quantification not allowing for accurate quantification of CCL20, statistical testing between infection conditions was unable to be performed.

Although IL-17C was detected at 6 h and 24 h, this cytokine was not detected in the majority of samples at 48 h. Very low levels of IL-17C were measured in two co-infected samples, however these values were below the LLOQ (Figure 6.22C). Release of the other measured neutrophil chemoattractant, IL-8/CXCL8 was significantly higher from co-infected MDM compared to uninfected MDM (p=0.0087). The general inflammatory proteins TNF-α, IL-1β and IL-6 were also

most significantly elevated in response to co-infection compared to uninfected MDM (Figure 6.22D; p=0.0014 for TNF-α, Figure 6.22E; p=0.0036 for IL-1β and Figure 6.22F; p=0.0423 for IL-6). MDM infected with NTHi-alone also released higher amounts of IL-1β (p=0.0036), IL-6 (p=0.0858) and TNF-α (not significant) compared to uninfected MDM. Although TNF-α release in response to IAV infection alone was detected, IAV infection did not stimulate significant release of IL-1β or IL-6.

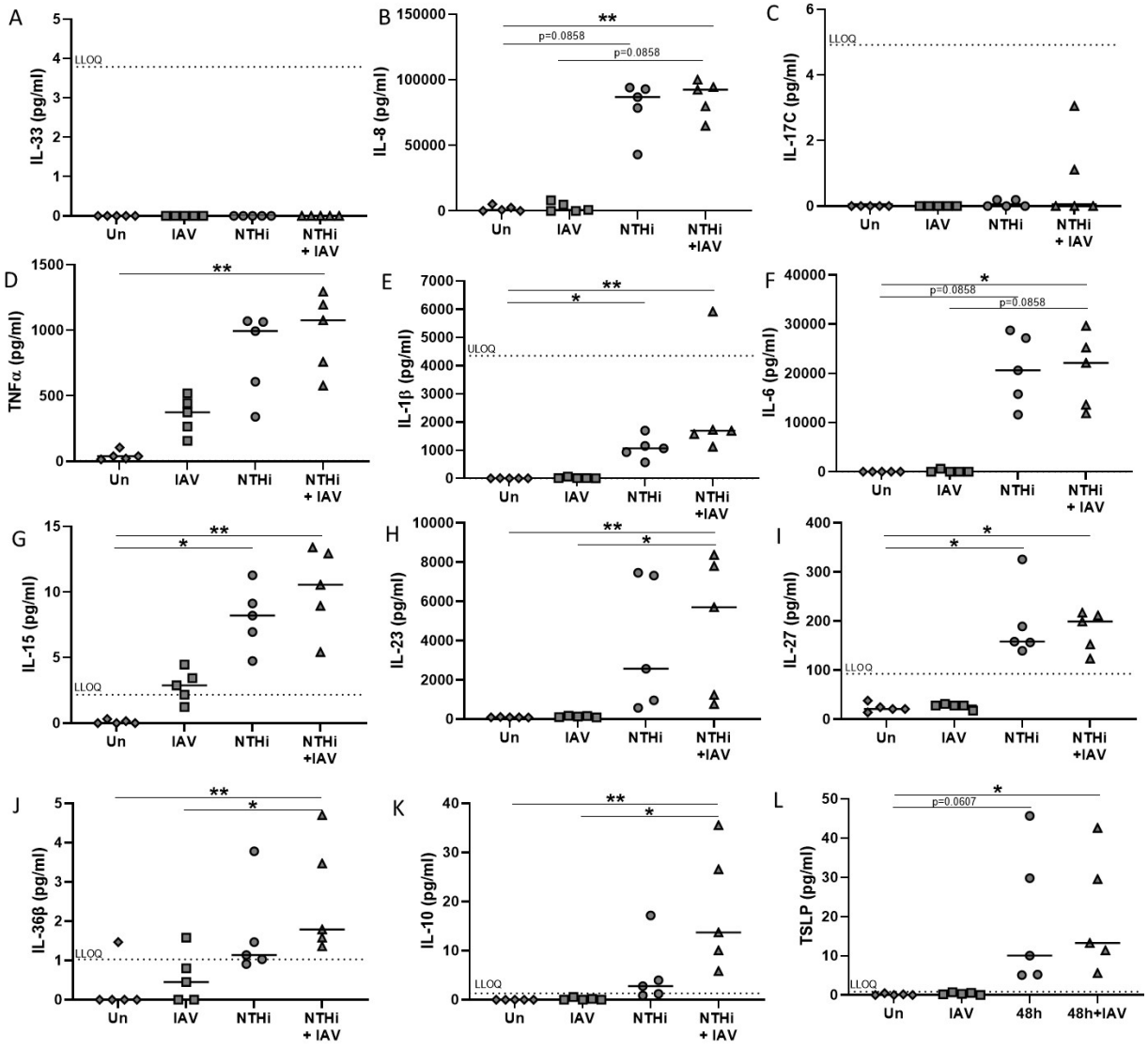

Figure 6.22. MDM release of mediators at 48 h in response to IAV, NTHi or co-infection. MDM were infected with NTHi ST14 or media control (Un), followed by addition of IAV at 24 h as described in Figure 6.1. MDM mediator of (A) IL-33, (B) IL-8, (C) IL-17C, (D) TNF-α, (E) IL-1β, (F) IL-6, (G) IL-15, (H) IL-23, (I) IL-27, (J) IL-36β, (K) IL-10 and (L) TSLP into harvested cell culture supernatants at 48 h in response to NTHi, IAV or co-infection was measured by Luminex or ELISA (IL-6 and IL-8 only), with horizontal dashed lines on graphs indicating the upper limit of quantification (ULOQ) or lower limit of quantification (LLOQ) of the Luminex assay for each specific analyte. N=5. Graphs show paired data and bars indicate median values. Data were analysed by Friedman test with Dunn's multiple comparisons; *p<0.05, **p<0.01

Similarly, the four lymphocyte-related cytokines IL-15, IL-23, IL-27 and IL-36β (Figure 6.22G-J) were all released in higher amounts by co-infected MDM compared to uninfected controls (IL-15; p=0.0036, IL-23; p=0.0036, IL-27; p=0.0423, IL-36β; p=0.0036). Unlike the earlier 6 h and 24 h time points, levels of IL-36β release for all infection conditions were below the LLOQ at 48 h, therefore differences in release must be interpreted with caution, even though IL-36β release followed the same trend observed for the other measured mediators (Figure 6.22J).

Increased release of the inflammatory regulators IL-10 and TSLP was detected from co-infected MDM compared to uninfected MDM at 48 h (Figure 6.22K & L; p=0.0057 and p=0.0291 respectively). Infection with IAV alone did not stimulate significant levels of pro-inflammatory mediator release, indicating that MDM release of these select mediators was NTHi-specific. This was likely due to selection of these mediators from the dual RNASeq analysis, which although evidence led, would have introduced bias against selection for mediators regulated by MDM in response to IAV alone. It was next assessed whether MDM release of these mediators was sustained in response to NTHi persistence across the time points tested (Table 6.4).

Table 6.4. Summary of MDM pro-inflammatory mediator release to NTHi and NTHi-IAV co-infection. Median concentration of each MDM analyte (all pg/ml) in response to NTHi ST14 infection at 6 h, 24 h, 48 h or co-infection with IAV at 48 h (48h +IAV). N=5. Mediator release was measured by a Luminex assay except for IL-6 and IL-8 which were measured by a DuoSet® ELISA kit. Values are median pg/ml, [IQR]. Concentration of CCL20 was unable to be extrapolated due to values above the upper limit of quantification of the Luminex assay, so was designated as concentration not available (NA)

Analyte	6 h	24 h	48 h	48 h + IAV
CCL20	NA	NA	NA	NA
IL-1β	258.6 [112 – 537]	1609 [940 – 1609]	1062 [752 – 1426]	1688 [1346 – 3821]
IL-10	817.3 [25 – 3081]	216.1 [53 - 602]	2.78 [1 - 11]	13.73 [8 - 31]
IL-15	1.08 1.08 – 1.67	8.15 [5.69 – 9.65]	8.21 [5.85 – 10.21]	10.56 [7.18 – 13.18]
IL-17C	11.08 [10.2 – 11.2]	12.84 [11.3 – 15.4]	0 [0 – 0.2]	0 [0 – 2.1]
IL-23	1949 [930 – 3490]	42664 [23968 - 101765]	2573 [774 – 7392]	5700 [1004 – 8088]
IL-27	34.49 [26.1 – 36.1]	149.5 [116.1 – 186.4]	158.1 [148 – 257.6]	199.0 [137.9 – 214.3]
IL-33	0	0	0	0
IL-36β	1.3 [1.1 – 3.3]	2.11 [1.63 - 4]	1.14 [0.97 – 2.625]	1.79 [1.47 – 4.085]
IL-6	23950 [17715 - 33585]	37110 [27630 - 61680]	20610 [13705 - 27970]	22130 [12755 - 27445]
IL-8	11520 [9542 - 19478]	88960 [60600 - 107670]	86860 [60850 - 93520]	92440 [72380 - 10000]
TLSP	17.12 [12.78 – 22.36]	120.3 [76 – 374.6]	10.06 [5.17 – 37.77]	13.25 [8.5 – 36.08]
TNF-α	9150 [8604 – 11294]	8828 [8019 - 13303]	994.0 [475 - 1067]	1077 [669 - 1246]

MDM release of mediators such as IL-23, IL-36β, IL-6 and TNF-α appeared to peak at 24 h, with higher release of these mediators measured at 24 h compared to 48 h (Table 6.4). Conversely, release of IL-1β, IL-15, IL-27 and IL-8 was generally significantly higher at 24 h and 48 h compared to 6 h, though this was likely due to the differences in time point; '6 h' samples were collected after 6 h of incubation, whereas '48 h' time point samples were harvested after 22 h incubation following removal of IAV or uninfected media control.

However, release of IL-1β, IL-15, IL-27 and IL-8 remained elevated and did not decrease over time, with no significant changes in protein levels measured between 24 h and 48 h, regardless of IAV presence at 48 h (Figure 6.23A-D). As these four mediators were not significantly upregulated in response to IAV infection alone at 48 h, the sustained release of these mediators during co-infection was likely due to NTHi modulation of MDM responses.

In contrast, although MDM release of IL-10 and TSLP was higher in samples with persistent NTHi infection compared to MDM infected with IAV alone at 48 h (Figure 6.22K & L), MDM release of these two immune regulators at 48 h was significantly lower compared to amount of protein released earlier in the infection time course (Table 6.4). In response to NTHi at 6 h, IL-10 release was 817.3 pg/ml, which fell to 216 pg/ml at 24 h (Figure 6.23E). However, despite the continued presence of NTHi at 48 h, only 2.78 pg/ml IL-10 was detected. Although higher levels of IL-10 were detected in co-infected samples (13.73 pg/ml), this was still lower compared to the earlier time points.

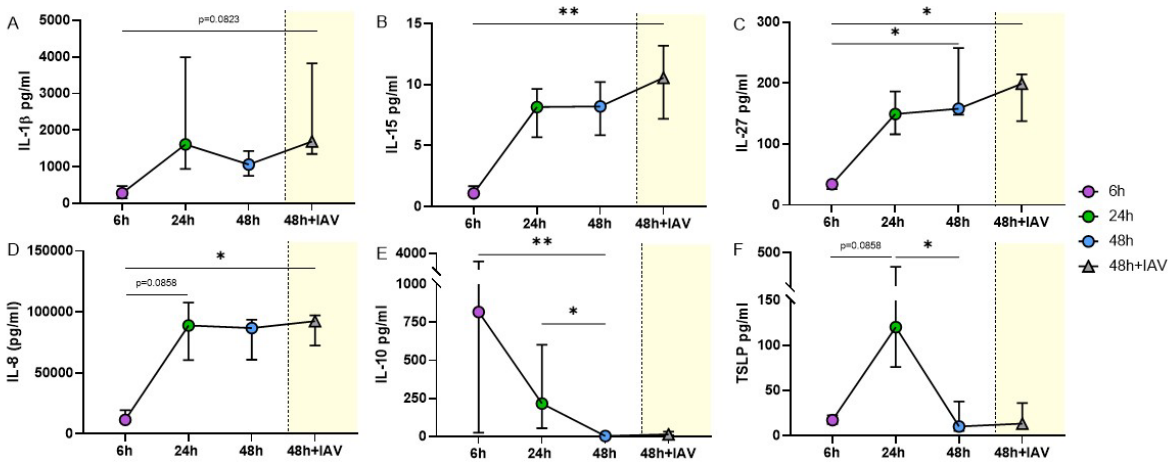

Figure 6.23. Modulation of MDM inflammatory mediator release in response to NTHi persistence.

Sustained release of (A) IL-1β, (B) IL-15, (C) IL-27 and (D) IL-8 at 24 h, 48 h and during NTHi ST14-IAV co-infection (48h + IAV). In contrast, release of (E) IL-10 and (F) TSLP peaked during the early phase of infection and were no longer significantly upregulated at 48 h regardless of the presence or absence of IAV. Dots show medians (n=5) and error bars indicate IQR. Yellow box indicates co-infected samples. Data were analysed by Friedman test with Dunn's multiple comparisons; *p<0.05, **p<0.01.

For TSLP, the highest level of release was 120.3 pg/ml at 24 h in response to NTHi (Figure 6.23F). However TSLP release at 48 h was almost ten times lower at 48 h in co-infected samples (13.25 pg/ml), despite the presence of two pathogens, with lower amounts of TSLP released by NTHi alone MDM (10.06 pg/ml).

Although these data indicate differences in modulation of macrophage inflammatory processes to different pathogens and pathogen combinations, the individual dynamics of each mediator from initial upregulation of gene expression to protein production to protein release to eventual uptake and recycling of protein requires further exploration to ensure any intricacies that differ between each protein is not overlooked and generalised. Nonetheless, the confirmation of increased pro-inflammatory mediator release corroborates the sustained inflammatory gene expression data in co-infected samples, indicating that persistent NTHi infection of macrophages resulted in a sustained inflammatory response that was not sufficient to completely clear either pathogen by 48 h. As such, NTHi modulation of macrophage responses may perpetuate the inflammatory environment during and prior to viral infection, potentially inducing dysregulated inflammatory responses which may contribute to exacerbation of disease.

6.3 Discussion

Studies investigating host-pathogen interactions often consider the interaction of a single pathogen with a host. Although this is important in exploring the precise mechanisms of the host-specific pathogen interaction, it does not necessarily reflect the *in vivo* lung landscape. The last decade has heralded a surge in lung microbiome studies, ending the original notion of lung sterility and increasing our understanding that the lung harbours a rich, unique profile of microbes. Cataloguing differences in lung microbiome composition between healthy and diseased states have been useful in identifying the organisms potentially responsible for contributing to disease pathogenesis[71]. Several studies have identified *Haemophilus influenzae* to be associated with asthma development, progression and steroid resistance[24,25,462], with presence of this species detected during both stable state and disease exacerbations[65,86]. To further complicate matters, Iikura *et al.* (2015) identified bacteria and virus co-infection in approximately one-fifth of asthma patients during exacerbations, including co-infection of *H. influenzae* and influenza[65]. Although the lung microbiome can be perturbed following use of antibiotics, administration of vaccines or respiratory tract infections[500–502], the reverse impact of the resident microbes perturbing the pathogen infection process and subsequent immune response of host cells has not been as extensively studied. Thus one of the main aims of this thesis was to model NTHi intracellular infection of MDM to determine the impact of a subsequent IAV infection on the MDM response and the NTHi already present within the model, rather than modelling an acquired secondary bacterial infection.

The working hypothesis for this thesis was that prior NTHi infection of macrophages would compromise the ability of the macrophage to respond to a subsequent viral challenge. In fact, the opposite of this hypothesis was observed. The work described in this chapter demonstrated that co-infection of MDM with NTHi and IAV resulted in two distinct alterations in the infection process: the IAV infection levels decreased, whereas NTHi load increased, compared to infection of each pathogen in isolation. This NTHi-IAV co-infection resulted in a differential immune response compared to infection of macrophages by each pathogen independently. NTHi-IAV co-infection of macrophages has not been widely studied, however studies have used different combinations of pathogens and host cells to investigate co-infection dynamics. Two murine studies investigating IAV and *S. pneumoniae* co-infection both observed similar results to the work in this chapter; decreased viral load and increased bacterial load[503,504]. In contrast, a study by Ouyang *et al.* (2014), found no difference in IAV replication following pre-treatment of epithelial cells with NTHi or *S. pneumoniae*[344]. The conflicting results of these studies are likely due to a number of factors including the experimental host model used, cell type, pathogen combinations and sequence of infection. As such, Ouyang and colleagues postulate that the outcome of their *in vitro* work would be different if higher bacterial loads were used. Therefore, conclusions derived from co-infection

studies must carefully consider the experimental model and infection protocol used to address the desired question or hypothesis.

Distinguishing between prior colonisation and acquired secondary bacterial infection was important, given that NTHi has been detected within the airway of individuals with chronic respiratory disease during stable periods. A murine study investigating the interactions between *Haemophilus influenzae* type b (Hib) and influenza found that all mice survived when infected with Hib 3 days prior to influenza challenge[261]. Timing of macrophage responses appeared to be crucial in this current work. Once it was identified that co-infected MDM did not upregulate type I IFN responses to the same extent as IAV-only infected MDM at 48 h, it was hypothesised that the NTHi infection activated macrophage anti-viral pathways prior to addition of IAV. This hypothesis was confirmed by re-analysis of the dual RNASeq transcriptomic data which identified enrichment of macrophage anti-viral pathways in response to NTHi at both 6 h and 24 h. This observation was further validated using a small number of anti-viral genes by qPCR and measuring the release of anti-viral immune mediators into the cell culture supernatants by a Luminex assay.

Recent work has shown that prophylactic administration of IFN-β to MDM, alveolar macrophages and primary bronchial epithelial cells resulted in reduced IAV infection of all three cell types[497]. Notably, this work showed time-dependent effects of IFN-β stimulation, with a 16 h window prior to IAV challenge being crucial for modulation of infection. As NTHi infection of MDM stimulated type I IFN production after 6 h and 24 h of infection, it can be postulated that a similar phenomenon is occurring in this current work. Although induction of *IFNA/B* gene expression and IFN-α/β release were both measured in IAV-only infected MDM at 48 h, the release of IFNs between 24 h and 48 h was not enough to restrict IAV infection compared to co-infected cells, which experienced NTHi-mediated upregulation of IFN pathways at least up to 18 h prior to IAV challenge. In contrast, the lack of a priming effect on MDM not previously infected with NTHi rendered them more susceptible to IAV infection.

NTHi-induced interferon signalling has been previously demonstrated by Tuvim *et al.* (2009) to be beneficial for host survival during viral infection[505]. Mice treated with aerosolised NTHi lysate prior to influenza A challenge showed reduced mortality and viral titres, which were suggested to be due to the NTHi lysate-induced early stimulation of lung mucosal innate immunity, including interferon signalling and increased levels of BAL IL-6 and TNF-α. However, 3 days post IAV challenge, significantly lower levels of BAL cytokines were recovered from mice that had been pre-treated with NTHi lysates, therefore priming cells with NTHi lysate resulted in faster resolution of infection and inflammation. As the work in this chapter uses a final endpoint of 48 h, resolution of inflammation following co-infection was not able to be assessed. However as Tuvim *et al.* did not use live NTHi, interaction of NTHi with the host during co-infection was not explored, and it is

possible that the presence of live NTHi may have resulted in a sustained inflammatory response, as observed in this current chapter.

Building on this observation, Hartwig and colleagues demonstrated that live, whole NTHi infection of epithelial cells inhibited RSV infection and postulated that prior exposure to bacteria such as NTHi can be protective against a subsequent viral infection[345]. However, this aforementioned study did not consider the impact of co-infection on the cumulative inflammatory response, only viral titres. Therefore, caution must be taken when suggesting these results are 'protective' and the impact of a sustained inflammatory response driven by NTHi persistence and potential subsequent bacterial outgrowth following viral infection within the airway must be considered; both of which were detected in this current work. This consideration is particularly important for individuals with chronic respiratory disease who may already have a dysregulated airway immune response.

Furthermore, anti-viral immunity is impaired in asthma, with several studies showing deficient type I interferon responses[312,506,507]. Although an IFN response to NTHi was observed in this current *in vitro* work, this IFN response may not be activated during longer, chronic NTHi airway colonisation *in vivo.* The end point of the 'priming' effect of NTHi intracellular infection on MDM anti-viral immunity was not determined in this current work. If IAV was added at later intervals, such as 48 h, 5 days, 1 week etc., it is possible that MDM would no longer be primed into an anti-viral state and return to a more IAV-permissible phenotype. Watson *et al.* (2020) demonstrated that MDM incubated with IFN-β for 16 h had elevated levels of ISG expression including *MX1*, *OAS1* and *DDX58* for up to 1 week after removal of IFN-β, which also resulted in reduced percentage of IAV-infected MDM. After 2 weeks however, the prophylactic benefit of IFN-β administration was lost. Although Watson *et al.* demonstrated that MDM remained responsive to IFN-β after 3 weeks of chronic administration, this current work shows that levels of IFN-β released by MDM decreased at 24 h and 48 h in response to NTHi-alone, indicating that NTHi persistence may not chronically stimulate IFN-β protein release. Thus, given that the length of NTHi chronic airway colonisation is suggested to be longer than the suggested optimum window of priming observed in this thesis[421], it may be likely that IFN and ISG expression will have returned to baseline prior to any viral challenge *in vivo*.

Conversely, instead of beneficially activating IFN pathways, the chronic presence of NTHi in the airway may instead contribute to the diminished IFN response detected in asthma as a result of sustained stimulation. Impaired airway IFN immunity has been demonstrated in the lung epithelium, with bronchial epithelial cells obtained from individuals with asthma unable to mount an efficient antiviral immune response when challenged *in vitro* with rhinovirus[312]. This observation has been extended further to innate immune cells. Sykes *et al.* (2012) reported that BAL cells, of which were 95% predominantly macrophages, obtained from asthmatic patients infected with rhinovirus *ex vivo* exhibited a delayed IFN response compared to healthy controls[508]. The delayed response was not observed in matched PBMC, suggesting the immune defect was specific to the

lung. It has been suggested that imprinting of macrophage function and phenotype is influenced by the lung microenvironment, with Aegerter *et al.* (2020) demonstrating that following respiratory tract infection, epigenetic modifications were not similar for all airway macrophages, with differences identified between recruited and resident macrophages[509]. It is possible that the inflammatory milieu characteristic of the asthmatic airway may promote the development of a specific epigenetic programme of innate immune training, in which intracellular infection may play a role. As such, the result of sustained inflammation by persistent bacterial presence may contribute to the deficient IFN responses to a viral infection *in vivo*[312].

It has been well documented that secondary bacterial infection following viral infection results in increased morbidity and mortality[252] with *H. influenzae* isolated from individuals suffering from pneumonia during numerous influenza epidemics and pandemics over the last century[510]. Due to the original notions of lung sterility, it was believed that bacteria isolated from the lower respiratory tract represented an acquired/secondary infection[71]. As such, the impact of airway microbiota presence prior to influenza infection has not been extensively investigated. Rather, NTHi-host interactions following IAV infection have typically been investigated in the context of secondary bacterial infections, with NTHi- IAV co-infection performed either simultaneously or sequentially in the hours or days following IAV challenge. Although an increasing number of studies have begun to consider NTHi infection prior to viral challenge, these studies do not necessarily prioritise measuring NTHi load as an experimental outcome[345,511].

This chapter identified increased presence of NTHi following co-infection, which was observed for all three NTHi strains used. The original hypothesis for this project stated that NTHi infection would compromise the ability of the macrophage to respond to a viral infection. Although it appears that this hypothesis was disproved as IAV infection levels actually decreased instead, the consequence of co-infection was macrophage loss of NTHi control, resulting in NTHi proliferation. Importantly, loss of control was not due to cell death, as MDM viability did not significantly change, as determined by use of a LDH assay. Therefore, although the hypothesis was specifically addressing the impact of the NTHi infection on the progression of IAV infection, co-infection dynamics are much more complex and co-infection does result in compromising the macrophage ability to respond – but to the bacterium and not the virus as originally hypothesised. Although the results showing bacterial outgrowth as a consequence of viral infection may be reminiscent of an acquired secondary bacterial infection, the data in this chapter have important implications for individuals with chronic NTHi airway colonisation prior to arrival of a virus. Expansion of NTHi following viral co-infection could contribute to increased exacerbation, hospitalisation and pneumonia risk in asthmatic individuals.

The mechanisms of increased NTHi proliferation during co-infection were not clear, however the dual RNASeq analysis of NTHi-MDM intracellular infection identified a transcriptomic signature of

macrophage immune responses important for NTHi infection at 6 h and 24 h. When investigating the expression of a selection of these genes at 48 h, all genes except for *CASP4* remained upregulated in co-infected samples. Specifically, levels of *CASP4* gene expression in co-infected samples were lower compared to both IAV-alone and NTHi-alone MDM. *CASP4* encodes for caspase-4, an component of the noncanonical inflammasome which can be activated upon detection of intracellular, cytosolic LPS[213]. As *CASP4* was the top hub gene in the blue module most highly associated with NTHi infection, downregulation of *CASP4* during co-infection could potentially explain how NTHi is able to escape the macrophage response.

Upstream of *CASP4* activation is *GBP1*, which has been shown to be important for inhibiting IAV replication *in vitro*[512]. To overcome the host defence response, the IAV NS1 protein interacts with the GBP1 protein, resulting in decreased anti-viral activity[512]. Although the gene expression data in this chapter indicates upregulation of *GBP1* in response to all three pathogen combinations, this does not indicate whether inhibition of protein activity is occurring during infection. However, the transcriptomic data in this thesis does suggest that *GBP1* is important in the macrophage response to intracellular NTHi infection. As such, it is tempting to speculate that IAV inhibition of GBP1 protein to promote viral survival, may in fact benefit and enhance NTHi persistence and escape by preventing intracellular NTHi detection and subsequent noncanonical inflammasome activation. As influenza viruses have evolved many strategies to evade or overcome the host anti-viral response, it is possible that other strategies used by the virus may also enhance the survival of both pathogens.

One of the aims of this thesis was to identify changes in NTHi gene expression associated with intracellular infection of MDM. As the DEGs identified in the NTHi transcriptomic analysis were suggested to be involved in this intracellular persistence, it was important to determine whether the expression of these DEGs were differentially regulated during co-infection. Although the expression of *bioC, mepM* and *dps* during intracellular persistence was strain-dependent, the pattern of expression of each gene for the individual strains remained consistent between 24 h and 48 h. However, transcriptomic adaptations during co-infection were particularly evident for NTHi ST14. The expression of the top two upregulated genes (*bioC* and *mepM*) during intracellular persistence at 24 h were decreased during co-infection at 48 h, compared to NTHi infection in the absence of IAV. Lower levels of these genes could suggest that although these genes were important for intracellular persistence, they are less important for NTHi adaptation to co-infection. As the expression of only three NTHi genes during co-infection was investigated, it is not clear whether a global transcriptomic shift occurs, resulting in a different transcriptomic profile expressed by NTHi during co-infection. As a similar transcriptomic shift may be occurring in co-infected MDM, further sequencing of the co-infected samples at 48 h would be extremely useful.

While the scope of this current project only allowed for investigation of a select number of NTHi and MDM genes at 48 h by qPCR, it was still important to determine whether these genes, which were identified as important for the initial interplay between NTHi and MDM, were dysregulated during co-infection, potentially facilitating NTHi proliferation and loss of MDM bacterial control. However, the bias of using a selection of genes deemed to be important under different conditions (single pathogen infection) may result in more biologically relevant transcriptomic responses in co-infected samples at 48 h being overlooked. Interestingly, a recent pioneering study utilising triple RNASeq demonstrated the feasibility of sequencing host cells co-infected with two pathogens[513]. Moreover, this study identified a subset of genes that were only activated during co-infection, compared to single-pathogen infections. As such, the changes in expression of a small number of MDM and NTHi genes during co-infection shown in this chapter provide a rationale for expanding the sequencing experiment to include IAV and co-infection conditions to better explore transcriptomic modulations that differ between single- and co-infections for both host and pathogen.

Although studies have focussed on how influenza infection results in the development and progression of secondary bacterial infections, rather than how influenza perturbs the status of the already present bacteria, the mechanism of influenza-associated impairment of macrophage responses may be similar. It has been suggested that the induction of type I interferons crucial for restricting IAV infection also promotes bacterial colonisation and increased susceptibility to secondary bacterial infection[514]. A study by Cooper *et al.* (2016) found that prior treatment of MDM with IFN-β resulted in decreased phagocytosis of *S. pneumoniae* [240]. Furthermore, Yang *et al.* (2019) showed that macrophage phagocytosis and bacterial killing was diminished in mice with functional IFNAR1, compared to IFNAR1$^{-/-}$ mice[515]. Other studies have shown that IFNAR1 deletion restored host defence to other bacteria *including F. novicida*[516]*, Listeria monocytogenes*[517]*, Salmonella enterica* serovar Typhimurium[518]*,* and *Mycobacterium tuberculosis*[519] whereas, an efficient IFN response was beneficial for clearance of some bacterial species including *L. pneumophila*[520]*, K. pneumoniae*[521]*,* and *S. pneumoniae*[522]. The inconsistency in these findings could be due to the experimental model used and the ability of each individual bacterial species to subvert or adapt to the host immune defence.

Other than type I IFNs, it has been suggested that influenza induced IFN-γ production results in impairment of alveolar macrophages to phagocytose and effectively clear bacteria[523]. In the murine lung, it was determined that T cells were the source of the IFN-γ responsible for inhibiting alveolar macrophage clearance of bacteria[524]. Furthermore, levels of virally-induced CXCL10 were found to be associated with increased bacterial load in a human challenge model of live attenuated virus infection followed by *S. pneumoniae* infection[525]. *CXCL10* is an IFN-γ inducible gene and was found in this current work to be upregulated early at the transcript and protein level by NTHi, but more

highly at 48 h by IAV infection alone. MDM upregulation of both *IFNG* gene expression but also IFN-γ release was also measured in response to NTHi, with higher IFN-γ detected in co-infected samples. Detection of IFN-γ and CXCL10 protein at 24 h and 48 h in response to NTHi, IAV and co-infection could suggest that MDM-derived IFN-γ may impair macrophage control of NTHi during co-infection in this experimental model by signalling in an autocrine or paracrine manner. However, given that macrophages have historically not been considered to be the main cellular source of IFN-γ, this observation may not be reflective of the *in vivo* immune response. It has been demonstrated that autologous T cells produce IFN-γ in response to NTHi-infected MDM and T cell derived IFN-γ was measured in response to NTHi infection in explant lung tissue[199,234]. As IFN responses, macrophage phagocytosis and bacterial clearance appear to be functionally linked[515,525], it is clear that the downstream impact of IFN signalling on macrophage bacterial clearance mechanisms requires further clarification.

Furthermore, a potential role for IFN-γ in steroid-resistant airway hyper-responsiveness has been suggested. Li *et al.* (2010) used a murine model to demonstrate that signalling by IFN-γ and IL-27 inhibited translocation of the glucocorticoid receptor to the nucleus, and thus prevented suppression of inflammation by glucocorticoid treatment[526]. Li *et al.* (2010) also identified increased sputum *IFNG* and *IL27* gene expression in patients with neutrophilic asthma, compared to eosinophilic asthma, implicating a role for these two cytokines in mediating steroid resistance and responsiveness *in vivo*. Given that IL-27 was upregulated and sustained in this current MDM model in response to NTHi, it is possible that macrophage release of IFN-γ and IL-27 during NTHi intracellular infection is a mechanism by which steroid-resistance develops.

Although the complex intricacies underlying the differential macrophage immune responses to each pathogen and during co-infection needs deeper exploration, this work indicated that NTHi persistence resulted in a sustained MDM pro-inflammatory response, which altered the subsequent response to IAV infection. Although prior NTHi infection resulted in decreased IAV levels, IAV infection was not completely inhibited and the presence of both pathogens elicited a pro-inflammatory response from MDM. Transcriptomic upregulation of this inflammatory response was confirmed by release of macrophage pro-inflammatory mediators into cell culture supernatants. In agreement with the data in this chapter, Bellinghausen *et al.* (2016) demonstrated that prior NTHi infection of epithelial cells resulted in an altered inflammatory response to RSV, with increased release of IL-6 and IL-8 detected from epithelial cells co-infected with both pathogens[511].

In this current work, no significant differences between NTHi-alone and co-infected MDM release of pro-inflammatory mediators were detected, which could be due to the single 48 h time point used for harvesting supernatants. The experimental limitation of only harvesting supernatants 22 h after challenge with IAV (48 h time point) may have resulted in accumulation of cytokines over 22 h, with any differences in mediator release across the infection period obscured or generalised due

to the single time point used. For example, it is possible that IL-8 release from co-infected MDM at 48 h may have achieved maximal release at an earlier point in the 22 h incubation, whereas MDM infected with NTHi alone may have released a similar amount of IL-8 over a longer period of time throughout the 22 h incubation. Yet, due to the single time point harvest, the release of IL-8 appeared to be very similar for both infection conditions. Thus, ascertaining the dynamic regulation of cytokines during NTHi persistence would require more regular sampling of intermediate time points and may better detect differences between NTHi and co-infected MDM mediator release.

The sustained release of pro-inflammatory mediators during co-infection could potentially be damaging to the airway *in vivo*, as mediators involved in recruitment of other inflammatory immune cells such as CCL20, IL-1β, IL-8, IL-15 and IL-27 may further contribute to inflammatory milieu characteristic of an asthma exacerbation. As such, determining whether MDM continually release low levels of pro-inflammatory mediators during NTHi persistence over 48 h (and longer) could increase our understanding of NTHi contribution to the low level chronic inflammation in the asthmatic airway. Interestingly, the aforementioned study by Lee *et al.* (2010) found that even when low doses of influenza were combined with Hib infection of mice, 55% lethality was still observed[261]. This observation of low levels of influenza in combination with Hib being detrimental to the host could be a consequence of Hib modulating the immune response. Bacterial modulation of host responses could be similarly observed in this chapter; macrophage responses in co-infected samples were distinct to the macrophage response elicited by IAV infection alone. This suggests that during co-infection, macrophage responses are still modulated largely by the colonising bacteria.

The potential for NTHi persistence to promote low levels of chronic inflammation has clinical relevance. Increased inflammation and NTHi presence has been observed *in vivo*, with a higher bacterial load associated with increased inflammation and decreased lung function during COPD exacerbations[339]. The presence of NTHi also increases exacerbation risk in COPD[332], with co-infection with bacteria and virus found to result in more severe exacerbation and more likely to result in hospital readmission[334]. Given that up 80% of asthma exacerbations are virally driven[58,70] and up to 60% of patients are chronically colonised with potentially pathogenic bacteria such as NTHi[44,87], it will be important to determine the contribution of NTHi to airway inflammation or the dysregulated immune response during an asthma exacerbation that would potentially be deemed ‘virally driven’ following positive confirmation of a viral respiratory tract infection.

6.4 Summary

This chapter has shown that adaptation of the NTHi-MDM infection model to include IAV allows for investigation of host-pathogen interactions during co-infection of host cells by clinically relevant pathogens. NTHi-IAV co-infection of MDM results in decreased IAV infection, but increased NTHi load. The increased presence of NTHi detected during co-infection with IAV, could potentially be as

a result of NTHi modulation of bacterial gene expression in response to the addition of IAV during infection of macrophages. Early induction of anti-viral responses by NTHi, as identified in the dual RNASeq data and validated by qPCR and the Luminex assay, suggests NTHi-priming of macrophages via activation of IFN pathways prior to addition of IAV. Despite sustained, upregulated transcriptomic activation of MDM inflammatory processes and release of inflammatory mediators, macrophages were unable to completely clear either pathogen by 48 h. Persistent infection and inflammation could potentially lead to exacerbation of disease states in individuals colonised by such pathogens. The next chapter will use severe asthmatic BAL samples to determine whether NTHi colonisation of host macrophages can be detected *in vivo* and whether NTHi modulation of macrophage gene expression can be detected and correlated with patient clinical characteristics.

Chapter 7 Clinical relevance of NTHi infection of macrophages in severe asthma

7.1 Introduction

The work in this thesis so far has optimised an NTHi-MDM infection model for investigation of NTHi and macrophage transcriptomic changes during intracellular infection. Analysis of transcriptomic changes identified an enrichment of macrophage immune processes, specifically upregulation of an intracellular immune response. Importantly, validation in the MDM model demonstrated that this macrophage response was conserved against multiple NTHi strains. In contrast, the expression of intracellular NTHi DEGs identified in the dual RNASeq analysis was strain-dependent, suggesting the ability to persist *in vitro* varies between NTHi strains. NTHi-MDM interactions modulated responses to subsequent viral challenge; prior activation of antiviral immunity by NTHi resulted in restriction of IAV infection, whereas NTHi presence increased during co-infection. Co-infected samples displayed sustained inflammation compared to samples infected with IAV-alone, which has potential ramifications for individuals chronically colonised with NTHi prior to viral infection.

In particular, NTHi colonisation of the asthmatic airway is associated with severe, neutrophilic, steroid resistant asthma[46,86,347]. Therefore it was important to next assess the clinical relevance of the dual RNASeq transcriptomic analysis of NTHi-infected MDM, to determine whether the *in vitro* gene signature could be detected *in vivo*. FISH will first be used to ascertain the NTHi colonisation status of BAL samples obtained from severe asthma patients. Differences in clinical characteristics and asthma inflammatory phenotypes will be assessed to determine the impact of NTHi presence. The expression of select MDM and NTHi genes identified in the dual RNASeq analysis will be measured in BAL cell pellets to determine whether NTHi-associated modulation of airway gene expression can be detected.

7.2 Results

7.2.1 Clinical characteristics of severe asthma patients

For this work, BAL RNA in TRizol was available for use from a subgroup of 25 severe asthmatics enrolled onto the WATCH study[355]. Patient demographics and clinical characteristics were recorded and matched sputum cell counts were obtained by the members of the WATCH study team. The general demographics of the 25 individuals indicated a higher number of males (15) than females (10) were present in this subgroup, with a median age of 56 and a BMI of 27.6 (Table 7.1). None of the 25 patients were current smokers at the time of sampling, with 11 declaring themselves as ex-smokers (44%) and the remainder being never-smokers (56%). Individuals suffered from a range of comorbidities with 35 different comorbidities identified across the 16 patients with 1 or more comorbidities. The most frequently occurring comorbidities in the 16 individuals were eczema (44%), GORD (25%) and sleep apnoea (25%), with 10/25 (40%) patients reported as being atopic to at least one common aeroallergen following a positive skin prick test.

Table 7.1. Demographics and clinical characteristics of the 25 severe asthmatic BAL samples available for analysis. Values reported are medians [IQR] or (%). # indicates missing patient data; pre-bronchodilator spirometry measures and asthma duration history was not available for 3 patients. Atopy was determined as a positive skin prick test, however this was not performed, or data were missing, for 10 patients. ACQ = asthma control questionnaire, BDP = beclometasone dipropionate, BD = bronchodilator, BMI = body mass index, FEV_1 = forced expiratory volume in one second, FVC = forced vital capacity, ICS = Inhaled corticosteroids, LAMA = long acting muscarinic antagonists, LABA = long acting beta agonist.

Severe asthmatic BAL samples	*n* = 25
General demographics	
Age (yr)	56 [47 – 67.5]
Gender (M/F)	15/10
BMI (kg/m^2)	27.6 [24.8 – 32.7]
Smoking status (Ex/Never)	11/14
Pack years	0 [0 – 4.9]
Clinical characteristics	
Comorbidities (Y)	16
Eczema	7/16 (44%)
GORD	4/16 (25%)
Sleep Apnoea	4/16 (25%)
Atopy (positive skin prick test)	10 (40%)#
Asthma duration (years)	21 [7.5 – 42.5]#
ACQ score	2.3 [1.5 – 2.9]
Number of exacerbations (past 1 year)	1 [1-2.5]
Pulmonary function	
Pre-BD FEV1 %	83.5% [71% - 92.25%]#
Post BD FEV1 %	93% [84.5%– 104.5%]
Pre-BD FEV1/FVC %	69.5% [64.42% - 77.01%]#
Post BD FEV1/FVC	75.89% [67.76% – 77.26%]
Asthma management	
Inhaled corticosteroids (ICS)	18 (72%)
Daily BDP equivalent dose(μg)	2000 [2000 - 2000]
Bronchodilator (LAMA/LABA)	18 (72%)
Combination therapy	24 (100%)
Daily BDP equivalent dose(μg)	2000 [1000 - 2000]
Long term antibiotics	4 (13%)
Biologics	3 (10.3%)

The Asthma Control Questionnaire (ACQ) median score was 2.3, above the recommended 1.5 cut-off score that indicates poor asthma control[527,528]. All 25 patients (100%) were using daily combination inhalers (ICS and bronchodilator), in addition to LAMA/LABA (72%) and/or ICS (72%) therapy alone. Despite this level of treatment, individuals still experienced exacerbations, with a median of 1 exacerbation recorded over the 12 months prior to the recorded study visit. Although spirometry testing indicated an increase in FEV_1 from 83.5% to 93% (p=0.0152) following bronchodilator use, this 9.5% increase was below the clinically significant airflow reversibility measure of 12%[57].

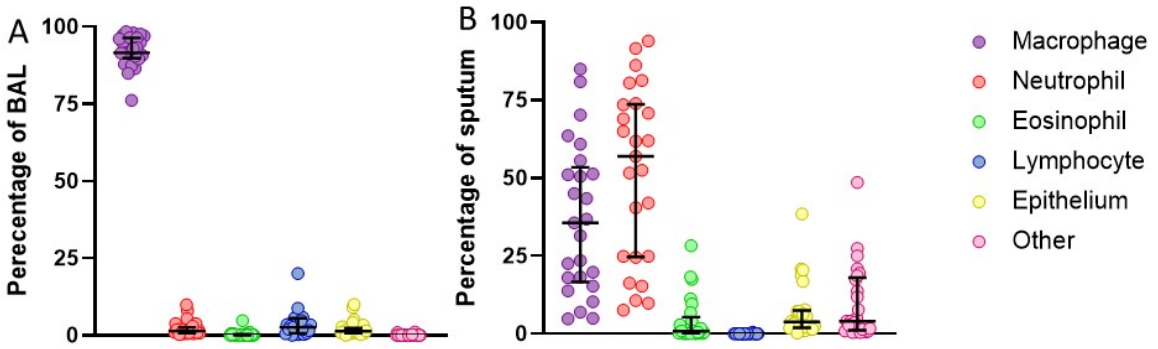

Figure 7.1. Proportion of cell types isolated from the airways of severe asthma patients. The cells recovered from BAL were predominantly macrophages (A), whereas a higher number of neutrophils were isolated from sputum (B), with a smaller percentage of eosinophils, epithelium and other cells such as squamous cells also isolated.

Differential cell counting of BAL cytospins identified macrophages as the predominant cell type in all 25 patients (Figure 7.1A), indicating that BAL was a good sample type to use to investigate macrophage gene expression in the airways of severe asthmatic patients. In contrast, neutrophils were the most abundant cell type present in sputum (57%), followed by macrophages (35.6%) (Figure 7.1B). Sputum inflammatory cell counts have been used to phenotype asthma into neutrophilic, eosinophilic, mixed granulocytic and paucigranulocytic inflammatory sub-phenotypes[529,530].

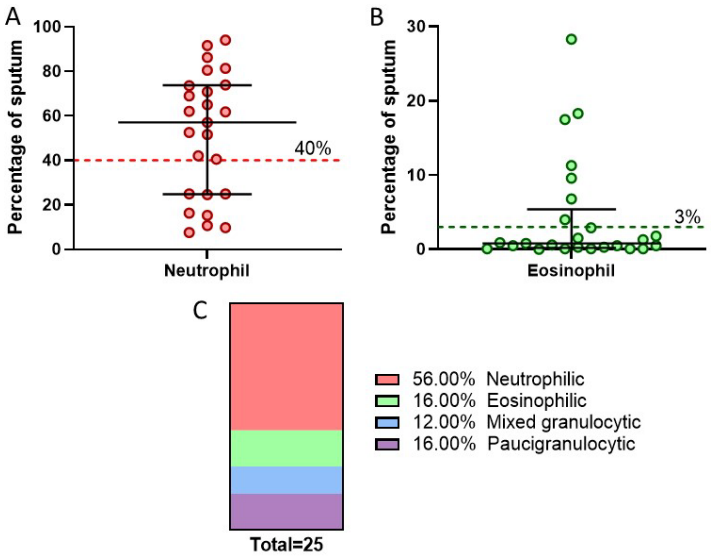

Figure 7.2.Stratification of severe asthma patients into defined asthma inflammatory phenotypes. (A) The neutrophil cut off was set at 40% and (B) the eosinophil cut off was set at 3%. (C) As a result, the 25 patients were stratified into neutrophilic (≥40% neutrophils, <3% eosinophils), eosinophilic (<40% neutrophils, ≥3% eosinophils), mixed granulocytic (≥40% neutrophils, ≥3% eosinophils) or paucigranulocytic (<40% neutrophils, <3% neutrophils) inflammatory phenotypes, indicating over half (56%) of patients were neutrophilic at the time of sampling.

The 25 severe asthma patients were stratified into these sub-groups based on neutrophil (40%) and eosinophil (3%) cell count cut offs[361–363] (Figure 7.2A & B). Although 17 individuals had sputum neutrophil counts ≥40% and 7 had eosinophil counts ≥3%, 3 individuals had counts of both inflammatory immune cells above these cut off percentage values. As such, more than half (14/25, 56%) of the individuals in this cohort were neutrophilic (≥40% neutrophils, <3% eosinophils), whereas only 4/25 (16%) were eosinophilic (<40% neutrophils, ≥3% eosinophils), 3/25 (12%) were mixed granulocytic (≥40% neutrophils, ≥3% eosinophils) and 4/25 (16%) were paucigranuloyctic (<40% neutrophils, <3% neutrophils) (Figure 7.2C).

7.2.2 Detection of NTHi colonisation of severe asthma cells by FISH

To ascertain the presence of NTHi for each patient, FISH was performed on 25 pre-prepared cytospins (as described in Section 2.24). FISH has previously been used by Olszewska-Sosińska *et al.* to identify NTHi in CD14+ adenoid and tonsillar cells[348]. The universal bacterial EUB338A RNA FISH probe, which targets a conserved region of the 16s rRNA gene, was used to detect presence of bacteria in BAL and the NTHi-specific bacterial 16s rRNA probe (HAIN16S1251) was used to specifically identify NTHi presence.

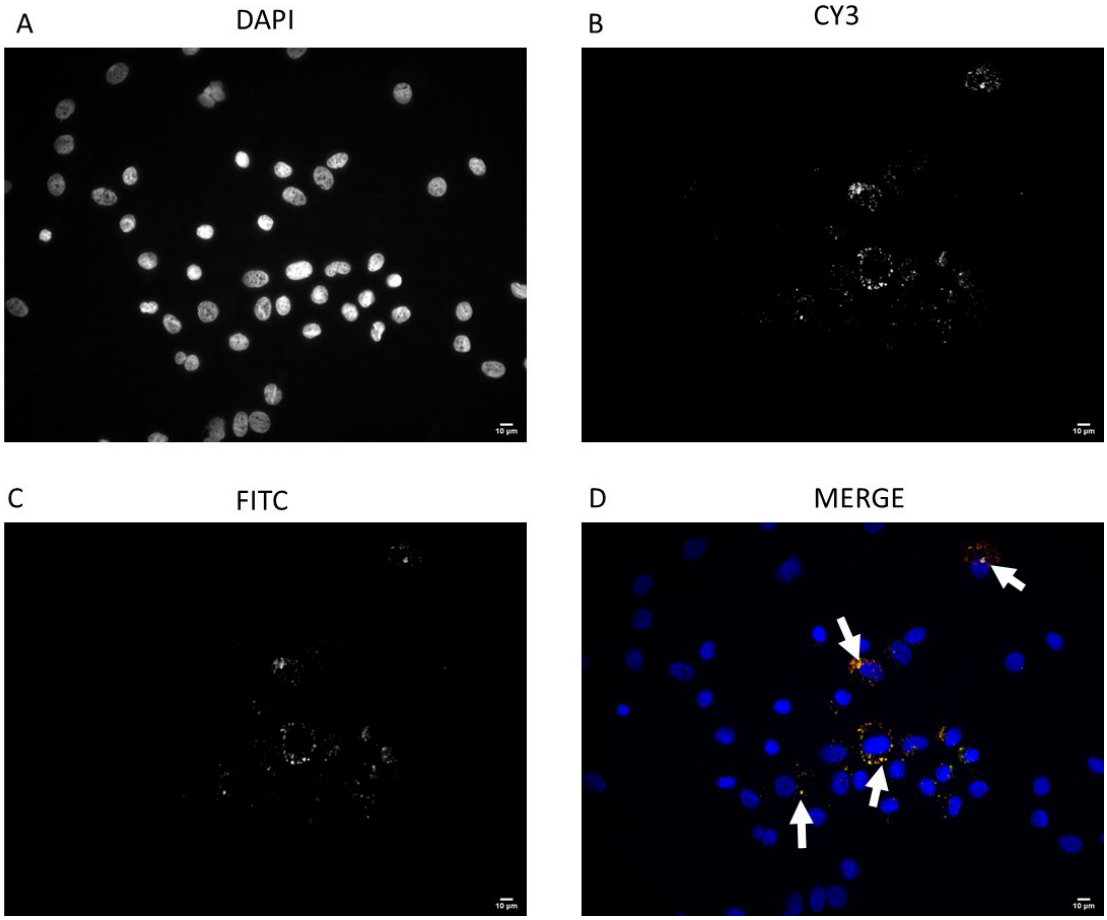

Figure 7.3. Detection of NTHi colonisation of asthmatic BAL cells. Cytospin slides of BAL cells were stained with DAPI (A) an NTHi-specific CY3 probe (B) and a pan-bacteria FITC probe. (D) Colour composite of all three channels. The white arrows indicate fluorescent signal indicating NTHi presence. Representative image of an NTHi-positive sample. Images were acquired using a x40 magnification immersion oil objective. Scale bar shows 10 µm.

The NTHi-specific CY3 signal and pan-bacteria FITC signal were both detectable (Figure 7.3B & C). By overlaying the individual host and bacteria fluorescent signals, it can be seen that the NTHi signal closely associated with host cell single-lobed nuclei (Figure 7.3A), indicating NTHi was closely associated with host macrophages in the airway (Figure 7.3D). NTHi also appeared to be co-colonising host cells (Figure 7.4A) with other, unidentified bacteria (Figure 7.4D). The FITC-pan bacteria probe highlighted the presence of bacteria that were not detected by the NTHi-specific CY3 probe (Figure 7.4B & C).

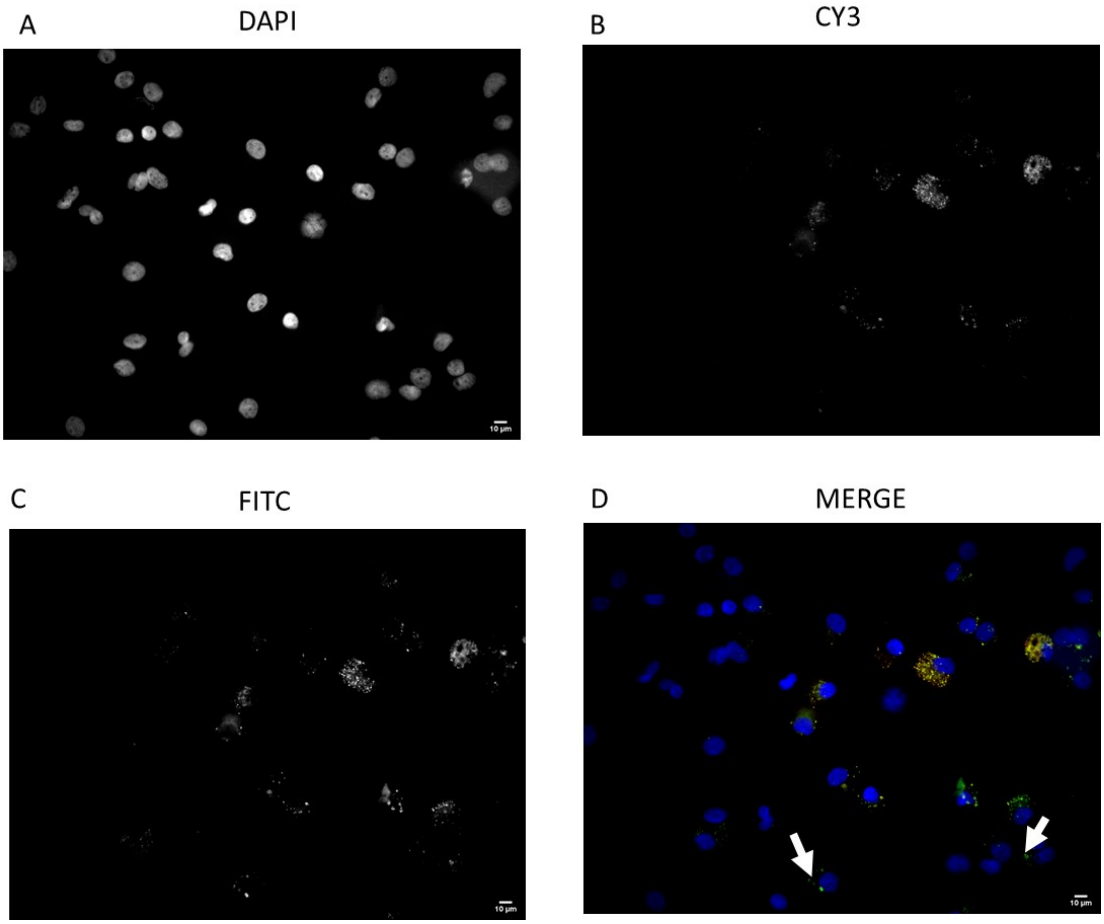

Figure 7.4. Co-colonisation of asthmatic BAL cells with bacteria. Slides were stained with an NTHi-specific CY3 probe, a pan-bacteria FITC probe and counter-stained with DAPI. (A) DAPI stain, (B) NTHi-specific CY3 probe, (C) pan-bacteria FITC probe and (D) colour composite of all three channels. The white arrows indicate FITC positive bacteria that were not CY3-NTHi +, suggesting co-colonisation of an unknown bacterium/bacteria with NTHi. Representative image of a co-colonised sample. Images were acquired using a x40 magnification immersion oil objective. Scale bar shows 10 µm.

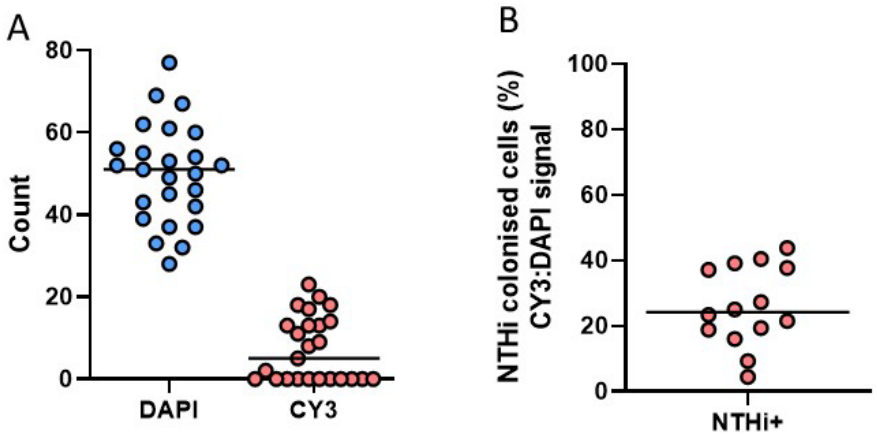

Figure 7.5. Quantification of NTHi-colonisation of asthmatic BAL cells. The DAPI (cell) and CY3 (NTHi) signals detected in 25 asthma BAL cytospins were quantified in Image J. (A) DAPI quantification was performed using the in-built 'Analyse Particles' function. CY3 quantification was performed using the in-built 'Find Maxima' function following use of the 'Gaussian Blur' tool. (B) The percentage cells colonised with NTHi was determined using the DAPI and CY3 cell count values for each sample. Only samples that returned a CY3 count, indicating NTHi presence were included here. Median values are indicated on each graph.

To determine the percentage of NTHi-associated cells for each sample, the DAPI and CY3 signals were quantified in ImageJ. Quantification of the DAPI signal resulted in a median host cell count of 51 cells per field of view (Figure 7.5A). The CY3 signal was quantified by identifying only a single CY3-signal per host cell (Section 2.24.1). This was to calculate the percentage of host cells infected, rather than bacterial load, as the representative nature of image acquisition for each field could incorrectly inflate the amount of NTHi colonisation for each patient sample. Only 56% of patient samples (14/25) were deemed to have a detectable CY3 signal following quantification and therefore presence of NTHi (herein referred to as NTHi+). The NTHi-CY3 counts and host cell DAPI counts were used to determine the percentage of NTHi-colonisation within each patient sample. For the 14 samples with detectable NTHi presence, the median percentage of colonised cells per field was 23.4% (Figure 7.5B).

7.2.3 Impact of NTHi presence on the clinical characteristics of severe asthma patients

When comparing the clinical characteristics between the 14 NTHi+ patients and the 11 NTHi- patients, only the increased duration of asthma for NTHi+ individuals (45 years), compared to NTHi- individuals (22.5 years) was determined as statistically significant (Table 7.2, p=0.0436). Although those colonised with NTHi had an older median age of 59 compared to 50 in the NTHi- group, this difference was not statistically significant (p=0.2). Similarly, the NTHi+ group had lower spirometry lung function measures but were also not significant. Both groups had no significant differences in ACQ score, number of exacerbations over the past year and steroid use/dose, perhaps as a result of the similar severity of disease exhibited by all patients, independent of NTHi colonisation status.

Table 7.2. Comparison of demographics and clinical characteristics between NTHi+ and NTHi- samples. The 25 severe asthma patients were split based on the outcome of the FISH analysis into NTHi+ (14) and NTHi- (11) groups. Values reported are medians [IQR] or (%). # indicates missing patient data; pre-bronchodilator spirometry measures and asthma duration history was not available for 3 patients. Atopy was determined as a positive skin prick test, however this was not performed, or data were missing for 10 patients. Continuous data were analysed by Mann-Whitney U test, categorical data were analysed by Fisher's exact test. Bold indicates p-values determined as statistically significant ($p<0.05$). ACQ = asthma control questionnaire, BD = bronchodilator, BDP = beclometasone dipropionate, BMI = body mass index, FEV_1 = forced expiratory volume in one second, FVC = forced vital capacity, ICS = Inhaled corticosteroids LAMA = long acting muscarinic antagonist, LABA = long acting beta agonist

	NTHi +	NTHi -	p-value
n	**14**	**11**	
General demographics			
Age (yr)	59 [54.25 – 67.25]	50 [41 – 68]	0.2167
Gender (M/F)	10/4	5/6	0.240
BMI (kg/m^2)	27.75 [24.48 – 33.28]	27.8 [25 – 32.9]	0.8508
Smoking status (Ex/Never)	7/7	4/7	0.6887
Pack years	0 [0 – 7.625]	0 [0 – 2]	0.6805
Asthma-related characteristics			
Comorbidities (Y/N):	9/5	7/4	>0.999
Asthma duration (years)[#]	45 [27.5 – 57]	22.5 [9.25 – 37.5]	**0.0436**
ACQ score	2.25 [1.3 – 3.1]	2.3 [1.5 – 2.8]	0.6959
Exacerbation (last 12 months)	1 [1 – 1.5]	2[0 – 4]	0.4918
Atopy (positive skin prick test)[#]	6 (42.9%)	4 (37.4%)	0.6084
Pulmonary function			
Pre-BD FEV1 %[#]	81.5 [47 – 90.75]	83.5 [90 – 93.5]	0.3207
Post BD FEV1 %	88 [73 – 104]	93 [89 – 106]	0.3101
Pre-BD FEV1/FVC %[#]	67.2 [54.9 – 75.3]	73.68 [67.41 – 77.88]	0.1802
Post BD FEV1/FVC	73.5 [59.4 – 82.5]	75.89 [68.24 – 77.92]	0.9786
Asthma management			
Inhaled corticosteroids (ICS)	10/14 (71.4%)	8/11 (72.7%)	>0.99
BDP equivalent dose(μg)	2000 [1000 - 2000]	2000 [2000 – 2000]	0.2279
Bronchodilator (LAMA/LABA)	8/14 (57.1%)	10/11 (90.9%)	0.09
Combination therapy	14/14 (100%)	11/11 (100%)	>0.99
BDP equivalent dose(μg)	2000 [1000 - 2000]	1000 [1000 – 2000]	0.1607
Long term antibiotics	1/14 (7%)	3/11 (27%)	0.2878
Biologics	3/14 (21.4%)	0/11 (0%)	0.23

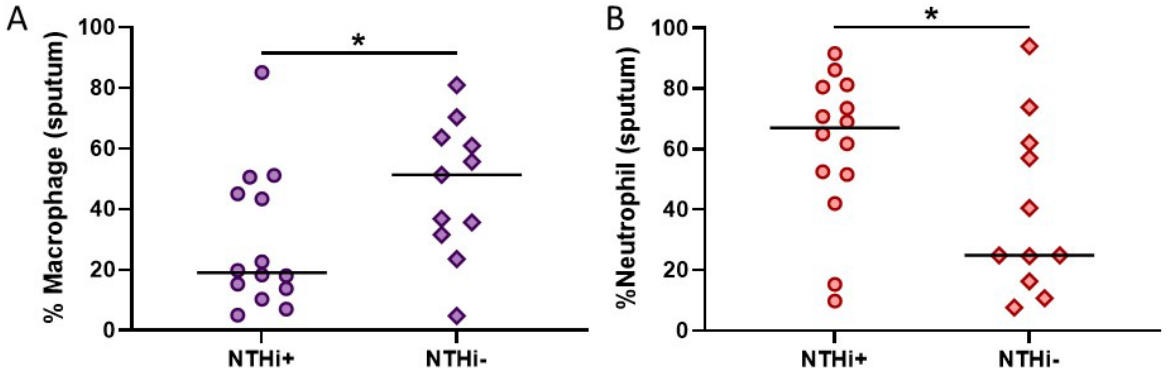

Figure 7.6. Differences in sputum cell proportions between NTHi+ and NTHi- severe asthmatic patients. (A) Decreased macrophage cell counts and (B) increased neutrophil cell counts in sputum from NTHi + patients. Lines on graph indicate medians. Data were analysed by Mann-Whitney U test, * = p<0.05.

In line with previously published literature, NTHi+ individuals had an increased proportion of sputum neutrophils (p=0.0462, Figure 7.6B) which corresponded with a decrease in macrophage sputum cell proportion (p=0.0221, Figure 7.6A). In contrast, no differences in BAL inflammatory cell proportions was detected. When assessing the relationship between sputum cell proportion and clinical characteristics, neutrophil sputum proportion was positively correlated with asthma duration, whereas the corresponding macrophage sputum proportion was negatively correlated with asthma duration, which appeared to be driven by the presence of NTHi (Figure 7.7A & B, NTHi+ samples in blue).

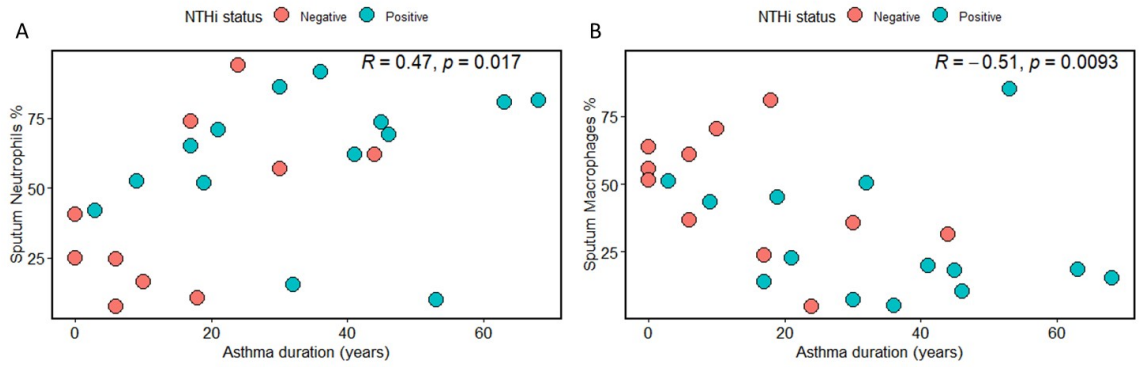

Figure 7.7. Asthma duration correlates with altered sputum inflammatory immune cell populations. (A) Sputum neutrophil proportion and (B) sputum macrophage proportion were both significantly correlated with asthma duration. Each dot represents a sample, red = NTHi -, blue = NTHi +. Data were analysed using Spearman's correlation, with R indicating the Spearman's correlation coefficient value, *rho*.

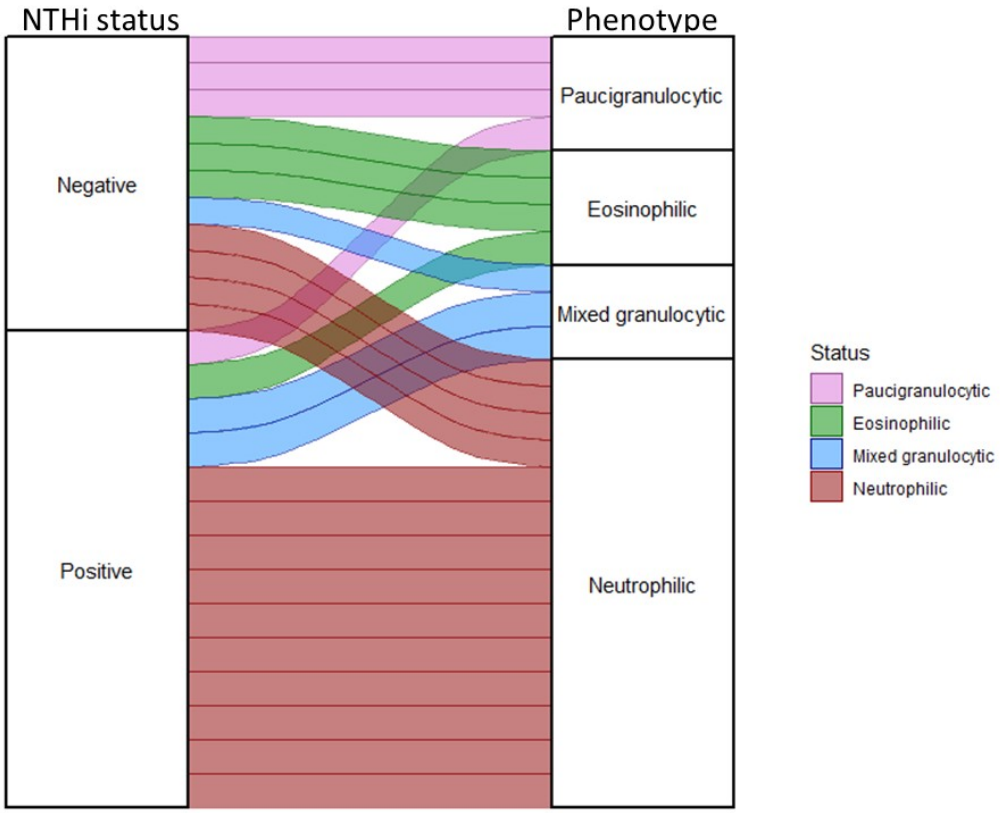

	NTHi+	NTHi-	p-value
Neutrophilic	10	4	0.1160
Eosinophilic	1	3	0.2878
Mixed Granulocytic	2	1	>0.9999
Paucigranulocytic	1	3	0.2878

Figure 7.8. Stratification of the 25 severe asthma BAL samples by NTHi colonisation and inflammatory phenotype status. Patients were stratified into neutrophilic (≥40% neutrophils, <3% eosinophils), eosinophilic (<40% neutrophils, ≥3% eosinophils), mixed granulocytic (≥40% neutrophils, ≥3% eosinophils) or paucigranulocytic (<40% neutrophils, <3% neutrophils) inflammatory phenotypes. Accompanying Table (bottom) indicates the significance (p-value) between NTHi+ and NTHi- groups as performed by Fisher's exact test.

Stratification of patients into sputum inflammatory phenotypes found a higher number (10/14; 71%) of NTHi-colonised individuals were neutrophilic (≥40% neutrophils, <3% eosinophils), compared to only 4/11 (36%) individuals not colonised with NTHi (Figure 7.8). Only 1 NTHi+ individual (4%) was eosinophilic (<40% neutrophils, ≥3% eosinophils). Although neutrophil percentage was significantly increased in NTHi+ individuals, the number of NTHi+ individuals determined as neutrophilic compared to NTHi- individuals was not significant (p=0.116). This could be due to a small number of NTHi+ individuals being determined as mixed granulocytic (≥40% neutrophils, ≥3% eosinophils).

7.2.4 Detection of macrophage intracellular immune response macrophage genes in NTHi-colonised samples

To determine whether a transcriptomic signal of intracellular infection of macrophages could be detected *in vivo,* the expression of macrophage and NTHi genes identified in the intracellular NTHi-MDM infection model by dual RNASeq were measured by qPCR. For this, BAL RNA matched to the 25 BAL cytospin samples were used. Unfortunately, expression of the NTHi genes identified in chapter 5 (*bioC, mepM,* and *dps*) were not reliably detected in BAL, perhaps due to the low bacterial load present in BAL samples. However, the expression of all eight macrophage genes identified and validated in chapter 4 (*CASP4, SGPP2, PNRC1, IL1B, GBP1, LAMP3, IRF1* and *ACOD1)* were detected in the 25 severe asthma BAL samples (Figure 7.9). Of these eight genes, *SGPP2*, *IL1B* and *GBP1* expression was higher in NTHi+ compared to NTHi- samples (Figure 7.9B, D & E respectively). The expression of *CASP4*, *PNRC1*, *IRF1* and *ACOD1* did not significantly differ between groups (p>0.05). Although it appeared that *LAMP3* expression was higher in NTHi- samples, this increase was not statistically significant (Figure 7.9F, p=0.1656).

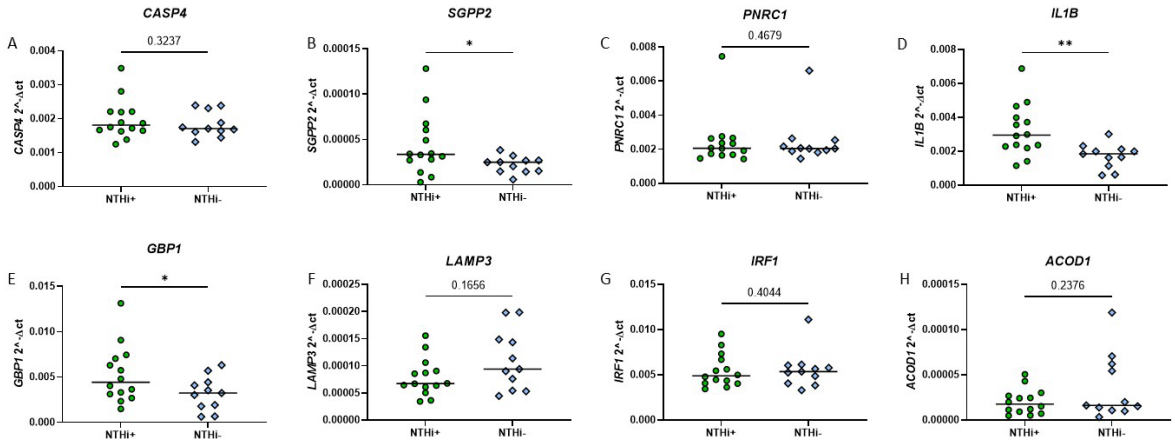

Figure 7.9. Modulation of macrophage gene expression by NTHi in BAL samples. Differences in the gene expression of (A) *CASP4*, (B) *SGPP2*, (C) *PNRC1*, (D) *IL1B*, (E) *GBP1*, (F) *LAMP3*, (G) *IRF1* and (H) *ACOD1* between NTHi+ and NTHi- colonised individuals were measured by qPCR. Gene expression was normalised to *B2M*. Graphs show medians, n=25. Data were analysed by Mann-Whitney U test, *p<0.05, **p<0.01

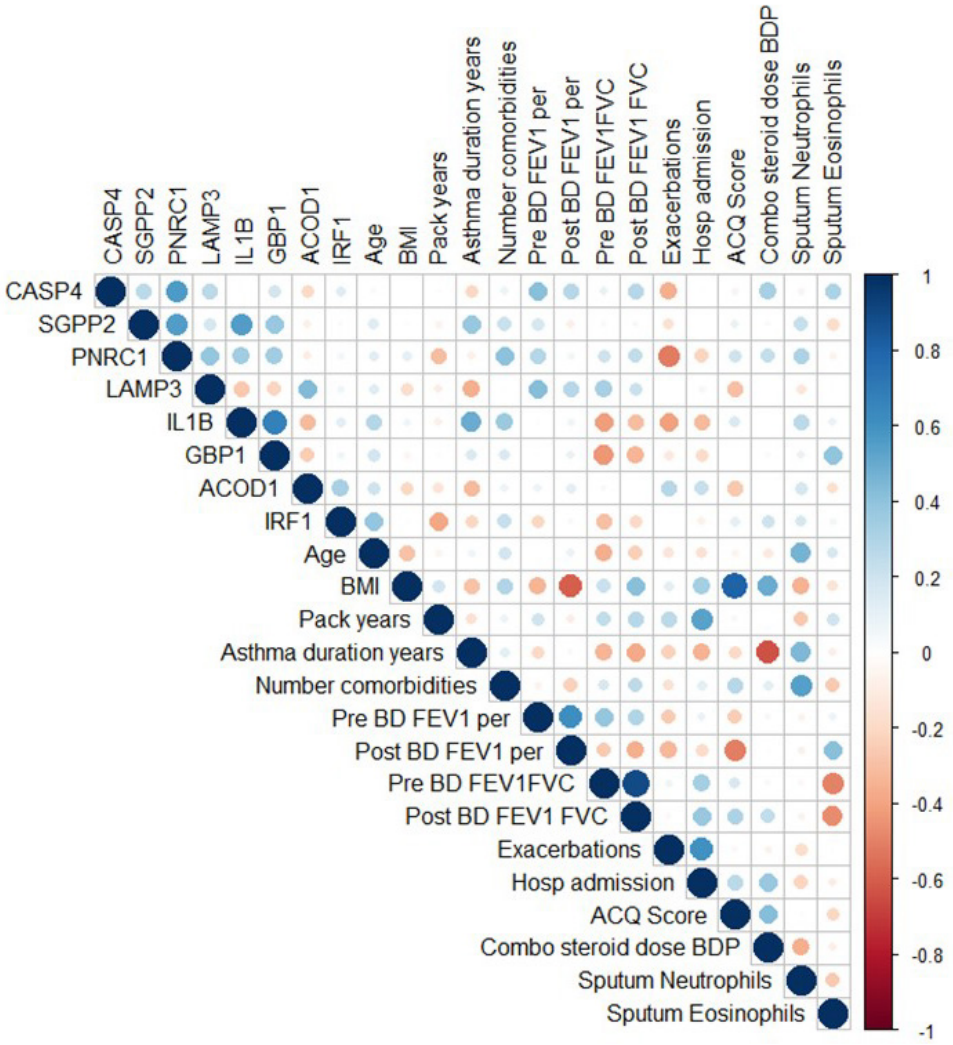

Figure 7.10. Correlation matrix of BAL gene expression and patient clinical characteristics. Spearman's correlation was used to determine correlations between the level of gene expression and clinical characteristics. Larger sized dots indicate more significant correlations, with the correlation coefficient (*rho*) represented by the coloured bar (right), with blue representing positive correlations and red representing negative correlations. Per = percentage.

To investigate correlations between the expression of macrophage genes and patient demographics, Spearman's correlation analysis was performed and a correlation matrix was produced (Figure 7.10). A moderate correlation between *IL1B* gene expression and asthma duration was identified (Figure 7.11A; *rho* = 0.41, p=0.041). A moderate negative correlation between *IL1B* and lung function (pre-bronchodilator (BD) FEV_1/FVC %) was observed, but was not statistically significant (Figure 7.11B; p=0.055). Similarly, the top hub gene, *CASP4* was moderately positively correlated with pre-BD FEV_1% which was also not statistically significant (Figure 7.11C; p=0.056). Similarly to *IL1B*, *GBP1* expression negatively moderately correlated with pre-BD FEV_1/FVC% (Figure 7.11D, p=0.046. Finally, significant positive moderate correlations between *LAMP3* and *IRF1* gene expression with pre-BD FEV_1% and age, respectively, were also found (Figure 7.11E & F).

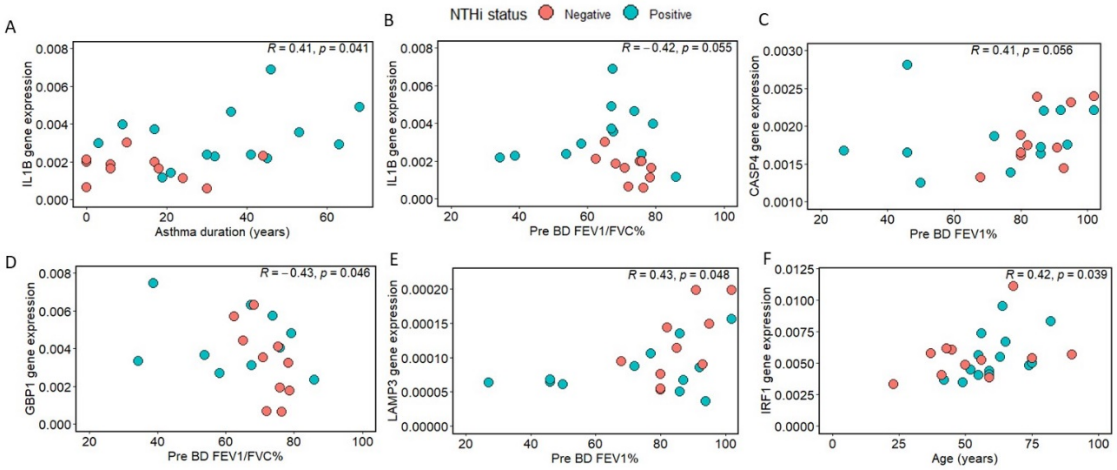

Figure 7.11. Correlations between select BAL genes and patient characteristics. Individual correlations identified in the correlation matrix were plotted to include the presence of NTHi (NTHi + = blue, NTHi- = red). *IL1B* gene expression correlated with (A) asthma duration and (B) pre-BD FEV_1. (C) *CASP4* gene expression correlated with pre-BD FEV_1, (D) *GBP1* correlated with pre-BD FEV_1/FVC, (E) *LAMP3* correlated with pre-BD FEV_1 and (F) *IRF1* correlated with age. N=22-25, as pre-bronchodilator measures were not taken for 3 patients (B-F). Data were analysed using Spearman's correlation. R indicates Spearman's *rho* correlation coefficient value.

A correlation matrix of gene expression and BAL cells was produced to determine whether the expression of macrophage genes was associated with BAL immune cell proportions (Figure 7.12A). No significant correlations of gene expression with BAL macrophage or neutrophil cell proportion were identified, however increased proportion of BAL lymphocytes correlated with increased ACOD1 gene expression (Figure 7.12B; *rho* = 0.57, p=0.0027). In contrast, *IL1B* expression negatively correlated with BAL lymphocyte proportion (Figure 7.12C; *rho* = -0.39, but this was not significant (p=0.056).

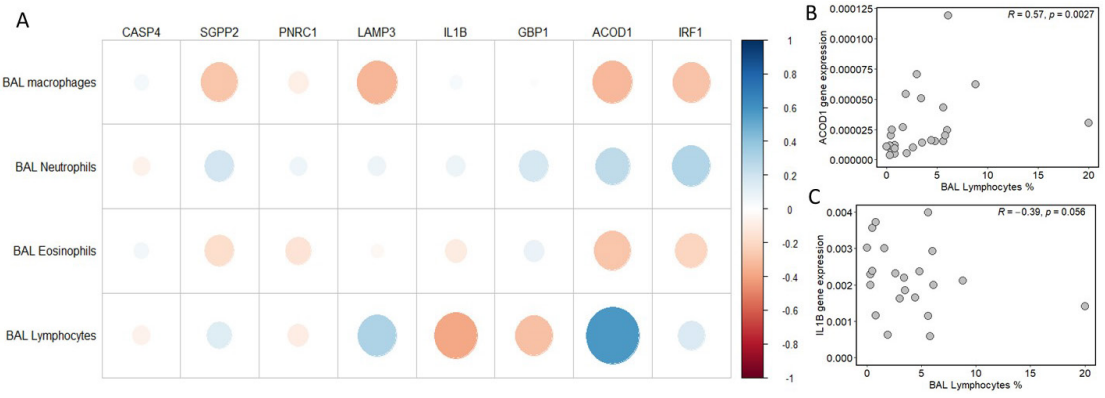

Figure 7.12. Correlation matrix of BAL gene expression and BAL immune cell counts. (A) Larger sized dots indicate more significant correlations, with the correlation coefficient (*rho*) represented by the coloured bar (right), with blue showing positive correlations and red showing negative correlations. (B) *ACOD1* gene expression positively correlated with BAL lymphocyte percentage, (C) *IL1B* negatively correlated with BAL lymphocytes. N=25. Data were analysed using Spearman's correlation. R = Spearman's *rho* correlation coefficient value.

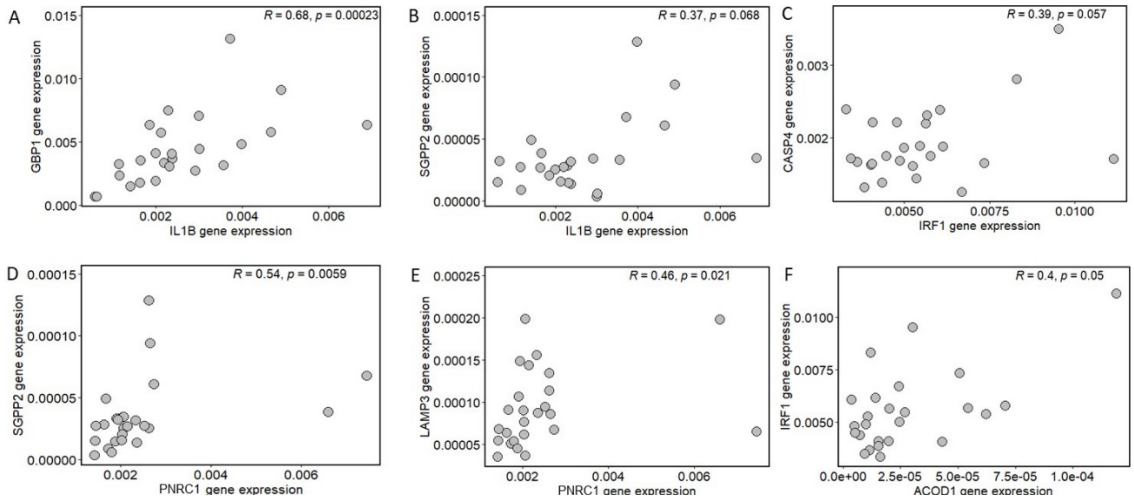

Figure 7.13. Co-expression of macrophage genes in the severe asthmatic airway. (A) *GBP1* strongly correlated with *IL1B*, (B) *SGPP2* weakly-moderately correlated with *IL1B*, (C) *CASP4* moderately correlated with *IRF1*, (D) *SGPP2* moderately correlated with *PNRC1*, (E) *LAMP3* correlated with *PNRC1* and (F) *IRF1* moderately correlated with *ACOD1*.Data were analysed by Spearman's correlation, R indicates Spearman's *rho* correlation coefficient value.

The co-expression of the eight genes in BAL was assessed, which identified a strong positive correlation of *IL1B* expression with *GBP1* (Figure 7.13A; *rho* = 0.67, p=0.00031). *IL1B* gene expression weakly to moderately correlated with a number of other genes including *SGPP2* (Figure 7.13B; *rho* = 0.37, p=0.068), *PNRC1* (*rho* 0.305, p=0.139), *LAMP3* (-0.302, p=0.143) and *ACOD1* (*rho*=-0.308, p=0.135) but these correlations were not statistically significant (Figure 7.10).

Despite identification of *CASP4* as the top blue module network hub gene in the dual RNASeq analysis, *CASP4* only weakly-moderately correlated with one gene, *IRF1* (Figure 7.13C; *rho*=0.39, p=0.057). Correlations between the expression of other genes included *SGPP2* and *PNRC1* (Figure 7.13D; *rho*=0.54, p=0.0059), *LAMP3* and *PNRC1* (Figure 7.13E; *rho*=0.46) and *ACOD1* and *IRF1* (Figure 7.13F; *rho* = 0.4, p=0.05).

7.2.5 NTHi modulation of IFN pathways was not detected in severe asthma

As up to 80% of asthma exacerbations are virally driven and NTHi colonisation occurs during a stable period of disease, it was important to determine whether NTHi modulation of macrophage IFN pathways could be detected *in vivo*. Modulation of IFN pathways was assessed by measuring the gene expression of six IFN pathway genes differentially regulated in response to NTHi infection in chapter 6: *IFNA, IFNB, IFNG, IRF3, IRF7* and *CXCL10*. The expression of all six genes were detected in the severe asthma BAL samples, however, no differences in expression levels for any gene were detected between NTHi+ and NTHi- patients (Figure 7.14).

The expression of *IFNG* and *CXCL10* in the BAL samples was highly positively correlated (Figure 7.15A; *rho*=0.8, p<0.001), which is not unexpected given that *CXCL10* expression is induced by *IFNG*. *IRF7* expression was moderately positively correlated with *IFNA* expression (Figure 7.15B; *rho* = 0.57, p=0.0029), which was also not unexpected given that *IRF7* is suggested to be a master regulator of the type I IFN response. *IRF7* was negatively correlated with *IFNG* expression (Figure 7.15C; *rho* = -0.45, p=0.023).

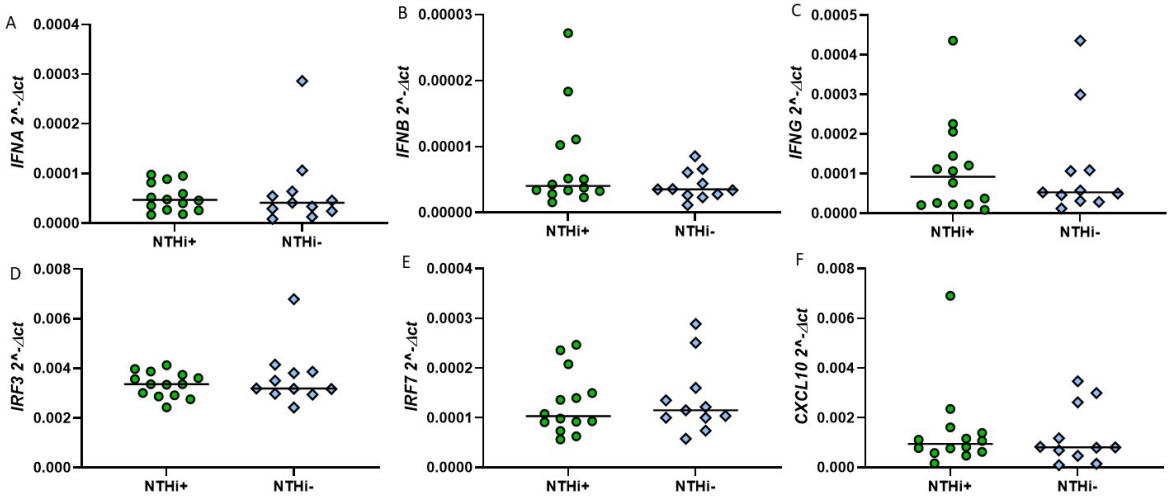

Figure 7.14. No NTHi modulation of IFN gene expression was detected in severe asthma. Gene expression of (A) *INFA*, (B) *IFNB*, (C) *IFNG*, (D) *IRF3*, (E) *IRF7*, and (F) *CXCL10* between NTHi+ and NTHi- colonised individuals were measured by qPCR. Gene expression was normalised to *B2M*. Graphs show medians, n=25. Data were analysed by Mann-Whitney U test.

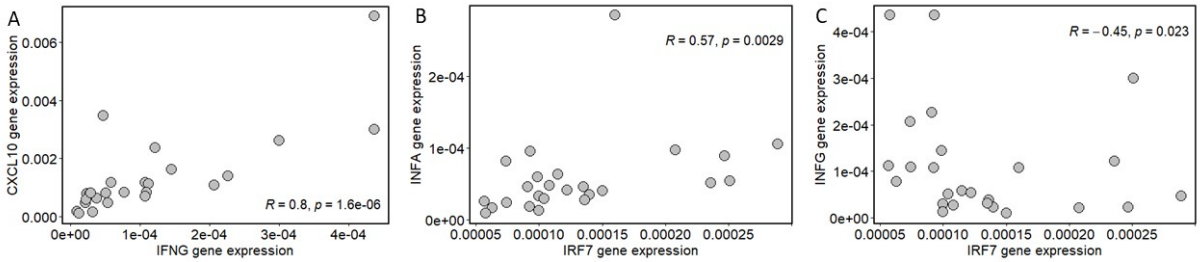

Figure 7.15. Co-expression of IFN genes in the severe asthmatic airway. (A) *CXCL10* strongly correlated with *IFNG*, (B) *IFNA* moderately correlated with *IRF7* and (C) *IFNG* moderately negatively correlated with *IRF7*. Data were analysed by Spearman's correlation, R indicates Spearman's *rho* correlation coefficient value.

To determine whether the expression of these genes correlated with any clinical characteristics, a correlation matrix was produced. Only *IFNB* gene expression correlated with sputum cell counts, which negatively correlated with sputum eosinophil percentage (Figure 7.16, *rho* -0.58, p=0.002). Differences in steroid dose between individuals did correlate with IFN gene expression (Figure 7.16). Both *IRF7* and *IFNG* gene expression correlated with several clinical characteristics (Figure 7.16). Specifically, higher *IRF7* gene expression moderately correlated with increased lung function measures such as pre-BD FEV_1% (Figure 7.17A), pre-BD FEV1/FVC% (Figure 7.17B) and post-BD FEV_1/FVC% (Figure 7.17C). In contrast, increased *IFNG* gene expression weakly-moderately correlated with decreased lung function, which trended towards significance (Figure 7.17D-F).

Figure 7.16. Correlation matrix of BAL IFN gene expression and patient clinical characteristics. Spearman's correlation was used to determine correlations between the level of gene expression and patient symptoms. Larger sized dots indicate more significant correlations, with the correlation coefficient (*rho*) represented by the coloured bar (right), with blue representing positive correlations and red representing negative correlations.

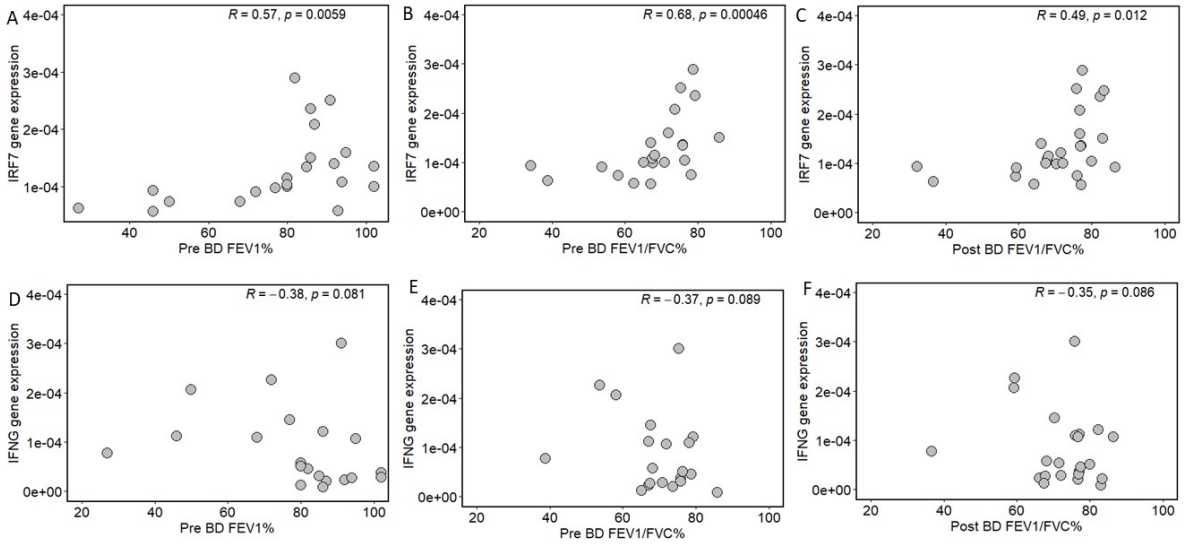

Figure 7.17. Correlations between IFN genes and patient characteristics. Correlations identified in the correlation matrix previously were plotted individually. N=22-25. As pre-bronchodilator measures were not taken for 3 patients Data were analysed using Spearman's correlation. R indicates Spearman's *rho* correlation coefficient value. *IRF7* moderately-strongly positively correlated with (A) Pre-BD FEV_1, (B) Pre-BD FEV_1/FVC and (C) Post-BD FEV_1/FVC, whereas *IFNG* weakly-moderately negatively correlated with (D) Pre-BD FEV_1, (E) Pre-BD FEV_1/FVC and (F) Post-BD FEV_1/FVC.

The relationship between gene expression and the proportion of immune cells in BAL samples was assessed, which found the expression of different IFN genes correlated with the proportion of different BAL cells (Figure 7.18A). Gene expression of the type I IFNs, *IFNA* and *IFNB* only correlated with BAL eosinophils, with increased expression of both genes associated with increased BAL eosinophils (Figure 7.18B & C).

In contrast the regulators of the type I interferons, *IRF3* and *IRF7* displayed differential associations; *IRF3* expression was not correlated with any BAL cells, however *IRF7* positively correlated with macrophage percentage, and negatively correlated with BAL neutrophil percentage counts (Figure 7.18A; *rho*=0.41; p=0.042 and *rho*=-0.48; p=0.015, respectively). However, the strongest correlations again included *IFNG* and *CXCL10* gene expression. Both genes negatively correlated with BAL macrophages (Figure 7.19A & D) but positively correlated with BAL neutrophils (Figure 7.19B & E) and BAL lymphocytes (Figure 7.19C & F).

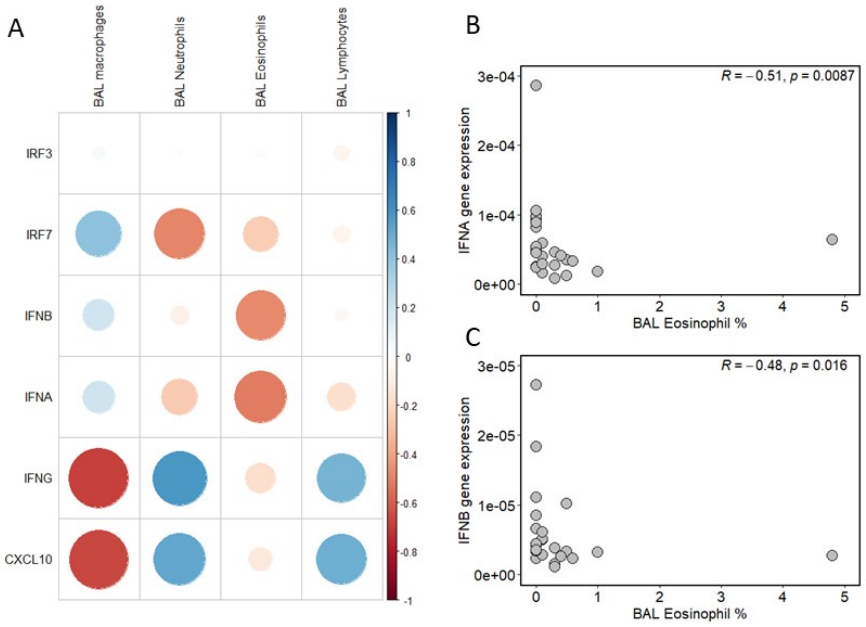

Figure 7.18. Correlation matrix of BAL IFN gene expression and BAL immune cell counts.(A) Spearman's correlation was used to determine correlations between the level of gene expression and BAL cell counts. Larger sized dots indicate more significant correlations, with the correlation coefficient (*rho*) represented by the coloured bar (right), with blue representing positive correlations and red representing negative correlations. (B) The presence of BAL eosinophils negatively correlated with *IFNA* (B) and *IFNB* (C) gene expression. N=25. Data were analysed using Spearman's correlation. R indicates Spearman's *rho* correlation coefficient value.

These data suggest that NTHi presence did not impact on the expression of select genes from the type I and II IFN pathways, however the expression of IFN genes in severe asthma correlated with clinical characteristics and inflammatory immune cell infiltration into the airways, potentially suggesting modulation of these pathways in severe asthma, independent of NTHi presence.

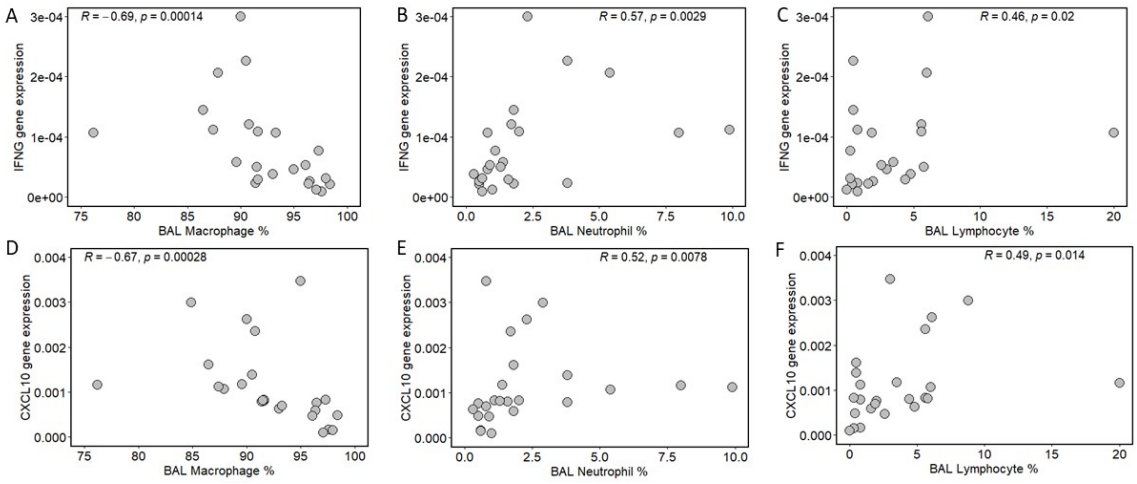

Figure 7.19. BAL *IFNG* and *CXCL10* gene expression correlated with BAL immune cell counts. *IFNG* and *CXCL10* gene expression negatively correlated with BAL macrophage counts (A & D) and correlated positively with both BAL neutrophil counts (B & E) and BAL lymphocyte counts (C & F). N=25. Data were analysed using Spearman's correlation. R indicates Spearman's *rho* correlation coefficient value.

7.3 Discussion

The work in this chapter focussed on determining the clinical relevance of intracellular NTHi infection of macrophages in severe asthma. Although bacterial infections by respiratory tract pathogens such as NTHi have been implicated in asthma exacerbations[65], NTHi was detected by FISH in this current work in 56% of individuals during a stable period of disease. In agreement with this observation, a study by Wood *et al.* (2010) identified that individuals with stable asthma were colonized with potentially pathogenic bacteria, with *H. influenzae* isolated from 60% of colonized individuals, with no respiratory symptoms reported[86]. Although only a single time point was used in this current work and by Wood and colleagues, longitudinal studies of individuals with chronic respiratory disease have shown NTHi persistence in the airway over an extended period of time[421,531], suggesting the capacity of NTHi to persist within a complex inflammatory environment such as the asthmatic airway.

The data in this chapter indicate NTHi presence in severe asthma is associated with increased sputum neutrophil proportion, supported by previous work demonstrating that individuals possessing a *Haemophilius*-dominant microbiome were more likely to be neutrophilic[64,87]. It is not clear why NTHi is associated with more severe disease, however this work found that NTHi presence was associated with increased asthma duration. A murine study exposing mice to long-term doses of *H. influenzae* found that over time, airway remodeling occurred following a bacteria-induced switch from a T2 eosinophilic inflammatory phenotype to T17, neutrophilic inflammation[462]. In agreement with this, Essilfie *et al.* demonstrated that the combination of NTHi infection and allergic airways disease promoted a steroid resistant, neutrophilic inflammatory phenotype in mice[154,532]. As these aforementioned studies used murine models of allergic airways disease, investigating the role of NTHi persistence in the airway of asthmatics prior to severe disease development could better elucidate the contribution of NTHi to severe asthma progression. This current work only uses asthmatic BAL samples obtained at a single time point and although these data indicate NTHi colonization of the airway during stable disease, this work was not designed to inform on whether NTHi presence drives the switch from mild to severe disease, or if the inflammatory nature of the severe asthmatic airway promotes NTHi persistence. Given the evidence of NTHi contributing to disease progression in murine models, human longitudinal studies tracking the progression of mild to severe asthma and identifying the role of NTHi would be informative. Due to the complex, multifactorial nature of asthma, it is likely that additional factors contribute to severe disease progression, rather than a single transitional event. Therefore, unpicking the complex relationship between NTHi persistence, the host immune response and severe asthma pathogenesis over an extended period of time could reveal therapeutic targets and the opportune moment to intervene to prevent disease progression.

Despite studies linking NTHi and neutrophils in asthma, the FISH data in this chapter indicate NTHi is more likely to be physically associated with macrophages, the predominant immune cell in the airway. The BAL samples used for this work were mainly comprised of macrophages (91.6%), suggesting NTHi interacts with macrophages in the airway to promote persistence. NTHi persistence *in vivo* has been shown previously by Olszewska-Sosiǫska *et al.* (2018), who identified a reservoir of NTHi within macrophages in adenoid tissue[348]. However, it is not clear how NTHi interactions with macrophages *in vivo* facilitate airway persistence. Therefore, qPCR was used to measure the expression of genes identified in the dual RNASeq analysis in severe asthmatic BAL samples. Unfortunately, NTHi gene expression was not able to be reliably detected in these samples. This could have been due to the potentially low total bacterial biomass present in BAL samples[533]; as demonstrated in chapter 3, a MOI of 100 was required to ensure a sufficient amount of live, viable NTHi was present within MDM for dual RNASeq.

Furthermore, rRNA depletion was performed on sequenced samples, to ensure that NTHi transcripts could not only be detected and sequenced, but sequenced in enough depth to allow for differential gene expression analysis to be performed. Together, these optimization steps may have allowed for more sensitive detection and analysis of gene expression that could be harder to replicate in more complex and limited samples, such as BAL, using qPCR. Although a combination of the top upregulated (*bioC, mepM*) and downregulated (*yadA, dps*) NTHi genes identified in chapter 5 were used, it may be possible that *in vivo* NTHi gene expression may differ from *in vitro* gene expression during infection. A further limiting factor of this current work was the long-term colonization status of these samples was unknown. As the MDM infection model only measured NTHi gene expression up to 24 h, longer intracellular persistence may result in further transcriptomic adaptations of both NTHi and macrophages that were not identified in the dual RNASeq analysis.

In contrast, all eight macrophage genes identified and validated in chapter 4 were detected in the 25 asthmatic BAL samples. The expression of *IL1B* in particular was significantly elevated in samples that were NTHi+ and correlated with a number of clinical characteristics, presence of airway immune cells and the expression of the other genes. Elevated BAL *IL1B* gene expression in this chapter is in agreement with previously published studies identifying elevated *IL1B* expression in both BAL and sputum from asthma, with protein levels of IL-1β also increased in asthma[53,55,362,534–536]. BAL IL-1β protein levels could not be determined in this current study as BAL fluid was not available for analysis of airway protein concentrations. However, measuring IL-1β protein levels would confirm whether the elevation of *IL1B* mRNA correlates with increased IL-1β protein in these particular samples. Interestingly, a study by Kim *et al.* (2017) found that inhibiting IL-1β in mice suppressed airway inflammation and the development of a steroid resistant phenotype[54]. Together, the work in this thesis demonstrated upregulation of *IL1B* gene expression and protein release by

NTHi-infected MDM and elevated *IL1B* gene expression in NTHi+ BAL samples. Therefore, it is possible that NTHi-infected macrophages may be the source of IL-1β induced inflammation in the asthmatic airway. As such, this could be a mechanism by which NTHi contributes to airway inflammation and the development of a steroid resistant asthma phenotype[54].

IL1B was identified as one of the top connected genes in the blue module in chapter 4, which was most highly associated with NTHi infection of MDM, along with the top hub gene *CASP4.* However, BAL *CASP4* gene expression did not differ between NTHi+ and NTHi- individuals. Simpson and colleagues (2014) identified increased *CASP4* gene expression in the sputum of neutrophilic asthmatics compared to eosinophilic and paucigranulocytic asthmatics[55]. Although these differences could be explained by sample source; this current study measured BAL *CASP4* gene expression, whereas Simpson and colleagues used sputum. The lack of difference in *CASP4* expression between NTHi groups could also be due to the predominant neutrophilic inflammatory phenotype of the 25 patients in the BAL cohort. One limitation of this current work is due to the small sample size, comparison of *CASP4* gene expression levels between neutrophilic (n=14), eosinophilic (n=4), mixed granulocytic (n=3) and paucigranulocytic (n=4) individuals was not able to be performed. Macrophages were highly likely to be the cellular source of *CASP4* expression as a recent study found elevated levels of *CASP4* expressed by alveolar macrophages from asthmatic patients compared to healthy controls[537]. As such, *CASP4* expression may already be elevated in the current BAL samples when compared to healthy individuals or eosinophilic/paucigranulocytic asthma, independently of NTHi presence.

The absence of *CASP4* gene expression upregulation despite the presence of NTHi could in fact be a mechanism by which NTHi is able to persist in the airway. Transcriptomic analysis identified *CASP4* as a hub gene, which was also upregulated in MDM by additional clinical strains of NTHi. However, levels of *CASP4* expression were lower in response to ST201, which was able to be recovered at a higher CFU at both 6 h and 24h, suggesting *CASP4* is an important gene for macrophage control of NTHi intracellular infection. The lack of *CASP4* upregulation in BAL samples despite NTHi presence could indicate an impairment in the macrophage ability to control NTHi infection in the asthmatic airway.

The GBPs are involved in activation and recruitment of the caspase-4 inflammasome[538], of which all 7 GBPs were upregulated by MDM in response to NTHi infection. The *GBP1* gene was chosen to be investigated in asthma BAL samples as it was present in the blue module gene network and is the initial GBP involved in the detection of cytosolic bacteria and recruitment of GBPs 2-4[216]. The upregulation of *GBP1* in NTHi+ BAL samples suggests the intracellular presence of NTHi in the macrophage cytosol, resulting in activation of an intracellular immune response. However, as *CASP4* gene expression was not similarly elevated in NTHi+ samples, it is not clear whether the non-

canonical inflammasome pathway is important for the macrophage immune response to intracellular NTHi infection *in vivo*.

The previous chapter demonstrated that infection with either NTHi, IAV or IAV following prior NTHi infection of MDM resulted in different immune response profiles to the three pathogen combinations. The activation of an anti-viral response, specifically a type I IFN response by NTHi appeared to prime macrophages to better respond to a subsequent viral infection. However, unlike the increased expression of macrophage intracellular immune response genes in NTHi+ samples, modulation of IFN pathways by NTHi *in vivo* was not detected. It has been documented that IFN responses in asthma are impaired so it is possible that NTHi intracellular persistence *in vivo* does not activate IFN pathways to the same extent observed in healthy MDM[312,508].

The lack of IFN responses may also be linked to the lack of *CASP4* expression. A recent study has identified that IFN-γ signalling is required for rapid and robust GBP-independent activation of caspase-11 – the murine homolog of the human caspase-4[215]. Thus, impaired *in vivo* IFN responses may not only increase susceptibility to a viral infection but may also contribute to the inability of macrophages to control airway microbial colonisation by pathogens such as NTHi. Prior activation of IFN responses in chapter 6 was associated with decreased IAV infection, but the presence of even low levels of IAV combined with NTHi appeared to modulate the macrophage inflammatory response. Due to the single time point sampling of the asthma patients used in this thesis, these samples were not appropriate to investigate the impact of NTHi colonisation on a subsequent viral infection.

However, modulation of host responses during dual infection in chronic respiratory disease has been reported following experimental rhinovirus infection of healthy and COPD volunteers[539]. The majority of COPD patients experimentally infected with rhinovirus developed an exacerbation, but those with evidence of secondary bacterial outgrowth had higher levels of total sputum inflammatory cells, sputum neutrophil elastase and lower peak expiratory flow and FEV_1 measures[539]. This study indicates that modulation of host responses during co-infection of the airway results in an altered inflammatory profile and worse clinical symptoms. Given the results of the experimental rhinovirus challenge study and the increased presence of NTHi in the severe asthmatic airway[66,86,87], it would be important to ascertain whether NTHi airway colonisation and subsequent IAV infection modulates the host immune response *in vivo* as observed in the MDM model.

Despite the absence of IFN gene modulation between NTHi+ and NTHi- BAL samples, *IFNG* and *CXCL10* gene expression were both correlated with lower lung function and *IFNG* correlated with increased number of exacerbations over the past 1 year. This current work previously reported in chapter 6 that IAV infection did not upregulate the expression and release of IFN-γ to the same

extent as co-infected samples. As such, NTHi-airway colonisation may contribute to disease progression and lung damage during viral infection by synergistically upregulating immune responses biased more towards IFN-γ compared to a type I IFN response. However, T cells and NK cells are the main cellular sources of IFN-γ in the airway, with T cells shown to produce IFN-γ in response to NTHi-infected MDM[199]. As increased *IFNG* expression in BAL samples correlated with increased lymphocyte percentage, it is possible that the cellular source of this gene expression was T cells. Nonetheless, increased *IFNG* expression could mean increased risk of airway damage. As the co-infected *in vitro* work indicated upregulation of *IFNG* responses, even detecting release of IFN-γ from NTHi-infected macrophages, who are not generally considered the primary *in vivo* source of IFN-γ, the synergistic contribution of IFN-γ expression and release during co-infection could be why individuals colonised with NTHi suffer from reduced lung function and dysregulated inflammation. Comparing the inflammatory profile of individuals chronically colonised with NTHi during a viral-induced exacerbation to individuals not colonised with NTHi could help address this possibility, as one of the limitations of this current work was that it was unable to address the co-infection dynamics and host immune responses modelled *in vitro* during asthma exacerbation.

Due to the increasing association between NTHi presence and severe asthma, the main aim of the work in this current chapter was to identify the clinical relevance of NTHi presence and NTHi-associated modulation of macrophage intracellular immune response genes in severe asthmatic BAL samples specifically. However, further work using healthy controls or samples from mild disease would be useful in determining whether the expression of these identified genes, such as *CASP4* or the IFNs, were already modulated in severe disease independent of NTHi presence. For example, the high use of steroids in this sample population could account for the differences observed between MDM and BAL gene expression. All 25 individuals included in this work were treated with combination (ICS and LABA) therapy, with some patients also treated with individual ICS or LAMA/LABA therapies. It is therefore tempting to speculate that steroid treatment may be dampening the expression of some of the identified upregulated MDM genes in the NTHi+ BAL samples.

The immunosuppressive effects of corticosteroids could influence the ability of NTHi to persist in the airway. However, a study by Marri *et al.* (2012) showed that a higher abundance of Proteobacteria were present in asthmatic individuals, 80% of whom were not using inhaled corticosteroids[92]. In this current work, no significant differences in steroid dose or use were observed between NTHi+ or NTHi- groups, suggesting colonisation of the airway by NTHi was independent of treatment. In fact, the increased expression of macrophage inflammatory genes in BAL despite steroid use suggests continual NTHi presence may result in the development of a steroid-resistant phenotype. Using the MDM model to determining whether steroid treatment

impacts on the macrophage immune response, specifically regulation of the identified genes in this thesis, would be of interest.

In this current work, *SGPP2* was also one of the top hub genes in the blue module most associated with NTHi infection and was found to be elevated in NTHi+ severe asthma BAL samples. Despite this, the role of *SGPP2* in the macrophage immune response to NTHi infection has not been well investigated. *SGPP2* encodes for Sphingosine-1-Phosphatase 2, which is involved in degradation of the sphingosine 1-phosphate (S1P) signalling molecule. S1P has increasingly been suggested to play a role in inflammation, phagocytosis and immune responses, with knockdown of *SGPP2* resulting in reduced cytokine production[540,541]. Recently, Hodge *et al.* (2020) investigated the gene expression of members of the S1P pathway in children with bronchiectasis and protracted bacterial bronchitis and found no correlation between NTHi presence and *SGPP2* expression[542]. However, Barnawi *et al.* (2015) have suggested a link between the S1P pathway and impaired phagocytosis by alveolar macrophages from COPD patients, suggesting a disease-associated impairment in the S1P pathway, rather than a pathogen-associated impairment[543]. Numerous studies have identified that phagocytosis is dysfunctional in airway macrophages in chronic respiratory disease but the exact mechanism is not well understood[247,250,454]. Therefore, determining the role of *SGPP2* and the S1P pathway in phagocytosis by alveolar macrophages in severe asthma could reveal a novel mechanism potentially allowing for NTHi persistence in the airway.

Work using isolated alveolar macrophages from the severe asthmatic airway would be important to confirm the transcriptomic MDM analysis and BAL gene expression results. As blood samples are more readily available, the MDM model has been extensively used to model healthy airway macrophages[250]. Although MDM have shown to be phenotypically similar to AM, there are still differences between the two cell types which must be considered. The regulation of AM function is influenced by the microenvironment of the lung and although GM-CSF is abundant in the lung, particularly in the asthmatic lung, other cytokines, chemokines and growth factors may affect macrophage steady state phenotype. As such, transcriptional and functional responses may differ *in vivo* and the *in vitro* MDM culture may be too simplistic to reflect the dynamic lung environment. Future work using isolated AM could determine whether AM are capable of mounting a similar intracellular immune response to NTHi as was identified in the dual RNASeq analysis. However, removing AM from the lung environment and stimulating *ex vivo* may also influence AM phenotype and functional responses[544]. Thus, determining AM responses to NTHi within a culture system which attempts to retain the 3D lung architecture may allow for a better understanding of NTHi-macrophage interactions occurring *in vivo*. This could include models such as a lung tissue explant model[545], a 3D lung organoid model[546], which can be further integrated with microfluidics to produce a lung-on-a-chip model[547], a murine model[261,462,532] or a human challenge model[548].

Investigating NTHi-macrophage interactions in the context of a 3D environment may also elucidate the importance of cellular cross-talk in the immune response to NTHi. Ongoing bidirectional cross-talk between macrophages and airway epithelial cells ensure homeostatic balance, whilst ensuring appropriate inflammatory responses are initiated. For example, epithelial cells are a source of regulatory cytokines such as IL-10 and TGF-β, which allows for maintenance of AM in an anti-inflammatory state, which can also occur through direct cell-cell interactions[549]. Conversely, stimulation of epithelial cells by macrophage-derived cytokines such as IL-1β, can upregulate epithelial cell pro-inflammatory responses, such as release of IL-8, which promotes recruitment of airway immune cells[550]. Infiltration of immune cells can amplify immune responses, with neutrophil recruitment following influenza virus infection important for activation of the NLRP3 inflammasome and IL-1β release from macrophages[551]. As such, it must be considered that the macrophage immune response to NTHi may be different when present within the dynamic lung microenvironment containing a milieu of airway cells, paracrine and autocrine signalling and inflammatory or regulatory stimuli.

As identification of bacterial colonisation of BAL samples was performed specifically for NTHi, it is not clear whether samples were colonised with other respiratory tract pathogens. The pan-bacterial probe was used and did identify the possibility of co-colonising bacteria, however due to the non-specific nature of this probe, these additional bacterial species were not identifiable. Additionally, extra steps during the FISH procedure, such as lysozyme treatment to permeabilise the cell wall of gram positive bacteria, have been suggested to allow better identification of gram positive bacteria by FISH[552]. However as extended periods of lysozyme treatment have shown to cause lysis of gram negative bacteria, using FISH to identify mixed populations of bacteria colonising host samples may not be accurate[552]. Therefore, full characterisation of BAL samples by unbiased sequencing approaches would better identify the microbial composition of BAL and whether specific microbial signatures were more associated with the inflammatory responses observed in this chapter. Further *in vitro* comparative work assessing MDM responses to additional respiratory tract pathogens such as *M. catarrhalis* and *S. pneumoniae* would also allow for better determination of specific responses unique to each pathogen.

Furthermore, although the BAL samples used for the work in this chapter primarily consisted of macrophages, BAL contains a mixed cell population. As such, it may be possible that certain gene signatures were from a cellular source other than macrophages. A limitation of this current work was that only the BAL cell pellet resuspended in QIAzol was available for this analysis. Sorting of BAL cells by FACS prior to addition of QIAzol would allow for the isolation of a pure macrophage population, which could then be used for RNA isolation and analysis of gene expression.

Nonetheless, the *in vitro* modelling of NTHi with MDM and subsequent transcriptomic analysis indicated that NTHi infection resulted in specific upregulation of the genes assessed in this chapter.

Thus, it is likely that macrophages were the cellular source of the gene expression measured in these current samples. Therefore, this work has identified NTHi-associated modulation of macrophage intracellular immune response genes in severe asthma BAL samples. Given that the previous chapter identified increased MDM inflammatory responses in co-infected MDM compared to IAV-alone infected MDM, the contribution of NTHi to airway immune response modulation during chronic colonisation requires further exploration.

7.4 Summary

The work in this chapter has demonstrated presence of NTHi in severe asthmatic BAL samples during a stable period of disease, in agreement with other previously published studies. NTHi was highly associated with host cell nuclei staining, and as the BAL cell pellets were mainly composed of macrophages, this indicated NTHi association with airway macrophages. The expression of host genes (*IL1B, GBP1, and SGPP2*) found to be highly associated with intracellular NTHi infection of MDM by dual RNASeq were elevated in NTHi+ BAL samples, indicating modulation of BAL macrophage gene expression by NTHi. Conversely, no modulation of IFN pathways were detected, however this could be due to the length and severity of disease in the patient cohort used. Nonetheless, this work suggests NTHi modulates airway macrophage gene expression in severe asthma. This observation potentially has serious ramifications for a subsequent viral respiratory tract infection, which is the main driver of exacerbations and worsening of disease symptoms in asthma, given the sustained inflammatory response and bacterial outgrowth observed previously during co-infection of MDM.

Chapter 8 Discussion and Future Work

8.1 Introduction

Asthma is a complex, heterogeneous disease, with asthma exacerbations resulting in up to 65,000 annual hospital admissions in the UK[59]. Exacerbations of disease can be mild, moderate, severe or life-threatening, which negatively impact quality of life and accelerate lung function decline[56]. NTHi colonisation of the severe asthmatic airway is associated with more severe, neutrophilic and steroid-resistant disease and has been implicated in asthma exacerbations[44,45,334,532]. Yet, virally driven exacerbations still account for the majority of asthma exacerbations[67,69]. However, as NTHi has been detected during both stable asthma and exacerbations[65,86], it is becoming clear that NTHi presence in the airway precedes the appearance of a virus and subsequent development of a virally driven exacerbation. The mechanisms of NTHi persistence in the respiratory tract are not well understood, but NTHi has been identified to reside and replicate within macrophages from adenoid tissue[147,348], with NTHi infection of macrophages also demonstrated *in vitro*[149]. Given that macrophages are the predominant immune cell in the airway, it is not clear whether NTHi colonisation of the airway influences the progression of a viral respiratory tract infection and asthma exacerbation. In this thesis, it was hypothesised that NTHi infection of macrophages would compromise the ability of macrophages to respond to a subsequent viral infection.

As such, the aim of this thesis was to explore NTHi-macrophage interactions and the impact of these interactions on a subsequent IAV infection. This aim was achieved by first optimising an NTHi-MDM intracellular infection model to characterise transcriptomic changes associated with intracellular persistence by dual RNASeq of both host and pathogen. Transcriptomic analysis found that although macrophages upregulated innate intracellular immune response pathways, this was not sufficient to completely clear NTHi infection. NTHi transcriptomic changes were associated with modulation of metabolic pathways, likely as a result of adaptation to intracellular residence within MDM. Although the macrophage response to NTHi intracellular infection by additional clinical strains was conserved, changes in NTHi gene expression appeared to be strain-dependent.

This prior NTHi modulation of the MDM response had consequences for a subsequent IAV infection. MDM upregulation of anti-viral pathways known to be crucial for an anti-IAV response resulted in macrophage priming and restriction of IAV infection. This data therefore did not support the primary hypothesis that this work set out to test. However, although levels of IAV were lower compared to MDM infected by IAV alone, IAV was still present in this co-infection model system and together with NTHi, stimulated a sustained macrophage inflammatory response. Co-infection also impacted on NTHi-infection dynamics, with NTHi presence increasing following co-infection. Thus, even though NTHi infection did not appear to compromise the ability of macrophages to respond to IAV infection, the macrophage response during co-infection was dysregulated which resulted in loss of bacterial control. Importantly, NTHi-macrophage interactions were of clinical

relevance, as modulation of the host macrophage response was observed in severe asthma BAL samples obtained from patients that were colonised with NTHi, and NTHi presence was also associated with increased neutrophilic inflammation. This chapter will discuss the overall findings from this thesis in further depth, considering the wider clinical implications of these results, limitations of the study and outline outstanding questions and areas of interest that require further exploration.

8.1.1 NTHi intracellular persistence within macrophages: implications for chronic airway colonisation

Numerous studies have identified chronic *H. influenzae* presence in the airway of individuals with chronic respiratory disease, not just in asthma[65,86], but also COPD[531,553], idiopathic pulmonary fibrosis (IPF)[554] and cystic fibrosis (CF)[555]. Despite evidence for NTHi persistence, the mechanisms of how a respiratory tract pathogen can persist within the airway for a sustained period of time in the face of host immune responses are not clear. Persistent colonisation of environmental surfaces has been suggested to be as a result of biofilm formation[556]. Although biofilms have been identified in CF, with *P. aeruginosa* being the predominant identified species, NTHi biofilm formation in the asthmatic lung is less clear. However, previous clinical studies have identified NTHi intracellular persistence in macrophages from adenoid tissue suggesting that host cells such as macrophages could act as reservoirs of NTHi infection[147,348]. NTHi intracellular infection and persistence within host cells has been shown *in vitro* for monocytes, macrophages and epithelial cells[123,133,149], with intracellular infection of macrophages further demonstrated in the data presented in this thesis. Although the MDM *in vitro* modelling demonstrated NTHi persistence within macrophages in this work, detection of NTHi associated with host macrophages in severe asthma BAL samples further confirmed the ability of NTHi to utilise host cells *in vivo*. Unfortunately, due to the nature of the patient cohort used, this work was unable to ascertain how long patients had been colonised with NTHi. Nonetheless, these patients were sampled at a period of stable disease and not during exacerbation, indicating NTHi presence in severe asthma during stable disease, in line with previous studies[65,86].

One of the key aims of this thesis was to explore NTHi transcriptomic changes associated with intracellular infection of MDM, which was why careful optimisation of the NTHi-MDM infection model was required in order to perform dual RNASeq on NTHi-infected MDM. Comparison of the top regulated NTHi genes between planktonic state and intracellularly-located NTHi by qPCR confirmed that these genes were differentially regulated during intracellular infection. This work identified an enrichment of NTHi metabolic pathways during intracellular infection, suggesting adaptation of NTHi to the intracellular environment within MDM. Diverse metabolic adaptations during infection of epithelial cells were also identified using dual RNASeq by Baddal *et al.* (2015), indicating that regulation of metabolism is key for successful NTHi infection of host cells[151].

Restriction of nutrients required for bacterial survival is a host immune response mechanism, with pathogens capable of successfully scavenging nutrients from restricted environments better able to survive and persist intracellularly[557]. The top upregulated NTHi gene was a member of the biotin pathway. Biotin is an essential cofactor required for enzymes involved in metabolic pathways such as fatty acid biosynthesis and amino acid metabolism[558]. Other pathogens including *Francisella tularensis, Mycobacterium* spp and *Candida* spp, have been shown to require biotin or biotin synthesis pathways for intracellular survival[478–480]. Biotin is a limited intracellular resource, particularly in the macrophage phagosome, which could explain the increased requirement for this gene if NTHi was located in the phagosome during infection[478]. However, biotin is also important for the immune response as increased levels of pro-inflammatory cytokines, including IL-1β, have been observed in biotin deficiency[559,560]. Although the role of other vitamins in asthma, such as vitamin D, have been explored[561], the role of biotin in development and maintenance of immunity in the asthmatic lung – or indeed the healthy lung - has not been investigated in such depth.

Although the transcriptomic data presented in chapter 5 suggests NTHi adaptation to intracellular survival required activation of biotin synthesis genes, the *bioC* gene was not significantly differentially expressed by one of the other tested NTHi strains (ST201). Only one gene involved in the biotin pathway was assessed in the additional clinical strains of NTHi during infection, so it is possible that other members of the biotin pathway were differentially expressed for ST201. Conversely, the intracellular location of ST201 may differ to that of ST14 and ST408 and it may not be in a less nutrient-restricted environment, such as the cytosol. Expanding the sequencing work performed in this thesis to include additional strains of NTHi would allow for enhanced characterisation of conserved pathways and genes during NTHi intracellular infection of MDM.

Differences between NTHi phenotypes *in vivo* would be important to identify. The intracellular NTHi transcriptomic changes detailed in this thesis differ to changes in the expression of genes during biofilm growth identified in other studies. A number of genes identified as important for biofilm growth[490] were downregulated by NTHi during intracellular persistence in this current model. In fact one of these genes, *dps*, was the top downregulated gene at 24 h. Pang and colleagues identified *dps* to be important for biofilm growth with *dps* mutant NTHi strains exhibiting reduced biofilm development[490]. The NTHi expression profile in this work is therefore likely to represent adaptation to an intracellular environment, as opposed to a switch to biofilm formation. It would be of importance to determine whether this NTHi intracellular gene signature can be detected *in vivo*, as this could confirm therapeutic targets to reduce the burden of NTHi airway colonisation.

NTHi strains isolated from different anatomical locations have demonstrated varying affinities for substrates, with the increased ability of two invasive strains of NTHi (C188, a blood isolate and R2866, a strain isolated from a child with meningitis following otitis media complications) to metabolise diverse substrates compared to Hi2019, a COPD isolate[562]. The COPD Hi2019 strain was

also demonstrated to be better able to invade and reside within bronchial epithelial cells compared to the two invasive NTHi strains[562]. This comparative analysis suggests that differences in metabolic adaptation could underpin the ability of NTHi to persist in certain anatomical niches. The three strains used in this current work were all obtained from different samples: lung protected bronchial brushing (ST14), sputum (ST201) and nasal brushing (ST408), which could account for the differences in gene expression measured between these strains. Deeper transcriptomic analysis of these three strains – and additional clinical strains – could better identify conserved genes regulated during intracellular infection and also identify similarities between strains from the same disease or location. Thus, stratifying NTHi strains by transcriptomic adaptations during infection, rather than by genomics, could be a better method by which to identify strains better able to persist *in vivo*.

Furthermore, *in vitro* studies have shown that different clinical NTHi isolates vary in their abilities to tolerate antibiotics[149]. The β-lactam family of antibiotics, including penicillin, ampicillin and cephalosporins, have long been used to treat bacterial infections and act by inhibiting bacterial cell wall synthesis. However, bacteria such as NTHi have developed strategies to overcome the action of antibiotics, such as expression of β-lactamases, which inactivate this family of antibiotics[563]. Previous antimicrobial characterisation of the strains used in this thesis demonstrated that ST14 was resistant to benzylpenicillin and cefotaxime, but was sensitive to ampicillin and did not produce β-lactamase (personal communication with Dr. K. Osman). In the absence of β-lactamases, it has been suggested that penicillin binding protein 3 (PBP3, encoded by the *ftsI* gene[564]) mediates resistance to members of the β-lactam family of antibiotics[108,565]. Presence of the *ftsI* gene was detected in ST14.No differential expression of *ftsI* was detected during intracellular infection of MDM, however this was likely due to intracellular residence of NTHi at 24 h. Instead, transcriptomic modulation of NTHi metabolic and stress response pathways was detected, consistent with adaptation of the persister phenotype[566].

It is tempting to speculate that efficient and successful intracellular residence within host cells is a method of persistence better utilised by NTHi strains that are more susceptible to antibiotic action. In chapter 3, the highest amount of bacteria recovered from MDM was when using ST201. This particular strain was susceptible to all antibiotics tested, including benzylpencillin (personal communication with Dr. K. Osman). In contrast, the lowest amount of recovery was ST408, however this strain was resistant to the majority of β-lactam antibiotics tested and was also β-lactamase positive (personal communication with Dr. K. Osman). Thus, some strains may have better developed the ability to infect and persist within host cells as an alternative means of escaping antibiotic action. Evidence for an alternate mechanism to antibiotic resistance includes a study by Olszewska-Sosińska *et al.* (2016) who demonstrated intracellular persistence of NTHi in macrophages isolated from children who were treated with azithromycin. Of interest, the

recovered persistent NTHi isolates were not deemed to be azithromycin resistant by use of minimum inhibitory concentration (MIC) measures. Rather than active resistance to antibiotics conferred by specific antibiotic resistance genes, the maintenance of persister cells and drug tolerance may occur by other mechanisms, such as intracellular persistence[567]. The transcriptomic analysis in this thesis demonstrated that during intracellular persistence within MDM, NTHi ST14 modulated bacterial stress response pathways and downregulated ribosomal protein genes, which are often targets of antibiotics, such as the aforementioned azithromycin antibiotic. Therefore, identifying conserved pathways that are modulated during intracellular persistence across multiple strains of NTHi, not just the additional strains used herein, could uncover novel therapeutic targets to reduce the burden of persistent airway colonisation.

8.1.2 Implications of NTHi-macrophage interactions for host immune responses in chronic respiratory disease

In agreement with other studies, this thesis indicates that NTHi presence *in vivo* was associated with increased sputum neutrophilic inflammation. Neutrophilic asthma is an inflammatory sub-phenotype associated with steroid-resistance, frequent exacerbations and more severe forms of disease. Corticosteroids have been shown to promote neutrophil survival *in vitro*[568], which could account for the increased neutrophilic asthma phenotype in the severe asthma cohort used for this study as all patients were on high dose steroid therapy. Given the accumulating evidence of associations between neutrophilic asthma and NTHi[64,86,87,347], and the data presented in this thesis providing further evidence for this, it raises the issue of the cause and effect paradox. Does neutrophilic inflammation, steroid use and associated airway damage promote NTHi colonisation, or does NTHi colonisation promote neutrophilic inflammation and the development of steroid-resistant asthma?

To try and unpick the complex mechanisms to this question, murine studies have investigated the development of neutrophilic disease following NTHi colonisation. NTHi infection of ovalbumin (OVA)-sensitised mice resulted in an influx of IL-17 expressing macrophages, neutrophils and lymphocytes, with eosinophilic inflammation reduced[532]. Despite an influx of immune cells during infection, NTHi infection was sustained in mice with allergic airways disease compared to non-allergic mice[154]. The combination of allergic airways disease contributed to the emergence of a steroid resistant neutrophilic phenotype, suggesting the synergy between prior host allergic sensitisation and subsequent NTHi infection promotes development of neutrophilic disease. However, these aforementioned murine studies may be too short to ascertain whether the neutrophilic phenotype persists or if the neutrophilic inflammation was a transient event with inflammatory resolution occurring after the chosen study endpoint. Yang *et al.* (2018) extended the experimental endpoint to two months in a study using OVA-sensitised mice and repeated low dose infections of NTHi to model NTHi chronic colonisation of the airway[462]. As a consequence, by the 2 month (56 day) endpoint, the inflammatory profile had switched from Th2-associated eosinophilic

inflammation to a Th17-associated neutrophilic inflammatory phenotype accompanied by Treg immunosuppression and impaired macrophage phagocytosis. Together, these murine studies suggest that the combination of allergic airways disease and NTHi infection drives the neutrophilic inflammation, with this inflammatory phenotype still present 2 months after the first NTHi exposure.

As such, the development of neutrophilic asthma and chronic NTHi colonisation has implications for co-infection and exacerbations. In asthma patients, frequent, severe exacerbations are predicted to accelerate lung function decline over time[569,570]. Not only are neutrophils rapidly recruited to the lung during viral infection, they undergo degranulation causing cell lysis and airway damage[47,68]. Continual viral infection by influenza or RSV has been shown to increase neutrophil inflammation, a state which has been suggested to contribute to asthma exacerbations[245,571]. Furthermore, the presence of neutrophils prior to viral infection have also shown to influence infection outcomes. A recent study by Habibi *et al.* (2020) identified a transcriptomic signature of neutrophil activation was associated with increased susceptibility for RSV symptomatic infection using experimental RSV nasal inoculation of healthy volunteers[572].

This current work demonstrated significant upregulation of macrophage genes and enrichment of macrophage functional pathways for neutrophil recruitment in response to NTHi infection, with confirmation of protein release of IL-8, IL-17C and CCL20. The substantial release of CCL20 was such that it was unable to be quantified. In contrast, IAV infection alone did not induce release of IL-8, IL-17C or CCL20 from MDM to the same extent as NTHi infection alone. Furthermore, IL-8 in particular was released in significantly greater amounts from co-infected samples compared to IAV-infected MDM. It could be postulated that NTHi-modulation of macrophage-neutrophil interactions may have dual consequences for respiratory tract viral infections. Firstly, the increased presence of neutrophils in severe, neutrophilic asthma may be driven by NTHi-infected macrophages during a stable period of disease. This neutrophil influx prior to viral challenge may result in delayed or impaired responses to a subsequent viral infection, as reported by Habibi *et al.*[572]. Secondly, macrophages may propagate the excessive inflammatory responses and airway damage characteristic of an asthma exacerbation by sustained and further recruitment of neutrophils. The interplay between NTHi-infected macrophages and other cells of the immune system, such as neutrophils, requires further exploration given the multi-faceted immune response.

The cytokine IL-1β and the NLRP3 inflammasome have also been linked to neutrophilic asthma[54,55]. In this current work, upregulation of IL-1β gene and protein expression by NTHi-infected MDM and increased *IL1B* gene expression in NTHi+ BAL samples was detected. Thus, macrophages may play a prominent role in IL-1β-mediated inflammation in response to NTHi. Associations between NTHi and IL-1β are not limited to asthma, with higher levels of IL-1β measured in BAL samples from NTHi+ COPD patients compared to NTHi- COPD patients[364]. A recent study found increased neutrophils in

the airways of COPD patients colonised with *H. influenzae*[573]. As such, targeting the IL-1β pathway in chronic respiratory disease could attenuate the chronic inflammation caused by persistent NTHi colonisation. The notion of therapeutically targeting IL-1β in neutrophilic asthma has already progressed to clinical trials[574]. Use of an IL-1 receptor agonist reduced IL-1β, IL-6 and IL-8 sputum levels in healthy volunteers challenged with LPS[575]. However, further work is required to determine whether upregulation of inflammasome responses and IL-1β in chronic respiratory disease is NTHi-specific or pan-bacterial, as IL-1 pathway interventions may only benefit a subset of patients with airway inflammation associated with NTHi-mediated IL-1 pathway activation.

Additionally, macrophages are not the only target of IAV infection, with airway epithelial cells a primary target of IAV and release inflammatory mediators during infection[576]. Therefore, if similar mechanisms of macrophage restriction of IAV infection following NTHi challenge occurs *in vivo*, it is possible that the total viral load in the airway would not significantly decrease. In combination with increased NTHi load and sustained macrophage inflammation, the total inflammatory milieu present in the airway could contribute to an exacerbation. An epithelial-macrophage co-infection co-culture model could be useful in determining the cellular cross-talk that may occur during NTHi-IAV co-infection in the airway.

8.1.3 NTHi-IAV co-infection dynamics: friend or foe?

Modelling colonisation of the airway preceding a viral infection, rather than a secondary bacterial infection from a new, opportunistic pathogen not previously present, was an important concept for this thesis. Although the role of commensals in modulating the host immune response has been explored[340], it is less well known how the colonising potentially pathogenic bacteria influences and modulates the immune response to viral infection. In this thesis, NTHi modulation of the macrophage response resulted in activation of anti-viral immune responses which likely primed macrophages to better respond to the subsequent IAV infection, at least at the early time point studied. However, other mechanisms impacting on the infection processes may have resulted in the observed outcome of decreased IAV levels.

A study by Gulraiz *et al.* (2015) found that pre-incubation of epithelial cells with NTHi subsequently resulted in increased rhinovirus infection, which was associated with NTHi-mediated upregulation of ICAM-1, which is the main cellular receptor for rhinovirus[346]. Previous work has shown that NTHi-infection of MDM also causes ICAM-1 upregulation at the cell surface level[234]. Thus, NTHi-infected MDM may also be susceptible to infection with rhinovirus, however this possibility requires further exploration in this current model. Conversely, IAV binds to sialic acids present on host cells to facilitate attachment and entry into host cells[577]. NTHi also possesses a number of outer membrane proteins that bind to sialic acid, including Hia and HMW1/2 [119,578,579]. NTHi also utilises host sialic acid as a carbon source or to decorate NTHi LOS for immune evasion[578]. It has been established that human IAV strains generally preferentially bind to α2,6-linked sialic acid residues[577], with NTHi

binding to α2,6- or α2,3-linked sialic acid residues depending on the differential expression of outer membrane proteins (HMW1/2 or Hia) by NTHi strains[128,129]. Therefore it is possible that sialic acid residues on receptors were occupied or utilised by NTHi in this current model, resulting in fewer sialylated receptors available for IAV entry into host cells. The modulation of macrophage or host cell responses and expression of cell surface receptors by colonising bacteria may indirectly alter the ability of viruses to attach and enter cells. Variation in respiratory tract virus tropism could partly explain the differences in results reported by co-infection studies using different combinations of pathogens. However, an intriguing concept is that the use of sialic acid by both NTHi and IAV to establish infection could in fact predispose the airway to infection by other respiratory tract pathogens such as *S. pneumoniae,* which has shown to co-infect the airway with NTHi[580]. Desialylation of epithelial cells following IAV infection was shown to result in increased *S. pneumoniae* adhesion to host cells[581]. This postulation of multiple pathogen interactions benefiting the contributing pathogens adds another layer of complexity to investigating bacterial-viral co-infection in the respiratory tract.

In contrast, the increased presence of NTHi following IAV co-infection was similar to the bacterial outgrowth observed during secondary bacterial infections[252]. Elucidating the mechanisms which result in bacterial proliferation following viral infection could help inform on how viruses compromise the ability of the immune system to control bacteria, not just in chronic respiratory disease, but also in the development of bacterial pneumonia in healthy individuals. Although activation of anti-viral immunity by NTHi appears to prime macrophages to better respond to a subsequent viral infection, it also indicates similarities in the macrophage response between NTHi and IAV, such as the similar induction of IFN responses. Thus, it is tempting to speculate that immune evasion strategies utilised by IAV will also be of benefit to NTHi. One such immune evasion strategy involves IAV NS1 protein binding to GBP1 to prevent macrophage intracellular inhibition of IAV replication[512]. GBP1 is also involved in the anti-microbial response by binding to bacteria or bacterial-containing vacuoles[445], with *GBP1* expression upregulated in response to all three pathogen combinations in this thesis. Unfortunately due to the transcriptomic nature of this work, protein-level inhibition of GBP1 by IAV or GBP1 binding to NTHi cannot be confirmed. However, given that the transcriptomic analysis identified *GBP1* to be important in the MDM immune response to intracellular NTHi infection, it is tempting to speculate that IAV inhibition of GBP1 facilitates NTHi escape from macrophage immune control.

8.1.4 Host-pathogen cellular cross talk during infection may modulate immune responses

This work has shown that NTHi infection of macrophages activated anti-viral immune responses that appeared to prime macrophages to better respond to the subsequent IAV infection. A recent study found that rhinovirus infection of epithelial cells 3 days prior to IAV infection effectively induced ISG expression and protected cells in an interferon-dependent manner[582]. Timing of IFN-β

responses have been shown to be crucial for restriction of viral infection. Addition of exogenous IFN-β to cell culture 16 h prior to IAV infection found that inhibitory effects on IAV replication were maintained up to 1 week in MDM[497]. Furthermore, a murine model of IAV and subsequent Influenza B virus (IBV) infection demonstrated significant protection to secondary IBV infection 3 weeks post primary infection, with protective immunity still detected, albeit reduced, at 6 weeks post initial infection[583]. Differences between these studies could be due to the experimental model used, with the murine model allowing for immune responses, such as IFN-β signalling[497], to be explored in the context of the whole lung environment. As persistent NTHi infection *in vivo* has been detected for longer than the time frames used in these aforementioned studies, activation or priming of IFN pathways may wane, resulting in the loss of any 'protective' effect of NTHi modulation of macrophage immune responses by the time a viral infection occurs.

Due to increased MDM release of cytokines and chemokines measured during NTHi infection, it is likely that the macrophages within this model system are communicating and signalling via these pro-inflammatory mediators. Moreover, this signalling may act to prime neighbouring cells prior to IAV infection. In addition to cytokine release, it has also become apparent that both host cells and pathogens are able to communicate through release of extracellular vesicles[584]. By packaging various lipids, proteins and RNA into vesicles, cells can effectively communicate the presence of an infectious agent either locally or systemically[584]. Studies using *Mycobacterium tuberculosis* (Mtb) and *Mycobacterium avium* have shown that *Mycobacterium* PAMPs packaged into extracellular vesicles were detected in neighbouring cells and were associated with stimulation of a pro-inflammatory response in these uninfected/neighbouring cells[585,586].

Although uninfected/neighbouring cell activation could be due to extracellular vesicle-derived PAMP recognition, host mRNA and microRNA (miRNA) packaged and released in extracellular vesicles can have transcriptional and translational functional effects on host target cells[584]. miRNA are small non coding RNA which epigenetically regulate gene expression[587]. It has been identified that disease-associated changes in the miRNA composition of extracellular vesicles isolated from BALF in COPD and asthma, which could suggest secreted vesicles contribute to the dysregulation of airway inflammation and disease progression[588,589]. However, pathogens such as Mtb have developed mechanisms to disrupt a variety of host responses; interference with extracellular vesicles are no exception. Mehra *et al.* (2013) demonstrated the ability of Mtb to disrupt part of the machinery in the macrophage endolysosomal pathway involved in directing cargo destined for multivesicular bodies, which may alter the formation of exosomes[590]. As a lack of MDM transcriptomic data for late endosomal markers was found in chapter 4, the possibility of NTHi subverting extracellular vesicle development is an interesting prospect and cannot be excluded.

Similarly to miRNA, long non-coding RNA (lncRNA) can also be transported in extracellular vesicles and epigenetically regulate gene expression, despite initially being considering as 'junk RNA'[587]. Ilott

et al. (2014) characterised the lncRNA transcriptome in LPS-stimulated monocytes and identified a variety of lncRNAs to be differentially expressed, including two lncRNA which regulated the transcription of *IL1B* and *IL8* and subsequent mediator release by a yet to be identified mechanism[591]. Given that these two inflammatory mediators were highly upregulated during both NTHi and co-infection, and are elevated in severe, neutrophilic asthmatics, determining their regulation by lncRNA could provide useful insights into how to reduce inflammation in the chronically colonised asthmatic airway.

Gram-negative bacteria also have the capacity to release outer membrane vesicles (OMVs). Respiratory tract pathogens including NTHi and *M. catarrhalis* secrete OMVs containing virulence factors which are able to modulate host responses whilst avoiding direct bacteria-host cell contact [592,593]. *M. catarrhalis* OMVs have been shown to contain β-lactamase, which conferred protection to NTHi from β-lactamase antibiotic action during co-culture of NTHi with *M. catarrhalis* OMVs[594]. As only up to 55% of NTHi strains express β-lactamases, co-infection of the airway with other bacteria such as *M. catarrhalis* could be beneficial for enhanced survival[108]. NTHi OMVs specifically have been shown to contain DNA, OMP P5, IgA endopeptidase, serine protease, and heme utilization protein which stimulates release of IL-8 from epithelial cells[593]. However, as the majority of studies on bacterial OMVs have focussed on extracellular bacteria, the role of NTHi OMVs during intracellular residence is relatively unknown. Release of NTHi OMVs may be a mechanism more involved in the initial stages of host cell entry and invasion, rather than intracellular persistence. Nonetheless, the release of extracellular vesicles by macrophages and NTHi has important implications for host-pathogen cross talk during infection in the respiratory tract and requires further exploration.

8.1.5 Potential role for trained innate immunity during co-infection

The mechanism of immune paralysis or tolerance is one such process that could result in NTHi proliferation following co-infection. Immune paralysis/tolerance arises from epigenetic modifications of immune response genes, which can include histone modifications or DNA methylation[587]. Other recognised epigenetic modifications now include the role of miRNA and lncRNA, which were discussed previously in 8.1.4. Immune paralysis/tolerance results in cells less responsive to a secondary stimulation; exposure of monocytes to LPS for 24 h resulted in lower amounts of TNF-α and IL-6 production upon secondary immune stimulation[177]. Transcriptomic analysis of monocytes from sepsis patients and in a sepsis mouse model demonstrated that tolerance was not due to failure of signalling pathways, but rather that immunosuppressive signalling following primary infection contributed to the inability for cells to effectively respond to a second infectious challenge[595]. More specifically, a further study found that following stimulation with LPS, macrophages undergo histone modifications at the promoter regions of IL-1β and TNF-α, which reduces the ability of macrophages to respond to second LPS challenge[596]. A study has

recently demonstrated that immune paralysis/tolerance contributes to reduced phagocytosis in monocytes isolated from patients cured from sepsis and then stimulated *ex vivo* with *E. coli* and *S. aureus*[597]. This same study also showed mouse alveolar macrophages (AM) from a murine model of pneumonia also exhibited a phagocytic defect up to 28 days after onset of the first pneumonia[597].

In contrast, studies have shown that monocyte/macrophage exposure to a specific challenge such as β-glucan, a component of the cell wall of bacteria and fungi, induced immune training. Immune training for lung macrophages is a relatively unexplored topic, with immune training or memory more associated with the adaptive arm of the immune response[598]. Priming with β-glucan induced trained immune cells with enhanced inflammatory responses, with secondary exposure to β-glucan resulting in reversal of the tolerance phenotype induced by LPS[595]. Comparisons between LPS and β-glucan challenge found that macrophages undergo differential 'training' resulting in diverse transcriptomic and epigenetic profiles depending on the type of stimulus, with the local inflammatory environment involved in the maintenance of this trained immunity[595,597].

Such a phenomenon may be occurring during NTHi-IAV co-infection, however the time points used in this current work may have been too acute. The data could suggest that infection of MDM with NTHi for 6 h, and the continued presence of NTHi until 24 h induces trained MDM immunity prior to IAV challenge, shown by inhibition of IAV infection at 48 h. However, the increased NTHi presence in this model following co-infection was more reminiscent of immune tolerance, with dysregulated inflammatory responses resulting in bacterial outgrowth. One caveat to this postulation is that the MDM would have already been exposed and cultured in GM-CSF for the 12 days prior to NTHi infection. Therefore, MDM used in this current work may respond differently to NTHi, IAV and co-infection compared to the naïve monocytes used in the aforementioned studies that were first stimulated with LPS or β-glucan. Novakovic *et al.* showed that β-glucan reversed the LPS-induced tolerance of macrophages, hence, it is possible that stimulation with NTHi and/or IAV may be re-writing the original GM-CSF generated macrophage phenotype[595].

Furthermore, the concept of trained immunity highlights potential further differences between the MDM used in this work and AM; macrophages resident in the lung environment may have already been 'trained' by previous exposure *in vivo* and may therefore respond differently to MDM[177]. For example, Watson *et al.* (2020), required a higher PFU of the same IAV strain to achieve AM infection levels comparable to MDM[497]. GM-CSF is commonly used to differentiate monocytes into lung-like macrophages, as GM-CSF is important for maintenance of AM function and phenotype *in vivo*[166,357]. Roquilly *et al.* (2020) demonstrated that the local inflammatory environment was responsible for maintenance of trained immunity[597]. Therefore, the inflammatory lung environment in asthma, which could involve the chronic presence of potentially pathogenic bacteria, may be compromising macrophage function through dysfunctional or impaired trained immunity. Roquilly *et al.* also found that a lower number of monocytes were able to phagocytose bacteria even 6 months after

resolution of systemic inflammation in sepsis patients. Given that numerous studies have shown dysfunctional macrophage phagocytosis in asthma[247,454], the impact of chronic NTHi presence on the balance between macrophage immune tolerance and trained immunity requires further exploration, as this could help explain why respiratory tract pathogens are able to persist in the lung.

8.1.6 Implications of bacteria-virus co-infection in the respiratory tract

This work has identified unique patterns of MDM immune responses depending on the pathogen or pathogen combinations used. A sustained macrophage inflammatory response was measured in co-infected macrophages that was not present in IAV-infected macrophages, whereas independent NTHi and IAV infection resulted in two distinct inflammatory responses. This indicates that NTHi infection of macrophages prior to IAV infection alters the subsequent MDM immune response to a different profile that would not be elicited if IAV infection occurred independently. This has important implications for studying host-pathogen interactions; responses observed and measured *in vitro* may in fact be distinct from and may not necessarily reflect *in vivo* biology. Of course, this work only uses macrophages in cell culture and as the respiratory tract is composed of a multitude of cell types in a 3D lung architecture, additional factors may influence co-infection progression *in vivo*. Nonetheless, this raises the question of whether the dysregulated inflammation occurring during exacerbations normally deemed to be 'virally-driven' is actually driven by the previously colonising bacteria, the virus or a combination of both. Elucidating the main driver of airway inflammation during exacerbations may influence the course of treatment or therapies given to patients during exacerbations.

As previously discussed in chapter 5, the responses observed in this thesis are reminiscent of secondary bacterial infection following viral infection. Secondary bacterial infections were commonly identified as the cause of death during the 1918 IAV pandemic, rather than the virus itself, which also appeared to disproportionally effect younger, 'healthier' individuals[252]. As such, the results of this thesis are not just relevant for co-infection contributing to exacerbations of chronic respiratory diseases, but also the impairment of lung immunity following viral infection resulting in bacterial outgrowth and bacterial pneumonia. A study by Murphy *et al.* (2004) demonstrated the difficulty in accurately detecting persistent airway microbial colonisation; their longitudinal study sampling the adult COPD lung found evidence of NTHi colonisation that appeared to disappear during subsequent sampling but the same initial strain reappeared during later sampling[134]. The method used to confirm positive NTHi samples was microbiological culture of sputum samples. It is possible that NTHi adaptation to persistent infection resulted in difficulty in culturing the isolated pathogen. Or perhaps, NTHi load was too low to be accurately detected by culture, a limitation overcome by recent advances in microbiome profiling by sequencing techniques. Nonetheless, it is clear that rather than focussing on the acquisition of bacterial

pathogens following viral infection, future studies need to consider the outgrowth of already present colonising bacteria in the lung, which due to low biomass in the lower respiratory tract, can often be difficult to detect.

Although NTHi and IAV used in this thesis are both clinically relevant pathogens for severe asthma, individuals – both healthy and with chronic respiratory disease – can be colonised and infected by a wide array of pathogen combinations which can influence the host immune response. NTHi co-infection with other viruses, such as RSV has also been identified, with *in vitro* work demonstrating that RSV infection was reduced in epithelial cells pre-incubated with NTHi[345]. However, this same study did not find any differences when epithelial cells were infected with IAV after NTHi infection. Potential airway interactions between NTHi and rhinovirus have also been suggested, with the AERIS COPD cohort study identifying increased risk of exacerbation was associated with presence of both NTHi and rhinovirus[332]. This cohort study demonstrates the real-life applications of the bacteria-virus co-infection *in vitro* studies, indicating the potential for NTHi chronic colonisation of the airway to modulate host responses to viral infection *in vivo*.

Although potentially pathogenic bacteria such as NTHi, *S. pneumoniae* and *M. catarrhalis* are present in increased abundance in the airways of individuals with chronic respiratory disease, such pathogens have also been suggested to be members of the 'heathy' lung microbiome. It is not clear how multiple potentially pathogenic bacteria colonise the same niche and whether they are in direct competition or facilitate co-colonisation. Associations between these potentially pathogenic bacteria *in vivo* are apparent, with a whole genome study identifying increased NTHi carriage in children following the introduction of the pneumococcal vaccine[502]. Co-carriage of bacteria can be beneficial to both pathogens, with *in vitro* work demonstrating that *M. catarrhalis* secreted OMVs contained *M. catarrhalis*-derived proteins which were able to protect NTHi from complement-mediated killing[599]. This cross-pathogen protection provides further evidence of pathogens modulating the immune response to a co-infecting pathogen, in this instance allowing for enhanced survival of NTHi. Multiple pathogen dynamics have also been demonstrated in a chinchilla model of OM. Animals challenged with NTHi, *M. catarrhalis* and RSV were found to exhibit more severe disease characteristics and enhanced persistence of *M. catarrhalis* in the middle ear of chinchillas[600]. Thus, considering the impact of multiple bacteria colonisation of the airway on the host immune response may also include modulation of responses to resident bacteria, not just viruses.

8.1.7 Implications of NTHi airway persistence and viral coinfections for early life asthma development

Although this work focuses specifically on NTHi and subsequent viral infection of macrophages and the implications for asthma exacerbations, NTHi presence at a young age has been associated with development of asthma in later life[24]. One of the seminal papers sequencing the lung microbiome

in asthma was published by Hilty *et al.* (2010), who identified increased abundance of *Haemophilus* in both adult and children[25]. However previous work had identified rhinovirus to be significantly predictive of asthma development, which has resulted in more of a focus on early life viral infections[601–603]. Retrospective studies have identified children with early life RSV infection, particularly those requiring hospitalisation, to be more at risk of asthma development [604]. Although early life RSV and rhinovirus infection had been associated with the increased risk of asthma development in later life, emerging studies and the co-infection data in this thesis indicate that the modulation of the immune response to viral infection by the pre-colonising airway microbiota, such as NTHi, requires consideration and further investigation.

The potential role of trained immunity in the macrophage response to secondary infection was discussed in Section 8.1.5. As mentioned previously, an efficient and timely IFN response is crucial in restricting viral infection, with epigenetic modifications also involved in modulation of IFN responses. Pre-treatment of human bronchial epithelial cells with IFN-γ inhibited RSV infection, which was shown to be associated with reduced methylation of the RIG-I promoter, with elevated RIG-I mRNA levels detected for up to 4 days after removal of IFN-γ[605]. Similarly, IFN-β stimulation of cells resulted in increased histone chromatin marks on numerous ISGs and immune memory that was sustained in macrophages[606]. Although this macrophage immune memory was associated with a faster induction of ISGs in cells exposed to a second IFN-β stimulation, the memory response was different to the initial response, with a number of ISGs not responding following a secondary stimulation.

The local environment appears to be important for maintenance of trained immunity or tolerance, with different stimuli altering the overall programme of macrophage immune defences[177]. It is not clear whether the epigenetic profile induced by one stimulus would provide an enhanced or even detrimental response to a different, secondary stimulus. Thus, the early life colonisation of the airway by bacteria such as NTHi, may modify the epigenetic profile of macrophages, resulting in an altered response to a virus. As mentioned previously, this current model was too acute to derive any conclusions surrounding the longer term implications of NTHi persistence on macrophage epigenetic modifications and the response to a subsequent viral infection *in vivo*. NTHi *in vivo* airway persistence occurs over months and years[421], so it will be important to ascertain how NTHi persistence over this long duration impacts on the epigenetic modifications of macrophage immune responses.

Conversely, rather than increased abundance of potentially pathogenic bacteria, the absence of commensal bacteria may result in impaired immune development and responses to viral infection in early life. The importance of the commensal bacteria members of the microbiome for efficient immune responses to infection has been shown in antibiotic-treated mice which displayed altered immune responses to respiratory viral infection[88,340]. Specific commensal lung bacteria, such as

Prevotella, elicit lower levels of inflammation compared to NTHi[607], with *Prevotella* spp. able to modulate dendritic cell responses to NTHi during co-culture, suggesting host cell-commensal bacteria cross-talk modulating the immune response to a pathogen[608]. Therefore, the loss of commensal species and gain of potentially pathogenic bacteria may modulate host immune responses. Removal of species from an environmental niche alters the ecological structure of the microbiome. Consequently a new pathogen colonising the now-vacant niche arrives and dominates; the removal of Hib through a successful vaccination programme has likely resulted in the increased prevalence of NTHi in disease[114]. Given that the presence of *Prevotella* spp. was sufficient to dampen aspects of the host response[607], it poses the question whether complete eradication of NTHi (by vaccine for example) is required, when instead promoting the restoration of commensal species may result in more favourable outcomes.

8.1.8 Role for macrophage immunometabolism during infection

Immunometabolism is an rapidly emerging field, with rewiring of macrophage metabolic pathways fundamental for key macrophage functions[420]. This work initially demonstrated increased metabolic activity in response to NTHi infection using a MTS assay and measurement of LDH release into culture supernatants. WGCNA also identified transcriptomic modulation of metabolic pathways, with a specific cluster (cluster III) significantly functionally enriched. This cluster included specific biological process GO:terms such as oxidative phosphorylation, mitochondrial ATP synthesis and cellular respiration, with cellular component GO:terms relating to the mitochondrion similarly enriched.

Moreover, *ACOD1* was one of the top most significantly upregulated MDM genes at 6 h and 24 h, which encodes for a cis-aconitate decarboxylase involved in the production of itaconate from cis-aconitate produced in the TCA (Kreb) cycle[609]. Itaconate inhibits succinate dehydrogenase (SDH), resulting in accumulation of succinate and diversion of macrophage metabolism towards aerobic glycolysis[610]. *ACOD1* was previously designated *IRG1* (immune responsive gene 1) as it appeared to play an unknown function in the inflammatory immune response, with increased gene expression in LPS stimulated macrophages[611]. However, Michelucci *et al.* (2013) confirmed itaconate is an antimicrobial metabolite, capable of restricting growth of Mtb and *Salmonella enterica*[609]. Studies by Nair *et al.* (2019) and Hoffman *et al.* (2019) also demonstrated that *ACOD1* expression was important for the host response to Mtb infection[612,613]. Recent work by Hersch and Navarre (2020) demonstrated the ability of *Salmonella* to sense and respond to macrophage itaconate by expression of itaconate degradation proteins[614]. It is not known whether NTHi is similarly able to interfere with *ACOD1*/itaconate regulation of macrophage inflammatory processes, however the presence of genes for itaconate degradation in numerous other bacteria suggests this possibility[615].

Other than direct antibacterial properties, a role for itaconate in modulating inflammatory processes has been suggested. Itaconate activates the Nrf2 pathway to induce the transcription of

anti-inflammatory and antioxidant genes[616] and can inhibit activation of the NLRP3 inflammasome to reduce IL-1β cleavage and release[617]. Itaconate and interferon regulation is also linked, with Mills *et al.* (2018) suggesting a feedback mechanism of itaconate regulating interferon signalling, which in turn limits further gene expression and production of itaconate[616]. This current work could indicate the immunoregulatory properties of *ACOD1*; *ACOD1* was highly upregulated at 6 h and 24 h, whereas expression of the type I IFNs were more lowly expressed or downregulated at 24 h in response to NTHi. However, in contrast to itaconate-mediated blocking of NLRP3 activation and IL-1β release observed by Hooftman *et al.* (2020), IL-1β release was not restricted and was upregulated during NTHi and co-infection of macrophages at 48 h[617]. This difference could be due to the high MOI of NTHi used to infect MDM. Muri *et al.* (2020) demonstrated that high dose of Nrf2 activators resulted in increased apoptosis and IL-1β release, whereas low dose inhibited pro-inflammatory cytokine transcription[618]. The role of macrophage-derived itaconate in chronic lung disease has not been fully explored. Recently, airway itaconate levels and expression levels of *ACOD1* were found to be decreased in AM from patients with IPF compared to controls[619]. Given the impaired AM immune response in asthma, investigating the role of itaconate in regulating inflammatory responses could elucidate a mechanism behind this impairment.

8.2 Translational impact of the study

The findings of this study may have important applications for developing and designing further studies, therapeutics or trials to address clinical needs and improve health outcomes in individuals with chronic respiratory disease. The translational impact of this work is discussed below.

Firstly, the host-pathogen dynamics occurring between MDM, NTHi and IAV identified potential mechanisms underlying chronic airway inflammation and exacerbations in chronic respiratory disease. This work suggests that NTHi persistence following invasion of macrophages may contribute to the chronic airway inflammation characteristic of chronic respiratory diseases such as asthma and COPD. Macrophages continued to elicit a pro-inflammatory responses up to 48 h after initial NTHi challenge, with certain macrophage inflammatory genes also found to be more highly expressed in severe asthmatics determined to have presence of NTHi. Furthermore, this work not only demonstrated differences in macrophage responses to IAV and NTHi individually, but the presence of both pathogens further alters the macrophage response. As the highest levels of macrophage inflammation were present in co-infected samples when compared to uninfected, it is possible that NTHi presence may predispose individuals to an exacerbation following viral infection. For example, the AERIS COPD cohort study identified increased exacerbation risk to be associated with presence of both NTHi and rhinovirus[332]. The AERIS cohort study demonstrates the potential for NTHi chronic colonisation of the airway to modulate host responses to viral infection *in vivo,* which can be explored further by bacteria-virus co-infection *in vitro* models, as developed in this current work. The implication of NTHi modulation of host responses is important; although it is

believed that the majority of exacerbations are virally-driven, it is possible that bacteria such as NTHi contribute to the excessive and dysregulated inflammatory response occurring during exacerbation of disease. As such, these findings suggest that reducing NTHi burden in the lung may reduce airway inflammation and risk of exacerbation.

Secondly, this work identified potential NTHi therapeutic targets to reduce airway bacterial burden. Although commonly used, antibiotic therapy has shown to be ineffective at completely clearing NTHi[348]. The AMAZES trial demonstrated that azithromycin treatment reduced asthma exacerbations[620] and *H. influenzae* load[621]. However, the work in this thesis showed that NTHi downregulated expression of ribosomal protein genes, which are the target of azithromycin. Thus, it is possible that azithromycin will not be effective against intracellularly located and adapted NTHi. Worryingly, the AMAZES study also found increased carriage of antibiotic-resistance genes[621], a reminder that with increasing rates of AMR, it is important to investigate other avenues of antimicrobial therapy. The findings detailed in this thesis could contribute to designing better antimicrobial therapies against NTHi, with numerous NTHi genes and pathways upregulated during intracellular persistence which could be investigated further as targets for therapeutic intervention. As previously mentioned, the top upregulated NTHi gene during intracellular persistence, *bioC*, is involved in biotin synthesis pathway, components of which are absent in humans and could therefore be attractive targets to interfere with the ability of NTHi to persist within the airway. Although identification of initial targets of interest through to eventual use as therapeutics can take years, the dual RNASeq data set generated in this work can be used as a resource to identify potential targets that can be taken forward into drug development pipelines for validation.

Finally, the findings of this work could provide a rationale for stratifying asthma patients based on NTHi presence. Transcriptomic analysis of the macrophage response to NTHi identified upregulation of IL-1 and non-canonical inflammasome signalling pathways. Components of the IL-1 and inflammasome pathways are also upregulated in asthma[55], but the mechanisms accounting for this upregulation have not been identified. Given that *IL1B* gene expression was higher in severe asthmatics with detected NTHi presence, it is possible that NTHi intracellular invasion of macrophages is the source of inflammasome activation and enrichment of IL-1 signalling pathways *in vivo*. Thus, it could be useful to stratify patients based on NTHi presence, which could improve the efficacy of IL-1 therapies that so far have shown to be ineffective in asthma[622]. In particular, individuals with airway NTHi presence who have not yet developed a T17 inflammatory phenotype may benefit from anti-IL-1β therapy, to prevent the progression towards neutrophilic, steroid resistant disease. Ascertaining whether the transcriptomic signal identified in this work is predictive of a switch to T17 inflammation using a larger, longitudinal cohort could identify a subset of asthmatics who could benefit from IL-1 therapy.

8.3 Limitations of the study

One of the main limitations of this study was the use of MDM to model lung macrophages. Although MDM have been extensively used and display similar phenotypes and responses to AM[250,356,357], there are dissimilarities between the two cell types. As previously mentioned, in order to achieve comparable levels of infection, Watson *et al.* (2020) infected AM with just over ten times higher PFU/ml of IAV compared to MDM[497]. Therefore, AM do not appear to be as permissive to IAV infection as MDM[277,623]. The more restrictive phenotype of AM isolated from the lung could be a consequence of the lung environment 'training' of lung-resident macrophages, as discussed previously. Hence, responses of AM to NTHi-IAV co-infection may differ to MDM, with potential disease impairment, such as diminished IFN responses and phagocytic impairment, also likely to contribute to different responses between cell types from health and disease. However, as obtaining AM by bronchoscopy is invasive for patients and can potentially result in too low a yield for infection model optimisation, the majority of work in this thesis was performed using the more readily available and accessible blood-derived MDM model.

Furthermore, the model may be too acute to consider long term implications of NTHi infection and subsequent viral infection. Due to technical and financial limitations, only two time points were able to be taken forward for sequencing. As 6 h and 24 h allowed for exploration of NTHi transcriptomic adaption to intracellular infection, these two time points were chosen. Subsequently, as macrophage responses to the NTHi infection were characterised at the 24 h time point by dual RNASeq, this time point was chosen to add IAV to assess the impact of co-infection. However, as discussed previously, the timing of immune responses and pathogen challenge could influence infection outcomes. Therefore, the results observed in this thesis may not be representative of a chronic infection *in vivo*. Similar short time periods between co-infecting pathogens have been used in previously published studies[345,511], however longer time courses determining the point at which modulation of the macrophage by chronic NTHi no longer restricts the IAV infection is warranted.

In this study, three time points were investigated in the optimised infection model (6 h, 24 h and 48 h). Due to the time periods of infection (6 h NTHi infection, 2 h IAV infection), gentamicin wash and subsequent culturing, the 6 h time point represented supernatants harvested after 6 h incubation, the 24 h time point represented supernatants harvested after 16.5 h of incubation and the 48 h time point represented supernatants harvested after 22 h of incubation. Exploring longer or multiple intermediate time points would overcome the limitation surrounding the dynamics of gene expression and protein synthesis and release. For example, IL-17C is suggested to function as an innate-like cytokine as it is induced during the early phases of infection[624]. This early role was mirrored in this current work, as IL-17C was only detected at 6 h and 24 h in response to NTHi, but not at 48 h. Conversely, the release of some cytokines may not 'peak' until later in the time course.

Some inflammatory mediators may accumulate in the cell culture supernatant and may not undergo the rapid recycling that might occur *in vivo*, resulting in saturation of the infection model system. As such, these proteins would be measured in higher abundance in cell culture supernatants harvested after 22 h of infection, compared to harvest after only 6 h. These limitations must be considered when determining absence or presence of cytokines and their contribution to the MDM inflammatory response. The wide range of mediators analysed in this work are likely to have a range of different regulatory processes, of which this current work was not designed to assess.

To try and overcome the limitations of the MDM model, BAL samples obtained from severe asthma patients were used to confirm the results of the transcriptomic analysis of NTHi-MDM infection. However, there are a number of cofounding variables when using these samples. Firstly, the low sample number combined with the heterogeneous nature of asthma could have resulted in difficulties determining significant changes between samples colonised due to the underlying disease differences. As previously discussed, Simpson *et al.* (2014) found higher levels of *CASP4* and *IL1B* in neutrophilic asthmatics compared to eosinophilic or paucigranulocytic inflammatory phenotypes[55]. The small cohort size in this thesis did not allow for stratification based on inflammatory status. Similarly, although this work was primarily concerned with differences in immune responses in severe asthma, the lack of available healthy controls did not allow for determination of whether gene pathways in asthma were already dysregulated (e.g. IFN responses).

Another drawback of only having access to RNA from the BAL cell pellet was that the impact of NTHi-IAV infection of AM from severe asthma patients could not be assessed. Functional work using freshly isolated AM from asthma patients could better determine whether similar responses to MDM co-infection occur in AM. Comparing responses between AM from healthy and asthma individuals would also give a better indication as to whether the differences would be due to the cell type (AM vs MDM) or intrinsic disease impairments (e.g. IFN responses). Similarly, the impact of steroids on the expression of the genes identified in the dual RNASeq was not able to be assessed. As all BAL samples were obtained from severe asthmatic patients, the potential impact of high dose inhaled steroid use on BAL gene expression must be appreciated when considering these results.

The expression of a small set of genes identified as important for NTHi persistence between 6 h and 24 h remained consistent at 48 h, however this time point could still be too early to be defined as persistence. Although these genes appeared to be crucial in establishing the persistent infection within macrophages between 6 h and 24 h, extending the duration of infection would confirm whether these genes remain stably expressed throughout longer intracellular persistence of MDM. As such, this could be why no expression of NTHi genes in BAL samples could be reliably detected; further transcriptomic changes may have occurred past the time points chosen in this current study

and the genes identified in the dual RNASeq analysis were no longer differentially expressed *in vivo*. Extending the NTHi intracellular persistence MDM model would allow for exploration of this possibility, as would sequencing the asthmatic BAL samples, which would allow for better coverage of NTHi transcripts and evaluation of NTHi gene expression during airway colonisation.

8.4 Further work

One of the main outstanding questions from this work is to determine whether AM isolated from NTHi-colonised asthmatic individuals respond to IAV infection in line with the results observed for MDM co-infection. Sorting of AM from BAL by fluorescence-activated cell sorting (FACS) would allow for a pure population of AM cells to be isolated and stimulated *ex vivo* with IAV as previously described[497]. Depending on the number of AM available, RNA could be harvested for transcriptomic analysis, cells harvested for flow cytometry analysis of IAV infection levels and relevant cell surface marker expression and cell culture supernatants harvested to assess AM inflammatory mediator release.

Similarly, the MDM *in vitro* experimental work in this thesis was performed using healthy volunteers, however all of the asthma patients in the WATCH study were taking steroids. As such, it was not clear whether the lack of differences in the expression of some genes between NTHi+/- groups was due to the immunosuppressive effects of steroids. Although steroids are a commonly used treatment in chronic respiratory diseases such as asthma and COPD, steroid used is linked to increased incidence of community-acquired pneumonia[625]. A recent study concluded that having asthma was associated with three times higher risk of being hospitalised for pneumonia, with particular ICS compounds identified as a risk factor[626]. Although there is good evidence for ICS in reducing exacerbations[627], inhibition of immune responses and inflammation via ICS therapy may have an undesired effect of suppressing immune responses to potentially pathogenic bacteria present in the airway. One of the suggested actions of ICS is to inhibit NF-Kb activation[625], a central transcription factor important for the response to respiratory pathogens such as NTHi and *S. pneumoniae*, two pathogens implicated in community acquired pneumonia[625,628].

Therefore, it would be of interest to perform further work assessing whether the presence of steroids alters the MDM response to NTHi infection, and what impact this may have on a subsequent IAV infection. Previous work has demonstrated that incubation of NTHi-infected MDM with either fluticasone propionate or budesonide resulted in decreased macrophage cell surface expression antigen presenting molecules and decreased release of IL-1β[199,234]. It is tempting to speculate that NTHi-induced priming of MDM anti-viral responses may not occur due to immunosuppressive effects of steroids, thus IAV infection may not be decreased.

It would be important to ascertain whether the transcriptomic changes identified during infection were functionally relevant. The majority of the work in this thesis is transcriptomic data and would

greatly benefit from functional work confirming the role of specific genes or pathways identified in this thesis. As early NTHi activation of MDM anti-viral pathways – namely type I IFN pathways – and release of IFNs likely primed MDM to respond to a subsequent viral infection, it would be important to confirm this analysis by blocking MDM release of IFNs during NTHi infection, to prevent IFN stimulation of MDM prior to IAV challenge. Blocking IFN-β signalling could be achieved by addition of an IFN-β neutralising antibody to capture soluble IFN-β, preventing secreted IFN-β from binding to cells and inducing cellular signalling using a similar technique described by Wallington *et al.* (2018)[352].

A different approach may be to silence *IFNB* expression by transfecting MDM with short interfering (si)RNA to inhibit IFN-β mRNA expression as previously used by Staples *et al.* (2015)[351]. Alternatively, the CRISPR-Cas9 gene editing technology could be utilised to knock out the IFN-β gene. The feasibility of using CRISP-Cas9 genome editing in human macrophages has recently been reported by Freund *et al.* (2020), who optimised a protocol targeting *B2M* in monocytes obtained from the blood of healthy volunteers using a CRISPR-Cas9 system[629]. Monocytes were first nucleofected with *B2M*-specific Cas9 complexes and were subsequently differentiated into macrophages in the presence of M-CSF. This methodology resulted in a *B2M* KO efficacy of ~90%, without the need for further cell selection or purification. Alternatively, the interferon-αβ receptor could be knocked down. Receptor knockdown in MDM has been demonstrated by Cooper *et al.* (2016) who used siRNA to reduce both CD36 mRNA and subsequent cell surface expression levels in MDM[240]. However, receptor knockdown may also prevent IFN-α signalling, which could mean that any changes observed may not solely be due to inhibition of IFN-β signalling.

Functionally confirming the role of the top identified NTHi genes during intracellular infection would be important when considering these genes or pathways as potential therapeutic targets. Mutagenesis methods include introducing a mutation into a target gene of interest to generate bacteria that no longer express the gene of interest, in order to confirm or further explore the suggested role of the target gene. For example, Murphy *et al.* (2006) constructed an OMP P6 *H. influenzae* mutant to assess the proposed cell wall structural role of OMP P6 in maintaining bacterial viability[630]. Generation of NTHi mutants lacking the top gene *bioC,* and then comparing the ability of NTHi *bioC* KO mutants and NTHi expressing *bioC* to infect and persist within MDM, would aid in confirming the importance of the *bioC* gene and the biotin pathway for NTHi intracellular persistence.

As discussed previously, the lung microbiome is a rich environment, with many commonly isolated pathogens appearing to cohabit the lung. It has been suggested that NTHi and *M. catarrhalis* co-culture results in protective benefits from host-mediated immune responses. This current work identified potential NTHi co-infection of asthma BAL samples with other unidentified bacteria. Together with *S. pneumoniae,* NTHi and *M. catarrhalis* are the most commonly isolated pathogens

from individuals with chronic respiratory disease. As such, these bacteria have also been implicated in exacerbations and have been found to be co-infecting with IAV, RSV and rhinovirus, all viral drivers of exacerbations. The MDM model has previously been used to investigate host responses to other pathogens including *S. pneumoniae*, *M. catarrhalis* and RSV[240,350]. Furthermore, it has been shown that the duration of *M. catarrhalis* carriage in individuals with COPD is much shorter than that of NTHi. The median carriage of M. catarrhalis was reported to be only 34 days[631], whereas another study found NTHi persisted for a median of 161 days[421]. Given the clinical relevance of these pathogens, the current optimised infection model and associated techniques used in this thesis could be utilised to investigate whether these various pathogens and different pathogen combinations uniquely modulate MDM responses.

The transcriptomic data set produced in this thesis provides a rich resource for exploration of other research questions focussed on investigating host-pathogen interactions. The MDM analysis in this thesis was only performed using the protein coding genes. However, the full read count list included over 60,000 transcripts, some of which were lncRNA. As mentioned in Section 8.1.4, lncRNAs were originally considered 'junk' RNA but have since been demonstrated to have diverse functional effects[632]. Determining the expression of lncRNA in response to NTHi may increase our understanding of how macrophage gene expression is regulated during intracellular infection. Future work analysing the differentially expressed lncRNAs in this data set may unveil lncRNAs that are master regulators of the upregulated MDM intracellular immune response pathways. This analysis could provide useful insights into which pathways to therapeutically target to reduce inflammation in the chronically colonised asthmatic airway.

Similarly, mapping of transcripts to the NTHi ST14 draft genome assembly by Novogene identified a number of novel NTHi genes in the dual RNASeq data set. Unfortunately, determining the relevance and potential function of these genes was beyond the scope of this current project, however the presence of these genes could be explored further. Likewise, the NTHi genome still contains a number of hypothetical protein coding genes that have not yet been assigned a function. A number of hypothetical protein coding genes were found to be differentially expressed during intracellular infection and confirmation of function by additional experimental work could identify novel gene targets for therapeutic intervention.

During co-infection, the three NTHi strains differentially modulated gene expression, whereas the MDM gene expression profile was unique for all three pathogen combinations. Although gene selection was evidence-led based on the outcome of the transcriptomic analysis, these select genes were identified as unique for NTHi-MDM interactions at 6 h and 24 h any may not represent the most important set of genes at 48 h during co-infection. Nonetheless, this preliminary analysis of NTHi and MDM gene expression at 48 h provides rationale to explore global transcriptomic differences of host and pathogen during co-infection by triple RNASeq[513].

A recently published study has demonstrated the feasibility of triple RNASeq and also found differences in host immune responses depending on the pathogen(s) used for infection[513]. Triple RNASeq of this current model would allow for better exploration of transcriptomic changes that are shared between, or are unique to each pathogen and co-infection. Extension of the co-infection model would also allow for exploration of whether IAV is able to overcome the initial priming of macrophages, and if NTHi load continues to increase. For the MDM response, it would be of interest to ascertain whether co-infection synergistically extends the inflammatory process or if resolution of inflammation occurs earlier when compared to single pathogen infections. Transcriptomic analysis of NTHi following co-infection would be extremely used to provide insights into the transcriptional regulation involved in bacterial outgrowth following viral co-infection, a process still poorly understood. Due to strain-dependent expression of the top regulated NTHi genes that were validated by qPCR, sequencing additional NTHi strains would ensure comparable analysis of transcriptomic adaptations during co-infection between strains.

An important and useful development in sequencing technology of recent times is single cell RNA sequencing (scRNASeq), which is able to provide resolution of cellular changes at the single cell level. As discussed previously, one of the limitations of this current work – and limitations of RNASeq in general – is that bulk transcriptomics provides a global view of gene expression changes. If a precise question or hypothesis is being addressed or the sequenced sample involves a purified population of cells, bulk RNASeq is useful. However, even in the MDM system which contains a single cell type, it is possible that a variety of macrophage phenotypes are present during NTHi infection. For example, in any given infected well, there may be NTHi-infected macrophages, macrophages that are not infected but have been cytokine-activated by neighbouring infected macrophages, macrophages that were previously NTHi infected and effectively cleared the infection and even perhaps uninfected and unstimulated macrophages. These possibilities become even more complex when considering the addition of IAV for co-infection. It would be of interest for future work to determine whether the activation of anti-viral immunity and type I IFN pathways was common for all macrophages, subsets of macrophages, or exclusively only MDM intracellularly infected with NTHi. Use of scRNASeq would also allow further exploration of NTHi outgrowth during co-infection. After identification of NTHi genes associated with NTHi proliferation following co-infection, MDM containing NTHi differentially expressing these genes could be identified. This technique could indicate whether proliferating NTHi are associated with macrophages infected with NTHi-only or co-infected with both pathogens. Determining this could help to unpick the mechanisms of macrophage loss of bacterial control during co-infection.

Furthermore, scRNASeq of asthmatic BAL samples would better allow for clarification of NTHi-host interactions and confirmation of NTHi associated with macrophages *in vivo*. The BAL samples used for this thesis contained a mixed cell population and although FISH analysis indicated association of

NTHi with host cells, further work is need to confirm this. The use of scRNASeq would not only allow for elucidation of BAL cell composition in asthma, but unearth transcriptomic profiles associated with different disease states (e.g. colonised vs not colonised). Subsequently, scRNASeq would help determine whether specific subsets of macrophages were associated with NTHi, which could be as a result of NTHi modulation of host gene expression. The finer complexity of scRNASeq allowing for resolution of host-pathogen interactions at the single cell level could provide a clearer picture of the multiple process and outcomes that can occur during infection[633].

Use of chromatin immunoprecipitation followed by sequencing (ChIP-seq) could be used to investigate epigenetic modulation of macrophages following infection[634]. It has been shown that different stimuli can induce either a tolerised or trained immune cell population[177,595]. Thus elucidating the potentially diverse epigenetic profiles associated with the different NTHi-alone, IAV alone and co-infection combinations could further our understanding of pathogen-mediated influences on macrophage immune activation and innate memory. Characterising epigenetic regulation of MDM following *in vitro* infection with multiple pathogen combinations could generate an epigenetic fingerprint associated with infection, which would allow for several questions to be addressed.

The first question would be whether persistent colonisation of the asthmatic or COPD airway results in epigenetic modifications resulting in tolerised/paralysed AM displaying the characterised phagocytic defect in these chronic respiratory diseases[247,250,454]. Roquilly *et al.* (2020) showed that acute inflammation resulted in prolonged impaired phagocytosis. Altered expression of monocyte phagocytosis receptors was detectable for months following the initial inflammatory stimulation, with the local environment responsible for long-term maintenance of the phagocytic paralysis defect[597]. Thus, sustained NTHi-induced macrophage inflammation, as shown in this thesis, during persistence may be contributing to the phagocytic defect in asthma and COPD via maintenance of macrophage epigenetic modifications. ChIP-seq could be used to characterise the epigenetic changes associated with this sustained inflammation caused by NTHi persistence *in vitro.* Subsequent comparison of epigenetic markers from infected MDM to freshly isolated AM, as well as ascertaining epigenetic differences between healthy and diseased AM, would contribute to understanding whether epigenetic regulation is involved in the mechanism of macrophage impairment in chronic respiratory disease

Secondly, future work could explore whether a subsequent IAV infection causes substantial epigenetic rewriting of MDM, resulting in the tolerised/paralysed state unable to respond to outgrowth of colonising NTHi. Such identification of an epigenetic signal in AM from patients following exacerbation and outgrowth of bacteria following a respiratory tract viral infection could identify genes or pathways that could be therapeutically targeted to prevent macrophage paralysis.

Finally, as previously mentioned, early life NTHi colonisation is associated with development of asthma, with links between number of respiratory tract viral infections and asthma development[335]. It has been demonstrated that immune cells isolated from children who later developed asthma exhibited aberrant immune responses to potentially pathogenic bacteria, including NTHi[155]. As such, it would be important to investigate the role of immune training and epigenetic regulation of macrophages in early life immune development, airway bacterial colonisation, respiratory tract viral infections and development of asthma.

As previously discussed, NTHi persistence in the airway is associated with steroid resistant, neutrophilic, severe asthma, but it is not clear whether NTHi contributes to disease progression or if the asthmatic airway facilitates NTHi colonisation. Although murine studies have attempted to study the relationship between NTHi colonisation and Th17/neutrophilic inflammation[462,532], the murine lung and allergic airways disease models are unable to completely recapitulate human asthma and infection of human-restricted pathogens. A longitudinal cohort study tracking individuals with mild, steroid naïve asthma and the progression to severe disease could better identify whether NTHi colonisation of the airway facilitates the transition to more severe disease. A prospective, observational cohort study of COPD patients identified associations between NTHi, rhinovirus and exacerbation risk[332], indicating the success of repeated observations for profiling disease and clinical outcomes. Performing a similar study in a population of mild, steroid naïve asthmatics with the intention of identifying the events leading to the development of severe, neutrophilic asthma could identify risk factors that could be targeted at an earlier stage of disease to reduce the burden of severe asthma. Tracking the stability of the microbiome and bacterial load before, during and after a viral infection or exacerbation would confirm whether the co-infection dynamics between NTHi and IAV observed in this thesis are reflective of the *in vivo* co-infection process, such as outgrowth of bacteria that are present prior to viral infection and synergistic modulation of inflammation.

8.5 Summary

The dynamics of host-pathogen interactions are complex, and are even more complex when considering multiple pathogens and underlying deficiencies in host responses. This thesis has characterised NTHi-MDM interactions during intracellular infection and found NTHi adaptation to intracellular persistence through modulation of metabolic and stress response pathways (Figure 8.1). NTHi appeared to avoid macrophage degradation pathways as transcriptional lack of MDM markers for late endosomes/phagosomes were identified, with enrichment of cytosolic signalling pathways suggesting NTHi was present in the cytosol. The downregulation of oxidative stress response pathways by NTHi further suggested that by 24 h, NTHi had escaped the macrophage degradation pathways.

In response to NTHi intracellular infection, MDM upregulated intracellular immune response pathways, that were found to be reminiscent of a response to a virus. Modulation of MDM genes identified from dual RNASeq analysis of the NTHi-MDM infection was identified in severe asthma BAL samples. NTHi appeared to be physically associated with host BAL cells and was associated with neutrophilic inflammation. Subsequently, co-infection of MDM with IAV following NTHi infection resulted in diminished IAV infection but conversely, increased NTHi recovery from MDM. Increased NTHi presence may be due to transcriptomic changes of NTHi genes required for intracellular persistence. However, the strain-dependent expression of NTHi genes could indicate how some strains are better able to persist. Inhibition of IAV infection was suggested to be as a result of the prior NTHi infection priming MDM via activation of anti-viral pathways, namely the type I IFN pathway. Despite lower IAV presence, the MDM inflammatory response was sustained in co-infected cells, with modulation of some inflammatory processes not observed in MDM infected with IAV alone.

The findings of this thesis have important ramifications not only for asthmatic individuals chronically colonised with NTHi, but also healthy individuals who develop bacterial pneumonia following viral infection. Future studies investigating host-pathogen interactions in airway diseases need to consider the impact of the resident lung microbiome on modulation of host responses when designing experimental models to address a research question, as it is becoming clear that single host-pathogen interactions are not reflective of the *in vivo* lung biology.

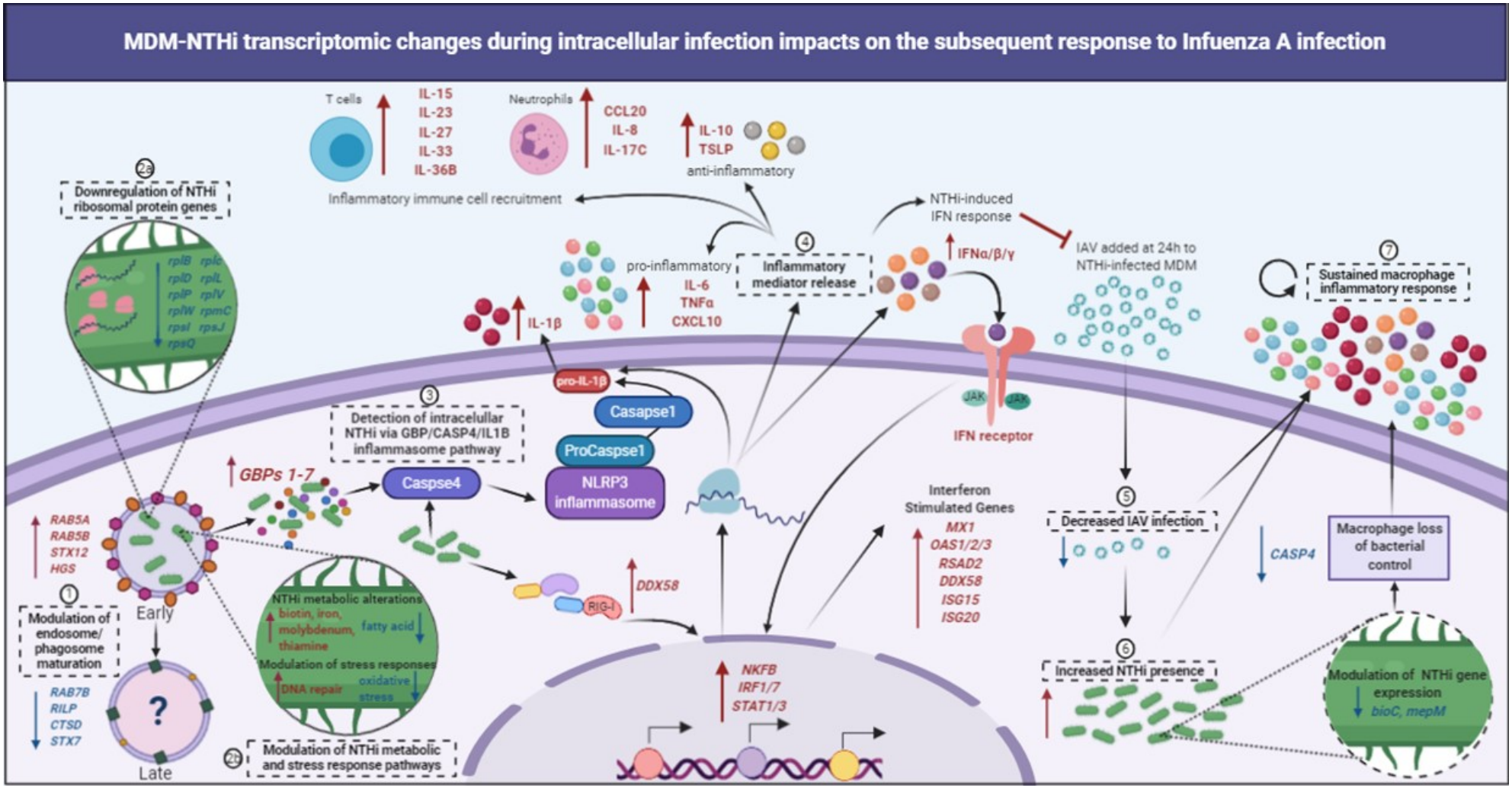
MDM-NTHi transcriptomic changes during intracellular infection impacts on the subsequent response to Infuenza A infection
T cells
IL-15
IL-23
IL-27
IL-33
IL-36B
Neutrophils
CCL20
IL-8
IL-17C
IL-10
TSLP
anti-inflammatory
Inflammatory immune cell recruitment
2a
Downregulation of NTHi ribosomal protein genes
rplB rplC
rplD rplL
rplP rplV
rplW rpmC
rpsI rpsJ
rpsQ
pro-inflammatory
IL-6
TNFα
CXCL10
4
Inflammatory mediator release
IL-1β
pro-IL-1β
Casapse1
ProCaspse1
NLRP3 inflammasome
3
Detection of intracelullar NTHi via GBP/CASP4/IL1B inflammasome pathway
GBPs 1-7
Caspse4
RIG-I
DDX58
NTHi-induced IFN response
IFNα/β/γ
IFN receptor
JAK
JAK
IAV added at 24h to NTHi-infected MDM
7
Sustained macrophage inflammatory response
Interferon Stimulated Genes
MX1
OAS1/2/3
RSAD2
DDX58
ISG15
ISG20
5
Decreased IAV infection
CASP4
Macrophage loss of bacterial control
RAB5A
RAB5B
STX12
HGS
1
Modulation of endosome/ phagosome maturation
Early
RAB7B
RILP
CTSD
STX7
Late
?
NTHi metabolic alterations
biotin, iron, molybdenum, thiamine
fatty acid
Modulation of stress responses
DNA repair
oxidative stress
2b
Modulation of NTHi metabolic and stress response pathways
NKFB
IRF1/7
STAT1/3
6
Increased NTHi presence
Modulation of NTHi gene expression
bioC, mepM

Figure 8.1. MDM-NTHi transcriptomic changes during intracellular infection impacts on the subsequent response to Influenza A infection. Summary of the proposed mechanisms of MDM-NTHi interactions and the subsequent response to IAV infection. (1) Modulation of macrophage gene expression of early and late endosomal markers suggests lack of late endosomal compartments. Residence within early endosomal compartments or within the cytosol could be a mechanism by which NTHi is able to resist macrophage intracellular degradation pathways. (2a) NTHi adaptation to intracellular residence involved downregulation of ribosomal protein genes and (2b) modulation of metabolic pathways. In addition, downregulation of oxidative response genes indicates NTHi escape from macrophage degradation pathways at 24 h. (3) Upregulation of *GBP1-7* gene expression suggest cytosolic presence of NTHi, which in combination with upregulation of *CASP4* and *IL1B*, indicates activation of the noncanonical inflammasome, resulting in increased IL-1β secretion. (4) Enrichment of cytosolic DNA sensing pathway and NOD-like signalling KEGG pathways indicate activation of other immune intracellular sensors, such as RIG-I (*DDX58*) which cause signalling cascades involving transcription factors, to upregulate the transcription of pro-inflammatory cytokines and interferons. Secreted pro-inflammatory mediators include cytokines and chemokines involved in recruitment of other immune cells such as neutrophils and T cells. Increased IFN release resulted in activation of MDM anti-viral immunity and upregulation of ISGs. (5) Prior activation of IFN immunity was suggested to inhibit subsequent IAV infection, however (6) NTHi presence increased following co-infection, which may have been due to further modulation of NTHi gene expression. Additionally, macrophage loss of bacterial control may be due to changes in the expression of genes, such as *CASP4*, which was previously identified to be important in the intracellular response to NTHi. (7) Together, the presence of both NTHi and IAV in co-infected MDM resulted in a sustained inflammatory responses which was higher compared to MDM infected with IAV alone. The modulation of MDM inflammatory responses by NTHi before and during co-infection with IAV has potential ramifications for individuals chronically colonised with NTHi. Created using BioRender.com

List of References

1. Jackson, D. J., Sykes, A., Mallia, P. & Johnston, S. L. (2011). Asthma exacerbations: Origin, effect, and prevention. *J Allergy Clin Immunol*. **128,** 1165–1174

2. Edwards, M. R., Saglani, S., Schwarze, J., Skevaki, C., Smith, J. A., Ainsworth, B., Almond, M., Andreakos, E., Belvisi, M. G., Chung, K. F., Cookson, W., Cullinan, P., Hawrylowicz, C., Lommatzsch, M., Jackson, D., Lutter, R., Marsland, B., Moffatt, M., Thomas, M., Virchow, J. C., Xanthou, G., Edwards, J., Walker, S. & Johnston, S. L. (2017). Addressing unmet needs in understanding asthma mechanisms: From the European Asthma Research and Innovation Partnership (EARIP) Work Package (WP) 2 collaborators. *Eur Respir J*. **49,** 1602448

3. McCracken, J. L., Veeranki, S. P., Ameredes, B. T. & Calhoun, W. J. (2017). Diagnosis and management of asthma in adults a review. *J Am Med Assoc*. **318,** 279–290

4. Platts-Mills, T. A. (2001). The role of immunoglobulin E in allergy and asthma. *Am J Respir Crit Care Med*. **164,** S1-5

5. Pearce, N., Pekkanen, J. & Beasley, R. (1999). How much asthma is really attributable to atopy? *Thorax*. **54,** 268–272

6. Ahmad Al Obaidi, A. H., Mohamed Al Samarai, A. G., Yahya Al Samarai, A. K. & Al Janabi, J. M. (2008). The predictive value of IgE as biomarker in asthma. *J Asthma*. **45,** 654–663

7. Pembrey, L., Barreto, M. L., Douwes, J., Cooper, P., Henderson, J., Mpairwe, H., Ardura-Garcia, C., Chico, M., Brooks, C., Cruz, A. A., Elliott, A. M., Figueiredo, C. A., Langan, S. M., Nassanga, B., Ring, S., Rodrigues, L. & Pearce, N. (2018). Understanding asthma phenotypes: the World Asthma Phenotypes (WASP) international collaboration. *ERJ Open Res*. **4,** 00013–02018

8. Bosnjak, B., Stelzmueller, B., Erb, K. J. & Epstein, M. M. (2011). Treatment of allergic asthma: Modulation of Th2 cells and their responses. *Respir Res*. **12,** 114

9. Wadhwa, R., Dua, K., Adcock, I. M., Horvat, J. C., Kim, R. Y. & Hansbro, P. M. (2019). Cellular mechanisms underlying steroid-resistant asthma. *Eur Respir Rev*. **28,** 190096

10. Wenzel, S. E. (2012). Asthma phenotypes: The evolution from clinical to molecular approaches. *Nat Med*. **18,** 716–725

11. O'Byrne, P. M. (2013). Role of monoclonal antibodies in the treatment of asthma. *Can Respir J*. **20,** 23–25

12. Lambrecht, B. N. & Hammad, H. (2015). The immunology of asthma. *Nat Immunol*. **16,** 45–56

13. Mukherjee, M., Stoddart, A., Gupta, R. P., Nwaru, B. I., Farr, A., Heaven, M., Fitzsimmons, D., Bandyopadhyay, A., Aftab, C., Simpson, C. R., Lyons, R. A., Fischbacher, C., Dibben, C., Shields, M. D., Phillips, C. J., Strachan, D. P., Davies, G. A., McKinstry, B. & Sheikh, A. (2016). The epidemiology, healthcare and societal burden and costs of asthma in the UK and its member nations: analyses of standalone and linked national databases. *BMC Med*. **14,** 113

14. Wolfe, I. (2011). How can we improve child health services? *BMJ*. **342,** 901–904

15. Levy, M. L. (2015). The national review of asthma deaths: What did we learn and what needs to change? *Breathe*. **11,** 15–24

16. Gupta, R. P., Mukherjee, M., Sheikh, A. & Strachan, D. P. (2018). Persistent variations in national asthma mortality, hospital admissions and prevalence by socioeconomic status and region in England. *Thorax*. **73,** 706–712

17. Eder, W., Ege, M. J. & von Mutius, E. (2006). The Asthma Epidemic. *N Engl J Med*. **355,** 2226–2235

18. Adami, A. J. & Bracken, S. J. (2016). Breathing better through bugs: Asthma and the microbiome. *Yale J Biol Med*. **89,** 309–324

19. Strachan, D. P. (2000). Family size, infection and atopy: the first decade of the 'hygiene hypothesis'. *Thorax*. **55 Suppl 1,** S2-10

20. Von Ehrenstein, O. S., Von Mutius, E., Illi, S., Baumann, L., Böhm, O. & Von Kries, R. (2000). Reduced risk of hay fever and asthma among children of farmers. *Clin Exp Allergy*. **30,** 187–193

21. Ege, M. J., Mayer, M., Normand, A.-C., Genuneit, J., Cookson, W. O. C. M., Braun-Fahrländer, C., Heederik, D., Piarroux, R. & von Mutius, E. (2011). Exposure to Environmental Microorganisms and Childhood Asthma. *N Engl J Med*. **364,** 701–709

22. Holgate, S. T. (2012). Innate and adaptive immune responses in asthma. *Nat Med*. **18,** 673–683

23. Von Mutius, E. (2014). Environmental microorganisms and lung health. *Ann Am Thorac Soc*. **11,** S13–S15

24. Bisgaard, H., Hermansen, M. N., Buchvald, F., Loland, L., Halkjaer, L. B., Bønnelykke, K., Brasholt, M., Heltberg, A., Vissing, N. H., Thorsen, S. V., Stage, M. & Pipper, C. B. (2007). Childhood Asthma after Bacterial Colonization of the Airway in Neonates. *N Engl J Med*. **357,** 1487–1495

25. Hilty, M., Burke, C., Pedro, H., Cardenas, P., Bush, A., Bossley, C., Davies, J., Ervine, A., Poulter, L., Pachter, L., Moffatt, M. F. & Cookson, W. O. C. (2010). Disordered microbial

communities in asthmatic airways. *PLoS One*. **5,** e8578

26. Kim, H. Y., Dekruyff, R. H. & Umetsu, D. T. (2010). The many paths to asthma: Phenotype shaped by innate and adaptive immunity. *Nat Immunol*. **11,** 577–584

27. Pavord, I. D., Beasley, R., Agusti, A., Anderson, G. P., Bel, E., Brusselle, G., Cullinan, P., Custovic, A., Ducharme, F. M., Fahy, J. V., Frey, U., Gibson, P., Heaney, L. G., Holt, P. G., Humbert, M., Lloyd, C. M., Marks, G., Martinez, F. D., Sly, P. D., von Mutius, E., Wenzel, S., Zar, H. J. & Bush, A. (2018). After asthma: redefining airways diseases. *Lancet*. **391,** 350–400

28. Baos, S., Calzada, D., Cremades-Jimeno, L., Sastre, J., Picado, C., Quiralte, J., Florido, F., Lahoz, C. & Cárdaba, B. (2018). Nonallergic asthma and its severity: Biomarkers for its discrimination in peripheral samples. *Front Immunol*. **9,** 1416

29. Ishmael, F. T. (2011). The inflammatory response in the pathogenesis of asthma. *J Am Osteopath Assoc*. **111,** S11-7

30. Deckers, J., Branco Madeira, F. & Hammad, H. (2013). Innate immune cells in asthma. *Trends Immunol*. **34,** 540–547

31. Fahy, J. V. (2015). Type 2 inflammation in asthma--present in most, absent in many. *Nat Rev Immunol*. **15,** 57–65

32. Barnes, P. J. (2008). Immunology of asthma and chronic obstructive pulmonary disease. *Nat Rev Immunol*. **8,** 183–192

33. Chang, H. C., Sehra, S., Goswami, R., Yao, W., Yu, Q., Stritesky, G. L., Jabeen, R., McKinley, C., Ahyi, A. N., Han, L., Nguyen, E. T., Robertson, M. J., Perumal, N. B., Tepper, R. S., Nutt, S. L. & Kaplan, M. H. (2010). The transcription factor PU.1 is required for the development of IL-9-producing T cells and allergic inflammation. *Nat Immunol*. **11,** 527–534

34. Koch, S., Sopel, N. & Finotto, S. (2017). Th9 and other IL-9-producing cells in allergic asthma. *Semin Immunopathol*. **39,** 55–68

35. Bradding, P. (2008). Asthma: eosinophil disease, mast cell disease, or both? *Allergy Asthma Clin Immunol*. **4,** 84–90

36. Barnes, P. J. (2008). The cytokine network in asthma and chronic obstructive pulmonary disease. *J Clin Invest*. **118,** 3546–56

37. Amin, K. (2012). The role of mast cells in allergic inflammation. *Respiratory Medicine*. **106,** 9–14

38. Djukanović, R., Lai, C. K. W., Wilson, J. W., Britten, K. M., Wilson, S. J., Roche, W. R., Howarth, P. H. & Holgate, S. T. (1992). Bronchial mucosal manifestations of atopy: a

comparison of markers of inflammation between atopic asthmatics, atopic nonasthmatics and healthy controls. *Eur Respir J*. **5,** 538–44

39. Kearley, J., Robinson, D. S. & Lloyd, C. M. (2008). CD4+CD25+ regulatory T cells reverse established allergic airway inflammation and prevent airway remodeling. *J Allergy Clin Immunol*. **122,** 617-624.e6

40. Baatjes, A. J., Smith, S. G., Watson, R., Howie, K., Murphy, D., Larché, M., Denburg, J. A., Inman, M. D. & O'Byrne, P. M. (2015). T regulatory cell phenotypes in peripheral blood and bronchoalveolar lavage from non-asthmatic and asthmatic subjects. *Clin Exp Allergy*. **45,** 1654–1662

41. Hartl, D., Koller, B., Mehlhorn, A. T., Reinhardt, D., Nicolai, T., Schendel, D. J., Griese, M. & Krauss-Etschmann, S. (2007). Quantitative and functional impairment of pulmonary CD4+CD25hi regulatory T cells in pediatric asthma. *J Allergy Clin Immunol*. **119,** 1258–1266

42. Douwes, J., Gibson, P., Pekkanen, J. & Pearce, N. (2002). *Non-eosinophilic asthma: Importance and possible mechanisms*. *Thorax*. **57,**

43. Ordoñez, C. L., Shaughnessy, T. E., Matthay, M. A. & Fahy, J. V. (2000). Increased neutrophil numbers and IL-8 levels in airway secretions in acute severe asthma: Clinical and biologic significance. *Am J Respir Crit Care Med*. **161,** 1185–90

44. Yang, X., Li, H., Ma, Q., Zhang, Q. & Wang, C. (2018). Neutrophilic Asthma Is Associated with Increased Airway Bacterial Burden and Disordered Community Composition. *Biomed Res Int*. **2018,** 1–11

45. Huang, Y. J., Nariya, S., Harris, J. M., Lynch, S. V., Choy, D. F., Arron, J. R. & Boushey, H. (2015). The airway microbiome in patients with severe asthma: Associations with disease features and severity. *J Allergy Clin Immunol*. **136,** 874–884

46. Zhang, J., Zhu, Z., Zuo, X., Pan, H., Gu, Y., Yuan, Y., Wang, G., Wang, S., Zheng, R., Liu, Z., Wang, F. & Zheng, J. (2020). The role of NTHi colonization and infection in the pathogenesis of neutrophilic asthma. *Respir Res*. **21,** 170

47. Jasper, A. E., McIver, W. J., Sapey, E. & Walton, G. M. (2019). Understanding the role of neutrophils in chronic inflammatory airway disease. *F1000Research*. **8,**

48. Wenzel, S. E., Szefler, S. J., Leung, D. Y. M., Sloan, S. I., Rex, M. D. & Martin, R. J. (1997). Bronchoscopic evaluation of severe asthma: Persistent inflammation associated with high dose glucocorticoids. *Am J Respir Crit Care Med*. **156,** 737–743

49. Song, C., Luo, L., Lei, Z., Li, B., Liang, Z., Liu, G., Li, D., Zhang, G., Huang, B. & Feng, Z.-H. (2008). IL-17-Producing Alveolar Macrophages Mediate Allergic Lung Inflammation Related

to Asthma. *J Immunol*. **181,** 6117–6124

50. Pène, J., Chevalier, S., Preisser, L., Vénéreau, E., Guilleux, M.-H., Ghannam, S., Molès, J.-P., Danger, Y., Ravon, E., Lesaux, S., Yssel, H. & Gascan, H. (2008). Chronically Inflamed Human Tissues Are Infiltrated by Highly Differentiated Th17 Lymphocytes. *J Immunol*. **180,** 7423–7430

51. Newcomb, D. C. & Peebles, R. S. (2013). Th17-mediated inflammation in asthma. *Current Opinion in Immunology*. **25,** 755–760

52. Roussel, L., Houle, F., Chan, C., Yao, Y., Bérubé, J., Olivenstein, R., Martin, J. G., Huot, J., Hamid, Q., Ferri, L. & Rousseau, S. (2010). IL-17 Promotes p38 MAPK-Dependent Endothelial Activation Enhancing Neutrophil Recruitment to Sites of Inflammation. *J Immunol*. **184,** 4531–4537

53. Hosoki, K., Ying, S., Corrigan, C., Qi, H., Kurosky, A., Jennings, K., Sun, Q., Boldogh, I. & Sur, S. (2015). Analysis of a Panel of 48 Cytokines in BAL Fluids Specifically Identifies IL-8 Levels as the Only Cytokine that Distinguishes Controlled Asthma from Uncontrolled Asthma, and Correlates Inversely with FEV1. *PLoS One*. **10,** e0126035

54. Kim, R. Y., Pinkerton, J. W., Essilfie, A. T., Robertson, A. A. B., Baines, K. J., Brown, A. C., Mayall, J. R., Ali, M. K., Starkey, M. R., Hansbro, N. G., Hirota, J. A., Wood, L. G., Simpson, J. L., Knight, D. A., Wark, P. A., Gibson, P. G., O'Neill, L. A. J., Cooper, M. A., Horvat, J. C. & Hansbro, P. M. (2017). Role for NLRP3 inflammasome-mediated, IL-1β-dependent responses in severe, steroid-resistant asthma. *Am J Respir Crit Care Med*. **196,** 283–297

55. Simpson, J. L., Phipps, S., Baines, K. J., Oreo, K. M., Gunawardhana, L. & Gibson, P. G. (2014). Elevated expression of the NLRP3 inflammasome in neutrophilic asthma. *Eur Respir J*. **43,** 1067–76

56. Sears, M. R. (2008). Epidemiology of asthma exacerbations. *J Allergy Clin Immunol*. **122,** 662–668

57. Global Initiative for Asthma. (2020). *Global Strategy for Asthma Management and Prevention Updated 2020*. *Global Initiative for Asthma*.

58. Wark, P. A. B. & Gibson, P. G. (2006). Asthma exacerbations. 3: Pathogenesis. *Thorax*. **61,** 909–15

59. Bloom, C. I., Nissen, F., Douglas, I. J., Smeeth, L., Cullinan, P. & Quint, J. K. (2018). Exacerbation risk and characterisation of the UK's asthma population from infants to old age. *Thorax*. **73,** 313–320

60. Ko, F. W. S., Tam, W., Wong, T. W., Lai, C. K. W., Wong, G. W. K., Leung, T. F., Ng, S. S. S. &

Hui, D. S. C. (2007). Effects of air pollution on asthma hospitalization rates in different age groups in Hong Kong. *Clin Exp Allergy*. **37,** 1312–1319

61. Thomson, N. C., Chaudhuri, R. & Livingston, E. (2004). Asthma and cigarette smoking. *Eur Respir J*. **24,** 822–833

62. Murray, C. S., Simpson, A. & Custovic, A. (2004). Allergens, viruses, and asthma exacerbations. *Proc Am Thorac Soc*. **1,** 99–104

63. Sutherland, E. R. & Martin, R. J. (2007). Asthma and atypical bacterial infection. *Chest*. **132,** 1962–1966

64. Green, B. J., Wiriyachaiporn, S., Grainge, C., Rogers, G. B., Kehagia, V., Lau, R., Carroll, M. P., Bruce, K. D. & Howarth, P. H. (2014). Potentially pathogenic airway bacteria and neutrophilic inflammation in treatment resistant severe asthma. *PLoS One*. **9,** e100645

65. Iikura, M., Hojo, M., Koketsu, R., Watanabe, S., Sato, A., Chino, H., Ro, S., Masaki, H., Hirashima, J., Ishii, S., Naka, G., Takasaki, J., Izumi, S., Kobayashi, N., Yamaguchi, S., Nakae, S. & Sugiyama, H. (2015). The importance of bacterial and viral infections associated with adult asthma exacerbations in clinical practice. *PLoS One*. **10,** e0123584

66. Zhang, Q., Cox, M., Liang, Z., Brinkmann, F., Cardenas, P. A., Duff, R., Bhavsar, P., Cookson, W., Moffatt, M. & Chung, K. F. (2016). Airway microbiota in severe asthma and relationship to asthma severity and phenotypes. *PLoS One*. **11,** 1–16

67. Johnston, S. L., Pattemore, P. K., Sanderson, G., Smith, S., Lampe, F., Josephs, L., Symington, P., Toole, S. o., Myint, S. H., Tyrrell, D. A. J. & Holgate, S. T. (1995). Community study of role of viral infections in exacerbations of asthma in 9-11 year old children. *BMJ*. **310,** 1225

68. Wark, P. A. B., Johnston, S. L., Moric, I., Simpson, J. L., Hensley, M. J. & Gibson, P. G. (2002). Neutrophil degranulation and cell lysis is associated with clinical severity in virus-induced asthma. *Eur Respir J*. **19,** 68–75

69. Papadopoulos, N. G. & Johnston, S. L. (1998). Viruses and asthma exacerbations: Editorial. *Thorax*. **53,** 913–914

70. Papadopoulos, N. G., Christodoulou, I., Rohde, G., Agache, I., Almqvist, C., Bruno, A., Bonini, S., Bont, L., Bossios, A., Bousquet, J., Braido, F., Brusselle, G., Canonica, G. W., Carlsen, K. H., Chanez, P., Fokkens, W. J., Garcia-Garcia, M., Gjomarkaj, M., Haahtela, T., Holgate, S. T., Johnston, S. L., Konstantinou, G., Kowalski, M., Lewandowska-Polak, A., Lødrup-Carlsen, K., Mäkelä, M., Malkusova, I., Mullol, J., Nieto, A., Eller, E., Ozdemir, C., Panzner, P., Popov, T., Psarras, S., Roumpedaki, E., Rukhadze, M., Stipic-Markovic, A., Todo

Bom, A., Toskala, E., Van Cauwenberge, P., Van Drunen, C., Watelet, J. B., Xatzipsalti, M., Xepapadaki, P. & Zuberbier, T. (2011). Viruses and bacteria in acute asthma exacerbations - A GA 2LEN-DARE* systematic review. *Allergy Eur J Allergy Clin Immunol*. **66,** 458–468

71. Dickson, R. P., Erb-Downward, J. R., Martinez, F. J. & Huffnagle, G. B. (2016). The Microbiome and the Respiratory Tract. *Annu Rev Physiol*. **78,** 481–504

72. Beck, J. M., Young, V. B. & Huffnagle, G. B. (2012). The microbiome of the lung. *Transl Res*. **160,** 258–266

73. Aguiar-Pulido, V., Huang, W., Suarez-Ulloa, V., Cickovski, T., Mathee, K. & Narasimhan, G. (2016). Metagenomics, metatranscriptomics, and metabolomics approaches for microbiome analysis. *Evol Bioinform*. **12,** 5–16

74. Bashiardes, S., Zilberman-Schapira, G. & Elinav, E. (2016). Use of metatranscriptomics in microbiome research. *Bioinform Biol Insights*. **10,** 19–25

75. Eisenhofer, R., Minich, J. J., Marotz, C., Cooper, A., Knight, R. & Weyrich, L. S. (2019). Contamination in Low Microbial Biomass Microbiome Studies: Issues and Recommendations. *Trends Microbiol*. **27,** 105–117

76. Dickson, R. P., Erb-Downward, J. R., Freeman, C. M., McCloskey, L., Falkowski, N. R., Huffnagle, G. B. & Curtis, J. L. (2017). Bacterial topography of the healthy human lower respiratory tract. *MBio*. **8,**

77. Salter, S. J., Cox, M. J., Turek, E. M., Calus, S. T., Cookson, W. O., Moffatt, M. F., Turner, P., Parkhill, J., Loman, N. J. & Walker, A. W. (2014). Reagent and laboratory contamination can critically impact sequence-based microbiome analyses. *BMC Biol*. **12,** 87

78. Erb-Downward, J. R., Thompson, D. L., Han, M. K., Freeman, C. M., McCloskey, L., Schmidt, L. A., Young, V. B., Toews, G. B., Curtis, J. L., Sundaram, B., Martinez, F. J. & Huffnagle, G. B. (2011). Analysis of the lung microbiome in the 'healthy' smoker and in COPD. *PLoS One*. **6,** e16384

79. Dominguez-Bello, M. G., Costello, E. K., Contreras, M., Magris, M., Hidalgo, G., Fierer, N. & Knight, R. (2010). Delivery mode shapes the acquisition and structure of the initial microbiota across multiple body habitats in newborns. *Proc Natl Acad Sci U S A*. **107,** 11971–11975

80. Lal, C. V., Travers, C., Aghai, Z. H., Eipers, P., Jilling, T., Halloran, B., Carlo, W. A., Keeley, J., Rezonzew, G., Kumar, R., Morrow, C., Bhandari, V. & Ambalavanan, N. (2016). The Airway Microbiome at Birth. *Sci Rep*. **6,** 31023

81. Aagaard, K., Ma, J., Antony, K. M., Ganu, R., Petrosino, J. & Versalovic, J. (2014). The

placenta harbors a unique microbiome. *Sci Transl Med*. **6,** 237–65

82. Kuperman, A. A., Zimmerman, A., Hamadia, S., Ziv, O., Gurevich, V., Fichtman, B., Gavert, N., Straussman, R., Rechnitzer, H., Barzilay, M., Shvalb, S., Bornstein, J., Ben-Shachar, I., Yagel, S., Haviv, I. & Koren, O. (2020). Deep microbial analysis of multiple placentas shows no evidence for a placental microbiome. *BJOG An Int J Obstet Gynaecol*. **127,** 159–169

83. Charlson, E. S., Bittinger, K., Haas, A. R., Fitzgerald, A. S., Frank, I., Yadav, A., Bushman, F. D. & Collman, R. G. (2011). Topographical continuity of bacterial populations in the healthy human respiratory tract. *Am J Respir Crit Care Med*. **184,** 957–963

84. Garzoni, C., Brugger, S. D., Qi, W., Wasmer, S., Cusini, A., Dumont, P., Gorgievski-Hrisoho, M., Mühlemann, K., Garnier, C. Von & Hilty, M. (2013). Microbial communities in the respiratory tract of patients with interstitial lung disease. *Thorax*. **68,** 1150–1156

85. Dickson, R. P., Martinez, F. J. & Huffnagle, G. B. (2014). The role of the microbiome in exacerbations of chronic lung diseases. *Lancet*. **384,** 691–702

86. Wood, L. G., Simpson, J. L., Hansbro, P. M. & Gibson, P. G. (2010). Potentially pathogenic bacteria cultured from the sputum of stable asthmatics are associated with increased 8-isoprostane and airway neutrophilia. *Free Radic Res*. **44,** 146–154

87. Simpson, J. L., Daly, J., Baines, K. J., Yang, I. A., Upham, J. W., Reynolds, P. N., Hodge, S., James, A. L., Hugenholtz, P., Willner, D. & Gibson, P. G. (2016). Airway dysbiosis: Haemophilus influenzae and Tropheryma in poorly controlled asthma. *Eur Respir J*. **47,** 792–800

88. Ichinohe, T., Pang, I. K., Kumamoto, Y., Peaper, D. R., Ho, J. H., Murray, T. S. & Iwasaki, A. (2011). Microbiota regulates immune defense against respiratory tract influenza a virus infection. *Proc Natl Acad Sci U S A*. **108,** 5354–5359

89. Abt, M. C., Osborne, L. C., Monticelli, L. A., Doering, T. A., Alenghat, T., Sonnenberg, G. F., Paley, M. A., Antenus, M., Williams, K. L., Erikson, J., Wherry, E. J. & Artis, D. (2012). Commensal Bacteria Calibrate the Activation Threshold of Innate Antiviral Immunity. *Immunity*. **37,** 158–170

90. Følsgaard, N. V., Schjørring, S., Chawes, B. L., Rasmussen, M. A., Krogfelt, K. A., Brix, S. & Bisgaard, H. (2013). Pathogenic bacteria colonizing the airways in asymptomatic neonates stimulates topical inflammatory mediator release. *Am J Respir Crit Care Med*. **187,** 589–595

91. Huang, Y. J., Nelson, C. E., Brodie, E. L., Desantis, T. Z., Baek, M. S., Liu, J., Woyke, T., Allgaier, M., Bristow, J., Wiener-Kronish, J. P., Sutherland, E. R., King, T. S., Icitovic, N., Martin, R. J., Calhoun, W. J., Castro, M., Denlinger, L. C., Dimango, E., Kraft, M., Peters, S.

P., Wasserman, S. I., Wechsler, M. E., Boushey, H. A., Lynch, S. V. & National Heart, Lung, and B. I. A. C. R. N. (2011). Airway microbiota and bronchial hyperresponsiveness in patients with suboptimally controlled asthma. *J Allergy Clin Immunol*. **127,** 372-381.e1–3

92. Marri, P. R., Stern, D. A., Wright, A. L., Billheimer, D. & Martinez, F. D. (2013). Asthma-associated differences in microbial composition of induced sputum. *J Allergy Clin Immunol*. **131,** 346-352.e3

93. Rooks, M. G. & Garrett, W. S. (2016). Gut microbiota, metabolites and host immunity. *Nat Rev Immunol*. **16,** 341–352

94. Franzosa, E. A., Morgan, X. C., Segata, N., Waldron, L., Reyes, J., Earl, A. M., Giannoukos, G., Boylan, M. R., Ciulla, D., Gevers, D., Izard, J., Garrett, W. S., Chan, A. T. & Huttenhower, C. (2014). Relating the metatranscriptome and metagenome of the human gut. *Proc Natl Acad Sci U S A*. **111,** E2329-38

95. Castro-Nallar, E., Shen, Y., Freishtat, R. J., Pérez-Losada, M., Manimaran, S., Liu, G., Johnson, W. E. & Crandall, K. A. (2015). Integrating microbial and host transcriptomics to characterize asthma-associated microbial communities. *BMC Med Genomics*. **8,** 50

96. Pérez-Losada, M., Castro-Nallar, E., Bendall, M. L., Freishtat, R. J. & Crandall, K. A. (2015). Dual transcriptomic profiling of host and microbiota during health and disease in pediatric asthma. *PLoS One*. **10,** e0131819

97. Erwin, A. L. & Smith, A. L. (2007). Nontypeable Haemophilus influenzae: understanding virulence and commensal behavior. *Trends Microbiol*. **15,** 355–362

98. Evans, N. M., Smith, D. D. & Wicken, A. J. (1974). Haemin and nicotinamide adenine dinucleotide requirements of Haemophilus influenzae and Haemophilus parainfluenzae. *J Med Microbiol*. **7,** 359–365

99. King, P. (2012). Haemophilus influenzae and the lung (Haemophilus and the lung). *Clin Transl Med*. **1,** 10

100. Swords, W. E. (2012). Nontypeable Haemophilus influenzae biofilms: role in chronic airway infections. *Front Cell Infect Microbiol*. **2,** 97

101. Ahearn, C. P., Gallo, M. C. & Murphy, T. F. (2017). Insights on persistent airway infection by non-typeable Haemophilus influenzae in chronic obstructive pulmonary disease. *Pathog Dis*. **75,**

102. Schumacher, S. K., Marchant, C. D., Loughlin, A. M., Bouchet, V., Stevenson, A. & Pelton, S. I. (2012). Prevalence and genetic diversity of nontypeable Haemophilus influenzae in the respiratory tract of infants and primary caregivers. *Pediatr Infect Dis J*. **31,** 145–149

103. Jalalvand, F. & Riesbeck, K. (2018). Update on non-typeable Haemophilus influenzae-mediated disease and vaccine development. *Expert Rev Vaccines*. **17,** 503–512

104. Hogg, J. S., Hu, F. Z., Janto, B., Boissy, R., Hayes, J., Keefe, R., Post, J. C. & Ehrlich, G. D. (2007). Characterization and modeling of the Haemophilus influenzae core and supragenomes based on the complete genomic sequences of Rd and 12 clinical nontypeable strains. *Genome Biol*. **8,** R103

105. Pinto, M., González-Díaz, A., Machado, M. P., Duarte, S., Vieira, L., Carriço, J. A., Marti, S., Bajanca-Lavado, M. P. & Gomes, J. P. (2019). Insights into the population structure and pan-genome of Haemophilus influenzae. *Infect Genet Evol*. **67,** 126–135

106. Van Der Woude, M. W. & Bäumler, A. J. (2004). Phase and antigenic variation in bacteria. *Clinical Microbiology Reviews*. **17,** 581–611

107. Reyes Ruiz, L. M., Williams, C. L. & Tamayo, R. (2020). Enhancing bacterial survival through phenotypic heterogeneity. *PLoS Pathog*. **16,** e1008439

108. Van Eldere, J., Slack, M. P. E., Ladhani, S. & Cripps, A. W. (2014). Non-typeable Haemophilus influenzae, an under-recognised pathogen. *Lancet Infect Dis*. **14,** 1281–1292

109. McCann, J. R., Mason, S. N., Auten, R. L., St. Geme, J. W. & Seed, P. C. (2016). Early-life intranasal colonization with nontypeable Haemophilus influenzae exacerbates juvenile airway disease in mice. *Infect Immun*. **84,** 2022–2030

110. Finney, L. J., Ritchie, A., Pollard, E., Johnston, S. L. & Mallia, P. (2014). Lower airway colonization and inflammatory response in COPD: A focus on Haemophilus influenza. *Int J COPD*. **9,** 1119–1132

111. Wang, S., Tafalla, M., Hanssens, L. & Dolhain, J. (2017). A review of Haemophilus influenzae disease in Europe from 2000–2014: challenges, successes and the contribution of hexavalent combination vaccines. *Expert Rev Vaccines*. **16,** 1095–1105

112. Adam, H. J., Richardson, S. E., Jamieson, F. B., Rawte, P., Low, D. E. & Fisman, D. N. (2010). Changing epidemiology of invasive Haemophilus influenzae in Ontario, Canada: Evidence for herd effects and strain replacement due to Hib vaccination. *Vaccine*. **28,** 4073–4078

113. Peltola, H., Aavitsland, P., Hansen, K. G., Jónsdóttir, K. E., Nøkleby, H. & Romanus, V. (1999). Perspective: A five-country analysis of the impact of four different Haemophilus influenzae type b conjugates and vaccination strategies in Scandinavia. *J Infect Dis*. **179,** 223–229

114. Langereis, J. D. & De Jonge, M. I. (2015). Invasive disease caused by nontypeable Haemophilus influenzae. *Emerg Infect Dis*. **21,** 1711–1718

115. Cerquetti, M. & Giufrè, M. (2016). Why we need a vaccine for non-typeable Haemophilus influenzae. *Hum Vaccines Immunother*. **12,** 2357–2361

116. WHO. (2017). *GLOBAL PRIORITY LIST OF ANTIBIOTIC-RESISTANT BACTERIA TO GUIDE RESEARCH, DISCOVERY, AND DEVELOPMENT OF NEW ANTIBIOTICS*.

117. St. Geme, J. W., Pinkner, J. S., Krasan, G. P., Heuser, J., Bullitt, E., Smith, A. L. & Hultgren, S. J. (1996). Haemophilus influenzae pili are composite structures assembled via the HifB chaperone. *Proc Natl Acad Sci U S A*. **93,** 11913–11918

118. Fink, D. L., Green, B. A. & St. Geme, J. W. (2002). The Haemophilus influenzae Hap autotransporter binds to fibronectin, laminin, and collagen IV. *Infect Immun*. **70,** 4902–4907

119. St Geme, J. W., Falkow, S. & Barenkamp, S. J. (1993). High-molecular-weight proteins of nontypable Haemophilus influenzae mediate attachment to human epithelial cells. *Proc Natl Acad Sci U S A*. **90,** 2875–9

120. St. Geme, J. W. & Cutter, D. (2000). The Haemophilus influenzae Hia adhesin is an autotransporter protein that remains uncleaved at the C terminus and fully cell associated. *J Bacteriol*. **182,** 6005–6013

121. Avadhanula, V., Rodriguez, C. A., Ulett, G. C., Bakaletz, L. O. & Adderson, E. E. (2006). Nontypeable Haemophilus influenzae adheres to intercellular adhesion molecule 1 (ICAM-1) on respiratory epithelial cells and upregulates ICAM-1 expression. *Infect Immun*. **74,** 830–838

122. Hill, D. J., Toleman, M. A., Evans, D. J., Villullas, S., Van Alphen, L. & Virji, M. (2001). The variable P5 proteins of typeable and non-typeable Haemophilus influenzae target human CEACAM1. *Mol Microbiol*. **39,** 850–862

123. Swords, W. E., Ketterer, M. R., Shao, J., Campbell, C. A., Weiser, J. N. & Apicella, M. A. (2001). Binding of the non-typeable Haemophilus influenzae lipooligosaccharide to the PAF receptor initiates host cell signalling. *Cell Microbiol*. **3,** 525–536

124. Duell, B. L., Su, Y. C. & Riesbeck, K. (2016). Host–pathogen interactions of nontypeable Haemophilus influenzae: from commensal to pathogen. *FEBS Lett*. **590,** 3840–3853

125. Su, Y. C., Mukherjee, O., Singh, B., Hallgren, O., Westergren-Thorsson, G., Hood, D. & Riesbeck, K. (2016). Haemophilus influenzae p4 interacts with extracellular matrix proteins promoting adhesion and serum resistance. *J Infect Dis*. **213,** 314–323

126. Novotny, L. A. & Bakaletz, L. O. (2016). Intercellular adhesion molecule 1 serves as a primary cognate receptor for the Type IV pilus of nontypeable Haemophilus influenzae.

Cell Microbiol. **18,** 1043–1055

127. Kubiet, M., Ramphal, R., Weber, A. & Smith, A. (2000). Pilus-mediated adherence of Haemophilus influenzae to human respiratory mucins. *Infect Immun*. **68,** 3362–7

128. St. Geme, J. W. (1994). The HMW1 adhesin of nontypeable Haemophilus influenzae recognizes sialylated glycoprotein receptors on cultured human epithelial cells. *Infect Immun*. **62,** 3881–3889

129. Atack, J. M., Day, C. J., Poole, J., Brockman, K. L., Timms, J. R. L., Winter, L. E., Haselhorst, T., Bakaletz, L. O., Barenkamp, S. J. & Jennings, M. P. (2020). The nontypeable haemophilus influenzae major adhesin hia is a dual-function lectin that binds to human-specific respiratory tract sialic acid glycan receptors. *MBio*. **11,** 1–15

130. Shinya, K. & Kawaoka, Y. (2006). Influenza virus receptors in the human airway. *Uirusu J Virol*. **56,** 85–89

131. Morey, P., Viadas, C., Euba, B., Hood, D. W., Barberán, M., Gil, C., Grilló, M. J., Bengoechea, J. A. & Garmendia, J. (2013). Relative contributions of lipooligosaccharide inner and outer core modifications to nontypeable haemophilus influenzae pathogenesis. *Infect Immun*. **81,** 4100–4111

132. Apicella, M. A., Coffin, J., Ketterer, M., Post, D. M. B., Day, C. J., Jen, F. E. C. & Jennings, M. P. (2018). Nontypeable Haemophilus influenzae lipooligosaccharide expresses a terminal ketodeoxyoctanoate in vivo, which can be used as a target for bactericidal antibody. *MBio*. **9,** e01401-18

133. Swords, W. E., Buscher, B. A., Ver Steeg Li, K., Preston, A., Nichols, W. A., Weiser, J. N., Gibson, B. W. & Apicella, M. A. (2000). Non-typeable Haemophilus influenzae adhere to and invade human bronchial epithelial cells via an interaction of lipooligosaccharide with the PAF receptor. *Mol Microbiol*. **37,** 13–27

134. Murphy, T. F., Brauer, A. L., Schiffmacher, A. T. & Sethi, S. (2004). Persistent colonization by haemophilus influenzae in chronic obstructive pulmonary disease. *Am J Respir Crit Care Med*. **170,** 266–272

135. Gallo, M. C., Kirkham, C., Eng, S., Bebawee, R. S., Kong, Y., Pettigrew, M. M., Tettelin, H. & Murphy, T. F. (2018). Changes in IgA protease expression are conferred by changes in genomes during persistent infection by nontypeable Haemophilus influenzae in chronic obstructive pulmonary disease. *Infect Immun*. **86,** e00313-18

136. Román, F., Cantón, R., Pérez-Vázquez, M., Baquero, F. & Campos, J. (2004). Dynamics of Long-Term Colonization of Respiratory Tract by Haemophilus influenzae in Cystic Fibrosis

Patients Shows a Marked Increase in Hypermutable Strains. *J Clin Microbiol*. **42,** 1450–1459

137. Flemming, H. C., Wingender, J., Szewzyk, U., Steinberg, P., Rice, S. A. & Kjelleberg, S. (2016). Biofilms: An emergent form of bacterial life. *Nat Rev Microbiol*. **14,** 563–575

138. Høiby, N., Ciofu, O. & Bjarnsholt, T. (2010). Pseudomonas aeruginosa biofilms in cystic fibrosis. *Future Microbiol*. **5,** 1663–1674

139. Starner, T. D., Zhang, N., Kim, G. H., Apicella, M. A. & McCray, P. B. (2006). Haemophilus influenzae forms biofilms on airway epithelia: Implications in cystic fibrosis. *Am J Respir Crit Care Med*. **174,** 213–220

140. Morey, P., Cano, V., Martí-Lliteras, P., López-Gómez, A., Regueiro, V., Saus, C., Bengoechea, J. A. & Garmendia, J. (2011). Evidence for a non-replicative intracellular stage of nontypable Haemophilus influenzae in epithelial cells. *Microbiology*. **157,** 234–250

141. Shapiro, R., Welcher, M., Nelson, V. & Di Fate, V. (1976). *Reaction of uracil and thymine derivatives with sodium bisulfite. Studies on the mechanism and reduction of the adduct*. *BBA Section Nucleic Acids And Protein Synthesis*. **425,**

142. Ahrén, I. L., Williams, D. L., Rice, P. J., Forsgren, A. & Riesbeck, K. (2001). The importance of a β-glucan receptor in the nonopsonic entry of nontypeable Haemophilus influenzae into human monocytic and epithelial cells. *J Infect Dis*. **184,** 150–158

143. Ketterer, M. R., Shao, J. Q., Hornick, D. B., Buscher, B., Bandi, V. K. & Apicella, M. A. (1999). Infection of primary human bronchial epithelial cells by Haemophilus influenzae: macropinocytosis as a mechanism of airway epithelial cell entry. *Infect Immun*. **67,** 4161–70

144. Hardison, R. L., Heimlich, D. R., Harrison, A., Beatty, W. L., Rains, S., Moseley, M. A., Thompson, J. W., Justice, S. S. & Mason, K. M. (2018). Transient Nutrient Deprivation Promotes Macropinocytosis-Dependent Intracellular Bacterial Community Development. *mSphere*. **3,** 286–304

145. Van Schilfgaarde, M., Eijk, P., Regelink, A., Van Ulsen, P., Everts, V., Dankert, J. & Van Alphen, L. (1999). Haemophilus influenzae localized in epithelial cell layers is shielded from antibiotics and antibody-mediated bactericidal activity. *Microb Pathog*. **26,** 249–262

146. Ren, D., Nelson, K. L., Uchakin, P. N., Smith, A. L., Gu, X. X. & Daines, D. A. (2012). Characterization of extended co-culture of non-typeable Haemophilus influenzae with primary human respiratory tissues. *Exp Biol Med*. **237,** 540–547

147. Forsgren, J., Samuelson, A., Ahlin, A., Jonasson, J., Rynnel-Dagoo, B. & Lindberg, A. (1994).

Haemophilus influenzae resides and multiplies intracellularly in human adenoid tissue as demonstrated by in situ hybridization and bacterial viability assay. *Infect Immun*. **62,** 673–679

148. Martí-Lliteras, P., Regueiro, V., Morey, P., Hood, D. W., Saus, C., Sauleda, J., Agustí, A. G. N., Bengoechea, J. A. & Garmendia, J. (2009). Nontypeable Haemophilus influenzae clearance by alveolar macrophages is impaired by exposure to cigarette smoke. *Infect Immun*. **77,** 4232–4242

149. Craig, J. E., Cliffe, A., Garnett, K. & High, N. J. (2001). Survival of nontypeable Haemophilus influenzae in macrophages. *FEMS Microbiol Lett*. **203,** 55–61

150. Craig, J. E., Nobbs, A. & High, N. J. (2002). The extracytoplasmic sigma factor, σE, is required for intracellular survival of nontypeable Haemophilus influenzae in J774 macrophages. *Infect Immun*. **70,** 708–715

151. Baddal, B., Muzzi, A., Censini, S., Calogero, R. A., Torricelli, G., Guidotti, S., Taddei, A. R., Covacci, A., Pizza, M., Rappuoli, R., Soriani, M. & Pezzicoli, A. (2015). Dual RNA-seq of nontypeable haemophilus influenzae and host cell transcriptomes reveals novel insights into host-pathogen cross talk. *MBio*. **6,** 1–13

152. Langereis, J. D., Zomer, A., Stunnenberg, H. G., Burghout, P. & Hermans, P. W. M. (2013). Nontypeable Haemophilus influenzae carbonic anhydrase is important for environmental and intracellular survival. *J Bacteriol*. **195,** 2737–2746

153. Nagayama, Y., Tsubaki, T., Toba, T., Kawakami, H. & Okusu, K. (1999). Role of bacterial infection in the exacerbation of acute or prolonged asthma attack in children. *Allergol Int*. **48,** 137–144

154. Essilfie, A. T., Simpson, J. L., Dunkley, M. L., Morgan, L. C., Oliver, B. G., Gibson, P. G., Foster, P. S. & Hansbro, P. M. (2012). Combined Haemophilus influenzae respiratory infection and allergic airways disease drives chronic infection and features of neutrophilic asthma. *Thorax*. **67,** 588–599

155. Larsen, J. M., Brix, S., Thysen, A. H., Birch, S., Rasmussen, M. A. & Bisgaard, H. (2014). Children with asthma by school age display aberrant immune responses to pathogenic airway bacteria as infants. *J Allergy Clin Immunol*. **133,** 1008-1013.e4

156. Sato, S. & Kiyono, H. (2012). The mucosal immune system of the respiratory tract. *Curr Opin Virol*. **2,** 225–232

157. Iwasaki, A., Foxman, E. F. & Molony, R. D. (2017). Early local immune defences in the respiratory tract. *Nat Rev Immunol*. **17,** 7–20

158. Martin, T. R. & Frevert, C. W. (2005). Innate immunity in the lungs. *Proc Am Thorac Soc*. **2,** 403–11

159. Nicod, L. P. (2005). Lung defences: An overview. *Eur Respir Rev*. **14,** 45–50

160. Byrne, A. J., Mathie, S. A., Gregory, L. G. & Lloyd, C. M. (2015). Pulmonary macrophages: Key players in the innate defence of the airways. *Thorax*. **70,** 1189–1196

161. Varol, C., Mildner, A. & Jung, S. (2015). Macrophages: Development and tissue specialization. *Annu Rev Immunol*. **33,** 643–675

162. Wynn, T. A., Chawla, A. & Pollard, J. W. (2013). Macrophage biology in development, homeostasis and disease. *Nature*. **496,** 445–455

163. Guilliams, M., De Kleer, I., Henri, S., Post, S., Vanhoutte, L., De Prijck, S., Deswarte, K., Malissen, B., Hammad, H. & Lambrecht, B. N. (2013). Alveolar macrophages develop from fetal monocytes that differentiate into long-lived cells in the first week of life via GM-CSF. *J Exp Med*. **210,** 1977–1992

164. Tan, S. Y. S. & Krasnow, M. A. (2016). Developmental origin of lung macrophage diversity. *Dev*. **143,** 1318–1327

165. Hussell, T. & Bell, T. J. (2014). Alveolar macrophages: Plasticity in a tissue-specific context. *Nat Rev Immunol*. **14,** 81–93

166. Shibata, Y., Berclaz, P. Y., Chroneos, Z. C., Yoshida, M., Whitsett, J. A. & Trapnell, B. C. (2001). GM-CSF regulates alveolar macrophage differentiation and innate immunity in the lung through PU.1. *Immunity*. **15,** 557–567

167. Borie, R., Danel, C., Debray, M. P., Taille, C., Dombret, M. C., Aubier, M., Epaud, R. & Crestani, B. (2011). Pulmonary alveolar proteinosis. *European Respiratory Review*. **20,** 98–107

168. Mosser, D. M. & Edwards, J. P. (2008). Exploring the full spectrum of macrophage activation. *Nat Rev Immunol*. **8,** 958–969

169. Takeda, K. & Akira, S. (2005). Toll-like receptors in innate immunity. *International Immunology*. **17,** 1–14

170. Aderem, A. & Underhill, D. M. (1999). Mechanisms of phagocytosis in macrophages. *Annu Rev Immunol*. **17,** 593–623

171. Korns, D., Frasch, S. C., Fernandez-Boyanapalli, R., Henson, P. M. & Bratton, D. L. (2011). Modulation of macrophage efferocytosis in inflammation. *Front Immunol*. **2,** 57

172. Watanabe, S., Alexander, M., Misharin, A. V. & Budinger, G. R. S. (2019). The role of

macrophages in the resolution of inflammation. *Journal of Clinical Investigation*. **129,** 2619–2628

173. Yamada, M., Fujino, N. & Ichinose, M. (2016). Inflammatory responses in the initiation of lung repair and regeneration: their role in stimulating lung resident stem cells. *Inflamm Regen*. **36,** 15

174. Connolly, E. & Hussell, T. (2020). The Impact of Type 1 Interferons on Alveolar Macrophage Tolerance and Implications for Host Susceptibility to Secondary Bacterial Pneumonia. *Frontiers in Immunology*. **11,** 495

175. Butcher, S. K., O'Carroll, C. E., Wells, C. A. & Carmody, R. J. (2018). Toll-like receptors drive specific patterns of tolerance and training on restimulation of macrophages. *Front Immunol*. **9,** 933

176. Didierlaurent, A., Goulding, J., Patel, S., Snelgrove, R., Low, L., Bebien, M., Lawrence, T., Van Rijt, L. S., Lambrecht, B. N., Sirard, J. C. & Hussell, T. (2008). Sustained desensitization to bacterial Toll-like receptor ligands after resolution of respiratory influenza infection. *J Exp Med*. **205,** 323–329

177. Saeed, S., Quintin, J., Kerstens, H. H. D., Rao, N. A., Aghajanirefah, A., Matarese, F., Cheng, S.-C., Ratter, J., Berentsen, K., van der Ent, M. A., Sharifi, N., Janssen-Megens, E. M., Ter Huurne, M., Mandoli, A., van Schaik, T., Ng, A., Burden, F., Downes, K., Frontini, M., Kumar, V., Giamarellos-Bourboulis, E. J., Ouwehand, W. H., van der Meer, J. W. M., Joosten, L. A. B., Wijmenga, C., Martens, J. H. A., Xavier, R. J., Logie, C., Netea, M. G. & Stunnenberg, H. G. (2014). Epigenetic programming of monocyte-to-macrophage differentiation and trained innate immunity. *Science*. **345,** 1251086

178. Stout, R. D., Jiang, C., Matta, B., Tietzel, I., Watkins, S. K. & Suttles, J. (2005). Macrophages Sequentially Change Their Functional Phenotype in Response to Changes in Microenvironmental Influences. *J Immunol*. **175,** 342–349

179. Varol, C., Mildner, A. & Jung, S. (2015). Macrophages: Development and tissue specialization. *Annu Rev Immunol*. **33,** 643–675

180. Xue, J., Schmidt, S. V., Sander, J., Draffehn, A., Krebs, W., Quester, I., DeNardo, D., Gohel, T. D., Emde, M., Schmidleithner, L., Ganesan, H., Nino-Castro, A., Mallmann, M. R., Labzin, L., Theis, H., Kraut, M., Beyer, M., Latz, E., Freeman, T. C., Ulas, T. & Schultze, J. L. (2014). Transcriptome-Based Network Analysis Reveals a Spectrum Model of Human Macrophage Activation. *Immunity*. **40,** 274–288

181. Sudan, B., Wacker, M. A., Wilson, M. E. & Graff, J. W. (2015). A Systematic Approach to Identify Markers of Distinctly Activated Human Macrophages. *Front Immunol*. **6,** 253

182. Martinez, F. O. & Gordon, S. (2014). The M1 and M2 paradigm of macrophage activation: time for reassessment. *F1000Prime Rep*. **6,** 13

183. Staples, K. J., Hinks, T. S. C., Ward, J. A., Gunn, V., Smith, C. & Djukanović, R. (2012). Phenotypic characterization of lung macrophages in asthmatic patients: Overexpression of CCL17. *J Allergy Clin Immunol*. **130,** 1404-1412.e7

184. Akira, S., Uematsu, S. & Takeuchi, O. (2006). Pathogen recognition and innate immunity. *Cell*. **124,** 783–801

185. Vijay, K. (2018). Toll-like receptors in immunity and inflammatory diseases: Past, present, and future. *Int Immunopharmacol*. **59,** 391–412

186. Shuto, T., Xu, H., Wang, B., Han, J., Kai, H., Gu, X. X., Murphy, T. F., Lim, D. J. & Li, J. D. (2001). Activation of NF-κB by nontypeable Hemophilus influenzae is mediated by toll-like receptor 2-TAK1-dependent NIK-IKKα/β-IκBα and MKK3/6-p38 MAP kinase signaling pathways in epithelial cells. *Proc Natl Acad Sci U S A*. **98,** 8774–8779

187. Berenson, C. S., Wrona, C. T., Grove, L. J., Maloney, J., Garlipp, M. A., Wallace, P. K., Stewart, C. C. & Sethi, S. (2006). Impaired alveolar macrophage response to Haemophilus antigens in chronic obstructive lung disease. *Am J Respir Crit Care Med*. **174,** 31–40

188. Wang, X., Moser, C., Louboutin, J.-P., Lysenko, E. S., Weiner, D. J., Weiser, J. N. & Wilson, J. M. (2002). Toll-Like Receptor 4 Mediates Innate Immune Responses to Haemophilus influenzae Infection in Mouse Lung . *J Immunol*. **168,** 810–815

189. Wieland, C. W., Florquin, S., Maris, N. A., Hoebe, K., Beutler, B., Takeda, K., Akira, S. & van der Poll, T. (2005). The MyD88-Dependent, but Not the MyD88-Independent, Pathway of TLR4 Signaling Is Important in Clearing Nontypeable Haemophilus influenzae from the Mouse Lung . *J Immunol*. **175,** 6042–6049

190. Lester, S. N. & Li, K. (2014). Toll-like receptors in antiviral innate immunity. *J Mol Biol*. **426,** 1246–1264

191. Kurt-Jones, E. A., Popova, L., Kwinn, L., Haynes, L. M., Jones, L. P., Tripp, R. A., Walsh, E. E., Freeman, M. W., Golenbock, D. T., Anderson, L. J. & Finberg, R. W. (2000). Pattern recognition receptors TLR4 and CD14 mediate response to respiratory syncytial virus. *Nat Immunol*. **1,** 398–401

192. Arbour, N. C., Lorenz, E., Schutte, B. C., Zabner, J., Kline, J. N., Jones, M., Frees, K., Watt, J. L. & Schwartz, D. A. (2000). TLR4 mutations are associated with endotoxin hyporesponsiveness in humans. *Nat Genet*. **25,** 187–191

193. Awomoyi, A. A., Rallabhandi, P., Pollin, T. I., Lorenz, E., Sztein, M. B., Boukhvalova, M. S.,

Hemming, V. G., Blanco, J. C. G. & Vogel, S. N. (2007). Association of TLR4 Polymorphisms with Symptomatic Respiratory Syncytial Virus Infection in High-Risk Infants and Young Children. *J Immunol*. **179,** 3171–3177

194. Shepardson, K. M., Schwarz, B., Larson, K., Morton, R. V., Avera, J., McCoy, K., Caffrey, A., Harmsen, A., Douglas, T. & Rynda-Apple, A. (2017). Induction of antiviral immune response through recognition of the repeating subunit pattern of viral capsids is toll-like receptor 2 dependent. *MBio*. **8,** e01356-17

195. Murawski, M. R., Bowen, G. N., Cerny, A. M., Anderson, L. J., Haynes, L. M., Tripp, R. A., Kurt-Jones, E. A. & Finberg, R. W. (2009). Respiratory Syncytial Virus Activates Innate Immunity through Toll-Like Receptor 2. *J Virol*. **83,** 1492–1500

196. Tan, A. C. L., Mifsud, E. J., Zeng, W., Edenborough, K., McVernon, J., Brown, L. E. & Jackson, D. C. (2012). Intranasal administration of the TLR2 agonist pam2Cys provides rapid protection against influenza in mice. *Mol Pharm*. **9,** 2710–2718

197. Sajjan, U. S., Jia, Y., Newcomb, D. C., Bentley, J. K., Lukacs, N. W., LiPuma, J. J., Hershenson, M. B., Sajjan, U. S., Jia, Y., Newcomb, D. C., Bentley, J. K., Lukacs, N. W., LiPuma, J. J. & Hershenson, M. B. (2006). H. influenzae potentiates airway epithelial cell responses to rhinovirus by increasing ICAM-1 and TLR3 expression. *FASEB J*. **20,** 2121–2123

198. Teng, F., Slavik, V., Duffy, K. E., San Mateo, L. & Goldschmidt, R. (2010). Toll-like receptor 3 is involved in airway epithelial cell response to nontypeable Haemophilus influenzae. *Cell Immunol*. **260,** 98–104

199. Hinks, T. S. C., Wallington, J. C., Williams, A. P., Djukanovic, R., Staples, K. J. & Wilkinson, T. M. A. (2016). Steroid-induced deficiency of mucosal-associated invariant T cells in the chronic obstructive pulmonary disease lung implications for nontypeable haemophilus influenzae infection. *Am J Respir Crit Care Med*. **194,** 1208–1218

200. Mogensen, T. H. (2006). Live Streptococcus pneumoniae, Haemophilus influenzae, and Neisseria meningitidis activate the inflammatory response through Toll-like receptors 2, 4, and 9 in species-specific patterns. *J Leukoc Biol*. **80,** 267–277

201. Wieland, C. W., Florquin, S. & van der Poll, T. (2010). Toll-like receptor 9 is not important for host defense against Haemophilus influenzae. *Immunobiology*. **215,** 910–914

202. Barton, G. M. (2007). Viral recognition by Toll-like receptors. *Semin Immunol*. **19,** 33–40

203. Dixit, E. & Kagan, J. C. (2013). Intracellular Pathogen Detection by RIG-I-Like Receptors. *Adv Immunol*. **117,** 99–125

204. Monroe, K. M., McWhirter, S. M. & Vance, R. E. (2009). Identification of host cytosolic

sensors and bacterial factors regulating the type I interferon response to Legionella pneumophila. *PLoS Pathog*. **5,** e1000665

205. Schmolke, M., Patel, J. R., de Castro, E., Sánchez, M. T. A., Uccellini, M. B., Miller, J. C., Manicassamy, B., Satoh, T., Kawai, T., Akira, S., Merad, M. & García-Sastre, A. (2014). RIG-I detects mRNA of intracellular Salmonella enterica serovar typhimurium during bacterial infection. *MBio*. **5,** e01006-14

206. Franchi, L., Warner, N., Viani, K. & Nuñez, G. (2009). Function of Nod-like receptors in microbial recognition and host defense. *Immunological Reviews*. **227,** 106–128

207. Leber, J. H., Crimmins, G. T., Raghavan, S., Meyer-Morse, N. P., Cox, J. S. & Portnoy, D. A. (2008). Distinct TLR- and NLR-mediated transcriptional responses to an intracellular pathogen. *PLoS Pathog*. **4,** 0084–0095

208. Lee, J., Leichtle, A., Zuckerman, E., Pak, K., Spriggs, M., Wasserman, S. I. & Kurabi, A. (2019). NOD1/NOD2-mediated recognition of non-typeable Haemophilus influenzae activates innate immunity during otitis media. *Innate Immun*. **25,** 503–512

209. de Zoete, M. R., Palm, N. W., Zhu, S. & Flavell, R. A. (2014). Inflammasomes. *Cold Spring Harb Perspect Biol*. **6,** a016287

210. Kayagaki, N., Wong, M. T., Stowe, I. B., Ramani, S. R., Gonzalez, L. C., Akashi-Takamura, S., Miyake, K., Zhang, J., Lee, W. P., Muszyński, A., Forsberg, L. S., Carlson, R. W. & Dixit, V. M. (2013). Noncanonical inflammasome activation by intracellular LPS independent of TLR4. *Science*. **341,** 1246–9

211. Casson, C. N., Yu, J., Reyes, V. M., Taschuk, F. O., Yadav, A., Copenhaver, A. M., Nguyen, H. T., Collman, R. G. & Shin, S. (2015). Human caspase-4 mediates noncanonical inflammasome activation against gram-negative bacterial pathogens. *Proc Natl Acad Sci U S A*. **112,** 6688–6693

212. Shi, J., Zhao, Y., Wang, Y., Gao, W., Ding, J., Li, P., Hu, L. & Shao, F. (2014). Inflammatory caspases are innate immune receptors for intracellular LPS. *Nature*. **514,** 187–192

213. Viganò, E., Diamond, C. E., Spreafico, R., Balachander, A., Sobota, R. M. & Mortellaro, A. (2015). Human caspase-4 and caspase-5 regulate the one-step non-canonical inflammasome activation in monocytes. *Nat Commun*. **6,** 8761

214. Tretina, K., Park, E. S., Maminska, A. & MacMicking, J. D. (2019). Interferon-induced guanylate-binding proteins: Guardians of host defense in health and disease. *Journal of Experimental Medicine*. **216,** 482–500

215. Meunier, E., Dick, M. S., Dreier, R. F., Schürmann, N., Broz, D. K., Warming, S., Roose-

Girma, M., Bumann, D., Kayagaki, N., Takeda, K., Yamamoto, M. & Broz, P. (2014). Caspase-11 activation requires lysis of pathogen-containing vacuoles by IFN-induced GTPases. *Nature*. **509,** 366–370

216. Santos, J. C., Boucher, D., Schneider, L. K., Demarco, B., Dilucca, M., Shkarina, K., Heilig, R., Chen, K. W., Lim, R. Y. H. & Broz, P. (2020). Human GBP1 binds LPS to initiate assembly of a caspase-4 activating platform on cytosolic bacteria. *Nat Commun*. **11,** 3276

217. Rotta detto Loria, J., Rohmann, K., Droemann, D., Kujath, P., Rupp, J., Goldmann, T. & Dalhoff, K. (2013). Nontypeable Haemophilus Influenzae Infection Upregulates the NLRP3 Inflammasome and Leads to Caspase-1-Dependent Secretion of Interleukin-1β - A Possible Pathway of Exacerbations in COPD. *PLoS One*. **8,** e66818

218. Brown, G. D., Willment, J. A. & Whitehead, L. (2018). C-type lectins in immunity and homeostasis. *Nat Rev Immunol*. **18,** 374–389

219. Raymond, B. B. A., Neyrolles, O. & Rombouts, Y. (2020). C-type Lectins in Immunity to Lung Pathogens. *Curr Top Microbiol Immunol*. **429,** 19–62

220. Heyl, K. A., Klassert, T. E., Heinrich, A., Müller, M. M., Klaile, E., Dienemann, H., Grünewald, C., Bals, R., Singer, B. B. & Slevogt, H. (2014). Dectin-1 is expressed in human lung and mediates the proinflammatory immune response to nontypeable Haemophilus influenzae. *MBio*. **5,** e01492-14

221. Kawai, T. & Akira, S. (2010). The role of pattern-recognition receptors in innate immunity: Update on toll-like receptors. *Nat Immunol*. **11,** 373–384

222. Reid, D. M., Gow, N. A. & Brown, G. D. (2009). Pattern recognition: recent insights from Dectin-1. *Current Opinion in Immunology*. **21,** 30–37

223. Moreira, L. O. & Zamboni, D. S. (2012). NOD1 and NOD2 Signaling in Infection and Inflammation. *Front Immunol*. **3,** 328

224. Rehwinkel, J. & Gack, M. U. (2020). RIG-I-like receptors: their regulation and roles in RNA sensing. *Nature Reviews Immunology*. **20,** 537–551

225. Berenson, C. S., Murphy, T. F., Wrona, C. T. & Sethi, S. (2005). Outer membrane protein p6 of nontypeable Haemophilus influenzae is a potent and selective inducer of human macrophage proinflammatory cytokines. *Infect Immun*. **73,** 2728–2735

226. King, P. T. & Sharma, R. (2015). The Lung Immune Response to Nontypeable Haemophilus influenzae (Lung Immunity to NTHi). *J Immunol Res*. **2015,** 706376

227. Yan, N. & Chen, Z. J. (2012). Intrinsic antiviral immunity. *Nat Immunol*. **13,** 214–222

228. Pfeffer, L. M. (2011). The role of nuclear factor κb in the interferon response. *Journal of*

Interferon and Cytokine Research. **31,** 553–559

229. Killip, M. J., Fodor, E. & Randall, R. E. (2015). Influenza virus activation of the interferon system. *Virus Res*. **209,** 11–22

230. Schneider, W. M., Chevillotte, M. D. & Rice, C. M. (2014). Interferon-stimulated genes: A complex web of host defenses. *Annu Rev Immunol*. **32,** 513–545

231. Lu, C., Zhang, X., Ma, C., Xu, W., Gan, L., Cui, J., Yin, Y. & Wang, H. (2018). Nontypeable Haemophilus influenzae DNA stimulates type I interferon expression via STING signaling pathway. *Biochim Biophys acta Mol cell Res*. **1865,** 665–673

232. Dufour, J. H., Dziejman, M., Liu, M. T., Leung, J. H., Lane, T. E. & Luster, A. D. (2002). IFN-γ-Inducible Protein 10 (IP-10; CXCL10)-Deficient Mice Reveal a Role for IP-10 in Effector T Cell Generation and Trafficking. *J Immunol*. **168,** 3195–3204

233. Trifilo, M. J., Montalto-Morrison, C., Stiles, L. N., Hurst, K. R., Hardison, J. L., Manning, J. E., Masters, P. S. & Lane, T. E. (2004). CXC Chemokine Ligand 10 Controls Viral Infection in the Central Nervous System: Evidence for a Role in Innate Immune Response through Recruitment and Activation of Natural Killer Cells. *J Virol*. **78,** 585–594

234. Wallington, J. C. (2017). The Responses Of Conventional T Cells And Mucosal- Associated Invariant T Cells To Nontypeable Haemophilus Influenzae Infection. *University of Southampton Research Repository ePrints Soton*. **PhD Thesis,**

235. Aderem, A. (2003). Phagocytosis and the inflammatory response. *J Infect Dis*. **187 Suppl,** S340-5

236. Shapouri-Moghaddam, A., Mohammadian, S., Vazini, H., Taghadosi, M., Esmaeili, S. A., Mardani, F., Seifi, B., Mohammadi, A., Afshari, J. T. & Sahebkar, A. (2018). Macrophage plasticity, polarization, and function in health and disease. *J Cell Physiol*. **233,** 6425–6440

237. Gordon, S. (2016). Phagocytosis: An Immunobiologic Process. *Immunity*. **44,** 463–475

238. Areschoug, T. & Gordon, S. (2009). Scavenger receptors: Role in innate immunity and microbial pathogenesis. *Cell Microbiol*. **11,** 1160–1169

239. Canton, J., Neculai, D. & Grinstein, S. (2013). Scavenger receptors in homeostasis and immunity. *Nat Rev Immunol*. **13,** 621–634

240. Cooper, G. E., Pounce, Z. C., Wallington, J. C., Bastidas-Legarda, L. Y., Nicholas, B., Chidomere, C., Robinson, E. C., Martin, K., Tocheva, A. S., Christodoulides, M., Djukanovic, R., Wilkinson, T. M. A. & Staples, K. J. (2016). Viral inhibition of bacterial phagocytosis by human macrophages: Redundant role of CD36. *PLoS One*. **11,** e0163889

241. Provost, K. A., Smith, M., Arold, S. P., Hava, D. L. & Sethi, S. (2015). Calcium restores the

macrophage response to nontypeable Haemophilus influenzae in chronic obstructive pulmonary disease. *Am J Respir Cell Mol Biol*. **52,** 728–737

242. Tridandapani, S., Siefker, K., Teillaud, J. L., Carter, J. E., Wewers, M. D. & Anderson, C. L. (2002). Regulated expression and inhibitory function of FcγRIIb in human monocytic cells. *J Biol Chem*. **277,** 5082–5089

243. Vieira, O. V., Bucci, C., Harrison, R. E., Trimble, W. S., Lanzetti, L., Gruenberg, J., Schreiber, A. D., Stahl, P. D. & Grinstein, S. (2003). Modulation of Rab5 and Rab7 Recruitment to Phagosomes by Phosphatidylinositol 3-Kinase. *Mol Cell Biol*. **23,** 2501–2514

244. Pope, S. M., Zimmermann, N., Stringer, K. F., Karow, M. L. & Rothenberg, M. E. (2005). The Eotaxin Chemokines and CCR3 Are Fundamental Regulators of Allergen-Induced Pulmonary Eosinophilia. *J Immunol*. **175,** 5341–5350

245. Nagarkar, D. R., Bowman, E. R., Schneider, D., Wang, Q., Shim, J., Zhao, Y., Linn, M. J., McHenry, C. L., Gosangi, B., Bentley, J. K., Tsai, W. C., Sajjan, U. S., Lukacs, N. W. & Hershenson, M. B. (2010). Rhinovirus Infection of Allergen-Sensitized and -Challenged Mice Induces Eotaxin Release from Functionally Polarized Macrophages. *J Immunol*. **185,** 2525–2535

246. Beal, D. R., Stepien, D. M., Natarajan, S., Kim, J. & Remick, D. G. (2013). Reduction of eotaxin production and eosinophil recruitment by pulmonary autologous macrophage transfer in a cockroach allergen-induced asthma model. *Am J Physiol - Lung Cell Mol Physiol*. **305,** L866-77

247. Liang, Z., Zhang, Q., Thomas, C. M. R., Chana, K. K., Gibeon, D., Barnes, P. J., Chung, K. F., Bhavsar, P. K. & Donnelly, L. E. (2014). Impaired macrophage phagocytosis of bacteria in severe asthma. *Respir Res*. **15,** 72

248. Huynh, M. L. N., Malcolm, K. C., Kotaru, C., Tilstra, J. A., Westcott, J. Y., Fadok, V. A. & Wenzel, S. E. (2005). Defective apoptotic cell phagocytosis attenuates prostaglandin E 2 and 15-hydroxyeicosatetraenoic acid in severe asthma alveolar macrophages. *Am J Respir Crit Care Med*. **172,** 972–979

249. Berenson, C. S., Garlipp, M. A., Grove, L. J., Maloney, J. & Sethi, S. (2006). Impaired phagocytosis of nontypeable Haemophilus influenzae by human alveolar macrophages in chronic obstructive pulmonary disease. *J Infect Dis*. **194,** 1375–1384

250. Taylor, A. E., Finney-Hayward, T. K., Quint, J. K., Thomas, C. M. R., Tudhope, S. J., Wedzicha, J. A., Barnes, P. J. & Donnelly, L. E. (2010). Defective macrophage phagocytosis of bacteria in COPD. *Eur Respir J*. **35,** 1039–1047

251. Cox, N. J. & Subbarao, K. (2000). Global epidemiology of influenza: past and present. *Annu Rev Med*. **51,** 407–21

252. Morris, D. E., Cleary, D. W. & Clarke, S. C. (2017). Secondary bacterial infections associated with influenza pandemics. *Front Microbiol*. **8,** 1041

253. WHO. (2018). Influenza (Seasonal). Available at: https://www.who.int/news-room/fact-sheets/detail/influenza-(seasonal).

254. Tellier, R. (2006). Review of aerosol transmission of influenza A virus. *Emerg Infect Dis*. **12,** 1657–1662

255. Gerke, A. K., Yang, M., Tang, F., Foster, E. D., Cavanaugh, J. E. & Polgreen, P. M. (2014). Association of hospitalizations for asthma with seasonal and pandemic influenza. *Respirology*. **19,** 116–121

256. Memoli, M. J., Athota, R., Reed, S., Czajkowski, L., Bristol, T., Proudfoot, K., Hagey, R., Voell, J., Fiorentino, C., Ademposi, A., Shoham, S. & Taubenberger, J. K. (2014). The natural history of influenza infection in the severely immunocompromised vs nonimmunocompromised hosts. *Clin Infect Dis*. **58,** 214–224

257. Taubenberger, J. K. & Morens, D. M. (2009). Pandemic influenza--including a risk assessment of H5N1. *Rev Sci Tech*. **28,** 187–202

258. Hale, B. G., Albrecht, R. A. & García-Sastre, A. (2010). Innate immune evasion strategies of influenza viruses. *Future Microbiol*. **5,** 23–41

259. Horimoto, T. & Kawaoka, Y. (2001). Pandemic threat posed by avian influenza A viruses. *Clin Microbiol Rev*. **14,** 129–149

260. Saunders-Hastings, P. R. & Krewski, D. (2016). Reviewing the History of Pandemic Influenza: Understanding Patterns of Emergence and Transmission. *Pathog (Basel, Switzerland)*. **5,**

261. Lee, L. N., Dias, P., Han, D., Yoon, S., Shea, A., Zakharov, V., Parham, D. & Sarawar, S. R. (2010). A mouse model of lethal synergism between influenza virus and Haemophilus influenzae. *Am J Pathol*. **176,** 800–811

262. Delaney, K. R. & Ferguson, J. (2011). Psychiatric Mental Health Nursing: A Dialogue on the Nature of Our Practice. *Arch Psychiatr Nurs*. **25,** 148–150

263. Breen, M., Nogales, A., Baker, S. F. & Martínez-Sobrido, L. (2016). Replication-competent influenza a viruses expressing reporter genes. *Viruses*. **8,** 1–28

264. Das, K., Aramini, J. M., Ma, L. C., Krug, R. M. & Arnold, E. (2010). Structures of influenza A proteins and insights into antiviral drug targets. *Nat Struct Mol Biol*. **17,** 530–538

265. Noda, T. & Kawaoka, Y. (2010). Structure of influenza virus ribonucleoprotein complexes and their packaging into virions. *Rev Med Virol*. **20,** 380–391

266. Turrell, L., Lyall, J. W., Tiley, L. S., Fodor, E. & Vreede, F. T. (2013). The role and assembly mechanism of nucleoprotein in influenza A virus ribonucleoprotein complexes. *Nat Commun*. **4,** 1591

267. Bouvier, N. M. & Palese, P. (2008). The biology of influenza viruses. *Vaccine*. **26,** D49–D53

268. Schnell, J. R. & Chou, J. J. (2008). Structure and mechanism of the M2 proton channel of influenza A virus. *Nature*. **451,** 591–595

269. Rossman, J. S. & Lamb, R. A. (2011). Influenza virus assembly and budding. *Virology*. **411,** 229–236

270. Vasin, A. V., Temkina, O. A., Egorov, V. V., Klotchenko, S. A., Plotnikova, M. A. & Kiselev, O. I. (2014). Molecular mechanisms enhancing the proteome of influenza A viruses: An overview of recently discovered proteins. *Virus Res*. **185,** 53–63

271. Skehel, J. J. & Wiley, D. C. (2000). Receptor binding and membrane fusion in virus entry: The influenza hemagglutinin. *Annu Rev Biochem*. **69,** 531–569

272. Pinto, L. H. & Lamb, R. A. (2006). The M2 proton channels of influenza A and B viruses. *J Biol Chem*. **281,** 8997–9000

273. Robb, N. C., Smith, M., Vreede, F. T. & Fodor, E. (2009). NS2/NEP protein regulates transcription and replication of the influenza virus RNA genome. *J Gen Virol*. **90,** 1398–1407

274. Zhang, J., Pekosz, A. & Lamb, R. A. (2000). Influenza Virus Assembly and Lipid Raft Microdomains: a Role for the Cytoplasmic Tails of the Spike Glycoproteins. *J Virol*. **74,** 4634–4644

275. Nayak, D. P., Hui, E. K. W. & Barman, S. (2004). Assembly and budding of influenza virus. *Virus Res*. **106,** 147–165

276. Short, K. R., Brooks, A. G., Reading, P. C. & Londrigan, S. L. (2012). The fate of influenza A virus after infection of human macrophages and dendritic cells. *J Gen Virol*. **93,** 2315–2325

277. van Riel, D., Leijten, L. M. E., van der Eerden, M., Hoogsteden, H. C., Boven, L. A., Lambrecht, B. N., Osterhaus, A. D. M. E. & Kuiken, T. (2011). Highly pathogenic avian influenza virus H5N1 infects alveolar macrophages without virus production or excessive TNF-alpha induction. *PLoS Pathog*. **7,** e1002099

278. Yu, W. C. L., Chan, R. W. Y., Wang, J., Travanty, E. A., Nicholls, J. M., Peiris, J. S. M., Mason, R. J. & Chan, M. C. W. (2011). Viral Replication and Innate Host Responses in Primary

Human Alveolar Epithelial Cells and Alveolar Macrophages Infected with Influenza H5N1 and H1N1 Viruses. *J Virol*. **85,** 6844–6855

279. Tate, M. D., Brooks, A. G. & Reading, P. C. (2011). Correlation between sialic acid expression and infection of murine macrophages by different strains of influenza virus. *Microbes Infect*. **13,** 202–207

280. Reading, P. C., Miller, J. L. & Anders, E. M. (2000). Involvement of the Mannose Receptor in Infection of Macrophages by Influenza Virus. *J Virol*. **74,** 5190–5197

281. Upham, J. P., Pickett, D., Irimura, T., Anders, E. M. & Reading, P. C. (2010). Macrophage Receptors for Influenza A Virus: Role of the Macrophage Galactose-Type Lectin and Mannose Receptor in Viral Entry. *J Virol*. **84,** 3730–3737

282. Rodgers, B. & Mims, C. A. (1981). *Interaction of influenza virus with mouse macrophages*. *Infection and Immunity*. **31,**

283. Tate, M. D., Pickett, D. L., van Rooijen, N., Brooks, A. G. & Reading, P. C. (2010). Critical Role of Airway Macrophages in Modulating Disease Severity during Influenza Virus Infection of Mice. *J Virol*. **84,** 7569–7580

284. Westenius, V., Mäkelä, S. M., Julkunen, I. & Österlund, P. (2018). Highly pathogenic H5N1 influenza A virus spreads efficiently in human primary monocyte-derived macrophages and dendritic cells. *Front Immunol*. **9,** 1664

285. Marvin, S. A., Russier, M., Huerta, C. T., Russell, C. J. & Schultz-Cherry, S. (2017). Influenza Virus Overcomes Cellular Blocks To Productively Replicate, Impacting Macrophage Function. *J Virol*. **91,**

286. Le, V. L., Courtney, C. L., Steel, J. & Compans, R. W. (2013). Closely Related Influenza Viruses Induce Contrasting Respiratory Tract Immunopathology. *PLoS One*. **8,** e76708

287. Campbell, G. M., Nicol, M. Q., Dransfield, I., Shaw, D. J., Nash, A. A. & Dutia, B. M. (2015). Susceptibility of bone marrow-derived macrophages to influenza virus infection is dependent on macrophage phenotype. *J Gen Virol*. **96,** 2951–2960

288. Ison, M. G. (2011). Antivirals and resistance: Influenza virus. *Curr Opin Virol*. **1,** 563–573

289. van der Vries, E. & Ison, M. G. (Springer International Publishing., 2017). Antiviral Resistance in Influenza Viruses: Clinical and Epidemiological Aspects. in *Antimicrobial Drug Resistance*. 1165–1183 doi:10.1007/978-3-319-47266-9_23

290. Goldhill, D. H., Te Velthuis, A. J. W., Fletcher, R. A., Langat, P., Zambon, M., Lackenby, A. & Barclay, W. S. (2018). The mechanism of resistance to favipiravir in influenza. *Proc Natl Acad Sci U S A*. **115,** 11613–11618

291. Broadbent, A. J. & Subbarao, K. (2011). Influenza virus vaccines: Lessons from the 2009 H1N1 pandemic. *Curr Opin Virol*. **1,** 254–262

292. WHO. (2020). WHO Consultation and Information Meeting on the Composition of Influenza Virus Vaccines for Use in the 2021 Southern Hemisphere Influenza Season. *Who*. Available at: http://www.who.int/influenza/vaccines/virus/recommendations/consultation201502/en/.

293. Vasileiou, E., Sheikh, A., Butler, C., El Ferkh, K., Von Wissmann, B., McMenamin, J., Ritchie, L., Schwarze, J., Papadopoulos, N. G., Johnston, S. L., Tian, L. & Simpson, C. R. (2017). Efectiveness of influenza vaccines in Asthma: A systematic review and meta-analysis. *Clin Infect Dis*. **65,** 1388–1395

294. Blank, P. R., Schwenkglenks, M. & Szucs, T. D. (2009). Disparities in influenza vaccination coverage rates by target group in five European countries: Trends over seven consecutive seasons. *Infection*. **37,** 390–400

295. Eggo, R. M., Scott, J. G., Galvani, A. P. & Meyers, L. A. (2016). Respiratory virus transmission dynamics determine timing of asthma exacerbation peaks: Evidence from a population-level model. *Proc Natl Acad Sci U S A*. **113,** 2194–2199

296. King, J. C., Stoddard, J. J., Gaglani, M. J., Moore, K. A., Magder, L., McClure, E., Rubin, J. D., Englund, J. A. & Neuzil, K. (2006). Effectiveness of school-based influenza vaccination. *N Engl J Med*. **355,** 2523–32

297. Izurieta, H. S., Thompson, W. W., Kramarz, P., Shay, D. K., Davis, R. L., DeStefano, F., Black, S., Shinefield, H. & Fukuda, K. (2000). Influenza and the Rates of Hospitalization for Respiratory Disease among Infants and Young Children. *N Engl J Med*. **342,** 232–239

298. Peltola, V., Ziegler, T. & Ruuskanen, O. (2003). Influenza A and B virus infections in children. *Clin Infect Dis*. **36,** 299–305

299. Poehling, K. A., Edwards, K. M., Weinberg, G. A., Szilagyi, P., Staat, M. A., Iwane, M. K., Bridges, C. B., Grijalva, C. G., Zhu, Y., Bernstein, D. I., Herrera, G., Erdman, D., Hall, C. B., Seither, R. & Griffin, M. R. (2006). The Underrecognized Burden of Influenza in Young Children. *N Engl J Med*. **355,** 31–40

300. Silvennoinen, H., Peltola, V., Vainionpää, R., Ruuskanen, O. & Heikkinen, T. (2012). Admission diagnoses of children 0-16 years of age hospitalized with influenza. *Eur J Clin Microbiol Infect Dis*. **31,** 225–231

301. Reed, C., Chaves, S. S., Perez, A., D'Mello, T., Daily Kirley, P., Aragon, D., Meek, J. I., Farley, M. M., Ryan, P., Lynfield, R., Morin, C. A., Hancock, E. B., Bennett, N. M., Zansky, S. M.,

Thomas, A., Lindegren, M. L., Schaffner, W. & Finelli, L. (2014). Complications among adults hospitalized with influenza: A comparison of seasonal influenza and the 2009 H1N1 pandemic. *Clin Infect Dis*. **59,** 166–174

302. Puig-Barberà, J., Natividad-Sancho, A., Trushakova, S., Sominina, A., Pisareva, M., Ciblak, M. A., Badur, S., Yu, H., Cowling, B. J., El Guerche-Séblain, C., Mira-Iglesias, A., Kisteneva, L., Stolyarov, K., Yurtcu, K., Feng, L., López-Labrador, X., Burtseva, E., Afanasieva, V., Aktaş, F., Borekci, S., Buigues-Vila, A., Buzitskaya, Z., Cai, J., Çakir, B., Carballido-Fernández, M., Carratalá-Munuera, C., Chai, C., Chen, E., Çelebi, S., Cui, Y., Deniz, D. B., Dong, H., Dong, X., Durusu, M., Fadeev, A., Feng, S., Garina, E., Gencer, S., Gil-Guillén, V., Hacimustafaoğlu, M., Hancerli, S., Huang, L., Ip, D. K., Kolobukhina, L., Krasnoslobotsev, K., Li, C., Limón-Ramírez, R., Mahé, C., Merkulova, L., Mollar Maseres, J., Mukasheva, E., Ozisik, L., Otero-Reigada, M. C., Özer, S., Qin, Y., Eren-Şensoy, A., Smorodintseva, E., Sukhovetskaya, V., Sun, G., Tang, Y., Tormos, A., López-Labrador, F. X., Tortajada-Girbés, M., Vartanyan, R., Voloshchuk, L., Wang, Q., Wen, D., Wu, P., Yang, P., Yi, B., Zhang, S., Zhang, Y. & Zheng, J. (2016). Epidemiology of hospital admissions with influenza during the 2013/2014 Northern hemisphere influenza season: Results from the Global Influenza Hospital Surveillance Network. *PLoS One*. **11,** e0154970

303. Teichtahl, H., Buckmaster, N. & Pertnikovs, E. (1997). The incidence of respiratory tract infection in adults requiring hospitalization for asthma. *Chest*. **112,** 591–596

304. Dawood, F. S., Kamimoto, L., D'Mello, T. A., Reingold, A., Gershman, K., Meek, J., Arnold, K. E., Farley, M., Ryan, P., Lynfield, R., Morin, C., Baumbach, J., Zansky, S., Bennett, N., Thomas, A., Schaffner, W., Kirschke, D., Finelli, L. & Emerging Infections Program Network. (2011). Children with asthma hospitalized with seasonal or pandemic influenza, 2003-2009. *Pediatrics*. **128,** e27-32

305. Dawood, F. S., Iuliano, A. D., Reed, C., Meltzer, M. I., Shay, D. K., Cheng, P. Y., Bandaranayake, D., Breiman, R. F., Brooks, W. A., Buchy, P., Feikin, D. R., Fowler, K. B., Gordon, A., Hien, N. T., Horby, P., Huang, Q. S., Katz, M. A., Krishnan, A., Lal, R., Montgomery, J. M., Mølbak, K., Pebody, R., Presanis, A. M., Razuri, H., Steens, A., Tinoco, Y. O., Wallinga, J., Yu, H., Vong, S., Bresee, J. & Widdowson, M. A. (2012). Estimated global mortality associated with the first 12 months of 2009 pandemic influenza A H1N1 virus circulation: A modelling study. *Lancet Infect Dis*. **12,** 687–695

306. Simonsen, L., Spreeuwenberg, P., Lustig, R., Taylor, R. J., Fleming, D. M., Kroneman, M., Van Kerkhove, M. D., Mounts, A. W., Paget, W. J., Echenique, H., Savy, V., Muscatello, D., MacIntyre, C. R., Dwyer, D. E., Azziz-Baumgartner, E., Homaira, N., Moura, F. E. A., Schuck, C., Akwar, H., Schanzer, D., Fuentes, R., Olea, A., Sotomayor, V., Feng, L., Yu, H., Mazick, A.,

Mølbak, K., Nielsen, J., Carrat, F., Lemaitre, M., Buchholz, U., Schweiger, B., Höhle, M., Vesenbeckh, S., Cowling, B., Leung, G., Tsang, T., Chuang, S. K., Bromberg, M., Kaufman, Z., Sugaya, N., Oka Ezoe, K., Hayashi, S., Matsuda, M., Lopez-Gatell, H., Alpuche-Aranda, C., Noyola, D., Chowell, G., van Asten, L., Meijer, A., van den Wijngaard, K., van der Sande, M., Baker, M., Zhang, J., Benavides, J. G., Munayco, C., Laguna-Torres, A., Rabczenko, D., Wojtyniak, B., Park, S. H., Lee, Y. K., Zolotusca, L., Popovici, O., Popescu, R., Ang, L. W., Cutter, J., Lin, R., Ma, S., Chen, M., Lee, V. J., Prosenc, K., Socan, M., Cohen, C., Larrauri, A., de Mateo, S., Méndez, L. S., Sanz, C. D., Andrews, N., Green, H. K., Pebody, R., Saei, A., Shay, D. & Viboud, C. (2013). Global Mortality Estimates for the 2009 Influenza Pandemic from the GLaMOR Project: A Modeling Study. *PLoS Med*. **10,** e1001558

307. CDC. (2010). CDC H1N1 Flu | Underlying Health Conditions among Hospitalized Adults and Children. Available at: https://www.cdc.gov/H1N1flu/eip_underlying_conditions.htm.

308. Busse, W. W., Peters, S. P., Fenton, M. J., Mitchell, H., Bleecker, E. R., Castro, M., Wenzel, S., Erzurum, S. C., Fitzpatrick, A. M. & Teague, W. G. (2011). Vaccination of patients with mild and severe asthma with a 2009 pandemic H1N1 influenza virus vaccine. *J Allergy Clin Immunol*. **127,** 130-137.e3

309. Veerapandian, R., Snyder, J. D. & Samarasinghe, A. E. (2018). Influenza in Asthmatics: For Better or for Worse? *Front Immunol*. **9,** 1843

310. Jain, S., Kamimoto, L., Bramley, A. M., Schmitz, A. M., Benoit, S. R., Louie, J., Sugerman, D. E., Druckenmiller, J. K., Ritger, K. A., Chugh, R., Jasuja, S., Deutscher, M., Chen, S., Walker, J. D., Duchin, J. S., Lett, S., Soliva, S., Wells, E. V., Swerdlow, D., Uyeki, T. M., Fiore, A. E., Olsen, S. J., Fry, A. M., Bridges, C. B. & Finelli, L. (2009). Hospitalized Patients with 2009 H1N1 Influenza in the United States, April–June 2009. *N Engl J Med*. **361,** 1935–1944

311. O'Riordan, S., Barton, M., Yau, Y., Read, S. E., Allen, U. & Tran, D. (2010). Risk factors and outcomes among children admitted to hospital with pandemic H1N1 influenza. *Cmaj*. **182,** 39–44

312. Wark, P. A. B., Johnston, S. L., Bucchieri, F., Powell, R., Puddicombe, S., Laza-Stanca, V., Holgate, S. T. & Davies, D. E. (2005). Asthmatic bronchial epithelial cells have a deficient innate immune response to infection with rhinovirus. *J Exp Med*. **201,** 937–947

313. Londrigan, S. L., Wakim, L. M., Smith, J., Haverkate, A. J., Brooks, A. G. & Reading, P. C. (2020). IFITM3 and type I interferons are important for the control of influenza A virus replication in murine macrophages. *Virology*. **540,** 17–22

314. Kim, H. M., Lee, Y.-W., Lee, K.-J., Kim, H. S., Cho, S. W., van Rooijen, N., Guan, Y. & Seo, S. H. (2008). Alveolar Macrophages Are Indispensable for Controlling Influenza Viruses in

Lungs of Pigs. *J Virol*. **82,** 4265–4274

315. Schneider, C., Nobs, S. P., Heer, A. K., Kurrer, M., Klinke, G., van Rooijen, N., Vogel, J. & Kopf, M. (2014). Alveolar Macrophages Are Essential for Protection from Respiratory Failure and Associated Morbidity following Influenza Virus Infection. *PLoS Pathog*. **10,** e1004053

316. Huang, F. F., Barnes, P. F., Feng, Y., Donis, R., Chroneos, Z. C., Idell, S., Allen, T., Perez, D. R., Whitsett, J. A., Dunussi-Joannopoulos, K. & Shams, H. (2011). GM-CSF in the Lung Protects against Lethal Influenza Infection. *Am J Respir Crit Care Med*. **184,** 259–268

317. Huang, H., Li, H., Zhou, P. & Ju, D. (2010). Protective effects of recombinant human granulocyte macrophage colony stimulating factor on H1N1 influenza virus-induced pneumonia in mice. *Cytokine*. **51,** 151–157

318. Wang, J., Nikrad, M. P., Travanty, E. A., Zhou, B., Phang, T., Gao, B., Alford, T., Ito, Y., Nahreini, P., Hartshorn, K., Wentworth, D., Dinarello, C. A. & Mason, R. J. (2012). Innate immune response of human alveolar macrophages during influenza a infection. *PLoS One*. **7,** e29879

319. Iwasaki, A. & Pillai, P. S. (2014). Innate immunity to influenza virus infection. *Nat Rev Immunol*. **14,** 315–328

320. Ichinohe, T., Pang, I. K. & Iwasaki, A. (2010). Influenza virus activates inflammasomes via its intracellular M2 ion channel. *Nat Immunol*. **11,** 404–410

321. Hoeve, M. A., Nash, A. A., Jackson, D., Randall, R. E. & Dransfield, I. (2012). Influenza virus A infection of human monocyte and macrophage subpopulations reveals increased susceptibility associated with cell differentiation. *PLoS One*. **7,** e29443

322. Woo, P. C. Y., Tung, E. T. K., Chan, K. H., Lau, C. C. Y., Lau, S. K. P. & Yuen, K. Y. (2010). Cytokine profiles induced by the novel swine-origin influenza A/H1N1 virus: Implications for treatment strategies. *J Infect Dis*. **201,** 346–353

323. Kaufmann, A., Salentin, R., Meyer, R. G., Bussfeld, D., Pauligk, C., Fesq, H., Hofmann, P., Nain, M., Gemsa, D. & Sprenger, H. (2001). Defense against influenza A virus infection: Essential role of the chemokine system. *Immunobiology*. **204,** 603–613

324. Perrone, L. A., Plowden, J. K., García-Sastre, A., Katz, J. M. & Tumpey, T. M. (2008). H5N1 and 1918 pandemic influenza virus infection results in early and excessive infiltration of macrophages and neutrophils in the lungs of mice. *PLoS Pathog*. **4,** e1000115

325. Cheung, C. Y., Poon, L. L. M., Lau, A. S., Luk, W., Lau, Y. L., Shortridge, K. F., Gordon, S., Guan, Y. & Peiris, J. S. M. (2002). Induction of proinflammatory cytokines in human

macrophages by influenza A (H5N1) viruses: A mechanism for the unusual severity of human disease? *Lancet*. **360,** 1831–1837

326. Baskin, C. R., Bielefeldt-Ohmann, H., Tumpey, T. M., Sabourin, P. J., Long, J. P., García-Sastre, A., Tolnay, A.-E., Albrecht, R., Pyles, J. A., Olson, P. H., Aicher, L. D., Rosenzweig, E. R., Murali-Krishna, K., Clark, E. A., Kotur, M. S., Fornek, J. L., Proll, S., Palermo, R. E., Sabourin, C. L. & Katze, M. G. (2009). Early and sustained innate immune response defines pathology and death in nonhuman primates infected by highly pathogenic influenza virus. *Proc Natl Acad Sci U S A*. **106,** 3455–60

327. Fujimoto, I., Pan, J., Takizawa, T. & Nakanishi, Y. (2000). Virus clearance through apoptosis-dependent phagocytosis of influenza A virus-infected cells by macrophages. *J Virol*. **74,** 3399–403

328. Hashimoto, Y., Moki, T., Takizawa, T., Shiratsuchi, A. & Nakanishi, Y. (2007). Evidence for Phagocytosis of Influenza Virus-Infected, Apoptotic Cells by Neutrophils and Macrophages in Mice. *J Immunol*. **178,** 2448–2457

329. Lehtinen, P., Jartti, T., Virkki, R., Vuorinen, T., Leinonen, M., Peltola, V., Ruohola, A. & Ruuskanen, O. (2006). Bacterial coinfections in children with viral wheezing. *Eur J Clin Microbiol Infect Dis*. **25,** 463–469

330. Kloepfer, K. M., Lee, W. M., Pappas, T. E., Kang, T. J., Vrtis, R. F., Evans, M. D., Gangnon, R. E., Bochkov, Y. A., Jackson, D. J., Lemanske, R. F. & Gern, J. E. (2014). Detection of pathogenic bacteria during rhinovirus infection is associated with increased respiratory symptoms and asthma exacerbations. *J Allergy Clin Immunol*. **133,** 1301-1307.e3

331. Kloepfer, K. M., Sarsani, V. K., Poroyko, V., Lee, W. M., Pappas, T. E., Kang, T., Grindle, K. A., Bochkov, Y. A., Janga, S. C., Lemanske, R. F. & Gern, J. E. (2017). Community-acquired rhinovirus infection is associated with changes in the airway microbiome. *J Allergy Clin Immunol*. **140,** 312-315.e8

332. Wilkinson, T. M. A., Aris, E., Bourne, S., Clarke, S. C., Peeters, M., Pascal, T. G., Schoonbroodt, S., Tuck, A. C., Kim, V., Ostridge, K., Staples, K. J., Williams, N., Williams, A., Wootton, S. & Devaster, J. M. (2017). A prospective, observational cohort study of the seasonal dynamics of airway pathogens in the aetiology of exacerbations in COPD. *Thorax*. **72,** 919–927

333. DeMuri, G. P., Gern, J. E., Eickhoff, J. C., Lynch, S. V & Wald, E. R. (2018). Dynamics of Bacterial Colonization With Streptococcus pneumoniae, Haemophilus influenzae, and Moraxella catarrhalis During Symptomatic and Asymptomatic Viral Upper Respiratory Tract Infection. *Clin Infect Dis*. **66,** 1045–1053

334. Wark, P. A. B., Tooze, M., Powell, H. & Parsons, K. (2013). Viral and bacterial infection in acute asthma and chronic obstructive pulmonary disease increases the risk of readmission. *Respirology*. **18,** 996–1002

335. Bønnelykke, K., Vissing, N. H., Sevelsted, A., Johnston, S. L. & Bisgaard, H. (2015). Association between respiratory infections in early life and later asthma is independent of virus type. *J Allergy Clin Immunol*. **136,** 81-86.e4

336. Blyth, C. C., Webb, S. A. R., Kok, J., Dwyer, D. E., van Hal, S. J., Foo, H., Ginn, A. N., Kesson, A. M., Seppelt, I., Iredell, J. R., Bennett, G., Ong, L., Nand, K., Reece, G., Sara, T., Bishop, G., Festa, M., Li, F., Blythe, D., Palermo, A., Parr, M., Micallef, S., Hoyling, L., Weisbrodt, L., Shehabi, Y., Campbell, M., Stockdale, V., Erickson, S., Chamberlain, J., Gould, A., McEntaggart, G., Webb, S., Inskip, D., Lamb, D., Myburgh, J., Sidoli, R., Numa, A., Williams, G., Young, J., Boyd, R., Nayyar, V., Skelly, C., Stachowski, E., Sterba, M., Johnson, B., van Hal, S. J., Branley, J., Rawlinson, W. D., Outhred, A., Flexman, J., Dwyer, D. E., Foo, H., Kok, J., McPhie, K., Patterson, J. & Foo, H. (2013). The impact of bacterial and viral co-infection in severe influenza. *Influenza Other Respi Viruses*. **7,** 168–176

337. Klein, E. Y., Monteforte, B., Gupta, A., Jiang, W., May, L., Hsieh, Y. H. & Dugas, A. (2016). The frequency of influenza and bacterial coinfection: a systematic review and meta-analysis. *Influenza Other Respi Viruses*. **10,** 394–403

338. Dao, C. N., Kamimoto, L., Nowell, M., Reingold, A., Gershman, K., Meek, J., Arnold, K. E., Farley, M., Ryan, P., Lynfield, R., Morin, C., Baumbach, J., Hancock, E., Zansky, S., Bennett, N. M., Thomas, A., Vandermeer, M., Kirschke, D. L., Schaffner, W. & Finelli, L. (2010). Adult hospitalizations for laboratory-positive influenza during the 2005-2006 through 2007-2008 seasons in the United States. *J Infect Dis*. **202,** 881–888

339. Wilkinson, T. M. A., Hurst, J. R., Perera, W. R., Wilks, M., Donaldson, G. C. & Wedzicha, J. A. (2006). Effect of interactions between lower airway bacterial and rhinoviral infection in exacerbations of COPD. *Chest*. **129,** 317–324

340. Abt, M. C., Osborne, L. C., Monticelli, L. A., Doering, T. A., Alenghat, T., Sonnenberg, G. F., Paley, M. A., Antenus, M., Williams, K. L., Erikson, J., Wherry, E. J. & Artis, D. (2012). Commensal Bacteria Calibrate the Activation Threshold of Innate Antiviral Immunity. *Immunity*. **37,** 158–170

341. Wang, J., Li, F., Sun, R., Gao, X., Wei, H., Li, L.-J. & Tian, Z. (2013). Bacterial colonization dampens influenza-mediated acute lung injury via induction of M2 alveolar macrophages. *Nat Commun*. **4,** 2106

342. Rowe, H. M., Meliopoulos, V. A., Iverson, A., Bomme, P., Schultz-Cherry, S. & Rosch, J. W.

(2019). Direct interactions with influenza promote bacterial adherence during respiratory infections. *Nat Microbiol*. **4,** 1328–1336

343. David, S. C., Norton, T., Tyllis, T., Wilson, J. J., Singleton, E. V., Laan, Z., Davies, J., Hirst, T. R., Comerford, I., McColl, S. R., Paton, J. C. & Alsharifi, M. (2019). Direct interaction of whole-inactivated influenza A and pneumococcal vaccines enhances influenza-specific immunity. *Nat Microbiol*. **4,** 1316–1327

344. Ouyang, K., Woodiga, S. A., Dwivedi, V., Buckwalter, C. M., Singh, A. K., Binjawadagi, B., Hiremath, J., Manickam, C., Schleappi, R., Khatri, M., Wu, J., King, S. J. & Renukaradhya, G. J. (2014). Pretreatment of epithelial cells with live Streptococcus pneumoniae has no detectable effect on influenza a virus replication in vitro. *PLoS One*. **9,** e90066

345. Hartwig, S. M., Ketterer, M., Apicella, M. A. & Varga, S. M. (2016). Non-typeable Haemophilus influenzae protects human airway epithelial cells from a subsequent respiratory syncytial virus challenge. *Virology*. **498,** 128–135

346. Gulraiz, F., Bellinghausen, C., Bruggeman, C. A. & Stassen, F. R. (2015). Haemophilus influenzae increases the susceptibility and inflammatory response of airway epithelial cells to viral infections. *FASEB J*. **29,** 849–858

347. Taylor, S. L., Leong, L. E. X., Choo, J. M., Wesselingh, S., Yang, I. A., Upham, J. W., Reynolds, P. N., Hodge, S., James, A. L., Jenkins, C., Peters, M. J., Baraket, M., Marks, G. B., Gibson, P. G., Simpson, J. L. & Rogers, G. B. (2018). Inflammatory phenotypes in patients with severe asthma are associated with distinct airway microbiology. *J Allergy Clin Immunol*. **141,** 94-103.e15

348. Olszewska-Sosińska, O., Zielnik-Jurkiewicz, B., Stępińska, M., Antos-Bielska, M., Lau-Dworak, M., Kozłowska, K. & Trafny, E. A. (2016). Persistence of non-typeable Haemophilus Influenzae in the pharynx of children with adenotonsillar hypertrophy after treatment with azithromycin. *Pathog Dis*. **74,** ftv106

349. Cooper, G. E., Ostridge, K., Khakoo, S. I., Wilkinson, T. M. A. & Staples, K. J. (2018). Human CD49a+ lung natural killer cell cytotoxicity in response to influenza A virus. *Front Immunol*. **9,** 1671

350. Ackland, J., Wallington, J., Cleary, D., Christodoulides, M. & Staples, K. (European Respiratory Society., 2017). The response of macrophages to Moraxella catarrhalis infection. in *European Respiratory Journal*. **50,** PA4127

351. Staples, K. J., Nicholas, B., McKendry, R. T., Spalluto, C. M., Wallington, J. C., Bragg, C. W., Robinson, E. C., Martin, K., Djukanović, R. & Wilkinson, T. M. A. (2015). Viral infection of human lung macrophages increases PDL1 expression via IFNβ. *PLoS One*. **10,** e0121527

352. Wallington, J. C., Williams, A. P., Staples, K. J. & Wilkinson, T. M. A. (2018). IL-12 and IL-7 synergize to control mucosal-associated invariant T-cell cytotoxic responses to bacterial infection. *Journal of Allergy and Clinical Immunology*. **141,** 2182-2195.e6

353. Robinson, M. D., McCarthy, D. J. & Smyth, G. K. (2009). edgeR: A Bioconductor package for differential expression analysis of digital gene expression data. *Bioinformatics*. **26,** 139–140

354. Anders, S. & Huber, W. (2010). Differential expression analysis for sequence count data. *Genome Biol*. **11,** R106

355. Azim, A., Mistry, H., Freeman, A., Barber, C., Newell, C., Gove, K., Thirlwall, Y., Harvey, M., Bentley, K., Knight, D., Long, K., Mitchell, F., Cheng, Y., Varkonyi-Sepp, J., Grabau, W., Dennison, P., Haitchi, H. M., Arshad, S. H., Djukanovic, R., Wilkinson, T., Howarth, P. & Kurukulaaratchy, R. J. (2019). Protocol for the Wessex AsThma CoHort of difficult asthma (WATCH): A pragmatic real-life longitudinal study of difficult asthma in the clinic. *BMC Pulm Med*. **19,** 99

356. Tudhope, S. J., Finney-Hayward, T. K., Nicholson, A. G., Mayer, R. J., Barnette, M. S., Barnes, P. J. & Donnelly, L. E. (2008). Different mitogen-activated protein kinase-dependent cytokine responses in cells of the monocyte lineage. *J Pharmacol Exp Ther*. **324,** 306–312

357. Akagawa, K. S., Komuro, I., Kanazawa, H., Yamazaki, T., Mochida, K. & Kishi, F. (2006). Functional heterogeneity of colony-stimulating factor-induced human monocyte-derived macrophages. *Respirology*. **11,** 27–34

358. Winkler, A. R., Nocka, K. H., Sulahian, T. H., Kobzik, L. & Williams, C. M. M. (2008). In vitro modeling of human alveolar macrophage smoke exposure: Enhanced inflammation and impaired function. *Exp Lung Res*. **34,** 599–629

359. Ritz, S. A., Stämpfli, M. R., Davies, D. E., Holgate, S. T. & Jordana, M. (2002). On the generation of allergic airway diseases: From GM-CSF to Kyoto. *Trends Immunol*. **23,** 396–402

360. Bezrukov, A. V. (2017). Romanowsky staining, the Romanowsky effect and thoughts on the question of scientific priority. *Biotech Histochem*. **92,** 29–35

361. Pavord, I. D., Brightling, C. E., Woltmann, G. & Wardlaw, A. J. (1999). Non-eosinophilic corticosteroid unresponsive asthma. *Lancet*. **353,** 2213–2214

362. Hastie, A. T., Moore, W. C., Meyers, D. A., Vestal, P. L., Li, H., Peters, S. P. & Bleecker, E. R. (2010). Analyses of asthma severity phenotypes and inflammatory proteins in subjects stratified by sputum granulocytes. *J Allergy Clin Immunol*. **125,** 1028-1036.e13

363. Barber, C., Ward, J., Elliott, S., Lau, L., Azim, A., Gove, K., Rupani, H., Brown, T., Chauhan, A., Staples, K. J. & Howarth, P. H. (European Respiratory Society (ERS)., 2020). Comparison of two published definitions of sputum neutrophilia show clinical measures of disease are more severe in neutrophilic asthma (NA) than non-neutrophilic asthma (NNA) using >40% sputum neutrophils as the definition of disease. in *European Respiratory Journal*. **56,** 1255

364. Staples, K. J., Taylor, S., Thomas, S., Leung, S., Cox, K., Pascal, T. G., Ostridge, K., Welch, L., Tuck, A. C., Clarke, S. C., Gorringe, A. & Wilkinson, T. M. A. (2016). Relationships between mucosal antibodies, non-typeable Haemophilus influenzae (NTHi) infection and airway inflammation in COPD. *PLoS One*. **11,** e0167250

365. Hood, D. W., Makepeace, K., Deadman, M. E., Rest, R. F., Thibault, P., Martin, A., Richards, J. C. & Moxon, E. R. (1999). Sialic acid in the lipopolysaccharide of Haemophilus influenzae: Strain distribution, influence on serum resistance and structural characterization. *Mol Microbiol*. **33,** 679–692

366. Cody, A. J., Field, D., Feil, E. J., Stringer, S., Deadman, M. E., Tsolaki, A. G., Gratz, B., Bouchet, V., Goldstein, R., Hood, D. W. & Moxon, E. R. (2003). High rates of recombination in otitis media isolates of non-typeable Haemophilus influenzae. *Infect Genet Evol*. **3,** 57–66

367. Osman, K. L. (2017). Characterisation of Haemophilus influenzae and Haemophilus haemolyticus in Chronic Obstructive Pulmonary Disease (COPD). *University of Southampton Research Repository ePrints Soton*. **PhD Thesis,**

368. Osman, K. L., Jefferies, J. M. C., Woelk, C. H., Devos, N., Pascal, T. G., Mortier, M.-C., Devaster, J.-M., Wilkinson, T. M. A., Cleary, D. W., Clarke, S. C. & AERIS Study Group. (2018). Patients with Chronic Obstructive Pulmonary Disease harbour a variation of Haemophilus species. *Sci Rep*. **8,** 14734

369. Kirkham, L.-A. S., Corscadden, K. J., Wiertsema, S. P., Currie, A. J. & Richmond, P. C. (2013). A practical method for preparation of pneumococcal and nontypeable Haemophilus influenzae inocula that preserves viability and immunostimulatory activity. *BMC Res Notes*. **6,** 522

370. Treangen, T. J., Ondov, B. D., Koren, S. & Phillippy, A. M. (2014). The Harvest suite for rapid core-genome alignment and visualization of thousands of intraspecific microbial genomes. *Genome Biol*. **15,** 524

371. Harrison, A., Dyer, D. W., Gillaspy, A., Ray, W. C., Mungur, R., Carson, M. B., Zhong, H., Gipson, J., Gipson, M., Johnson, L. S., Lewis, L., Bakaletz, L. O. & Munson, R. S. (2005). Genomic sequence of an otitis media isolate of nontypeable Haemophilus influenzae:

Comparative study with H. influenzae serotype d, strain KW20. *J Bacteriol*. **187,** 4627–4636

372. De Chiara, M., Hood, D., Muzzi, A., Pickard, D. J., Perkins, T., Pizza, M., Dougan, G., Rappuoli, R., Moxon, E. R., Soriani, M. & Donati, C. (2014). Genome sequencing of disease and carriage isolates of nontypeable Haemophilus influenzae identifies discrete population structure. *Proc Natl Acad Sci U S A*. **111,** 5439–5444

373. Marsh, J. W., Humphrys, M. S. & Myers, G. S. A. (2017). A laboratory methodology for dual RNA-sequencing of bacteria and their host cells in vitro. *Front Microbiol*. **8,** 1830

374. Dobin, A., Davis, C. A., Schlesinger, F., Drenkow, J., Zaleski, C., Jha, S., Batut, P., Chaisson, M. & Gingeras, T. R. (2013). STAR: Ultrafast universal RNA-seq aligner. *Bioinformatics*. **29,** 15–21

375. Langmead, B. & Salzberg, S. L. (2012). Fast gapped-read alignment with Bowtie 2. *Nat Methods*. **9,** 357–359

376. Seemann, T. (2014). Prokka: Rapid prokaryotic genome annotation. *Bioinformatics*. **30,** 2068–2069

377. Conesa, A., Madrigal, P., Tarazona, S., Gomez-Cabrero, D., Cervera, A., McPherson, A., Szcześniak, M. W., Gaffney, D. J., Elo, L. L., Zhang, X. & Mortazavi, A. (2016). A survey of best practices for RNA-seq data analysis. *Genome Biol*. **17,** 13

378. Love, M. I., Huber, W. & Anders, S. (2014). Moderated estimation of fold change and dispersion for RNA-seq data with DESeq2. *Genome Biol*. **15,** 550

379. Langfelder, P. & Horvath, S. (2008). WGCNA: An R package for weighted correlation network analysis. *BMC Bioinformatics*. **9,** 559

380. Chin, C. H., Chen, S. H., Wu, H. H., Ho, C. W., Ko, M. T. & Lin, C. Y. (2014). cytoHubba: Identifying hub objects and sub-networks from complex interactome. *BMC Syst Biol*. **8,** S11

381. Chen, J., Bardes, E. E., Aronow, B. J. & Jegga, A. G. (2009). ToppGene Suite for gene list enrichment analysis and candidate gene prioritization. *Nucleic Acids Res*. **37,** 305–311

382. Ge, S. X., Jung, D., Jung, D. & Yao, R. (2020). ShinyGO: A graphical gene-set enrichment tool for animals and plants. *Bioinformatics*. **36,** 2628–2629

383. Matsuzaki, Y., Umemoto, T., Tanaka, Y., Okano, T. & Yamato, M. (2015). β2-Microglobulin is an appropriate reference gene for RT-PCR-based gene expression analysis of hematopoietic stem cells. *Regen Ther*. **1,** 91–97

384. Piehler, A. P., Grimholt, R. M., Øvstebø, R. & Berg, J. P. (2010). Gene expression results in lipopolysaccharide-stimulated monocytes depend significantly on the choice of reference genes. *BMC Immunol*. **11,** 21

385. Stephens, A. S., Stephens, S. R. & Morrison, N. A. (2011). Internal control genes for quantitative RT-PCR expression analysis in mouse osteoblasts, osteoclasts and macrophages. *BMC Res Notes*. **4,** 410

386. Coughtrie, A. L., Morris, D. E., Anderson, R., Begum, N., Cleary, D. W., Faust, S. N., Jefferies, J. M., Kraaijeveld, A. R., Moore, M. V., Mullee, M. A., Roderick, P. J., Tuck, A., Whittaker, R. N., Yuen, H. M., Doncaster, C. P. & Clarke, S. C. (2018). Ecology and diversity in upper respiratory tract microbial population structures from a cross-sectional community swabbing study. *J Med Microbiol*. **67,** 1096–1108

387. Abràmoff, M. D., Magalhães, P. J. & Ram, S. J. (2004). Image processing with imageJ. *Biophotonics International*. **11,** 36–41

388. Schindelin, J., Arganda-Carreras, I., Frise, E., Kaynig, V., Longair, M., Pietzsch, T., Preibisch, S., Rueden, C., Saalfeld, S., Schmid, B., Tinevez, J. Y., White, D. J., Hartenstein, V., Eliceiri, K., Tomancak, P. & Cardona, A. (2012). Fiji: An open-source platform for biological-image analysis. *Nature Methods*. **9,** 676–682

389. Galili, T. (2015). dendextend: An R package for visualizing, adjusting and comparing trees of hierarchical clustering. *Bioinformatics*. **31,** 3718–3720

390. Walter, W., Sánchez-Cabo, F. & Ricote, M. (2015). GOplot: An R package for visually combining expression data with functional analysis. *Bioinformatics*. **31,** 2912–2914

391. Kucera, M., Isserlin, R., Arkhangorodsky, A. & Bader, G. D. (2016). AutoAnnotate: A Cytoscape app for summarizing networks with semantic annotations. *F1000Research*. **5,** 1717

392. Morris, J. H., Apeltsin, L., Newman, A. M., Baumbach, J., Wittkop, T., Su, G., Bader, G. D. & Ferrin, T. E. (2011). ClusterMaker: A multi-algorithm clustering plugin for Cytoscape. *BMC Bioinformatics*. **12,** 436

393. Shannon, P., Markiel, A., Ozier, O., Baliga, N. S., Wang, J. T., Ramage, D., Amin, N., Schwikowski, B. & Ideker, T. (2003). Cytoscape: A software Environment for integrated models of biomolecular interaction networks. *Genome Res*. **13,** 2498–2504

394. Merico, D., Isserlin, R., Stueker, O., Emili, A. & Bader, G. D. (2010). Enrichment Map: A Network-Based Method for Gene-Set Enrichment Visualization and Interpretation. *PLoS One*. **5,** e13984

395. Oesper, L., Merico, D., Isserlin, R. & Bader, G. D. (2011). WordCloud: A Cytoscape plugin to create a visual semantic summary of networks. *Source Code Biol Med*. **6,** 7

396. Ignatchenko, V., Ignatchenko, A., Sinha, A., Boutros, P. C. & Kislinger, T. (2015). VennDIS: A

JavaFX-based Venn and Euler diagram software to generate publication quality figures. *Proteomics*. **15,** 1239–1244

397. Rusinova, I., Forster, S., Yu, S., Kannan, A., Masse, M., Cumming, H., Chapman, R. & Hertzog, P. J. (2013). Interferome v2.0: an updated database of annotated interferon-regulated genes. *Nucleic Acids Res*. **41,** D1040-6

398. Kumar, K., Chakraborty, A. & Chakrabarti, S. (2020). PresRAT: a server for identification of bacterial small-RNA sequences and their targets with probable binding region. *RNA Biol*. **00,** 1–8

399. Oliveros, J. C. (2007). VENNY. An interactive tool for comparing lists with Venn Diagrams. Available at: http://bioinfogp.cnnb.csic.es/tools/venny/index.html.

400. Taylor, S. L., Leong, L. E. X., Choo, J. M., Wesselingh, S., Yang, I. A., Upham, J. W., Reynolds, P. N., Hodge, S., James, A. L., Jenkins, C., Peters, M. J., Baraket, M., Marks, G. B., Gibson, P. G., Simpson, J. L. & Rogers, G. B. (2018). Inflammatory phenotypes in patients with severe asthma are associated with distinct airway microbiology. *J Allergy Clin Immunol*. **141,** 94-103.e15

401. Westermann, A. J., Gorski, S. A. & Vogel, J. (2012). Dual RNA-seq of pathogen and host. *Nat Rev Microbiol*. **10,** 618–630

402. Rapaport, F., Khanin, R., Liang, Y., Pirun, M., Krek, A., Zumbo, P., Mason, C. E., Socci, N. D. & Betel, D. (2013). Comprehensive evaluation of differential gene expression analysis methods for RNA-seq data. *Genome Biol*. **14,** R95

403. Cooper, G. E. (2018). Natural Killer Cell Responses to Influenza A Virus in the Human Lung. *University of Southampton Research Repository ePrints Soton*. **PhD Thesis,** 163

404. Kihlström, E. & Andåker, L. (1985). Inability of gentamicin and fosfomycin to eliminate intracellular enterobacteriaceae. *J Antimicrob Chemother*. **15,** 723–728

405. Volgers, C., Benedikter, B. J., Grauls, G. E., Savelkoul, P. H. M. & Stassen, F. R. M. (2017). Immunomodulatory role for membrane vesicles released by THP-1 macrophages and respiratory pathogens during macrophage infection. *BMC Microbiol*. **17,** 216

406. King, P., Ngui, J., Oppedisano, F., Robins-Browne, R., Holmes, P. & Holdsworth, S. (2008). Effect of interferon gamma and CD40 ligation on intracellular monocyte survival of nontypeable Haemophilus influenzae. *APMIS*. **116,** 1043–9

407. Pickering, J. L., Prosser, A., Corscadden, K. J., de Gier, C., Richmond, P. C., Zhang, G., Thornton, R. B. & Kirkham, L.-A. S. (2016). Haemophilus haemolyticus Interaction with Host Cells Is Different to Nontypeable Haemophilus influenzae and Prevents NTHi Association

with Epithelial Cells. *Front Cell Infect Microbiol*. **6,** 50

408. Raza, S., Barnett, M. W., Barnett-Itzhaki, Z., Amit, I., Hume, D. A. & Freeman, T. C. (2014). Analysis of the transcriptional networks underpinning the activation of murine macrophages by inflammatory mediators. *J Leukoc Biol*. **96,** 167–183

409. Rex, J., Albrecht, U., Ehlting, C., Thomas, M., Zanger, U. M., Sawodny, O., Häussinger, D., Ederer, M., Feuer, R. & Bode, J. G. (2016). Model-Based Characterization of Inflammatory Gene Expression Patterns of Activated Macrophages. *PLoS Comput Biol*. **12,** e1005018

410. Yadav, M. C., Chakraborti, A., Ray, P., Sapru, S., Majumdar, S. & Narang, A. (2003). Rapid detection of Haemophilus influenzae by hel gene polymerase chain reaction. *Lett Appl Microbiol*. **37,** 190–195

411. Kelly, B. & O'Neill, L. A. J. (2015). Metabolic reprogramming in macrophages and dendritic cells in innate immunity. *Cell Res*. **25,** 771–784

412. Erwin, A. L., Sandstedt, S. A., Bonthuis, P. J., Geelhood, J. L., Nelson, K. L., Unrath, W. C. T., Diggle, M. A., Theodore, M. J., Pleatman, C. R., Mothershed, E. A., Sacchi, C. T., Mayer, L. W., Gilsdorf, J. R. & Smith, A. L. (2008). Analysis of genetic relatedness of Haemophilus influenzae isolates by multilocus sequence typing. *J Bacteriol*. **190,** 1473–1483

413. Clementi, C. F. & Murphy, T. F. (2011). Non-typeable Haemophilus influenzae invasion and persistence in the human respiratory tract. *Front Cell Infect Microbiol*. **1,** 1

414. Szelestey, B. R., Heimlich, D. R., Raffel, F. K., Justice, S. S. & Mason, K. M. (2013). Haemophilus Responses to Nutritional Immunity: Epigenetic and Morphological Contribution to Biofilm Architecture, Invasion, Persistence and Disease Severity. *PLoS Pathog*. **9,** e1003709

415. Neupane, A. S., Willson, M., Chojnacki, A. K., Vargas E Silva Castanheira, F., Morehouse, C., Carestia, A., Keller, A. E., Peiseler, M., DiGiandomenico, A., Kelly, M. M., Amrein, M., Jenne, C., Thanabalasuriar, A. & Kubes, P. (2020). Patrolling Alveolar Macrophages Conceal Bacteria from the Immune System to Maintain Homeostasis. *Cell*. **183,** 110-125.e11

416. Fotakis, G. & Timbrell, J. A. (2006). In vitro cytotoxicity assays: Comparison of LDH, neutral red, MTT and protein assay in hepatoma cell lines following exposure to cadmium chloride. *Toxicol Lett*. **160,** 171–177

417. Mitchell, D. B., Santone, K. S. & Acosta, D. (1980). Evaluation of cytotoxicity in cultured cells by enzyme leakage. *J Tissue Cult Methods*. **6,** 113–116

418. Song, Y. J., Kim, A., Kim, G. T., Yu, H. Y., Lee, E. S., Park, M. J., Kim, Y. J., Shim, S. M. & Park, T. S. (2019). Inhibition of lactate dehydrogenase A suppresses inflammatory response in

RAW 264.7 macrophages. *Mol Med Rep*. **19,** 629–637

419. Daifuku, M., Nishi, K., Okamoto, T. & Sugahara, T. (2014). Activation of J774.1 murine macrophages by lactate dehydrogenase. *Cytotechnology*. **66,** 937–943

420. Russell, D. G., Huang, L. & VanderVen, B. C. (2019). Immunometabolism at the interface between macrophages and pathogens. *Nat Rev Immunol*. **19,** 291–304

421. Pettigrew, M. M., Ahearn, C. P., Gent, J. F., Kong, Y., Gallo, M. C., Munro, J. B., D'Mello, A., Sethi, S., Tettelin, H. & Murphy, T. F. (2018). Haemophilus influenzae genome evolution during persistence in the human airways in chronic obstructive pulmonary disease. *Proc Natl Acad Sci U S A*. **115,** E3256–E3265

422. Jiang, D., Tikhomirova, A. & Kidd, S. P. (2016). Haemophilus influenzae strains possess variations in the global transcriptional profile in response to oxygen levels and this influences sensitivity to environmental stresses. *Res Microbiol*. **167,** 13–19

423. Twigg, H. L., Morris, A., Ghedin, E., Curtis, J. L., Huffnagle, G. B., Crothers, K., Campbell, T. B., Flores, S. C., Fontenot, A. P., Beck, J. M., Huang, L., Lynch, S., Knox, K. S. & Weinstock, G. (2013). Use of bronchoalveolar lavage to assess the respiratory microbiome: Signal in the noise. *Lancet Respir Med*. **1,** 354–356

424. Segal, L. N. & Blaser, M. J. (2014). A brave new world: The lung microbiota in an era of change. *Ann Am Thorac Soc*. **11,** S21-7

425. Jaskowiak, P. A., Campello, R. J. G. B. & Costa, I. G. (2014). On the selection of appropriate distances for gene expression data clustering. *BMC Bioinformatics*. **15,** 17–19

426. Jolliffe, I. T. & Cadima, J. (2016). Principal component analysis: a review and recent developments. *Philos Trans A Math Phys Eng Sci*. **374,** 20150202

427. Koch, C. M., Chiu, S. F., Akbarpour, M., Bharat, A., Ridge, K. M., Bartom, E. T. & Winter, D. R. (2018). A beginner's guide to analysis of RNA sequencing data. *Am J Respir Cell Mol Biol*. **59,** 145–157

428. Dillies, M. A., Rau, A., Aubert, J., Hennequet-Antier, C., Jeanmougin, M., Servant, N., Keime, C., Marot, N. S., Castel, D., Estelle, J., Guernec, G., Jagla, B., Jouneau, L., Laloë, D., Le Gall, C., Schaëffer, B., Le Crom, S., Guedj, M. & Jaffrézic, F. (2013). A comprehensive evaluation of normalization methods for Illumina high-throughput RNA sequencing data analysis. *Brief Bioinform*. **14,** 671–683

429. Robinson, M. D. & Oshlack, A. (2010). A scaling normalization method for differential expression analysis of RNA-seq data. *Genome Biol*. **11,** R25

430. Yendrek, C. R., Ainsworth, E. A. & Thimmapuram, J. (2012). The bench scientist's guide to

statistical analysis of RNA-Seq data. *BMC Res Notes*. **5,** 506

431. Dalman, M. R., Deeter, A., Nimishakavi, G. & Duan, Z.-H. (2012). Fold change and p-value cutoffs significantly alter microarray interpretations. *BMC Bioinformatics*. **13 Suppl 2,** S11

432. Aprianto, R., Slager, J., Holsappel, S. & Veening, J.-W. (2016). Time-resolved dual RNA-seq reveals extensive rewiring of lung epithelial and pneumococcal transcriptomes during early infection. *Genome Biol*. **17,** 198

433. Pisu, D., Huang, L., Grenier, J. K. & Russell, D. G. (2020). Dual RNA-Seq of Mtb-Infected Macrophages In Vivo Reveals Ontologically Distinct Host-Pathogen Interactions. *Cell Rep*. **30,** 335-350.e4

434. Gillis, J. & Pavlidis, P. (2013). Assessing identity, redundancy and confounds in Gene Ontology annotations over time. *Bioinformatics*. **29,** 476–482

435. Houri, N., Huang, K.-C. & Nalbantoglu, J. (2013). The Coxsackievirus and Adenovirus Receptor (CAR) undergoes ectodomain shedding and regulated intramembrane proteolysis (RIP). *PLoS One*. **8,** e73296

436. Ge, S. X., Jung, D., Jung, D. & Yao, R. (2020). ShinyGO: A graphical gene-set enrichment tool for animals and plants. *Bioinformatics*. **36,** 2628–2629

437. Li, T., Qin, K., Li, N., Han, C. & Cao, X. (2019). An endosomal LAPF is required for macrophage endocytosis and elimination of bacteria. *Proc Natl Acad Sci U S A*. **116,** 12958–12963

438. Huynh, K. K., Eskelinen, E. L., Scott, C. C., Malevanets, A., Saftig, P. & Grinstein, S. (2007). LAMP proteins are required for fusion of lysosomes with phagosomes. *EMBO J*. **26,** 313–324

439. Clemans, D. L., Bauer, R. J., Hanson, J. A., Hobbs, M. V., St. Geme, J. W., Marrs, C. F. & Gilsdorf, J. R. (2000). Induction of proinflammatory cytokines from human respiratory epithelial cells after stimulation by nontypeable Haemophilus influenzae. *Infect Immun*. **68,** 4430–4440

440. Brewer, S. M., Brubaker, S. W. & Monack, D. M. (2019). Host inflammasome defense mechanisms and bacterial pathogen evasion strategies. *Curr Opin Immunol*. **60,** 63–70

441. Martinon, F., Burns, K. & Tschopp, J. (2002). The Inflammasome: A molecular platform triggering activation of inflammatory caspases and processing of proIL-β. *Mol Cell*. **10,** 417–426

442. Clark, S. E., Snow, J., Li, J., Zola, T. A. & Weiser, J. N. (2012). Phosphorylcholine allows for evasion of bactericidal antibody by Haemophilus influenzae. *PLoS Pathog*. **8,** e1002521

443. Ngo, C. C. & Man, S. M. (2017). Mechanisms and functions of guanylate-binding proteins and related interferon-inducible GTPases: Roles in intracellular lysis of pathogens. *Cell Microbiol*. **19,** e12791

444. Kim, B.-H., Shenoy, A. R., Kumar, P., Das, R., Tiwari, S. & MacMicking, J. D. (2011). A family of IFN-γ-inducible 65-kD GTPases protects against bacterial infection. *Science*. **332,** 717–21

445. Meunier, E., Wallet, P., Dreier, R. F., Costanzo, S., Anton, L., Rühl, S., Dussurgey, S., Dick, M. S., Kistner, A., Rigard, M., Degrandi, D., Pfeffer, K., Yamamoto, M., Henry, T. & Broz, P. (2015). Guanylate-binding proteins promote activation of the AIM2 inflammasome during infection with Francisella novicida. *Nat Immunol*. **16,** 476–484

446. Duncan, M. J., Shin, J. S. & Abraham, S. N. (2002). Microbial entry through caveolae: Variations on a theme. *Cell Microbiol*. **4,** 783–791

447. Sun, J., Deghmane, A.-E., Soualhine, H., Hong, T., Bucci, C., Solodkin, A. & Hmama, Z. (2007). Mycobacterium bovis BCG disrupts the interaction of Rab7 with RILP contributing to inhibition of phagosome maturation. *J Leukoc Biol*. **82,** 1437–1445

448. Binker, M. G., Cosen-Binker, L. I., Terebiznik, M. R., Mallo, G. V., Mccaw, S. E., Eskelinen, E. L., Willenborg, M., Brumell, J. H., Saftig, P., Grinstein, S. & Gray-Owen, S. D. (2007). Arrested maturation of Neisseria -containing phagosomes in the absence of the lysosome-associated membrane proteins, LAMP-1 and LAMP-2. *Cell Microbiol*. **9,** 2153–2166

449. Lamothe, J., Huynh, K. K., Grinstein, S. & Valvano, M. A. (2007). Intracellular survival of Burkholderia cenocepacia in macrophages is associated with a delay in the maturation of bacteria-containing vacuoles. *Cell Microbiol*. **9,** 40–53

450. Lee, E. J., Park, K. S., Jeon, I. S., Choi, J. W., Lee, S. J., Choy, H. E., Song, K. D., Lee, H. K. & Choi, J. K. (2016). LAMP-3 (lysosome-associated membrane protein 3) promotes the intracellular proliferation of Salmonella typhimurium. *Mol Cells*. **39,** 566–572

451. De Saint-Vis, B., Vincent, J., Vandenabeele, S., Vanbervliet, B., Pin, J. J., Aït-Yahia, S., Patel, S., Mattei, M. G., Banchereau, J., Zurawski, S., Davoust, J., Caux, C. & Lebecque, S. (1998). A novel lysosome-associated membrane glycoprotein, DC-LAMP, induced upon DC maturation, is transiently expressed in MHC class II compartment. *Immunity*. **9,** 325–336

452. Becker, M., De Bastiani, M. A., Parisi, M. M., Guma, F. T. C. R., Markoski, M. M., Castro, M. A. A., Kaplan, M. H., Barbé-Tuana, F. M. & Klamt, F. (2015). Integrated Transcriptomics Establish Macrophage Polarization Signatures and have Potential Applications for Clinical Health and Disease. *Sci Rep*. **5,** 1–12

453. Jubrail, J., Morris, P., Bewley, M. A., Stoneham, S., Johnston, S. A., Foster, S. J., Peden, A.

A., Read, R. C., Marriott, H. M. & Dockrell, D. H. (2016). Inability to sustain intraphagolysosomal killing of Staphylococcus aureus predisposes to bacterial persistence in macrophages. *Cell Microbiol*. **18,** 80–96

454. Fitzpatrick, A. M., Holguin, F., Teague, W. G. & Brown, L. A. S. (2008). Alveolar macrophage phagocytosis is impaired in children with poorly controlled asthma. *J Allergy Clin Immunol*. **121,** 1372-1378.e3

455. Tanno, A., Fujino, N., Yamada, M., Sugiura, H., Hirano, T., Tanaka, R., Sano, H., Suzuki, S., Okada, Y. & Ichinose, M. (2020). Decreased expression of a phagocytic receptor Siglec-1 on alveolar macrophages in chronic obstructive pulmonary disease. *Respir Res*. **21,** 1–11

456. Droemann, D., Goldmann, T., Tiedje, T., Zabel, P., Dalhoff, K. & Schaaf, B. (2005). Toll-like receptor 2 expression is decreased on alveolar macrophages in cigarette smokers and COPD patients. *Respir Res*. **6,** 68

457. Provost, K. A., Smith, M., Miller-Larsson, A., Gudleski, G. D. & Sethi, S. (2019). Bacterial regulation of macrophage bacterial recognition receptors in COPD are differentially modified by budesonide and fluticasone propionate. *PLoS One*. **14,** e0207675

458. Arango Duque, G. & Descoteaux, A. (2014). Macrophage cytokines: involvement in immunity and infectious diseases. *Front Immunol*. **5,** 491

459. Soehnlein, O. & Lindbom, L. (2010). Phagocyte partnership during the onset and resolution of inflammation. *Nature Reviews Immunology*. **10,** 427–439

460. Larché, M., Robinson, D. S. & Kay, A. B. (2003). The role of T lymphocytes in the pathogenesis of asthma. *Journal of Allergy and Clinical Immunology*. **111,** 450–463

461. Mosmann, T. R. & Coffman, R. L. (1989). TH1 and TH2 cells: different patterns of lymphokine secretion lead to different functional properties. *Annu Rev Immunol*. **7,** 145–73

462. Yang, X., Wang, Y., Zhao, S., Wang, R. & Wang, C. (2018). Long-term exposure to low-dose Haemophilus influenzae during allergic airway disease drives a steroid-resistant neutrophilic inflammation and promotes airway remodeling. *Oncotarget*. **9,** 24898–24913

463. Singhania, A., Wallington, J. C., Smith, C. G., Horowitz, D., Staples, K. J., Howarth, P. H., Gadola, S. D., Djukanović, R., Woelk, C. H. & Hinks, T. S. C. (2018). Multitissue transcriptomics delineates the diversity of airway T cell functions in asthma. *American Journal of Respiratory Cell and Molecular Biology*. **58,** 261–270

464. Busse, P. J., Birmingham, J. M., Calatroni, A., Manzi, J., Goryachokovsky, A., Fontela, G., Federman, A. D. & Wisnivesky, J. P. (2017). Effect of aging on sputum inflammation and asthma control. *J Allergy Clin Immunol*. **139,** 1808-1818.e6

465. Atack, J. M., Winter, L. E., Jurcisek, J. A., Bakaletz, L. O., Barenkamp, S. J. & Jennings, M. P. (2015). Selection and Counterselection of Hia Expression Reveals a Key Role for Phase-Variable Expression of Hia in Infection Caused by Nontypeable Haemophilus influenzae. *J Infect Dis*. **212,** 645–653

466. Vuong, J., Wang, X., Theodore, J. M., Whitmon, J., de Leon, P. G., Mayer, L. W., Carlone, G. M. & Romero-Steiner, S. (2013). Absence of high molecular weight proteins 1 and/or 2 is associated with decreased adherence among non-typeable Haemophilus influenzae clinical isolates. *J Med Microbiol*. **62,** 1649–1656

467. Euba, B., Moleres, J., Viadas, C., De Los Mozos, I. R., Valle, J., Bengoechea, J. A. & Garmendia, J. (2015). Relative contribution of P5 and Hap surface proteins to nontypable Haemophilus influenzae interplay with the host upper and lower airways. *PLoS One*. **10,** e0123154

468. Harrison, A., Ray, W. C., Baker, B. D., Armbruster, D. W., Bakaletz, L. O. & Munson, R. S. (2007). The OxyR regulon in nontypeable Haemophilus influenzae. *J Bacteriol*. **189,** 1004–1012

469. Stapels, D. A. C., Hill, P. W. S., Westermann, A. J., Fisher, R. A., Thurston, T. L., Saliba, A. E., Blommestein, I., Vogel, J. & Helaine, S. (2018). Salmonella persisters undermine host immune defenses during antibiotic treatment. *Science (80-)*. **362,** 1156–1160

470. Groeneveld, K., van Alphen, L., Eijk, P. P., Visschers, G., Jansen, H. M. & Zanen, H. C. (1990). Endogenous and exogenous reinfections by Haemophilus influenzae in patients with chronic obstructive pulmonary disease: The effect of antibiotic treatment on persistence. *Journal of Infectious Diseases*. **161,** 512–517

471. Möller, L. V. M., Regelink, A. G., Grasselier, H., Dankert-Roelse, J. E., Dankert, J. & van Alphen, L. (1995). Multiple Haemophilus influenzae strains and strain variants coexist in the respiratory tract of patients with cystic fibrosis. *J Infect Dis*. **172,** 1388–92

472. Fleischmann, R. D., Adams, M. D., White, O., Clayton, R. A., Kirkness, E. F., Kerlavage, A. R., Bult, C. J., Tomb, J. F., Dougherty, B. A. & Merrick, J. M. (1995). Whole-genome random sequencing and assembly of Haemophilus influenzae Rd. *Science*. **269,** 496–512

473. Ahrén, I. L., Williams, D. L., Rice, P. J., Forsgren, A. & Riesbeck, K. (2001). The importance of a β-glucan receptor in the nonopsonic entry of nontypeable Haemophilus influenzae into human monocytic and epithelial cells. *J Infect Dis*. **184,** 150–158

474. Ahrén, I. L., Janson, H., Forsgren, A. & Riesbeck, K. (2001). Protein D expression promotes the adherence and internalization of non-typeable Haemophilus influenzae into human monocytic cells. *Microb Pathog*. **31,** 151–158

475. Cholon, D. M., Cutter, D., Richardson, S. K., Sethi, S., Murphy, T. F., Look, D. C. & St. Geme, J. W. (2008). Serial isolates of persistent Haemophilus influenzae in patients with chronic obstructive pulmonary disease express diminishing quantities of the HMW1 and HMW2 adhesins. *Infect Immun*. **76,** 4463–4468

476. Sprenger, M., Kasper, L., Hensel, M. & Hube, B. (2018). Metabolic adaptation of intracellular bacteria and fungi to macrophages. *International Journal of Medical Microbiology*. **308,** 215–227

477. Lin, S. & Cronan, J. E. (2012). The BioC O-methyltransferase catalyzes methyl esterification of malonyl-acyl carrier protein, an essential step in biotin synthesis. *J Biol Chem*. **287,** 37010–37020

478. Sprenger, M., Hartung, T. S., Allert, S., Wisgott, S., Niemiec, M. J., Graf, K., Jacobsen, I. D., Kasper, L. & Hube, B. (2020). Fungal biotin homeostasis is essential for immune evasion after macrophage phagocytosis and virulence. *Cell Microbiol*. **22,**

479. Yu, J., Niu, C., Wang, D., Li, M., Teo, W., Sun, G., Wang, J., Liu, J. & Gao, Q. (2011). MMAR_2770, a new enzyme involved in biotin biosynthesis, is essential for the growth of Mycobacterium marinum in macrophages and zebrafish. *Microbes Infect*. **13,** 33–41

480. Napier, B. A., Meyer, L., Bina, J. E., Miller, M. A., Sjöstedt, A. & Weiss, D. S. (2012). Link between intraphagosomal biotin and rapid phagosomal escape in Francisella. *Proc Natl Acad Sci U S A*. **109,** 18084–18089

481. Othman, D. S. M. P., Schirra, H., McEwan, A. G. & Kappler, U. (2014). Metabolic versatility in Haemophilus influenzae: A metabolomic and genomic analysis. *Front Microbiol*. **5,**

482. Koeppen, K., Hampton, T. H., Jarek, M., Scharfe, M., Gerber, S. A., Mielcarz, D. W., Demers, E. G., Dolben, E. L., Hammond, J. H., Hogan, D. A. & Stanton, B. A. (2016). A Novel Mechanism of Host-Pathogen Interaction through sRNA in Bacterial Outer Membrane Vesicles. *PLoS Pathog*. **12,** e1005672

483. Petráčková, D., Farman, M. R., Amman, F., Linhartová, I., Dienstbier, A., Kumar, D., Držmíšek, J., Hofacker, I., Rodriguez, M. E. & Večerek, B. (2020). Transcriptional profiling of human macrophages during infection with Bordetella pertussis. *RNA Biol*. **17,** 731–742

484. Dillon, L. A. L., Suresh, R., Okrah, K., Corrada Bravo, H., Mosser, D. M. & El-Sayed, N. M. (2015). Simultaneous transcriptional profiling of Leishmania major and its murine macrophage host cell reveals insights into host-pathogen interactions. *BMC Genomics*. **16,** 1108–1108

485. Wilson, D. N. & Nierhaus, K. H. (2007). The weird and wonderful world of bacterial

ribosome regulation. *Crit Rev Biochem Mol Biol*. **42,** 187–219

486. Boutte, C. C. & Crosson, S. (2013). Bacterial lifestyle shapes stringent response activation. *Trends Microbiol*. **21,** 174–180

487. Loveland, A. B., Bah, E., Madireddy, R., Zhang, Y., Brilot, A. F., Grigorieff, N. & Korostelev, A. A. (2016). Ribosome•RelA structures reveal the mechanism of stringent response activation. *Elife*. **5,**

488. Sureka, K., Ghosh, B., Dasgupta, A., Basu, J., Kundu, M. & Bose, I. (2008). Positive feedback and noise activate the stringent response regulator rel in mycobacteria. *PLoS One*. **3,** e1771

489. Wong, S. M. S., Alugupalli, K. R., Ram, S. & Akerley, B. J. (2007). The ArcA regulon and oxidative stress resistance in Haemophilus influenzae. *Mol Microbiol*. **64,** 1375–1390

490. Pang, B., Hong, W., Kock, N. D. & Swords, W. E. (2012). Dps promotes survival of nontypeable Haemophilus influenzae in biofilm communities in vitro and resistance to clearance in vivo. *Front Cell Infect Microbiol*. **2,** 58

491. Groisman, E. A., Parra-Lopez, C., Salcedo, M., Lipps, C. J. & Heffron, F. (1992). Resistance to host antimicrobial peptides is necessary for Salmonella virulence. *Proc Natl Acad Sci U S A*. **89,** 11939–43

492. Mason, K. M., Munson, R. S. & Bakaletz, L. O. (2005). A mutation in the sap operon attenuates survival of nontypeable Haemophilus influenzae in a chinchilla model of otitis media. *Infect Immun*. **73,** 599–608

493. Mason, K. M., Bruggeman, M. E., Munson, R. S. & Bakaletz, L. O. (2006). The non-typeable Haemophilus influenzae Sap transporter provides a mechanism of antimicrobial peptide resistance and SapD-dependent potassium acquisition. *Mol Microbiol*. **62,** 1357–1372

494. Su, Y. C., Resman, F., Hörhold, F. & Riesbeck, K. (2014). Comparative genomic analysis reveals distinct genotypic features of the emerging pathogen Haemophilus influenzae type f. *BMC Genomics*. **15,** 1–23

495. Singh, S. K., Saisree, L., Amrutha, R. N. & Reddy, M. (2012). Three redundant murein endopeptidases catalyse an essential cleavage step in peptidoglycan synthesis of Escherichia coli K12. *Mol Microbiol*. **86,** 1036–1051

496. Nicholson, K. G., Kent, J. & Ireland, D. C. (1993). Respiratory viruses and exacerbations of asthma in adults. *Br Med J*. **307,** 982–986

497. Watson, A., Spalluto, C. M., McCrae, C., Cellura, D., Burke, H., Cunoosamy, D., Freeman, A., Hicks, A., Hühn, M., Ostridge, K., Staples, K. J., Vaarala, O. & Wilkinson, T. (2020). Dynamics

of IFN-β responses during respiratory viral infection insights for therapeutic strategies. *Am J Respir Crit Care Med*. **201,** 83–94

498. Lonsdale, R., Pau, M. G., Oerlemans, M., Ophorst, C., Vooys, A., Havenga, M., Goudsmit, J., UytdeHaag, F. & Marzio, G. (2003). A rapid method for immunotitration of influenza viruses using flow cytometry. *J Virol Methods*. **110,** 67–71

499. Ning, S., Pagano, J. S. & Barber, G. N. (2011). IRF7: Activation, regulation, modification and function. *Genes and Immunity*. **12,** 399–414

500. Dickson, R. P., Erb-Downward, J. R. & Huffnagle, G. B. (2015). Homeostasis and its disruption in the lung microbiome. *Am J Physiol Lung Cell Mol Physiol*. **309,** L1047-55

501. Hanada, S., Pirzadeh, M., Carver, K. Y. & Deng, J. C. (2018). Respiratory Viral Infection-Induced Microbiome Alterations and Secondary Bacterial Pneumonia. *Front Immunol*. **9,** 2640

502. Cleary, D., Devine, V., Morris, D., Osman, K., Gladstone, R., Bentley, S., Faust, S. & Clarke, S. (2018). Pneumococcal vaccine impacts on the population genomics of non-typeable Haemophilus influenzae. *Microb genomics*. **4,** 27

503. Diavatopoulos, D. A., Short, K. R., Price, J. T., Wilksch, J. J., Brown, L. E., Briles, D. E., Strugnell, R. A. & Wijburg, O. L. (2010). Influenza A virus facilitates Streptococcus pneumoniae transmission and disease . *FASEB J*. **24,** 1789–1798

504. Smith, A. M., Adler, F. R., Ribeiro, R. M., Gutenkunst, R. N., McAuley, J. L., McCullers, J. A. & Perelson, A. S. (2013). Kinetics of Coinfection with Influenza A Virus and Streptococcus pneumoniae. *PLoS Pathog*. **9,** e1003238

505. Tuvim, M. J., Evans, S. E., Clement, C. G., Dickey, B. F. & Gilbert, B. E. (2009). Augmented lung inflammation protects against influenza A pneumonia. *PLoS One*. **4,** e4176

506. Zhu, J., Message, S. D., Mallia, P., Kebadze, T., Contoli, M., Ward, C. K., Barnathan, E. S., Mascelli, M. A., Kon, O. M., Papi, A., Stanciu, L. A., Edwards, M. R., Jeffery, P. K. & Johnston, S. L. (2019). Bronchial mucosal IFN-α/β and pattern recognition receptor expression in patients with experimental rhinovirus-induced asthma exacerbations. *J Allergy Clin Immunol*. **143,** 114-125.e4

507. Pritchard, A. L., White, O. J., Burel, J. G., Carroll, M. L., Phipps, S. & Upham, J. W. (2014). Asthma is associated with multiple alterations in anti-viral innate signalling pathways. *PLoS One*. **9,** e106501

508. Sykes, A., Edwards, M. R., MacIntyre, J., Del Rosario, A., Bakhsoliani, E., Trujillo-Torralbo, M. B., Kon, O. M., Mallia, P., McHale, M. & Johnston, S. L. (2012). Rhinovirus 16-induced

IFN-α and IFN-β are deficient in bronchoalveolar lavage cells in asthmatic patients. *J Allergy Clin Immunol*. **129,** 1506-1514.e6

509. Aegerter, H., Kulikauskaite, J., Crotta, S., Patel, H., Kelly, G., Hessel, E. M., Mack, M., Beinke, S. & Wack, A. (2020). Influenza-induced monocyte-derived alveolar macrophages confer prolonged antibacterial protection. *Nat Immunol*. **21,** 145–157

510. Brundage, J. F. (2006). Interactions between influenza and bacterial respiratory pathogens: implications for pandemic preparedness. *Lancet Infect Dis*. **6,** 303–12

511. Bellinghausen, C., Gulraiz, F., Heinzmann, A. C. A., Dentener, M. A., Savelkoul, P. H. M., Wouters, E. F., Rohde, G. G. & Stassen, F. R. (2016). Exposure to common respiratory bacteria alters the airway epithelial response to subsequent viral infection. *Respir Res*. **17,** 68

512. Zhu, Z., Shi, Z., Yan, W., Wei, J., Shao, D., Deng, X., Wang, S., Li, B., Tong, G. & Ma, Z. (2013). Nonstructural Protein 1 of Influenza A Virus Interacts with Human Guanylate-Binding Protein 1 to Antagonize Antiviral Activity. *PLoS One*. **8,** 55920

513. Seelbinder, B., Wallstabe, J., Marischen, L., Weiss, E., Wurster, S., Page, L., Löffler, C., Bussemer, L., Schmitt, A.-L., Wolf, T., Linde, J., Cicin-Sain, L., Becker, J., Kalinke, U., Vogel, J., Panagiotou, G., Einsele, H., Westermann, A. J., Schäuble, S. & Loeffler, J. (2020). Triple RNA-Seq Reveals Synergy in a Human Virus-Fungus Co-infection Model. *Cell Rep*. **33,** 108389

514. Nakamura, S., Davis, K. M. & Weiser, J. N. (2011). Synergistic stimulation of type I interferons during influenza virus coinfection promotes Streptococcus pneumoniae colonization in mice. *J Clin Invest*. **121,** 3657–3665

515. Yang, S., Yin, Y., Xu, W., Zhang, X., Gao, Y., Liao, H., Hu, X., Wang, J. & Wang, H. (2019). Type I interferon induced by DNA of nontypeable Haemophilus influenza modulates inflammatory cytokine profile to promote susceptibility to this bacterium. *Int Immunopharmacol*. **74,** 105710

516. Zhu, Q., Man, S. M., Karki, R., Malireddi, R. K. S. & Kanneganti, T. D. (2018). Detrimental Type I Interferon Signaling Dominates Protective AIM2 Inflammasome Responses during Francisella novicida Infection. *Cell Rep*. **22,** 3168–3174

517. Rayamajhi, M., Humann, J., Penheiter, K., Andreasen, K. & Lenz, L. L. (2010). Induction of IFN-αβ enables Listeria monocytogenes to suppress macrophage activation by IFN-γ. *J Exp Med*. **207,** 327–337

518. Robinson, N., McComb, S., Mulligan, R., Dudani, R., Krishnan, L. & Sad, S. (2012). Type i

interferon induces necroptosis in macrophages during infection with Salmonella enterica serovar Typhimurium. *Nat Immunol*. **13,** 954–962

519. Antonelli, L. R. V., Rothfuchs, A. G., Gonçalves, R., Roffê, E., Cheever, A. W., Bafica, A., Salazar, A. M., Feng, C. G. & Sher, A. (2010). Intranasal poly-IC treatment exacerbates tuberculosis in mice through the pulmonary recruitment of a pathogen-permissive monocyte/macrophage population. *J Clin Invest*. **120,** 1674–1682

520. Naujoks, J., Tabeling, C., Dill, B. D., Hoffmann, C., Brown, A. S., Kunze, M., Kempa, S., Peter, A., Mollenkopf, H. J., Dorhoi, A., Kershaw, O., Gruber, A. D., Sander, L. E., Witzenrath, M., Herold, S., Nerlich, A., Hocke, A. C., van Driel, I., Suttorp, N., Bedoui, S., Hilbi, H., Trost, M. & Opitz, B. (2016). IFNs Modify the Proteome of Legionella-Containing Vacuoles and Restrict Infection Via IRG1-Derived Itaconic Acid. *PLoS Pathog*. **12,** e1005408

521. Ivin, M., Dumigan, A., de Vasconcelos, F. N., Ebner, F., Borroni, M., Kavirayani, A., Przybyszewska, K. N., Ingram, R. J., Lienenklaus, S., Kalinke, U., Stoiber, D., Bengoechea, J. A. & Kovarik, P. (2017). Natural killer cell-intrinsic type I IFN signaling controls Klebsiella pneumoniae growth during lung infection. *PLoS Pathog*. **13,** e1006696

522. LeMessurier, K. S., Häcker, H., Chi, L., Tuomanen, E. & Redecke, V. (2013). Type I Interferon Protects against Pneumococcal Invasive Disease by Inhibiting Bacterial Transmigration across the Lung. *PLoS Pathog*. **9,** e1003727

523. Verma, A. K., Bansal, S., Bauer, C., Muralidharan, A. & Sun, K. (2020). Influenza Infection Induces Alveolar Macrophage Dysfunction and Thereby Enables Noninvasive Streptococcus pneumoniae to Cause Deadly Pneumonia . *J Immunol*. **205,** 1601–1607

524. Sun, K. & Metzger, D. W. (2008). Inhibition of pulmonary antibacterial defense by interferon-γ during recovery from influenza infection. *Nat Med*. **14,** 558–564

525. Jochems, S. P., Marcon, F., Carniel, B. F., Holloway, M., Mitsi, E., Smith, E., Gritzfeld, J. F., Solórzano, C., Reiné, J., Pojar, S., Nikolaou, E., German, E. L., Hyder-Wright, A., Hill, H., Hales, C., de Steenhuijsen Piters, W. A. A., Bogaert, D., Adler, H., Zaidi, S., Connor, V., Gordon, S. B., Rylance, J., Nakaya, H. I. & Ferreira, D. M. (2018). Inflammation induced by influenza virus impairs human innate immune control of pneumococcus. *Nat Immunol*. **19,** 1299–1308

526. Li, J. J., Wang, W., Baines, K. J., Bowden, N. A., Hansbro, P. M., Gibson, P. G., Kumar, R. K., Foster, P. S. & Yang, M. (2010). IL-27/IFN-γ Induce MyD88-Dependent Steroid-Resistant Airway Hyperresponsiveness by Inhibiting Glucocorticoid Signaling in Macrophages. *J Immunol*. **185,** 4401–4409

527. Juniper, E. F., O'Byrne, P. M., Guyatt, G. H., Ferrie, P. J. & King, D. R. (1999). Development

and validation of a questionnaire to measure asthma control. *Eur Respir J*. **14,** 902–907

528. Juniper, E. F., Bousquet, J., Abetz, L. & Bateman, E. D. (2006). Identifying 'well-controlled' and 'not well-controlled' asthma using the Asthma Control Questionnaire. *Respir Med*. **100,** 616–621

529. Simpson, J. L., Scott, R., Boyle, M. J. & Gibson, P. G. (2006). Inflammatory subtypes in asthma: Assessment and identification using induced sputum. *Respirology*. **11,** 54–61

530. Rossall, M. R. W., Cadden, P. A., Molphy, S. D., Plumb, J. & Singh, D. (2014). Repeatability of induced sputum measurements in moderate to severe asthma. *Respir Med*. **108,** 1566–1568

531. Wilkinson, T. M. A., Aris, E., Bourne, S. C., Clarke, S. C., Peeters, M., Pascal, T. G., Taddei, L., Tuck, A. C., Kim, V. L., Ostridge, K. K., Staples, K. J., Williams, N. P., Williams, A. P., Wootton, S. A. & Devaster, J.-M. (2019). Drivers of year-to-year variation in exacerbation frequency of COPD: analysis of the AERIS cohort. *ERJ Open Res*. **5,** 00248–02018

532. Essilfie, A. T., Simpson, J. L., Horvat, J. C., Preston, J. A., Dunkley, M. L., Foster, P. S., Gibson, P. G. & Hansbro, P. M. (2011). Haemophilus influenzae infection drives IL-17-mediated neutrophilic Allergic airways disease. *PLoS Pathog*. **7,** e1002244

533. Dickson, R. P., Erb-Downward, J. R. & Huffnagle, G. B. (2013). The role of the bacterial microbiome in lung disease. *Expert Rev Respir Med*. **7,** 245–257

534. Simpson, J. L., Grissell, T. V., Douwes, J., Scott, R. J., Boyle, M. J. & Gibson, P. G. (2007). Innate immune activation in neutrophilic asthma and bronchiectasis. *Thorax*. **62,** 211–218

535. Baines, K. J., Simpson, J. L., Wood, L. G., Scott, R. J. & Gibson, P. G. (2011). Transcriptional phenotypes of asthma defined by gene expression profiling of induced sputum samples. *J Allergy Clin Immunol*. **127,** 153-160.e9

536. Goleva, E., Jackson, L. P., Harris, J. K., Robertson, C. E., Sutherland, E. R., Hall, C. F., Good, J. T., Gelfand, E. W., Martin, R. J. & Leung, D. Y. M. (2013). The effects of airway microbiome on corticosteroid responsiveness in asthma. *Am J Respir Crit Care Med*. **188,** 1193–1201

537. Zasłona, Z., Flis, E., Wilk, M. M., Carroll, R. G., Palsson-McDermott, E. M., Hughes, M. M., Diskin, C., Banahan, K., Ryan, D. G., Hooftman, A., Misiak, A., Kearney, J., Lochnit, G., Bertrams, W., Greulich, T., Schmeck, B., McElvaney, O. J., Mills, K. H. G., Lavelle, E. C., Wygrecka, M., Creagh, E. M. & O'Neill, L. A. J. (2020). Caspase-11 promotes allergic airway inflammation. *Nat Commun*. **11,** 1055

538. Santos, J. C., Dick, M. S., Lagrange, B., Degrandi, D., Pfeffer, K., Yamamoto, M., Meunier, E., Pelczar, P., Henry, T. & Broz, P. (2018). LPS targets host guanylate-binding proteins to the

bacterial outer membrane for non-canonical inflammasome activation. *EMBO J*. **37,**

539. Mallia, P., Footitt, J., Sotero, R., Jepson, A., Contoli, M., Trujillo-Torralbo, M. B., Kebadze, T., Aniscenko, J., Oleszkiewicz, G., Gray, K., Message, S. D., Ito, K., Barnes, P. J., Adcock, I. M., Papi, A., Stanciu, L. A., Elkin, S. L., Kon, O. M., Johnson, M. & Johnston, S. L. (2012). Rhinovirus infection induces degradation of antimicrobial peptides and secondary bacterial infection in chronic obstructive pulmonary disease. *Am J Respir Crit Care Med*. **186,** 1117–1124

540. Kusner, D. J., Thompson, C. R., Melrose, N. A., Pitson, S. M., Obeid, L. M. & Iyer, S. S. (2007). The localization and activity of sphingosine kinase 1 are coordinately regulated with actin cytoskeletal dynamics in macrophages. *J Biol Chem*. **282,** 23147–23162

541. Zhang, Y., Willis-Owen, S. A. G., Spiegel, S., Lloyd, C. M., Moffatt, M. F. & Cookson, W. O. C. M. (2019). The ORMDL3 asthma gene regulates ICAM1 and has multiple effects on cellular inflammation. *Am J Respir Crit Care Med*. **199,** 478–488

542. Hodge, S., Macowan, M., Liu, H., Hamon, R., Chen, A. C. H., Marchant, J. M., Pizzutto, S. J., Upham, J. W. & Chang, A. B. (2020). Sphingosine signaling dysfunction in airway cells as a potential contributor to progression from protracted bacterial bronchitis to bronchiectasis in children. *Pediatr Pulmonol*. **55,** 1414–1423

543. Barnawi, J., Tran, H., Jersmann, H., Pitson, S., Roscioli, E., Hodge, G., Meech, R., Haberberger, R. & Hodge, S. (2015). Potential link between the sphingosine-1-phosphate (S1P) system and defective alveolar macrophage phagocytic function in chronic obstructive pulmonary disease (COPD). *PLoS One*. **10,** e0122771

544. Tomlinson, G. S., Booth, H., Petit, S. J., Potton, E., Towers, G. J., Miller, R. F., Chain, B. M. & Noursadeghi, M. (2012). Adherent human alveolar macrophages exhibit a transient pro-inflammatory profile that confounds responses to innate immune stimulation. *PLoS One*. **7,** e40348

545. Nicholas, B., Staples, K. J., Moese, S., Meldrum, E., Ward, J., Dennison, P., Havelock, T., Hinks, T. S. C., Amer, K., Woo, E., Chamberlain, M., Singh, N., North, M., Pink, S., Wilkinson, T. M. A. & Djukanović, R. (2015). A Novel Lung Explant Model for the Ex Vivo Study of Efficacy and Mechanisms of Anti-Influenza Drugs. *J Immunol*. **194,** 6144–6154

546. Porotto, M., Ferren, M., Chen, Y. W., Siu, Y., Makhsous, N., Rima, B., Briese, T., Greninger, A. L., Snoeck, H. W. & Moscona, A. (2019). Authentic modeling of human respiratory virus infection in human pluripotent stem cell-derived lung organoids. *MBio*. **10,** 1–13

547. Huh, D., Matthews, B. D., Mammoto, A., Montoya-Zavala, M., Hsin, H. Y. & Ingber, D. E. (2010). Reconstituting organ-level lung functions on a chip. *Science*. **328,** 1662–8

548. Winokur, P. L., Chaloner, K., Doern, G. V., Ferreira, J. & Apicella, M. A. (2013). Safety and immunological outcomes following human inoculation with nontypeable haemophilus influenzae. *J Infect Dis*. **208,** 728–738

549. Bissonnette, E. Y., Lauzon-Joset, J. F., Debley, J. S. & Ziegler, S. F. (2020). Cross-Talk Between Alveolar Macrophages and Lung Epithelial Cells is Essential to Maintain Lung Homeostasis. *Front Immunol*. **11,** 1–12

550. Marriott, H. M., Gascoyne, K. A., Gowda, R., Geary, I., Nicklin, M. J. H., Iannelli, F., Pozzi, G., Mitchell, T. J., Whyte, M. K. B., Sabroe, I. & Dockrell, D. H. (2012). Interleukin-1β regulates CXCL8 release and influences disease outcome in response to Streptococcus pneumoniae, defining intercellular cooperation between pulmonary epithelial cells and macrophages. *Infect Immun*. **80,** 1140–1149

551. Peiró, T., Patel, D. F., Akthar, S., Gregory, L. G., Pyle, C. J., Harker, J. A., Birrell, M. A., Lloyd, C. M. & Snelgrove, R. J. (2018). Neutrophils drive alveolar macrophage IL-1β release during respiratory viral infection. *Thorax*. **73,** 546–556

552. Rocha, R., Almeida, C. & Azevedo, N. F. (2018). Influence of the fixation/permeabilization step on peptide nucleic acid fluorescence in situ hybridization (PNA-FISH) for the detection of bacteria. *PLoS One*. **13,** e0196522

553. Mayhew, D., Devos, N., Lambert, C., Brown, J. R., Clarke, S. C., Kim, V. L., Magid-Slav, M., Miller, B. E., Ostridge, K. K., Patel, R., Sathe, G., Simola, D. F., Staples, K. J., Sung, R., Tal-Singer, R., Tuck, A. C., Van Horn, S., Weynants, V., Williams, N. P., Devaster, J. M. & Wilkinson, T. M. A. (2018). Longitudinal profiling of the lung microbiome in the AERIS study demonstrates repeatability of bacterial and eosinophilic COPD exacerbations. *Thorax*. **73,** 422–430

554. Han, M. L. K., Zhou, Y., Murray, S., Tayob, N., Noth, I., Lama, V. N., Moore, B. B., White, E. S., Flaherty, K. R., Huffnagle, G. B. & Martinez, F. J. (2014). Lung microbiome and disease progression in idiopathic pulmonary fibrosis: An analysis of the COMET study. *Lancet Respir Med*. **2,** 548–556

555. Razvi, S., Quittell, L., Sewall, A., Quinton, H., Marshall, B. & Saiman, L. (2009). Respiratory microbiology of patients with cystic fibrosis in the United States, 1995 to 2005. *Chest*. **136,** 1554–1560

556. Hall-Stoodley, L. & Stoodley, P. (2009). Evolving concepts in biofilm infections. *Cell Microbiol*. **11,** 1034–1043

557. Weiss, G. & Schaible, U. E. (2015). Macrophage defense mechanisms against intracellular bacteria. *Immunol Rev*. **264,** 182–203

558. Salaemae, W., Booker, G. W. & Polyak, S. W. (2016). The Role of Biotin in Bacterial Physiology and Virulence: a Novel Antibiotic Target for Mycobacterium tuberculosis. *Microbiol Spectr*. **4,**

559. Agrawal, S., Agrawal, A. & Said, H. M. (2016). Biotin deficiency enhances the inflammatory response of human dendritic cells. *Am J Physiol Cell Physiol*. **311,** C386-91

560. Kuroishi, T., Kinbara, M., Sato, N., Tanaka, Y., Nagai, Y., Iwakura, Y., Endo, Y. & Sugawara, S. (2009). Biotin status affects nickel allergy via regulation of interleukin-1β production in mice. *J Nutr*. **139,** 1031–1036

561. Lange, N. E., Litonjua, A., Hawrylowicz, C. M. & Weiss, S. (2009). Vitamin D, the immune system and asthma. *Expert Rev Clin Immunol*. **5,** 693–702

562. Muda, N. M., Nasreen, M., Dhouib, R., Hosmer, J., Hill, J., Mahawar, M., Schirra, H. J., McEwan, A. G. & Kappler, U. (2019). Metabolic analyses reveal common adaptations in two invasive Haemophilus influenzae strains. *Pathog Dis*. **77,** 15

563. Epand, R. M., Walker, C., Epand, R. F. & Magarvey, N. A. (2016). Molecular mechanisms of membrane targeting antibiotics. *Biochim Biophys Acta*. **1858,** 980–7

564. Tristram, S., Jacobs, M. R. & Appelbaum, P. C. (2007). Antimicrobial resistance in Haemophilus influenzae. *Clinical Microbiology Reviews*. **20,** 368–389

565. Ubukata, K., Shibasaki, Y., Yamamoto, K., Chiba, N., Hasegawa, K., Takeuchi, Y., Sunakawa, K., Inoue, M. & Konno, M. (2001). Association of amino acid substitutions in penicillin-binding protein 3 with β-lactam resistance in β-lactamase-negative ampicillin-resistant Haemophilus influenzae. *Antimicrob Agents Chemother*. **45,** 1693–1699

566. Amato, S. M., Fazen, C. H., Henry, T. C., Mok, W. W. K., Orman, M. A., Sandvik, E. L., Volzing, K. G. & Brynildsen, M. P. (2014). The role of metabolism in bacterial persistence. *Front Microbiol*. **5,** 70

567. Cohen, N. R., Lobritz, M. A. & Collins, J. J. (2013). Microbial persistence and the road to drug resistance. *Cell Host and Microbe*. **13,** 632–642

568. Cox, G. (1995). Glucocorticoid treatment inhibits apoptosis in human neutrophils. Separation of survival and activation outcomes. *J Immunol*. **154,** 4719–25

569. Bai, T. R., Vonk, J. M., Postma, D. S. & Boezen, H. M. (2007). Severe exacerbations predict excess lung function decline in asthma. *Eur Respir J*. **30,** 452–456

570. O'Byrne, P. M., Pedersen, S., Lamm, C. J., Tan, W. C. & Busse, W. W. (2009). Severe exacerbations and decline in lung function in asthma. *Am J Respir Crit Care Med*. **179,** 19–24

571. Sakai, S., Kawamata, H., Mantani, N., Kogure, T., Shimada, Y., Terasawa, K., Sakai, T., Imanishi, N. & Ochiai, H. (2000). Therapeutic Effect of Anti-Macrophage Inflammatory Protein 2 Antibody on Influenza Virus-Induced Pneumonia in Mice. *J Virol*. **74,** 2472–2476

572. Habibi, M. S., Thwaites, R. S., Chang, M., Jozwik, A., Paras, A., Kirsebom, F., Varese, A., Owen, A., Cuthbertson, L., James, P., Tunstall, T., Nickle, D., Hansel, T. T., Moffatt, M. F., Johansson, C., Chiu, C. & Openshaw, P. J. M. (2020). Neutrophilic inflammation in the respiratory mucosa predisposes to RSV infection. *Science*. **370,**

573. Beech, A. S., Lea, S., Kolsum, U., Wang, Z., Miller, B. E., Donaldson, G. C., Wedzicha, J. A., Brightling, C. E. & Singh, D. (2020). Bacteria and sputum inflammatory cell counts; a COPD cohort analysis. *Respir Res*. **21,** 289

574. Kalchiem-Dekel, O., Yao, X. & Levine, S. J. (2020). Meeting the Challenge of Identifying New Treatments for Type 2-Low Neutrophilic Asthma. *Chest*. **157,** 26–33

575. Hernandez, M. L., Mills, K., Almond, M., Todoric, K., Aleman, M. M., Zhang, H., Zhou, H. & Peden, D. B. (2015). IL-1 receptor antagonist reduces endotoxin-induced airway inflammation in healthy volunteers. *J Allergy Clin Immunol*. **135,** 379–385

576. Denney, L. & Ho, L. P. (2018). The role of respiratory epithelium in host defence against influenza virus infection. *Biomedical Journal*. **41,** 218–233

577. Edinger, T. O., Pohl, M. O. & Stertz, S. (2014). Entry of influenza A virus: Host factors and antiviral targets. *J Gen Virol*. **95,** 263–277

578. Ng, P. S. K., Day, C. J., Atack, J. M., Hartley-Tassell, L. E., Winter, L. E., Marshanski, T., Padler-Karavani, V., Varki, A., Barenkamp, S. J., Apicella, M. A. & Jennings, M. P. (2019). Nontypeable Haemophilus influenzae Has Evolved Preferential Use of N-Acetylneuraminic Acid as a Host Adaptation. *MBio*. **10,**

579. Heise, T., Langereis, J. D., Rossing, E., de Jonge, M. I., Adema, G. J., Büll, C. & Boltje, T. J. (2018). Selective Inhibition of Sialic Acid-Based Molecular Mimicry in Haemophilus influenzae Abrogates Serum Resistance. *Cell Chem Biol*. **25,** 1279-1285.e8

580. Damasio, G. A. C., Pereira, L. A., Moreira, S. D. R., Duarte dos Santos, C. N., Dalla-Costa, L. M. & Raboni, S. M. (2015). Does virus-bacteria coinfection increase the clinical severity of acute respiratory infection? *J Med Virol*. **87,** 1456–1461

581. Nita-Lazar, M., Banerjee, A., Feng, C., Amin, M. N., Frieman, M. B., Chen, W. H., Cross, A. S., Wang, L. X. & Vasta, G. R. (2015). Desialylation of airway epithelial cells during influenza virus infection enhances pneumococcal adhesion via galectin binding. *Mol Immunol*. **65,** 1–16

582. Wu, A., Mihaylova, V. T., Landry, M. L. & Foxman, E. F. (2020). Interference between rhinovirus and influenza A virus: a clinical data analysis and experimental infection study. *The Lancet Microbe*. **1,** e254–e262

583. Hamilton, J. R., Sachs, D., Lim, J. K., Langlois, R. A., Palese, P. & Heaton, N. S. (2016). Club cells surviving influenza A virus infection induce temporary nonspecific antiviral immunity. *Proc Natl Acad Sci U S A*. **113,** 3861–3866

584. Schorey, J. S., Cheng, Y., Singh, P. P. & Smith, V. L. (2015). Exosomes and other extracellular vesicles in host–pathogen interactions. *EMBO Rep*. **16,** 24–43

585. Beatty, W. L. & Russell, D. G. (2000). Identification of mycobacterial surface proteins released into subcellular compartments of infected macrophages. *Infect Immun*. **68,** 6997–7002

586. Bhatnagar, S. & Schorey, J. S. (2007). Exosomes released from infected macrophages contain Mycobacterium avium glycopeptidolipids and are proinflammatory. *J Biol Chem*. **282,** 25779–25789

587. Chen, S., Yang, J., Wei, Y. & Wei, X. (2020). Epigenetic regulation of macrophages: from homeostasis maintenance to host defense. *Cellular and Molecular Immunology*. **17,** 36–49

588. Burke, H., Freeman, A., Ostridge, K., Staples, K. J., Spalluto, M. & Wilkinson, T. (European Respiratory Society (ERS)., 2019). Lung exosomal miRNAs discriminate between healthy ex-smokers and COPD. in PP212 doi:10.1183/23120541.lungscienceconference-2019.pp212

589. Levänen, B., Bhakta, N. R., Torregrosa Paredes, P., Barbeau, R., Hiltbrunner, S., Pollack, J. L., Sköld, C. M., Svartengren, M., Grunewald, J., Gabrielsson, S., Eklund, A., Larsson, B.-M., Woodruff, P. G., Erle, D. J. & Wheelock, Å. M. (2013). Altered microRNA profiles in bronchoalveolar lavage fluid exosomes in asthmatic patients. *J Allergy Clin Immunol*. **131,** 894–903

590. Mehra, A., Zahra, A., Thompson, V., Sirisaengtaksin, N., Wells, A., Porto, M., Köster, S., Penberthy, K., Kubota, Y., Dricot, A., Rogan, D., Vidal, M., Hill, D. E., Bean, A. J. & Philips, J. A. (2013). Mycobacterium tuberculosis Type VII Secreted Effector EsxH Targets Host ESCRT to Impair Trafficking. *PLoS Pathog*. **9,** e1003734

591. Ilott, N. E., Heward, J. A., Roux, B., Tsitsiou, E., Fenwick, P. S., Lenzi, L., Goodhead, I., Hertz-Fowler, C., Heger, A., Hall, N., Donnelly, L. E., Sims, D. & Lindsay, M. A. (2014). Long non-coding RNAs and enhancer RNAs regulate the lipopolysaccharide-induced inflammatory response in human monocytes. *Nat Commun*. **5,** 3979

592. Schaar, V., De Vries, S. P. W., Perez Vidakovics, M. L. A., Bootsma, H. J., Larsson, L.,

Hermans, P. W. M., Bjartell, A., Mörgelin, M. & Riesbeck, K. (2011). Multicomponent Moraxella catarrhalis outer membrane vesicles induce an inflammatory response and are internalized by human epithelial cells. *Cell Microbiol*. **13,** 432–449

593. Sharpe, S. W., Kuehn, M. J. & Mason, K. M. (2011). Elicitation of epithelial cell-derived immune effectors by outer membrane vesicles of nontypeable haemophilus influenzae. *Infect Immun*. **79,** 4361–4369

594. Schaar, V., Nordström, T., Mörgelin, M. & Riesbeck, K. (2011). Moraxella catarrhalis outer membrane vesicles carry β-lactamase and promote survival of Streptococcus pneumoniae and Haemophilus influenzae by inactivating amoxicillin. *Antimicrob Agents Chemother*. **55,** 3845–3853

595. Novakovic, B., Habibi, E., Wang, S. Y., Arts, R. J. W., Davar, R., Megchelenbrink, W., Kim, B., Kuznetsova, T., Kox, M., Zwaag, J., Matarese, F., van Heeringen, S. J., Janssen-Megens, E. M., Sharifi, N., Wang, C., Keramati, F., Schoonenberg, V., Flicek, P., Clarke, L., Pickkers, P., Heath, S., Gut, I., Netea, M. G., Martens, J. H. A., Logie, C. & Stunnenberg, H. G. (2016). β-Glucan Reverses the Epigenetic State of LPS-Induced Immunological Tolerance. *Cell*. **167,** 1354-1368.e14

596. Gazzar, M. El, Yoza, B. K., Chen, X., Garcia, B. A., Young, N. L. & McCall, C. E. (2009). Chromatin-Specific Remodeling by HMGB1 and Linker Histone H1 Silences Proinflammatory Genes during Endotoxin Tolerance. *Mol Cell Biol*. **29,** 1959–1971

597. Roquilly, A., Jacqueline, C., Davieau, M., Mollé, A., Sadek, A., Fourgeux, C., Rooze, P., Broquet, A., Misme-Aucouturier, B., Chaumette, T., Vourc'h, M., Cinotti, R., Marec, N., Gauttier, V., McWilliam, H. E. G., Altare, F., Poschmann, J., Villadangos, J. A. & Asehnoune, K. (2020). Alveolar macrophages are epigenetically altered after inflammation, leading to long-term lung immunoparalysis. *Nat Immunol*. **21,** 636–648

598. Netea, M. G., Joosten, L. A. B., Latz, E., Mills, K. H. G., Natoli, G., Stunnenberg, H. G., O'Neill, L. A. J. & Xavier, R. J. (2016). Trained immunity: A program of innate immune memory in health and disease. *Science*. **352,** aaf1098

599. Thuan, T. T., Mörgelin, M., Forsgren, A. & Riesbeck, K. (2007). Haemophilus influenzae survival during complement-mediated attacks is promoted by Moraxella catarrhalis outer membrane vesicles. *J Infect Dis*. **195,** 1661–1670

600. Brockson, M. E., Novotny, L. A., Jurcisek, J. A., McGillivary, G., Bowers, M. R. & Bakaletz, L. O. (2012). Respiratory syncytial virus promotes Moraxella catarrhalis-induced ascending experimental otitis media. *PLoS One*. **7,** e40088

601. Kotaniemi-Syrjänen, A., Vainionpää, R., Reijonen, T. M., Waris, M., Korhonen, K. & Korppi,

M. (2003). Rhinovirus-induced wheezing in infancy - The first sign of childhood asthma? *J Allergy Clin Immunol*. **111,** 66–71

602. Lemanske, R. F., Jackson, D. J., Gangnon, R. E., Evans, M. D., Li, Z., Shult, P. A., Kirk, C. J., Reisdorf, E., Roberg, K. A., Anderson, E. L., Carlson-Dakes, K. T., Adler, K. J., Gilbertson-White, S., Pappas, T. E., DaSilva, D. F., Tisler, C. J. & Gern, J. E. (2005). Rhinovirus illnesses during infancy predict subsequent childhood wheezing. *J Allergy Clin Immunol*. **116,** 571–577

603. Jackson, D. J., Gangnon, R. E., Evans, M. D., Roberg, K. A., Anderson, E. L., Pappas, T. E., Printz, M. C., Lee, W. M., Shult, P. A., Reisdorf, E., Carlson-Dakes, K. T., Salazar, L. P., DaSilva, D. F., Tisler, C. J., Gern, J. E. & Lemanske, R. F. (2008). Wheezing rhinovirus illnesses in early life predict asthma development in high-risk children. *Am J Respir Crit Care Med*. **178,** 667–672

604. Wu, P. & Hartert, T. V. (2011). Evidence for a causal relationship between respiratory syncytial virus infection and asthma. *Expert Rev Anti Infect Ther*. **9,** 731–745

605. Spalluto, C. M., Singhania, A., Cellura, D., Woelk, C. H., Sanchez-Elsner, T., Staples, K. J. & Wilkinson, T. M. A. (2017). IFN-g influences epithelial antiviral responses via histone methylation of the RIG-I promoter. *Am J Respir Cell Mol Biol*. **57,** 428–438

606. Kamada, R., Yang, W., Zhang, Y., Patel, M. C., Yang, Y., Ouda, R., Dey, A., Wakabayashi, Y., Sakaguchi, K., Fujita, T., Tamura, T., Zhu, J. & Ozato, K. (2018). Interferon stimulation creates chromatin marks and establishes transcriptional memory. *Proc Natl Acad Sci U S A*. **115,** E9162–E9171

607. Larsen, J. M., Musavian, H. S., Butt, T. M., Ingvorsen, C., Thysen, A. H. & Brix, S. (2015). Chronic obstructive pulmonary disease and asthma-associated Proteobacteria, but not commensal Prevotella spp., promote Toll-like receptor 2-independent lung inflammation and pathology. *Immunology*. **144,** 333–342

608. Larsen, J. M., Steen-Jensen, D. B., Laursen, J. M., Søndergaard, J. N., Musavian, H. S., Butt, T. M. & Brix, S. (2012). Divergent pro-inflammatory profile of human dendritic cells in response to commensal and pathogenic bacteria associated with the airway microbiota. *PLoS One*. **7,** e31976

609. Michelucci, A., Cordes, T., Ghelfi, J., Pailot, A., Reiling, N., Goldmann, O., Binz, T., Wegner, A., Tallam, A., Rausell, A., Buttini, M., Linster, C. L., Medina, E., Balling, R. & Hiller, K. (2013). Immune-responsive gene 1 protein links metabolism to immunity by catalyzing itaconic acid production. *Proc Natl Acad Sci U S A*. **110,** 7820–7825

610. O'Neill, L. A. J. & Artyomov, M. N. (2019). Itaconate: the poster child of metabolic

reprogramming in macrophage function. *Nature Reviews Immunology*. **19,** 273–281

611. Lee, C. G. L., Jenkins, N. A., Gilbert, D. J., Copeland, N. G. & O'Brien, W. E. (1995). Cloning and analysis of gene regulation of a novel LPS-inducible cDNA. *Immunogenetics*. **41,** 263–270

612. Nair, S., Huynh, J. P., Lampropoulou, V., Loginicheva, E., Esaulova, E., Gounder, A. P., Boon, A. C. M., Schwarzkopf, E. A., Bradstreet, T. R., Edelson, B. T., Artyomov, M. N., Stallings, C. L. & Diamond, M. S. (2018). Irg1 expression in myeloid cells prevents immunopathology during M. tuberculosis infection. *J Exp Med*. **215,** 1035–1045

613. Hoffmann, E., Machelart, A., Belhaouane, I., Deboosere, N., Pauwels, A. M., Saint-André, J. P., Song, O. R., Jouny, S., Poncet, A., Marion, S., Beyaert, R., Majlessi, L. & Brodin, P. (2019). Irg1 controls immunometabolic host response and restricts intracellular mycobacterium tuberculosis infection: Immunometabolic host response to tuberculosis. *bioRxiv*. doi:10.1101/761551

614. Hersch, S. J. & Navarre, W. W. (2020). The Salmonella LysR Family Regulator RipR Activates the SPI-13-Encoded Itaconate Degradation Cluster. *Infect Immun*. **88,**

615. Sasikaran, J., Ziemski, M., Zadora, P. K., Fleig, A. & Berg, I. A. (2014). Bacterial itaconate degradation promotes pathogenicity. *Nat Chem Biol*. **10,** 371–377

616. Mills, E. L., Ryan, D. G., Prag, H. A., Dikovskaya, D., Menon, D., Zaslona, Z., Jedrychowski, M. P., Costa, A. S. H., Higgins, M., Hams, E., Szpyt, J., Runtsch, M. C., King, M. S., McGouran, J. F., Fischer, R., Kessler, B. M., McGettrick, A. F., Hughes, M. M., Carroll, R. G., Booty, L. M., Knatko, E. V., Meakin, P. J., Ashford, M. L. J., Modis, L. K., Brunori, G., Sévin, D. C., Fallon, P. G., Caldwell, S. T., Kunji, E. R. S., Chouchani, E. T., Frezza, C., Dinkova-Kostova, A. T., Hartley, R. C., Murphy, M. P. & O'Neill, L. A. (2018). Itaconate is an anti-inflammatory metabolite that activates Nrf2 via alkylation of KEAP1. *Nature*. **556,** 113–117

617. Hooftman, A., Angiari, S., Hester, S., Corcoran, S. E., Runtsch, M. C., Ling, C., Ruzek, M. C., Slivka, P. F., McGettrick, A. F., Banahan, K., Hughes, M. M., Irvine, A. D., Fischer, R. & O'Neill, L. A. J. (2020). The Immunomodulatory Metabolite Itaconate Modifies NLRP3 and Inhibits Inflammasome Activation. *Cell Metab*. **32,** 468-478.e7

618. Muri, J., Wolleb, H., Broz, P., Carreira, E. M. & Kopf, M. (2020). Electrophilic Nrf2 activators and itaconate inhibit inflammation at low dose and promote IL-1β production and inflammatory apoptosis at high dose. *Redox Biol*. **36,** 101647

619. Ogger, P. P., Albers, G. J., Hewitt, R. J., O'Sullivan, B. J., Powell, J. E., Calamita, E., Ghai, P., Walker, S. A., McErlean, P., Saunders, P., Kingston, S., Molyneaux, P. L., Halket, J. M., Gray, R., Chambers, D. C., Maher, T. M., Lloyd, C. M. & Byrne, A. J. (2020). Itaconate controls the

severity of pulmonary fibrosis. *Sci Immunol*. **5,**

620. Gibson, P. G., Yang, I. A., Upham, J. W., Reynolds, P. N., Hodge, S., James, A. L., Jenkins, C., Peters, M. J., Marks, G. B., Baraket, M., Powell, H. & Simpson, J. L. (2019). Efficacy of azithromycin in severe asthma from the AMAZES randomised trial. *ERJ Open Res*. **5,** 00056–02019

621. Taylor, S. L., Leong, L. E. X., Mobegi, F. M., Choo, J. M., Wesselingh, S., Yang, I. A., Upham, J. W., Reynolds, P. N., Hodge, S., James, A. L., Jenkins, C., Peters, M. J., Baraket, M., Marks, G. B., Gibson, P. G., Rogers, G. B. & Simpson, J. L. (2019). Long-Term Azithromycin Reduces Haemophilus influenzae and Increases Antibiotic Resistance in Severe Asthma. *Am J Respir Crit Care Med*. **200,** 309–317

622. Osei, E. T., Brandsma, C., Timens, W., Heijink, I. H. & Hackett, T. (2020). Current perspectives on the role of interleukin-1 signalling in the pathogenesis of asthma and COPD. *Eur Respir J*. **55,** 1900563

623. Cline, T. D., Beck, D. & Bianchini, E. (2017). Influenza virus replication in macrophages: Balancing protection and pathogenesis. *J Gen Virol*. **98,** 2401–2412

624. Song, X., He, X., Li, X. & Qian, Y. (2016). The roles and functional mechanisms of interleukin-17 family cytokines in mucosal immunity. *Cellular and Molecular Immunology*. **13,** 418–431

625. Singanayagam, A., Chalmers, J. D. & Hill, A. T. (2010). Inhaled corticosteroids and risk of pneumonia: evidence for and against the proposed association. *QJM*. **103,** 379–85

626. Ekbom, E., Quint, J., Schöler, L., Malinovschi, A., Franklin, K., Holm, M., Torén, K., Lindberg, E., Jarvis, D. & Janson, C. (2019). Asthma and treatment with inhaled corticosteroids: Associations with hospitalisations with pneumonia. *BMC Pulm Med*. **19,** 1–8

627. O'Byrne, P., Fabbri, L. M., Pavord, I. D., Papi, A., Petruzzelli, S. & Lange, P. (2019). Asthma progression and mortality: The role of inhaled corticosteroids. *Eur Respir J*. **54,** 1–14

628. Slack, M. P. E. (2015). A review of the role of Haemophilus influenzae in community-acquired pneumonia. *Pneumonia*. **6,** 26–43

629. Freund, E. C., Lock, J. Y., Oh, J., Maculins, T., Delamarre, L., Bohlen, C. J., Haley, B. & Murthy, A. (2020). Efficient gene knockout in primary human and murine myeloid cells by non-viral delivery of CRISPR-Cas9. *J Exp Med*. **217,**

630. Murphy, T. F., Kirkham, C. & Lesse, A. J. (2006). Construction of a mutant and characterization of the role of the vaccine antigen P6 in outer membrane integrity of nontypeable Haemophilus influenzae. *Infect Immun*. **74,** 5169–5176

631. Murphy, T. F., Brauer, A. L., Grant, B. J. B. & Sethi, S. (2005). Moraxella catarrhalis in chronic obstructive pulmonary disease: Burden of disease and immune response. *Am J Respir Crit Care Med*. **172,** 195–199

632. Shirahama, S., Miki, A., Kaburaki, T. & Akimitsu, N. (2020). Long Non-coding RNAs Involved in Pathogenic Infection. *Front Genet*. **11,** 454

633. Avital, G., Avraham, R., Fan, A., Hashimshony, T., Hung, D. T. & Yanai, I. (2017). scDual-Seq: Mapping the gene regulatory program of Salmonella infection by host and pathogen single-cell RNA-sequencing. *Genome Biol*. **18,** 200

634. Schmidt, S. V., Krebs, W., Ulas, T., Xue, J., Babler, K., Günther, P., Hardt, A. L., Schultze, H., Sander, J., Klee, K., Theis, H., Kraut, M., Beyer, M. & Schultze, J. L. (2016). The transcriptional regulator network of human inflammatory macrophages is defined by open chromatin. *Cell Res*. **26,** 151–170